

AIR QUALITY MODELING

Theories, Methodologies,
Computational Techniques, and
Available Databases and Software

Volume III - Special Issues

Editor

Paolo Zannetti

Chapter Authors

Maureen E. Buono
Brad Cochran
Aaron Daly
Phyllis G. Diosey
Frank R. Freedman

J.D. McAlpine
Ronald L. Petersen
Michael Ruby
Ananthakrishna Sarma
Douglas Solomon

Jesse Thé
Robert J. Yamartino
Paolo Zannetti

AIR QUALITY MODELING

Theories, Methodologies, Computational Techniques,
and Available Databases and Software

Volume III – Special Issues

Blank Page

Dedicated to my brothers Roberto and Gino

PZ

Blank Page

AIR QUALITY MODELING
Theories, Methodologies, Computational Techniques,
and Available Databases and Software
Volume III – Special Issues

Editor

Paolo Zannetti

Chapter Authors

Maureen E. Buono, Brad Cochran, Aaron Daly, Phyllis G. Diosey,
Frank R. Freedman, J.D. McAlpine, Ronald L. Petersen,
Michael Ruby, Ananthakrishna Sarma, Douglas Solomon,
Jesse Thé, Robert J. Yamartino, Paolo Zannetti

Published by

The EnviroComp Institute
Air & Waste Management Association



AIR & WASTE MANAGEMENT
A S S O C I A T I O N

◆
SINCE 1907

Copyright © 2008 The EnviroComp Institute and Air & Waste Management Association. All rights reserved.

Notice regarding copyrights: Chapter authors retain copyrights to their original materials. All requests for permission to reproduce chapter material should be directed to the appropriate author(s); all other requests should be directed to the Air & Waste Management Association, One Gateway Center, 3rd Floor, 420 Ft. Duquesne Blvd., Pittsburgh, PA 15222-1435, USA.

ISBN 978-1-9334740-0-7 (CD-ROM version).

Printed in the United States of America.

Copies of this CD-ROM may be purchased by visiting the EnviroComp Institute site at <http://www.envirocomp.org/aqm>, the Air & Waste Management Association's online library at www.awma.org, or by contacting the A&WMA directly at 1-800-270-3444 or 1-412-232-3444 (please reference A&WMA Order Code OTHP-26-CD).

This book is also available from the A&WMA in hard copy format: Order Code OTHP-26 (ISBN 978-0-9232049-9-0).

For updates, additional information, and online discussion regarding this book series, please visit www.envirocomp.org/aqm.

Table of Contents – Volume III^{1, 2}

	<u>Preface</u>	<u>xi</u>
	<u>About the Editor</u>	<u>xiii</u>
	<u>About the Publishers</u>	<u>xv</u>
	<u>About the Chapter Authors/Contributors</u>	<u>xvii</u>
<u>1</u>	<u>The Problem – Air Pollution</u>	<u>1</u>
<u>2</u>	<u>The Tool – Mathematical Modeling</u>	<u>3</u>
<u>3</u>	<u>Emissions Modeling and Inventory</u>	<u>5</u>
1	<u>Introduction to Emissions Inventory and Emissions Modeling</u>	<u>6</u>
2	<u>Overview of Inventories</u>	<u>10</u>
3	<u>Process-Level Codes Used in Emissions Inventories</u>	<u>18</u>
4	<u>Emissions Estimation Techniques</u>	<u>21</u>
5	<u>Characterization of Emissions</u>	<u>28</u>
6	<u>Characterization of Point Sources</u>	<u>37</u>
7	<u>Area Sources</u>	<u>66</u>
8	<u>Fire Emissions</u>	<u>90</u>
9	<u>Biogenic and Geogenic</u>	<u>92</u>
10	<u>Available Emissions Models</u>	<u>93</u>
11	<u>Estimating Emissions for Use in Air Quality Modeling</u>	<u>95</u>
12	<u>Estimating Emissions for Air Toxic Human Health Risk Assessment</u>	<u>97</u>
13	<u>Emissions Inventory Quality Control</u>	<u>100</u>
14	<u>Greenhouse Gases</u>	<u>102</u>
15	<u>Data Quality Objectives (DQO)</u>	<u>107</u>
16	<u>Data Gap Filling</u>	<u>108</u>
17	<u>Rule Effectiveness, Rule Penetration, and Control Efficiency</u>	<u>108</u>
18	<u>Pollutant Monitoring and Fuel Analysis Methodologies</u>	<u>110</u>
19	<u>Emissions Inventory Terms</u>	<u>116</u>
<u>4</u>	<u>Air Pollution Meteorology</u>	<u>127</u>
<u>5</u>	<u>Meteorological Modeling</u>	<u>129</u>

¹ Chapters in italics will be provided in subsequent volumes.

² The table of contents for Volumes I and II can be found in this book on pages [473](#) and [477](#), respectively.

<u>5A</u>	<u>Meteorological Modeling for Air Quality Applications</u>	<u>131</u>
1	<u>Introduction</u>	<u>131</u>
2	<u>Modeling Approaches</u>	<u>137</u>
3	<u>Modeling Framework</u>	<u>142</u>
4	<u>Dynamical and Thermodynamical Processes</u>	<u>145</u>
5	<u>Physics Parameterizations</u>	<u>146</u>
6	<u>Model Numerics</u>	<u>160</u>
7	<u>Data Ingest</u>	<u>162</u>
8	<u>Model Verification and Validation</u>	<u>163</u>
9	<u>Symbols</u>	<u>164</u>
10	<u>List of Acronyms</u>	<u>165</u>
<u>5B</u>	<u>Large-Eddy Simulations of the Atmospheric Boundary Layer</u>	
<u>5C</u>	<u>Computational Fluid Dynamics of Microscale Meteorological Flows for Air Quality Applications</u>	<u>169</u>
1	<u>Introduction</u>	<u>170</u>
2	<u>Synopsis of CFD: the Math, Assumptions, and Availability</u>	<u>171</u>
3	<u>Simulating the Atmosphere in CFD</u>	<u>189</u>
4	<u>Industry Opinion and Guidelines</u>	<u>207</u>
5	<u>Validation and Verification</u>	<u>215</u>
6	<u>Conclusion</u>	<u>229</u>
<u>6</u>	<u>Plume Rise</u>	<u>235</u>
<u>7</u>	<u>Gaussian Plume Models</u>	<u>237</u>
<u>7A</u>	<u>Introduction to Gaussian Plume Models</u>	
<u>7B</u>	<u>Simulation Algorithms in Gaussian Plume Modeling</u>	<u>239</u>
1	<u>Introduction</u>	<u>239</u>
2	<u>Theoretical Background</u>	<u>241</u>
3	<u>Extending the Plume Formulation Beyond Point Sources</u>	<u>253</u>
4	<u>Removal Processes in Gaussian Plume Modeling</u>	<u>268</u>
<u>8</u>	<u>Gaussian Puff Modeling</u>	<u>281</u>
1	<u>Introduction</u>	<u>281</u>
2	<u>Theoretical Background</u>	<u>285</u>
3	<u>Puff Model Enhancements</u>	<u>301</u>
<u>9</u>	<u>Special Applications of Gaussian Models</u>	<u>315</u>
<u>10</u>	<u>Eulerian Dispersion Models</u>	<u>317</u>
<u>11</u>	<u>Lagrangian Particle Models</u>	<u>319</u>
<u>12</u>	<u>Atmospheric Transformations</u>	<u>321</u>
<u>13</u>	<u>Deposition Phenomena</u>	<u>323</u>

<u>14</u>	<u>Indoor Air Pollution Modeling</u>	<u>325</u>
<u>15</u>	<u>Modeling of Adverse Effects</u>	<u>327</u>
<u>15A</u>	<u>Modeling of Health Risks Associated with Combustion Facility Emissions</u>	
<u>15B</u>	<u>Odor Modeling</u>	<u>329</u>
1	<u>Modeling for Odors in the Atmosphere</u>	<u>329</u>
2	<u>Odor Measurement</u>	<u>330</u>
3	<u>Odor Modeling-Related Issues</u>	<u>333</u>
4	<u>Odor Criteria</u>	<u>338</u>
5	<u>Odor Models and Modeling Techniques</u>	<u>340</u>
6	<u>Summary</u>	<u>349</u>
<u>15C</u>	<u>Climate Change - An Introduction to Atmosphere-Ocean General Circulation Modeling</u>	<u>353</u>
1	<u>Introduction</u>	<u>353</u>
2	<u>AOGCM Formulation</u>	<u>355</u>
3	<u>Applications of AOGCMs</u>	<u>365</u>
4	<u>Future Development Needs and Further Readings</u>	<u>370</u>
<u>16</u>	<u>Statistical Modeling</u>	<u>379</u>
<u>16A</u>	<u>Air Quality Forecast and Alarm Systems</u>	
<u>16B</u>	<u>Receptor Models</u>	
<u>17</u>	<u>Evaluation of Air Pollution Models</u>	<u>381</u>
<u>18</u>	<u>Regulatory Modeling</u>	<u>383</u>
<u>18A</u>	<u>A Historical Look at the Development of Regulatory Air Quality Models for the United States Environmental Protection Agency</u>	
<u>19</u>	<u>Case Studies – Air Pollution Modeling at Local, Regional, Continental, and Global Scales</u>	<u>385</u>
<u>20</u>	<u>The Future of Air Pollution Modeling</u>	<u>387</u>
<u>21</u>	<u>Active Groups in Air Pollution Modeling</u>	<u>389</u>
<u>22</u>	<u>Available Software</u>	<u>391</u>
<u>23</u>	<u>Available Databases</u>	<u>393</u>
<u>24</u>	<u>Physical Modeling of Air Pollution</u>	<u>395</u>

<u>24A</u>	<u>Wind Tunnel Modeling of Pollutant Dispersion</u>	<u>397</u>
1	<u>Introduction</u>	<u>397</u>
2	<u>Theoretical Basis</u>	<u>399</u>
3	<u>Experimental Methods and Instrumentation</u>	<u>406</u>
4	<u>Typical Applications</u>	<u>418</u>
<u>25</u>	<u>Tracer Studies</u>	<u>433</u>
<u>26</u>	<u>Air Quality Modeling: Pre-Processing and Post-Processing</u>	<u>435</u>
1	<u>Introduction</u>	<u>435</u>
2	<u>Pre-Processing</u>	<u>436</u>
3	<u>Post-Processing</u>	<u>440</u>
4	<u>GIS in Air Quality Modeling</u>	<u>449</u>
5	<u>Summary</u>	<u>452</u>
<u>27</u>	<u>Air Quality Modeling Resources on the Web</u>	<u>453</u>
1	<u>Introduction</u>	<u>453</u>
2	<u>Regulatory Issues</u>	<u>454</u>
3	<u>Books</u>	<u>456</u>
4	<u>Available Software</u>	<u>456</u>
5	<u>Dispersion Models</u>	<u>459</u>
6	<u>Photochemical Models</u>	<u>460</u>
7	<u>Receptor Models</u>	<u>462</u>
8	<u>Air Quality Forecast and Resources</u>	<u>463</u>
9	<u>Visibility Modeling</u>	<u>464</u>
10	<u>Publications and Information Online</u>	<u>465</u>
11	<u>Courses Online</u>	<u>467</u>
12	<u>Case Studies</u>	<u>468</u>
13	<u>Resources and lists of References</u>	<u>470</u>
14	<u>Calculation Sites</u>	<u>471</u>
	<u>Table of Contents – Volume I</u>	<u>473</u>
	<u>Table of Contents – Volume II</u>	<u>477</u>
	<u>Authors’/Contributors’ Index for Volumes I, II and III</u>	<u>481</u>
	<u>Subject Index for Volumes I, II and III</u>	<u>485</u>

Preface

This is the third volume of our book series on air quality modeling published by the EnviroComp Institute and the Air & Waste Management Association (A&WMA). The series seeks to provide environmental scientists, engineers, researchers, and students with a comprehensive, organized, and evolving body of information in virtually all aspects of computer simulation of air pollution and related atmospheric phenomena. Each volume in the series expands the scope of our efforts by presenting new chapter topics and updates of material included in previous volumes.

All volumes in this series are available in both a traditional book format and an electronic format (CD-ROM). The electronic version is not a simple digital copy of the printed files, but includes additional material, such as active Internet pointers. In addition, the CD-ROM material can be quickly and easily searched by keywords. The book series also has its own Web page, www.envirocomp.org/aqm, which readers are encouraged to visit for additional information.

Volume I primarily presented introductory material and Volume II focused on more advanced topics. Volume III presents special air quality issues, such as emission modeling, mesoscale meteorology, computational fluid dynamics for microscale flows, Gaussian plume and puff models, odor modeling, greenhouse gasses and global climate change, modeling pre-processors and post-processors, and resources on the Web.

As a whole, the three volumes now provide a comprehensive description of almost all technical topics related to air quality modeling. Future volumes in the book series are expected to complete the effort and update previous chapters.

I want to express my sincere thanks to the chapter authors for their competence, dedication, and patience in the production of this volume. Thanks are also due to A&WMA Publications Director Andy Knopes for his help and support in the preparation of the entire book series. Sincere appreciation is again extended to Ji Ohm and Scott Cragin who, as with previous volumes, provided extremely valuable editorial and organizational assistance throughout the entire book production cycle.

Paolo Zannetti
Fremont, California

BRITISH
LIBRARY

About the Editor

Dr. Paolo Zannetti is the President of the EnviroComp Institute and EnviroComp Consulting, Inc. in Fremont, California. He received a Doctoral Degree in Physics from the University of Padova (Italy) and has managed a range of environmental projects throughout his professional career. With a specialization in air pollution and environmental modeling and software, Dr. Zannetti's experience has covered research and development studies, teaching, consulting, modeling, software development, project management, editorial activities, and expert testimony. In addition to authoring in 1990 the first comprehensive textbook, *Air Pollution Modeling — Theories, Computational Methods and Available Software*, Dr. Zannetti has authored more than 200 publications, primarily for peer-reviewed journals and conference proceedings. For more information, visit <http://www.envirocomp.org/html/meetus/zannetti.htm>.

Blank Page

About the Publishers

The EnviroComp Institute

The International Institute of Environmental Sciences and Environmental Computing (EnviroComp) is a nonprofit, Internet-based institute and software laboratory dedicated to the study of environmental sciences and pollution phenomena. Founded in 1996, the EnviroComp Institute also promotes the publication of a unique, new-generation series of environmental books in electronic format. For more information, visit the institute's website at <http://www.envirocomp.org>.

The Air & Waste Management Association

The Air & Waste Management Association (AWMA) is a nonprofit, nonpartisan professional organization that provides information, training, and networking opportunities to thousands of environmental professionals around the world. AWMA was founded in 1907 and is headquartered in Pittsburgh, Pennsylvania. For more information, visit the association's Web site at <http://www.awma.org>.

Blank Page

About the Chapter Authors/Contributors for Volumes I, II and III
([Additional information](#) is provided in the CD-ROM version)

Anfossi

Dr. Domenico Anfossi
CNR - ISAC, Sezione di Torino
Corso Fiume 4
I-10133 - Torino
ITALY

Phone: +39 011 6606376
Phone direct: +39 011 3839826
Fax: +39 011 6600364
Email: anfossi@to.infn.it or d.anfossi@isac.cnr.it
Work site: <http://www.isac.cnr.it>

Builtjes

Dr. Peter J.H. Builtjes
Professor
TNO Environment, Energy and Process Innovation
Department of Environmental Quality
Laan van Westenenk 501
P.O. Box 342
7300 AH Apeldoorn
THE NETHERLANDS

Phone: +31 555493038
Fax: +31 555493252
Email: p.j.h.builtjes@mep.tno.nl

Buono

Maureen E. Buono
Malcolm Pirnie, Inc.
104 Corporate Park Drive
White Plains, NY 11102
USA

Byun

Dr. Daewon W. Byun
Professor
312 Science & Research Bldg. 1
Geoscience Department
University of Houston
Houston, Texas 77204-5007
USA

Email: dwbyun@math.uh.edu

Canepa

Elisa Canepa, Ph.D.
Atmospheric and Oceanic Physics Group
INFN - Department of Physics
University of Genova
Via Dodecaneso 33
I-16146 Genova
ITALY

Phone: +39 010 353 6354
Fax: +39 010 353 6354
Email: elisa.canepa@fisica.unige.it or
canepae@libero.it

Work site: <http://www.fisica.unige.it/~atmosfe/>
Personal site: <http://www.fisica.unige.it/~canepae/>

Carrington

David B. Carrington, Ph.D.
Los Alamos National Laboratory
CCS-4 Transport Methods
P.O. Box 1663 MS D409
Los Alamos, NM 87545
USA

Phone: (505) 667-3569
Email: dcrrngtn@lanl.gov

Chow

Judith C. Chow, Sc.D.
Department of Atmospheric Sciences
Desert Research Institute
University of Nevada, Reno
2215 Raggio Parkway
Reno, NV 89512
USA

Phone direct: (775) 674-7050
Fax: (775) 674-7009
Email: judy.chow@dri.edu
Work site: <http://www.das.dri.edu/>
Personal site: <http://www.dri.edu/People/judyc/>

Cochran

Mr. Brad Cochran
Sr. Associate, CPP, Inc.
1415 Blue Spruce Drive
Fort Collins, CO 80524
USA

Phone: (970) 221-3371
Fax: (970) 221-3124
Email: bcochran@cppwind.com
Work site: www.cppwind.com

Daly

Aaron Daly
EnviroComp Consulting, Inc.
2298 Ocaso Camino
Fremont, CA 94539
USA

Phone: (408) 893-1874
Fax: (408) 351-8400
Email: daly@envirocomp.com
Work site: <http://www.envirocomp.com>

Degrazia

Dr. Gervásio A. Degrazia
Universidade Federal de Santa Maria
Departamento de Física
97105900 Santa Maria – RS
BRASIL

Phone: +55 55 2208616
+55 55 2208032
Email: degrazia@ccne.ufsm.br

Diosey

Phyllis G. Diosey
Malcolm Pirnie, Inc.
104 Corporate Park Drive
White Plains, NY 11102
USA

Phone: (914) 641-2646
Fax: (914) 641-2645
Email: pdiosey@pirnie.com
Work site: <http://www.pirnie.com>

Eastman

Joseph L. Eastman, Ph.D.
Research Faculty
UMBC/GEST
Hydrological Sciences Branch
NASA/GSFC Code 974
Building 33, Room A322
Greenbelt, MD 20771
USA

Phone: (410) 279-9702
Fax: (301) 614-5808
Email: eastman@hsb.gsfc.nasa.gov or
jleastman@comcast.net
Work site: <http://gest.umbc.edu/directory.html>

Ferrero

Dr. Enrico Ferrero, Ph.D.
Dip. di Scienze e Tecnologie Avanzate
Universita' del Piemonte Orientale "A. Avogadro"
Via Bellini, 25/G
15100 Alessandria
ITALY

Phone: +39 013 136 0151
Fax: +39 013 136 0199
Email: enrico.ferrero@unipmn.it
Work site: <http://dista.unipmn.it/>
Personal site: <http://www.mfn.unipmn.it/~ferrero>

Finzi

Prof. Giovanna Finzi
Dipartimento di Elettronica per l'Automazione
Università degli Studi di Brescia
Via Branze 38
25123 Brescia
ITALY

Phone: +39 030 371 5459
Fax: +39 030 380014
Email: finzi@ing.unibs.it
Personal site: <http://www.ing.unibs.it/~finzi>

Freedman

Frank R. Freedman, Ph.D.
The EnviroComp Institute
2298 Ocaso Camino
Fremont, CA 94539
USA

Phone: (408) 291-0933
Email: freedman@envirocomp.com
Website: <http://www.air-basics.com/>

González Barras

Prof. Dr. Rosa M. González Barras
Department of Geophysics and Meteorology
Faculty of Physics, Complutense University of Madrid (UCM)
Ciudad Universitaria
28040 Madrid
SPAIN

Phone: +34 91 394 4513
Fax: +34 91 394 4798
Email: rgbarras@fis.ucm.es
Work site: <http://www.ucm.es/info/Geofis/>

Hibberd

Dr. Mark Hibberd
CSIRO Atmospheric Research
PMB1
Aspendale VIC 3195
AUSTRALIA

Phone: +61 3 9239 4400
Phone direct: +61 3 9239 4545
Fax: +61 3 9239 4444
Email: mark.hibberd@csiro.au
Work site: <http://www.dar.csiro.au>
Personal site: <http://www.dar.csiro.au/profile/hibberd.html>

Hurley

Dr. Peter Hurley
CSIRO Atmospheric Research
PMB1
Aspendale VIC 3195
AUSTRALIA

Phone: +61 3 9239 4400
Phone direct: +61 3 9239 4547
Fax: +61 3 9239 4444
Email: peter.hurley@csiro.au
Work site: <http://www.dar.csiro.au>
Personal site: <http://www.dar.csiro.au/profile/hurley.html>

Irwin

John S. Irwin, CCM
John S. Irwin and Associates
1900 Pony Run Road
Raleigh, NC 27615-7415
USA

Phone: (919) 541-5682
Email: irwin.john@epa.gov or
jsirwinetal@nc.rr.com

Keen

Prof. Cecil S. Keen
Atmospheric Sciences / Geography (c/o Box 2)
Minnesota State University
Mankato, MN 56002-8400
USA

Phone: (507) 389-5169
Fax: (507) 345-1283
Email: cecil.keen@mnsu.edu
Work site: <http://www.mnsu.edu/weather>

Lacser

Avraham Lacser, Ph.D.
Israel Institute for Biological Research (IIBR)
POB 19
NESS ZIONA 74100
ISRAEL

Phone: +972 8 9381488
Fax: +972 8 9401404
Email: lacser@iibr.gov.il
Work site: <http://www.iibr.gov.il>

Lee

Russell Lee
Meteorologist
5806 Prosperity Church Road
Suite A2-128
Charlotte, NC 28269
USA

Phone: (704) 947-8024
Fax: (704) 947-8024
Email: Russell.Lee@RFLee.com
Work site: <http://www.RFLee.com>

Luhar

Dr. Ashok Luhar
CSIRO Atmospheric Research
PMB1
Aspendale VIC 3195
AUSTRALIA

Phone: +61 3 9239 4400
Phone direct: +61 3 9239 4624
Fax: +61 3 9239 4444
Email: ashok.luhar@csiro.au
Work site: <http://www.dar.csiro.au>
Personal site: <http://www.dar.csiro.au/profile/luhar.html>

Lyons

Walter A. Lyons, Ph.D., CCM
FORENSIC METEOROLOGY ASSOCIATES, Inc. (FMA)
46050 Weld County Road 13
Fort Collins, CO 80524
USA

Phone: (800) 854-7219
Fax: (970) 482-8627
Email: walyons@frie.com
Work site: <http://www.forensic-weather.com>

McAlpine

J.D. McAlpine
Meteorologist
Envirometrics, Inc.
4128 Burke Ave N
Seattle, WA 98103
USA

Phone: (206) 633-4456
Email: jdmac6@gmail.com
Work site: www.envirometrics.com

Michelsen

Dr. Hope Michelsen
Combustion Research Facility
Sandia National Labs
P. O. Box 969; MS 9055
Livermore, CA 94551
USA

Phone direct: (925) 294 2335
Fax: (925) 294 2276
Email: hamiche@ca.sandia.gov
Work site: <http://www.ca.sandia.gov/CRF/>

Moon

Dennis A. Moon, Ph.D.
Chief Scientist
WindLogics, Inc.
Itasca Technology Exchange
201 NW 4th St.
Grand Rapids, MN 55744
USA

Phone: (651) 556-4281
Email: dmoon@WindLogics.com
Work site: <http://www.WindLogics.com>

Moussiopoulos

Dr. Eng. Nicolas Moussiopoulos
Professor and Laboratory Director
Laboratory of Heat Transfer and Environmental Engineering
Box 483, Aristotle University
GR-54124 Thessaloniki
GREECE

Phone: +30 2310 996011
Fax: +30 2310 996012
Email: moussio@vergina.eng.auth.gr
Work site: <http://aix.meng.auth.gr/lhtee/>
Personal site: <http://www.envirocomp.org/html/meetus/moussio.htm>

Nelson

Thomas E. Nelson
FMA Research, Inc.
Yucca Ridge Field Station
46050 Weld County Road
Fort Collins, CO 80524
USA

Email: tnelson@frii.com

Nunnari

Prof. Giuseppe Nunnari
Dipartimento di Ingegneria, Elettrica, Elettronica e dei Sistemi
Viale A. Doria, 6
95125 Catania
ITALY

Phone: +39 095 738 2306
Fax: +39 095 330793
Email: gunnari@diees.unict.it
Work sites: <http://www.dees.unict.it/users/gunnari/>
<http://www.diees.unict.it>
Group site: <http://www.scg.dees.unict.it/>

Oettl

Dietmar Oettl
Institute for Internal Combustion Engines and
Thermodynamics
Graz University of Technology
Inffeldgasse 25
A-8010 Graz
AUSTRIA

Phone: +43 316 873 8081
Email: oettl@vkmb.tu-graz.ac.at
Work site: <http://fvkma.tu-graz.ac.at>

Pepper

Dr. Darrell W. Pepper
Professor and Director, NCACM
Department of Mechanical Engineering
University of Nevada Las Vegas
4505 Maryland Parkway
Las Vegas, NV 89154-4027
USA

Phone: (702) 895-1056
Fax: (702) 895-0498
Cell: (702) 528-7213
Email: dwpepper@nscee.edu
Work site: www.unlv.edu/Research_Centers/NCACM

Pérez

Dr. Juan L. Pérez
Environmental Software and Modelling Group
Computer Science School, Technical University of Madrid
(UPM)
Campus de Montegancedo, Boadilla del Monte
28660 Madrid
SPAIN

Phone: +34 91 336 7465
Fax: +34 91 336 7412
Email: jlperez@fi.upm.es
Work site: <http://artico.lma.fi.upm.es>

Petersen

Ronald L. Petersen, CCM
Vice President, CPP, Inc.
1415 Blue Spruce Drive
Fort Collins, CO 80524
USA

Phone: (970) 221 3371
Fax: (970) 221 3124
Email: rpetersen@cppwind.com
Work site: www.cppwind.com

Physick

Dr. William Physick
CSIRO Atmospheric Research
PMB1
Aspendale VIC 3195
AUSTRALIA

Phone: +61 3 9239 4400
Phone direct: +61 3 9239 4636
Fax: +61 3 9239 4444
Email: bill.physick@csiro.au
Work site: <http://www.dar.csiro.au>
Personal site: <http://www.dar.csiro.au/profile/physick.html>

Pun Dr. Betty K. Pun
Air Quality Division
Atmospheric and Environmental Research, Inc
2682 Bishop Drive, Suite 120
San Ramon, CA 94583
USA

Phone: (925) 244-7125
Fax: (925) 244 7129
Email: pun@aer.com
Work site: <http://www.aer.com>

Reynolds Steven D. Reynolds
Envair
12 Palm Avenue
San Rafael, CA 94901
USA

Email: steve@sreynolds.com
Personal site: <http://www.sreynolds.com>

Richter Dr. Richard O. Richter, P.E.
Exponent, Inc.
320 Goddard, Suite 200
Irvine, CA 92612
USA

Phone: (949) 341-6015
Fax: (949) 341-6059
Email: rrichter@exponent.com
Work site: <http://www.exponent.com>

Roth³ Philip M. Roth, Ph.D.

Ruby Michael Ruby, Ph.D., P.E.
President
Envirometrics, Inc.
4128 Burke Ave N
Seattle WA 98103
USA

Phone: (206) 633-4456
Email: mruby@envirometrics.com
Work site: www.envirometrics.com

³ Deceased. See page 639 of Volume II.

San José

Prof. Dr. Roberto San José
Environmental Software and Modelling Group
Computer Science School - Technical University of Madrid
(UPM)
Campus de Montegancedo - Boadilla del Monte
28660 Madrid
SPAIN

Phone: +34 91 336 7465
Fax: +34 91 336 7412
Email: roberto@fi.upm.es
Work site: <http://artico.lma.fi.upm.es>

Sarma

Dr. Ananthakrishna Sarma
Senior Research Scientist
Center for Atmospheric Physics
SAIC, MS T2-3-1
1710 SAIC Dr.
McLean, VA 22102
USA

Phone: (703) 676-7017
Cell: (703) 589-0847
Fax: (703) 676-5509
Email: sarmaa@saic.com
Work site: <http://vortex.saic.com>

Seigneur

Dr. Christian Seigneur
Air Quality Division
Atmospheric and Environmental Research, Inc.
2862 Bishop Drive, Suite 120
San Ramon, CA 94583
USA

Phone direct: (925) 244-7121
Fax: (925) 244-7129
Email: seigneur@aer.com
Work site: <http://www.aer.com>

Sheehan Dr. Patrick J. Sheehan
Exponent, Inc.
1970 Broadway, Suite 250
Oakland, CA 94612
USA

Phone: (510) 208-2008
Fax: (510) 208-2039
Email: psheehan@exponent.com
Work site: <http://www.exponent.com>

Solomon Douglas Solomon
US EPA - Emission Inventory and Analysis Group
USA

Phone: (919) 541-4132
Fax: (919) 685-3185
Email: solomon.douglas@epa.gov

Sorbjan Prof. Zbigniew Sorbjan
Department of Physics
Marquette University
Milwaukee, WI 53201
USA

Phone: (414) 288-7458
Fax: (414) 288-3989
Email: sorbjanz@mu.edu
Work site: <http://www.mu.edu/~sorbjanz>

Thé Jesse Thé, Ph.D., P.Eng.
Lakes Environmental Software Inc. and University of Waterloo
419 Phillip Street, Unit 3
Waterloo - Ontario - N2L 3X2
CANADA

Phone: (519) 746-5995
Fax: (519) 746-0793
Email: Jesse@WEBLAKES.com
Work site: <http://www.WEBLAKES.com>

Tourlou

Dr. Eng. Paraskevi-Maria Tourlou
Hellenic Ministry of Transport and Communications
Land Transport Safety Directorate
Anastaseos 2 & Tsigante str.
GR-10191 Papagos, Athens
GREECE

Phone: +30 210 6508468 and 2310 996011
Fax: +30 210 6508493 and 2310 996012
Email: evelina@aix.meng.auth.gr
Work site: <http://aix.meng.auth.gr/lhtee/>

Trini Castelli

Dr. Silvia Trini Castelli
CNR - ISAC, Sezione di Torino
Corso Fiume 4
I-10133 - Torino
ITALY

Phone: +39 011 660 6376
Phone direct: +39 011 383 9828
Fax: +39 011 660 0364
Email: S.TriniCastelli@isac.cnr.it
Work site: <http://www.isac.cnr.it>

van Dop

Dr. Han van Dop
Institute for Marine and Atmospheric Research Utrecht
Utrecht University
P.O. Box 80.005
3508 TA Utrecht
THE NETHERLANDS

Phone: +31 30 253 3154
Fax: +31 30 254 3163
Email: h.vandop@phys.uu.nl
Personal site: <http://www.phys.uu.nl/~dop/>

Venkatram

Akula Venkatram, Ph.D.
Professor of Mechanical Engineering
A343 Bourns Hall
Riverside, CA 92521
USA

Phone: (909) 787-2195
Fax: (909) 787-2899
Email: venky@engr.ucr.edu
Personal sites: <http://www.engr.ucr.edu/mechanical/people/venkatram.html>
<http://www.engr.ucr.edu/~venky/>

Watson

John G. Watson, Ph.D.
Department of Atmospheric Sciences
Desert Research Institute
University of Nevada, Reno
2215 Raggio Parkway
Reno, NV 89512
USA

Phone direct: (775) 674-7046
Fax: (775) 674-7009
Email: john.watson@dri.edu
Work Site: <http://www.das.dri.edu/>
Personal site: <http://www.dri.edu/People/johnw/>

Yamartino

Robert J. Yamartino, Ph.D.
Integrals Unlimited
509 Chandler's Wharf
Portland, ME 04101
USA

Phone: (207) 780-0594
Email: rjy@maine.rr.com or
rjy@stanfordalumni.org

Zannetti

Dr. Paolo Zannetti, QEP
President, EnviroComp Consulting, Inc. and
The EnviroComp Institute
2298 Ocaso Camino
Fremont, CA 94539
USA

Phone: (510) 490-3438
Fax: (510) 490-3357
Email: zannetti@envirocomp.com
Work site: <http://www.envirocomp.com> and
<http://www.envirocomp.org>
Personal site: <http://www.envirocomp.org/html/meetus/zannetti.htm>

Blank Page

Chapter 1

The Problem – Air Pollution

A chapter dedicated to the topic “The Problem – Air Pollution” was presented in Volume I of this book series.

For additional introductory information, the reader can visit:

- http://en.wikipedia.org/wiki/Air_pollution
A detailed description in the well-known free encyclopedia.
- <http://www.epa.gov/ebtpages/airairpollution.html#subtopics>
A very useful list of air quality subtopics.
- http://encarta.msn.com/encyclopedia_761577413/Air_Pollution.html
Another encyclopedia article on this theme.
- <http://www.weather.com/activities/health/airquality/airquality101/index.html?from=airqfl>
Air Quality 101.

BRANK
P
e

Chapter 2

The Tool – Mathematical Modeling

A chapter dedicated to the topic “The Tool – Mathematical Modeling” was presented in Volume I of this book series.

For additional information, the reader can visit:

- <http://epa.gov/ttn/scram/>
<http://www.aqmd.gov/CEQA/models.html>
<http://www.arb.ca.gov/html/soft.htm>
Sites for downloading available models.
- http://en.wikipedia.org/wiki/Atmospheric_dispersion_modeling
Introductory information.
- http://en.wikipedia.org/wiki/Air_Quality_Modeling_Group
The Air Quality Modeling Group at the US EPA.

BRANKLEY
PAPER

Thé, J. and D. Solomon. 2008. *Emissions Modeling and Inventory*. Chapter 3 of *AIR QUALITY MODELING - Theories, Methodologies, Computational Techniques, and Available Databases and Software. Vol. III - Special Issues* (P. Zannetti, Editor). Published by The EnviroComp Institute (<http://www.envirocomp.org/>) and the Air & Waste Management Association (<http://www.awma.org/>).

Chapter 3

Emissions Modeling and Inventory

Jesse Thé⁽¹⁾ and Douglas Solomon⁽²⁾

⁽¹⁾ *Lakes Environmental and University of Waterloo, Waterloo - Ontario (Canada)*

Jesse.The@weblakes.com

⁽²⁾ *United States Environmental Protection Agency - OAQPS - RTP, NC (USA)*

Solomon.Douglas@epamail.epa.gov

Abstract: Emissions Inventory (EI) has rapidly evolved from an art to a science. More complex emissions estimates techniques have been developed in the past decade, even against reduction in investment in the same period. More accurate industrial and regional emissions inventory are under development every year, with coordination by various regulatory agencies, such as state, tribal, and the USEPA. There are 3 main factors for increased emissions inventory accuracy, which are listed below:

1. Improved and expanded regulatory requirements
2. Better emissions inventory models and methods
3. Accumulated experiences in conducting emissions inventory

This Chapter will describe existing approaches to creating emissions inventories.

Key Words: Emissions inventory, emissions modeling, emissions tools, inventory preparation plan.

Disclaimer: This Emissions Inventory Chapter is a summary of many publicly available documents referenced at the end of the Chapter. The main references are based mostly on USEPA publications, which are available at <http://www.epa.gov/chief>. The authors did not develop any of the emissions inventory models or emissions factors presented in this Chapter. One of the authors, J. Thé, produces commercial emissions inventory software packages which are not mentioned in the Chapter to avoid the perception of conflict of interest. The other author, D. Solomon, is currently the group leader of the Emissions Inventory Analysis Group at the USEPA.

1 Introduction to Emissions Inventory and Emissions Modeling

Emissions Inventory is the process of capturing information on atmospheric releases of pollutant matter. Some of this information can be actual measurements from Continuous Emissions Monitors (CEMs) placed directly at the emissions point. This may be the most accurate way, but may not be feasible to occur on all types of sources. As an example, current technology does not support measuring emissions on a continuous basis from each vehicle, lawn mower, barbeque, construction equipment, and other thousands of types of emissions. For this reason, emissions methods exist to estimate total atmospheric releases. Some estimation methods are simple linear equations, while others require complex emissions models.

According to the USEPA, emission inventories are most often developed to support regulations. Emission inventory data are used to evaluate the status of existing air quality as related to air quality standards, air pollution problems, to assess the effectiveness of air pollution policy, and to initiate changes as needed. The USEPA (USEPA, 1999) present the following reasons to conduct an emissions inventory:

1. Meet the Clean Air Act (CAA) mandate for specific inventories as part of the State Implementation Plans (SIPs)
2. Tracking progress towards the National Ambient Air Quality Standards (NAAQS) attainment and emission reductions
3. Determine compliance with emission regulations and set the baseline for policy planning
4. Identifying sources and general emission levels, patterns, and trends to develop control strategies and new regulations
5. Serve as the basis for modeling of predicted pollutant concentrations in ambient air
6. Provide input for human health risk assessment studies
7. Conduct environmental impact assessments for proposed new sources
8. Serve as the basis for construction and operating permits
9. Serve as a tool to support emissions trading programs
10. Siting ambient air monitors

1.1 Regulations Basis for Emissions Inventories

In order to comply with various federal and state regulations, sources must initiate an emissions estimation effort. This section primarily focuses on the federal requirements for reporting emissions, while typical state requirements are also briefly discussed.

Figure 1 provides an overview of some of the key emissions estimation relationships among industry and state and federal agencies (EPA, 1993a).

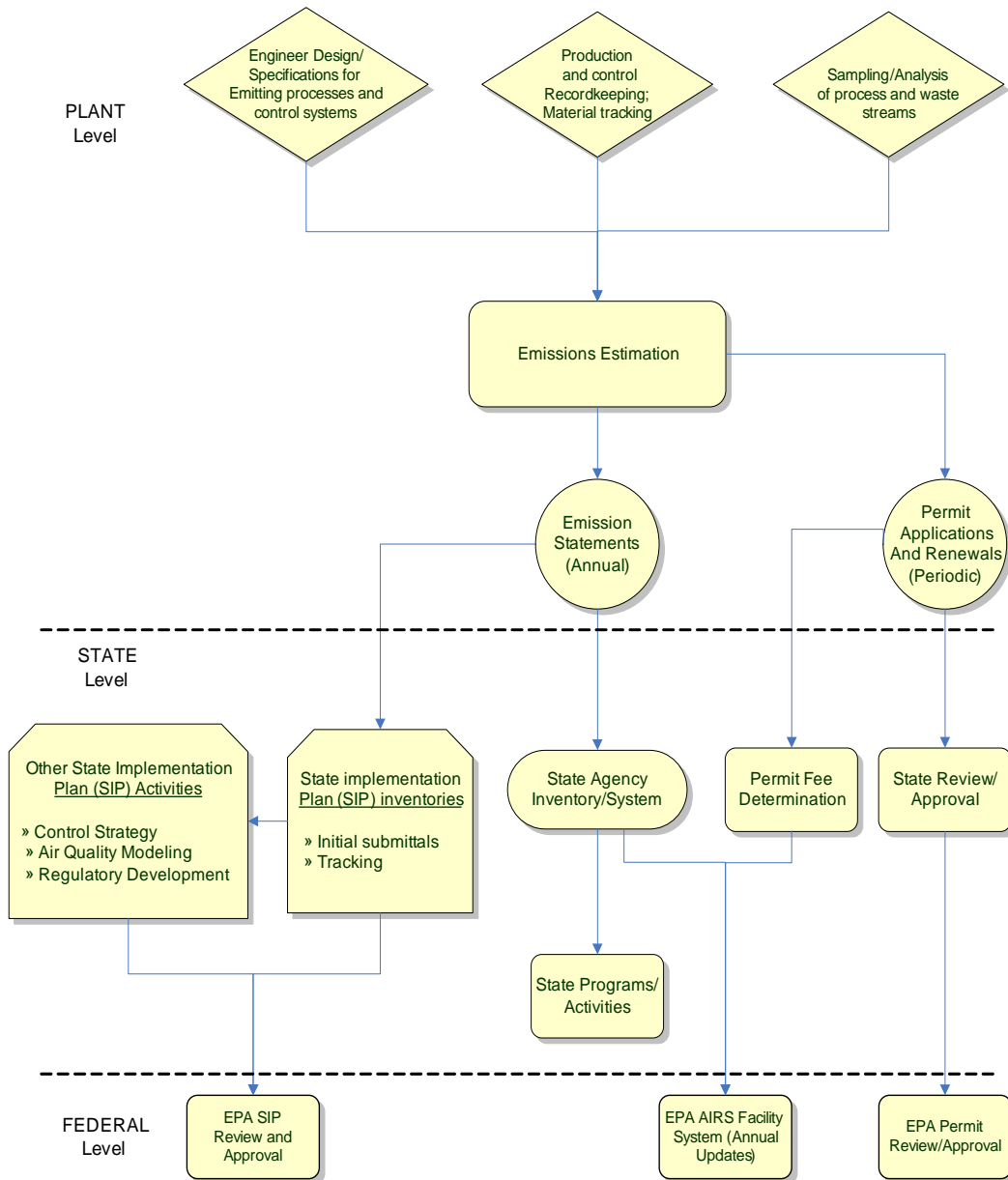


Figure 1. Emissions inventory data flow through regulatory requirements.

Regulatory requirements stem mainly from the Clean Air Act and other legislation such as the National Environmental Policy Act (NEPA). Additional requirements stem from policy issued by the EPA, the Department of Energy (DOE), and the Department of Defense (DoD).

1.2 Clean Air Act Requirements

The Clean Air Act is the major legislation addressing air pollution in the United States. It mandates a wide variety of programs to manage air quality. The federal air quality management effort begins with the national ambient air quality standards (NAAQS). The NAAQS set nationwide minimum air quality goals.

Each state must assess all areas' air quality relative to the NAAQS. For those areas meeting the standard, the state is required to submit plans showing prevention of significant deterioration (PSD).

For non-attainment areas, the state must develop and submit to EPA a detailed, comprehensive and legally binding plan to meet the NAAQS by a specified date and to continue to meet the NAAQS beyond that date. This legally binding plan is called a state implementation plan (SIP). In the SIP, each state has the responsibility for selecting a control strategy that determines which sources must control emissions and the degree of control needed to achieve and/or maintain the NAAQS. If the state fails to submit an adequate plan, the EPA will impose its own plan called a federal implementation plan (FIP).

1.3 Operating Permits Program (CAA Amendments, Title V)

Title V of the Clean Air Act mandates that states establish operating permits programs, requiring the owners or operators of major and other sources to obtain permits addressing all applicable pollution control obligations under the CAA. These obligations include emissions limitations and standards, monitoring, recordkeeping, and reporting requirements. Such requirements are to be contained in an operating permit, which is issued to the source for a period of no more than five years before renewal. In general, the operating permits program, as defined in Part 70 regulations, includes the following sources regulated under the Clean Air Act:

1. Major sources of air toxics as defined in Section 112 with the potential to emit 10 tpy or more of any single HAP listed in Section 112(b); or 25 tpy or more of any combination of HAPs; or a lesser quantity if specified by the USEPA.
2. Any other source, including an area source, subject to the HAP provisions of Section 112. An area source is any source not considered to be a major source.
3. Sources subject to the preconstruction permits requirements of the Prevention of Significant Deterioration (PSD) program under Title I, Part C or the non-attainment area NSR program under Title I, Part D.
4. Major sources as defined in Section 302 of the Act with the potential to emit 100 tpy or more of any pollutant.
5. Sources subject to the acid rain provisions contained in Title IV.
6. Any source designated by the EPA in whole or in part, by regulation, after notice and comment.

1.4 New Source Review (CAA Amendments, Title I)

For non-attainment areas, the CAA requires preconstruction permits for the construction and operation of new or modified major stationary sources anywhere within the non-attainment area. The CAA also requires that new or modified sources in attainment areas must also secure preconstruction permits. These

permits must contain certain basic elements, including legal authority, technical specifications (including an estimate of emissions of each pollutant that the source would have the potential to emit in significant amounts), emission compliance methods, a definition of excess emissions, and other administrative and miscellaneous conditions (EPA, 1992e). Once the source begins operating, it will be necessary to determine source emissions under design operating conditions in order to demonstrate compliance or noncompliance with the allowable levels of emissions. Sources obtaining permits for new sources often use trading transactions, which also require emissions estimations.

1.5 Hazardous Air Pollutants (CAA Amendments, Title III)

Section 112 of the CAA requires EPA to promulgate regulations for reducing the emissions of HAPs. Section 112(b) contains a list of 189 pollutants which are to be regulated as HAPs. Section 112(d) requires that emissions standards be established for each source category listed. A draft schedule for issuance of these standards was published on September 24, 1992 (57 FR 44147) and the emissions standards must be technology-based and must require the maximum achievable degree of reduction possible in emissions of HAPs from the source category. This technology is referred to as maximum achievable control technology (MACT) and the emissions standards are called MACT standards. In general, MACT standards may include: process changes; material substitutions; reuse or recycling; enclosure of systems or processes to eliminate emissions; pollution collection, capture or treatment systems; design, equipment, work practice or operational methods; operator training requirements; or a combination of these methodologies.

Section 112 may lead to additional emission estimation or inventory requirements for sources. All sources subject to Section 112 are also subject to the Title V requirements.

1.6 Urban Air Toxics Study

Under the Urban Air Toxics Study, EPA is required to conduct a program of research on sources of HAPs in urban areas. This program must include an analysis to characterize sources of such pollution with a focus on area sources. EPA, in implementing this program, may request specific emissions estimates and other relevant information from sources.

1.7 Great Lakes and Coastal Waters Program

Under the Great Lakes and Coastal Waters program (often referred to as the Great Waters Program), EPA is required to assess the extent of atmospheric deposition of HAPs into the Great Lakes, Chesapeake Bay, Lake Champlain, and coastal waters. In addition to numerous monitoring and sampling efforts, this assessment will include an investigation of the deposited chemicals, their precursors, and sources.

1.8 Requirements under Other EPA Regulations

A number of other EPA requirements, which are not directly related to the CAA, necessitate some form of emissions estimation. These requirements are a result of the following federal laws: NEPA, CERCLA, SARA, RCRA, and the Pollution Prevention Act. This subsection briefly highlights these requirements.

1.9 National Environmental Policy Act (NEPA)

The National Environmental Policy Act (NEPA) requires that, where a federal agency action may result in a significant environmental impact, an environmental assessment be prepared before such policy can be implemented. An environmental assessment (EA) is a study that provides background information and preliminary analyses of the potential impact of a new policy. Generally, industries are not required to prepare an environmental impact statement (EIS), but EPA may require industry input, including emissions estimates, for its evaluation of the impact of proposed rulings (EPA, 1993a).

1.10 Federal Requirements outside EPA

In addition to the EPA, two other federal agencies have requirements that may lead to emissions estimates for certain sources. The Department of Energy (DOE) requires electric power plants to report information on fuels, cooling equipment, environmental control equipment, and other information from which air emissions may be estimated. It should also be noted that each facility subject to any DOE or DoD requirements is also subject to any relevant EPA requirements.

1.11 State Requirements

As previously described, the EPA places several requirements on states which may indirectly lead to reporting requirements for sources. These include the requirements that the states update emissions inventories on an annual basis and that the states develop Title V Operating Permits programs.

2 Overview of Inventories

Emissions inventories are commonly developed using eight general steps:

1. Planning
2. Gathering emissions and related information
3. Estimating emissions
4. Compiling data into a database
5. Data augmentation
6. Quality control/quality assurance
7. Documenting the EI
8. Providing access to EI data

Figure 2 below displays the necessary steps required to complete a large emissions inventory. Such inventory covers point sources (e.g., stacks), area sources (e.g., landfills and small point sources too small to be investigated individually), mobile sources (road traffic and off-road mobile equipment), and biogenic sources (e.g., forest fires).

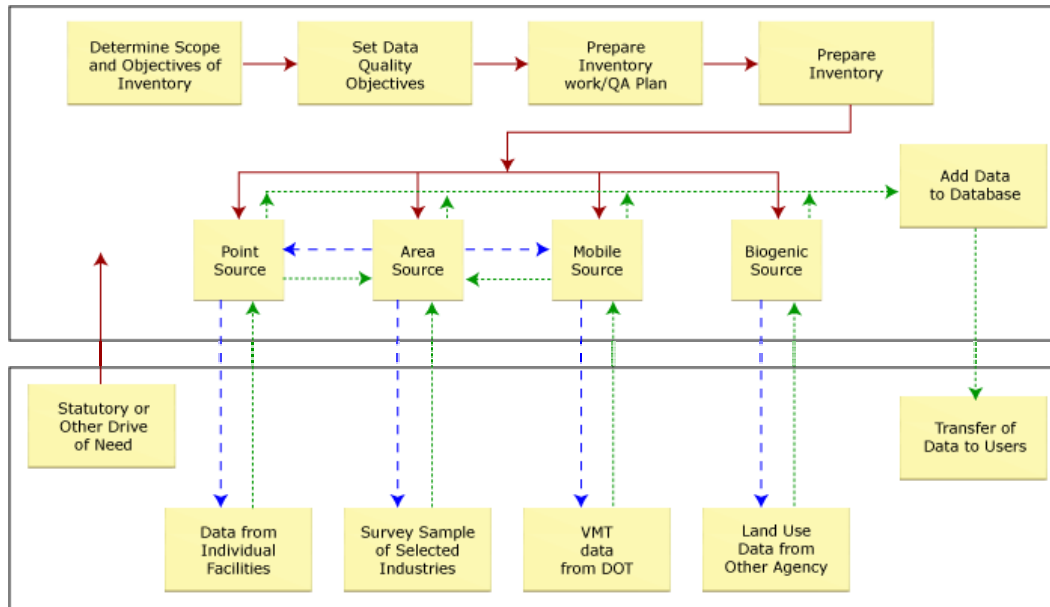


Figure 2. Complete emissions inventory process.

Each of the major steps employed in guiding emissions inventories are further described in the following subsections.

2.1 Planning

Emissions inventory preparation plans ensure focused and streamlined processes, reduced costs and prevention of potential mistakes. The Inventory Preparation Plan (IPP) is developed during the planning stage and is the overarching guidance document for the entire emission inventory development process. The IPP identifies:

1. The end-uses of the inventory (e.g., to support a risk assessment)
2. The acceptable data quality level
3. The resources available to conduct the inventory

The steps taken to develop an Inventory preparation Plan (IPP) are listed below:

1. Identify the end-uses of the inventory
2. Determine Data Quality Objectives
3. Define the inventory to be created
4. Select an inventory data management and reporting system
5. Summarize data reporting and documentation
6. Establish QA/QC procedures

7. Determine staffing and resource requirements
8. Develop a schedule
9. Identify partners and develop a communication plan

The level of precision for emissions data required may differ among different tiers of analysis.

2.1.1 Gathering Information

A comprehensive information search should include guidance documents, preliminary studies for the sources with existing emissions data, emission factors, models, and activity data references. The information gathered in an emissions inventory should include:

1. Pollutant name - chemical name, CAS numbers, and phase
2. Pollutant sources
3. Emission rates over time for each chemical

For air dispersion modeling and air toxic exposure risk assessments the following additional information is required:

1. Source coordinate location (ideally in latitude/longitude or UTM coordinates)
2. Source parameters - exit temperature, exit velocity, diameter at release point, and release height.
3. Building size and shape for assessing downwash

2.2 Estimating Emissions

There are two main approaches for estimating emissions: the top-down approach and the bottom-up approach.

In the **top-down approach**, national- or regional data are allocated to a state or county based on a surrogate parameter such as population or employment in a specific sector. The top-down approach requires minimum resources, but at the expense of emissions accuracy. This approach is used for non-point sources when:

1. Local data are not available
2. The cost to gather local information is prohibitive
3. The end-use of the data does not justify the required cost

In the **bottom-up approach**, the inventory is developed from site-specific information on emissions sources, activity levels, and emission factors. This approach, typically used for point sources, requires more resources, but results in more accurate estimates than the top-down approach.

2.3 Direct Measurement

Direct measurement of source-specific emission rates is infrequent except for permitted facilities with monitoring requirements written into their permits. Source monitoring is available for large point source releases at facilities covered under the Title IV emissions tracking system associated with the acid rain control program.

Source testing may also be required as part of the process of obtaining a permit. To ensure continued compliance, regulatory agencies may require continuous monitoring of stack emissions on some sources.

2.4 Emission Estimation Models

Most emissions estimations are estimated using simple linear relationships, such as:

$$\text{Emissions Rate} = \text{Emissions Factor} * \text{Activity} * (1 - ER / 100)$$

where,

- Activity* = Activity level such as throughput, material produced, or employment in industry.
- ER* = Overall emissions reduction efficiency (e.g., by a control device) [%]
- Emissions Factor* = “Uncontrolled” emissions factor

However, there are situations where many factors are involved and the system may not even have any linear relationships. This way, emission estimation models are used when a large number of complex calculations must be undertaken in order to estimate a given emission, or when a combination of parameters has been identified that affect emissions but individually do not provide a direct correlation. The USEPA provides a variety of peer-reviewed approved emissions models to determine point, non-point, and mobile source emissions based on a variety of known input parameters. These models are described later in this chapter.

2.5 Emissions Inventory Pollutants

There are thousands of types of substances emitted into the atmosphere at any moment. These substances can be in the solid, liquid, or gaseous (or vapor) phase. To facilitate regulatory framework, pollutants are classified into three major categories: criteria, toxics, and greenhouse. This classification is further explained below.

2.5.1 Criteria Pollutants

Criteria Pollutants are carbon monoxide (CO), lead (Pb), nitrogen oxides (NO_x), sulfur dioxide (SO₂), volatile organic compounds (VOCs), and particulate matter of aerodynamic diameter less than or equal to 10 micrometers (PM₁₀) and less than or equal to 2.5 micrometers (PM_{2.5}). The National Ambient Air Quality Standards (NAAQS) were mandated by the Clean Air Act of 1970, and are based on criteria including adverse health or welfare effects. The NAAQS are currently used to establish air pollutant concentration limits for the six air pollutants listed above.

2.5.2 Air Toxics

Air toxics are pollutants generally emitted in smaller quantities than criteria pollutants but may be reasonably anticipated to cause cancer, developmental effects, reproductive dysfunctions, neurological disorders, inheritable gene mutations, or other chronically or acutely toxic effects in humans. Air toxics are commonly referred to as Hazardous Air Pollutants (HAPs). There are 188 HAPs listed in Section 112(b) of the 1990 Clean Air Act Amendments (CAAA), including relatively common pollutants such as formaldehyde, chlorine, methanol, and asbestos, as well as numerous less-common substances.

2.5.3 Greenhouse Gases

Certain gases have a stronger opacity to infrared radiation than others. These gases are denoted as Greenhouse Gases (GHGs), and may be emitted by natural and anthropogenic (man-made) sources. The main GHGs are carbon dioxide (CO₂), methane (CH₄), nitrous oxide (N₂O), and chlorofluorocarbons (CFCs).

2.6 Allocating Emissions to Sources and Processes in the Inventory

The level of detail and effort in an emissions inventory is strongly dependent on the final objective of the inventory. However, as the use of inventory data is expanding, it is important to allocate emissions to the unit that actually generates them. It is common, but not appropriate, to have emissions broken only to a complete industrial facility level. To obtain the maximum use and value of emission inventory projects, emissions must be identified at the process level, not at emissions point level.

In Figure 3, an industrial facility is presented with various processes and stacks. Note that each stack can emit pollutants from many other processes. This makes it difficult to estimate emissions, establish control policies, and audit.

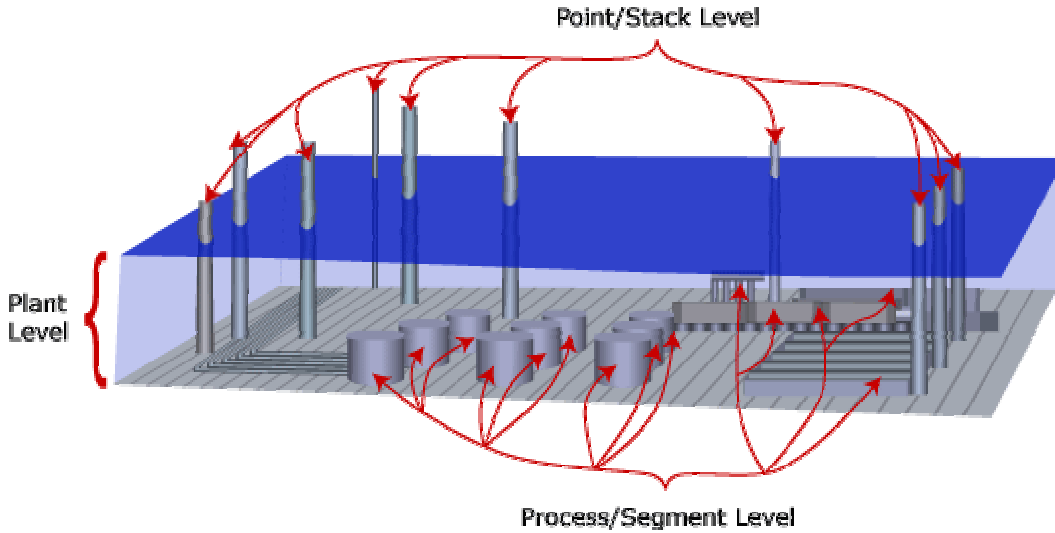


Figure 3. Plant, release point (stack), and process levels in an industrial facility.

Figure 4 presents a situation where different chemicals are produced on two separate processes. In this case, all chemicals are then emitted by a single source. Therefore, it would not be easy or accurate to segregate emissions from processes.

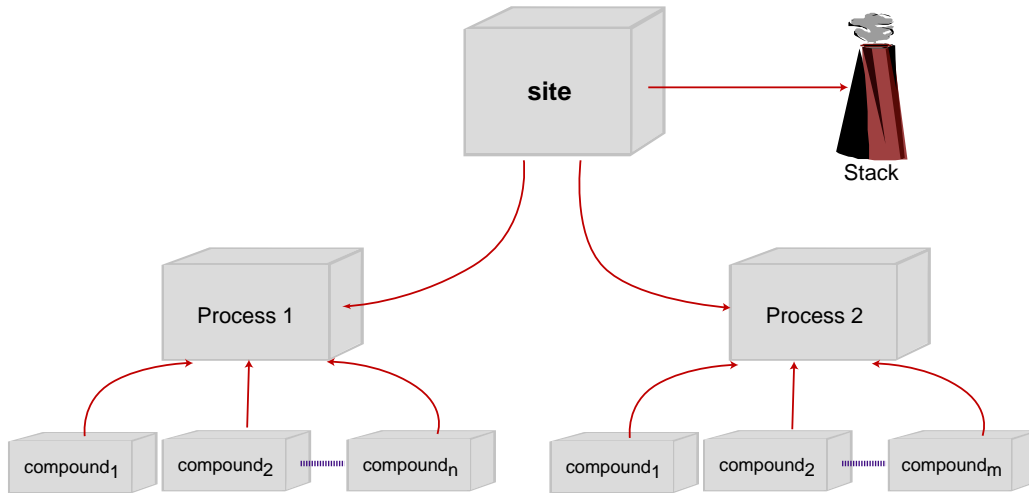


Figure 4. Multiple processes emitting to the atmosphere from a single release point.

In the example presented in Figure 5, each process has its own release point (stack). This situation would allow the emissions to be allocated at the stack level, but it still requires calculations to be performed at process level due to existing estimation methods. Note that in both cases, reporting emissions at the site level would add many uncertainties on emissions, such as release location and changes in emissions due to process throughput.

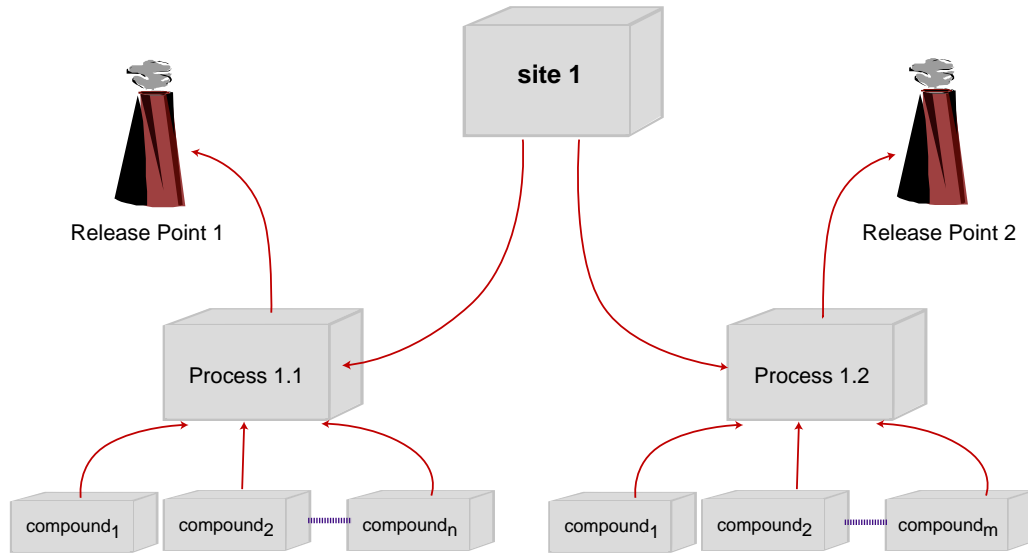


Figure 5. Segregation of site emissions from processes into individual stacks.

Additional needs for inventories data may include air dispersion modeling, identification of processes that drive environmental risks, and others. Figure 6 presents a comprehensive description of process level and data requirements that would satisfy the most complex emissions inventory data quality objectives.

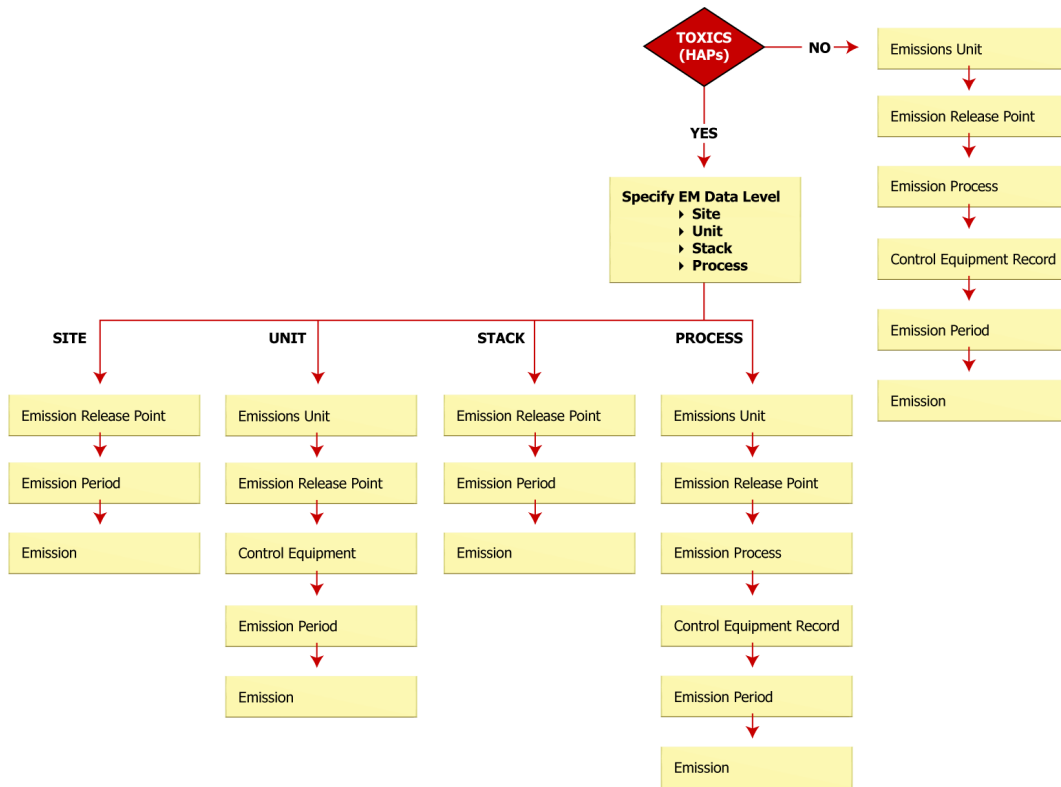


Figure 6. Comprehensive data requirements for EI.

2.6.1 Top-Down Emissions Inventories

Top down emissions inventories employ national statistics on economic activity, material flows, employment, and population to obtain estimates over large areas such as states or an entire country. One advantage of the top-down emissions inventory is the reduction resource requirements since it can be done in short time period with few trained staff. However, the results from the top-down approach lack both spatial and temporal resolution, which may be very essential to policy making and detailed atmospheric studies.

2.6.2 Bottom-Up Emissions Inventory

Bottom-up inventories derive emissions at the plant or county level (for area sources). These types of inventories are extremely useful in many applications, such as creating inputs into atmospheric dispersion and visibility models.

2.7 Emissions Inventory Preparation Plan (IPP)

An inventory preparation plan (IPP) lays the groundwork that the Emissions Inventory (EI) professional will follow to plan and execute the emission inventory steps. It describes how the professional intends to develop and present the EI. The IPP should include inventory objectives, input data quality, and general procedures. Also, it should clearly detail how the inventory preparer will present and document the inventory for submission to the EPA and others. The IPP will give EI reviewers an idea of what EI preparer intends to do with the EI, who will do the work, how one will gather information, and the resources need to complete the work.

Reasons to start an emissions inventory with a Preparation Plan:

- Emissions inventory is the foundation of many decisions
- Mistakes early in the process interject errors in downstream calculations
- Redoing work is costly and embarrassing

These are the major steps in the Inventory Preparation Plan (IPP):

- Identify required staffing levels and resources
- Identify all steps in compiling an inventory
- Specify methods and procedures to be used in compiling an inventory
- Consider the following points:
 - End uses of the data
 - Scope of the inventory
 - Availability and usefulness of existing data
 - Strategy for data collection and management
- Define uses of inventory and acceptable data quality for uses of inventory
- Identify pollutants and source categories, geographic area, and time interval to be included in inventory

- Define all procedures that will be used to estimate emissions
 - Data collection
 - Emission estimation methodology
- Select inventory data management system
- Input data
- Manage data
- Output data
- Summarize data reporting and documentation
- Data analysis
- Complete files with all data fields
- Data summaries
- Documentation
- Define QA/QC procedures
- Establish resource requirements and schedule
- Identify partners and develop communication plan
 - Industry
 - Trade Associations
 - Agencies
 - Community groups

2.7.1 Base Case

Atmospheric emissions change with time, when some compounds are reducing due to regulations of efficiency gains, while other increase. Every emissions inventory type requires a base year of reference. This base year is used to assess how emissions are changing with time, or in planning studies to evaluate the impact of emissions growth

3 Process-Level Codes Used in Emissions Inventories

Emissions inventory calculations are conducted at the process level. Information on emissions inventory must uniquely identify the processes. To address this issue, the USEPA created the Source Classification Codes (SCC). These codes are used to provide emissions factors, speciation profiles, temporal allocation profiles, and general reporting of processes in the inventory. Some details on the SCC are presented below:

- Approximately 10,300 codes
- Maintained by the USEPA
- Point Sources => 8-characters
- Area, Non-Road, On-Road, and Biogenic Sources => 10-characters
- Used as a primary identifying data element in the EPA's National Emission Inventory (NEI)

The Source Classification Codes (SCC) for the point sources contain 8 characters:

- Example: 10100202
- 1-01-002-02 = 8-characters
- For each SCC, there are four levels of descriptions:
 - SCC 1 Description (1): External Combustion Boilers
 - SCC 3 Description (1-01): Electric Generation
 - SCC 6 Description (1-01-002): Bituminous/Subbituminous Coal
 - SCC 8 Description (1-01-002-02): Pulverized Coal: Dry Bottom (Bituminous Coal)

The SCC for area and other non-point sources use 10-characters:

- Example: 2610030000
- 26-10-030-000 = 10-characters
- The 10-character SCCs are used for Area, Non-Road, On-Road, and Biogenic sources
- For each SCC, there are four levels of descriptions:
 - SCC 2 Description (26): Waste Disposal, Treatment, and Recovery
 - SCC 4 Description (26-10): Open Burning
 - SCC 7 Description (26-10-030): Residential
 - SCC 10 Description (26-10-030-000): Household Waste

The first two digits in the area SCC codes describe the category of the source, as shown below:

Major Categories by SCC2 Description:

- 21-XX-XXX-XXX: Stationary Source Fuel Combustion
- 22-XX-XXX-XXX: Mobile Sources
- 23-XX-XXX-XXX: Industrial Processes
- 24-XX-XXX-XXX: Solvent Utilization
- 25-XX-XXX-XXX: Storage and Transport
- 26-XX-XXX-XXX: Waste Disposal, Treatment, and Recovery
- 27-XX-XXX-XXX: Natural Sources
- 28-XX-XXX-XXX: Miscellaneous Area Sources

The SCC4 in the NON-POINT source categories define sub-categories. The example below for Mobile source is useful for the understanding:

22-XX-XXX-XXX: Mobile Sources

1. On-Road Mobile Sources by SCC4 Category

22-01 Highway Vehicles - Gasoline
 22-30 Highway Vehicles - Diesel

2. Non-Road Mobile Sources by SCC4 Category

22-60	Off-Highway Vehicle Gasoline, 2-Stroke
22-65	Off-Highway Vehicle Gasoline, 4-Stroke
22-67	LPG
22-68	CNG
22-70	Off-highway Vehicle Diesel
22-75	Aircraft
22-80	Marine Vessels, Commercial
22-82	Pleasure Craft
22-83	Marine Vessels, Military
22-85	Railroad Equipment

3. The following Mobile Sources SCCs are reported under AREA Sources

22-94	Paved Roads
22-96	Unpaved Roads

3.1 SIC and NAICS CODES

The Standard Industrial Classification (SIC) codes provide categorization of business main field of operation. The SIC was developed and maintained by the U.S. Department of Commerce to identify businesses by their products and services. The SIC codes are being replaced by the North American Information Classification System (NAICS). A short summary of the SIC and NAICS codes are presented below:

SIC - Standard Industrial Classification

- Economic Sectors of the Economy
- Beginning in 1997, the **SIC** was replaced by the **NAICS** - North American Industry Classification System
- **NAICS** reorganizes the categories on a production/process-oriented basis.

NAICS Codes - North American Information Classification System

- Consists of 6-digits:
 - 2 digits - Economic sector
 - 3 digits - Economic sub-sector
 - 4 digits - Group of related industries
 - 5 digits - An industry within the economy
 - 6 digits - A subdivision of an industry

3.2 FIPS CODES

Databases require unique identifiers for electronically stored information. This way, emissions inventory experts use the Federal Information Processing Standard (FIPS) to uniquely identify the state and county where emissions occur.

Example of FIPS codes:

- Arizona = 04
- Yavapai County = 025

4 Emissions Estimation Techniques

There are four main techniques to estimate emissions. These techniques include emissions factors, material balance, fuel analysis, and continuous emissions monitoring systems (CEMS). These are explained in the following sub-sections.

Emissions modeling comprise of methodologies to estimate emissions when direct measurement are not available. These models can be one simple linear equation relating throughput with emissions, or much more complex models, such as those that predict traffic pollution of urban areas.

Five basic factors are used to estimate emissions:

1. Throughput, such as fuel consumption
2. Emission factor, which relates the throughput (such quantity of fuel burned) to the quantity of pollutant emitted
3. Throughput characteristics, such as sulfur content, ash content, and heating value of fuels
4. Control efficiency, which indicates the percent of pollutant emissions removed through control methods
5. Rule effectiveness, which is the regulatory program's ability to achieve all the emission reductions that could be achieved by full compliance with the applicable regulations at all sources at all times

4.1 Emissions Factors (EFs)

Emission factors (EFs) are simple ratios that relate the emission of a pollutant to an activity level. This activity level should be easily measured, such as an amount of fuel burned for point source or population for area sources. Emission calculations are obtained by a simple multiplication of an emission factor and a known activity level. This is shown below:

$$\text{Emissions from a Process} = (\text{Emissions Factor}) * (\text{Activity Level}) * (1 - ER / 100)$$

where,

Activity = Activity level such as throughput, material produced, population, or employment.

ER = Emission reduction efficiency [%]

Emissions Factor = Uncontrolled emission factor

For example, releases from a coal burning combustion device are represented as pounds of pollutant emitted per BTU coal burned. Depending on the emission source, there may be a lot of emissions testing data, just one or two measurements (the usual case), or none. For a screening-level assessment, it may be possible to obtain an estimate of maximum emissions in one of several ways:

- If sufficient data are available, the assessment could use the highest available value.
- If only one or two measurements are available, the assessment could assume that all the emissions occur in a short period of time (such as only for 8 hours a day) and/or assume that all sources of emissions are co-located.
- If no data are available, the assessor may need to rely on professional judgment based on similar types of sources.

Frequently, emission factors contain an associated confidence level by species, which assists in determining the appropriate emission factor. In some cases, accurate measurements of the activity rates are not available and estimates of activity rates can also contribute uncertainty to the release rate estimate for any particular source type.

Emission factors are used extensively in point and area sources inventories. The main underlying assumption for the emissions factors is that linear relationship exists between emissions and the process activity level over the similar processes. Emission factors are developed from separate facilities within an industry category. This way, emission factors may represent only typical values for an industry, not necessarily represent a specific source. Published emission factors, available in numerous sources, are listed below:

- **AP-42:** One of the most frequently cited resources for emission factor information is the EPA document, *Compilation of Air Pollutant Emission Factors (AP-42)*. This document contains criteria pollutant emission factors for point and area sources. *AP-42* is available on the World Wide Web at:
 - <http://www.epa.gov/ttn/chief/ap42.html>
 - *AP-42* is also available on the *Air CHIEF* CD-ROM.
- **FIRE:** Factor Information REtrieval Data System, contains an extensive set of emissions factors organized by the Source Category Code (SCC). FIRE includes emission factors from the EPA documents (such as *Compilation of Air Pollutant Emission Factors [AP-42]* and the *Locating and Estimating Air Emission Series*), factors derived from state-reported test data, and factors taken from literature searches. The FIRE Data System is available at:
 - <http://cfpub.epa.gov/oarweb/index.cfm?action=fire.main>
- Air Clearinghouse for Inventories and Emission Factors web site is located at:

- o <http://www.epa.gov/ttn/chief/efpac/>

The use of emission factors is straightforward when the relationship between process data and emissions is direct and relatively uncomplicated. Note, however, that emission factors may be developed assuming no control device is in place. These are referred to as “uncontrolled emission factors.” When emission factors are derived from data that was obtained from facilities with a control device in place, then emission factors are referred to as “controlled emission factors.”

4.1.1 Emission Factors Rating

Emission factors are averages obtained from data with wide ranges and varying degrees of accuracy. The USEPA commonly publish emission factors associated with a Rating classification to express the quality of the published values. This way, an “A” rating indicates emission factors of high quality, while an “E” rating indicates an Emissions Factor (EF) that is not very trustworthy. For example, emissions calculated using national emission factors are rated poorly as “C”, “D”, or “E”, since considerable variability will be present from actual values at a specific source or within a geographic area.

The following emission factor quality ratings are used for the emission factors found in *AP-42*, FIRE, or any U.S. EPA published document:

A - Excellent - The emission factor was developed only from A-rated test data taken from many randomly chosen facilities in the industry population. The source category is specific enough to minimize variability within the source category population.

B - Above Average - The emission factor was developed only from A-rated test data from a reasonable number of facilities. Although no specific bias is evident, it is not clear if the facilities tested represent a random sample of the industry. As with the A-rating, the source category is specific enough to minimize variability within the source category population.

C - Average - The emission factor was developed only from A- and B-rated test data from a reasonable number of facilities. Although no specific bias is evident, it is not clear if the facilities tested represent a random sample of the industry. As with the A-rating, the source category is specific enough to minimize variability within the source category population.

D - Below Average - The emission factor was developed only from A- and B-rated test data from a small number of facilities, and there may be reason to suspect that these facilities do not represent a random sample of the industry. There also may be evidence of variability within the source category population.

E - Poor - The emission factor was developed from C- and D-rated test data, and there may be reason to suspect that the facilities tested do not represent a random sample of the industry. There also may be evidence of variability within the source category population.

Each emission factor in the FIRE database includes the following information:

1. Pollutant name and its unique Chemical Abstract Service [CAS] numbers
2. Source codes using the Standard Industrial Classification [SIC]. Note that the SIC is being replaced by the NAICS (North America Industrial Classification Codes)
3. Process level information using the Source Classification Code
4. Data quality rating for the emissions factor (A to E, U for Unrated)

Each emission factor entry includes comments about its development, in terms of the calculation methods and/or source conditions, as well as the references where the data were obtained. The emission factor entry also includes a data quality rating. Data in the FIRED database can be searched in many different ways and can be downloaded to data files, or can be printed in a report format that is designed by the user.

4.1.2 Recommendation for Emissions Factors Use

As recommended by the USEPA, national emission factors should be used when:

- No locally derived factor exists
- The local mix of individual sources in the category is similar to the national average
- The source is a low priority in the inventory

Locally derived emission factors are preferred when:

- A national level emission factor does not account for local variations
- The category is a high priority in the area

4.1.3 Emission Factors Accuracy Components

The accuracy of the emission estimate is dependent upon the relative accuracy of the following components:

1. Emissions calculated using emission factors for a given process are likely to differ from that facility's actual emissions because the estimate is less precise than source test measurements.
2. The use of emission factors will produce higher emissions estimates than are actual for some sources and lower for others.
3. Emission factors are often based on limited data, and may not truly represent the facility of interest.
4. If emission factors are used to predict emissions from new or proposed sources, users should review the latest literature and technology to

determine if such sources would likely exhibit emissions characteristics different from those of typical existing sources.

5. In order to calculate emissions using emission factors, the following information is required:
 - Activity information for the process as specified by the relevant emission factor;
 - Emission factors to translate activity information into controlled or uncontrolled emission estimates
 - Capture device and control device efficiencies to provide the basis for estimating emissions to the atmosphere after passage through the control devices(s) if using an uncontrolled emission factor.

4.2 Material Balance

Assume that a quick mass balance of major emissions can be determined based on the amount of material that enters a process, the amount that leaves the process, the amount retained on residue, and the amount incorporated at a potential final product. For example, one can assume that all the sulfur present in the fuel will be emitted by the stack. This way, a mass balance will indicate that all the sulfur in coal will be burned and emitted to the atmosphere, and all metals are emitted as fly ash. This may not be the case, since some metal mass is retained as bottom ash.

The material balance method can be used where source test data, emission factors, or other developed methods are not available. It is more appropriate in cases where measurements can be made of all process parameters except the air emission component.

Note that the material balance emissions method is equally applicable to point and area sources. However, one serious limitation of the mass balance approach is that it cannot be used where material reacts to form secondary products. This is the case for some very toxic Hazardous Air Pollutants (HAPs), such as Dioxin and Furans.

4.2.1 Material Balance - Accuracy Components

The accuracy of the Material Balance is dependent upon the relative accuracy of the following components:

1. The material balance method should not be used for processes where material is reacted to form products or the material otherwise undergoes significant chemical change, unless the process is well-characterized.
2. Because the emissions are estimated to be the difference between the material input and the known material output, a small percentage error in estimating the input or output can result in a large percentage error in the emission estimate. Therefore, material balances may be inappropriate

when considering a small difference (i.e., loss) between two rather large input and output values.

4.3 Fuel Analysis

Emissions are determined based on the application of mass conservation laws. The presence of specific elements in fuels may be used to predict their presence in emission streams. For example, mercury contained in coal can be assumed to be completely emitted to the atmosphere as a result of the combustion process. Another common example where the Fuel Analysis method is used is the conversion of sulfur in the fuel. One can safely assume the complete conversion of sulfur to SO₂. Therefore, for every pound of sulfur in the fuel burned, two pounds of SO₂ are emitted (molecular weight of sulfur is 32g and the molecular weight of SO₂ is 64g).

4.4 Source Tests / Stack Tests

Source tests provide emission rates from short-term emission measurements taken at a point of release, such as a stack or vent. Emission data can then be extrapolated to estimate long-term emissions from the same or similar sources.

4.5 Continuous Emissions Monitoring Systems - CEMS

CEMS are devices which continuously measure and record actual emissions from release points. CEM measurements are also used to estimate emissions factors to similar emission units, or processes, without this monitoring equipment.

Figure 7, shown below helps define the range of emissions data quality obtained by applying the estimation methodology described above.

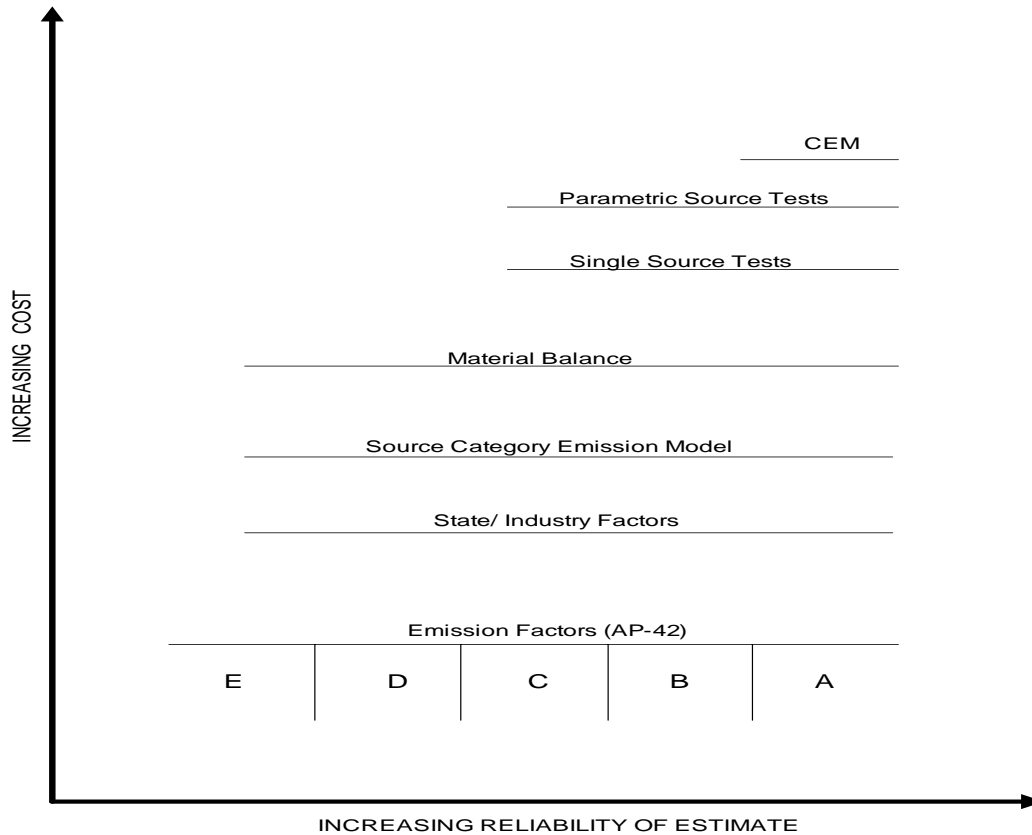


Figure 7. Emissions estimate reliability.

4.6 Emission Estimation Models

Emission estimation models are empirically developed process equations used to estimate emissions from certain sources. An example of emission estimation model is the TANKS software for estimating volatile organic compounds emitted from fixed- and floating-roof storage tanks.

Several emission estimation models are available for download free-of-charge.

- LandGEM - Estimates emissions from municipal landfills, and it is available at:
 - <http://www.epa.gov/ttn/catc/products.html#software>
- TANKS - Estimates emissions from fixed- and floating-roof storage tanks and is available at:
 - <http://www.epa.gov/ttn/chief/software/tanks/index.html>
- WATER9 and CHEMDAT - Estimates air emissions from wastewater collection and treatment systems, and it is available at:
 - <http://www.epa.gov/ttn/chief/software/index.html>
- PM Calculator - Calculates controlled emissions for filterable PM_{2.5} and filterable PM₁₀, and it is available at:
 - <http://www.epa.gov/ttn/chief/software/pmcalc/index.html>

These models are further described later in this Chapter.

4.6.1 Emissions Models - Accuracy Components

The accuracy of the Material Balance is dependent upon the relative accuracy of the following components:

1. Models generally require more data than emission factors.
2. The data needed will be dependent upon the particular emission source as well as the model. For example, emission models for wastewater treatment operations may require wastewater flow rate, pollutant concentration, and temperature, while emission models for storage tanks may require tank capacity, dimensions, throughput, and vapor pressure.
3. The accuracy of the emission estimate is dependent upon the accuracy of the individual data input entry.

5 Characterization of Emissions

Emissions in an emissions inventory are more than the pollutant emissions rate. Information on the temporal and spatial variations is important along with the determination of an actual emission that occurred or an emission amount that is allowed by a regulatory agency. The following sections illustrate the different ways of describing emissions.

5.1 Types of Emissions in an Emissions Inventory

Actual Emissions: Defined as the actual rate of emissions of a pollutant from a source (or emission unit within a source) calculated using actual operating hours, production rate, and materials used during the period of interest. Actual emissions are used in base year inventories in support of a SIP, or to define permit fees and the end of the period.

Allowable Emissions: The product of a permitted and enforceable emissions rate. Allowable emissions can be:

- The anticipated operating rate or activity level (e.g., gallons of solids applied per hour)
- The anticipated operating schedule (hours per day)

Allowable emissions are used in permits, enforcements, and in the development of SIP modeling.

Potential Emissions: As the name describes, this emission type describes the capability of a source, at maximum design capacity, to emit a pollutant after the application of air pollution control equipment. Potential to emit estimates are based on the maximum capacity of a source after taking into consideration the permit conditions such as:

- The type of materials consumed (e.g., combusted fuel)
- The type of material processed
- The annual hours of operation

In general, potential emissions are estimated and reported in inventories in support of permitting activities under Title V of the CAA.

5.2 Temporal Allocation

Temporal allocation of emissions considers the emissions profile over periods of time. Example of temporal profiles includes hourly, daily, monthly, seasonal and annual variations. Emissions inventory objectives dictate the temporal resolution of the emissions inventory. Regulatory air management programs until 2004 required annual total emissions. Recent needs for airshed evaluation require emissions data on hourly or monthly basis. For example, occurrence of smog and high ground level concentration of ozone and particulates in the summer months require specific photochemical model, which uses the best available hourly and monthly emissions data.

Temporal allocation factor databases are available from the EPA's Emissions Characterization and Prevention Branch, in text and MS-Access database formats. These temporal allocation factors may be used as default values for temporal allocation when no local data are available.

Temporal adjustments are made because of seasonal differences in the rate of emissions or high activity, or to apportion emissions to a particular season or day. For example, high photochemical ozone levels are generally associated with the warmer months of the year, while CO emission levels are generally associated with the colder months of the year.

- Activity level: The level of activity of some area sources varies throughout the calendar year. Some industrial activities are conducted only five days per week. Some operations, such as architectural surface coating, are more active in Spring through Fall, because of the warmer temperatures and the increased number of daylight hours. Other sources, such as residential heating, are active only in the colder months.
- Rate of emissions: Seasonal variations in temperature can impact the rate of emissions, even for sources that maintain constant activity levels. For example, at petroleum product handling and storage operations, breathing losses from fixed-roof tanks are significantly influenced by changes in the temperature of the product.

Emission estimates or activity data for point sources are often presented as a rate per unit time (e.g., pounds per hour or tons per year). Temporal allocation methodologies adjust emission or activity to apportion the variations over time for the inventory period. Default temporal profiles (i.e., hours/day, days/week, weeks/year) are often used to develop hourly estimates from annual estimates. Under

actual conditions, steady-state emission sources are not the rule. Instead, emission sources may operate only in the summer, only on working week days, or their activity may peak during certain hours of the day. Examples of these sources are electric power plant, food processing, and industries that operate in batch mode.

The best way to calculate daily or seasonal emission estimates is to obtain activity data that are specific for the period of interest. When this is not possible, an estimate of seasonal activity can be calculated using an adjustment factor applied to the annual activity.

In cases where a surrogate activity factor is used to calculate emission estimates, an adjustment factor is applied to the calculated annual emission estimates. Factors for making seasonal adjustments may be expressed as fractions, percentages, or ratios. Therefore, an adjustment factor is typically expressed as:

1. **A fraction:** Seasonal Activity Factor (SAF) representing the amount of annual activity or emissions within a season, say summer (such as $4/12 = 0.33$)
2. **A percentage:** percent period throughput, the percent value of the SAF for a period (such as $0.33 * 100 = 33$)
3. **A ratio:** SAF, the ratio of seasonal activity or emissions to average period activity or emissions (such as $0.33/0.25 = 1.33$)

The following sub-sections present a summary of variable emission rates. Note that the best situation is to obtain activity data that are specific for the season or period of interest.

5.2.1 Annual Emissions

Most regional or national inventories are reported in terms of total emissions in a year. This situation precludes the use of these emissions by many types of applications, such as air dispersion modeling and air quality event analysis, since it lacks temporal information. Very few sources actually emit at a near constant rate throughout the year. These include chemical facilities operating in favorable marketing conditions and processes that cannot stop operating, such as blast furnaces and nuclear power plants. Even in these cases, the operation may oscillate, but emissions variability is usually small, as shown in Figure 8.

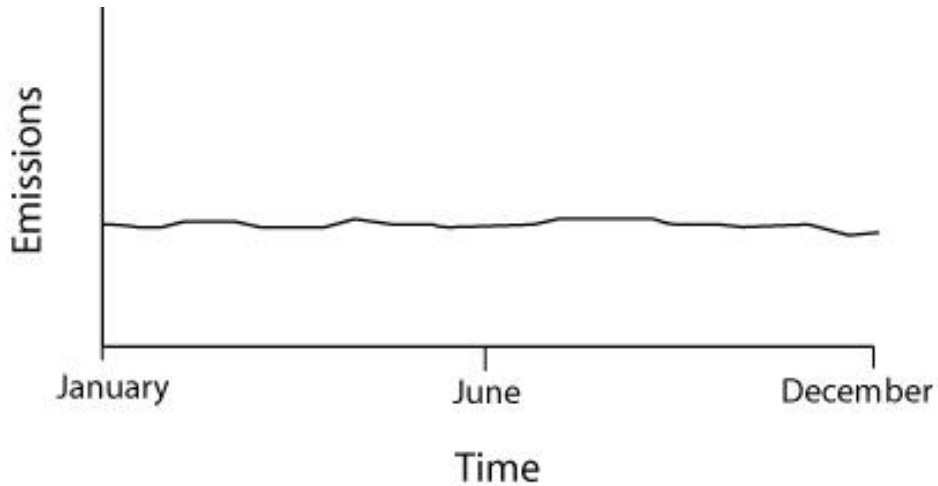


Figure 8. Quasi-constant emissions are accurately accounted as annual.

5.2.2 Average Week Day

Many source categories have significant emission variations during the day. Mobile sources on urban road networks and thermal electric power stations are good examples of these sources. Most sources with a daily variation of emissions will also change the emissions during the year or even during the week. Traffic on weekends is different than on regular business week days, and power plants burn more fuel during hot summer days than in the spring. Figure 9 presents an approximation of a power plant emissions daily adjustment to meet electrical demand.

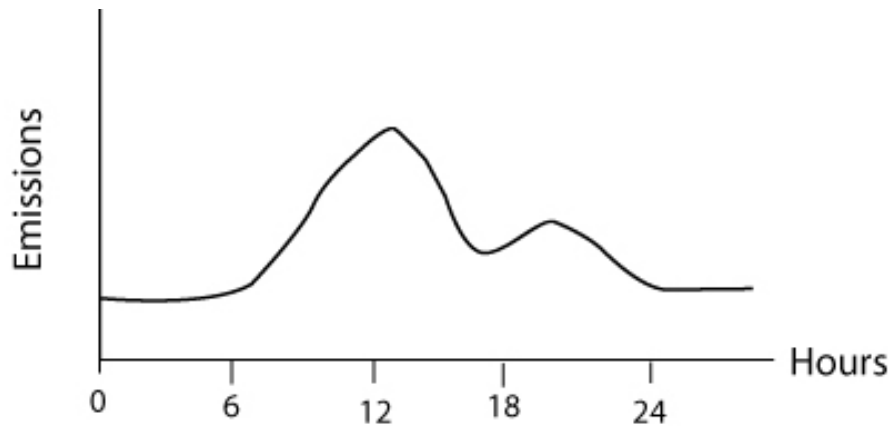


Figure 9. Power plant emissions variation on a typical summer week day.

5.2.3 Seasonal Emission Variation

There are many source categories that emit more during warmer months. This may be caused by higher biological activity (e.g., forest VOC emissions), agricultural production that requires tractor and other equipments, and industries that depend on agricultural production, such as soup manufacturing in Canada.

Figure 10 depicts a typical emissions growth and decrease for agricultural non-road mobile sources, which occurs during the year in the Northern Hemisphere.

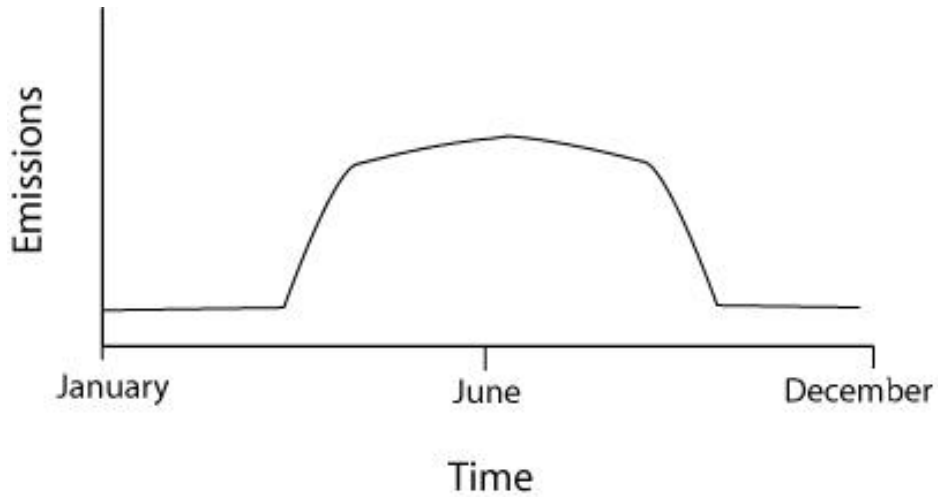


Figure 10. Agricultural non-road mobile emissions variations in the year.

5.3 Spatial Allocation

Spatial allocation is the adjustment of activity levels or emission estimates to an area of different size than the one for where estimates were prepared. Spatial allocation requires the definition of a defensible surrogate indicator that will be used in the scaling procedure.

Spatial allocation of emissions considers geographical shifts of sources, both in size and intensity. This consideration is critical for area, mobile, and geogenic sources. Point source emissions for industrial facilities may only require the spatial location of release points.

Surrogate indicators for the spatial allocation adjustments include:

- Local activity level data
- State or national data
- Population data
- Employment data

Spatial resolution prescribes the resolution that the geographic location of pollution sources must be defined. For example, area source emission inventories provide pollutants' totals over an entire county. However, more air quality modeling efforts will require a more detailed description of emissions distribution over a much smaller spatial scale.

Spatial allocation of regional or county-level emission estimates is accomplished through the use of spatial surrogates or Spatial Allocation Factors (SAFs) for each emission source category or group of source categories. Spatial surrogates are

typically based on the proportion of a known region-wide characteristic variable that exists within the region of interest. Traditionally, the development of spatial gridding surrogates for dispersion modeling applications has been performed by a variety of methods depending on the emission source category being considered, the required spatial resolution, the geographic extent of the domain, and the particular characteristics of the geospatial data available. The same spatial allocation methodologies can also be applied to general arbitrary regions.

Spatial surrogates can be developed from several sources of spatial data describing the Land Use/Land Cover (LULC), transportation networks and population characteristics. The processing and development of gridding surrogates is performed using GIS. To develop Spatial Allocation Factors (SAFs), the following geospatial coverages are imported:

- The appropriate surrogate databases (e.g., land use, population, roadways, and railways)
- The user-specified region
- The regional/county boundaries

5.4 Chemical Speciation

Speciation is the process of disaggregating inventory pollutants into individual chemical species. The need for speciation is determined by the inventory purpose. Inventory applications that require detailed speciation include photochemical modeling, air toxics inventories, chemical mass balance modeling, and visibility modeling. The major types of speciation are:

- Total suspended particulate matter (TSP), where the particle diameter and density are missing
- NO_x emissions may need to be specified as NO and NO₂
- Total Volatile Organic Compounds (VOCs) are reported
- Mobile source inventories report organic emissions as total hydrocarbons.

It is a common practice to report volatile organic compounds (VOCs) as total VOC or Non-methane. VOCs are composed of chemicals with orders of magnitude difference in toxicity, fate and transport on various media (e.g., atmosphere, soils, water, animal tissue, milk, and eggs). In projecting future emissions, it is necessary to take speciation into account since changes in fuel and solvent can dramatically change environmental and human health impacts.

The two main considerable factors in temporal changes in the spatial allocation are the evolution of land use patterns and higher activity rates on the sources. For example, urbanization of farmlands will change the area emissions profile and the increase in traffic on roads will cause higher emissions (accounted as higher activity rate).

Species resolution refers to disaggregating an inventory pollutant into its individual chemical components. Species resolution is primarily performed using speciation profiles that describe the fraction of individual chemical species.

Air toxics inventories seek to quantify the amount of hazardous air pollutants (HAPs) that are emitted. Ideally, this would be performed using emission factors for individual HAPs. Although there are some HAP emission factors for combustion and other sources, emission factors often do not exist. As a result, individual HAP species frequently are disaggregated from TOG and PM by using speciation profiles. This is not the preferred approach for estimating HAPs emissions. If this approach is used, it often results in an overestimation of HAPs.

SPECIATE is EPA's repository of Total Organic Compound (TOC) and Particulate Matter (PM) speciated profiles for a variety of sources for use in source apportionment studies. No new profiles have been added to SPECIATE since the October 1999 release. The SPECIATE software tool is available at: <http://www.epa.gov/ttn/chief/software/speciate/index.html>.

5.5 Double Counting

Double counting occurs when the emissions from one source are included twice in the same inventory.

Double counting can result from:

Overlap between point and area sources: In this case, double counting occurs when some of the area categories are partially included in the point area inventory. For example, large dry cleaning facilities can emit above the minimal threshold for point sources. Therefore, these large dry cleaning facilities' emissions must be subtracted from the total estimated dry cleaning area source emissions to avoid double counting. Emissions inventory methodology should include comparison of point and area emission sources to evaluate sources that may be included in both inventories.

Overlap between area source categories: In this second case, double counting occurs when two categories are fairly similar. Two examples are given here. The first is the commercial use of solvent category and auto body refinishing one. Another example would be burning emissions estimate for the prescribed burning area source category, which could potentially include emissions from agricultural burning. To avoid this type of double counting, you must become very familiar with the definitions of each area source category and understand the various processes.

5.6 Air Pollution Control Devices

To properly estimate emissions, the effectiveness of an existing Air Pollution Control Device (APCD) must be applied in the emission calculations. Control devices for reducing particulate and volatile organic compound (VOC) emissions generally employ physical collection or combustion processes. Sulfur oxides and nitrogen oxides are more often controlled by chemical transformation. Control devices for carbon monoxide are typically not used by stationary sources. Ammonia emissions may be controlled by physical, combustion, or chemical processes.

5.6.1 Emissions Reduction - Control Efficiency (CE)

The Emissions Reduction (ER), also known as the control device efficiency (CE), is the percentage of the air pollutant that is removed from the emission stream before release to the atmosphere. In addition to control device efficiency, emissions will be determined by capture efficiency of a system. The capture efficiency indicates the percentage of the emission stream that is taken into the control system.

Control efficiency (CE) is a measure of emission reduction efficiency. It is a percentage value representing the amount of emissions that are controlled by a control device, process change, or reformulation. Control efficiency is calculated as:

$$CE = (UER - CER) / UER * 100 \quad [\%]$$

where,

<i>CE</i>	= Control Efficiency
<i>UER</i>	= Uncontrolled Emission Rate
<i>CER</i>	= Controlled Emission Rate

Note that some facilities do not always operate devices at their maximum level of efficiency. Although Air Pollution Control Device (APCD) should be designed to accommodate reasonable process variation and some deterioration, some types of control devices vary in efficiency based on process equipment operating rates, fuel quality, and age. Usually, an emission limit must be met and the primary goal of the facility is to meet that limit. It may or may not be necessary to operate the control device at its maximum level of efficiency in order to meet that limit.

In general, when estimating the overall control efficiency for a combination of control devices in series, inventory preparers should not assume the overall efficiency is additive or cumulative. This is because control efficiency for a particular device is often dependent on the inlet concentration. The overall control efficiency of a series of APCDs is typically higher than the efficiencies of

the individual control devices, but smaller than the sum of the individual control efficiencies. However, in some cases the control efficiencies of multiple devices in series may be assumed to be additive. In this case, the overall control efficiency of a series of "n" devices is:

$$CE (overall) = 1 - [(1 - CE_1 / 100) * (1 - CE_2 / 100) * * (1 - Ce_n / 100)]$$

When the last device in a series of control devices is a fabric filter, you should assume that the control efficiency of the APCDs is equal to the control efficiency of the fabric filter, and the other devices help to reduce the load on the fabric filter. For example, suppose a wood boiler is equipped with a multicyclone designed to operate at a control efficiency of 60 percent and a fabric filter designed to operate at 99 percent, then the overall control efficiency is likely to be around 99 percent, and for all practical purposes, can be assumed to be 99 percent.

The capture efficiency is defined as the fraction of pollutant emitted from the processing point that is actually gathered by baffles, hoods, or other capturing devices, and routed to the control device. Capture efficiency can be estimated by tests performed at the facility for which emissions are being estimated. Capture device efficiency is estimated on the basis of tests performed on similar equipment at other facilities. Capture efficiency is also estimated from manufacturer's specifications or literature values.

Three different ways to determine control device efficiency are presented below in order of preference.

Source Test: Control device efficiency may be determined for specific equipment and operating conditions by source tests measuring pollutant concentrations before and after application of the control device. However, because of possible variation in control device operation with process, control device malfunction, and deterioration over time, the measurement is subject to the potential limitations of all source tests.

Manufacturer Specification: A second method of obtaining control efficiency is to use the manufacturer's design specification or guaranteed performance specification. However, the design collection efficiency reported by manufacturers is the efficiency obtainable under optimum conditions and may not represent actual conditions. In addition, a control device may be improperly sized for effective control of the process under consideration. Some assessment of design efficiency will be required to adjust for these source conditions.

Literature Values: When test data or manufacturer's specifications are not available for estimating control efficiency of a specific control device, literature values may be used. Table 1 lists control devices commonly used at stationary

point sources, applicable pollutants controlled, and their typical control efficiencies

Control device efficiency estimates will also need to be adjusted for downtime or control device condition (e.g., degradation of fabric filter bags). If control devices are shut down periodically for maintenance or by upset conditions, the emissions released in a given hour may far exceed those released in the controlled mode over many hours of operation. The table below was obtained from the work created by the Western Governors' Association titled "Mexico Emissions Inventory Program Manuals".

Table 1. Typical Control Devices and Control Efficiencies (%).

Device/Technique	Pollutant Reduction Efficiency (%)			
	Particulate Matter	VOC	SOx	NOx
Cyclone	80-90+			
Fabric Filter	80-99+			
Electrostatic Precipitator	95-99+			
Scrubber	80-95	--	80-98	--b
Absorption		90-99	--	--b
Adsorption		50-99	--b	--b
Condensation	--	50-95		
Thermal Incineration	--	95-99+		
Catalytic Incineration		95-99+		--
Selective Catalytic Reduction				40-90
Selective Noncatalytic Reduction			*	40-60

Sources: Emission Inventory Improvement Program (EIIP), July 1995a.

6 Characterization of Point Sources

Point Sources are defined as large, stationary, identifiable sources of emissions that release pollutants into the atmosphere. Point sources are often defined by state or local air regulatory agencies as point sources when they annually emit more than a specified amount of a given pollutant, and how state and local agencies define point sources can vary. Point sources are typically large manufacturing or production plants. They typically include both confined "stack" emission points as well as individual unconfined "fugitive" emission sources.

A more technical point source definition is presented below:

- 100 tons/year of any compound
- Stationary sources that release 10 tons per year (TPY) of any one HAP or 25 TPY of a combination of HAPs
- Emissions from equipment leaks, materials transferred from one location to another, or during discharge through emissions stacks or vents

Point source emissions can be obtained by various methods, including the following:

- Direct facility reporting
- The use of emission factors
- Incorporating data from the United States Superfund Toxics Release Inventory.

Point source locations can be determined by:

- Facility self-reporting
- Global positioning system (GPS)
- Geographic information system (GIS) addressing matching

Point source stack parameters information may come from the following:

- Regulatory agency files
- Default values from the National Emissions Inventory

Within a given facility, stack-by-stack emissions were not available. Therefore, each facility was represented as a single stack whose location was taken as the centroid of the facility (when available) or as the location of the front entrance. Similarly, stack parameters were taken as averages across all emission points at the facility, weighted by the throughput for the emission point.

Regardless of how complete an emissions inventory is, four major considerations must remain in focus:

- 1) Process upset conditions with elevated air toxic emissions for specific processes and facilities. Upset conditions may contribute a substantial increase on emissions into the atmosphere. Such episodes may last from a few minutes to days.
- 2) Site characterization information. This characterization is very desirable for an emissions inventory database. The type of data that would help better define the air dispersion model include:
 1. Surrounding building details - Buildings may cause significant increase in ground level concentrations.
 2. Stack location and facility fence line coordinates - It is usual that facilities sum all the emissions data and report the accumulated value. This way, each individual source contribution is hidden from view. Ideally, individual source locations would be provided for the risk assessment. Additionally, for very high-resolution

studies (e.g., neighborhood level), it would be ideal to be able to associate specific sources to sensitive receptors. These issues were not as significant as initially thought, since the air model does not accurately predict the impact position.

3) Actual, allowable, or reported emissions for the point sources.

6.1 Stationary Point Source Emissions from Combustion of Fuel

Combustion of fuel is the greatest source of atmospheric emissions. The list below indicates a few of the types of fuels commonly used by stationary sources:

- Coal
 - Anthracite Coal
 - Bituminous / Sub-bituminous Coal
- Distillate Oil:
 - Total - Boilers & Internal Combustion (IC) Engines
 - All Boiler Types
 - All IC Engine Types
 - Kerosene
 - Gasoline
 - Diesel
- Residual Oil
- Waste Oil
- Natural Gas
 - Total - Boilers & IC Engines
 - All Boiler Types
 - All IC Engine Types
- Liquefied Petroleum Gas (LPG)
- Process Gas
- Wood
- Coke

Three of the above fuels are predominant in stationary sources, and therefore will be further discussed in the following sections.

6.2 Coal Combustion

Coals are classified by rank according to their progressive alteration in the natural metamorphosis from lignite to anthracite. Coal rank depends on the volatile matter, fixed carbon, inherent moisture, and oxygen. Typically, coal rank increases as the amount of fixed carbon increases and the amount of volatile matter and moisture decreases.

Bituminous coals are by far the largest group and are characterized as having lower fixed carbon and higher volatile matter than anthracite. Sub-bituminous coals have higher moisture and volatile matter and lower sulfur content than

bituminous coals, and may be used as an alternative fuel in some boilers originally designed to burn bituminous coals. Anthracite coal is a high-ranking coal with more fixed carbon and less volatile matter than bituminous, sub-bituminous, or lignite varieties.

6.2.1 Emissions

Emissions from coal combustion depend on the rank and composition of the fuel, type and size of the boiler, firing conditions, load, type of control technologies, and the level of equipment maintenance. The major pollutants of concern from coal combustion are particulate matter (PM), sulfur oxides (SO_x), and nitrogen oxides (NO_x). Some unburned combustibles, including carbon monoxide (CO) and numerous organic compounds, are generally emitted even under proper boiler operating conditions.

6.2.2 Particulate Matter - PM

Particulate matter (PM) composition and emission levels are complex functions of boiler firing configuration, boiler operation, pollution control equipment, and coal properties. Uncontrolled PM emissions from coal-fired boilers include the ash from combustion of the fuel, as well as unburned carbon resulting from incomplete combustion. In pulverized coal systems, combustion is almost complete; thus, the emitted PM is primarily composed of inorganic ash residues.

Coal ash may either settle out in the boiler (bottom ash) or entrain in the flue gas (fly ash). The distribution of particulates between the bottom ash and fly ash fractions directly affects the PM emission rate. Furthermore, these fractions depend on the boiler firing method and furnace type (wet or dry bottom). Boiler load also affects the PM emissions as decreasing load tends to reduce PM emissions. However, the magnitude of the reduction varies considerably depending on boiler type, fuel, and boiler operation.

Soot blowing is also a source of intermittent PM emissions in coal-fired boilers. Steam soot and air soot blowing is periodically used to dislodge ash from heat transfer surfaces in the furnace, convective section, economizer, and air pre-heater.

Particulate emissions may be categorized as either filterable or condensable. Filterable emissions are generally considered to be the particles that are trapped by the glass fiber filter in the front half of a Reference Method 5 or Method 17 sampling train. Vapors and particles less than 0.3 microns pass through the filter. Condensable particulate matter is material that is emitted in the vapor state that later condenses to form homogeneous and/or heterogeneous aerosol particles. The condensable particulate emitted from boilers fueled on coal or oil is primarily inorganic in nature.

6.2.3 Sulfur Oxides - SO_x

Gaseous sulfur oxides (SO_x) from coal combustion are primarily sulfur dioxide (SO₂), with a much lower quantity of sulfur trioxide (SO₃) and gaseous sulfates. These compounds form as the organic and pyretic sulfur in the coal are oxidized during the combustion process. On average, about 95 percent of the sulfur present in bituminous coal will be emitted as gaseous SO_x, whereas somewhat less will be emitted when sub-bituminous coal is fired. The more alkaline nature of the ash in some sub-bituminous coals causes some of the sulfur to react in the furnace to form various sulfate salts that are retained in the boiler or in the fly ash.

6.2.4 Nitrogen Oxides - NO_x

Nitrogen oxide (NO_x) emissions from coal combustion are primarily nitric oxide (NO), with only a few volume percent as nitrogen dioxide (NO₂). Nitrous oxide (N₂O) is also emitted at a few parts per million. NO_x formation results from thermal fixation of atmospheric nitrogen in the combustion flame and from oxidation of nitrogen bound in the coal. Experimental measurements of thermal NO_x formation have shown that the NO_x concentration is exponentially dependent on temperature and is proportional to nitrogen concentration in the flame, the square root of oxygen concentration in the flame, and the gas residence time. Cyclone boilers typically have high conversion of nitrogen to NO. Typically, only 20 to 60 percent of the fuel nitrogen is converted to NO_x. Bituminous and sub-bituminous coals usually contain from 0.5 to 2 weight percent nitrogen, mainly present in aromatic ring structures. Fuel nitrogen can account for up to 80 percent of total NO_x from coal combustion.

6.2.5 Carbon Monoxide - CO

The rate of carbon monoxide (CO) emissions from combustion sources depends on the fuel oxidation efficiency of the source. By controlling the combustion process carefully, CO emissions can be minimized. Thus, if a unit is operated improperly or is not well-maintained, the resulting concentrations of CO (as well as organic compounds) may increase by several orders of magnitude. Smaller boilers, heaters, and furnaces typically emit more CO and organics than larger combustors. This is because smaller units usually have less high-temperature residence time and, therefore, less time to achieve complete combustion than larger combustors. Combustion modification techniques and equipment used to reduce NO_x can increase CO emissions if the modification techniques are improperly implemented or if the equipment is improperly designed.

6.2.6 Organic Compounds

As with CO emissions, the rate at which organic compounds are emitted depends on the combustion efficiency of the boiler. Therefore, combustion modifications

that change combustion residence time, temperature, or turbulence may increase or decrease concentrations of organic compounds in the flue gas.

Organic emissions include volatile, semi-volatile, and condensable organic compounds either present in the coal or formed as a product of incomplete combustion (PIC). Organic emissions are primarily characterized by the criteria pollutant class of unburned vapor-phase hydrocarbons. These emissions include alkanes, alkenes, aldehydes, alcohols, and substituted benzenes (e.g., benzene, toluene, xylene, and ethyl benzene).

Emissions of polychlorinated dibenzo-p-dioxins and polychlorinated dibenzofurans (PCDD/PCDF) also result from the combustion of coal. Environmentally, tetrachloro- through octachloro- dioxins and furans are of primary interest. Dioxin and furan emissions are influenced by the extent of destruction of organics during combustion and through reactions in the air pollution control equipment. The formation of PCDD/PCDF in air pollution control equipment is primarily dependent on flue gas temperature, with maximum potential for formation occurring at flue gas temperatures of 450 - 650 °F.

The remaining organic emissions are composed largely of compounds emitted from combustion sources in a condensed phase. These compounds can almost exclusively be classified into a group known as polycyclic organic matter (POM), and a subset of compounds called polynuclear aromatic hydrocarbons (PNA or PAH). Polycyclic organic matter is more prevalent in the emissions from coal combustion because of the more complex structure of coal.

6.2.7 Trace Metals

Trace metals are also emitted during coal combustion. The quantity of any given metal emitted, in general, depends on:

- Physical and chemical properties of the metal itself
- Concentration of the metal in the coal
- Combustion conditions
- Type of particulate control device used, and its collection efficiency as a function of particle size.

6.2.8 Acid Gases

In addition to SO₂ and NO_x emissions, combustion of coal also results in emissions of chlorine and fluorine, primarily in the form of hydrogen chloride (HCl) and hydrogen fluoride (HF). Lesser amounts of chlorine gas and fluorine gas are also emitted. A portion of the chlorine and fluorine in the fuel may be absorbed onto fly ash or bottom ash. Both HCl and HF are water soluble and are readily controlled by acid gas scrubbing systems.

6.2.9 Fugitive Emissions

Fugitive emissions are defined as pollutants, which escape from an industrial process due to leakage, materials handling, inadequate operational control, transfer, or storage. The fly ash handling operations in most modern utility and industrial combustion sources consist of pneumatic systems, or enclosed and hooded systems, which are vented through small fabric filters or other dust control devices. The fugitive PM emissions from these systems are therefore minimal. Fugitive particulate emissions can sometimes occur during fly ash transfer operations from silos to trucks or rail cars.

6.2.10 Greenhouse Gases

Carbon dioxide (CO₂), methane (CH₄), and nitrous oxide (N₂O) emissions are all produced during coal combustion. Nearly all of the fuel carbon (99 percent) in coal is converted to CO₂ during the combustion process. This conversion is relatively independent of firing configuration. Although the formation of CO acts to reduce CO₂ emissions, the amount of CO produced is insignificant compared to the amount of CO₂ produced. The majority of the fuel carbon not converted to CO₂ is entrained in bottom ash. CO₂ emissions for coal vary with carbon content, and carbon content varies between the classes of bituminous and sub-bituminous coals. Further, carbon content also varies within each class of coal based on the geographical location of the mine.

Formation of N₂O during the combustion process is governed by a complex series of reactions, and its formation is dependent upon many factors. Formation of N₂O is minimized when combustion temperatures are kept high (above 1575 °F) and excess air is kept to a minimum (less than 1 percent). N₂O emissions for coal combustion are not significant except for fluidized bed combustion (FBC), where the emissions are typically two orders of magnitude higher than all other types of coal firing due to areas of low temperature combustion in the fuel bed.

Methane emissions vary with the type of coal being fired and firing configuration, but are highest during periods of incomplete combustion, such as the start-up or shut-down cycle for coal-fired boilers. Typically, conditions that favor formation of N₂O also favor emissions of CH₄.

6.2.11 Calculation Example - Coal Combustion in Stationary Point Sources

In the following example, the emissions inventory practitioner is required to estimate emissions from a pulverized coal dry bottom and wall fired boiler. This unit burned 750,000 tons last year using sub-bituminous coal, with 4% sulfur.

To complete the emissions estimate, the first action is to identify the Source Classification Code (SCC) for the boiler, which in this case is 1-01-002-02. Using Table 2 presented below, one can obtain the emission factors for SO_x,

NO_x, and CO. Note that Table 2 was extracted from Chapter 1 in AP-42. The calculations for these pollutants are expressed below:

$$\text{Emissions [lb]} = \text{Activity} * \text{Emissions Factor}$$

$$SO_x = 750,000 \times 38S \quad [\text{lb}]$$

$$SO_x = 750,000 \times (38 \times 4) = 114 \text{ million pounds}$$

$$NO_x = 750,000 \times 22 = 16.5 \text{ million pounds}$$

$$CO = 750,000 \times 0.5 = 375,000 \text{ lb}$$

Table 3 contains emissions factors for PAHs. As an example, one can compute the emissions of Benzo(A)Pyrene as follows:

$$\text{Benzo(A)Pyrene} = 750,000 \times 3.8E-8 = 2.85 \text{ lb}$$

Table 4 presents emission factors for metals, as indicated in AP-42. Note that in this case it would be more accurate to know the exact composition of the mineral content of the ash. Calculations for arsenic and mercury are as follows:

$$\text{Arsenic} = 750,000 \times 4.1E-4 = 307.5 \text{ lb}$$

$$\text{Mercury} = 750,000 \times 8.35E-5 = 62.25 \text{ lb}$$

Figure 11 presents a summary of the steps required for the emissions estimation for coal combustion. In this example, we did not use the information on ash content and mineral content, as presented in Figure 11.

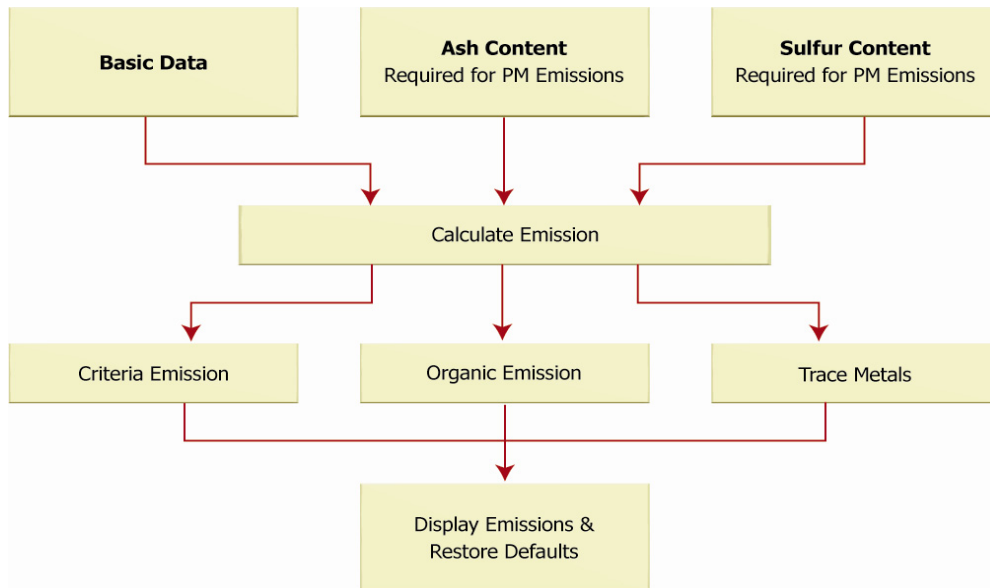


Figure 11. Emissions estimation flowchart for coal burning.

Table 2. Emission factors for SO_x, NO_x, and CO from bituminous coal combustion.

Firing Configuration	SCC	SO _x		NO _x		CO	
		Emission Factor (lb/ton)	Emission Factor Rating	Emission Factor (lb/ton)	Emission Factor Rating	Emission Factor (lb/ton)	Emission Factor Rating
PC, dry bottom, wall-fired, bituminous Pre-NSPS	1-01-002-02 1-02-002-02 1-03-002-06	38S	A	22	A	0.5	A

Source: AP-42 Chapter 1.

Emissions factor above for SO_x is 38S, where S is the percentage in weight of sulfur in coal.

Table 3. EF for polynuclear aromatic hydrocarbons (PAH) from coal combustion.

Pollutant	Emission Factor (lb/ton)	Emission Factor rating
Acenaphthene	5.1E-07	B
Acenaphthylene	2.5E-07	B
Anthracene	2.1E-07	B
Benzo(a)anthracene	8.0E-08	B
Benzo(a)pyrene	3.8E-08	D
Benzo(b,j,k)fluoranthene	1.1E-07	B
Benzo(g,h,i)perylene	2.7E-08	D
Chrysene	1.0E-07	C
Fluoranthene	7.1E-07	B
Fluorene	9.1E-07	B
Indeno(1,2,3-cd)pyrene	6.1E-08	C

Table 4. Emission factors for trace metals for controlled coal combustion.

Pollutant	Emission Factor (lb/ton)	Emission Factor Rating
Arsenic	4.1E-04	A
Beryllium	2.1E-05	A
Cadmium	5.1E-05	A
Chromium	2.6E-04	A
Chromium (VI)	7.9E-05	D
Cobalt	1.0E-04	A
Lead	4.2E-04	A
Mercury	8.3E-05	A

6.3 Fuel Oil Combustion

Two major categories of fuel oil are burned by combustion sources: distillate oils and residual oils. These oils are further distinguished by grade numbers:

- No. 1 and No. 2 are distillate oils
- No. 4 being either distillate oil or a mixture of distillate and residual oils
- No. 5 and No. 6 are residual oils. Note that No. 6 fuel oil is sometimes referred to as Bunker C.

Distillate oils are more volatile and less viscous than residual oils. They have negligible nitrogen and ash contents and usually contain less than 0.3 percent sulfur (by weight). Distillate oils are used mainly in domestic and small commercial applications, and include kerosene and diesel fuels. Being more viscous and less volatile than distillate oils, the heavier residual oils (Nos. 5 and 6) may need to be heated for ease of handling and to facilitate proper atomization. Because residual oils are produced from the residue remaining after the lighter fractions (gasoline, kerosene, and distillate oils) have been removed from the crude oil, they contain significant quantities of ash, nitrogen, and sulfur. Residual oils are used mainly in utility, industrial, and large commercial applications.

6.3.1 Emissions

Emissions from fuel oil combustion depend on the grade and composition of the fuel, the type and size of the boiler, the firing and loading practices used, and the level of equipment maintenance. Because the combustion characteristics of distillate and residual oils are different, their combustion can produce significantly different emissions. In general, the baseline emissions of criteria and non-criteria pollutants are those from uncontrolled combustion sources. Uncontrolled sources are those without add-on air pollution control (APC)

equipment, or other combustion modifications designed for emission control. Baseline emissions for sulfur dioxide (SO₂) and particulate matter (PM) can also be obtained from measurements taken upstream of APC equipment.

6.3.2 Particulate Matter Emissions - PM

Particulate matter (PM) emissions may be categorized as either filterable or condensable. Filterable emissions are generally considered to be the particles that are trapped by the glass fiber filter in the front half of a Reference Method 5 or Method 17 sampling van. Vapors and particles less than 0.3 microns pass through the filter. Condensable PM is material that is emitted in the vapor state, which later condenses to form homogeneous and/or heterogeneous aerosol particles. The condensable particulate, emitted from boilers fueled on coal or oil, is primarily inorganic in nature. Filterable particulate matter emissions depend predominantly on the grade of fuel fired. Combustion of lighter distillate oils results in significantly lower PM formation than combustion of heavier residual oils. Among residual oils, firing of No. 4 or No. 5 oil usually produces less PM than firing of heavier No. 6 oil.

In general, filterable PM emissions depend on the completeness of combustion as well as on the oil ash content. The PM emitted by distillate oil-fired boilers primarily comprises carbonaceous particles resulting from incomplete combustion of oil, and is not correlated to the ash or sulfur content of the oil. However, PM emissions from residual oil burning are related to the oil sulfur content. This is because low-sulfur No. 6 oil, either from naturally low-sulfur crude oil or desulfurized by one of several processes, exhibits substantially lower viscosity and reduced asphaltene, ash, and sulfur contents, which results in better atomization and more complete combustion.

Boiler load can also affect filterable particulate emissions in units firing No. 6 oil. At low load (50 percent of maximum rating) conditions, particulate emissions from utility boilers may be lowered by 30 to 40 percent, and by as much as 60 percent from small industrial and commercial units. However, no significant particulate emission reductions have been noted at low loads from boilers firing any of the lighter grades. At very low load conditions (approximately 30 percent of maximum rating), proper combustion conditions may be difficult to maintain and particulate emissions may increase significantly.

6.3.3 Sulfur Oxides Emissions - SO_x

Sulfur oxides (SO_x) emissions are generated during oil combustion from the oxidation of sulfur contained in the fuel. The emissions of SO_x from conventional combustion systems are predominantly in the form of SO₂. Uncontrolled SO_x emissions are almost entirely dependent on the sulfur content of the fuel and are not affected by boiler size, burner design, or grade of fuel being fired. On average, more than 95 percent of the fuel sulfur is converted to

SO₂, about 1 to 5 percent is further oxidized to sulfur trioxide (SO₃), and 1 to 3 percent is emitted as sulfate particulate. SO₃ readily reacts with water vapor (both in the atmosphere and in flue gases) to form a sulfuric acid mist.

6.3.4 Nitrogen Oxides Emissions - NO_x

Oxides of nitrogen (NO_x) formed in combustion processes are due either to thermal fixation of atmospheric nitrogen in the combustion air ("thermal NO_x"), or to the conversion of chemically bound nitrogen in the fuel ("fuel NO_x"). The term NO_x refers to the composite of nitric oxide (NO) and nitrogen dioxide (NO₂). Test data have shown that for most external fossil fuel combustion systems, over 95 percent of the emitted NO_x is in the form of nitric oxide (NO). Nitrous oxide (N₂O) is not included in NO_x, but it has recently received increased interest because of atmospheric effects.

Fuel nitrogen conversion is the more important NO_x-forming mechanism in residual oil boilers. It can account for 50 percent of the total NO_x emissions from residual oil firing. The percent conversion of fuel nitrogen to NO_x varies greatly; however, typically from 20 to 90 percent of nitrogen in oil is converted to NO_x. Except in certain large units having unusually high peak flame temperatures, or in units firing a low nitrogen content residual oil, fuel NO_x generally accounts for over 50 percent of the total NO_x generated. Thermal fixation, on the other hand, is the dominant NO_x-forming mechanism in units firing distillate oils, primarily because of the negligible nitrogen content in these lighter oils. Because distillate oil-fired boilers are usually smaller and have lower heat release rates, the quantity of thermal NO_x formed in them is less than that of larger units, which typically burn residual oil.

6.3.5 Carbon Monoxide Emissions - CO

The rate of carbon monoxide (CO) emissions from combustion sources depends on the oxidation efficiency of the fuel. By controlling the combustion process carefully, CO emissions can be minimized. Thus, if a unit is operated improperly or not well maintained, the resulting concentrations of CO (as well as organic compounds) may increase by several orders of magnitude. Smaller boilers, heaters, and furnaces tend to emit more of these pollutants than larger combustors. This is because smaller units usually have a higher ratio of heat transfer surface area to flame volume than larger combustors have; this leads to reduced flame temperature and combustion intensity and, therefore, lower combustion efficiency.

The presence of CO in the exhaust gases of combustion systems results principally from incomplete fuel combustion. Several conditions can lead to incomplete combustion, including: insufficient oxygen (O₂) availability; poor fuel/air mixing; cold-wall flame quenching; reduced combustion temperature; decreased combustion gas residence time; and load reduction (i.e., reduced combustion intensity). Since various combustion modifications for NO_x

reduction can produce one or more of the above conditions, the possibility of increased CO emissions is a concern for environmental, energy efficiency, and operational reasons.

6.3.6 Organic Compound Emissions

Small amounts of organic compounds are emitted from combustion. As with CO emissions, the rate at which organic compounds are emitted depends, to some extent, on the combustion efficiency of the boiler. Therefore, any combustion modification which reduces the combustion efficiency will most likely increase the concentrations of organic compounds in the flue gases.

Total organic compounds (TOCs) include VOCs, semi-volatile organic compounds, and condensable organic compounds. Emissions of VOCs are primarily characterized by the criteria pollutant class of unburned vapor phase hydrocarbons. Unburned hydrocarbon emissions can include essentially all vapor phase organic compounds emitted from a combustion source. These are primarily emissions of aliphatic, oxygenated, and low molecular weight aromatic compounds, which exist in the vapor phase at flue gas temperatures. These emissions include all alkanes, alkenes, aldehydes, carboxylic acids, and substituted benzenes (e.g., benzene, toluene, xylene, and ethyl benzene).

The remaining organic emissions are composed largely of compounds emitted from combustion sources in a condensed phase. These compounds can almost exclusively be classified into a group known as polycyclic organic matter (POM), and a subset of compounds called polynuclear aromatic hydrocarbons (PAH or PNA). There are also PAH-nitrogen analogs. Information available in the literature on POM compounds generally pertains to these PAH groups.

Formaldehyde is formed and emitted during combustion of hydrocarbon-based fuels including coal and oil. Formaldehyde is present in the vapor phase of the flue gas. Formaldehyde is subject to oxidation and decomposition at the high temperatures encountered during combustion. Thus, larger units with efficient combustion (resulting from closely regulated air-fuel ratios, uniformly high combustion chamber temperatures, and relatively long gas retention times) have lower formaldehyde emission rates than do smaller, less efficient combustion units.

6.3.7 Trace Element Emissions

The quantity of trace elements entering the combustion device depends solely on the fuel composition. The quantity of trace metals emitted from the source depends on combustion temperature, fuel feed mechanism, and the composition of the fuel. The temperature determines the degree of volatilization of specific compounds contained in the fuel. The fuel feed mechanism affects the separation of emissions into bottom ash and fly ash. In general, the quantity of any given metal emitted depends on the physical and chemical properties of the element itself, concentration

of the metal in the fuel the combustion conditions, the type of particulate control device used, and its collection efficiency as a function of particle size.

6.3.8 Greenhouse Gases (GHGs)

Carbon dioxide (CO₂), methane (CH₄), and nitrous oxide (N₂O) emissions are all produced during fuel oil combustion. Nearly all of the fuel carbon (99 percent) in fuel oil is converted to CO₂ during the combustion process. This conversion is relatively independent of firing configuration. Although the formation of CO acts to reduce CO₂ emissions, the amount of CO produced is insignificant compared to the amount of CO₂ produced. The majority of the fuel carbon not converted to CO₂ is due to incomplete combustion in the fuel stream.

Formation of N₂O during the combustion process is governed by a complex series of reactions, and its formation is dependent upon many factors. Formation of N₂O is minimized when combustion temperatures are kept high (above 1475 °F) and excess air is kept to a minimum (less than 1 percent). Emissions can vary widely from unit to unit, or even from the same unit at different operating conditions.

Methane emissions vary with the type of fuel and firing configuration, but are highest during periods of incomplete combustion or low-temperature combustion, (such as the start-up or shut-down cycle, or oil-fired boilers). Typically, conditions that favor formation of N₂O also favor emissions of CH₄.

6.3.9 Calculation Example - Fuel Oil Combustion in Stationary Point Sources

For this example, an industrial boiler burned 160,000 gallons of fuel oil No.6 (also known as Bunker C) in the previous year. The emissions must be calculated for regulatory reporting.

The first action is to identify the Source Classification Code (SCC) for this process. In this case the SCC is 1-02-04-01. Applying emission factors from Table 5 requires a careful attention to the units. Note that emission factors too often cause serious errors due to the different measuring units. In the case of fuel oil, all emission rates are based on 1,000 gallons of fuel oil. This way, we must divide our total fuel oil throughput by 1,000. The calculations for the different pollutant species are presented below:

1. From Table 5, we can estimate emissions for TOC, CH₄, and NMTOC:

$$TOC = 160,000 \text{ gallons} \times 1.28 / 1,000 \text{ [lb/1,000 gallons]} = 204.8 \text{ lb}$$

$$CH_4 = 160,000 \times 1.00 / 1,000 = 160 \text{ lb}$$

$$NMTOC = 160,000 \times 0.28 / 1,000 = 44.8 \text{ lb}$$

2. From Table 6, we can obtain emission factors to estimate emissions for N₂O, POM, and HCOH. Note that there are ranges of values for POM and HCOH in Table 6. In this example, the emissions factors will use a central value, as shown below:

$$N_2O = 160,000 \times 0.11 / 1,000 = 17.6 \text{ lb}$$

$$POM = 160,000 \times 1.2E-3 / 1,000 = 0.192 \text{ lb}$$

$$HCOH = 160,000 \times 3.3E-2 = 5.28 \text{ lb}$$

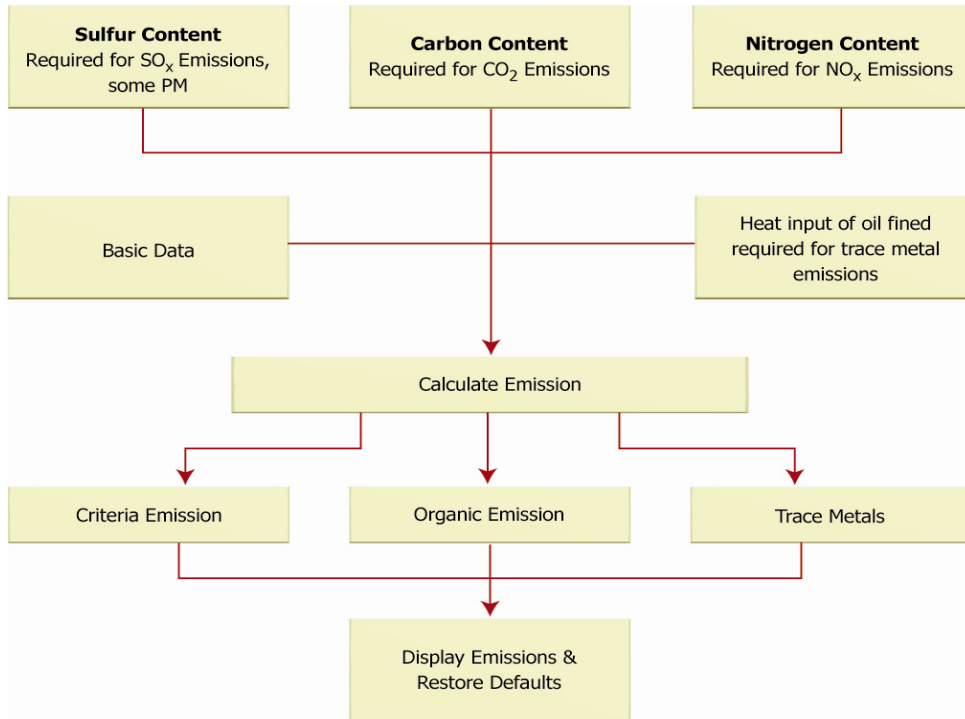


Figure 12. Summary of emissions estimation for Fuel Oil combustion.

Table 5. EF for TOC, methane (CH₄), and NMTOC for fuel oil combustion.

Firing Configuration (SCC)	TOC Emission Factor (lb/10³ gal)	Methane Emission Factor (lb/10³ gal)	NMTOC Emission Factor (lb/10³ gal)
<u>Utility boilers</u>			
No.4 (1-01-005-04), No.5 (1-01-004-05), and No.6 oil fired, normal firing (1-01-004-01)	1.04	0.28	0.76
No.4 (1-01-005-05), No.5 (1-01-004-06), and No.6 oil fired, tangential firing (1-01-004-04)	1.04	0.28	0.76
<u>Industrial boilers</u>			
No. 6 oil fired (1-02-004-01/02/03)	1.28	1.00	0.28
No. 5 oil fired (1-02-004-04)	1.28	1.00	0.28
Distillate oil fired (1-02-005-01/02/03)	0.252	0.052	0.2
No. 4 oil fired (1-02-005-04)	0.252	0.052	0.2

Source: USEPA AP-42 Chapter 1

TOC: Total Organic Compounds (TOC)

CH₄: Methane

NMTOC: Non-Methane TOC

Emissions rating factor for all devices in table: A

Table 6. EF for N₂O, (POM), and Formaldehyde (HCOH) from fuel oil combustion.

Firing Configuration (SCC)	Emission Factor (lb/10³ gal)		
	N₂O	POM	HCOH
Utility/industrial/commercial boilers			
No. 6 oil fired (1-01-004-01, 1-02-004-01, 1-03-004-01)	0.11	0.0011 - 0.0013	0.024 - 0.061
Distillate oil fired (1-01-005-01, 1-02-005-01, 1-03-005-01)	0.11	0.0033	0.035 - 0.061

Source: USEPA AP-42 Chapter 1

Emissions rating factor for all devices in table: E

Table 7. EF for Speciated organic compounds from fuel oil combustion.

Organic Compound	Emission Factor (lb/10 ³ Gal)	Emission Factor Rating
Benzene	2.14E-04	C
Ethylbenzene	6.36E-05	E
Formaldehyde	3.30E-02	C
Naphthalene	1.13E-03	C
1,1,1-Trichloroethane	2.36E-04	E
Toluene	6.20E-03	D
O-Xylene	1.09E-04	E
Acenaphthene	2.11E-05	C
Acenaphthylene	2.53E-07	D
Anthracene	1.22E-06	C
Benz(a)anthracene	4.01E-06	C
Benzo(b,k)fluoranthene	1.48E-06	C
Benzo(g,h,i)perylene	2.26E-06	C
Chrysene	2.38E-06	C

Table 8. Emissions factors for metals from No.6 fuel oil combustion.

Metal	Emission Factor (lb/10 ³ Gal)	Emission Factor rating
Arsenic	1.32E-03	C
Barium	2.57E-03	D
Beryllium	2.78E-05	C
Cadmium	3.98E-04	C
Chloride	3.47E-01	D
Chromium	8.45E-04	C
Chromium VI	2.48E-04	C
Cobalt	6.02E-03	D
Copper	1.76E-03	C
Fluoride	3.73E-02	D
Lead	1.51E-03	C
Manganese	3.00E-03	C
Mercury	1.13E-04	C

6.4 Natural Gas Combustion

Natural gas is one of the major combustion fuels used throughout the world. It is mainly used to generate industrial and utility electric power, produce industrial process steam and heat, and heat residential and commercial spaces. Natural gas consists of a high percentage of methane (generally above 85 percent) and varying

amounts of ethane, propane, butane, and inert gases (typically nitrogen, carbon dioxide, and helium).

6.4.1 Emissions

The emissions from natural gas-fired boilers and furnaces include nitrogen oxides (NO_x), carbon monoxide (CO), carbon dioxide (CO_2), methane (CH_4), nitrous oxide (N_2O), volatile organic compounds (VOCs), trace amounts of sulfur dioxide (SO_2), and particulate matter (PM).

6.4.2 Particulate Matter - PM

Because natural gas is a gaseous fuel, filterable particulate matter (PM) emissions are typically low. Particulate matter from natural gas combustion has been estimated to be less than 1 micrometer in size, and has filterable and condensable fractions. Particulate matter, produced during natural gas combustion, is composed of large molecular weight hydrocarbons that are not fully combusted. Increased PM emissions may result from poor air/fuel mixing or maintenance problems.

6.4.3 Sulfur Oxides - SO_x

Emissions of SO_2 from natural gas-fired boilers are low because pipeline quality natural gas typically has sulfur levels of 2,000 grains per million cubic feet. However, sulfur-containing odorants are added to natural gas for detecting leaks, leading to small amounts of SO_2 emissions. Boilers combusting unprocessed natural gas may have higher SO_2 emissions due to higher levels of sulfur in the natural gas. For these units, a sulfur mass balance should be used to determine SO_2 emissions.

6.4.4 Nitrogen Oxides - NO_x

Nitrogen oxide formation occurs by three fundamentally different mechanisms. The principal mechanism of NO_x formation in natural gas combustion is thermal NO_x . The thermal NO_x mechanism occurs through the thermal dissociation and subsequent reaction of nitrogen (N_2) and oxygen (O_2) molecules in the combustion air. Most NO_x formed through the thermal NO_x mechanism occurs in the high temperature flame zone near the burners. The formation of thermal NO_x is affected by three furnace-zone factors:

1. Oxygen concentration
2. Peak temperature
3. Time of exposure at peak temperature

As these three factors increase, NO_x emission levels increase. The emission changes caused by the above factors are fairly consistent for all types of natural gas-fired boilers and furnaces. Emission levels vary considerably with the type

and size of combustor and with operating conditions, such as combustion air temperature, volumetric heat release rate, load, and excess oxygen level.

The second mechanism of NO_x formation, called prompt NO_x, occurs through early reactions of nitrogen molecules in the combustion air and hydrocarbon radicals from the fuel. Prompt NO_x reactions occur within the flame and are usually negligible when compared to the amount of NO_x formed through the thermal NO_x mechanism. However, prompt NO_x levels may become significant with ultra-low NO_x burners.

The third mechanism of NO_x formation, called fuel NO_x, stems from the evolution and reaction of fuel-bound nitrogen compounds with oxygen. Due to the characteristically low fuel nitrogen content of natural gas, NO_x formation through the fuel NO_x mechanism is insignificant.

6.4.5 Carbon Monoxide - CO

The rate of carbon monoxide (CO) emissions from boilers depends on the efficiency of natural gas combustion. Improperly tuned boilers and boilers operating at off-design levels decrease combustion efficiency, resulting in increased CO emissions. In some cases, the addition of NO_x control systems, such as low NO_x burners and flue gas recirculation (FGR), may also reduce combustion efficiency, resulting in higher CO emissions relative to uncontrolled boilers.

6.4.6 Volatile Organic Compounds

The rate of volatile organic compound (VOC) emissions from boilers and furnaces also depends on combustion efficiency. VOC emissions are minimized by combustion practices that promote high combustion temperatures, long residence times at those temperatures, and turbulent mixing of fuel and combustion air. Trace amounts of VOC species in the natural gas fuel (e.g., formaldehyde and benzene) may also contribute to VOC emissions if they are not completely combusted in the boiler.

6.4.7 Greenhouse Gases

Natural gas combustion produces key greenhouse gases such as CO₂, CH₄, and N₂O. In properly tuned boilers, nearly all of the fuel carbon (99.9 percent) in natural gas is converted to CO₂ during the combustion process. This conversion is relatively independent of boiler or combustor type. Fuel carbon not converted to CO₂ results in CH₄, CO, and/or VOC emissions, and is due to incomplete combustion. Even in boilers operating with poor combustion efficiency, the amount of CH₄, CO, and VOC produced is insignificant compared to CO₂ levels.

Formation of N₂O during the combustion process is affected by two furnace-zone factors. N₂O emissions are minimized when combustion temperatures are kept high (above 1475°F) and excess oxygen is kept to a minimum (less than 1 percent).

Methane emissions are highest during low-temperature combustion or incomplete combustion, such as the start-up or shut-down cycle for boilers. Typically, conditions that favor formation of N₂O also favor emissions of methane.

6.4.8 Calculation Example - Natural Gas Combustion in Stationary Point Sources

A sport arena used 5 million cubic feet of natural gas for space heating last year using an uncontrolled burner (no control for NO_x). A monitor unit found high levels of NO_x and SO₂ close to the arena and decided to study the possibility that the burning of the natural gas was the culprit. Table 9 contains emission factors for the burning of natural gas. Note that the units for the emission factors are in pounds/million cubic feet of natural gas. This way, we must divide the throughput by 1.0E-6. The emissions calculations are as follows:

$$NO_x = 5.0 \times 2.2 = 10.1 \text{ lb}$$

$$SO_2 = 5.0 \times 0.6 = 3 \text{ lb}$$

Table 9. EF for criteria pollutants and greenhouse gases from natural gas combustion.

Pollutant	Emission Factor (lb/10 ⁶ scf)	Emission Factor Rating
CO ₂	120,000	A
Lead	0.0005	D
N ₂ O (Uncontrolled)	2.2	E
N ₂ O (low-NO _x burner)	0.64	E
PM (Total)	7.6	D
PM (Condensable)	5.7	D
PM (Filterable)	1.9	B
SO ₂	0.6	A
TOC	11	B
Methane	2.3	B
VOC	5.5	C

Source: USEPA AP-42 Chapter 1

For greenhouse gas calculations, one can also use Table 9 to obtain the emission factors and calculate the total greenhouse gas emissions as follows:

$$CO_2 = 5 \times 120,000 = 600,000 \text{ lb}$$

$$N_2O = 5 * 2.2 = 101. \text{ lb}$$

Note that Table 9 does not contain speciated hydrocarbons (volatile organic compounds). One can use the SPECIATE database to obtain individual emission factors. In this case, the emissions inventory professional would multiply the Total Organic Compounds (TOC) or the Non-Methane TOC (NMTOC) by a speciation profile factor (just like the emissions factor). A sample set of the hydrocarbons is presented in Table 10. The user of this table should always be aware that some factors, such as in Table 10, are applied directly on the actual throughput. For example, toluene emissions would be calculated as follows:

$$\text{Toluene} = 5E6 * 3.4E-3 / 1.0E6 = 1.7E-2 \text{ lb}$$

Table 10. EF for Speciated organic compounds from natural gas combustion.

CAS No.	Pollutant	Emission Factor (lb/10 ⁶ scf)	Emission Factor Rating
74-98-6	Propane	1.6E+00	E
129-00-0	Pyrene	5.0E-06	E
108-88-3	Toluene	3.4E-03	C

6.5 Level of Inventory Data Detail for Point Sources

Information on point sources is usually gathered by surveys. Point sources can be inventoried at the following three levels of detail:

1. Plant level, which denotes a plant or facility that could contain several pollutant-emitting activities
2. Point (stack) level, where emissions to the ambient air occur
3. Process segment level, representing the emission unit operations of a source category

The specific issues pertaining to each level are listed below, and depicted in Figure 13. Whenever possible, emissions should be inventoried at the process/segment level to enable support to air quality activities such as regulation, compliance, and permitting. For example, identifying the processes and devices to which a future regulation might apply and then estimating the impact (i.e., costs and benefits) of that regulation would typically require estimating emissions for each process/device.

Another equally important reason for collecting data at this level of detail is that it provides the agency with the information required to verify the emission estimates provided by the facility operators.

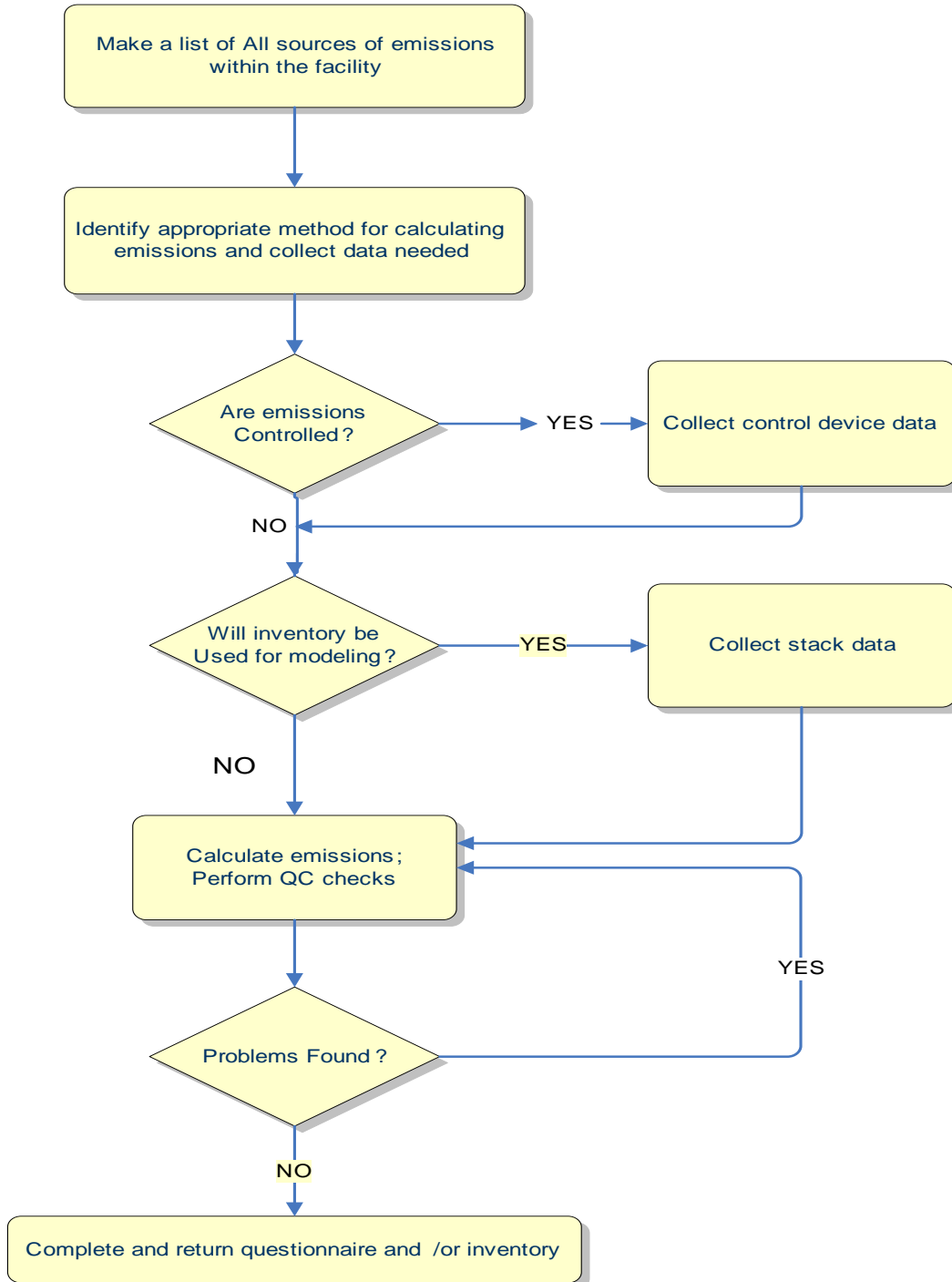


Figure 13. Facility level emissions inventory procedure.

6.5.1 Plant Level Data Detail

In a plant-level survey, the following issues apply:

- Each plant within the area should be identified and assigned a unique plant identification number
- The plant should be further identified by geographic descriptors such as state, municipality, street and/or mailing address, and universal transverse Mercator (UTM) map coordinates, or latitude / longitude
- A plant contact should be identified to facilitate communication and interaction with the plant

6.5.2 Point of Release - Stack Level Data Detail

In a point of emission level survey, each stack, vent, or other point of emission should receive identification:

- as a unique emission point within a plant
- as a unique point within the inventory

The following information should be recorded for each emission point in a comprehensive inventory, as well as for modeling programs:

1. Location (latitude/longitude or UTM coordinates)
2. Height of the emission point
3. Diameter of the emission point
4. Emission rate
5. Gas exit temperature
6. Gas exit velocity or volumetric flow rate from the emission point

6.5.3 Process Level Data Detail

A plant may include various processes or operations. The information necessary to establish an inventory at this level includes the following:

1. Process identification information
2. Process level data (e.g., raw materials, process streams, and product properties)
3. Operating rate data, including actual, maximum, and design operating rate or capacity
4. Fuel use and properties data (ash, sulfur, trace elements, heat content, etc.)
5. Identification of all air pollution control equipment and their associated collection and control efficiencies (measured or design)
6. Identification of the estimation method or reference used to develop each emissions estimate
7. Final emission information, proper speciation, as shown in Figure 14

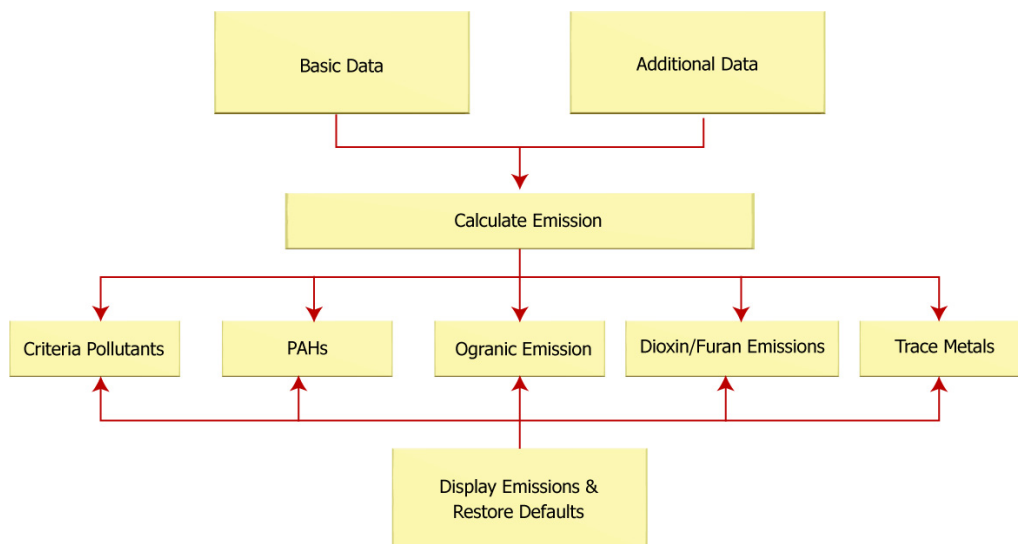


Figure 14. Emissions calculations with speciation of various components.

6.6 Additional Emission Sources at Facilities

Process Upset Emissions - Upset atmospheric emissions usually result from an upset in the process, and are often known as “Process Upset Emissions”. Upset emissions are generally expected to be greater than stack emissions because the process upset results in incomplete destruction of the wastes, or other physical or chemical conditions within the combustion system, that promote the formation and/or release of hazardous compounds from combustion stacks. Upset emissions usually occur during events and times when the hazardous waste combustion unit is not operating within the limits specified in a permit or regulation.

Fugitive Emissions - Fugitive emissions are typically associated with the release of compounds or pollutants from leaks in the combustion chamber (e.g., “puffs”); tanks, valves, flanges, and other material handling equipment used in the storage and handling of hazardous wastes; residues from the combustion process such as ash or quench water; and other treatment, storage, or disposal units.

Accidental Release - Accidental release is defined in Section 112(r) of the Clean Air Act as an unanticipated emission of a regulated substance or other extremely hazardous substance into the ambient air from a stationary source. Accidental releases are typically associated with non-routine emissions from facilities such as the failure of tanks or other material storage and handling equipment, or transportation accidents.

6.7 Emissions from Process Upsets

Non-combusted hazardous waste can be emitted through the stack as a result of various process upsets, such as start-ups, shutdowns, and malfunctions of the combustion unit or Air Pollution Control System (APCS). Emissions can also be

caused by operating upsets in other areas of the facility (e.g., an upset in a reactor, which vents gases to a boiler burning hazardous waste, could trigger a process upset in the boiler, resulting in increased emissions).

Process upsets occur when the hazardous waste combustion unit is not being operated as intended, or during periods of startup or shutdown. Upset emissions are generally expected to be greater than stack emissions (over short periods of time) because the process upset results in incomplete destruction of the wastes or other physical or chemical conditions within the combustion system that promote the formation and/or release of hazardous compounds from combustion stacks. Upset emissions usually occur during events and times when the hazardous waste combustion unit is not operating within the limits specified in a permit or regulation.

To account for the increased emissions associated with process upsets, the stack emission rate estimated from trial burn data is multiplied by an upset factor. When available, facilities should use site specific emissions or process data to estimate the upset factor. The following types of data may be considered and evaluated to derive the upset factor:

- Data for continuous emission monitoring systems that measure stack carbon monoxide, oxygen, total hydrocarbon (if required), or opacity
- Data on combustion chamber, APCS, or stack gas temperature
- APCS operating variables, such as baghouse pressure drop, liquid scrubber flow rate, or electrostatic precipitator voltage
- Stack test collected while the combustion unit was operated under upset conditions

This information may be analyzed with the objective of estimating the magnitude of the increase in emissions and the percentage of time on an annual basis that the unit operates during upset conditions.

When site specific data are not available or are inappropriate for deriving an upset factor, upset emissions should be estimated by using a procedure based on work by the California Air Resources Board (CARB, 1990).

Estimating Emissions from Process Upsets: To represent stack emission rates during process upsets, multiply the emission rate developed from the trial burn data by 2.8 for organics and 1.45 for metals. These factors are derived by assuming that emissions during process upsets are 10 times greater than emissions measured during the trial burn. Since the unit does not operate under upset conditions continually, the factor must be adjusted to account for only the period of time, on an annual basis, that the units operate under upset conditions. For organic compounds, the facility is assumed to operate as measured during the trial burn 80 percent of the year and operate under upset conditions 20 percent of the year $[(0.80)(1) + (0.20)(10) = 2.8]$. For metals, the combustion unit is assumed to operate as measured during the trial burn 95 percent of the year and operate under

upset conditions the remaining 5 percent of the year $[(0.95)(1) + (0.05)(10) = 1.45]$.

Catastrophic process upsets brought about by complete failure of combustion and air pollution control systems resulting from non-routine events (e.g., explosions, fires, and power failures) are considered accidental releases and are not addressed by this guidance.

6.7.1 Fugitive Emissions

This section contains guidance for quantitatively estimating fugitive emissions on the basis of procedures outlined by other U.S. EPA guidance.

6.7.2 Quantitative Estimation of Fugitive Emissions from Processes

Quantitative estimation of fugitive emissions requires:

1. Identifying equipment(s) to be evaluated as fugitive emission source(s)
2. Grouping equipments, as appropriate, into a combined source
3. Estimating compound-specific emission rates for each source

Step 1: Identifying Fugitive Emission Sources - fugitive emission sources include the following:

- Pumps
- Valves
- Connectors (flanges, unions, tees, etc.)
- Compressors
- Pressure-relief devices
- Open-ended lines
- Product accumulator vessels
- Sampling connecting systems
- Closed vent systems
- Agitators

Each fugitive emission source should be identified on a facility plot map with a descriptor and the location denoted with Universal Transverse Mercator (UTM) coordinates or LAT/LONG.

Step 2: Grouping Equipment into One Combined Source - To significantly reduce the effort required to complete air dispersion modeling and subsequent risk assessment, equipment in close proximity may be grouped and evaluated as a single combined source with speciated emission rates for each piece of equipment summed.

Step 3: Estimating Fugitive Emissions from Process Equipment - Based on guidelines provided in U.S. EPA (1995e), "Protocol for Equipment Leak Emission Estimates, EPA-453/R-93-017," fugitive emissions for each equipment

can be estimated by the following four approaches, in order of increasing refinement and data requirements:

- Average Emission Factor Approach (AEFA)
- Screening Ranges Approach (SRA)
- U.S. EPA Correlation Approach (EPACA)
- Unit-Specific Correlation Approach (USCA)

These four approaches can be used at any facility to estimate fugitive emission rates of volatile organic compounds (VOCs) from equipments. Except for the AEFA method, all of the approaches require screening data collected by using a portable monitoring device (PMD).

When this approach is used, equipments can be grouped by waste streams of similar characteristics and VOC composition. However, the AEFA approach does not account for different site-specific conditions, such as temperature, vapor pressure, or screening values, among process units within a source category. Site-specific factors can significantly influence fugitive emission rates of leaks from equipments.

The average emission factors for synthetic organic chemical manufacturing industry process units, refineries, and natural gas plants are presented in U.S. EPA (1995k). Table 11 is an excerpt from this guidance document. These emission factors are most valid for estimating rates of emissions from a grouping of equipments over a long time period.

Table 11. Emissions factor for fugitive emissions in pipelines.

Equipment type	Service	Emission factor (kg/hr/source)
Valves	Gas	0.00597
	Light liquid	0.00403
	Heavy liquid	0.00023
Pump seals	Light liquid	0.0199
	Heavy liquid	0.00862
Compressor seals	Gas	0.228
Pressure relief valves	Gas	0.104
Connectors	All	0.00183
Open-ended lines	All	0.0017
Sampling connectors	All	0.0150

Source: U.S. EPA (1993e).

6.7.3 Fugitive Emissions from Combustion Unit Leaks

Examples of fugitive emissions from combustion unit leaks include the following:

- Combustion units that operate under negative pressure may experience temporary positive pressures (“puffing”) that cause fugitive emissions. This condition can occur when a slug of high BTU waste is combusted, causing a rapid expansion in the volume of combustion gases that exceeds the volume of the combustion chamber.
- Fugitive emissions may occur as a result of routine operation of the combustion unit or the Air Pollution Control system (APCS). These emissions will typically include: (1) leaks that occur due to a positive pressure in the APCS and (2) routine maintenance activities such as replacement of baghouse collection bags.

6.7.4 Fugitive Ash Emissions

The combustion of fuels and waste materials may generate fly ash. Fugitive particle emissions may result from the subsequent collection, handling, and disposal of the fly ash. Typically, fugitive emissions of fly ash, collected from an air pollution control device (APCD), will occur during transfer into covered trucks or other conveyance mechanisms prior to disposal. Emissions generated during the loading process can be controlled by APCDs or other types equipment; however, a fraction of the fly ash may still escape into the atmosphere as fugitive emissions.

6.7.5 Quantitative Estimation of Fugitive Ash Emissions

Steps for the quantitative estimation of fugitive ash emissions include:

1. Determining an empirical emission factor
2. Estimating the fly ash generation rate
3. If applicable, accounting for air pollution control equipment

As demonstrated in the example calculation below, the fugitive ash emission rate can then be estimated by multiplying the empirical emission factor by the fly ash generation rate and the control deficiency of the air pollution control equipment, if applicable.

Step 1: Determining an Empirical Emission Factor - Particle emissions associated with fly ash loading and unloading can be estimated using an empirical emission factor of 1.07 lb per ton fly ash. This factor is based on a field testing program conducted at a coal fired power plant equipped with an electrostatic precipitator (ESP) (Muleski and Pendleton, 1986). Because the combustion of coal and hazardous wastes are similar activities, fly ash generated from similar control devices is expected to behave similarly under the same conditions with respect to fugitive emissions. In general, particle behavior is dependent more on the physical form of the fly ash than on the feed (or waste) stream being combusted. The emission factor determined during the empirical study (0.107 lb per ton fly ash) can be adjusted by a factor (e.g., 10) to account for the fact that the fly ash from the combustion of coal (as in the study) was “wetted”. Fly ash from the hazardous waste combustion facility may not be “wetted” depending on the facility.

Step 2: Estimating the Fly ash Generation Rate - The fly ash generation rate from the APCD can be obtained from Part B Permit Application and the total ash content of the “generic” waste streams created from the waste profile. Both values should be approximately the same. Since a major portion of ash fed to the combustor is converted to bottom ash, it is likely that this value is a conservatively high estimate of the actual fly ash generation rate.

Step 3: Accounting for Air Pollution Control Equipment - If an APCD is used for controlling emissions during fly ash handling operations, an efficiency factor (e.g., 99.5 percent) can be applied to the emission rate. An efficiency factor of 99.5 percent is based on U.S. EPA (1995a) for typical collection efficiencies of particulate matter control devices, for the particle sizes in the range of 2.5 to 10 μm .

Example Calculation

The fugitive ash emission rate is calculated by multiplying the empirical emission factor (1.07 lb per ton) times the estimated fly ash generation rate. For this example, if the generation rate is 5,000 tons per year,

$$1.07 \text{ lb per ton} \times 5,000 \text{ tons / year} = 5,350 \text{ lbs / year}$$

Account for the air pollution control equipment efficiency (99.5%, to obtain the final fugitive ash emission rate:

$$5,350 \text{ lbs / year} \times (1 - 0.995) = 26.75 \text{ lbs / year}$$

6.7.6 Cement Kiln Dust (CKD) Fugitive Emissions

Cement Kiln Dust (CKD) fugitive emissions are release of compounds or pollutants into the ambient air caused by the handling, storage, and disposal of cement kiln dust. CKD is the particulate matter (PM) that is removed from combustion gas leaving a cement kiln. This PM is typically collected by an APCS — such as a cyclone, baghouse, or ESP. Many facilities recycle a part of the CKD back into the kiln.

The extent to which dust is blown into the air by wind erosion depends on several site-specific characteristics, including:

1. The texture (particle size distribution) and moisture content of the CKD on the surface of piles
2. Non-erodible elements, such as clumps of grass or stones on the pile
3. A surface crust
4. Wind speeds

Mechanical disturbances that can suspend CKD constituents in the air include:

1. Vehicular traffic on and around CKD piles

2. CKD dumping and loading operations
3. Transportation of CKD around a plant site in uncovered trucks

Cement plants may use various control measures to limit the release of CKD to the air. For example, CKD may be pelletized in a pug mill, compacted, wetted, and covered to make the material less susceptible to wind erosion.

7 Area Sources

Sources that are not stationary, or are too small to be included as point sources, are grouped into a general category defined as Area Sources. This type of source is usually not subject to licensing or to other regulatory requirements, such as periodical reporting. As a result, most of these sources are estimated at a county level. For example, the use of solvents in paint can be estimated by the total volume annual sales. The area source category is defined as “Stationary sources of emissions that are too small and diffuse to be inventoried as individual sources; they are generally smaller in terms of the mass of contaminants emitted than major sources [CAA major source facility designation] and are often ubiquitous in developed areas” (U.S. EPA, 2000c).

To estimate emissions from area sources, the individual facilities or activities are grouped with like facilities or activities into broad source categories so that emissions can be collectively estimated using one methodology. Area source emission inventories are generally estimated by one of the following two methods:

1. Collecting data for a representative category of area sources. This type of information is composed of emission estimates or activity data for a subset of facilities or activities in the source category. Estimates are scaled to reflect the population of the area source
2. Emission factors or allocation of national or regional estimates to the local level

Area Sources are smaller sources that do not qualify as point sources under the relevant emission cutoffs. Area sources encompass more widespread sources that may be abundant, but individually, release small amounts of a given pollutant. These are sources for which emissions are estimated as a group rather than individually. Examples typically include dry cleaners, residential wood heating, auto body painting, and consumer solvent use. Area sources generally are not required to submit individual emission estimates.

The more technical definition of area source is presented below:

1. Stationary sources that emit:
 - o <10 tons/year of a single air toxic
 - o <25 tons/year of a combination of air toxics

2. Area sources tend to be smaller facilities:
 - Gasoline stations
 - Dry cleaners
 - Car painting shops
 - Small electroplaters

7.1 Ammonia

The ammonia inventory addresses industrial and animal husbandry operations. Ammonia generation by animals is accounted for operations that raise animals either in confined animal feeding or on pasture. Ammonia emissions inventory must account for the following animal operations:

1. Beef
2. Dairy
3. Swine
4. Poultry
5. Sheep and goat
6. Horse

Ammonia is produced as a by-product of microbial decomposition of the organic nitrogen compounds in manure, urea (mammals) or uric acid (poultry) in urine. Animal sources of ammonia occur from confinement buildings, open lots, stockpiles, anaerobic lagoons, and land application of manure. The volatilization of ammonia from any manure management operation can be highly variable and depends on temperature, PH, and storage time.

County-level farm animal populations can be obtained from state and national level departments of agriculture or national statistic services. Industrial, commercial, and municipal sources of ammonia include:

1. Industrial refrigeration units
2. Sewage Treatment
3. Bakeries
4. Pulp and Paper
5. Surface Coatings
6. Municipal Solid Waste Landfills
7. Portland Cement Kilns

Two other sources of ammonia are application of fertilizers and fire (wildfire and prescribed burns).

7.2 Mobile Sources

MOBILE6 is a road emissions estimating model. It was developed by the Office of Transportation and Air Quality (OTAQ) of the U.S. Environmental Protection Agency. Highway motor vehicle emission calculations include:

- Oxides of nitrogen (NO_x)

- Hydrocarbons (HC)
- Carbon monoxide (CO)

MOBILE6, available at <http://www.epa.gov/otaq/m6.htm>, was released in January of 2002 with significant improvements over previous versions (MOBILE5) for motor vehicle fleets under a range of conditions. This latest version accounts for, among other factors, the following:

- Vehicle age distribution
- Annual mileage accumulation rates
- Diesel gasoline and natural gas powered vehicle
- Vehicle activity patterns
 - Vehicle mile traveled (VMT) according to various classifications
 - Vehicle engine start patterns
- Fleet sub-classification - characteristics
 - There are currently 28 vehicle classifications, such as light-duty gasoline passenger cars to class 8b heavy-duty diesel truckers
- Fuel type and composition
 - Volatility
 - Oxygen content
 - Sulfur
 - Additives
- Emission type classifications (6 categories)
- Roadway Classifications

MOBILE6 requires extensive information on the vehicles. Specific data gathering for the mobile sources include the estimation of mileage accumulation rates, registration distributions, diurnal travel distributions, and regional vehicle miles traveled (VMT).

A sample of the main types of data that needs gathering is presented below:

1. Registration distributions and mileage accumulation rates from I/M program data
2. Diurnal travel distributions
3. VMT mix
4. Fleet registration information
5. I/M program status from remote sensing program data
6. Fuel consumption and VMT from tax revenue and other data sources

Note that OTAQ is working on a new mobile emissions model called MOVES, which is due by December 2007.

7.3 On-Road (MOBILE)

The major function of MOBILE6 is to calculate emission factors in the following on-road Gasoline- and diesel-fuelled vehicles:

1. Light-duty vehicles

2. Light-duty trucks
3. Heavy-duty vehicles
4. Motorcycles

These motor vehicle types are also grouped by low- and high-altitude areas of the United States. MOBILE6 requires the use of the following input data:

1. Temperature
2. Roadway speed

MOBILE6 is also capable of calculating emission factors for any calendar year between 1960 and 2020, and it includes provisions for modeling the effects of oxygenated fuels on exhaust CO emissions.

7.4 Off-Road (NONROAD/OFFROAD)

The U.S. EPA NONROAD model provides emission estimations for mobile non-road sources. Non-road emission sources encompass a wide variety of vehicles and equipments, and the NONROAD model enables emission estimation for:

- Recreational vehicles (i.e., all-terrain vehicles and off-road motorcycles)
- Logging equipment (i.e., chain saws)
- Agricultural equipment (i.e., tractors)
- Construction equipment (i.e., graders and back hoes)
- Industrial equipment (i.e., fork lifts and sweepers)
- Residential and commercial lawn and garden equipment (i.e., leaf and snow blowers)
- Recreation marine vessels

Non-road emission sources can be large contributors of VOC, NO_x, and PM emissions, and as a result should not be overlooked in emission inventories. The NONROAD model is currently distributed with a fully functional graphical user interface and reporting system. As a result, the NONROAD model, with its text-mode graphical user interface (GUI), can be readily learned and used in non-road emission inventory projects. Users will be able to launch the NONROAD model through the main menu and perform their analyses in the standard NONROAD graphical user interface. Emission estimation results will then be compiled and stored in the primary internal NONROAD database within the system for further analysis and visualization. Figure 15 presents the emissions calculated by the NONROAD EPA model.

The NONROAD model incorporates default values for regions from the national level to country level across the U.S. These default values will enable users who do not have access to specific non-road data to still perform emissions estimations for their geographic location of interest.

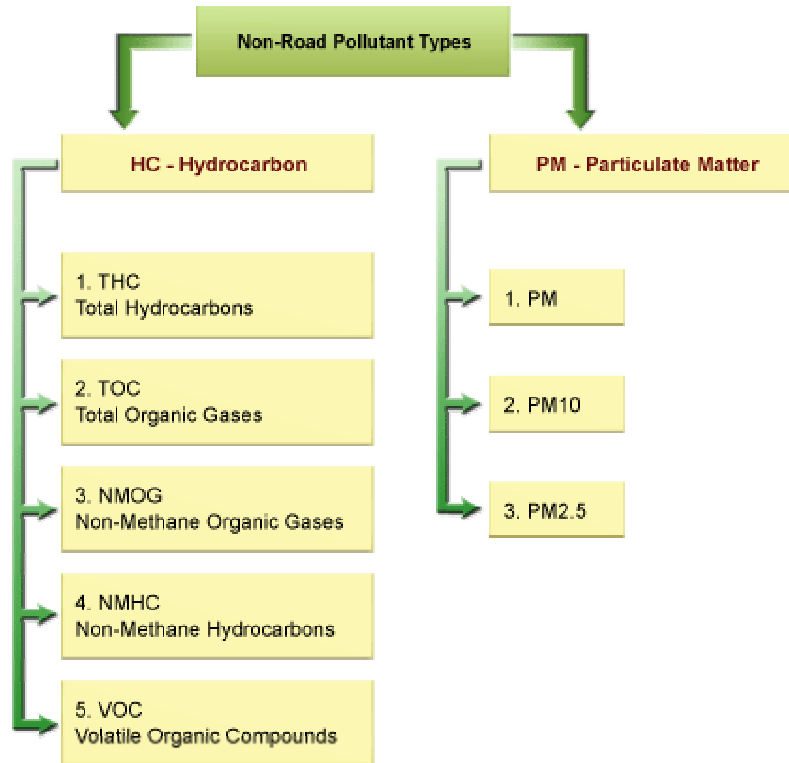


Figure 15. Emissions calculated by the NONROAD EPA model.

Fugitive emissions from non-road equipment, which are presented in Figure 16, include:

- Hot soak
- Diurnal
- Refueling
- Resting loss
- Running loss
- Crankcase emissions

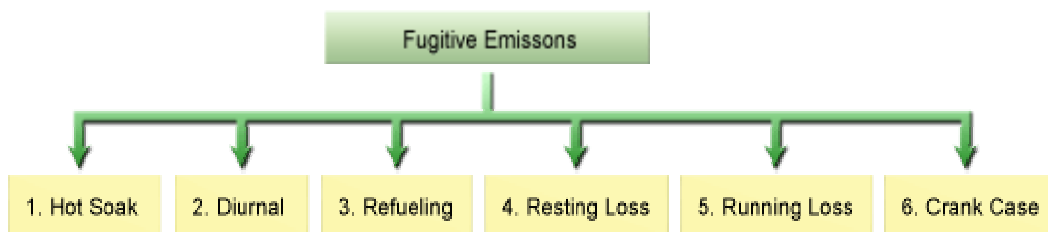


Figure 16. Types of fugitive emissions calculated by the USEPA NONROAD.

7.5 Airports

Civil aircrafts include all categories of fixed and rotary wing craft from the smallest single engine, privately owned and operated, to the largest commercial aircraft. Within the civil category, there are three subcategories: commercial

aircraft, air taxis, and general aviation aircraft. In the development of an emission inventory, it is necessary to account for the different types of aircraft using each airfield. Commercial aircrafts are used in regularly scheduled flights. Air taxis also fly scheduled service carrying passengers and/or freight, but usually they are smaller aircrafts and operate on a more limited basis than the commercial carriers. General aviation includes all nonmilitary aircraft not used in scheduled service. Business aircraft supports business travel, usually on an unscheduled basis. For the purpose of creating an emissions inventory, business aircraft are combined with general aviation aircraft because of their similar size, use frequency, and operating profiles. Types of aircraft operating in airports include:

- Aircraft Total
- Military
- Commercial Total
- Civil Aircraft

In this inventory guidance, they are referred to simply as general aviation. Similarly, air taxis are treated much like the general aviation category because they are typically the same types of aircraft. Helicopters, or rotary wing aircrafts, can be found in each of the categories. Their operation is distinct because they do not always operate from an airport, but may land and take off from a heliport at a hospital, police station, or similarly dispersed location.

Typically, commercial aircrafts are the largest source of aircraft emissions. Although they make up less than half of all aircraft in operation around a metropolitan area, their emissions usually represent a large percentage of the total emissions because of their size and operating frequency. This will not hold true, of course, for a city with no major civil airports.

Pollutants are emitted from aircraft whenever the engines are operating. In the context of emission inventory development, however, concern is limited to those portions of the flight that occur between ground level and an altitude defined as the above ground level inversion height. Within this layer, the air is fairly stable and emissions tend to diffuse rather than being transported away. As a result, emissions occurring below the ground level inversion height have an effect on air quality at ground level, owing to the mixing that occurs within the air cell.

Aircraft emissions are affected by the throttle power setting, that is, the percentage of maximum power that the engines are producing at a given time. However, the power setting is fairly predictable given the specific operating mode in which the aircraft is operating. For purposes of inventory development, five operating modes are of interest:

- Approach (30 - 40 percent throttle)
- Taxi/idle in (3 - 7 percent throttle)
- Taxi/idle out (3 - 7 percent throttle)
- Takeoff (100 percent throttle)
- Climb out (85 - 90 percent throttle)

Collectively, these five modes form the landing and takeoff (LTO) cycle, which provides a basis for allocating aircraft emissions to a specific region. The emissions for a given mode are calculated based on the period of time an aircraft spends in the specified mode. This period of time is called the Time In Mode (TIM).

Duration in approach and climbout depends largely on the local meteorology. Since the period of interest is during operation of the aircraft within the air modeling zone, the inversion layer thickness determines how long the aircraft is in this zone. The inversion layer thickness is also known as the mixing height or mixing zone since the air in this layer is completely mixed, and pollutants emitted anywhere within the layer will be carried down to ground level. When the aircraft is above the mixing layer, whether on descent or when climbing to cruising altitude, the emissions tend to disperse, rather than being trapped by the inversion, and have no ground level effect.

Taxi/idle time, whether from the runway to the gate (taxi/idle-in) or from the gate to the runway (taxi/idle-out), depends on the size and layout of the airport, the amount of traffic or congestion on the ground, and airport-specific operational procedures. Taxi/idle time is the most variable of the LTO modes. Taxi/idle time can vary significantly for each airport throughout the day, as aircraft activity changes, and seasonally, as general travel activity increases and decreases.

The takeoff period, characterized primarily by full-throttle operation, typically lasts until the aircraft reaches between 150 and 300 meters above ground level when the engine power is reduced and the climbout mode begins. This transition height is fairly standard and does not vary much from location to location or among aircraft categories.

The steps in the emission estimation methodology are basically the same for each aircraft classification and each location, although several factors used in creating an inventory are site specific. The steps are:

1. Identify all airports to be included in the inventory
2. Determine the mixing height to be applied to the LTO cycle
3. Define the fleet make-up for aircraft category using each airport
4. Determine airport activity as the number of LTOs for each aircraft category
5. Calculate emission rates from fuel flow rates and emission indexes for each category (presented later in this section)
6. Estimate a TIM for each aircraft category at each airport
7. Calculate emissions based on the airport activity, TIM, and aircraft emission factors.

The height of the mixing zone influences only the TIM for approach and climbout. Primarily, this factor is significant when calculating NO_x emissions rather than TOG or CO. If NO_x emissions are an important component of the

inventory, specific data must be gathered on mixing heights. If NO_x emissions are not important, mixing height will have little effect on the results, and the default value of 900 meters can be used for more generalized results.

The engines used on each aircraft type must be determined to select the emission factors for step 5. Many aircrafts use only a single engine model, while others have been certified to use engines from two or three different manufacturers. When a single engine is listed for an aircraft model, emission data for that engine should be used. For aircrafts with engines from more than one manufacturer, defining the specific engine mix used on the fleet of aircraft operating at a specific airport may be extremely difficult.

To develop a representative engine mix for aircrafts with more than one engine model, the percentage of each model likely to be found on those aircrafts must be identified. The recommended procedure for compensating for the lack of detailed engine data is using the percentages shown in the table as weighing factors. For example, Boeing 757-200 cargo aircrafts have been sold to U.S. airlines with Pratt & Whitney PW2040 engines as well as Rolls Royce RF.211-535E4 engines. The number of aircraft with each engine model is 15 and 43, respectively, to give the percentages shown in Table A of 26 and 74. These percentages can be used to divide the total LTOs for Boeing 757-200 cargo aircrafts into two groups representing the two engine types. This makes the inventory more representative than assigning a single engine for all cargo versions of Boeing 757-200, since the emission factors are different for each engine.

After identifying the engines included in the fleet, engine emission factors are used to calculate mass of emissions. For some of the engines, emission factors have never been determined. For these engines, it is necessary to use emission factors from a related alternative engine. For most of these engines, emission factors are available for a very similar engine, usually one of the same model or a related series. For a small number of engines, there is no emissions data available and there are no suggested alternatives. In these instances, there are three approaches available. First, the needed data may appear in the latest update of the Federal Aircraft Engine Emission Database (FAEED), located at:

<http://www.epa.gov/oar/omswww/aviation.html> .

The Federal Aviation Administration (FAA) should be contacted for the latest version of the data base. Second, for an aircraft with several potential engine types where no emissions data are available for one engine, the recommended procedure is to reallocate the market share among the engines for which data is available. Third, if emission rate information (fuel consumption and emission index) for an engine model still cannot be located, the engine manufacturer should be contacted directly.

The next step is to identify fuel flow rates and emission indexes for each engine type. Emission indexes are given for specific fuel flow rates that are

representative of the power settings used during the different operating modes. The emission index multiplied by the fuel flow rate yields an emission rate.

Step 6 is to specify a time-in-mode for each aircraft type. Take-off time is fairly standard for commercial aircraft and represents the time for initial climb from ground level to about 150 meters. The default take-off time for calculating emissions is 0.7 minutes (42 seconds) and, unless more specific data are available, it should be used in this methodology. The time in the approach and “climb out” modes depends on mixing height. As mentioned earlier, a default mixing height of 900 meters was assumed for calculating an approach time of 4 minutes and a climb out time of 2.2 minutes, which can be used if specific information on mixing height is not available. The procedure for adjusting these times to correspond to a different mixing height is shown below.

The mode most likely to vary by time for each specific airport is “Taxi/Idle” time. Total “taxi/idle” time for a very congested airport can be as much as three or four times longer than for an un-congested airport. Taxi/idle-in time typically is shorter than taxi/idle-out time because there are usually fewer delays for aircrafts coming into a gate than for aircrafts lining up to takeoff. For a large congested airport, the taxi/idle-out time can be three times longer than taxi/idle-in time. “Taxi/idle” time also may vary by aircraft type. For example, wide-body jets may all use special gates at the terminal that place them further from the runway than narrow-body jets or small regional commuter aircraft so their taxi/idle-in and taxi/idle-out times are longer.

Because of the variation in “taxi/idle” time, it is important to get data specific to the airports of interest in the inventory. Commercial airlines must keep track of their “taxi/idle” time at each airport for different aircraft types so that their flight schedules reflect anticipated daily and seasonal variations. Therefore, the airlines’ Flight Operations departments at their headquarter locations are the best source of data for “taxi/idle” time by aircraft type at a particular airport. Since all airlines using a particular airport will experience similar “taxi/idle” times, it is only necessary to get information from a single source. If “taxi/idle” times are not available for a particular airport, use default values of “taxi/idle” periods, as well as other modes, for different aircraft classifications. For commercial aircraft, this information is based on data collected prior to 1971 at large airports during periods of congestion. For the inventory calculations, taxi/idle-in and taxi/idle-out time are added together to get a total time for the “taxi/idle” mode.

7.6 Railroads

There are two types of locomotives used in most railway systems: electric and diesel-electric. Electric locomotives are powered by electricity generated at stationary power plants and distributed by either a third rail or overhead system. Emissions are produced only at the electrical generation plant and are not covered in a non-road inventory. Diesel-electric locomotives use a diesel engine and an

alternator or generator to produce the electricity required to power the traction motors.

7.6.1 Locomotive Line Haul Operations

For this source category, emissions are estimated based on the amount of fuel combusted. If the line haul locomotives only travel within the inventory area, fuel consumption can be determined directly from the amount of fuel dispensed. However, line haul locomotives do not necessarily limit their travel to an inventory area, and therefore do not necessarily consume the fuel in the same location where the fuel is dispensed. The amount of fuel combusted in the area of interest must be first determined in order to estimate emissions.

It is recommended that fuel consumption be allocated by track length so the percentage of fuel consumed is based on the percentage of track length within the inventory area, as noted in the following equation:

To estimate emissions, emission factors need to be applied to fuel consumption values, as noted in the following equation:

$$ELp_i = Fc_i \times EFl_p$$

where:

- ELp_i = Estimated annual emissions (kg) for pollutant p for inventory area i for long haul railroad operations
- Fc_i = Railroad fuel consumption for inventory area i (liter/year)
- EFl_p = Emission factor for pollutant p (kg/liter) (from data table)

Emission Factors:

TOG	0.0025 kg/liter
CO	0.0075 kg/liter
NO _x	0.0591 kg/liter
SO ₂	0.0043 kg/liter
PM	0.0014 kg/liter

Track length data can be obtained by measuring distance on local maps, or by using the U.S. Department of Transportation's Geographic Information System (GIS) study (<http://www.bts.gov>). For example, if it has been estimated that 10 percent of the national track length runs within the inventory area, multiply the total national fuel consumption for the railroad by 0.10 in order to apportion the total fuel consumed in the inventory area.

7.6.2 Locomotive Yard Operations

Yard locomotive emissions are derived by multiplying the number of yard locomotives operating within the inventory area by the emissions generated by each unit during the year. The equation is:

$$EYp_i = NY_i \times EFy_p$$

where:

- EYp_i = Estimated annual emissions (kg) for pollutant p for inventory area i for yard railroad operations
- NY_i = Number of yard locomotives that operate in inventory area i
- EFy_p = Yard locomotive emission factors for pollutant p (kg/year)

Emission Factors:

TOG	1,893 kg/locomotive/yr
CO	3,345 kg/locomotive/yr
NO _x	18,873 kg/locomotive/yr
SO ₂	1,395 kg/locomotive/yr
PM	516 kg/locomotive/yr

Because yard locomotives operate within the boundaries of the railway yard, it is possible to estimate the number of yard locomotives operating within the inventory area through interviews with the railway yard managers, who may maintain records of yard locomotive operations. If this approach proves to be unproductive, the number of yard locomotives can be determined by manually counting the units operating in each railway yard during a given day. This method is sufficient because the number of yard locomotives in operation each day remains relatively constant throughout the year.

7.7 Shipping - Commercial Marine Vessel

Commercial marine vessels include all boats and ships used either directly or indirectly in the conduct of commerce. These include vessels ranging in size from 7 meter charter boats to large tankers and military vessels which can exceed 300 meters in length. Despite the large range of vessels represented by this category, the majority of vessels in this category are powered either by diesel engines (motor vessels) or steam turbines (steamships). Gasoline powered engines are not typically used for commercial marine vessels.

The predominant fuel used in all motor vessels and most steamships is oil, both distillate and residual grades. In steamships, residual fuel such as heavy oil, typically Number 6 or Bunker C, is used. Moderate speed diesel engines usually require a blend of distillate and residual oil for satisfactory operation. Motor vessels use diesel engines that require distillate oil.

Two methods are available for estimating emissions from commercial marine vessels. The first method is based on the quantity of fuel sold for marine use. Emissions are estimated based on assumptions regarding the percentage of fuel sold that is actually used within the port area, and the emission rate associated with the use of the fuel. The second method attempts to provide a more accurate estimate based on ship movement data. Both methods are described here. Calculations need only be done using one method, not both. The method used will depend upon the availability of local data. Commercial marine vessels used throughout the world are expected to have similar emission characteristics.

7.7.1 Fuel Sales Method

The fuel sales method assumes that 25 percent of the residual oil and 75 percent of the distillate oil sold in port is used there, and that all distillate oil is used by motor vessels and all residual oil is used by steamships. The total estimated quantities of residual and distillate oil used in port are:

$$\begin{aligned} Q_{ri} &= 0.25 \times Q_{rs} \quad (\text{for residual oil}) \\ Q_{di} &= 0.75 \times Q_{ds} \quad (\text{for distillate oil}) \end{aligned}$$

where:

- Q_{ri} and Q_{di} = The quantities of residual and distillate oil, respectively, used in port i
- Q_{rs} and Q_{ds} = The total quantities of residual and distillate oil sold in the inventory area for marine use

To estimate emissions, an emission factor is applied to the quantities Q_{ri} and Q_{di} . The emission factors for motor vessels are shown in the data table. Emission factors are given for two general categories of vessels - river and coastal. A river port supports vessels that travel throughout a given river basin and a coastal port supports vessels that travel in and across an ocean. To calculate emissions for motor vessels and steamships, the following equation should be used:

$$E_{ip} = Q_{ri} \times EF_{rp} + Q_{di} \times EF_{dp}$$

where:

- E_{ip} = Quantity of emissions of pollutant p produced annually by vessels operating within area i waters
- Q_{ri} = Quantities of residual oil used in port i
- Q_{di} = Quantities of distillate oil used in port i
- EF_{rp} = Emission factors for pollutant p for residual oil
- EF_{dp} = Emission factors for pollutant p for distillate oil

7.7.2 Emission Factors

Steamships (Residual fuels)

TOGa	0.463 kg/1000 liter
ROG	0.383 kg/1000 liter (3.2 lb/103 gal)
CO	negligible
NO _x	4.362 kg/1000 liter (36.4 lb/103 gal)
SO _x	19 × % sulfur [kg/1000 liter] (159 × % sulfur [lb/103 gal])
PM	1.198 kg/1000 liter (10 lb/103 gal)

Motor Vessels (Diesel fuels) River Vessels

TOG	6.2 kg/1000 liter
ROG	6.0 kg/1000 liter
CO	12.0 kg/1000 liter
NO _x	33.0 kg/1000 liter
SO _x	3.2 kg/1000 liter

Coastal Vessels

TOG	6.2 kg/1000 liter
ROG	6.0 kg/1000 liter
CO	13.0 kg/1000 liter
NO _x	32.0 kg/1000 liter
SO _x	3.2 kg/1000 liter

7.7.3 Ship Movement Method

This method utilizes data concerning the number of vessels in various size categories that use a particular port, and assumptions about dockside activity and ship movements in and out of the harbor. This approach has two separate types of emissions associated with it:

- Underway emissions (i.e., emissions from vessels while in transit in the harbor)
- Dockside emissions (i.e., emissions from vessels that are tied up at docks unloading or loading cargo).

The methods to estimate emissions from underway and dockside emissions are discussed below.

a) Underway Emissions

The first data element required is the number of vessels, by size category, using the port. Four vessel size categories are of interest, based on “Draft”:

1. Less than 2 meters

2. Greater than 2 meters or less than 4 meters
3. Greater than 4 meters and less than 6 meters
4. Greater than 6 meters

These data are used to compute emissions for vessels underway and at dockside. Underway emissions occur while the vessel is entering, leaving, or maneuvering in port. Estimates of emissions produced by underway vessels can be developed based on the average travel time by vessels entering, maneuvering, and leaving the port, applying a fuel consumption factor to estimate fuel usage within the port, and applying an emission rate based on the quantity of fuel used.

Vessels with a draft of less than 6 meters (depth of water required for loaded vessel to operate in) are assumed to be powered by diesel engines using distillate fuels, while those vessels with a draft of 6 meters or more are assumed to be steam powered. Although large diesel powered vessels are capable of burning residual oil, it is assumed that distillate is used while underway or maneuvering in port. Furthermore, it is assumed that all steamships use residual oil at all times.

To estimate average travel time, the distance between the outer limits of the study area and a theoretical centroid of activity within the port is determined. This distance is increased by 120 percent to account for maneuvering and leaving port, and it is divided by an assumed average speed in port of 13 km per hour to yield the estimated average underway travel time of each vessel using the port. This is:

$$\begin{aligned} \bar{t} &= \text{Average travel time for vessels using the port (hr)} \\ d &= \text{Distance in km between the outer limit of the study area and the} \\ &\quad \text{assumed centroid of port activity} \end{aligned}$$

Average travel time data can be applied to fuel consumption rates to estimate underway fuel consumption as noted in the following equation:

$$Q_{ijd} = \bar{t} \times FC_{jd} \times N_{ijd}$$

where:

$$\begin{aligned} Q_{ijd} &= \text{Underway fuel consumption for vessel type } j \text{ (steamship, motor} \\ &\quad \text{vessels) with draft } d, \text{ for inventory area } i \text{ (liter)} \\ \bar{t} &= \text{Average travel time (hr)} \\ FC_{jd} &= \text{Fuel consumption rate for vessel type } j \text{ and draft } d \text{ (liter/hr)} \\ N_{ijd} &= \text{Number of vessels of vessel type } j \text{ and draft } d \text{ in inventory area } i \end{aligned}$$

Fuel consumption rates for vessels operating in a port are provided in the data table. Different rates are given for motor vessels and steamships. Once fuel use associated with underway operations has been computed, emissions can be calculated by applying emission factors from the data table. Emissions are calculated using the following equation:

$$E_{ijp} = Q_{ijd} \times EF_{jpd}$$

where:

- E_{ijp} = The quantity of emissions of pollutant p produced annually by category j vessels with draft d operating within area i waters
- Q_{ijd} = The quantity of fuel (residual or distillate), in liters, consumed by vessel type j with draft d
- EF_{jpd} = The emission factor for pollutant p and vessel type j with draft d, from the data table

b) Dockside Emissions

Large vessels (those with a draft of 6 meters or more) produce emissions while in dockside. These emissions are caused by either auxiliary diesel generator systems or the main boilers, which are operated to supply power for the vessels' utilities. Furthermore, the boilers on most steamships in port for less than 2 days are rarely shut down because of the relatively long time required to restart and prepare them for operation. To estimate the quantity of emissions produced by these vessels, an estimate of the average number of days in port must be developed and a fuel consumption rate must be determined. After the total quantity of fuel consumed in port is estimated, an emission factor is applied to derive the emission estimate.

The average duration of stay for large commercial vessels is from one to three days. An estimate for a particular port can be derived by inquiring to the port authority or shipping company, or a default value of three days can be used.

The fuel consumption rates for steamships and motor vessels are assumed to be 7,192 liters per day of residual oil, and 2,490 liters per day of distillate oil. Again, it is assumed that all U.S. registered vessels are steamships and all non-U.S. registered vessels are motor vessels. Fuel used by each type of vessel while in port is calculated from:

$$Q_{ij} = N_{ij} \times D_{ij} \times fc_j$$

where:

- Q_{ij} = Total annual fuel consumption (liters) of residual or distillate oil, in area i, by type j vessels (steamships or motor vessels) (liters)
- N_{ij} = Total number of type j vessels using the port i
- D_{ij} = Average duration of stay for vessel type j in area i (days)
- fc_j = Fuel consumption rate for vessel type j (assumed to be 7,192 liters per day of residual oil for steamships and 2,498 liters per day of distillate oil for motor vessels)

Emissions produced by the ships while at dockside are:

$$E_{ijp} = Q_{ij} \times EF_{jp}$$

where:

- E_{ijp} = The quantity of emissions of pollutant p produced annually by category j vessels while at dockside in area i waters
- Q_{ij} = The quantity of fuel, in 1,000 liters, consumed at dockside by vessel type j (1,000 liters)
- EF_{jp} = The emission factor for pollutant p and vessel type j

7.8 Industrial and Commercial/Institutional Fuel Combustion

Industrial fuel combustion includes the use of the following:

1. Coal
2. Fuel oil
3. Kerosene
4. Natural gas and liquefied petroleum gas (LPG)
5. Wood for heating and power at industrial facilities

These fuels can be burned using a number of different equipment types including boilers, internal combustion (IC) engines, furnaces, heaters, and other heating units too small to be included in a point source inventory. Electric utilities are excluded from this category and should be inventoried as point sources. Commercial and institutional facilities are establishments that engage in retail and wholesale trade, hotels, restaurants, schools, hospitals, government buildings, etc. The emissions from these facilities are not inventoried separately. Rather, the fuel consumption from all sources is aggregated to yield a total that is used in the emission calculation. This aggregation is done by fuel type because the emission factors vary by fuel.

7.9 Residential Combustion - Commercial Fuels

The residential fuel combustion area source category uses commercially available fuels such as:

1. Coal
2. Fuel oil
3. Natural gas and LPG used for heating of individual homes and apartment complexes

Non-commercially available fuels (e.g., wood, crop waste, waste oil, waste solvents, and tires) are excluded from this category and it should be inventoried as Non-Commercial Fuels - Residential.

7.10 Residential Combustion - Non-Commercial Fuels

The non-commercial residential combustion area source category uses wood, biomass, manure, scrap materials, tires, and other waste-derived fuels. These fuels are used for both residential heating and cooking purposes. Waste-derived fuels tend to be used by the lower socioeconomic classes of the population. For these reasons, assessing the amount of biomass and other waste-derived fuels used in a region can be somewhat problematic.

7.11 Industrial Surface Coating

Surface coating operations consist of applying a thin layer of coating such as paint, varnish, lacquer, or paint primer to an object for decorative or protective purposes. Surface coatings are applied during the manufacture of a wide variety of products, including furniture, cans, automobiles, airplanes and other transportation equipment, machinery, appliances, flat wood, wire, and other miscellaneous products. In addition, coatings are used in maintenance operations at industrial facilities. Emissions estimations for industrial surface coating are very complex, as shown in Figure 17.

Solvents contained in the surface coatings evaporate as the coating is applied and dries. Most inventory efforts assume that all of the coating solvents evaporate into the air.

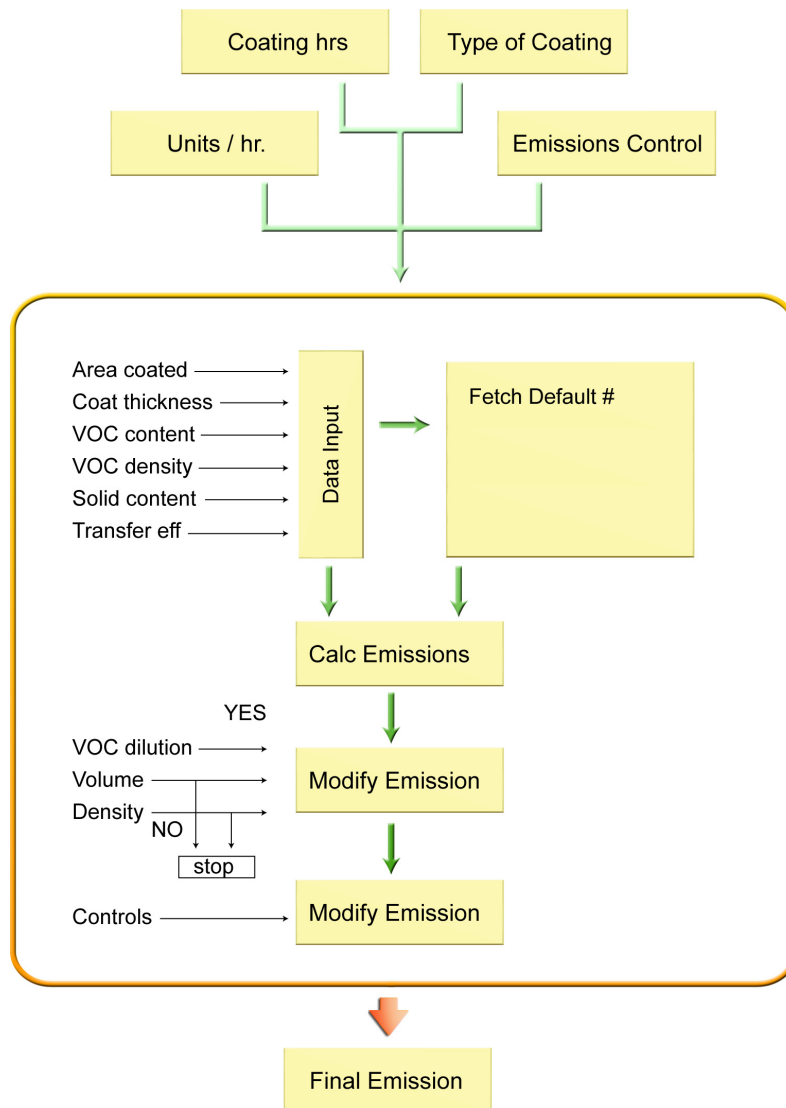


Figure 17. Industrial surface coating calculation flowchart.

7.12 Auto Body Refinishing

Auto body refinishing is the repair and restoration of automobile, light truck, and other vehicle bodies. Refinishing operations occur subsequent to those at original equipment manufacturer assembly plants. Most auto body refinishing jobs are performed as part of collision repair and involve only portions of a vehicle.

Emissions occur during surface cleaning, filling and priming, painting, and cleanup. Emissions from refinishing operations are influenced by the solvent content of the product, transfer efficiency of the spray equipment used to apply the coatings, and cleanup practices.

$$\text{Annual VOC Emissions} = (\text{Population}) \times (\text{Emission Factor})$$

or,

$$\text{Annual VOC Emissions} = (\text{Employment}) \times (\text{Emission Factor})$$

7.13 Architectural Surface Coating

Architectural surface coatings are used by painting contractors and individuals to protect and enhance building interior and exterior surfaces. Architectural surface coating involves spreading a thin layer of coating such as paint, paint primer, varnish, or lacquer to architectural surfaces, and the use of solvents for thinning and cleanup. VOCs that are used as solvents in the coatings are emitted during the application and as it dries.

$$\text{Annual VOC Emissions} = (\text{Population}) \times (\text{Emission Factor})$$

7.14 Traffic Paint

Traffic paint application is the painting of centerlines, edge stripes, directional markings, parking lot markings, and paved and unpaved surfaces to improve traffic flow. Traffic markings can include solvent-based and water-based paints, which are usually applied with a spray, or in the form of thermoplastics or preformed tapes that are epoxied to the road surface. Traffic paints are applied by maintenance crews and traffic paint contractors during road construction and repairs. Factors such as climatic conditions, the durability of the paint, pavement type, traffic density, and position of the marking will determine how often the paint will need to be re-applied, and thereby influence emissions.

$$\text{Annual VOC Emissions} = (\text{Population}) \times (\text{Emission Factor})$$

7.15 Degreasing - Industrial Surface Cleaning

Surface cleaning operations involve the use of solvent liquids or solvent vapors to remove water-insoluble contaminants such as grease, oils, waxes, carbon deposits, fluxes, and tars from metal, plastic, glass, and other surfaces. This process takes place in a large variety of manufacturing, scientific, and repair operations. Solvent cleaning operations involve the use of a number of different solvents and different solvent cleaning procedures.

Solvent cleaning equipment can be categorized as:

1. **Batch cold cleaning machines** - These machines are batch loaded and liquid solvent is sprayed, dipped, or brushed onto the surfaces that are to be cleaned.
2. **Batch vapor cleaning machines** - These machines are batch loaded, and the materials to be cleaned are exposed to vaporized solvent. The condensing solvent flushes the contaminants from the surfaces to be cleaned.

3. **In-line cleaning machines** - These machines are loaded on a continual basis and are often custom made for large-scale operations. An in-line solvent cleaning machine may use liquid solvent or vapor solvent.
4. **Cleanup solvent use** - This process involves wiping a surface with the solvent and a rag, mop, or sponge.

$$\text{Annual VOC Emissions} = \text{Employment in Group (SIC)} * \text{Emissions Factors}$$

7.16 Dry Cleaning

The dry cleaning industry is a service industry for the cleaning of clothing, draperies, leather goods, and other fabric items. Dry cleaning operations use halogenated or petroleum distillate organic solvents for cleaning. Dry cleaners can range in size from large industrial plants, which are typically treated as point sources, to very small operations with one unit, which may only be used intermittently. Commercial plants are the intermediate size between the two extremes.

Dry cleaning typically uses the following solvents:

- Perchloroethylene
- 1,1,1-trichloroethane
- Trichlorofluoroethane (CFC-113)
- Other petroleum solvents

Emissions occur from dry cleaning facilities when the solvents evaporate during the process from leaks in the equipment and from solvent recovery or disposal systems.

$$\text{Annual VOC Emissions} = \text{Employment in Dry Cleaning Group} * \text{Emissions Factors}$$

7.17 Graphic Arts

Graphic arts include operations that are involved in the printing of newspapers, magazines, books, and other printed materials. Printing may be performed on various substrates (e.g., coated or uncoated paper, metal, or fabric). The difference between printing on paper coating is that printing always involves the application of ink by a printing press. The five basic operations used in graphic arts are:

1. Web lithography
2. Rotogravure
3. Web letterpress
4. Flexography
5. Screen printing and manual or sheet-fed techniques

Printing inks vary widely in composition, but all consist of three major components: pigments, binders, and solvents. The majority of solvents used in graphic arts operations are consumed in printing ink formulations, with lesser amounts of solvents used for equipment cleaning or as a component in fountain solutions for dampening systems in lithographic printing. The solvents evaporate from the inks into the atmosphere during the drying process.

Figure 18 presents a sample calculation for emissions from the graphical arts source category.

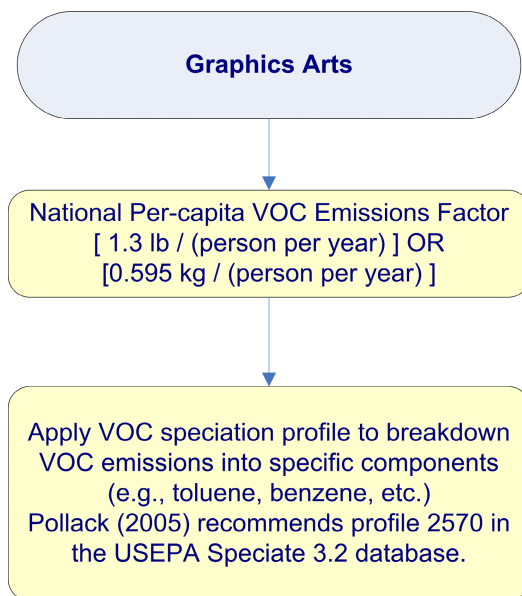


Figure 18. Sample calculations for emissions from the graphical arts source category.

7.18 Asphalt Applications

Asphalt surfaces and pavements are composed of compacted aggregate and an asphalt binder. The aggregate transmits the load from the surface to the base course, takes the abrasive wear of traffic, and provides a nonskid surface. The binder holds the aggregate together and prevents movement or loss of aggregate.

There are two types of liquefied asphalts: cutback asphalts and emulsified asphalts. Cutback asphalts are asphalt cement thinned or “cutback” with volatile petroleum distillates; they are generally categorized as rapid cure, medium cure, and slow cure. Asphalt characterization is based on the solvent used as a diluent and the corresponding time needed for curing (i.e., gasoline or naphtha is used as a diluent for rapid cure, whereas kerosene and other low volatile fuel oils are used for medium and slow cure). Emulsified asphalts use a blend of water and emulsifier (i.e., soap) instead of solvent diluent, and they rely on water evaporation or ionic bonding to cure. VOC emissions result from the evaporation of the petroleum distillate solvent used to liquefy the asphalt cement.

7.19 Commercial/Consumer Solvent Use

Hydrocarbons are ingredients of consumer and commercial products which serve as propellants, aid in product drying (through evaporation), act as co-solvents and cleaning agents, and are emitted during product use. Typically, these hydrocarbon sources are large in number, highly dispersed, and individually emit relatively small amounts of VOC. Commercial and consumer products which release VOC include aerosols, household products, personal care products, automotive aftermarket products, adhesives and sealants, and commercial and household pesticides.

Solvents contained in consumer and commercial products are primarily released during product use. Most inventory efforts assume that all VOC in consumer and commercial products volatilize to the air. Typical TOG constituents that are released to the atmosphere from this source category include special naphthas, alcohols and various solvents.

$$\text{Annual VOC Emissions} = (\text{Population}) \times (\text{Emission Factor})$$

7.20 Gasoline Distribution

In the gasoline distribution industry, gasoline is transported from refineries by tanker trucks to bulk plants and terminals, and ultimately to service stations. The procedures discussed below relate directly to the emissions that occur during the transportation and distribution of gasoline from bulk plants and terminals to service stations.

Evaporative emissions occur at all points in the gasoline distribution process. Those operations generally thought of as area sources are gasoline dispensing stations (service stations) and gasoline tank trucks in transit. Bulk terminals and gasoline bulk plants, which are intermediate distribution points between refineries and outlets, should be inventoried as point sources.

VOC emissions from the transportation and distribution of gasoline involve the following types of emissions:

1. Breathing losses

- Evaporation of gasoline from the tank truck during transportation of the gasoline from the bulk plant/terminal to the service station or other dispensing outlet
- Evaporation of gasoline from the empty tank truck on the return trip from the service station within an inventory area to the bulk plant/terminal
- Evaporation of gasoline from the underground storage tank(s) and the lines going to the gasoline dispensing outlet (pumps) when standing and not in use

2. Working losses

- Evaporation of gasoline during the transfer of gasoline from the tank truck to underground storage at the service station (often referred to as “Stage I”)
- Evaporation of gasoline during the transfer of gasoline from the pump to vehicles (often referred to as “Stage II”)
- Spillage of gasoline (and subsequent evaporation) during either delivery activity, described above. This loss is made up of contributions from pre-fill and post-fill nozzle drip and from spit-back and overflow from the filler pipe of the vehicle’s fuel tank during filling
- Evaporation of gasoline from the underground storage tank or the lines going to the pumps during transfer of gasoline

7.21 Construction Activities

Building, road, and other construction activities are potentially significant sources of fugitive PM emissions. These emissions can be generated by a variety of activities, including land clearing, drilling and blasting, ground excavation, earth moving, and actual building construction. Emissions due to construction activities vary by site due to different levels of activity, operations, and meteorological conditions.

This section focuses solely on fugitive PM emissions generated by construction activities. The following equation can be used to estimate fugitive dust emissions from overall regional construction activities:

$$Emissions = Area \times Time \times EF$$

7.22 Pesticide Application

Pesticides are used to kill or retard the growth of insects, weeds, or other pests. Most air emissions from pesticide use primarily occur because of the volatile nature of the active ingredients, carrier solvents, and other chemicals in pesticide formulations. Volatilization of pesticides can occur both during application and for some time after application.

Volatile pesticides usually are applied as liquid formulations, such as solutions, emulsions, or aerosols. In general, volatile pesticides consist of an “active” ingredient and various “inert” ingredients. The terms “active” and “inert” refer to a measure of compound toxicity. The active and inert fractions can vary depending upon the specific type of pesticide application.

The volatility of active ingredients can also be quite variable. Volatilization is typically assumed to occur during the first 30 days after application. After

approximately 30 days, degradation and surface runoff become the primary removal mechanisms for pesticides. Laboratory and field research indicates that active ingredient volatility appears to be dependent on three major parameters:

1. Physical and chemical properties of the active ingredient
2. Local meteorological conditions
3. Soil adsorption

7.23 Beef Cattle Feedlots

Beef cattle feedlots and stock yards are areas used for fattening or holding cattle prior to marketing or transfer to another location. The fattening process typically consists of feeding cattle a high energy ration of feed grains for a period of four or five months. Feedlots and stock yards can be a significant source of fugitive particulate matter. The primary generation mechanism is cattle movement over soil dust and dried manure. Vehicle traffic and wind action in the vicinity of the feedlot can also contribute to particulate emissions. Similar emissions are not expected to occur when cattle are put out to pasture for grazing because there will be minimal concentrated manure accumulation and disturbed surface area.

7.24 Fertilizer Application

Fertilizers are used extensively to add or replenish nutrients that are depleted or otherwise missing from agricultural soil. Because of the large number of soil and crop types, many different types of fertilizers have been formulated. After application, the nitrogen-based fertilizers release ammonia to the atmosphere. The amount of ammonia emissions is dependent upon the type of fertilizer applied and is typically expressed as some percent of the nitrogen content of the fertilizer. Some generalized ammonia emission factors have been developed. However, there are many influencing factors that have not been adequately addressed in these generalized emission factors. These influencing factors include:

1. Meteorological conditions
2. Soil properties
3. Application technique (surface or subsurface)
4. Application cycles

7.25 Animal Waste

In some locations, livestock and other domesticated farm animals constitute the largest single source of ammonia emissions. Ammonia emissions from livestock animals result from the conversion of excreted nitrogen to ammonia and its subsequent volatilization. Nitrogen contained in livestock urine is easily converted to ammonia and subsequently emitted to the atmosphere. In contrast, ammonia emissions from manure typically require considerable decomposition.

The factors that influence livestock animal ammonia emissions include:

1. Type of livestock

2. Animal size and weight
3. Manure storage practices
4. Nitrogen content of livestock feed
5. Meteorology.

7.26 Agricultural Tilling

Fugitive dust from agricultural operations can be a significant contributor of PM₁₀ emissions in some rural areas. Agricultural operations are typically divided into three classifications:

1. Soil preparation
2. Soil maintenance
3. Crop harvesting

The agricultural tilling source category focuses primarily on soil preparation, which includes such operations as plowing, harrowing, leveling, and dicing.

8 Fire Emissions

Seven essential components are necessary to consistently calculate fire emissions and to uniformly assess impacts to regional haze. These components are presented below, and are described in more detail as procedural steps:

1. Date of Burn
2. Burn Location
3. Area of Burn
4. Fuel Type
5. Pre-Burn Fuel Loading
6. Type of Burn
7. Classification: Anthropogenic or Natural

STEP 1 - Specify the Start and End of when the emissions start and cease.

STEP 2 - Specify the location of the burn area according to the Public Land survey System (PLSS). The Public Land Survey System (PLSS) is a way of subdividing and describing land in the United States. All lands in the public domain are subject to subdivision by this rectangular system of surveys, which is regulated by the U.S. Department of the Interior, Bureau of Land Management (BLM), at <http://www.blm.gov/nhp/index.htm>. The PLSS subdivides the land into (see Figure 19):

- Township
- Range
- Section
- Quarter Section
- Quarter-Quarter Section

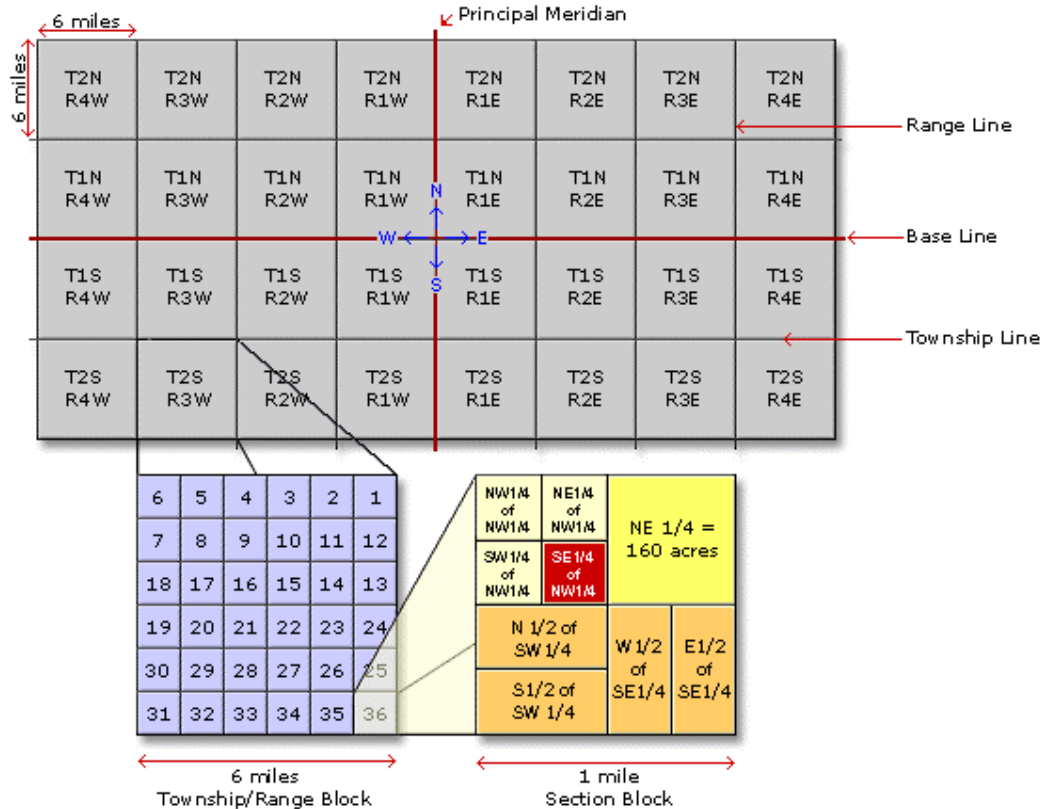


Figure 19. Public Land Survey System “land coordinate system” used in fire emissions.

STEP 3 - Area of Burn

1. Specify the burned area in acres.
2. Blackened areas should be determined post-burn.
3. For a pile burn, the area burned should be represented by the dimensions of the pile as well as the number of piles consumed.

STEP 4 - Define Fuel Type

1. Specify the fuel type that represents the predominant fuel or cover type consumed in the fire.
2. Emissions from fire are highly dependent upon the fuel or cover type (e.g., ponderosa pine, juniper, orchard residue, rice straw).

STEP 5 - Pre-Burn Fuel Loading

1. Specify the amount of fuel present at the burn location (tons/acre).
2. The more accurate the pre-burn fuel loading, the more refined the subsequent emissions estimates will be.

STEP 6 - Define Type of Burn

1. Specify the predominant configuration of the fuel burned (e.g., pile, windrow, broadcast, underburn).

STEP 7 - Classify the Fire

1. Anthropogenic: a human-caused source of fire
2. Natural: a natural source of fire

Optional Additional Inputs:

1. Fuel Consumption [%]
2. Fuel Moisture [%]
3. Purpose of Burn
4. Non-Burning Alternatives
5. Additional Tracking Information

Fire emissions calculations can now be performed, as follows:

Emission Mass (ton pollutant/day) = Fire Size (acre/day) * Fuel Loading (ton/acre) * Emission Factor (lb/ton) * 0.0005 (ton/lb)

- Emission Mass is calculated per day per pollutant.
- Fire Size is a site-specific input.
- Fuel Loading is selected from a 2D reference matrix (3 source types x 95 fuel classes).
- Emission Factors are selected from a 3D reference matrix (2 wildland burn types and 75 ag fuel classes x 12 pollutants).

9 Biogenic and Geogenic

In addition to anthropogenic (human) activities, soil, plant, and animal organisms can be important sources of air emissions. In some areas where natural source emissions may be significant to the overall inventory, it is important to understand the contribution of natural sources, since implementing control strategies generally cannot readily reduce these emissions. Two significant natural sources commonly considered in air emissions inventory efforts are described below.

Biogenic Emissions: A number of researchers have established that vegetation (e.g., grass, crops, shrubs, forests, etc.) emits significant quantities of hydrocarbons to the atmosphere. Several studies (e.g., Pierce et al., 1990 and Robinson and Robbins, 1968) have shown that biogenic emissions may be comparable to, or exceed, the emissions of non-methane hydrocarbons (NMHC) from anthropogenic sources in certain areas.

Emissions from Soils: Nitrous oxide (N₂O), largely emitted by soils, is produced by denitrification (i.e., the reduction of nitrite or nitrate to gaseous nitrogen as N₂ or NO_x) and nitrification (i.e., the oxidation of ammonia to nitrate).

Wind erosion is another natural phenomenon that generates emissions. However, because wind erosion emissions typically are associated with disturbed land, they are sometimes treated as area sources. Some other smaller categories of natural

sources include termites (CH₄), lightning (NO_x), volcanoes, and other geothermal activities (SO_x).

Note that some locations, such as Hawaii, contain two unique geogenic emissions sources: Volcanic and sea spray.

10 Available Emissions Models

There are currently various emission models that incorporate emissions estimation and projections. In addition to MOBILE6 and NONROAD, the following models are supported by the USEPA:

- **BEIS** - Estimates hourly emissions of biogenic volatile organic compound and soil nitrogen oxide emissions for any county in the contiguous United States.
- **TANKS** - A computer software program that estimates emissions of volatile organic compounds (VOCs) and hazardous air pollutants (HAPs) from fixed- and floating-roof organic liquid storage tanks. Estimation procedures follow the USEPA's *Compilation of Air Pollutant Emission Factors* (AP-42). Data input include tank physical parameters and its contents. The storage tank contents can consist of single or multiple liquid components. TANKS may be downloaded from:
<http://www.epa.gov/ttn/chief/software/tanks/index.html>.

The information required for estimating fugitive emission rates from storage tanks includes, but is not limited to, the following:

Dimensions of the tanks

- Shell height and diameter

Characteristics of the tank roof

- Color and shade
- Condition (e.g., poor, good)
- Type (e.g., cone, dome)
- Height
- Radius or slope
- Fixed or floating

Characteristics of the shell

- Color and shade
- Condition (e.g., poor, good)
- Heated

Settings on breathe vents

- Vacuum setting
- Pressure setting

Characteristics of the stored liquids

- Maximum and annual average liquid height
 - Working volume
 - Turnovers per year
 - Net throughput
 - Average annual temperature
 - Vapor pressures of speciated constituents (at annual average temperature)
- **WATER9** - Estimates air emissions of individual waste constituents in wastewater collection, storage, treatment, and disposal facilities. It contains a database listing for many of the organic compounds, and procedures for obtaining reports of constituent fates, including air emissions and treatment effectiveness. The models produce emission estimates for each individual compound that is identified as a constituent of the wastes leaving the facility based on the physical/chemical properties of the compound and its concentration in the wastes. Therefore, the analyst should be able to identify the constituent compounds and provide their respective concentrations. Estimates of the total air emissions from the wastes are obtained by summing the estimates for individual compounds. Program software may be downloaded from:
<http://www.epa.gov/ttn/chief/software/water/index.html>.
 - **LANDGEM** - The LANDfill Gas Emissions Model is a program that uses characteristics and capacity of a municipal solid waste (MSW) landfill to estimate air emissions. These emissions are generated by decomposition of refuse in landfills, which are methane, carbon dioxide, non-methane organic compounds, and hazardous air pollutants. The model is located at the Clean Air Technologies USEPA website:
<http://www.epa.gov/ttn/catc/products.html#software>.
 - **PM CALC** - Calculates controlled emissions for filterable PM₁₀ and PM_{2.5} for point sources with up to two control devices. It requires the user to input data parameters consisting of the Source Classification Code (SCC) for the point source, the primary and secondary particulate control device codes, and the uncontrolled PM-FIL or PM10-FIL emissions. The Calculator works by first calculating the PM10-FIL and PM25-FIL particle distribution for the input SCC's uncontrolled emissions. It then determines the control efficiencies for the primary and secondary particulate device code. The Calculator then calculates the final controlled PM10-FIL and PM25-FIL emissions and overall PM10-FIL and PM25-

FIL control efficiencies. PMCALC can be downloaded from the following USEPA web site:

<http://www.epa.gov/ttn/chief/software/pmcalc>.

- **MOBILE6** - It is an emission factor model for predicting emission factors for various vehicle types driving in different road classes. These emissions factors, gram per mile, cover the main types, such as hydrocarbons (HC), carbon monoxide (CO), nitrogen oxides (NO_x), carbon dioxide (CO₂), particulate matter (PM₁₀ and PM_{2.5}), and other toxics from cars, trucks, and motorcycles under various on-road conditions. Note that results from MOBILE6 still must be multiplied by the “Vehicle Mile Traveled” (VMT) to obtain the final emission rate. The program is available for download from <http://www.epa.gov/otaq/m6.htm>.
- **NONROAD** - NONROAD Model is a software program to estimate emissions from off-road mobile source. The program is available for download from <http://www.epa.gov/otaq/nonrdmdl.htm>.
- **MOVES** - The USEPA’s Office of Transportation and Air Quality (OTAG) is **currently** developing a new off-road mobile estimation modeling system, the Multi-scale mOtor Vehicles and equipment Emission System (MOVES) that will replace the existing MOBILE6 and NONROAD models. This new system will estimate emissions for onroad and nonroad sources, cover a broad range of pollutants, and allow multiple scale analysis from fine-scale analysis to national inventory estimation. For further information on MOVES, visit <http://www.epa.gov/otaq/ngm.htm>.

11 Estimating Emissions for Use in Air Quality Modeling

Emissions inventory methodologies are evolving to accommodate new objectives. Previously, regulatory data provided by industry and estimated by governmental agencies were used only to assess emissions reductions and analyze trends. New objectives include the application of emissions inventory on visibility impairment studies and even human health risk assessment for large areas, such as the ones conducted by the Minnesota Pollution Control Agency.

In addition to the common reporting by industry on total annual emissions by the whole facility, new requirements will include source specific information, such as presented in Table 12

Table 12. Source-Specific Emissions Data Needs for Model Input.

	Stack Source	Fugitive Source	Mobile Source
Physical Characteristics	<ul style="list-style-type: none"> - Stack height [m] - Base elevation [m] - Stack diameter [m] - Stack gas exit velocity [m/s] - Stack gas exit temp. [K] - Control device description - Location [NAD 83] 	<ul style="list-style-type: none"> - Area [m²] - Release height [m] - Base elevation [m] - Location [NAD-83] 	<ul style="list-style-type: none"> - Area [m²] - Release height [m] - Base elevation [m] - Location [NAD-83]
Emissions Characteristics	<ul style="list-style-type: none"> - Contaminant CAS number and name - Speciated emission rate [g/s] 	<ul style="list-style-type: none"> - Contaminant CAS number and name - Speciated emission rate [g/s] 	<ul style="list-style-type: none"> - Contaminant CAS number and name - Speciated emission rate [g/s]

Notes:

m	meters
m/s	meters/second
K	Kelvin
NAD-83	North American Datum 1983
g/s	grams/second
CAS	Chemical Abstract Service

11.1 Geographical Information Systems - GIS

Geographical Information Systems (GIS) use modern computer technology to store, retrieve, analyze, update, and display spatially arranged data (maps). Because the characterization of emissions is enhanced by knowledge of the location and spatial arrangement of all identified sources, the Geographical Information System can be a useful tool for emission inventories. Locating each point source, defining the boundaries around each area source, and mapping all road networks can provide valuable information for formulating, evaluating, and implementing emission reduction strategies. Mapping point and area sources are also important in defining, and subsequently modifying, non-attainment area boundaries. Map features are available in digital formats from transportation departments, tax offices, planning/zoning offices, and emergency response agencies.

11.2 Study Domain and Grid Definition

Traditionally, the development of spatial gridding surrogates for dispersion modeling applications has been performed by a variety of methods depending on:

1. The emission source category being considered
2. The required spatial resolution
3. Geographic extent of the domain
4. Particular characteristics of the geospatial data available

Spatial surrogates must define the percentage of regional or county level emissions from a particular source category that is to be allocated to some spatial region, such as Census Tract or a modeling grid cell. For most area and off-road sources, these percentages are based on areas of a particular land use/land cover type, while for on-road mobile source categories, the percentages are usually based on total length of a certain road type or a transportation network. Often, human population is also used as a spatial surrogate for certain emission source categories.

Spatial surrogates can be developed from several sources of spatial data, such as:

1. Land Use/Land Cover (LULC)
2. Transportation networks such as roadways or railroads
3. Population characteristics

The processing and development of gridding surrogates can be performed using GIS engines or GIS-based emissions Inventory systems, such Emissions View™ from Lakes Environmental Software. To develop Spatial Surrogates, or SAFs, the appropriate surrogate databases (i.e., land use, population, roadways, railways, etc.), the user-specified region, and the regional/county boundaries are first imported into the GIS as geospatial coverages. Through intersecting, or overlaying these coverages, the appropriate areal and/or linear percentages can be calculated as follows. The spatial data are first intersected with the regional boundaries to generate a new coverage that contains polygons, or arcs, with attributes associated with the spatial data and the regional boundaries. The total area, or length, of a particular land use, or roadway type, within each region or county can then be calculated. The resulting coverage is then overlaid with the arbitrary user-defined region to associate the spatial attributes of the region with the land use and regional/county boundary attributes. These procedures result in the generation of new polygons, each of which has all of these attributes as well as the corresponding areas, or lengths. The spatial allocation factors are then generated by forming ratios of the total area, or length, in each region and county to the corresponding total area, or length of the particular spatial data type within each county.

The resulting SAFs are then multiplied by the county-level emission estimates to obtain the emission estimate for the general user-defined region.

12 Estimating Emissions for Air Toxic Human Health Risk Assessment

Historically, risk assessments have focused on air toxics from point sources, and assessments of air emissions were performed for new and expanding facilities. These assessments typically are time consuming, resource intensive, and focused on plants that generally had the latest and best pollution control technology for air toxics. However, facility-level assessments are not capable of answering

questions concerning potential impacts from proposed plants, and the overall impacts when combined with existing pollutants in the air. To answer these questions, a large-scale risk assessment should be performed.

An air toxic emission inventory is a comprehensive listing, by source, of the air toxic pollutant emissions within a specific geographic area in a specific time period. EPA prepares a **National Emissions Inventory (NEI)** with input from numerous state, local, and tribal (S/L/T) air agencies. NEI data are used for air quality modeling, regional strategy development, regulation, air toxics risk assessment, and tracking trends in emissions over time. The NEI Input Format (NIF) is the standard format widely used by S/L/T agencies to transfer data to the NEI.

Air toxic emission inventories serve as the first step in quantifying exposure for an air toxics risk assessment. In addition to source information, such as location, chemicals released, and time of release, emission inventories provide most of the critical input data for air quality models used to predict air toxics fate and transport in the atmosphere.

To facilitate a systematic, more objective way of understanding and addressing impacts from emissions of air toxics, the risk assessment should integrate all types of source information (point, mobile and area), reported emissions from those sources, chemical information (i.e., how a chemical moves through the environment, its toxicity) as well as physical and meteorological information specific to the region.

Air toxics inventories are usually not at the quality that would provide the results desired in a modeling assessment, and improving the entire statewide toxics inventory may be unrealistic. An enhancement of the local air toxics inventory in the assessment area of interest may be beneficial for providing more accurate and precise risk assessment results and, consequently, a better basis for any air toxics risk or airshed-program management decisions. Also, local emission inventory work in specific areas of concern or study makes these air toxics efforts smaller and easier for agencies and participating facilities to manage and conduct.

The risk manager must define the inventory objectives, the required data, and quality objectives. The risk manager must then substantiate the reasons for allocation of resources and identify the necessary inventory components:

- The air toxics to be carried out through the risk assessment (the chemicals of potential concern or COPCs)
- The specific sources or source categories to be assessed
- The geographic area (scale) of the assessment area
- The time interval over which emissions are to be inventoried

12.1 Emission Speciation for Air Toxic Risk Assessments

Emission Speciation is a critical problem for human health and ecological risk assessment. The lack of adequately speciated emission data imposes a significant limit to emissions characterization, and subsequent inclusion in risk modeling. A review of the emission inventory's assessment area would be required to determine the degree of speciation reported:

- Speciated to specific contaminant, which enables risk modeling because contaminant-specific toxicity factors can be obtained (e.g., benzene, 1,3-butadiene)
- Speciated to contaminant class that is not acceptable for modeling because the toxicity factors for individual isomers may vary considerably and cannot be speciated without a source-specific apportionment scheme (e.g., total xylenes, including one or more of the ortho-, meta-, and para-isomers)
- Unspeciated as a product or process mixture that may be manually speciated with an appropriate apportionment scheme (e.g., gasoline, crude oil)
- Unspeciated as a categorical mixture that cannot be further speciated except possibly by the facility (e.g., non-methane VOCs, particulates)

12.2 Emissions Spatial Allocation for Air Toxic Risk Assessments

A risk assessment study can benefit by improved spatially defined area emissions allocation. Area sources are invariably defined at county level, which is a critical limitation on large scale risk assessments. The author strongly recommends that county level area sources be spatially allocated to census tracts level using emissions surrogates. Aircraft emissions, for example, can be apportioned to the census tracts in which the airports are located, depending upon the proportion of air traffic occurring at each airport. Likewise, railway emissions can be apportioned to census tracts according to the length of the railway in the census tract as a fraction of the county total length. Most of the other non-road mobile source emissions could be apportioned to census tract according to population. Figure 20 presents spatial re-allocation of emission estimates from county level to smaller census tract level.

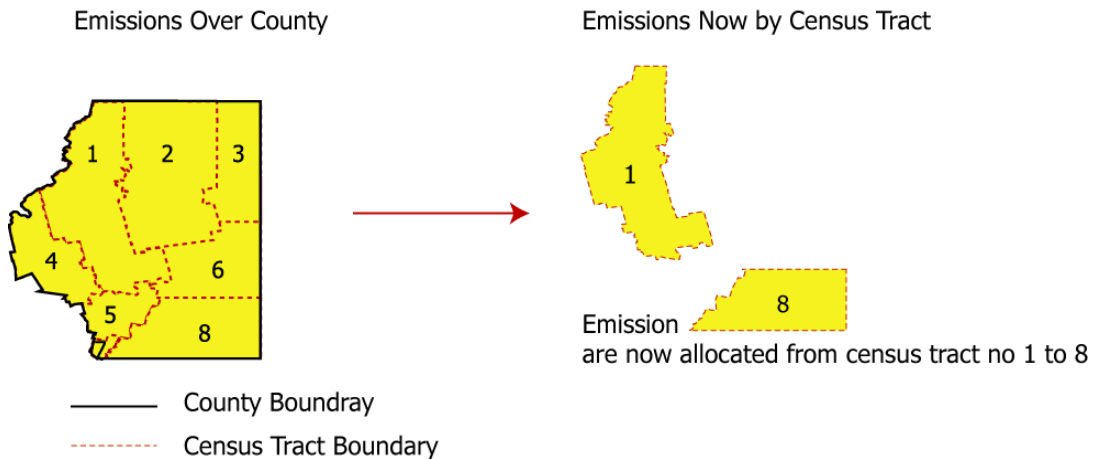


Figure 20. Allocating emissions from County level to smaller census tract level.

13 Emissions Inventory Quality Control

The focus of quality control (QA/QC) is the preparation and implementation of protocols designed to ensure that data input and output are accurate, complete, and verifiable. As with the USEPA Emissions Inventory Improvement Program (EIPP), it is also good practice to always prepare an emissions inventory Quality Assurance Project Plan (QAPP), prior to conducting the emissions inventory data collection.

The descriptions of the Quality Assurance and Quality Control (QA/QC) procedures to be implemented in the QAPP are drawn from the USEPA procedures established for the National Emissions Inventory (NEI) process. The QAPP should recommend the details and specifics of QA/QC checks. Briefly, these will include:

- Checks of file formats for completeness and referential integrity
- Checks for correctness of table and field names/types/properties
- Checks of data content for acceptable codes and values within acceptable ranges
- Cross field checks (e.g., county code vs. zip code, release point diameter, gas flow rate, and release point exit velocity)
- Checks that all location parameters are within the geographic boundaries for the state/locality/tribe

Some additional QA/QC efforts include:

- Verification of Lat/Long coordinates
- Checks for completeness of the data
- Use of accepted data gap filling procedures

The USEPA describe Emissions Projections as “*extrapolating baseline emission estimates to predict future emissions based upon expected future activity levels*”

and emissions controls. Projected emissions estimates are often used for planning, evaluation of potential control measures, analysis of new source impacts, modeling of future air quality, and assessment of the effectiveness of air pollution control strategies. A baseline emissions inventory is important because it represents a snapshot of emissions for a given baseline year". In this sense, emission projections are important to forecast emissions changes, impact of regulatory policies, and the effect of employment and population growth on air quality standards of prescribed airsheds.

An outstanding guidance document on emissions projections, developed by the USEPA, is titled *Procedures for Preparing Emissions Projections* (EPA, July 1991), and is located at <http://www.epa.gov/ttn/chief/publications.html>.

To meet the objectives stated above, emissions projections track past and future emission trends due to activity growth and implemented control strategies or defined policy. The USEPA has conducted extensive emissions projection studies. A large emission projection was conducted by the Western Regional Air Partnership (WRAP) to define policy to protect the visibility at national parks. This WRAP study estimates future motor vehicle emissions, use of solvents, and other source categories. Projections of emissions were based on changes expected to occur on surrogates such as population, employment, and economic activity. For more information on the WRAP emissions projections study refer to <http://www.wrapair.org>.

The USEPA also provides emission projection resources such as the Economic Growth Analysis System (EGAS). Note that the Multiple Projection System (MPS) is no longer supported. These electronic resources can be accessed on the World Wide Web at <http://www.epa.gov/ttn/chief/emch/projection/>.

There are two types of emission projections:

- Baseline emissions projections
- Control strategy emissions projections

13.1 Baseline Emissions Projections

Baseline emissions projections are estimates of future year emissions that are taken into account:

- Expected growth in an area
- Existing air pollution control regulations in effect at the time the projections are made

Promulgated regulations **expected to take effect at future intervals**.

Baseline projections provide a reference point for measuring reasonable further progress and determining if additional emission reductions are necessary to attain the air quality standards.

13.2 Control Strategy Emission Projections

Control strategy projections are estimates of future year emissions that also include the expected impact of **modified or additional control** regulations. Control strategy emission projections are used because while baseline emissions projections take into account promulgated regulations expected to take effect at future intervals, they often do not reflect all of the growth and control scenarios that the agency may wish to evaluate.

14 Greenhouse Gases

Atmospheric scientists believe current climatological data indicate that the planet is warming up. The most accepted theory for this warming trend is the trapping of solar radiation, which would be partially reflected to space in form of longer-wave radiation. Certain gases have a stronger opacity to infrared radiation than others. These gases are denoted as Greenhouse Gases (GHGs) and may be emitted by natural and anthropogenic (man-made) sources. The main GHGs are listed below:

- Carbon dioxide [CO₂]
- Methane [CH₄]
- Nitrous oxide [N₂O]
- Chlorofluorocarbons [CFCs]
- Nitrous oxide [N₂O]

14.1 Greenhouse Gases, Their Major Sources, and Atmospheric Concentrations

Naturally occurring greenhouse gases (GHGs) include water vapor, carbon dioxide (CO₂), methane (CH₄), nitrous oxide (N₂O), and ozone (O₃). Several classes of halogenated substances that contain fluorine, chlorine, or bromine are also greenhouse gases, but they are, for the most part, emitted solely by human activities. Chlorofluorocarbons (CFCs) and hydrochlorofluorocarbons (HCFCs) are halocarbons that contain chlorine. Halocarbons that contain bromine are referred to as halons. Other fluorine-containing halogenated substances include hydrofluorocarbons (HFCs), perfluorocarbons (PFCs), and sulfur hexafluoride (SF₆). There are also several gases that, although they do not have a direct radiative forcing effect, do influence the formation and destruction of ozone, which has a terrestrial radiation absorbing effect. These gases referred to here as ozone precursors include carbon monoxide (CO), oxides of nitrogen (NO_x), and non-methane volatile organic compounds (NMVOCs). Aerosols - extremely small particles or liquid droplets emitted directly or produced as a result of atmospheric reactions - can also affect the absorptive characteristics of the atmosphere.

A brief description of each GHG, its sources, and its role in the atmosphere is given below. The following section then explains the concept of Global Warming Potentials (GWPs), which are assigned to individual gases as a measure of their relative average global radiative forcing effect.

14.2 Water Vapor - H₂O

Overall, the most abundant and dominant greenhouse gas in the atmosphere is water vapor. Water vapor is neither long-lived nor well-mixed in the atmosphere, varying spatially from 0 to 2 percent (IPCC, 1996). In addition, atmospheric water can exist in several physical states, including gaseous, liquid, and solid. Human activities are not believed to directly affect the average global concentration of water vapor; however, the radiative forcing produced by the increased concentrations of other GHGs may indirectly affect the hydrologic cycle. A warmer atmosphere has an increased water holding capacity; yet, increased concentrations of water vapor affect the formation of clouds, which can both absorb and reflect solar and terrestrial radiation.

14.3 Carbon Dioxide - CO₂

In nature, carbon is cycled between various atmospheric, oceanic, land biotic, marine biotic, and mineral reservoirs. The largest fluxes occur between the atmosphere and terrestrial biota, and between the atmosphere and surface water of the oceans. In the atmosphere, carbon predominantly exists in its oxidized form, CO₂. Atmospheric carbon dioxide is part of this global carbon cycle, and therefore, its fate is a complex function of geochemical and biological processes. Carbon dioxide concentrations in the atmosphere, as of 1994, increased from approximately 280 parts per million by volume (ppmv) in pre-industrial times to 358 ppmv, which is more than 25 percent increase (IPCC, 1996). Forest clearing, other biomass burning, and some non-energy production processes (e.g., cement production) emit notable quantities of carbon dioxide.

14.4 Methane - CH₄

Methane is produced through anaerobic decomposition of organic matter in biological systems. Agricultural processes such as wetland rice cultivation, enteric fermentation in animals, and the decomposition of animal wastes emit CH₄, as does the decomposition of municipal solid wastes. Methane is also emitted during the production and distribution of natural gas and petroleum, and it is also released as a by-product of coal mining and incomplete fossil fuel combustion. The average global concentration of methane in the atmosphere was 1,720 parts per billion by volume (ppbv) in 1994, a 145 percent increase from the pre-industrial concentration of 700 ppbv (IPCC, 1996). It is estimated that 60 to 80 percent of current CH₄ emissions are the result of anthropogenic activities. Carbon isotope measurements indicate that roughly 20 percent of methane emissions are from fossil fuel consumption, and an equal percentage is produced

by natural wetlands, which will likely increase with rising temperatures and rising microbial action (IPCC, 1996).

14.5 Nitrous Oxide - N₂O

Anthropogenic sources of N₂O emissions include agricultural soils, especially the use of synthetic and manure fertilizers; fossil fuel combustion, especially from mobile sources; adipic (nylon) and nitric acid production; wastewater treatment and waste combustion; and biomass burning. The atmospheric concentration of nitrous oxide (N₂O) in 1994 was about 312 parts per billion by volume (ppbv), while pre-industrial concentrations were roughly 275 ppbv. The majority of this 13 percent increase has occurred after the pre-industrial period and is most likely due to anthropogenic activities (IPCC, 1996). Nitrous oxide is removed from the atmosphere primarily by the photolytic action of sunlight in the stratosphere.

14.6 Ozone - O₃

Ozone is present in both the stratosphere, where it shields the Earth from harmful levels of ultraviolet radiation, and at lower concentrations in the troposphere, where it is the main component of anthropogenic photochemical “smog”. During the last two decades, emissions of anthropogenic chlorine and bromine-containing halocarbons, such as chlorofluoro- carbons (CFCs), have depleted stratospheric ozone concentrations. This loss of ozone in the stratosphere has resulted in negative radiative forcing, representing an indirect effect of anthropogenic emissions of chlorine and bromine compounds (IPCC, 1996). Ozone in the troposphere has increased dramatically in the past 100 years, contributing to increased radiative forcing.

Tropospheric ozone, which is also a greenhouse gas, is produced from the oxidation of methane and from reactions with precursor gases such as carbon monoxide (CO), nitrogen oxides (NO_x), and non-methane volatile organic compounds (NMVOCs). The tropospheric concentrations of both ozone and these precursor gases are short-lived and therefore, spatially variable.

14.7 Halocarbons

Halocarbons are for the most part man-made chemicals that have both direct and indirect radiative forcing effects. Halocarbons that contain chlorine, such as chlorofluorocarbons (CFCs) and hydrochlorofluorocarbons (HCFCs), or bromine, such as halons and methyl bromide, result in stratospheric ozone depletion. Therefore, these halocarbons are controlled under the *Montreal Protocol on Substances that Deplete the Ozone Layer*. The United States and Western Europe phased out production and commercialization of halons and CFCs by 1996.

14.8 Carbon Monoxide - CO

Carbon monoxide has an indirect radiative forcing effect by elevating concentrations of CH₄ and tropospheric ozone through chemical reactions with other atmospheric constituents (e.g., the hydroxyl radical) that would otherwise assist in destroying CH₄ and tropospheric ozone. Carbon monoxide is created when carbon-containing fuels are burned incompletely. Through natural processes in the atmosphere, it is eventually oxidized to CO₂. Carbon monoxide concentrations are short-lived in the atmosphere and spatially variable.

14.9 Nitrogen Oxides - NO_x

The primary climate change effects of nitrogen oxides (i.e., NO and NO₂) are indirect and result from their role in promoting the formation of tropospheric ozone and, to a lesser degree, lower stratospheric ozone. NO_x emissions injected higher in the stratosphere can lead to stratospheric ozone depletion. Nitrogen oxides are created from lightning, soil microbial activity, biomass burning (both natural and anthropogenic fires), fossil fuel combustion, and in the stratosphere from nitrous oxide (N₂O). NO_x is relatively short-lived in the atmosphere and its concentrations are spatially variable.

14.10 Non-Methane Volatile Organic Compounds - NMVOCs

Non-methane volatile organic compounds include compounds such as propane, butane, and ethane. These compounds participate, along with NO_x, in the formation of tropospheric ozone and other photochemical oxidants. NMVOCs are emitted primarily from transportation and industrial processes, as well as biomass burning and non-industrial consumption of organic solvents. NMVOCs tend to be short-lived in the atmosphere and their concentrations are spatially variable.

14.11 Aerosols

Aerosols are extremely small particles or liquid droplets found in the atmosphere. They can be produced by natural events such as dust storms and volcanic activity, or by anthropogenic processes such as fuel combustion. Their effect upon radiative forcing is to both absorb radiation and to alter cloud formation, thereby affecting the reflectivity (i.e., albedo) of the Earth. Aerosols are removed from the atmosphere primarily by precipitation, and generally have short atmospheric lifetimes. Like ozone precursors, aerosol concentrations and composition vary by region (IPCC, 1996).

14.12 Global Warming Potentials of Greenhouse Gases

The Global Warming Potential (GWP) is a measure that quantifies the relative radiative forcing impacts of various GHGs. It is defined as the cumulative radiative forcing - both direct and indirect effects - over a specified time horizon resulting from the emission of a unit mass of gas relative to some reference gas (IPCC, 1996). Direct effects occur when the gas itself is a greenhouse gas. Indirect radiative forcing occurs when chemical transformations involving the original gas produce a gas or gases that are greenhouse gases, or when a gas influences the atmospheric lifetimes of other gases. The reference gas used is CO₂. GWP-weighted emissions are expressed in metric tons of carbon equivalent (MTCE). Carbon comprises 12/44ths of carbon dioxide by weight. In order to convert emissions reported in metric tons (MT) of a gas to MTCE, the following equation is used:

$$MTCE = (MT \text{ of gas}) \times (GWP) \times (12 / 44)$$

where:

MTCE = Metric Tons of Carbon Equivalent
GWP = Global Warming Potential
(12 / 44) = Ratio of Carbon mass to Carbon Dioxide mass

GWP values allow policy makers to compare the impacts of emissions and reductions of different gases. According to the IPCC, GWPs typically have an uncertainty of 35 percent. Greenhouse gases with long atmospheric lifetimes (e.g., CO₂, CH₄, N₂O, HFCs, PFCs, and SF₆) tend to be evenly distributed throughout the atmosphere, and consequently, global average concentrations can be determined. On the other hand, concentrations vary regionally for the short-lived gases such as water vapor, tropospheric ozone, ozone precursors (e.g., NO_x, CO, and NMVOCs), and tropospheric aerosols (e.g., SO₂ products). No GWP values are attributed to gases that are short-lived with spatially heterogeneous atmospheric concentrations.

Table 13. Global Warming Potentials (GWP) and Atmospheric Lifetime.

Gas	Lifetime (Years)	GWP
Carbon dioxide (CO ₂)	50-200	1
Methane (CH ₄) ^b	23	21
Nitrous oxide (N ₂ O)	120	310
HFC-23	264	11,700
HFC-125	32.6	2,800
HFC-134a	14.6	1,300
HFC-143a	48.3	3,800
HFC-152a	1.5	140
HFC-227ea	36.5	2,900
HFC-236fa	209	6,300
HFC-4310mee	17.1	1,300
CF ₄	50,000	6,500
C ₂ F ₆	10,000	9,200
C ₄ F ₁₀	2,600	7,000
C ₆ F ₁₄	3,200	7,400

15 Data Quality Objectives (DQO)

DQOs, data quality objectives, are qualitative and quantitative statements to identify the level of uncertainty that a decision maker is willing to accept. The purpose of DQOs is to ensure that the final data will be sufficient for the intended use. DQOs are identified as part of the inventory planning process. They are determined based on the end use of the inventory, but should realistically reflect the limitations resulting from time constraints, lack of data, and resource limitations of staff and funding. A statement of DQOs should be prepared as part of the inventory preparation plan.

The development of a DQO statement is an iterative process. The managers must work together to balance the quality objectives and the available resources. It is important to acknowledge the constraints that limit the ultimate quality of the inventory, especially if the achievable DQOs fall short of the desired DQOs.

16 Data Gap Filling

Data gaps in the inventory may be the result of:

1. Pollutants unaccounted for due to a lack of credible emission factors
2. Missing or unaccounted facilities due to incomplete source lists
3. Source categories that have not been considered due to a lack of credible emission factors or activity data

Filling data gaps is done on a case-by-case basis, and depends on the nature of the data gap and the importance of the source category under review. One should prioritize the gap filling effort. Tools available for gap filling include:

- Performing additional searches of databases to identify appropriate surrogate activity data and emission factors
- Using the NET database to spatially allocate emissions to the area of study
- Extrapolating emissions from other geographic areas
- Projecting emissions data from past inventories within the same geographic area

Emissions inventory practitioners must carefully document the gap filling actions, including all assumptions made and all resources used. Data quality issues may surface when filling data gaps. For example, one might derive emissions from a certain source category by projecting emissions from previous national inventories based upon growth indicators. These emissions estimates may not adequately capture facility shutdowns, new facilities, changes in operations relative to the previous inventory levels, or additions of new controls. Thus, while there are emission estimates available for gap filling, the data quality will not be of the same level as the emission estimates developed using actual and current data. One should discuss this tradeoff between accuracy and completeness with the task manager before making a decision on gap filling strategy.

17 Rule Effectiveness, Rule Penetration, and Control Efficiency

Control efficiency (CE), rule effectiveness (RE), and rule penetration (RP) are applied to area source emission estimates if regulations are in place, which may affect any of the individual sources within a source category. CE, RE, and RP are used to estimate the effect of controls being applied in the real world. Sources that are completely uncontrolled do not have CE, RE, or RP applied.

17.1 Control Efficiency - CE

Control Efficiency (CE) is the emission reduction efficiency. This reduction efficiency is a percentage value representing the amount of a source category's emissions that are controlled by a control device, process change, or

reformulation. For area sources in particular, controls can vary widely. CE values for area sources represent the weighted average control for the category.

17.2 Rule Effectiveness - RE

Regulatory programs often achieve fewer reductions than anticipated for most source categories. Rule effectiveness (RE), expressed as a fraction or percent, is an adjustment which reflects the ability of a regulatory program to achieve the required emission reductions.

RE is an adjustment to the CE to account for failures and uncertainties that affect the actual performance of the control. For example, control equipment performance may be adversely affected by age of the equipment, lack of maintenance, or improper use. The USEPA recommends the default value of 0.80 for RE when information cannot be acquired to substantiate the true value of RE.

The RE factor accounts for the fact that many emission control equipments do not achieve emission reductions at the designed rates, at all times, and under all conditions. Process upsets, control equipment malfunctions, operator errors, equipment maintenance, and other non-routine operations are examples of times when control device performance is expected to be less than optimal.

The basic emission estimation equation when RE is applied is shown below:

$$E_C = E \times (1 - C_E \times R_E)$$

where:

E_C = Emissions after control C

E = Emissions before control

C_E = Estimated control efficiency (expressed as a fraction, from 0 to 1)

R_E = Rule effectiveness (expressed as a fraction, from 0 to 1)

17.3 Rule Penetration (RP)

Rule penetration (RP) is the percentage of an area source category that is covered by an applicable regulation. For example, regulations on gasoline underground tank filling may apply only to stations above a specified size cutoff, or the regulation may apply to facilities built after a certain date. When estimating emissions using area source methods for source categories where a rule or regulation applies, agencies should incorporate an estimate of the amount of rule penetration.

$$\text{Rule Penetration} = \frac{(\text{Uncontrolled emissions covered by the regulation}) \times 100}{(\text{Total uncontrolled emissions})}$$

18 Pollutant Monitoring and Fuel Analysis Methodologies

This section describes available pollutant monitoring and fuel analysis methodologies. These methodologies were developed by the USEPA and are presented on the Emissions Measurement Center website:

<http://www.epa.gov/ttn/emc/>.

18.1 Stack Sampling (EPA Method 3)

This method is used to determine oxygen (O₂) and carbon dioxide (CO₂) concentrations in flue gas from fossil-fuel-fired combustion processes. A gas sample is extracted from the stack either from a single point or by multipoint integrated sampling. The sample is passed through an Orsat analyzer containing a solution of 45-percent potassium hydroxide (KOH) in one impinger and a solution of pyrogallol in the second impinger. CO₂ is absorbed by KOH, and O₂ is absorbed by pyrogallol. The decrease in sample volume due to this absorption is directly proportional to the concentration in the sample.

18.2 EPA Method 3A (CEM)

This method may be used to determine O₂ and CO₂ concentrations when CEM systems are in place. A gas sample is extracted continuously from the stack and conveyed to the O₂ and CO₂ analyzers. The sample can be wet or dry depending on the type of analyzer used.

CO₂ can only be measured using infrared analyzers such as non-dispersive infrared (NDIR) systems or gas filter correlation (GFC) analyzers. NDIR analyzers consist of sample and reference optical cells through which a beam of infrared light passes. This beam of light is modulated so that the infrared light passing through the optical cell pulses. The modulated infrared light then enters a two-chambered detector that is filled with the same gas that is being analyzed. The gas in the detector chambers absorbs the infrared light and heats up, causing it to expand. Separating the two chambers is a thin diaphragm which flexes as the pressure between the two chambers varies. Since the sample has absorbed some of the infrared light, the detector chamber associated with the sample cell does not heat up as much as the reference side. This causes a pressure difference between the two chambers deflecting the diaphragm. Because the infrared light is modulated, the diaphragm pulses. This degree of deflection in conjunction with the pulsing is converted into an electrical signal proportional to gas concentration.

O₂ analyzers generally use electrochemical cells. Porous platinum electrodes are attached to the inside and outside of the cell to provide the instrument voltage response. Zirconium oxide contained in the cell conducts electrons when it is hot due to the mobility of O₂ ions in its crystal structure. A difference in O₂ concentration between the sample side of the cell and the reference (outside) side

of the cell produces a voltage. This response is proportional to the logarithm of the O₂ concentration ratio. The reference gas is ambient air at 20.9 percent O₂ by volume.

18.3 EPA Method 5 Or 17 (Stack Sampling)

EPA Method 5 or 17 may be used to monitor emissions of particulate matter (PM) from boilers. In Method 5, PM is withdrawn isokinetically from the source and collected externally on a heated glass fiber filter maintained at 248°F ± 25°F. Method 17 employs an in-stack filter and particulate matter is collected at source temperature and pressure. The particulate mass is determined gravimetrically.

18.4 EPA Method 6 (Stack Sampling)

Method 6 is used to measure SO₂ emissions. A gas sample is extracted from the sampling point in the stack. The sample passes through a filter to remove PM, and sulfuric acid (including sulphur trioxide) and sulfur dioxide (SO₂) are separated in a series of impingers containing 80 percent isopropanol and 3 percent hydrogen peroxide. SO₂ is then measured by barium-thorin titration.

18.5 EPA Method 6C (CEM)

Method 6 is used to measure SO₂ emissions when CEM systems are in place. A gas sample is continuously extracted from a stack, and a portion of the sample is conveyed to a continuous analyzer in determining SO₂ gas concentration using an NDIR, ultraviolet (UV), or fluorescence analyzer.

UV analyzers work very similarly to NDIR instruments. A beam of UV light passes through the gas sample, which absorbs some of the light. The remaining light passes through the sample cell and is measured by the detector.

Fluorescence analyzers are typically used in ambient monitoring. The analyzer works by exposing the sample to a pulse of ultraviolet light. SO₂ molecules absorb this light, which "excites" the molecule into a higher energy state. The molecule loses some of this excess energy by fluorescing (detected by a photomultiplier tube), which in turn provides an SO₂ concentration value.

18.6 EPA Method 7 (Stack Sampling)

Method 7 is used to measure NO_x emissions. A grab sample is collected in an evacuated flask containing a diluted sulfuric acid-hydrogen peroxide absorbing solution, and the NO_x, except nitrous oxide (N₂O), is measured colorimetrically using phenoldisulfonic acid (PDS).

18.7 EPA Method 7E (CEM)

When CEM systems are in place, Method 7E is used. A gas sample is continuously extracted from the stack and a portion of the sample is conveyed to an instrument chemiluminescent analyzer for determination of NO_x concentration. This measurement technique uses a chemical reaction (ozone combining with nitric oxide [NO]) to cause light to be emitted. This light is measured with a photomultiplier tube, similar to the SO_2 fluorescence analyzer.

18.8 EPA Method 8 (Stack Sampling)

This method is applicable in determining sulfuric acid mist (including SO_3) and SO_2 emissions from stationary sources. A gas sample is extracted isokinetically from the stack. Sulfuric acid mist and SO_2 are separated, and both fractions are measured separately by the barium-thorium titration method.

18.9 EPA Method 10 (CEM)

When CEM systems are in place, Method 10 may be used to measure CO concentration. A gas sample is continuously extracted from the stack and a portion of the sample is conveyed to an instrumental NDIR analyzer for determination of CO concentration. The principle of operation is similar to the NDIR SO_2 analyzer.

18.10 EPA Method 10B (Stack Sampling)

An integrated bag sample is extracted from the sampling point and analyzed for CO. The sample is passed through a conditioning system to remove interferences and collected in a Tedlar® bag.

The CO is separated from the sample by a gas chromatograph (GC) and catalytically reduced to methane (CH_4) prior to analysis by flame ionization detection (FID).

18.11 EPA Method 19

This method is applicable for determining:

- PM, SO_2 , and NO_x emission rates
- Sulfur removal efficiencies of fuel pretreatment and SO_2 control devices
- Overall reduction of potential SO_2 emissions
- SO_2 rates based on fuel sampling and analysis procedures

Pollutant emission rates and SO_2 control device efficiencies are determined from concentrations of PM, SO_2 or NO_x , and O_2 or CO_2 , along with F factors (ratios of combustion gas volumes to heat inputs).

18.12 EPA Method 25 (Stack Sampling)

This method is applicable for the determination of total gaseous non-methane organic (TGNMO) emissions as carbon. A gas sample is extracted from the stack at a constant rate through a heated filter and a chilled condensate trap by means of an evacuated sample tank. After sampling is completed, the TGNMO emissions are determined by independent analysis of the condensate trap, the sample tank fractions and combining the analytical results. The organic content of the condensate trap fraction is determined by oxidizing the non-methane organics to CO₂, and quantitatively collecting the effluent in an evacuated vessel; then, a portion of the CO₂ is reduced to CH₄ and measured by flame ionization detection (FID). The organic content of the sample tank fraction is measured by injecting a portion of the sample into a GC equipped with a capillary column capable of separating the non-methane organic emissions from CO, CO₂, and CH₄.

18.13 EPA Method 25A (CEM)

This method applies to the measurement of total gaseous organic concentrations of vapors consisting primarily of alkanes, alkenes, and aromatic hydrocarbons. A gas sample is extracted continuously from the source through a heated sample line and directed to the total hydrocarbon analyzer that uses FID. The sample gas enters the detector and it is combusted in a hydrogen flame. The ions and electrons formed in the flame enter an electrode gap, decrease the gas resistance, and allow a current to flow in an external circuit. The resulting current is proportional to the instantaneous concentration of total hydrocarbons. Concentration values are expressed in terms of methane or propane.

18.14 EPA Method 29 (Stack Sampling)

This method is applicable for the determination of chromium, cadmium, arsenic, nickel, manganese, beryllium, copper, lead, selenium, silver, antimony, and mercury emissions from stationary sources. The stack gas sample is withdrawn isokinetically. Particulate emissions are collected in the probe and on a heated filter, while gaseous emissions are collected in solutions of acidic hydrogen peroxide and acidic potassium permanganate. The recovered samples are digested and the appropriate fractions are analyzed by atomic absorption spectrophotometry.

18.15 EPA Method 0030 (Stack Sampling)

Method 0030 is a manual method for collecting VOCs which are defined for purposes of this method as those organics with boiling points less than 100°C. The gas sample is collected from the sampling point and cooled to 20 °C by passing through a water-cooled condenser, and the volatile organics are collected on a pair of sorbent resin traps. The resin traps are then analyzed in the laboratory using a gas chromatograph equipped with an electron capture detector (ECD),

flame ionization detector (FID), or mass spectrometer to determine speciated organics.

18.16 EPA Methods 201 AND 202 (Stack Sampling)

In this method, a gas sample is isokinetically extracted from the source. An in-stack cyclone is used to separate PM with a diameter greater than 10 micrometers, and an in-stack glass fiber filter is used to collect the PM₁₀. The particulate mass is determined gravimetrically after removal of uncombined water. Method 202 is used to determine the condensable PM. The condensable PM is determined gravimetrically by analysis of the impinger fractions.

18.17 Continuous Flow Rate Monitors

A new monitoring requirement under Acid Rain regulations (Title IV of the CAAA) is the measurement of exhaust gas velocities. There are three velocity monitoring techniques applicable to utility stacks or exhaust ducts:

- Ultrasonic flow monitors
- Thermal flow monitors
- Differential pressure monitors

Ultrasonic monitors operate by passing a pulse of ultrasonic sound diagonally through the moving stack gas. The frequency of the ultrasonic pulse is changed in proportion to the velocity of the stack gas. This frequency shift is measured and gas velocity is then calculated.

Thermal flow monitors operate by inserting a heated element into the exhaust stream. As gas moves over the probe, the heated element is cooled, thus requiring additional power to be supplied to the heater in order to maintain a constant temperature. This additional power is proportional to the gas velocity being measured.

Differential pressure monitors measure the difference between the velocity head and static pressure. This difference is proportional to the velocity of the gas stream. The gas flow rate is then calculated using this pressure difference.

18.18 Fuel Analysis (ASTM D1552-83/D4507-81)

SO₂ emissions from combustion sources can also be estimated by fuel analysis. The fuel is analyzed for sulfur content and emissions are calculated based on the assumption that all of the sulfur is converted to SO₂. Depending on the characteristics of the fuel ash, a portion of the SO₂ may be absorbed onto the ash (generally less than 5 percent). The remainder is emitted.

18.19 Fuel Analysis (SW 846 Methods 3040/7090)

Metal emissions from combustion sources can also be estimated by fuel analysis. The fuel is analyzed for the metals of interest and emissions are calculated assuming all of the metals are emitted. Because most of the metals are associated with either boiler ash or PM, which may be collected by an air pollution control system, this approach will provide a conservative emission estimate.

18.20 Flux Chamber Measurement

Flux chamber measurement is a direct measurement technique used to estimate emissions from area sources of fugitive emissions such as contaminated soil, landfills, and lagoons. The approach employs an emission isolation flux chamber to obtain an estimate of the amount of pollutant, or pollutants, being emitted from a given surface area per unit time. A variety of flux chamber equipment designs and operating procedures have been employed. EPA has issued guidance identifying flux chamber measurement as a recommended method of estimating baseline air emissions from Superfund sites (USEPA, 1990).

18.21 Optical Remote Measurement

Another method used to estimate emissions from open areas, or otherwise inaccessible sources (e.g., plumes from smoke stacks, hazardous waste landfills), are the use of optical remote sensing (ORS). ORS is an open-path method of determining pollutant concentration using optical absorption spectroscopy. Pollutant concentration data combined with on-site meteorological data may then be used to estimate emissions. ORS techniques include:

- Fourier transform spectroscopy
- Differential optical absorption spectroscopy
- Laser long-path absorption
- Differential absorption lidar
- Gas cell correlation spectroscopy

18.22 Summary of USEPA Monitoring and Fuel Analysis Methods

Table 14 presents a summary of the methods described in this section.

Table 14. Summary of the USEPA Monitoring and Fuel Analysis Methods.

Parameter	Monitoring Methods		Fuel Analysis Method
	Stack Sampling	CEM	
SO ₂	EPA Method 6	EPA Method 6C	ASTM D-1552-83/ D4507-81 ^a
SO ₃	EPA Method 8	NA	
NO _x	EPA Method 7	EPA Method 7E	
O ₂ / CO ₂	EPA Method 3	EPA Method 3A	
CO	EPA Method 10B	EPA Method 10	
VOC	EPA Method 25	NA	
THC	EPA Method 25	EPA Method 25A	
Speciated organics	EPA Method 0030	NA	
Heavy metals	EPA Method 29	NA	SW 846 Methods 3040/7090 ^b
PM	EPA Method 5	NA	
PM ₁₀	EPA Method 201/202	NA	
Sulfuric acid mist	EPA Method 8	NA	
Flow rate	EPA Method 2	EPA Method 19, CFRM ^c	

References:

EPA, 1986; *Test Methods for Evaluating Solid Waste, SW-846, Third Edition*; ASTM, 1992; Title 40 CFR, Appendices A and B, September 1992. Title 40 CFR Part 60, Appendix A and Part 61, Appendix B.

^a For liquid fuels. ASTM D3177-75/D4239-85 is used for coal.

^b For liquid fuels.

^c Continuous flow rate monitoring.

NA = Not applicable; no CEM method exists.

19 Emissions Inventory Terms

Actual Emissions - The rate of emissions of a pollutant from an emissions unit, calculated using the unit's actual operating hours, production rates, and types of materials processed, stored, or combusted during the selected time period.

Allowable Emissions - Emission rate that represents a limit on the emissions that can occur from an emissions unit. This limit may be based on a federal, state, or local regulatory emission limit determined from state or local regulations.

Ambient Standards - Concentration limit of a given pollutant in the ambient air. Ambient standards are not emissions limitations on sources, but usually result in such limits being placed on source operation as part of a control strategy to achieve or maintain an ambient standard.

Area Sources - Smaller sources that do not qualify as point sources under the relevant emissions cutoffs. Area sources encompass more widespread sources that may be abundant, but individually, release small amounts of a given pollutant. These are sources for which emissions are estimated as a group rather than individually. Examples typically include dry cleaners, residential wood heating, auto body painting, and consumer solvent use. Area sources generally are not required to submit individual emissions estimates.

Condensable Emissions - Emissions that exist in the stack in the vapor phase and condenses after cooling outside the stack.

Continuous Emissions Monitoring (CEM) is any monitoring effort that continuously measures and records emissions. In addition, CEM data can be used to estimate emissions for different operating periods and longer averaging times.

Criteria Pollutants consist of carbon monoxide (CO), lead (Pb), nitrogen oxides (NO_x), sulfur dioxide (SO₂), volatile organic compounds (VOCs), and particulate matter of aerodynamic diameter less than or equal to 10 micrometers (PM₁₀). The National Ambient Air Quality Standards (NAAQS) were mandated by the Clean Air Act of 1970, and are based on criteria including adverse health or welfare effects. The NAAQS are currently used to establish air pollutant concentration limits for the six air pollutants listed above that are commonly referred to as **criteria pollutants**.

Design Standards impose certain hardware requirements. For example, it might require that leaks from compressors be collected and diverted to a control device. Design standards are typically used when an emissions limit is not feasible.

DQI - Data quality indicators (DQIs) are qualitative and quantitative descriptors used to interpret the degree of acceptability or utility of the data. The principal DQIs are:

1. **Accuracy:** The closeness of a measurement to the true value, or the degree of agreement between an observed value and an accepted reference value. Accuracy includes a combination of error (precision) and systematic error (bias) that are due to sampling and analytical operations.
2. **Comparability:** The degree to which different methods, data sets, or decisions agree or can be represented as similar.
3. **Completeness:** The amount of valid data obtained compared to the planned amount.
4. **Representativeness:** Degree to which an inventory is representative of the region and sources it is meant to cover.

Emission Concentration Standards limit the mass emissions of a pollutant per volume of air. Emission concentration standards are expressed in terms such as grams per dry standard cubic meter (g/dscm) or other similar units.

Emission Factors - Ratios that relate emissions of a pollutant to an activity level at a plant that can be easily measured, such as an amount of material processed or an amount of fuel used. Given an emission factor and a known activity level, a simple multiplication yields an estimate of the emissions. Emission factors are developed from separate facilities within an industry category, so they represent typical values for an industry, but they do not necessarily represent a specific source.

Emissions Reduction Standards - Standards that limit the amount of current emissions relative to the amount of emissions before application of a pollution control measure. For example, an emission reduction standard may require a source to reduce, within a specified time, its emissions to 50 percent of the present value.

Emission Standards - General type of standards that limit the mass of a pollutant that may be emitted by a source. The most straightforward emissions standard is a simple limitation on mass of pollutant per unit time (e.g., pounds of pollutant per hour).

Filterable Emissions - Portion of particulates (particle matter) that is captured by a filter. This term is applied for sampling trains.

FIPS (Federal Information Processing Standard) - Coding system for all states and counties in the USA.

Fugitive Emissions - Emissions from sources that are technically infeasible to collect and control (e.g., storage piles, wastewater retention ponds, pipeline leaks).

Hazardous Air Pollutants (HAPs) - Pollutants that are generally emitted in smaller quantities than criteria pollutants, but may be reasonably anticipated to cause cancer, developmental effects, reproductive dysfunctions, neurological disorders, inheritable gene mutations, or other chronically or acutely toxic effects in humans. The list of 188 HAPs in Section 112(b) of the 1990 Clean Air Act Amendments (CAAA) includes relatively common pollutants such as formaldehyde, chlorine, methanol, and asbestos, as well as numerous less-common substances.

Material Balance or **Mass Balance** - This method is used to estimate emissions by accounting for all the inputs and outputs of a given pollutant. When inputs of a material to a given process are known and all outputs except for air emissions

can be reasonably well quantified, then the remainder can be assumed to be an estimate of the amount lost to the atmosphere for the process.

Mobile Sources include all non-stationary sources, such as automobiles, trucks, aircraft, trains, construction and farm equipment, and others. Mobile sources are a subcategory of area sources, and are generally not required to submit individual emissions estimates. Mobile sources are commonly sub-divided into on-road and off-road sources.

NAICS - North America Industrial Classification System defines the economic sector of a facility.

National Ambient Air Quality Standards (NAAQS) - This is the main ambient standards for the following six criteria pollutants: carbon monoxide (CO), lead (Pb), nitrogen oxides (NO_x), sulphur oxides (SO_x), ozone (O₃), and particulate matter of aerodynamic diameter less than or equal to 10 micrometers (PM₁₀).

National Emissions Standards for Hazardous Air Pollutants (NESHAP) - This is a class of standards that limits emissions of HAPs. The common usage of NESHAP actually refers to two different sets of standards. First, there are 22 emissions standards promulgated prior to the 1990 Clean Air Act Amendments (CAAA). Some of these standards are pollutant-specific (e.g., the NESHAP for vinyl chloride), others are source-category specific (e.g., the NESHAP for benzene waste operations), and still others are both pollutant- and source-category specific (e.g., the NESHAP for inorganic arsenic emissions from glass manufacturing plants).

NEI - National Emissions Inventory from the USEPA. The NEI data is available at <http://www.epa.gov/ttn/chief/net/index.html>.

NET - National Emissions Trends.

New Source Performance Standards (NSPS) are promulgated for criteria, hazardous, and other pollutant emissions from new, modified, or reconstructed sources that the U.S. Environmental Protection Agency (EPA) determines contribute significantly to air pollution. These are typically emission standards, but may be expressed in other forms such as concentration and opacity. The NSPS are published in 40 Code of Federal Regulations (CFR) Part 60.

NIF - NEI Input Format. This is the USA National Emissions Inventory (NEI) data input format.

Nitrogen Oxides (NO_x) are a class of compounds that are respiratory irritants and react with volatile organic compounds (VOCs) to form ozone (O₃). The primary combustion product of nitrogen is nitrogen dioxide (NO₂). However, several other nitrogen compounds are usually emitted at the same time (nitric oxide [NO],

nitrous oxide [N_2O], etc.), and these may or may not be distinguishable in available test data. They are usually in a rapid state of flux, with NO_2 being in the short term, the ultimate product emitted or formed shortly downstream of the stack. The convention followed in emission factor documents is to report the distinctions wherever possible, but to report total NO_x on the basis of the molecular weight of NO_2 . NO_x compounds are also precursors to acid rain. Motor vehicles, power plants, and other stationary combustion facilities emit large quantities of NO_x .

NTI - National Toxic Inventory from the USEPA. NTI has been replaced by the NEI.

Opacity Standards limit the opacity (in units of percent opacity) of the pollutant discharge rather than the mass of a pollutant.

Operational Standards impose some requirements on the routine operation of the unit. Such standards include maintenance requirements or operator training certification requirements. Operational standards are typically used when an emission limit is not feasible.

Ozone (O_3) is a colorless gas that damages lungs and can damage materials and vegetation. It is the primary constituent of smog, and it is formed primarily when nitrogen oxides (NO_x) and volatile organic compounds (VOCs) react in the presence of sunlight. It is also emitted in insignificant quantities from motor vehicles, industrial boilers, and other minor sources.

Particulate Matter of aerodynamic diameter less than or equal to 10 micrometers (PM_{10}) is a measure of small solid matter suspended in the atmosphere. Small particles can penetrate deeply into the lung where they can cause respiratory problems. Emissions of PM_{10} are significant from fugitive dust, power plants, commercial boilers, metallurgical industries, mineral industries, forest and residential fires, and motor vehicles.

Particulate Matter of aerodynamic diameter less than or equal to 2.5 micrometers ($\text{PM}_{2.5}$) is a measure of fine particles of particulate matter that come from fuel combustion, agricultural burning, woodstoves, etc.

Plant Level Emissions are consolidated for an entire plant or facility. A plant may contain one or many pollutant-emitting sources.

Plant Level Reporting is generally required if total emissions from a plant (which may be composed of numerous individual emission points) meet the point source cut-off. The plant level reporting used by most air pollution control agencies generally requires that the facility provide data that apply to the facility as a whole. Such data include number of employees and the Standard Industrial Classification (SIC) code designated to the plant. A plant usually has only one

SIC code denoting the principal economic activity of the facility. The plant is also identified by geographic or jurisdictional descriptors such as air quality control region, county, address, and universal transverse Mercator (UTM) grid coordinates (or latitude/longitude) that identify a coterminous location.

Point Level Emissions typically represent single stack or vent individually large enough to be considered point sources.

Point Level Reporting includes specific data for individual emission points (typically stacks). These data are more detailed than that submitted in Plant Level Reporting, and may include emission-related and modeling information such as stack height of the release point, diameter of the stack, emission rate, method of determination, fugitive emissions, gas exit velocity from a stack, gas temperature, and operating schedule.

Point Sources are large, stationary, identifiable sources of emissions that release pollutants into the atmosphere. Sources are often defined by state or local air regulatory agencies as point sources when they annually emit more than a specified amount of a given pollutant. The way state and local agencies define point sources can vary. Point sources are typically large manufacturing or production plants. They typically include both confined "stack" emission points as well as individual unconfined "fugitive" emission sources.

Potential Emissions are the potential rate of emissions of a pollutant from an emissions unit, calculated using the unit's maximum design capacity. Potential emissions are a function of the unit's physical size and operational capabilities.

It is important to note that annual potential emissions from a unit are not necessarily the product of 8760 hours per year times the hourly potential emissions. For most processes, the operation of one piece of equipment is limited in some way by the operation of another piece of equipment upstream or downstream. It is also possible for the emission rate to vary over time. For instance, if a reaction requires 6 hours to reach completion, the emissions from the reaction vessel during the first hour will be different than those during the last hour. Thus, the highest hourly emission rate is not sustained during the entire cycle or for the entire year.

Primary Emissions - Pollutants emitted by the source that did not transform into other chemicals.

Process-based Emission Standards limit the mass emissions per unit of production. These standards may limit mass emissions per unit of material processed or mass emissions per unit of energy used. As process rate increases (e.g., an increase in tons of ore processed per hour), the allowable emissions increase (e.g., an increase in pounds of pollutant per hour).

Process Emissions are emissions from sources where an enclosure, collection system, duct system, and/or stack (with or without an emission control device) is in place for a process. Process emissions represent emissions from process equipment (other than leaks) where the emissions can be captured and directed through a controlled or uncontrolled stack for release into the atmosphere.

Process Fugitive Emissions occur as leaks from process equipment, including compressors, pump seals, valves, flanges, product sampling systems, pressure relief devices, and open-ended lines. Emissions from the process that are not caught by the capture system are also classified as process fugitive emissions.

Process or Segment Level Emissions usually represent a single process or unit of operation.

Process or Segment Level Reporting involves each process within a plant being identified by a U.S. Environmental Protection Agency (EPA) source classification code (SCC). For point sources, reporting guidelines may require that a plant identify, for each process or operation (designated by SCC), the periods of process operation (daily, weekly, monthly, annually); operating rate data including actual, maximum, and design operating rate or capacity; fuel use and fuel property data (ash, sulfur, trace elements, heat content, etc.); identification of all pollution control equipment and their associated control efficiencies (measured or designed); and emissions rates. Source identification information, as previously described under Plant Level Reporting, is usually also required at the process level to ensure that emissions data for a single plant are clearly identified.

Process-specific Empirical Relationships are similar to emission factors in that they relate emissions to easily identifiable process parameters. However, these relationships are represented by more detailed equations that relate emissions to several variables at once, rather than a simple ratio. An example is the estimate for volatile organic compound (VOC) emissions from storage tanks that is based on tank size and throughput, air temperature, vapor pressure, and other variables.

PTE - Potential to Emit.

Reported Emissions are those emission estimates that are submitted to a regulatory agency. Emissions inventories can be used for a variety of purposes such as State Implementation Plan (SIP) base year inventories, environmental compliance audits, air quality rule applicability, and reporting information in an air quality permit application. Emissions can be reported on an actual, potential, or maximum basis. Many state and local air pollution control agencies have rules and regulations that define an allowable emission value for a particular piece of equipment. Because of this, a facility should first define the purpose of the inventory and then choose the appropriate means of reporting emissions to the regulatory agency.

SIC - Source Industrial Codes, defines the economic sector of a facility. SIC is being phased out by the NAICS.

Source Tests are short-term tests used to collect emissions data that can then be extrapolated to estimate long-term emissions from the same or similar sources. Uncertainties arise when source test results are used to estimate emissions under process conditions that differ from those under which the test was performed.

Stratospheric Ozone-depleting Compounds are chlorofluorocarbons (CFCs), halons, carbon tetrachloride, methyl chloroform, and hydrochlorofluorocarbons (HCFCs). These pollutants are regulated by Title VI of the Clean Air Act Amendments (CAAA) because they may destroy stratospheric ozone.

Sulfur Oxides (SO_x) are a class of colorless, pungent gases that are respiratory irritants and precursors to acid rain. Sulfur oxides are emitted from various combustion or incineration sources, particularly from coal combustion.

Volatile Organic Compounds (VOCs) react with nitrogen oxides (NO_x) in the atmosphere to form ozone (O₃). Although they are not criteria pollutants, VOC emissions are regulated under criteria pollutant programs because they are ozone precursors. Large amounts of VOCs are emitted from motor vehicle fuel distribution, chemical manufacturing, and a wide variety of industrial, commercial, and consumer solvent uses.

References

ASTM. *Annual Book of ASTM Standards*, Volumes 06.01 and 15.05. September 1992.

EIA, 1999. *Coal Industry Annual 1999*, DOE/EIA-0584(99), Office of Coal, Nuclear, Electric and Alternate Fuels, Energy Information Administration, Washington DC, 1999.

EIIP, 2001b. *Asphalt Paving*. Volume III: Chapter 17. Emission Inventory Improvement Program, Area Sources Committee. January. Internet address:
http://www.epa.gov/ttn/chief/eiip/techreport/volume03/iii17_apr2001.pdf.

EIIP, 2001c. *Pesticides - Agricultural and Nonagricultural*, Volume III: Chapter 9. Emission Inventory Improvement Program, Area Sources Committee. Internet address:
http://www.epa.gov/ttn/chief/eiip/techreport/volume03/iii09_jun2001.pdf.

EIIP, 2001d. *Gasoline Marketing (Stage I and Stage II)*, Volume III: Chapter 11. Emission Inventory Improvement Program, Area Sources Committee. January. Internet address:
http://www.epa.gov/ttn/chief/eiip/techreport/volume03/iii11_apr2001.pdf.

EIIP, 2000a. *Auto Body Refinishing*, Volume III: Chapter 13. External Review Draft. Emission Inventory Improvement Program, Area Sources Committee. May. Internet address:
<http://www.epa.gov/ttn/chief/eiip/techreport/volume03/iii13.zip>.

EIIP, 1997a. *Traffic Markings*, Volume III: Chapter 14. Emission Inventory Improvement Program, Area Sources Committee. May. Internet address:
<http://www.epa.gov/ttn/chief/eiip/techreport/volume03/iii14.pdf>.

EIIP, 1997b. *Solvent Cleaning*, Volume III: Chapter 6. Emission Inventory Improvement Program, Area Sources Committee. September. Internet address: <http://www.epa.gov/ttn/chief/eiip/techreport/volume03/iii06fin.pdf>.

EIIP, 1997c. *Industrial Surface Coating*, Volume III: Chapter 8. Emission Inventory Improvement Program, Area Sources Committee. September. Internet address: <http://www.epa.gov/ttn/chief/eiip/techreport/volume03/iii08.pdf>.

EIIP, 1996a. *Consumer and Commercial Solvent Use*, Volume III: Chapter 5. Emission Inventory Improvement Program, Area Sources Committee. August. Internet address: <http://www.epa.gov/ttn/chief/eiip/techreport/volume03/iii05.pdf>.

EIIP, 1996b. *Graphic Arts*, Volume III: Chapter 7. Emission Inventory Improvement Program, Area Sources Committee. November. Internet address: <http://www.epa.gov/ttn/chief/eiip/techreport/volume03/iii07.pdf>.

EIIP, 1996c. *Dry Cleaning*. Volume III: Chapter 4. Emission Inventory Improvement Program, Area Sources Committee. May. Internet address: <http://www.epa.gov/ttn/chief/eiip/techreport/volume03/iii04fn2.pdf>.

EIIP, 1995. *Architectural Surface Coating*, Volume III: Chapter 3. Emission Inventory Improvement Program, Area Sources Committee. November. Internet address: <http://www.epa.gov/ttn/chief/eiip/techreport/volume03/archsfc.pdf>.

Lakes Environmental Consultants Inc. *Software Development Plan for Tribal Emissions Inventory Software Solution*. Lakes Environmental Consultants Inc., Waterloo, Ontario, 2002.

U.S. Census, 2001a. *State & County QuickFacts*. U.S. Census Bureau, Washington, D.C. Internet address: <http://quickfacts.census.gov/qfd/>.

U.S. Census, 2001b. *County Business Patterns*. U.S. Census Bureau, Washington, D.C. Internet address: <http://www.census.gov/epcd/cbp/view/cbpview.html>.

U.S. Census, 2000. *American FactFinder - Census 2000*. U.S. Census Bureau, Washington, D.C. URL: <http://factfinder.census.gov/servlet/BasicFactsServlet>.

USEPA. 1986. *Test Methods for Evaluating Solid Waste*, SW-846, Third Edition, U.S. Environmental Protection Agency, Office of Solid Waste and Emergency Response. Washington, D.C.

USEPA, 1989. "Procedures for Estimating and Applying Rule Effectiveness In Post-1987 Base Year Emissions Inventories for Ozone and Carbon Monoxide State Implementation Plans," United States Environmental Protection Agency, Office of Air Quality Planning and Standards, Technical Support Division, Research Triangle Park, NC. EPA-452/4-92-010.

USEPA. 1990. *Procedures for Conducting Air Pathway Analyses for Superfund Activities, Interim Final Documents: Volume 2 - Estimation of Baseline Air Emissions at Superfund Sites*. EPA-450/1-89-002a (NTIS PB90-270588), August.

USEPA, 1991. "Procedures for the Preparation of Emissions Inventories for Carbon Monoxide and Precursors of Ozone, Volume I: General Guidance for Stationary Sources," United States Environmental Protection Agency, Office of Air Quality Planning and Standards, Technical Support Division, Research Triangle Park, NC. EPA-450/4-91-016.

USEPA, 1995. *Compilation of Air Pollution Emission Factors (AP-42) - Volume I: Stationary Point and Area Sources*, Fifth Edition. U.S. Environmental Protection Agency, Office of Air Quality Planning and Standards, Research Triangle Park, North Carolina. January. Internet address: <http://www.epa.gov/ttn/chief/ap42/>.

USGS, 1999. "Mining and Quarrying Trends" in *Minerals Yearbook: Volume I Metals and Minerals*. Minerals Information, U.S. Geological Survey, Reston, Virginia.

USEPA, 1999. "Handbook for Criteria Pollutant Inventory Development: A Beginner's Guide for Point and Area Sources," United States Environmental Protection Agency, Office of Air Quality Planning and Standards, Research Triangle Park, NC. EPA-454/R-99-037. September. URL: <http://www.epa.gov/ttn/chief/eidocs/beginner.pdf>.

USEPA, 1995. "Compilation of Air Pollutant Emission Factors AP-42, Fifth Edition, Volume I: Stationary Point and Area Sources," United States Environmental Protection Agency, Office of Air Quality Planning and Standards, Research Triangle Park, NC. URL: <http://www.epa.gov/ttn/chief/ap42/>.

U.S. EPA. July 1995, *EIIP. Volume II. Chapter 1. Introduction to Stationary Point Sources Emission Inventory Development, revised working draft*. Point Sources Committee, Emission Inventory Improvement Program and Radian Corporation, Research Triangle Park, North Carolina.

U.S. EPA, July 1995, *EIIP. Volume II. Chapter 2. Preferred and Alternative Methods for Estimating Air Emissions from Boilers, final report*. Point Sources Committee, Emission Inventory Improvement Program and Radian Corporation. Research Triangle Park, North Carolina.

U.S. EPA, October 1995, *EIIP. Volume VI Quality Assurance Procedures for the Emission Inventory Improvement Program, external draft*. Quality Assurance Committee, Emission Inventory Improvement Program and Radian Corporation. Research Triangle Park, North Carolina.

U.S. EPA. 1995-1996. *Compilation of Air Pollutant Emission Factors, Volume I: Stationary Point and Area Sources, Fifth Edition and Supplements, AP-42*. U.S. Environmental Protection Agency, Office of Air Quality Planning and Standards. Research Triangle Park, North Carolina.

U.S. EPA, August 1996, *EIIP. Volume III Chapter 1. Introduction to Area Source Emission Inventory Development, Final Report*. Area Sources Committee, Emission Inventory Improvement Program and Eastern Research Group, Inc. Research Triangle Park, North Carolina.

USEPA, 2000. "AP-42: Compilation of Air Pollutant Emission Factors Mobile Sources," United States Environmental Protection Agency, Office of Transportation and Air Quality, Ann Arbor, MI. URL: <http://www.epa.gov/otaq/ap42.htm>.

USEPA, 2002. *Municipal Solid Waste in the United States: 2000 Facts and Figures*. EPA 530-R-02-001. U.S. Environmental Protection Agency, Office of Solid Waste and Emergency Response, Washington D.C. June. Internet address: <http://www.epa.gov/epaoswer/non-hw/muncpl/report-00/report-00.pdf>.

USEPA. 2002a. "Documentation for the 1999 National Emissions Inventory Version 2.0 for Criteria Air Pollutants and Draft Version 3.0 for HAPS - On-Road Sources." U.S. EPA, Emission Factor and Inventory Group, Office of Air Quality Planning and Standards, Research Triangle Park, NC. October.

USEPA. 2002b. “Documentation for Aircraft, Commercial Marine Vessel, Locomotive, and Other Nonroad Components of the National Emissions Inventory.” U.S. EPA, Emission Factor and Inventory Group, Office of Air Quality Planning and Standards, Research Triangle Park, NC. November.

Additional WEB References for Area Sources

1. Gasoline Sales Data

<http://www.fhwa.dot.gov/ohim/hs97/mf33ga.pdf>
<http://www.fhwa.dot.gov/ohim/hs97/mf21.pdf>
<http://www.fhwa.dot.gov/ohim/hs98/tables/mf21.pdf>

2. Pesticide Data

<http://www.aes.purdue.edu/agstat/annbul/9899/pg51.html>

3. Household Energy Data

<http://www.eia.doe.gov/emeu/recs/contents.html>
<http://www.eia.doe.gov/emeu/sep/in/frame.html>

4. Highway Expenditures

<http://www.fhwa.dot.gov/ohim/hs97/sf1.pdf>
<http://www.fhwa.dot.gov/ohim/hs98/tables/sf1.pdf>
<http://www.census.gov/ftp/pub/industry/1/ma28f97.pdf>

5. Population

http://www.census.gov/population/estimates/county/co-99-3/99C3_18.txt
<http://www.census.gov/population/estimates/state/st-99-3.txt>

6. County Business Patterns

<http://www.census.gov/epcd/cbp/map/97data/18/999.txt>

The Census Bureau (www.census.gov) does have data on number of employees per county per SIC code called County Business Patterns. This data can be obtained at:

www.census.gov/epcd/cbp/view/cbpview.html.

Chapter 4

Air Pollution Meteorology

A chapter dedicated to the topic “Air Pollution Meteorology” was presented in Volume I of this book series.

For additional information, the reader can visit:

- <http://www.shodor.org/metweb/index.html>
A comprehensive course on Air Quality Meteorology.
- http://yosemite.epa.gov/oaqps/eogtrain.nsf/DisplayView/SI_409_0-5?OpenDocument
US EPA course (SI:409) on Basic Air Pollution Meteorology.

BRANK
P
e

Chapter 5

Meteorological Modeling

A brief introduction to the topic “Meteorological Modeling” was presented in Volume I of this book series. “Chapter 5B – Large-Eddy Simulations of the Atmospheric Boundary Layer” was included in Volume II. In the following pages we present:

5A – Meteorological Modeling for Air Quality Applications

5C – Computational Fluid Dynamics of Microscale Meteorological Flows for Air Quality Applications

BRANK
P
e

Sarma, A. 2008. *Meteorological Modeling for Air Quality Applications*. Chapter 5A of *AIR QUALITY MODELING - Theories, Methodologies, Computational Techniques, and Available Databases and Software*. Vol. III – *Special Issues* (P. Zannetti, Editor). Published by The EnviroComp Institute (<http://www.envirocomp.org/>) and the Air & Waste Management Association (<http://www.awma.org/>).

Chapter 5A

Meteorological Modeling for Air Quality Applications

Ananthakrishna Sarma

*Center for Atmospheric Physics, Science Applications International Corporation,
McLean, Virginia (USA)*
sarmaa@saic.com

Abstract: The phrase “meteorological modeling” (or synonymously “atmospheric modeling” and “numerical weather prediction”) refers to the numerical representation of the atmosphere and its processes. This chapter describes the various processes that are usually included in numerical models that are relevant to air quality applications. Due to the mathematical complexities of many of these processes, parameterizations are used to simplify the numerical models. Many different parameterizations exist for these processes, and representative examples are presented.

Key Words: numerical modeling, algorithms, and parameterizations.

1 Introduction

Air quality is defined by the presence of pollutants that are deemed harmful to life and environment. Pollutants are released by industrial and other commercial activities, and also from natural sources such as volcanoes and dust storms. The atmosphere is an active chemical medium in which numerous chemical reactions are taking place continuously, with their rates governed by the concentrations of the participating species and the external factors (e.g., incident solar energy). The modeling of air quality requires an accurate modeling of all the factors that control the concentrations of these chemical species, including the movement of these airborne species from one location to another. Hence, accurate air quality modeling is predicated by accurate meteorological modeling.

The phrase “meteorological modeling” (or synonymously “atmospheric modeling” and “numerical weather prediction – NWP”) refers to the numerical representation of the atmosphere and its processes. This numerical representation is based on dynamical, thermodynamical, physical and chemical properties of the atmospheric system. Even though atmospheric modeling started out as examining just the atmospheric processes, it is commonly understood that the atmospheric motions depend on the properties of the earth’s surface as well as the dynamics of the oceans. Therefore, it is appropriate to extend the definition of “meteorological modeling” to include the effects of the surface of the earth and the oceans. In this chapter, we will explore the fundamentals of meteorological modeling and its current trends.

The initial work of Charney (1948), Charney and von Neumann (1950), and Arakawa (1966) form the foundations of meteorological modeling. In those early days, NWP played a significant role in the development of computer hardware.

1.1 Why are Models Necessary?

The ultimate goal of atmospheric scientists is to understand the behavior of the atmospheric system so that its behavior can be forecasted accurately in order to benefit the society. For some of the processes involved, a mathematical representation is possible. However, it is not mathematically feasible to solve all of the equations in an analytical framework. Hence, we have to resort to approximate numerical representations of the atmospheric system using computers. Also, at a given time, in-situ as well as remote instruments sense only a very small portion of the atmosphere. Numerical modeling helps to fill the gaps in the sensed data and complete the three-dimensional picture of the atmospheric system in a physically consistent manner.

1.2 Processes that are Modeled

The atmospheric system is a complex system driven by processes that span various disciplines of science. Solar radiation forms the primary energy source for the atmospheric system. The atmospheric gases and the surface of the Earth absorb the solar energy that is not reflected back to space. The absorbed energy is emitted back in the infrared wavelengths (long-wave) to be re-absorbed by atmospheric gases or to be emitted to space. This radiation exchange process is modulated by intervening clouds, aerosols, pollutant species, and also by the properties of the surface of the Earth. The properties of the Earth’s surface vary from water surfaces (e.g., oceans and lakes), dry and arid surfaces of the deserts, and moisture-laden vegetation (e.g., rain forests) to the reflective surfaces of the snow and ice of the polar and high mountainous regions. These variations impact the thermodynamic structure of the atmosphere, and in turn affect its dynamics. For the sake of clarity, it is helpful to classify the different processes into broad classes: 1) atmospheric dynamics, 2) microphysical processes of the water cycle, 3) atmospheric radiation, 4) atmospheric and aerosol chemistry, and 5) processes

that involve the air-surface interactions. The following paragraphs describe these processes in detail.

1.2.1 Atmospheric Dynamics

Atmospheric dynamics refers to the processes that directly impact the movement of air and airborne constituents. These processes are related to the fundamental forces acting on a parcel of air:

- The pressure gradient force - the force exerted by air, as it wants to move from a high-pressure region to a low-pressure region. This force acts perpendicular to the isobar through a given location and it is pointed towards the low pressure.
- The gravitational force - acts towards the center of the Earth (along the local vertical).
- The buoyancy force - the force related to difference in densities between the parcel of air and its surroundings. It acts along the local vertical.
- The frictional forces - forces caused as the parcel of air moves with a velocity different than that of the surrounding air. These forces are pointed against the direction of motion.
- The centrifugal – the force caused by the rotation of the Earth. This force is pointed along a direction perpendicular to the axis of rotation of the Earth through the air parcel.

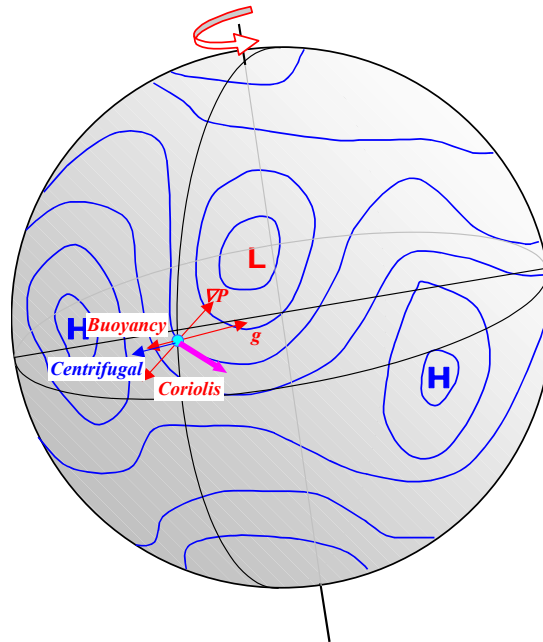


Figure 1. Primary forces acting on an air parcel indicated by the cyan dot. Note that the weather patterns shown in this figure are conceptual and are not intended to match the general circulation of the Earth's atmosphere.

1.2.2 Water Cycle and Cloud Microphysics

Water is a key component of the atmosphere. It makes the Earth's atmosphere unique in this solar system, and also makes life possible. The term water cycle refers to the set of processes that move water from the oceans to the atmosphere, in the form of water vapor, and then form clouds, generate precipitation that leads to runoff to streams and rivers, thus taking the water back to its source, the oceans. During this cycle, water manifests itself in all three of its phases – vapor, liquid and solid. The processes that comprise the water cycle include conceptually simple processes, such as evaporation and condensation, to complex processes that involve growth of ice crystals (and water droplets) on heterogeneous microscopic particle substrates called ice (and condensation) nuclei. These processes are collectively termed “microphysics”. The phase change that occurs in several of these processes results in the release of latent heat, which changes the thermodynamics of the environment significantly. For example, a thunderstorm that is initiated in a convectively unstable atmosphere can sustain itself from the energy released by these processes for several hours even after sundown. Several books have been written on these and related topics (e.g., Mason, 1976; Pruppacher and Klett, 1997; Rogers, 1976; and Young, 1993). Many of these processes are not completely understood.

Many of the microphysical processes are not easy to represent in simple mathematical terms to be incorporated into numerical models. In models, these processes are represented by parameterizations that have been derived empirically with theoretical considerations in which the parametric values are set from the results of numerous field and laboratory experiments and measurements. Even though significant progress has been achieved in the understanding of these processes in the last few decades, cloud microphysics still poses considerable challenge to researchers in the field of NWP.

1.2.3 Atmospheric Radiation

The Sun is the primary source of energy that drives the atmosphere. Solar energy reaches the Earth in the form of electromagnetic radiation. Some of this energy is reflected back to space and the rest is absorbed by the various constituents of the atmosphere as well as by various features on the Earth's surface. Part of this absorbed energy is re-emitted in longer wavelengths (in the infrared range). Gases such as carbon dioxide and methane reabsorb this emitted long wave radiation, thus trapping the energy and giving rise to the term “greenhouse effect”. Clouds also play a major role in reflecting some of the incoming solar radiation and absorbing some of the outgoing long wave radiation. This complex energy cycle along with the rotation of Earth about its axis, the tilt of the axis with respect to the plane of Earth's orbit, and the fact that the equatorial regions receive more direct insolation than the Polar Regions, give rise to the large-scale planetary waves and global circulations such as the Hadley cells.

As radiation directly impacts the temperature of both the atmosphere and the Earth's surface, it plays an important role in local circulations, especially thermally driven circulations such as land- and sea-breezes, drainage flows, and Katabatic winds. Atmospheric radiation is modeled at various levels of complexities ranging from simple bulk calculations and two-stream models to more complex models that treat different parts of the electromagnetic spectrum.

1.2.4 Atmospheric Chemistry

The atmosphere is a complex mixture of gases and aerosols. This mixture is augmented with chemical species that result from human activities. This mixture gives rise to numerous chemical reactions of varying strengths and speeds. Some of the chemical reactions are catalyzed by the presence of other chemicals (catalysts) or the presence of ultraviolet radiation. These reactions and their products are the topics of discussion in other chapters of this book. However, it is worthwhile noting that the previous two topics, cloud microphysics and atmospheric radiation, play a major role in atmospheric chemistry. Atmospheric radiation is a key process to several reactions of interest providing the actinic flux for the photochemical reactions. Heterogeneous reactions involve the presence of reactant species and catalysts dissolved in water. Also, water facilitates the transport of material spatially, especially in the vertical, due to washout by precipitation.

1.2.5 Atmosphere-Surface Interactions

Atmospheric conditions are significantly affected by the properties of the Earth's surface at any location. These interactions occur via several mechanisms – dynamical processes due to terrain forcing and friction, radiational processes through the absorption and emission of radiation, and physical and microphysical processes due to the injection into the atmosphere of water vapor as well as aerosol particles, which act as condensation and depositional nuclei. Atmospheric phenomena that are caused by these interactions can be found almost anywhere. Along the coastal areas, sea and land breezes are driven by the thermal gradient generated by the unequal heating of the land and water surfaces. Mountains block the mean wind. Down-slope winds that accelerate and warm the air are found in many places and are known by names such as Chinook and Föhn. Katabatic winds are found in the Antarctic and are believed to be caused by the rapid cooling at the surface due to the high albedo of the ice surface. It is a well-known fact that hurricanes are strengthened by the thermal energy and water vapor from the surface of warm oceans, and they rapidly decay if either of these sources is cut off. Urban areas impact the local meteorology by a complex interaction between the surface (including buildings and other urban scenery) and the atmosphere, which include the slowing down the mean wind by the increased resistance, and the input of moisture and heat. The urban landscape also provides cloud-forming aerosols and other pollutant species. This phenomenon is called the urban heat island.

1.3 Scales and Scale Interactions

Atmospheric processes are usually classified into different scales based on their spatial or temporal extent. Dynamical features in the atmosphere range from large-scale planetary waves to small-scale turbulent motions. The atmospheric scales of motion are generally divided in the following wavelength regimes: planetary, synoptic scale or continental scale, mesoscale, and local or cloud scale. These are depicted in the panels of Figure 2. These scales have typical wavelengths of 10,000, 1000, 100, and 1 km respectively. The wavelengths represent the spatial size of oscillations that are significant at those scales. Other scales can be easily defined depending on the processes of interest. For example, “urban scale” is of considerable interest due to the current threats involving terrorism and release of hazardous materials in an urban area. However, such a classification does not imply that atmospheric dynamical processes do not occur in between wavelengths. The scales have traditionally been defined to make the problem of modeling of the atmosphere tractable. The definitions of the scales themselves tend to change as faster computers become available. For example, global and mesoscale models continually increase their grid resolutions.

Even though the scales are defined for numerical convenience, it is widely accepted that the processes at one scale significantly affect processes in other scales. For example, the behavior of a hurricane that has a length scale $O(100 - 1000 \text{ km})$ is very much dependent on the individual convective elements surrounding its eye-wall and in the spiral bands. The water vapor vented by the convective elements in a hurricane can affect large-scale and small-scale circulations thousands of kilometers away. Very small-scale gravity waves generated by thunderstorm outflows trigger new thunderstorms hundreds of kilometers from the parent storm (Uccellini, 1975).

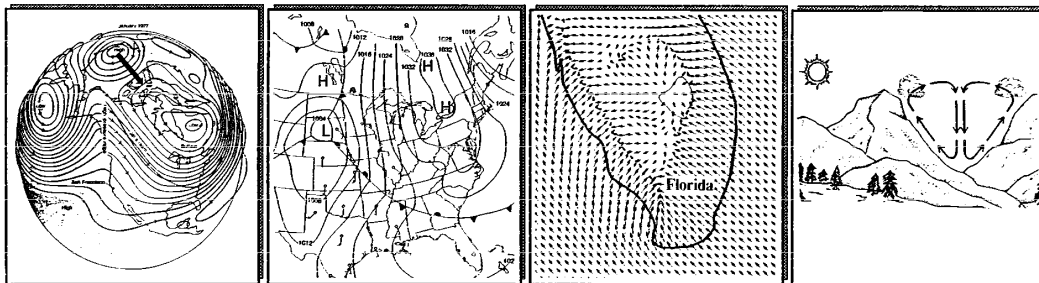


Figure 2. It is customary to divide the atmospheric motions into several scales. This figure shows four classifications – (from left to right) planetary, synoptic or regional scale, mesoscale and local scale.

2 Modeling Approaches

Numerical models of the atmosphere are derived fundamentally from the Taylor series approximation, which relates the value of a continuous function $f(x)$ to the known values of the function and its derivatives at a set of discrete points, x_i .

$$f(x) = f(x_i) + (x - x_i)f'_i + \frac{(x - x_i)^2}{2!}f''_i + \frac{(x - x_i)^3}{3!}f'''_i + \dots \quad (1)$$

where, f'_i , f''_i , f'''_i , etc. denote the spatial derivatives $\frac{\partial f}{\partial x}$, $\frac{\partial^2 f}{\partial x^2}$, $\frac{\partial^3 f}{\partial x^3}$, etc. respectively, evaluated at $x = x_i$. The general accuracy (or “order”) of the calculation depends upon the number of terms on the right hand side (RHS) of Equation 1 retained in the calculation. However, retention of more terms translates into greater requirement on computational resources for the evaluation of the higher order derivatives. Hence, it is customary to strike a balance by truncating the series at a suitable order of accuracy.

An examination of Equation 1 reveals that the error can also be minimized by reducing the magnitude of $(x - x_i)$. This is in fact attained by increasing the grid resolution. However, if the magnitudes of the spatial derivatives are small, there is no need to increase the grid resolution. This is the principle behind the concept of grid adaptation (or solution adaptive modeling technique) in which the higher resolutions are placed only in regions dictated by the gradients of principal variables. This will be discussed further in following sections.

Numerical models of the atmosphere can be divided into two major categories: 1) diagnostic models and 2) prognostic models. This classification is based solely on the functionality of the model. Diagnostic models are used to describe the state of the atmosphere at a particular instant in time or during a period of time, based on the known values of the state variables (variables that describe the state of an air parcel – pressure, temperature, moisture content and density), as well as the dynamical variables (speed and direction or the velocity components) during that time. In general, the equations in this modeling approach do not contain time differentials. Prognostic models, on the other hand, attempt to describe the atmospheric state at a future time based on the current and past conditions. The prognostic models are, hence, described by appropriate differential equations, which represent the time-variability of the state and dynamical variables. The choice among these models depends on the application at hand.

2.1 Diagnostic Models

In diagnostic models, as the name implies, the variables of interest are diagnosed or inferred from the state of the atmosphere, which has been described by other models and/or observational analyses. In most cases, atmospheric states at

various times are read into these models. The models make some fundamental assumptions regarding the behavior of the atmosphere in between these states. For example, the variables can be assumed to be constant, or vary linearly to the next state. In any case, the utility of these models are restricted to cases where the atmospheric states are well known at sufficiently high resolution in space and time. Diagnostic models are used in the air quality modeling and plume dispersion modeling arenas, primarily in conjunction with a prognostic model, which can provide the four-dimensional state of the atmosphere as an input to the diagnostic model.

2.2 Prognostic Models

Prognostic models use predictive equations to describe the model variables. The model variables are quantities that are conserved under spatial motion. A quantity is defined as conservative if it does not change in value with time as it moves through the computational grid. For example, in the atmosphere, linear momentum, potential temperature, and mass mixing ratios (ratios between the concentrations of the material to the density of air) of airborne material are conserved quantities. Hence, for a conserved quantity, Q ,

$$\frac{dQ}{dt} = 0 \quad (2)$$

Equation 1 can then be written as:

$$\frac{dQ}{dt} = \frac{\partial Q}{\partial t} + V \cdot \nabla Q = 0 \quad (3)$$

The equations are normally cast in the form

$$\frac{\partial Q}{\partial t} = -V \cdot \nabla Q + Q_s \quad (4)$$

where Q is the prognostic variable, t is time, V is the velocity vector and Q_s is a term describing the sources and sinks of the variable at that particular time. Such equations are often referred to as conservation equations as they describe the “conservation” of the variable Q .

2.3 Hierarchical Modeling

In a numerical model of the atmosphere, the spatial scales of motion that can be resolved are dependent on the grid spacing used to represent the computational domain. In general, effectively representing any feature requires that the feature be defined over four grid cells. Traditional numerical models use a constant grid spacing. This implies that these models have prescribed lower limits for the

spatial scale. However, atmospheric motions occur over various spatial scales. Hence, the concept of hierarchical modeling was created in which a set of numerical models is run, each addressing a specific range of motions.

The models are sometimes run in sequence with the lowest grid resolution model first followed by the higher grid resolution models, which derive boundary conditions from the solution of coarser grid resolution model. They can also be run in tandem with information exchanged from the lower to higher resolution model during each time step. This is referred to as “*nested-grid modeling*”. When the information transfer occurs only from the lower to higher resolution model, the models are termed “*one-way nesting*”. If the solution from the higher resolution model is used to update the lower resolution model, the models are termed “*two-way nesting*”. Almost all the operational, numerical forecast centers use this approach of nested-grid modeling. A few examples of nested-grid models include: the ETA model of the National Centers of Environmental Prediction (NCEP), Mesoscale Model 5 (MM5) of the National Center for Atmospheric Research (NCAR), the Regional Atmospheric Modeling System (RAMS) of Colorado State University (CSU), and the Coupled Ocean Atmospheric Mesoscale Prediction System (COAMPS) of the US Fleet Numerical Meteorological and Oceanographic Center (FNMOC). The new Weather Research and Forecast (WRF) model, under development under the leadership of NCAR and NCEP, is also a nested-grid model.

From the air quality standpoint, any of these models can be used to provide the environmental conditions required by atmospheric chemistry models. For example, the US Environmental Protection Agency’s (EPA) Models-3 system is comprised of MM5, the Community Multiscale Air Quality (CMAQ) modeling system, Sparse Matrix Operator Kernel Emissions (SMOKE) System and several pre- and post-processors (Byun and Ching, 1999).

Nesting provides an efficient method for operational models to place higher resolution over areas of interest, especially when uniform grid spacing is desired over all of the area of interest. However, when dealing with specific atmospheric phenomena such as hurricanes or the transport and diffusion of a toxic cloud, nested grids have some inherent disadvantages. Nested grid models require an a priori knowledge of the solution so that high-resolution nests can be strategically placed to capture the features of interest. Another problem with nested grids is the existence of internal boundaries in the computational domain, which can give rise to spurious features if not treated properly. Unstructured grid methods (discussed next) provide a paradigm to circumvent these problems.

2.4 Multiscale Modeling

Even though the nested grid models have shown considerable skill in forecasting atmospheric processes, the scales of motion that have to be addressed by the current needs pose considerable challenges to the modelers. Bacon et al. (2000) introduced a new paradigm with the ability to automatically vary the grid resolution based on physical features in the computational domain and in the evolving solution. The Operational Multiscale Environment model with Grid Adaptivity (OMEGA) is built upon an adaptive unstructured grid, where the fundamental computational element is a triangular prism (Figure 3). Such a grid takes advantage of the flexibility of unstructured grids as well as the vertical correlation of the atmosphere. The underlying mathematics and numerical implementation of unstructured adaptive grid techniques have been evolving rapidly, and in many fields of application, there is recognition that these methods are more efficient and accurate than the traditional structured grid approach (Baum and Löhner, 1994; Sarma et al., 1999; and Schnack et al., 1998). OMEGA represents the first attempt to use this CFD technique for atmospheric simulations.

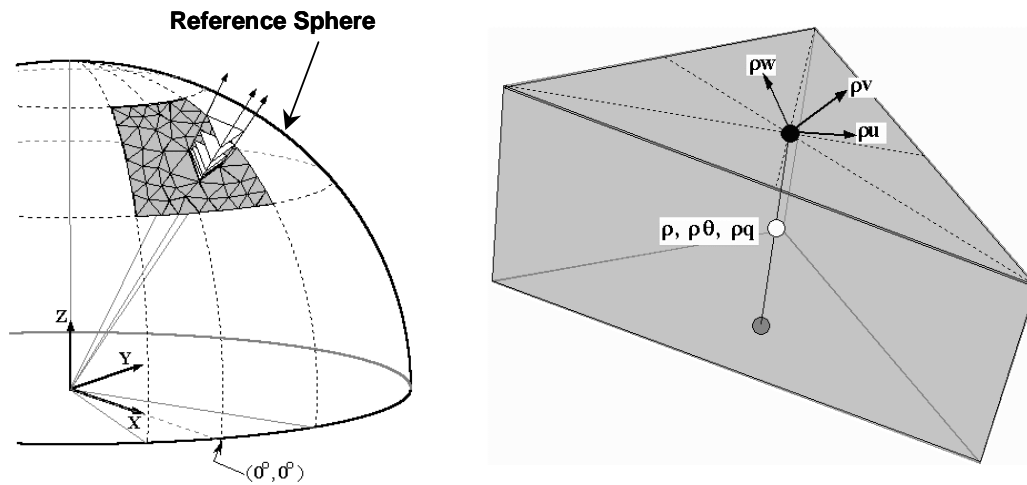


Figure 3. The OMEGA grid coordinate system with the grid layout (left) and a typical OMEGA grid element (right).

A fundamental difference between the traditional constant grid spacing modeling approach and the unstructured adaptive grid method is the fact that the unstructured grid method strives to reduce the numerical error by increasing the grid resolution in regions where the error has a potential to grow. This is evident from Equation 1 in which $(x - x_i)$ represents the spatial resolution. Such a multiscale approach provides great flexibility in modeling regional as well as global problems. For example, Figure 4 shows a grid that provides high resolution along the complex coastline of the Chesapeake Bay in order to better capture the land/sea breeze circulations.



Figure 4. An OMEGA grid for a domain covering the Chesapeake Bay provides high resolution along the coastline. The color fill represents elevation with its scale (values in meters) shown along the right edge.

A unique capability of unstructured grid used by OMEGA is its ability to adapt its resolution at run time. This is called solution-adaptation or dynamic adaptation. The grid resolution is changed over a part of the domain based on adaptivity criteria that are defined by the user. An example is given in Figure 5, which shows a global grid used for the simulation of the eruption of Mt. Etna in October of 2002. A noteworthy feature of this grid is that it is free of singularities (singularities are problems in structured rectilinear grids in which the grid lines converge to form zero-volume grid elements at the poles).

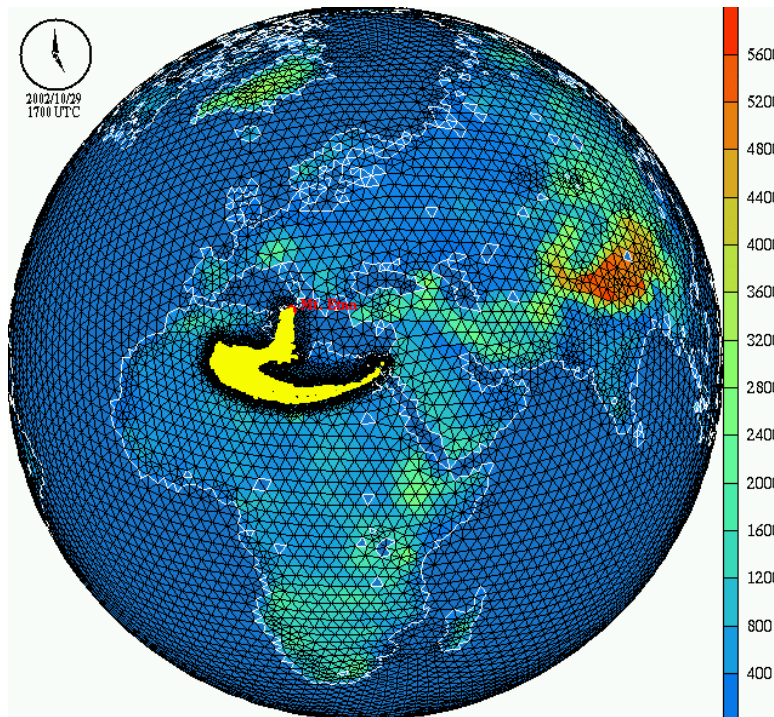


Figure 5. An OMEGA grid for a global run simulating the eruption of Mt. Etna uses dynamic grid adaptation to provide high resolution in the vicinity of the ash plume. In this case, the grid resolution varied from 5 km in the region of the plume to 100 km away from the plume. The yellow dots represent the centroids of the puffs that constitute the plume. The grid elements are colored based on their surface elevation (the scale is indicated in meters by the color bar on the right.)

3 Modeling Framework

A model consists of a set of equations or relationships between variables representing processes, which are defined on a well-specified computational domain. The structure of the computational domain is determined by the way in which the equations are solved. In general, models can be divided into two based on the frame of reference. If the frame of reference moves with an air parcel, the model is termed Lagrangian. If the frame of reference is fixed while the air parcel moves relative to it, the model is termed Eulerian.

3.1 Lagrangian Models

If the equations are solved following an air parcel, the model is said to be Lagrangian as the process solves the Lagrangian (or total) derivative $\frac{d}{dt}$.

Lagrangian models are also sometimes referred to as grid-free models as they do not depend on a specific grid for their solution. The Lagrangian framework has certain advantages. Usually, there are no spurious computational modes that can

make the calculations unstable. However, the accuracy of the calculations depends on the magnitude of the time steps used for integration as well as the fidelity of representation of the underlying environment. Long time steps make the calculations less accurate. The magnitude of the integration time step has to be chosen to represent the time-scales of the underlying physics.

Lagrangian models are ideally suited to treat localized problems such as plume dispersion where the plume itself covers a small volume compared to the dynamic environment. In this case, the plume can be represented as a collection of puffs and/or particles whose movement and growth (in the case of puffs) are determined by the dynamic and turbulent nature of the environment they are in. However, plume modeling using puffs also display the drawbacks of Lagrangian models. As the puffs are followed independently, it is difficult to compute interaction between the puffs, while in nature, the plume is a continuous field with concentrations tailing off towards zero in between puffs.

3.2 Eulerian Models

Eulerian models are grid based and integrate the partial derivative $\frac{\partial}{\partial t}$. Here, the prognostic variables are defined in an appropriate geometric grid and the time-behavior of the variables is represented by a truncated Taylor series as shown in Equation 1. The partial differential equations (PDEs) compute the rate of change of a quantity at a grid point. The integral of the PDE will yield a family of solutions for arbitrary values of the constant of integration. Hence, additional constraints are necessary to isolate a single solution. This can be done with appropriate choice of variables. It is preferred that the variables represent quantities that are conserved in the domain of integration so that at any time the sum of the variables over the domain is always known. For example, momentum of air is used in many models, as it is a conserved quantity. Other variables describing the state of the atmosphere include air density, energy density, and pollutant concentrations.

3.3 Semi-Lagrangian Techniques

Semi-Lagrangian techniques combine the Lagrangian and the Eulerian methods (discussed in the last two sections) to provide a method, which is unconditionally stable in a numerical sense. However, as for the Lagrangian schemes, accuracy does depend on the time step used. Longer time steps increase truncation errors resulting from interpolation of values from an Eulerian grid to the characteristic trajectory at any given time.

3.4 Plume Models

Plume models, as the name implies, describe the plume of material in a background flow. These models infer the background flow either as a constant or derived from data generated by other models. Plume models need to describe: 1) the source of the airborne material and 2) the transport and dispersion of this material in the ambient flow. In early plume models, the plumes were characterized by a Gaussian distribution of concentration in the transverse directions (across the direction of travel). Such a characterization was based on observations of power plant plumes fairly close to their source (Figure 6).

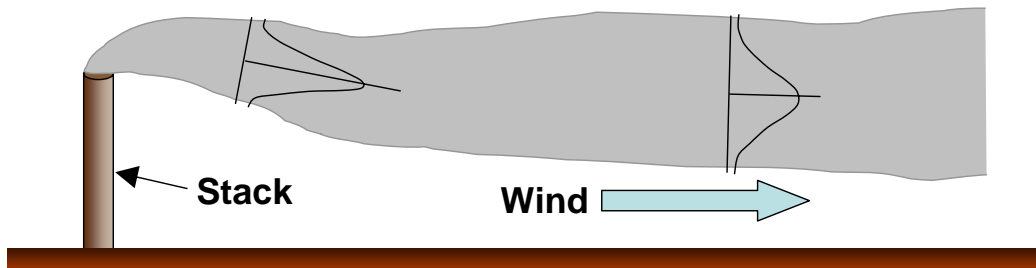


Figure 6. A Gaussian plume model assumes a Gaussian distribution of concentration across the plume.

The plume representation is valid for most cases near the source, where the plume is “pristine” or untouched by other effects, and is expanding only by diffusion. However, the planetary boundary layer (PBL), where most plumes originate, provides a very complex environment in which the plume can be moved around in many ways. Thermals in the PBL can cause entrainment and detrainment to the plume. Once the plume expands enough to touch the ground, some effects (such as ground reflection) have to be taken into account. Other complexities include plume splitting by geographical features such as hills or dynamical features such as eddies. In order to better represent the plume, researchers came up with the puff model in which the plume is considered as a collection of discrete puffs, with each puff having Gaussian attributes (Figure 7).

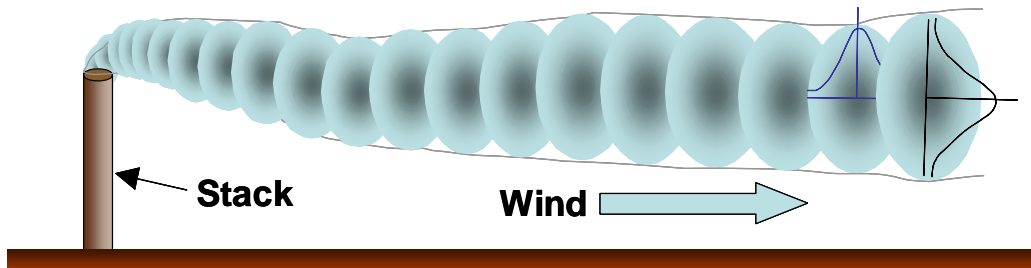


Figure 7. A Gaussian puff model characterizes the plume as a collection of discrete puffs, each displaying a Gaussian distribution of concentration.

The OMEGA model has an embedded Lagrangian plume model which has been used to simulate many plumes. One example is seen in Figure 5, which shows the

simulation of the Mt. Etna eruption of 2002. Figure 8 shows the simulation of a Saharan dust storm compared with the corresponding satellite imagery.

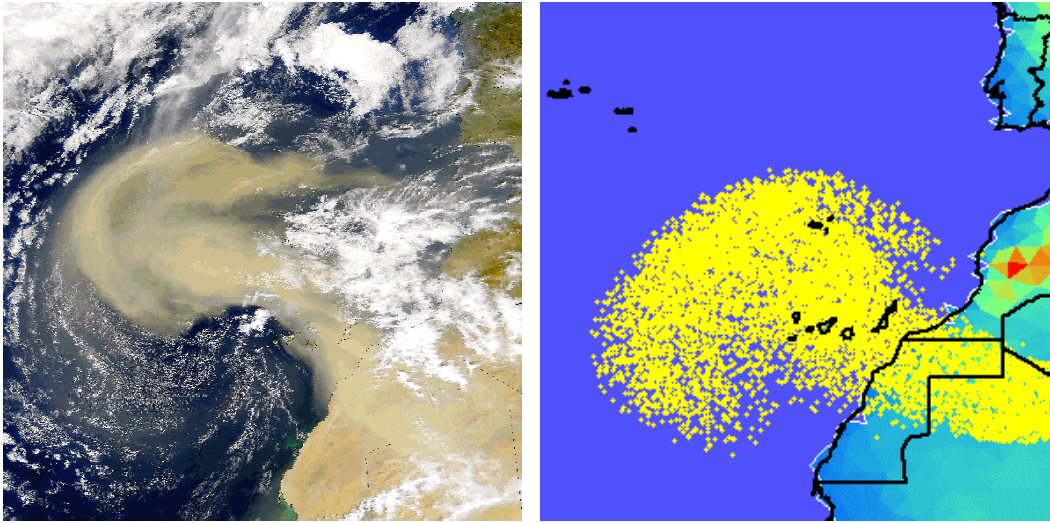


Figure 8. Simulation of a Saharan dust storm using OMEGA's embedded dispersion model. The yellow dots on the right hand panel represent the centroids of the puffs that constitute the plume. The left hand panel shows a satellite image of the storm.

4 Dynamical and Thermodynamical Processes

The processes that directly affect the state of the atmosphere at any given time can be broadly classified into two: 1) dynamic processes that determine the movement of air and 2) thermodynamic processes that control the transfer of thermal energy. The equations that make up a model are basically equations that describe these processes. They represent the behavior of the variables describing the state of the atmosphere.

4.1 Atmospheric Variables

Atmospheric variables can be classified into three broad classes: 1) variables representing the current state of an air parcel, known as the state variables; 2) variables representing the motion of air, or dynamic variables; and 3) variables describing the airborne constituents. The state variables include density, temperature and pressure. The dynamic variables include momentum (or velocities) and turbulent kinetic energy (in models that use high-order turbulence parameterizations). Airborne constituents are usually represented by their concentration (mass per unit volume) or mixing ratio (mass per unit mass of dry air).

4.2 Fundamental Equations

The equations that govern the circulations in the atmosphere are derived from the fundamental physical processes that are involved. For example, all of the advection and diffusion equations can be derived from Newton's equation of Motion and the laws of thermodynamics as explained in the following paragraphs.

4.3 Advection

Advection is the term used to refer to the process of transport of a material in the fluid flow solely due to the fluid's point-to-point movement. In Equation 3, the term $V \cdot \nabla Q$ refers to the local change in the concentration of the quantity Q due to advection. All predictive non-steady models at a minimum solve this equation.

4.4 Turbulent Diffusion

Turbulent diffusion refers to the seemingly random motions of air that occur in small scales. They are caused by processes ranging from molecular diffusion due to Brownian motion to eddy diffusion as eddies are generated by either velocity shear or buoyancy driven circulations. This is a very complex and challenging process to model. Representing these processes explicitly in a model requires very high spatial and temporal resolution, which will make the model unsuitable for forecasting. Most models resort to parameterizations to describe these processes. Turbulent diffusion plays a very important role in defining PBL, which is defined as the layer of the atmosphere closest to the Earth's surface that is dominated by the effects of the terrain surface. Processes in the PBL will be discussed in a subsequent section. Outside the PBL, turbulent diffusion is seen in boundaries between high-speed atmospheric layers in which waves are generated that break in a manner similar to ocean waves. Such waves can also be initiated downstream from high mountain ridges as air streams across them. These regions pose great danger in the form of clear air turbulence (CAT) to aircraft.

5 Physics Parameterizations

As mentioned earlier, the atmosphere undergoes a variety of physical processes ranging from the large-scale very-nearly steady influx of solar radiation to the rapidly changing turbulent eddy processes. For the accurate prediction of the atmosphere, it is necessary to accurately represent these processes. In most cases, explicitly representing these processes from first principles become numerically expensive. Hence, it is customary to simplify those equations using empirical relationships derived from field and laboratory experiments. Several parameters exist for the same processes. Most prognostic models differ in the type of parameterizations and the manner in which they are applied. Some of these processes and their parameterizations are discussed in the following sections.

5.1 Cloud Microphysics

Cloud microphysics refers to the collection of processes that define the water cycle, with an emphasis on the evolution of clouds and precipitation. Water is very unique in the sense that it can occur in the atmosphere in all three of its phases concurrently. Also, the phase changes exchange significant thermal energy with the ambient air. Most models will classify the water substance into several categories: water vapor, cloud droplets (non-precipitating), rain, ice crystals (non-precipitating), snow, and sometimes hail. However, models will differ in how each of these categories is represented. For example, some models treat each category in bulk as a total mass in each grid volume, while others will specify detailed distribution functions. Some models represent cloud ice (ice crystals) as a single species type in which the average size and number can vary with time. Other models will solve conservation equations for various ice crystal types – needles, plates, stellar crystals as well as hybrid shapes. Even though there are several cloud microphysics schemes in use, for purposes of discussion in this chapter, we will confine to the parameterization proposed by Lin *et al.* (1983).

Figure 11 shows a typical cloud microphysical scheme used in mesoscale models. This scheme is a bulk-water scheme and is derived from one that was suggested by Lin *et al.* (1983), which also included hail growth and associated processes. In this scheme, the cloud droplets and ice crystals are assumed to be monodispersed and non-precipitating. Marshall and Palmer (1948) type relationships are used in describing size distributions of raindrops and snow crystals. These are given as:

$$N(d_R) = N_{0R} \exp\left(-\frac{d_R}{\Lambda_R}\right)$$

and

$$N(d_S) = N_{0S} \exp\left(-\frac{d_S}{\Lambda_S}\right)$$
(5)

where $N(d)$ is number concentration at diameter d , and d_R and d_S are the particle diameters for rain and snow respectively. N_{0R} and N_{0S} are the y-intercepts of the distribution of rain and snow, and hence, represent the limiting number concentration as diameter tends to zero. Λ_R and Λ_S represent the slope of the respective inverse-exponential distribution.

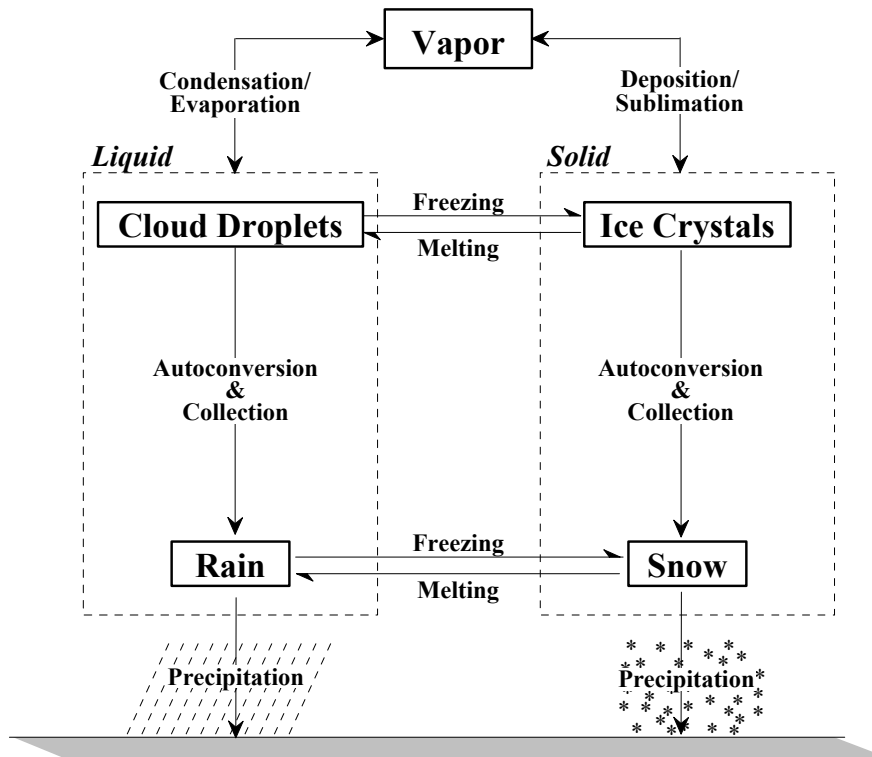


Figure 9. A conceptual layout of a microphysics scheme derived from the scheme developed by Lin *et al.* (1983).

This scheme includes processes driven by phase changes of water (condensation, evaporation, deposition, sublimation, freezing and melting) as well as processes driven by collection (autoconversion, and sweepout collection). These processes are explained in the following paragraphs.

Condensation / Evaporation: Water vapor condenses when the ambient vapor pressure exceeds the saturation vapor pressure at the ambient temperature. Saturation vapor pressure is represented by the Clausius-Clapeyron equation, which relates saturation vapor pressure to the ambient temperature.

$$\frac{de_s}{dT} = \frac{Le_s}{R_v T^2} \quad (6)$$

where e_s is the saturation vapor pressure of water, T is the temperature, L the latent heat of vaporization, and R_v the gas constant for water vapor. This equation represents the equilibrium condition for a system consisting of vapor and bulk liquid. Small water droplets exhibit strong surface tension forces that provide a “free energy barrier” between the droplets and the surrounding moist air. This means that for condensation to occur, the vapor pressure will have to significantly exceed that of saturation equilibrium so as to break the free energy barrier. In a pristine environment, water vapor will start condensing only when the relative humidity (the ratio of the actual vapor pressure to its saturated value) exceeds

well over hundred percent (supersaturated conditions). However, in the actual atmosphere, condensation can occur at significantly lower supersaturated condition due to the presence of small aerosol particles known as cloud condensation nuclei (CCN). These nuclei provide a mechanism to overcome the free energy barrier as water molecules can more readily attach themselves to surface of these particles. This process is called nucleation. The effectiveness of a particle as a CCN is dependent on its chemical and crystalline properties.

William Thomson (1870) and later Lord Kelvin investigated the effects of the curvature of a water surface on the saturation vapor pressure deriving the following equation:

$$e_s(r) = e_s \exp\left(\frac{2\sigma}{rR_v\rho_L T}\right) \quad (7)$$

where $e_s(r)$ is the saturation vapor pressure over the surface of a droplet with radius r , e_s is the saturation over a planar surface, σ is the surface tension, and ρ_L is the density of the liquid making up the droplet.

Another important relationship is derived from Raoult's law, which relates the reduction in vapor pressure to the amount of a solute dissolved in a liquid.

$$e' = e_s \left(1 - \frac{b}{r^3}\right) \quad (8)$$

where $b = (3im_v M)/(4\pi\rho_L m_s)$ in which m_v and m_s denote the molecular weights of water vapor and the solute, i is the degree of ionic dissociation, and M is the total mass of the solute in solution. Combining (6) and (7) yields a good approximation to the saturation vapor pressure over a solution droplet:

$$e'_s = e_s \left(1 + \frac{a}{r} - \frac{b}{r^3}\right) \quad (9)$$

where $a = \frac{2\sigma}{\rho_L R_v T}$.

When the actual vapor pressure exceeds the saturation vapor pressure, condensation occurs. However, during this process, latent heat of vaporization is released, increasing the temperature of the environment, which in turn increases the saturation vapor pressure. This feedback loop has to be correctly included in models as they use finite time steps.

The condensation adjustment equation can be derived by considering a closed volume of moist air. If supersaturation exists, the excess water vapor will start to

condense. As condensation proceeds, latent heat of vaporization is released, increasing the temperature and hence, the saturation vapor pressure of air. Thus, the initial water vapor excess ΔQ_V is used not only for condensation, but also for the increase in vapor capacity of the air. Let ΔQ_1 and ΔQ_2 denote the amount of water vapor condensed and the amount of extra vapor the air can hold due to the increase in temperature such that the total ΔQ is given by:

$$\Delta Q = \Delta Q_1 + \Delta Q_2 \quad (10)$$

The increase in temperature ΔT due to the release in latent heat when ΔQ_1 vapor is condensed is:

$$\Delta T = \frac{L_v \Delta Q_1}{c_p} \quad (11)$$

This increase in temperature increases the saturation vapor pressure as given by the Clausius-Clapeyron in Equation 5. In an isobaric process, we assume that in each grid cell the pressure does not change during the microphysical adjustments such that,

$$\frac{dQ_{sv}}{Q_{sv}} = \frac{de_s}{e_s} \quad (12)$$

Hence,

$$\Delta Q_2 = Q_{sv} \frac{L_v \Delta T}{R_v T^2} = \frac{L_v^2 Q_{sv} \Delta Q_1}{c_p R_v T^2} \quad (13)$$

Define a fraction r such that $\Delta Q_1 = r \Delta Q$. Then,

$$r = \frac{\Delta Q_1}{\Delta Q} = \frac{\Delta Q_1}{\Delta Q_1 + \Delta Q_2} = \Delta Q_1 \left\{ \Delta Q_1 + \frac{L_v^2 Q_{sv} \Delta Q_1}{c_p R_v T^2} \right\}^{-1} = \left\{ 1 + \frac{L_v^2 Q_{sv}}{c_p R_v T^2} \right\}^{-1} \quad (14)$$

Thus, the amount of water vapor to be condensed (or the maximum amount of cloud water that can be evaporated) can be written as

$$\Delta Q_{CCND} = r \Delta Q = \frac{Q_v - Q_{sv}}{1 + \frac{L_v^2 Q_{sv}}{c_p R_v T^2}} \quad (15)$$

Raindrops evaporate in sub-saturated conditions if enough cloud droplets are not present to alleviate the saturation deficit. The smaller cloud droplets are allowed to evaporate first as the saturation vapor pressure over a curved surface with

smaller radius of curvature is higher than over a surface with larger radius of curvature. Also, if the environment is supersaturated, vapor can condense onto the raindrops. The following expression takes into account the ventilation effect of the falling raindrop:

$$P_{RCND} = \frac{2\pi(Q_v - Q_{vs})N_{0R}\Lambda_R^2 \left(1 + 0.3194027N_{Sc}^{1/3} \sqrt{\frac{\Lambda_R W_R}{v_m}}\right)}{Q_{vs} \frac{L_v \rho}{k_T T} \left(\frac{L_v}{R_v T} - 1\right) + \frac{1}{D_v}} \quad (16)$$

where N_{Sc} is the Schmidt number, W_R is the fall velocity of raindrops, v_m is the molecular viscosity of air, k_T is the thermal conductivity of air, and D_v is the diffusivity of water vapor in air.

Deposition / Sublimation: A similar process leads to the formation of ice crystals on particulates called ice nuclei (IN). The maximum ice mixing ratio that can be generated by depositional growth, driven by the supersaturation, can be derived in a manner analogous to the condensation adjustment (Equation 15) by replacing L_v with L_s and Q_{vs} with Q_{si} . Thus,

$$\Delta Q_{I2} = \frac{Q_v - Q_{si}}{1 + \frac{L_s^2 Q_{si}}{c_p R_v T^2}} \quad (17)$$

However, this quantity has to be limited by the growth that is possible on the available number of ice nuclei.

The deposition onto (or sublimation of) snow is calculated in a manner similar to condensation on (or evaporation of) raindrops. The following formulation also takes into account the ventilation factor of falling snow:

$$P_{SDEP} = \frac{2\pi(Q_v - Q_{si})N_{0S}\Lambda_S^2 \left(0.86 + 0.21N_{Sc}^{1/3} \sqrt{\frac{\pi\Lambda_S W_S}{v_m}}\right)}{Q_{si} \frac{L_v \rho}{k_T T} \left(\frac{L_s}{R_v T} - 1\right) + \frac{1}{D_v}} \quad (18)$$

Freezing / Melting: These processes relate to the phase change between liquid and solid, and they are less complex than the other two processes discussed so far. Even though bulk water freezes at 0°C, water droplets in a cloud do not freeze until much lower temperatures are reached. The actual freezing temperature depends on impurities that are present in the drops. Pure water drops suspended in air will not freeze until -40°C. Melting, however, happens at 0°C.

Autoconversion: Autoconversion refers to a stochastic process by which a field of uniformly sized droplets/ice crystals may interact and collect to make larger drops/snow flakes that can precipitate. In most models, this is based on empirical formulations derived from observational data. Observations in clouds show that cloud droplet or ice-crystal mixing ratios rarely exceed certain thresholds, and above this threshold, precipitating hydrometeors (raindrops and snow) are seen. Even though most models assume the cloud droplets to be monodisperse, in reality, they exist in all sizes (small of course). They undergo inter-particle collisions and coalesce to form larger droplets or rain drops. This stochastic process of self-collection and growth to form rain is termed autoconversion. The rate of production of rain from cloud droplets via autoconversion, P_{RACV} , is given by (Berry and Reinhardt, 1974a and 1974b):

$$P_{RACV} = 7.26 \times 10^{-3} \left[10^{20} \left(\frac{\sigma}{0.38} \right) r_c^4 - 0.4 \right] \rho Q_C^2 \left[\left(\frac{\sigma_C}{0.38} \right)^{1/3} r_c 10^6 - 7.5 \right] \quad (19)$$

where $r_c = \left(\frac{3\rho Q_C}{4\pi N_C \delta_w} \right)^{1/3}$ is the mean cloud droplet radius, σ_C is the dispersion coefficient of the cloud droplet distribution, and, N_C the cloud condensation nuclei (CCN) concentration.

Cloud ice conversion to snow (via stochastic collection or autoconversion) occurs when the cloud ice mixing ratio exceeds a threshold Q_{IMAX} . A fraction of extra cloud ice is converted to snow according to the formula:

$$P_{SRCV} = (Q_I - Q_{IMAX}) E_{SCI} \frac{1}{\Delta t} \quad (20)$$

where E_{SCI} is the collection efficiency of snow for ice crystals given by:

$$E_{SCI} = \exp(0.03(T - T_m)) \quad (21)$$

where T_m is the melting temperature (0°C). Q_{IMAX} is usually set equal to 1×10^{-3} Kg/Kg.

Collection: Collection refers to the processes by which a large hydrometeor sweeps up smaller hydrometeors as it falls through the cloud.

Raindrops collect cloud droplets as the raindrops have a much higher fall speed than the cloud droplets. The collection efficiency is a function of the size of cloud droplets. Large droplets will have a collection efficiency of zero. The

production rate due to this collection mechanism is a high collection efficiency, whereas the very small droplets will flow around the raindrop is

$$P_{RAC} = \frac{15\pi}{38} \Lambda_R^3 N_{0R} W_R Q_C E_{RCD} \quad (22)$$

where E_{RCD} is computed from a polynomial fit to experimental data (Proctor, 1987) given by:

$$E_{RCD} = \begin{cases} 0 & \text{if } r_c < 1.2\mu\text{m} \\ \left. \begin{aligned} -0.27544 + 0.26249 \times 10^6 r_c \\ -1.8896 \times 10^{10} r_c^2 + 4.4626 \times 10^{14} r_c^3 \end{aligned} \right\} & \text{if } 1.2\mu\text{m} \leq r_c < 20\mu\text{m} \\ 1 & \text{if } 20\mu\text{m} < r_c \end{cases} \quad (23)$$

Just as raindrops collect cloud droplets by virtue of their difference in slip velocity, snowflakes collect ice crystals.

5.2 Convection

Convection is the process by which air moves upward due to the buoyancy forces. This upward motion cools the air adiabatically and can become saturated in the process, resulting in convective/cumulus clouds. The release of latent heat, associated with the condensation and deposition processes that occur, adds extra buoyancy which generates accelerating updrafts. Convection poses specific challenges to a numerical model. First, convection happens over relatively small scales, $O(1-10\text{km})$. This forces the models to resort to very small grid spacing if the convection is to be resolved more accurately. Second, the high-speed updrafts impose severe limitations on the time step of integration. Most mesoscale and regional-scale models use convective parameterizations to grossly represent the effects of the sub-grid scale convective clouds on the larger scale circulations. There are various convective parameterizations with varying complexities. Two commonly-used schemes, the Kuo scheme (Kuo, 1965 and 1974) and Kain-Fritsch (1990) scheme, are depicted in Figure 11.

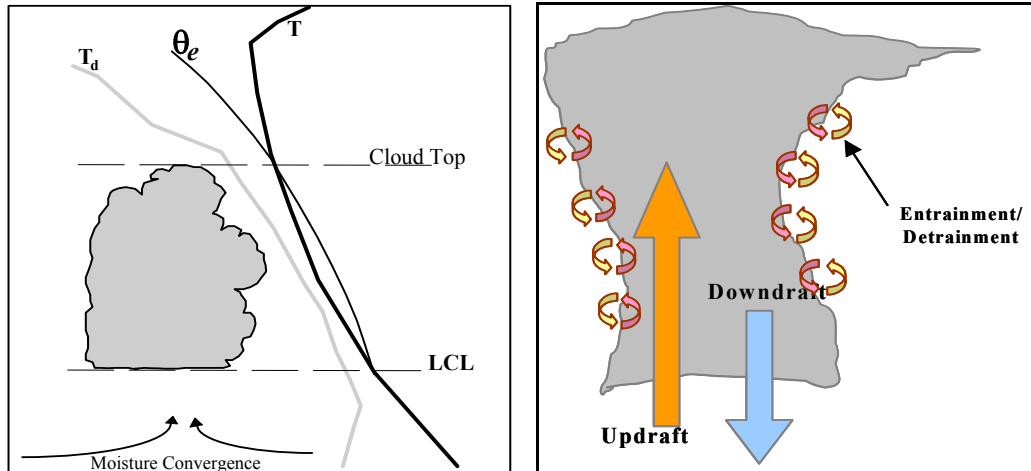


Figure 10. These diagrams depict conceptually two popular convective parameterization schemes. The left-hand panel represents the Kuo scheme in which the convective fluxes are calculated based on the low-level moisture convergence and the atmospheric stability. The right-hand panel depicts the Kain-Fritsch scheme where the strengths of updrafts and downdrafts, as well as entrainment along cloud edges are considered.

Other popular cumulus parameterization schemes include:

- 1) The Arakawa-Schubert parameterization, which assumes an ensemble of cumulus elements with the convection controlled by the buoyancy forces evaluated at grid-scale (Arakawa and Schubert, 1974).
- 2) The Betts-Miller scheme (Betts, 1986; Betts and Miller, 1986) uses a mixing line model which performs well over tropical oceans and in coarse grids.
- 3) The Anthes-Kuo parameterization is a modification of the Kuo scheme. An empirical heating and moistening profile has been added by Anthes (1977).
- 4) The Fritsch-Chappell scheme (Fritsch and Chappell, 1980) is a forerunner of the Kain-Fritsch scheme shown in Figure 5.
- 5) The Grell scheme (Grell et al., 1991; Grell, 1993) uses a closure on the Convective Available Potential Energy (CAPE) as in the Kain-Fritsch scheme. It does not allow for direct mixing with the environment via entrainment.

Pielke (2002) discusses these schemes in more detail.

5.2.1 Implementation of Convective Parameterization

Since convective parameterization is scale specific, particular attention has to be paid in its implementation, based on the typical spatial scales of the numerical model. For example, if the model is of sufficient resolution to be able to simulate convection at its coarsest levels, including a convective scheme will in effect double-count the energy and water vapor distributed via the convective scheme.

To circumvent this problem, nested-grid models selectively activate or deactivate the convective parameterization based on the grid scale; the cumulus scheme is kept active only in the coarse-resolution grids (usually with grid size > 10 km). In the high-resolution grids, only the explicit microphysics is kept active. This poses some interesting questions on implementation on variable-resolution (multiscale) models such as OMEGA, which is discussed in Section 2.4. In the grid cells larger than a few kilometers, convection is truly sub-gridscale, and in cells with size less than a kilometer, bulk of the convection may be explicitly captured. One would desire a behavior that smoothly varies from full impact of the convective parameterization at coarse-resolution to no impact at the high-resolution part of the grid. This is achieved in OMEGA by using a scale factor, f_c , to the cumulus contribution that is based on the cell area computed as follows:

$$f_c = \min\left(\frac{A}{A_c}, 1\right) \quad (24)$$

where A_c is a threshold cell area, which is set to 10 km^2 in OMEGA. This implementation appears to produce fairly accurate precipitation amounts in cumulus dominated systems such as hurricanes. Figure 11 shows a comparison of storm-total precipitation from Hurricane Floyd as predicted by OMEGA to the observed values.

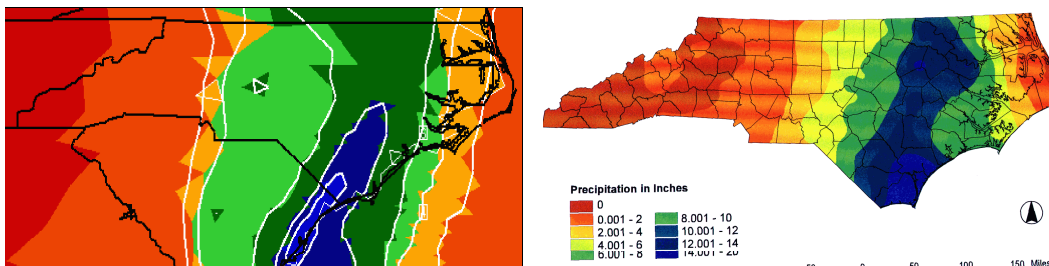


Figure 11 - Comparison of OMEGA forecast storm-total precipitation (left) with the observed precipitation field (right). Figure courtesy of Dr. Sethuraman, of North Carolina State University.

5.3 Planetary Boundary Layer

The Planetary Boundary Layer (PBL) is the layer closest to the surface of the Earth, which is directly impacted by the effects of the terrain. The thickness of this layer is not constant in space and time. It is, in general, shallow over homogeneous and water surfaces, and thicker over rough and land surfaces. The dynamics within the PBL is controlled by convective and turbulent processes, which in turn are controlled by the frictional forces and the thermal (sensible) and water vapor (latent heat) fluxes at the surface.

The effects of the PBL can be incorporated into a mesoscale model in two ways. One way is to parameterize the entire PBL as one layer. This involves identifying

and relating unresolved processes in the PBL with resolvable ones. The complexity of this single-layer PBL parameterization lies in the variety and interdependence of atmospheric processes acting on different scales. The second approach is to include several computational levels in the PBL in order to resolve the boundary layer structure effectively and explicitly. Such multi-level PBL formulations require near-surface turbulent fluxes of momentum, heat, and moisture within the PBL. Thus, they require some type of closure scheme to relate turbulent fluxes to mean quantities.

5.4 Atmospheric Radiation

The fundamental source of energy for the atmospheric engine is the Sun. To understand atmospheric dynamics and physics, it is essential to have a good understanding of the energy transformations, starting with the incoming solar radiation. Solar radiation plays a crucial role in atmospheric chemistry by enabling and modulating several key reactions commonly grouped under the term photochemical reactions.

5.4.1 Radiation Parameterizations

Radiation parameterization poses several major challenges. Even though we have classified the radiation broadly into two (short wave and long wave), the absorptivity and emissivity parameters can vary considerably based on the wavelength and the composition of the medium. Scattering by intervening aerosol and gases, as well as the presence of clouds, make the problem intractable to be explicitly solved. Another problem is posed by the delicate balance between two large quantities – the incoming solar radiation and the outgoing terrestrial radiation. If the balance is not computed accurately, it can result in major errors in circulation, especially in models integrating over long time domains such as climate models.

Most mesoscale models use variants of the 2-stream radiation scheme (Zdunkowski et al., 1980; King and Harshvardhan, 1986). These methods calculate the radiation fluxes in the upward and downward directions separately. They differ from each other mostly in the methodology used to describe the scatter and diffusion of radiation at each level.

The radiative source-sink term in the conservation of energy relation can be written as

$$S_R = \left(\frac{\partial T}{\partial t} \right)_{LW} + \left(\frac{\partial T}{\partial t} \right)_{SW} \quad (25)$$

where the terms on the right hand side represent the temperature change resulting from longwave and shortwave radiative divergence flux in the vertical direction.

The divergence of radiative energy in the horizontal direction is neglected, since its variation is much larger in the vertical direction on the mesoscale. The methods of parameterizing this vertical flux take into account the absorption of shortwave radiation by water vapor and the longwave energy emitted by water vapor and carbon dioxide. This is essentially similar to the one used by Mahrer and Pielke (1977). Because of the separation of wavelength in the atmospheric radiation spectra, it is convenient to develop separate parameterizations for long and short wavelengths.

5.4.2 Incoming Solar Short Wave Radiation

The Earth-Atmosphere system receives a total of 1380 W/m^2 of solar energy at the top of the atmosphere. This quantity is relatively constant and is termed as *solar constant*. There are several processes that take part in the energy budget that redistribute the energy received from the Sun. The following lists some of those in an aggregate sense.

Of the total 1380 W/m^2 of short wave radiation reaching the top of the atmosphere from the Sun,

- 17% is absorbed by the atmosphere,
- 44% reaches the surface (20% directly and 24% through clouds), with 4% being reflected back,
- 20% is absorbed by the surface,
- 20% is reflected by clouds,
- 3% is absorbed by clouds, and
- 6% is scattered by the atmosphere back to space, with an equal amount scattered towards the ground.

Thus, a total of 30% is reflected back to space, the atmosphere absorbs 20% and 50% is absorbed by the Earth's surface. Of course, this is an aggregated scenario; local situations can be different.

The diurnal variation of the solar flux on a horizontal surface at the top of the atmosphere is computed from

$$S = S_0 \cos Z \quad (26)$$

with

$$\cos Z = \cos \psi \cos \delta \cos H + \sin \psi \sin \delta \quad (27)$$

where S_0 is the solar constant, Z the zenith angle, ψ the latitude, δ the solar declination (a function of Julian day), and H the solar hour angle. Assuming that shortwave absorption in the atmosphere is only due to water vapor, the heating of the atmosphere by this radiation is then given by:

$$\left(\frac{\partial T}{\partial t}\right)_s = \begin{cases} 0.231 \frac{S_0 \cos Z}{\rho C_p} \left[\frac{r(z)}{\cos Z} \right]^{-0.7} \frac{dr}{dz}, & \cos Z > 0 \\ 0, & \cos Z \leq 0 \end{cases} \quad (28)$$

where $r(z)$ is the optical path length of water vapor above the layer z and is given by:

$$r(z) = \int_z^{top} \rho q dz \quad (29)$$

5.4.3 Outgoing Terrestrial Long Wave Radiation

The Earth's surface and the atmosphere emit radiation primarily in the infrared part of the spectrum. This is termed long wave radiation to differentiate it from the short wave radiation from the Sun. Some of the radiation emitted by the surface is absorbed by atmospheric components such as carbon dioxide (CO₂) and water vapor. Clouds also play a major role as they reflect back a good portion of the outbound radiation. Other factors that affect the radiant energy budget include aerosols and greenhouse gases (e.g., methane).

The parameterization of the long wave radiative flux in atmospheric models is typically treated as a function of the normal optical thickness, which when integrated over all wavelengths is represented by the broadband emissivity, ϵ . In clear or cloudy air, this emissivity is dominated by the water content of the air. Water vapor and carbon dioxide are considered as emitters of long wave radiation. The path length for water vapor (Δr_j) expressed in units of g cm⁻² is computed for each vertical layer by:

$$\Delta r_j = \rho_j q_j (z_{j+1} - z_j) = -\frac{(P_{j+1} - P_j)}{g} q_j \quad (30)$$

and the path length for carbon dioxide (Δc_j) expressed in units of millibars is

$$\Delta c_j = 0.4248329(P_{j+1} - P_j) \quad (31)$$

After these increments are obtained, they are summed up from the first level to the i^{th} level to give the total path length as follows:

$$r_{i+1} = \sum_{j=1}^i \Delta r_j \quad \text{and} \quad c_{i+1} = \sum_{j=1}^i \Delta c_j \quad (32)$$

where $r_1 = c_1 = 0$ at the surface. The emissivity for water vapor was derived from data in Kuhn (1963) and is given in Jacobs *et al.* (1974) by

$$\varepsilon_r(i, j) = \begin{cases} 0.113 \log_{10}(1 + 12.63\bar{r}) & \text{if } \log_{10} \bar{r} \leq -4 \\ 0.104 \log_{10} \bar{r} + 0.440 & \text{if } -4 < \log_{10} \bar{r} \leq -3 \\ 0.121 \log_{10} \bar{r} + 0.491 & \text{if } -3 < \log_{10} \bar{r} \leq -1.5 \\ 0.146 \log_{10} \bar{r} + 0.527 & \text{if } -1.5 < \log_{10} \bar{r} \leq -1.0 \\ 0.161 \log_{10} \bar{r} + 0.542 & \text{if } -1.0 < \log_{10} \bar{r} \leq 0 \\ 0.136 \log_{10} \bar{r} + 0.542 & \text{if } 0 < \log_{10} \bar{r} \end{cases} \quad (33)$$

where $\bar{r} = |r_i - r_j|$ is the optical path length between the i^{th} and j^{th} level. The emissivity function for carbon dioxide is given by Kondratyev (1969) as

$$\varepsilon_{CO_2}(i, j) = 0.185 \left[1 - \exp\left(-0.3919 |c_i - c_j|^{0.4}\right) \right] \quad (34)$$

Total emissivity for each depth between level i and level j is then given by

$$\varepsilon(i, j) = \varepsilon_r(i, j) + \varepsilon_{CO_2}(i, j) \quad (35)$$

The downward and upward radiative fluxes at level N can be computed using the above emissivity functions as

$$R \downarrow(N) = \sum_{j=N}^{top-1} \frac{\sigma}{2} (T_{j+1}^4 + T_j^4) [\varepsilon(N, j+1) - \varepsilon(N, j)] + \sigma T_{top}^4 [1 - \varepsilon(N, top)] \quad (36)$$

and

$$R \uparrow(N) = \sum_{j=1}^{n-1} \frac{\sigma}{2} (T_{j+1}^4 + T_j^4) [\varepsilon(N, j) - \varepsilon(N, j+1)] + \sigma T_G^4 [1 - \varepsilon(N, 1)] \quad (37)$$

where T_G and T_{top} are the temperatures at the ground level and model top, respectively and σ is the Stefan-Boltzman constant. Thus, the radiative cooling at each level N , except the ground level, is computed as

$$\left(\frac{\partial T}{\partial t} \right)_{LW} = \frac{1}{\rho C_p} \frac{[R \uparrow(N+1) - R \uparrow(N) + R \downarrow(N) - R \downarrow(N+1)]}{z(N+1) - z(N)} \quad (38)$$

where LW denotes the longwave radiation and z is the height.

Without simplification, radiative transfer is computationally expensive. Sasamori's technique (1972), which assumes an isothermal atmosphere for radiative transfer, simplifies the computing procedure. After this simplification,

the temperature change resulting from long wave radiative flux divergence at each level N is computed as

$$\left(\frac{\partial T}{\partial t}\right)_{LW} = \frac{1}{\rho C_p} \frac{(\sigma T_N^4 - \sigma T_G^4)[\varepsilon(N+1,1) - \varepsilon(N,1)] + (\sigma T_{top}^4 - \sigma T_N^4)[\varepsilon(N+1,top) - \varepsilon(N,top)]}{z(N+1) - z(N)} \quad (39)$$

6 Model Numerics

Model numerics represent the equations in the model's discretized domain. The discretization process involves the conversion of the continuous conservation equations into piecewise linear set of discrete representations. This happens in space (solving and computing gradients) as well as in time (solving the partial differential equations that form the prognostic equations).

6.1 Domain Discretization

Domain discretization methods depend very much on the complexity of the domain. The discretization can be separated functionally into two – spatial and time discretizations.

Spatial Discretization: A simple rectilinear box can be subdivided into a structured three-dimensional grid by sets of uniformly separated planes that are parallel to the sides of the domain. In fact, early cloud models used such a setting. Early mesoscale models also included the curvature of the Earth by changing the coordinate system such that one set of planes was parallel to the mean sea level. As models became more sophisticated, it was necessary to include detailed processes that involve the surface of the Earth and in which the altitude at each grid point is important so that the effects of terrain be included. This led to the development of terrain-following coordinate systems such as the sigma coordinates in which the vertical coordinate is represented as $\sigma_z = (z - z_0)/(z_T - z_0)$, where z_0 is the altitude of the surface and z_T is the altitude at the top of the model domain. This type of coordinate system is referred to as a sigma-Z system as it normalizes the altitude z . Other variations to this include sigma-P coordinate system, which uses a normalized pressure so that all calculations are done on pressure surfaces. This simplifies the calculation of processes involving the pressure gradient term, as the pressure gradient in the “horizontal” (along a pressure surface) is zero. However, this also poses a disadvantage as pressure surfaces can intersect with the terrain, thus introducing artificial boundaries and degenerate grid elements. Some models use a hybrid coordinate system in which a sigma-P system is used in the upper parts of the model domain (usually above the PBL) and a sigma-z system is used below that.

In the sigma coordinate system, all calculations depend on the accurate integration of a prognostic equation for the surface pressure.

In models such as OMEGA, the domain discretization is based upon an unstructured triangular grid. All integrations are performed using a finite volume calculation, which is somewhat immune to the choice of the coordinate system. In fact, that methodology allows one to choose a generic Cartesian system on a rotating frame of reference (cf. Figure 3). Bacon et al. (2003) provides a good discussion on the process of numerical integration on such a grid.

Temporal Discretization: Marching in time is performed by computing the rate of change of each prognostic variable at each instant in time, then calculating the difference from the last time step to the current time step. The rate of change over time in the variable Q , $\frac{\partial Q}{\partial t}$, is approximated by the expression $\frac{\Delta Q}{\Delta t}$. Hence one can write

$$Q^{new} = Q^{old} + \frac{\Delta Q}{\Delta t} \Delta t \quad (40)$$

where Q^{old} is the value of Q at the beginning of the time step and Q^{new} is the value at the end of the time step of duration Δt .

6.2 Computational Stability Considerations

The numerical models solve a set of finite difference equations, which are approximations to the partial differential equations. The approximate nature of these equations is due to the truncation of the Taylor series for the respective differentials. The truncation errors can accumulate in an unbounded manner depending on the numerical integration scheme chosen. In most cases, the error is directly linked to the local velocity, the spatial resolution and the time step used in the integration. The specific limits on time steps can be derived by performing an Eigen analysis on the numerical scheme employed. The occurrence of numerical instability can easily be demonstrated for the Euler method. Assume a differential equation of the form

$$\frac{dQ}{dt} = -AQ \quad (41)$$

Assume the function has a value of 1 at $x = 0$. This equation can be analytically integrated to yield

$$Q = \exp(-At) \quad (42)$$

which is a monotonically decreasing function for $A > 0$. For the Euler method, we choose a uniform time step, Δt . The original differential equation can be written as a finite difference equation,

$$\frac{\Delta Q}{\Delta t} = -AQ \quad \text{or} \quad \Delta Q = -A\Delta t Q \quad (43)$$

To evaluate the function at t_{n+1} (future state) from a known value at t_n (current state), one would calculate the change in Q , ΔQ , from the current state and compute $Q_{n+1} = Q_n + \Delta Q$. Thus,

$$\begin{aligned} Q_{n+1} &= Q_n - A\Delta t Q_n \\ &= (1 - A\Delta t)Q_n \end{aligned} \quad (44)$$

With $Q_0 = 1$, it is easily seen that $Q_n = (1 - A\Delta t)^n$. This is an oscillatory sequence in which the successive terms start increasing when $A\Delta t > 2$. Hence, if too large a time step is taken, the solution will become unstable.

7 Data Ingest

Atmospheric modeling is fundamentally an initial and boundary value problem. The fundamental equations are integrated with the constraint that the variables have known values at the initial time and also along the boundaries of the computational domain at all times. For the initial conditions, we depend on measurements of the key state variables. Ideally, the initial conditions should define the state of the atmosphere accurately at all points within the computational domain. This is impractical, if not impossible, to achieve and we have to be satisfied with a diverse set of measurements at a few finite points in space and time.

7.1 Data Types

The measured meteorological data can be broadly divided into two types: 1) in situ measurements and 2) remotely sensed measurements. In situ measurements, as the term implies, are measurements of the variables at the location of the measuring instrument. A thermometer, a pressure sensor, a wind-vane, and an anemometer are examples of in situ measurements. Remotely sensed measurements come from instruments that look into a region that is not collocated with them. These include systems like satellite based instruments, radars, sodars and lidars. In situ measurements are considered to constitute ground truth. Even though they have improved in accuracy over the years, remote measurements are still fraught with errors of various types.

7.2 Data Quality Control and Quality Assurance

Various types of data are needed to initialize and bound numerical models. Hence, the quality of data will directly impact the quality of model output. Errors in data come from various sources. First, it comes from the instrument errors. This manifests from the fundamental physical limitations of the instrument and from calibration errors. The second type of error is the data retrieval error. This is especially applicable for remote sensing platforms. For example, the most common remote sensing instrument is a radiometer, which actually measures the radiance of the atmospheric layer it sees. The radiances are then converted to temperature. The retrieval algorithms required for this process are only approximations.

7.3 Data Assimilation Techniques

The process of taking a set of data values to build a complete state of the atmosphere at a single point in time or during a time period is called data assimilation. The sparseness of atmospheric data makes it very challenging to build a three-dimensional state of the atmosphere only using the observations. Hence, it is an usual practice to start from a known state of the atmosphere at a time close to model initialization time and alter this first guess state based on the difference between the observations and corresponding first-guess values. This process has to include constraints based on fundamental physical principles. If these constraints are not met properly, the inclusion of the observations will only result in generating noise in the numerical modeling system.

The forecasts from a previous operational cycle can be used as the first guess. However, it should be noted that the data assimilation scheme would result in a more accurate analysis if the first guess field is as close to the analysis as possible. Data assimilation is a topic which has received lots of attention in the past two decades from various research organizations resulting in techniques of various complexities. These techniques include schemes such as 1) Optimum Interpolation, 2) Three-dimensional Variational Schemes, and 3) Four-dimensional Variational Schemes. A new class of assimilation technique receiving much attention by researchers is based on the ensemble approach.

8 Model Verification and Validation

Verification and validation are important steps in the development of any model. Verification refers to the process of checking whether a model indeed represents the relevant physics. Validation is the process by which the model results are checked for accuracy. Verification is usually performed during the model development. It also needs to be periodically performed to make sure that the processes that are supposed to be in a model are still included and have not been disabled for various testing and debugging procedures.

At times, model validation can be challenging. The greatest challenge in model validation is the disparity of the modeled variables and their observed counterpart. Most models output volume-averaged (averaged over a grid cell) values while most observations are point observations. However, it is important to note that some observations, as for some chemical species, may be single-point but time-averaged values.

9 Symbols

Δ	Change in a variable over a period of time
A_R	The slope of the inverse-exponential Marshall-Palmer size distribution for raindrops
A_S	The slope of the inverse-exponential Marshall-Palmer size distribution for snow
ν_m	Molecular viscosity of air
ρ	Density of air
ρ_L	Density of the liquid of a drop
ρ_w	Density of water
σ	Surface tension over a water drop
σ_C	Dispersion coefficient for cloud droplets
σ_Z	Sigma coordinate using altitude for reference
σ_P	Sigma coordinate using pressure for reference
c_p	Specific heat of air at constant pressure
d_R	Diameter of a raindrop
d_S	Equivalent diameter of a snow particle
D_v	Diffusivity of water vapor in air
e	Vapor pressure
e'	Vapor pressure over a solution
e_s	Saturation vapor pressure over a water surface.
E_{RCD}	Efficiency of raindrops collecting cloud droplets
E_{SCI}	Collection efficiency of ice crystals
k_T	Thermal conductivity of air
L	Latent heat
L_v	Latent heat of vaporization
L_f	Latent heat of freezing
L_s	Latent heat of sublimation
M	Mass of solute in a water drop or droplet
m_s	Molecular weight of the solute in a drop or droplet
m_v	Molecular weight of water vapor
N_{OR}	y-intercept of the inverse-exponential Marshall-Palmer size distribution for raindrops
N_{OS}	y-intercept of the inverse-exponential Marshall-Palmer size distribution for snow

N_C	Number concentration of CCN
N_{Sc}	Schmidt number
P	Pressure
P_{RAC}	Production rate of raindrops due to collection (accretion) of cloud droplets
P_{RACV}	Production rate of raindrops due to autoconversion of cloud droplets
P_{RCND}	Production rate of raindrops due to condensation/evaporation
P_{SACV}	Production rate of snow due to autoconversion of cloud ice
P_{SACI}	Production rate of snow due to collection of cloud ice
P_{SDEP}	Production rate of snow due to deposition/sublimation
Q	A generic variable
Q_I	Mixing ratio of cloud ice
Q_{IMAX}	Threshold maximum mixing ratio of cloud ice for autoconversion
Q_C	Mixing ratio of cloud droplets
Q_v	Mixing ratio of water vapor
Q_{vs}	Saturation mixing ratio of water vapor over a water surface
Q_{si}	Saturation mixing ratio of water vapor over an ice surface
r	Radius of a drop/droplet
R_v	Gas constant for water vapor
T	Temperature
t	Time
V	Velocity
W_R	Fall velocity of raindrops
W_S	Fall velocity of snow
z	Altitude, height
z_0	Altitude (MSL) at the surface of the Earth.
z_T	Altitude (MSL) at the top of a model domain.

10 List of Acronyms

CAPE	Convective Available Potential Energy
CAT	Clear Air Turbulence
CCN	Cloud Condensation Nuclei
CMAQ	Community Multiscale Air Quality model
COAMPS	Coupled Ocean Atmosphere Mesoscale Prediction System
CSU	Colorado State University
FNMOC	Fleet Numerical Meteorological and Oceanography Center
IN	Ice Nuclei
MM5	Mesoscale Model (Version 5)
MSL	Mean Sea Level
NCAR	National Center for Atmospheric Research
NCEP	National Centers for Environmental Prediction
NWP	Numerical Weather Prediction
OMEGA	Operational Multiscale Environment model with Grid Adaptivity
PBL	Planetary Boundary Layer
PDE	Partial Differential Equation

RAMS Regional Atmospheric Modeling System
 SMOKE Sparse Matrix Operator Kernel Emissions system
 WRF Weather Research and Forecast model

References

- Anthes, 1977. A cumulus parameterization scheme utilizing a one-dimensional cloud model. *Mon. Wea. Rev.*, **105**, 270-286.
- Arakawa, A., 1966. Computational design for long-term numerical integrations of the equations of atmospheric motion. *J. Comp. Phys.*, **1**, 119-143.
- Arakawa, A. and W.H. Schubert, 1974. Interaction of a cumulus cloud ensemble with the large-scale environment. Part I, *J. Atmos. Sci.*, **31**, 674-701.
- Bacon, D.P., N. Ahmad, Z. Boybeyi, T. Dunn, S.G. Gopalakrishnan, M.S. Hall, Y. Jin, P.C.S. Lee, D.E. Mays, A. Sarma, M.D. Turner, T.R. Wait, K.T. Waight III, S.H. Young, and J.W. Zack, 2003. Dynamically Adapting Unstructured Triangular Grids: A New Paradigm for Geophysical Fluid Dynamics Modeling, *Proc. of Indian Academy of Science*, 69, 457-471.
- Bacon, D.P., N.N. Ahmad, Z. Boybeyi, T.J. Dunn, M.S. Hall, P.C-S. Lee, R.A. Sarma, M.D. Turner, K.W. Waight, S.H. Young, and J.W. Zack, 2000. A Dynamically Adapting Weather and Dispersion Model: The Operational Multi-scale Environment model with Grid Adaptivity (OMEGA). *Mon. Wea. Rev.*, 128, 2044–2076.
- Baum, J.D. and R. Löhner, 1994. Numerical simulation of shock-elevated box interaction using an adaptive finite element shock capturing scheme. *AIAA Journal*, 32, 682-692.
- Berry, E.X. and R.L. Reinhardt, 1974a. An analysis of cloud drop growth by collection: Part I. Double distributions. *J. Atmos. Sci.*, **31**, 1814-1824.
- Berry, E.X. and R. L. Reinhardt, 1974b. An analysis of cloud drop growth by collection: Part II. Single initial distributions. *J. Atmos. Sci.*, **31**, 1825-1831.
- Betts, A.K., 1986. A new convective adjustment scheme. Part I: Observational and theoretical basis. *Quart. J. Roy. Meteor. Soc.*, **112**, 677-692.
- Betts, A.K. and M. J. Miller, 1986. A new convective adjustment scheme. Part II: Single column tests using GATE wave, BOMEX, ATEX, and Arctic air-mass data sets. *Quart. J. Roy. Meteor. Soc.*, **112**, 693-709.
- Byun, D.W. and J. K.S. Ching, 1999. Science algorithms of the EPA Models-3 Community Multiscale Air Quality (CMAQ) Modeling System, EPA Report EPA/600/R-99/030.
- Charney, J., 1948. On the scale of atmospheric motions. *Geophys. Publ.*, **17**, 17pp.
- Charney, J.G., R. Fjørtoft and J. von Neumann, 1950. Numerical integration of the barotropic vorticity equation. *Tellus*, **2**, 237-254.
- Fritsch, J.M. and C.F. Chappell, 1980. Numerical prediction of convectively driven mesoscale pressure systems. Part I: Convective Parameterization. *J. Atmos. Sci.*, **37**, 1722-1733.

- Grell, G.A., 1993. Prognostic evaluation of assumptions used by cumulus parameterizations. *Mon. Wea. Rev.*, **121**, 764-787.
- Grell, G.A., Y.-H. Kuo, and R. Pasch, 1991. Semi-prognostic test of cumulus parameterization schemes in middle latitudes. *Mon. Wea. Rev.*, **119**, 5-31.
- Kain, J.S. and J.M. Fritsch, 1990. A one-dimensional entraining/detraining plume model and its application in convective parameterization. *J. Atmos. Sci.*, **47**, 2784-2802.
- Kuo, H.L., 1965. On formation and intensification of tropical cyclones through latent heat release by cumulus convection. *J. Atmos. Sci.*, **22**, 40-63.
- Kuo, H.L., 1974. Further studies of the parameterization of the influence of cumulus on large scale flow. *J. Atmos. Sci.*, **31**, 1232-1240.
- Lin, Y.-L., R.D. Farley, and H.D. Orville, 1983. Bulk Parameterization of the Snow Field in a Cloud Model. *J. Appl. Meteor.*, **22**, 1065-1092.
- Marshall, J.S. and W.M. Palmer, 1948. The distribution of raindrops with size. *J. Meteor.*, **5**, 165-166.
- Mason, B.J., 1976. *Clouds, Rain and Rainmaking*, 2nd Edition, Cambridge Univ. Press, Cambridge, pp 189.
- Proctor, F.H., 1987: The Terminal Area Simulation System / Volume I: Theoretical Formulation, NASA Contractor Report 4046.
- Pruppacher, H.R. and J.D. Klett, 1997. *Microphysics of Clouds and Precipitation: An Introduction to Cloud Chemistry and Electricity*, 2nd Edition, Kluwer Academic Publishers, pp 976.
- Rogers, R.R., 1976: *A Short Course in Cloud Physics*, Pergamon Press, Oxford, pp 227.
- Sarma, A., N. Ahmad, D. Bacon, Z. Boybeyi, T. Dunn, M. Hall, and P. Lee, 1999. Application of adaptive grid refinement to plume modeling. In Air Pollution VII, WIT Press, Southampton, 59-68.
- Schnack, D.D., I. Lottati, Z. Mikic, and P. Satyanarayana, 1998. A finite-volume algorithm for three-dimensional magnetodynamics on an unstructured, adaptive grid in axially symmetric geometry. *J. Comp. Phys.*, **140**, 71-121.
- Thomson, W., 1870. *On the equilibrium of vapour at a curved surface of liquid*. Proc. Roy. Soc. Edinb., 63-68.
- Uccellini, L.W., 1975. A Case Study of Apparent Gravity Wave Initiation of Severe Convective Storms, *Monthly Weather Review*: **103**, 497-513.
- Young, K.C., 1993. *Microphysical Processes in Clouds*, Oxford University Press, New York, pp 427.

BRANK
P
e

McAlpine, J.D. and M. Ruby. 2008. *Computational Fluid Dynamics of Microscale Meteorological Flows for Air Quality Applications*. Chapter 5C of *AIR QUALITY MODELING - Theories, Methodologies, Computational Techniques, and Available Databases and Software*. Vol. III – *Special Issues* (P. Zannetti, Editor). Published by The EnviroComp Institute (<http://www.envirocomp.org/>) and the Air & Waste Management Association (<http://www.awma.org/>).

Chapter 5C

Computational Fluid Dynamics of Microscale Meteorological Flows for Air Quality Applications

J.D. McAlpine ⁽¹⁾ and Michael Ruby ⁽²⁾

⁽¹⁾ *Envirometrics, Inc., Seattle, Washington (USA)*

jdmcalpine@envirometrics.com

⁽²⁾ *Envirometrics, Inc., Seattle, Washington (USA)*

mruby@envirometrics.com

Abstract: There is an ever-increasing need to simulate airflow at the micro-meteorological scale for environmental applications. Dispersion of pollutants around buildings and pedestrian level wind-speeds are two applications that concern environmental planners. Wind tunnels are still the main tool used, but computational methods are becoming more popular as a way to address these issues. Computational Fluid Dynamics (CFD) simulations are being used more often to model the surface layer of the atmosphere for environmental application. The use of CFD in this field is still experimental in nature and inherent weaknesses are apparent, but advances in computing and simulation methods are continually driving it towards becoming a reliable tool for predicting local air quality and other environmental conditions.

This review addresses today's common method of simulating the atmospheric surface layer in an urban environment using CFD. The features of the surface layer that are important for flow modeling are discussed as well as different methods for applying them in CFD. Different turbulence models and techniques for simulating the surface layer in CFD are reviewed as well. Current guidelines and processes for conducting a project are also described and discussed.

This chapter is intended for environmental scientists or engineers as an overview of the basics of CFD and its application to the surface layer of the atmosphere so that one can know how to conduct or evaluate a CFD analysis for compliance with industry best practices.

Key Words: CFD, micrometeorology, air quality, atmosphere, surface layer, buildings, urban, turbulence, modeling, Computational Fluid Dynamics, K-epsilon, steady state flow, plume, pollution, guidelines, ERCOFTAC, QNET-CFD, dispersion, validation, Computational Wind Engineering, RNG, lab hood, stacks, airflow, Chen-Kim, Project EMU.

1 Introduction

Air quality modeling has become an important tool for environmental review. Gaussian dispersion models and puff models are now routinely used to model the dispersion of pollutants from industry and traffic as part of regulatory and voluntary efforts to ensure that we breathe healthy air. Air quality models are invaluable in their ability to help planners assess the likely environmental impacts from alternative configurations of sources.

Lately, there has been increasing interest in addressing air quality at the local scale, in and around homes and workplaces. Recent issues such as sick building syndrome, the carcinogenicity of diesel particulate matter, terrorist attacks using chemical or biological weapons, and accidental chemical spills have especially driven this interest. Air quality modeling of the dispersion of pollutants through the urban landscape is needed to study these issues.

Traditional air quality models such as the Industrial Source Complex-Short Term (ISCST3) model can not adequately handle dispersion around a building. The “PRIME” addition to these models has been applied to account for the influence of building wakes on pollutant concentrations downwind of buildings, but not concentrations on the building itself, such as at air intakes.

Atmospheric boundary layer wind tunnels have been the dominant tool for modeling the dispersion of exhaust at the local scale. The U.S. Environmental Protection Agency (EPA) has a set of standards for fluid modeling of the atmosphere that lends guidance for these efforts (Snyder, 1981), and it is today’s accepted method for local scale air quality and environmental analysis. Though proven and reliable, wind tunnel modeling can be expensive and time consuming, and thus unjustifiable for simpler studies. The number of installations available for wind tunnel modeling is also quite limited, with just a handful of commercial facilities available.

Computational Fluid Dynamics (CFD) shows promise as a tool for answering questions about local air quality in and around buildings by providing computerized simulation models. CFD works by solving the fundamental equations of motion using assumptions about local turbulence to obtain a steady-state or time-dependent airflow structure in a domain. Therefore, it is essentially a computerized, virtual wind tunnel.

For example, in a typical local-scale air quality project using CFD, one would first essentially “build” the domain of the project by assigning boundaries representing buildings, vegetation, pollutant sources, and other features. Second, additional boundary conditions would be assigned to represent air inlets and outlets to the domain, with careful attention to match incoming wind and turbulence profiles to a typical atmospheric condition. The domain is then “meshed”; that is, divided into a three dimensional grid of discrete volumes, as illustrated in Figure 1, that the CFD solver will use to compute changes in fluid motion through discrete finite difference calculations. After this, a field initialization would be prescribed. The CFD model solver is then run until a steady state solution is reached or for a set amount of time to an unsteady-state solution. The results would then be viewed in a graphical user interface for analysis. Wind vectors, plume paths, turbulent kinetic energy, and pollutant concentrations would be typical variables for exploration.

Modeling of flow around buildings is typically referred to as Computational Wind Engineering and covers several applications including pollutant dispersion, pedestrian wind evaluation, building wind loading, and snow loading. This chapter focuses primarily on the details of simulating the steady-state atmospheric surface layer in the CFD domain for the dispersion of pollutants in and around buildings.

This chapter is divided into four sections:

- Synopsis of CFD: the math, assumptions, and availability.
- Simulation of the atmosphere in CFD
- Application of the method and guidelines
- Verification and validation efforts

This chapter does not explore the mathematics behind CFD in depth, but rather, it is meant to help the environmental scientist or engineer understand the basics of CFD and its applications to the atmospheric boundary layer. It should provide sufficient information on the strengths and weaknesses of the method to allow a thorough review of a CFD project.

A more basic introduction to CFD modeling for air quality applications, with illustrations of example projects using CFD, has been provided previously by the authors (McAlpine and Ruby, 2004).

2 Synopsis of CFD: the Math, Assumptions, and Availability

To begin discussing the basics of CFD, we must first explore the nature of fluid flow, and thus, the basic equations of fluid motion as applied to the atmosphere. CFD works by solving the equations of motion using several assumptions about the local behavior of turbulence. First, in this section we will derive the equations

of motion and the turbulence terms that will make the solution possible. Then, we will explore the turbulence assumptions that are needed when solving the equations. We will discuss how CFD is set up to solve these equations, and finally, we will describe guidelines for modeling and validating a CFD code using a standard problem.

2.1 Equations of Motion

The basic equations of motion are applicable to any type of fluid flow, but we will focus on an atmospheric application of the equations in illustrating how CFD works. First, we will explore the fundamentals of what is happening at a point in a hypothetical two-dimensional atmosphere. We will consider a discrete volume of the atmospheric surface layer, as illustrated in Figure 1. The change in velocity across our volume will be influenced by several factors: 1) the local horizontal pressure gradient and the velocity of air entering our domain will influence our local velocity; 2) air above our volume will be moving at a higher velocity than the air below our volume since our volume is located in a horizontal wind that changes in the vertical with profile $U(z)$; and 3) diffusion of momentum into and out of our volume.

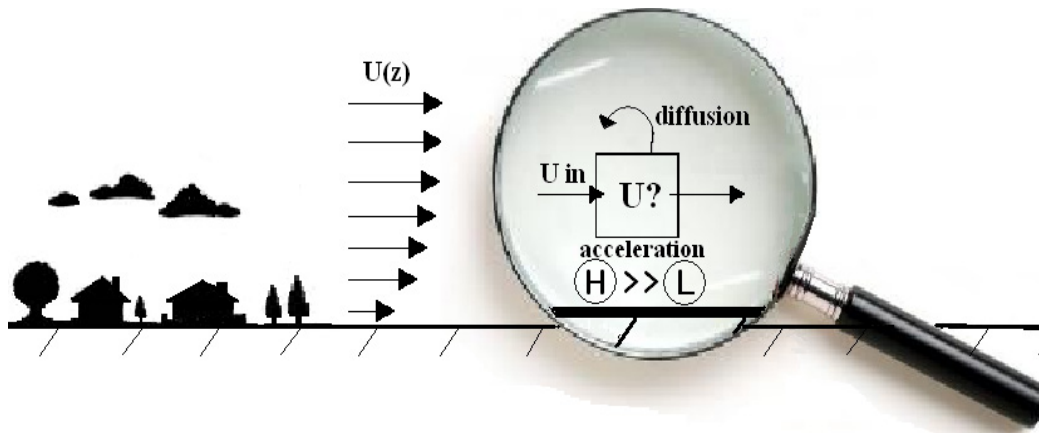


Figure 1. Examination of a volume of air in the atmospheric boundary layer of wind profile $U(z)$. The local change of velocity in our volume is dependent on the pressure gradient (represented in the graphic as Higher pressure going to Lower pressure) and transport of velocity through molecular and turbulent diffusion.

The higher velocity above and the slower velocity below, our volume will create stress that will force the kinetic energy in our volume to diffuse downward as turbulence. Similarly, turbulence will diffuse downward into our volume from above.

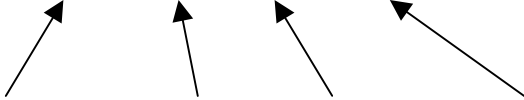
Since we are interested in modeling the velocity of wind flow in a discrete volume of the atmosphere, we need to establish equations of motion for the local change in velocity at this point. One of the more important features of our

atmospheric volume will be the difference in pressure in the horizontal due to local atmospheric weather systems.

This pressure difference is a force that results in advection of air and its velocity into our volume and an acceleration of the air mass, resulting in a change in velocity. Writing out the conservation of momentum equation for our volume, we have:

$$\begin{aligned} \text{Local change of velocity} = & \text{advection of velocity} + \text{turbulent diffusion of velocity} \\ & + \text{acceleration from pressure gradient} \end{aligned}$$

For the 2-D case, the equation for the u-component of velocity per unit density will be:

$$\frac{\partial \mathbf{u}}{\partial t} = -\mathbf{u} \frac{\partial \mathbf{u}}{\partial x} + \nu \frac{\partial^2 \mathbf{u}}{\partial z^2} - \frac{1}{\rho} \frac{\partial P}{\partial x} \quad (2.1)$$


Local change of velocity = advection + turbulent diffusion + acceleration

where \mathbf{u} is the velocity vector, P is the pressure, and ν is the sum of molecular and turbulent viscosity of air.

Conservation of mass comes into play through the continuity equation. Let us assume that in our hypothetical atmosphere the density variations are small enough to ignore. This is a good assumption for the neutral and stable atmospheric surface layer, where the flow is virtually incompressible and isothermal on a small scale. It is also reasonable to assume that air is an incompressible fluid in the atmospheric boundary layer (Garratt, 1992). Thus, we can write an equation that says the instantaneous velocity divergence is zero across the flow:

$$\frac{\partial \mathbf{u}}{\partial x} = 0 \quad (2.2)$$

These two equations (2.1 and 2.2) together are known as the Navier-Stokes equations. Variations of these two equations can be used for any type of fluid flow. Gravity and the Coriolis force are not included in these equations because at the local scale (i.e., not much more than 1 km) in the neutral atmosphere these terms are negligible. More importantly, these two equations, in this form, do not suggest any turbulence, a primary feature of local atmospheric flows.

2.2 Reynold's Averaging

Turbulent flow in the atmospheric boundary layer is, by its nature, one of chaos. Therefore, modeling the exact, turbulent velocity in the atmosphere at any given moment would be extremely difficult. Modeling only the mean flow at any given moment is the usual approach in larger scale modeling of atmospheric flows. However, mean flow does not tell us anything about the turbulent fluctuations in the flow. Because turbulence is the dominant feature of the boundary layer on the local scale, we must address it. A statistical approach has been found to be a good way to approach turbulent modeling.

“Reynold's decomposition” is the separation of the instantaneous velocity into its mean and fluctuating parts (Arya, 1988):

$$\mathbf{u} = \bar{\mathbf{u}} + \mathbf{u}' \quad (2.3)$$

where u' is the deviation from the mean flow (\bar{u}) and represents the turbulent flux of velocity. Figure 2 demonstrates the measurement of u' and the mean velocity in the atmosphere. The standard deviation of the flow (σ_u) is a measure of this variance:

$$\sigma_u = \sqrt{u'^2} \quad (2.4)$$

The turbulent fluctuations are extremely important, especially in air pollution modeling, because turbulent flux is the dominant transport term of scalar flux.

Reynold's averaging can now be incorporated into the Navier-Stokes equations by substituting the mean component and fluctuating component into each variable and then averaging each term. We will not here go through the mathematics of Reynold's averaging. We will just state that terms, such as $\overline{\mathbf{u} \mathbf{w}'}$ and $\overline{\mathbf{u} \mathbf{u}'}$, drop out of the equation because the average of a fluctuating component is zero. A good mathematical demonstration of Reynold's averaging of the conservation of momentum equation can be found in several textbooks (e.g., Stull, 1988).

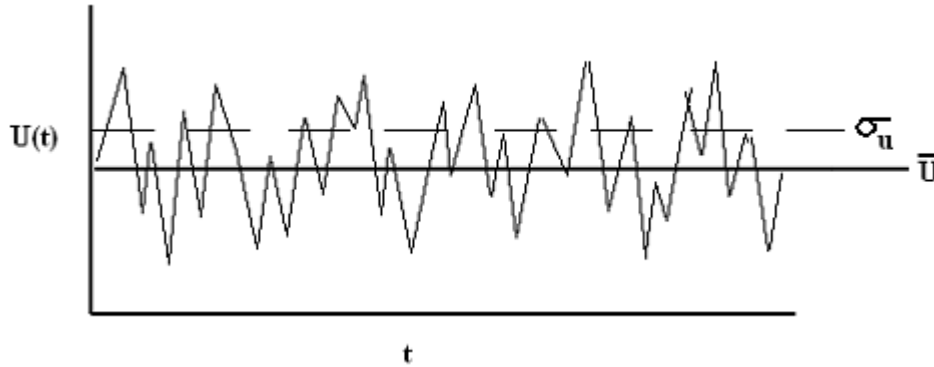
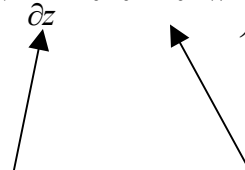


Figure 2. Graph of wind speed observation at a fixed point with time. Modeling of the flow can be simplified by Reynolds decomposition.

The result is the Reynold's averaged Navier-Stokes (RANS) equations, which contain two new unknowns representing turbulence, $\overline{u'u'}$ and $\overline{u'w'}$. These are known as the “Reynold's stresses”. The RANS equations now include the conservation of mass equation (2.2) and a rewritten conservation of momentum equation (2.5):

$$\frac{\partial \mathbf{u}}{\partial t} = -\overline{\mathbf{u}} \frac{\partial \overline{\mathbf{u}}}{\partial x} + \frac{\partial}{\partial z} \left(\nu \frac{\partial \overline{\mathbf{u}}}{\partial z} + \overline{\mathbf{u}'\mathbf{u}'} + \overline{\mathbf{u}'\mathbf{w}'} \right) - \frac{1}{\rho} \frac{\partial P}{\partial x} \quad (2.5)$$



 molecular diffusion turbulent diffusion

In this two-dimensional example, we now have two equations and 4 unknowns: \overline{u} , \overline{w} , $\overline{u'u'}$, and $\overline{u'w'}$. Vertical velocity, w , is still considered an unknown in the equation even though we are assuming it is zero, and thus not displaying the term $-\overline{w} \frac{\partial \overline{\mathbf{u}}}{\partial z}$ in the equation.

To make these equations solvable, we need to find additional equations that will relate the turbulence terms to the properties of the mean flow. This is known as “turbulence closure.” Several different turbulence closure techniques have been proposed using various assumptions about turbulence, but none has ever proved entirely satisfactory (Arya, 1988).

2.3 Turbulence Closure

Assumptions must be made about turbulence to model the turbulent fluctuations and solve the equations of motion. Equations that relate the unknown turbulent

variances to the mean flow must be proposed. We can first explore this by stepping back to our earlier discussion, where we noted that turbulent fluctuations are carried down-gradient from higher velocity to lower velocity. From this observation we are led to the assumption that the turbulent stress is proportional to the velocity gradient in some way:

$$\overline{\mathbf{u}'\mathbf{w}'} = ? \cdot \frac{\partial \overline{\mathbf{u}}}{\partial z} \quad (2.6)$$

where ? indicates an unknown proportionality constant or variable.

At a very small scale in viscous liquid fluids, Isaac Newton proposed and confirmed that molecular turbulent shearing stress is linearly proportional to the velocity gradient:

$$\frac{\tau}{\rho} = \nu \frac{\partial \overline{\mathbf{u}}}{\partial z} \quad (2.7)$$

where τ is the shear stress of the fluid, and ν is a constant known as molecular kinematic viscosity, which is unique for each fluid. If we assume that turbulent viscosity in the atmosphere is analogous to molecular viscosity, as J. Boussinesq did in 1877, then we have a solution relating the turbulent stresses to the mean flow (Arya, 1988):

$$\frac{\tau}{\rho} = \overline{\mathbf{u}'\mathbf{w}'} = -K \frac{\partial \overline{\mathbf{u}}}{\partial z} \quad (2.8)$$

Making this assumption is known as “K theory.” The constant K can be considered the turbulent viscosity of the fluid, ν_t . However, it has been found that this assumption by analogy is flawed; turbulent stress is not linearly proportional to the gradient of the flow in some cases. In the surface layer of the atmosphere, the linear assumption is acceptable in neutral and slightly stable conditions over open areas, but it breaks down as soon as the flow interacts with buildings and obstacles, or the atmosphere becomes unstable, generally because it cannot account for the energy stored in large eddies. Also, in some cases, turbulent fluctuations can transfer up-gradient to higher velocity due to large eddies. Therefore, to be more accurate and to ensure equation closure, the turbulent viscosity assumption must be able to change with location and still be defined by properties of the flow.

A different assumption can be derived from dimensional analysis, a favorite tool of engineers (and first used in exploring turbulent flow). Using dimensional analysis, we note that the units of K must be (length²/time) or m²/s. Prandtl hypothesized in 1925 that this mixing length scale can be defined as the average

distance a parcel of air moves when it is displaced, and that it is a function of height and atmospheric state. It was then proposed that a good estimate for this length in a neutral atmosphere is $L = kz$, where k is the Von Karmon constant ≈ 0.4 (Stull, 1988):

$$\nu_t = (kz)^2 \frac{\partial \bar{\mathbf{u}}}{\partial z} \quad (2.9)$$

Then, equation 2.8 can be rewritten as:

$$\frac{\tau}{\rho} = \overline{\mathbf{u}'\mathbf{w}'} = -((kz)^2 \frac{\partial \bar{\mathbf{u}}}{\partial z}) \frac{\partial \bar{\mathbf{u}}}{\partial z} \quad (2.10)$$

This assumption is reasonable for a neutral atmosphere; but, once again it breaks down as the flow interacts with buildings and other objects, and in unstable atmospheres.

Another common way of generating an assumption for this mixing length is using the Monin-Obukov length, which calculates a characteristic turbulent transfer length using several atmospheric factors, also derived from dimensional analysis. There are many other parameterization techniques that are based on atmospheric conditions. However, for urban microscale modeling, we must use a technique that will be based more on local conditions rather than parameterization because we must deal with both atmospheric flow and flow around obstacles.

A popular approach for obtaining a closure equation involves the parameterization of a local characteristic mixing length by including generation and transport equations for two new scalars: the turbulent kinetic energy (TKE) and the dissipation rate of TKE, labeled ε . Intuitively, one can get a sense of dissipation rate by imagining a turbulent eddy moving through the flow carrying turbulent kinetic energy. The distance that an eddy will travel before degrading into heat and lots of smaller eddies will be determined by the rate of dissipation, ε , of the TKE. The equation relating these two variables is known as the standard K- ε model and is the most widely used turbulence closure model in CFD. Since ε has the dimension inverse time, if we are to maintain the dimensionality of ν_t (see Equation 2.9) the relationship between TKE and ε will be:

$$\nu_t = C_\mu \frac{K^2}{\varepsilon} \quad (2.11)$$

where C_μ is a dimensionless constant, K is TKE, and ε is the dissipation rate of TKE.

The K- ε model introduces two new equations, one for turbulent kinetic energy production (from shear and buoyancy) and one for turbulent kinetic energy dissipation. Together they describe TKE transport. The production term will be discussed below in describing variations on the K- ε model, but this chapter will not explore the mathematics of these two equations. They are described in detail in several sources in the literature (e.g., Duynkerke, 1987; Richards and Hoxey, 1993).

With this K- ε model, we now have 4 equations and 4 unknowns that can be solved with boundary conditions applied:

- 4 unknowns: u , v , K , and ε
- 4 equations: conservation of mass, conservation of momentum, conservation of K , and conservation of ε

Because we have assumed the vertical pressure gradients are small in our local scale, P is not a variable; but, if it is to be included, the ideal gas law ($PV = nRT$) quickly provides an additional equation with no additional unknowns. Decomposing u and counting w , the vertical velocity, gives us six equations with six unknowns.

A variety of turbulence closure methods are available in most commercial CFD codes today. The most widely used for industrial applications is the standard K- ε model and variations of it (ERCOFTAC, 2000). However, the standard K- ε model has been found to be inadequate for computational wind engineering and only the K- ε variant models that have corrections for TKE generation/dissipation have shown reasonable results (Castro, 2003). This is generally due to over-predicting the eddy viscosity when the flow is highly rotational. The better performing variants of the K- ε model usually have terms that suppress the generation of TKE in regions of high vorticity (Murakami, 1998).

Besides the K- ε model and its variants, other closure models are also used in CFD. The K- ε and other major closure models used for atmospheric applications are listed in Table 1, which provides a simple description of each model. The estimate of computing power required is based on a typical small-scale modeling project of dilution of a plume around several buildings. The larger the size of the domain and accuracy needed, the more resolution would be needed in the model, and the more computing power would be needed. Modeling an entire city skyline with a modified K- ε model would require significant computing resources; it would also be inappropriate, as the scale would significantly exceed the region of validity of our assumptions.

Table 1. Various Turbulence Closure Models Used in CFD.

CFD Turbulence Closure Model	Method of Modeling Reynold's Stresses	Accuracy for environmental modeling	Use history	Computing Power required
Standard K- ϵ	Eddy viscosity parameterization	Problems with flow around bluff bodies: overproduction of TKE at sharp edges	Common earlier	Minimal: Standard PC
Variant K- ϵ	Eddy viscosity parameterization: correction term for TKE production/dissipation	Better accuracy than standard K- ϵ for various aspects of the flow. Problems still inherent.	Most common now	Minimal: Standard PC
Reynold's stress models (RSM)	Direct modeling of parameterized Reynold's stresses	Proven better accuracy than K- ϵ but not as good as LES on average.	Rare	Substantial: Parallel multiprocessor
Large Eddy Simulation (LES)	Large turbulent eddies modeled in incoming atmosphere - subgrid scale turbulence only parameterized	Best accuracy	Increasingly common use	Substantial: Fast parallel multiprocessor
Direct Numerical Simulation (DNS)	No parameterization of turbulence	Good accuracy	Extremely rare: only simple cases	Enormous: Large mainframe

More sophisticated turbulence modeling schemes include Reynold's stress models (RSMs) and Large-Eddy Simulation (LES). RSM is similar to K- ϵ in the sense that it uses extra equations that describe the production and transport of turbulence. However, instead of parameterized TKE, RSM models use separate equations for each separate Reynold's stress. LES works by parameterization of the local-scale (subgrid) turbulence and full representation of turbulence greater than the grid size. Therefore, LES is best used for unsteady state solutions.

The general trend, as one would expect, is that the more sophisticated the model, the greater accuracy it has when used for atmospheric flows. More in depth discussion of the various models and variants is provided in the following section.

2.4 CFD Models

The simplest closure scheme that can handle both atmospheric flow and flow around bluff (i.e., non-aerodynamic) bodies is the standard K- ϵ model. It has been the work-horse of the industry, despite its drawbacks. Validation efforts have demonstrated the model's weakness in simulating flow around simple shapes (bluff body modeling). Thus, many modeling projects today use variants of the K-

ε model. Though dynamic LES will eventually be the preferred method as computational resources increase, variant K- ε models will continue to be the favored tool for many more years.

For computational wind engineering, much of the attention of model validation and verification has been focused on flow around bluff bodies. The performance of a model is often rated by its ability to match its predictions of flow around a simple bluff body to the results of wind-tunnel tests. Flow around a simple cube is the common experiment used in validation. The simplified “flow around a cube” case is ideal because, even though the shape is simple, the flow around the shape is characterized by complex flow structures such as vortices, separation points, and unsteady flux of turbulence zones. Figure 3 offers a simple illustration of the typical re-circulation zones around a cube. Our discussion of these models will refer to this validation exercise because it has been the benchmark test for comparison of models.

2.4.1 Standard K- ε Model

The standard K- ε model has been the most common turbulence closure model used in the past due to its robustness and computational efficiency in a variety of applications. It has validated well for various applications, but it has had problems in computational wind engineering. The main problem that much of the literature discusses is its difficulty with predicting the flow at the sharp edges of bluff bodies, particularly at the sharp roof edge of a block building. It is reported that this is due to overproduction of turbulent kinetic energy in regions of stagnant flow (Franke et al., 2004b; Tsuchiya et al., 1996).

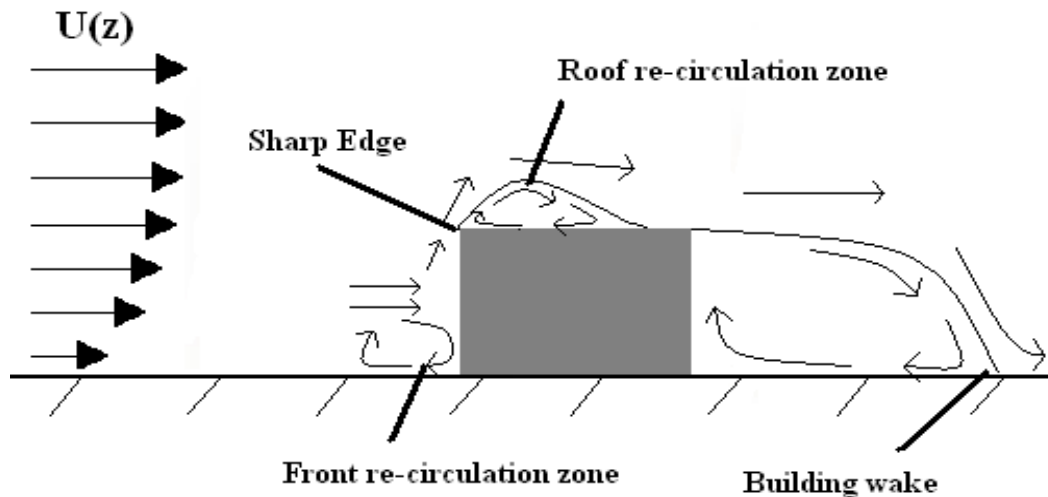


Figure 3. Illustration of the typical two-dimensional flow zones around a cube. Validation efforts using flow around a cube will involve comparing the qualities of these zones to physical tests.

This results in the model giving “mediocre” comparative results in areas of high anisotropy (Kim and Boysan, 1999). Generally, on a building, these areas are at the roof edge, in the wake at the windward edge of the building, and in the wake behind the building. Over/under predictions of TKE will travel downwind until dissipated, affecting the generation of TKE at points downwind, and resulting in errors in the dimensions of wakes and other flow features.

There are several modified K- ϵ model variants available. These variant models focus on changing aspects of the TKE, ϵ , and/or the constant C_μ (described below), to improve the predictability of turbulent viscosity at stagnant points in the flow. These models are, in essence, “ad hoc” for wind engineering. The changes limit the universality of the K- ϵ model, so what is good for bluff body flows might reduce the predictability of the model in other applications. And, even within bluff body studies, while they improve certain aspects of a flow description, they tend to worsen other aspects of the flow, leading to the conclusion that “ad hoc” models may not be the long-term solution for computational wind engineering (Easom, 2000). Nevertheless, these models do seem to perform better overall than the standard K- ϵ model. However, no matter how sophisticated the modified model is, the K- ϵ model is inherently limited by its assumption of isotropic eddy viscosity.

2.4.2 LK K- ϵ Model

The LK K- ϵ model (Kato and Laufer, 1993) was one of the early attempts to make an adjustment for the production of turbulent kinetic energy to coincide with vorticity of the flow. The model was developed strictly for bluff body flows to account for overproduction of TKE at sharp building edges. The production term for TKE in the standard K- ϵ model is:

$$P_k = \nu_t S^2 \quad (2.12)$$

where S is a scalar term related to the strain rate in the fluid. The LK model replaces this with:

$$P_k = \nu_t S \Omega \quad (2.13)$$

where Ω is vorticity. In simple shear flows, $\Omega \approx S$, and in stagnation regions $\Omega \approx 0$, so that the erroneous TKE production is limited in the vortex.

Lakehal and Rodi (1997) compared flows past a surface mounted cube modeled with the standard K- ϵ model and experimental results. They found improvement in the location and magnitude of the roof recirculation zone, and turbulent kinetic energy maxima. However, they noted that the model had poorer performance for the length of the re-circulation zone behind the block. The improved roof wake zone and longer building wake zones were also observed by Tominaga and Mochida (1999) using the LK model.

With less production of TKE at the building roof edge, less TKE advects into the building wake, which may account for the longer wakes. With higher TKE, vortexes would tend to dissipate more quickly. It was noted that vortex shedding behind the building contributes greatly to momentum exchange in the wake, leading to a smaller recirculation zone. The steady-state models cannot account for vortex shedding (Lakehal and Rodi, 1997).

2.4.3 MMK K- ε Model

The Murakami, Mochida, and Kondo (MMK) model is another example of ad-hoc models designed to improve the performance of the K- ε model for bluff body flows. The model itself is based on assumptions similar to the LK model, that is, that the production of TKE can be modified based on an observation of vorticity and strain at discrete points in the domain (Tsuchiya et al., 1996).

The author's approach with the MMK model begins by examining an inconsistency in the LK model - the production term of TKE is modified, but the loss of momentum to TKE term in the energy equation is not modified. Therefore, P_k in the TKE equation and P_k in the mean flow energy equation do not have the same form. Tsuchiya's approach is to deal with the eddy viscosity directly rather than tamper with the production of TKE.

The production term of TKE is dependent on the eddy viscosity:

$$P_k = \nu_t S^2 \quad (2.14)$$

Keeping the eddy viscosity equation in mind (Equation 2.11):

$$\nu_t = C_\mu \frac{K^2}{\varepsilon} \quad (2.15)$$

We see that we can alter the production of TKE by defining values of C_μ based on flow properties. The MMK model includes terms that define C_μ by the ratio of vorticity to strain rate:

$$C_\mu = C_\mu \Omega/S \text{ when } (\Omega/S < 1) \quad (2.16)$$

$$C_\mu = C_\mu \text{ when } (\Omega/S \geq 1) \quad (2.17)$$

Similarly to the LK model, TKE production will be limited when the Ω/S is low, such as in stagnant areas or centers of vortexes where the standard K- ε model has problems.

The authors note that the MMK model predicted the location and magnitude of the TKE maxima on the building roof better than the LK model did when

compared to the experiment. Also, the direction and magnitude of velocity vectors within the roof re-circulation zone were closer to the experiment than those calculated by the LK model. Other validation attempts have shown that the MMK model still over-predicts the length of the re-circulation zone behind the building (Easom, 2000).

2.4.4 Chen-Kim $K-\epsilon$ Model

The Chen-Kim model (Chen and Kim, 1987) is less of an ad-hoc model than the MMK model, but it is based on a similar assumption that production/dissipation of TKE can be altered to limit excessive TKE in regions of high vorticity. The Chen-Kim model contains a correction of the TKE equation by introducing a second time-scale of TKE production and dissipation dependent on the strain rate of the flow.

In general, the production rate of TKE is the product of turbulent viscosity and the strain rate of the flow. Chen and Kim argue that for rapidly evolving flow, such as in recirculation zones around bluff bodies, it is appropriate to restrain full production of the TKE to ensure that the energy generation rate is more realistic. They introduce two new time scales: the production time scale TKE/Pr_{TKE} and dissipation time scale TKE/ϵ . These two time scales are used in the expression for energy transfer rate from large scale turbulence to small scale turbulence in the dissipation equation. The inclusion of these terms enhances the development of dissipation rate, ϵ , when the mean strain rate is strong and suppresses it when the strain rate is weak. This allows the dissipation rate to respond more rapidly to control TKE development more effectively.

Chen and Kim compare modeling results of their alteration to the standard model for a number of common CFD validation exercises. The most applicable demonstration to our application is the flow over a backward facing step. The Chen-Kim model demonstrates superior performance in predicting reattachment length, surface pressures, velocity distributions, and turbulent kinetic energy magnitude and position when compared to the standard model.

Several studies are available in the literature that used the Chen-Kim model with varying success. One of these studies is Delauney (1996), who used the model for dispersion at an urban site and reported satisfactory results when compared to field data measurement of concentrations at the site. Delauney also conducted a validation exercise of flow around buildings and compared the standard $K-\epsilon$ model to the Chen-Kim model. He found overproduction of TKE in the standard model. He also reports the Chen-Kim model performed similar to the RNG model in the same comparison.

2.4.5 RNG K- ϵ Model

The Randomized Normal Group (RNG) K- ϵ model was developed based on RNG theory. RNG theory is a highly complex mathematical technique used to predict universal properties in distributions of chaotic phenomena such as turbulence. It originated in statistical physics and was used originally in quantum field theory (Kantha, 2000). It was first used in fluid turbulence to study fluctuations in a randomly stirred fluid at rest. Yakhot and Orszag (1986) were the first to use RNG to obtain equations and constants for fluid motion. The RNG K- ϵ model is identical to the standard K- ϵ model, except with an added term in the ϵ equation that limits the production of ϵ in areas of stagnation with rapid strain (areas of swirl). The model also uses revised constants. In this respect, the RNG model is similar in approach to the Chen-Kim model.

For simple flow around cubes and rectangular bluff bodies, the RNG model has shown superior performance compared to the standard K- ϵ model, more accurately predicting pressure distribution, TKE distribution, and flow (Kim, 1999). For flow over terrain, the RNG model has also been demonstrated to model flow and re-circulation better than other modified K- ϵ models (Kim and Patel, 2000).

There seems to be an overall consensus that the RNG model provides more accurate results (Franke et al., 2004b). However, the RNG model can be much more computationally expensive than other K- ϵ model variants, so its current use is still limited.

2.4.6 Reynold's Stress Models

Reynold's stress models (RSMs) are quite different in their approach to parameterizing turbulence. RSM uses the Navier Stokes equations and separate transport equations for each of the individual directional Reynold's stresses. This type of model will be quite useful for air quality analysis at the surface because it has the ability to incorporate the inherent anisotropy of the turbulence resulting from a boundary on one side (e.g., the earth's surface) and essentially unbounded flows on the other. However, the extra transport equations make this model much more computationally intensive than the standard K- ϵ model or its variants.

Although RSMs seemingly have a lot of promise, they have not been used extensively in computational wind engineering studies, most likely because of the added computational expense (Kim and Boysan, 1999). Some studies involving flow around a cube indicate that they perform with similar accuracy as the RNG model with only limited additional benefit. RSMs do show much promise for the future of computational wind engineering once the method is improved and larger, faster computers are more generally available (Easom, 2000).

2.4.8 Large-Eddy Simulation

Large-Eddy Simulation (LES) modeling is definitely the future of computational wind engineering as computer power increases and the modeling technique itself improves. LES has shown superior performance compared to all RANS modeling techniques. LES operates by parameterizing subgrid scale turbulence and by directly modeling the turbulence of larger scales. It is an unsteady state approach and is quite computationally intensive. More exquisite definition of the atmospheric boundary layer is needed since turbulence is directly modeled instead of parameterized by a TKE profile.

There is a temptation to use LES modeling over a larger scale than we are discussing in this chapter. When the scale of the domain is large enough that there is significant turning of the boundary layer due to Coriolis forces, the modeling must change fundamentally, as the atmosphere becomes distinctly nonlinear. When the basic assumptions used in deriving the Navier-Stokes equations no longer hold, the model cannot be expected to yield useful results. An alternative is an approach which models the atmosphere as organized large-eddies, developed by Brown (1991).

This chapter does not discuss LES in detail. The reader can refer to Chapter 5B of this volume for a detailed description of LES modeling of the atmospheric boundary layer.

2.5 Numerical Methods

One of the prime factors that led to the growth in the use of CFD is increased computational efficiency with the development of improved methods of solving the associated differential equations. Interestingly, some introductions to CFD focus almost entirely on these mathematical aspects, giving little attention to the physics.

For incompressible flow, which is what most civil engineering applications are concerned with, the Navier-Stokes equation and the mass continuity equation can be summed up as a relation between pressure and momentum, since velocity is dependent on the pressure gradient. Numerical schemes have been developed to solve the equations iteratively, known as pressure-velocity coupling schemes. In most commercial CFD codes, a variety of schemes are provided that the user can select. Most papers will report which pressure-velocity coupling method is used for their CFD project.

The two most popular methods are the Semi-Implicit Method for Pressure Linked Equations (SIMPLE) method and the Pressure Implicit with Splitting of Operators (PISO) method. There are several variants of the SIMPLE method also that are quite popular.

The SIMPLE method is a four stage process which involves a ‘guess, check, correction’ technique to solve the equations. The first step is to solve the momentum equation using the current pressure gradient computed from the last time step or initialization. It is highly unlikely that the first step generated velocity field will satisfy the conservation of mass and momentum. Next, pressure changes are estimated based on the new velocity. The SIMPLE approximation at this point is to assume that the velocity is dependent only on the pressure gradient across the cell, and ignore mass flux out of the cell faces. Third, the velocity is again adjusted to account for mass continuity. Fourth, the solution is repeated until the solution converges (Apsley, 2003).

There are several variants to SIMPLE that attempt to account for some of the weaknesses of the approach. In SIMPLE, it has been observed that correction equations are good for updating velocity, but not pressure since significant terms are ignored in the approximation of the pressure-velocity link. The variant SIMPLER is formulated to account for this by adding an additional equation for pressure used before the pressure-correction step. SIMPLEC is a variant that accounts for the velocities at the cell faces, rather than ignoring them as in the SIMPLE approximation.

The PISO method is other important type of pressure-velocity coupling scheme. It is similar to SIMPLE in many respects. However, it takes a different approach at estimating pressure and velocity, based on the surrounding flow properties rather than through steps of iteration.

The first few steps of PISO are essentially the same as SIMPLE, but with forward time marching. A solution to the velocity field is estimated by one time step forward and the pressure gradient and density is corrected to account for mass continuity. Instead of iteration, the PISO method takes into account conditions at neighboring cells from the time marching advection (Adaptive Research, 1997).

The general industry consensus is that a more advanced method than SIMPLE such as the SIMPLE variations or PISO should be used. This will not necessarily improve accuracy, but it may improve convergence behavior and lower numerical diffusion. In terms of model convergence performance, Jang et al. (1986) compared the performance of the SIMPLER, SIMPLEC, and PISO algorithms in a number of simplified CFD cases. The cases included expanding flow in a channel, swirling flow with scalar transport, and convection due to a heated wall in an enclosure. In general, no real advantage of using SIMPLER versus SIMPLEC is observed. The SIMPLEC algorithm tends to converge slightly faster than the SIMPLER method in some cases. PISO performs better than the SIMPLE derivatives in terms of quicker convergence at larger time steps with less computing effort in isothermal conditions. In the cases where temperature varies, the PISO algorithm converged slower and only at smaller time-steps than the SIMPLE variants.

2.5.1 Commercial CFD Codes

Computational Fluid Dynamics commercial packages usually consist of: 1) a solver program that performs the computations; 2) a graphical user interface where boundary conditions, mesh, and geometry are defined, and 3) a post-processor where the results are viewed in a graphical user interface. Most CFD solvers were originally developed by government laboratories and university research programs. Some of these have been developed into efficient graphical user interfaces.

Commercial CFD software packages are now available from many vendors. Most packages are general-purpose codes with various features. However, some application specific packages are available that are related to the environmental sciences. Application specific packages often contain the same features as the general-purpose package but with additional specialized boundary condition features. Specific applications range from aerospace engineering to electronic equipment cooling. Average cost for a commercial software license is about \$20,000 a year for the more popular packages. Several of the smaller firms offer packages for as low as \$3,000 - \$10,000 per year, which generally contain many of the same features as the more popular packages. For educational purposes, most firms offer substantial discounts and some firms offer limited-use student packages at very low prices.

The largest general-use CFD vendors are:

- Fluent[®] (www.fluent.com): Fluent general-purpose and application specific packages.
- CD-Adapco[®] (www.cd-adapco.com): Star-CFD general-purpose package.
- ANSYS-CFX[®] (www.ansys.com): CFX general-purpose package and application specific packages.

Some smaller CFD vendors offer packages that are often nearly equivalent in features and abilities to the larger vendors, at lower cost. These vendors include:

- Adaptive Research[®] (www.adaptive-research.com): CFD2000 general-purpose package
- CHAM[®] (www.cham.co.uk): PHOENICS general-purpose package

Several commercial vendors offer packages that have added features or adaptations for air quality applications at the local scale. The most popular of these are used more for indoor applications. They contain specialized boundary condition options for various HVAC equipments (e.g., diffusers, air conditioners, and heating apparatus). However, since these packages are geared towards building HVAC, they often do contain options for modeling the flow and air quality around the exterior of buildings. Two popular packages are:

- *Airpak*[®] from Fluent[®] (<http://www.fluent.com/software/airpak/index.htm>)
- Flovent[®] from Flomerics[®] (<http://www.flomerics.com/flovent>)

There are few commercial CFD packages that are custom-made for small-scale atmospheric environmental modeling. These models generally include the same functions as a general-purpose commercial CFD package, but with tools that allow easier topography definition, AutoCAD[®] import for building design, and wind data from meteorological files. The actual mathematics and turbulence models within the solver are no different from what can be found in a general-purpose package, usually utilizing the same standard K- ϵ or modified K- ϵ models.

Panache[®] from Fluidyn (www.fluidyn.com) is a CFD package for atmospheric dispersion, which is pre-packaged with several different turbulence models and a handy meteorological data input scheme. Surface wind data can be prescribed at different points in the domain for better initialization. Panache contains a standard K- ϵ model, as well as two one-equation models: a K-diff model that uses Monin-Obukov similarity for flow over flat terrain, and an LK model that can simulate different atmospheric stabilities. This model is even referenced by the EPA as an alternative to the official EPA dispersion models (www.epa.gov/ttn/scram001/dispersion_alt.htm).

Another commercial package is CFD-Urban developed by CFD Research Corporation (www.cfdrc.com). It was derived from the commercial CFD package CFD-ACE+, also from CFDRC. The model has the ability to use both LES and RANS turbulence models. The model has been validated against several field studies using the RNG K- ϵ model (Coirier, 2004), including the MUST, Kit Fox, and Prairie Grass dispersion field experiments.

Another is the FLACS-dispersion CFD model. The FLACS suite of models is developed by GexCon (www.gexcon.com), and is primarily used as an explosion simulator. The dispersion CFD model has been extensively validated and contains several features handy for atmospheric simulation - easy CAD import, and a “wind” boundary condition that maintains a wind and turbulence profile.

A number of urban dispersion simulators have also been developed by various government institutions. FEFLO, FAST3D, HIGRAD, and FEM3MP are several models that were developed primarily for military purposes. The high level of attention paid to terrorist attacks has driven the interest to accurately model the dispersion of chemicals in an urban area. FEFLO and FAST3D are Department of Defense models. FEM3MP is the Department of Energy model. HIGRAD is the model developed by the Los Alamos National Laboratory. All of these models are generally run as LES models, but some provide variant K- ϵ models. These models are actively being used in field studies such as the Urban2003 and Urban2000 studies, where tracer gases are released in urban areas in the United States to collect data for model verification.

Air quality modeling for regulatory purposes in the United States is generally the domain of the Environmental Protection Agency (EPA). The EPA has not developed its own CFD model for small scale modeling, but is actively exploring

the use of CFD for the future. Alan Huber's group at the EPA National Exposure Research Laboratory has been doing some work attempting to develop a method to use CFD for small-scale air quality studies. The work so far has generally focused on validation efforts, attempting to find the best way to simulate the atmosphere using the Fluent commercial software CFD package (Huber et al., 2004). Recent work has involved a comparison of CFD simulations to the Project Prairie Grass field experiment. This experiment was one of the main studies used to determine the properties of plume dispersion during different atmospheric conditions, giving rise to the Pasquill-Gifford stabilities and dispersion curves. They have found good agreement between the CFD simulations and the experimental data (Tang et al., 2005).

Additional detailed information on these and other CFD modeling codes, as well as links to a wide variety of the latest research, can be found on the portal website, www.cfd-online.com.

3 Simulating the Atmosphere in CFD

The EPA Guideline for fluid modeling of atmospheric dispersion (Snyder, 1981) provides guidance on atmospheric simulation that can be used for CFD studies. The guideline is intended mostly for wind tunnel modeling, and therefore, primarily discusses scaling.

An advantage of using CFD is that no scaling is necessary since the exact dimensions of the experiment can be represented in the computational domain. The important details in the Guideline for simulating the dispersion of exhaust around a building, not related to scaling, can be summarized as:

- The flow must be fully turbulent. This is ideal for RANS modeling, since the TKE is parameterized.
- The Coriolis force can be ignored at such a small scale (about 1 km).
- The incoming flow should be horizontally homogeneous, which will not be the case at larger scales.
- A logarithmic wind profile extending to the height of the boundary layer is needed, dependent on the friction element height, z_o .
- Turbulence intensity, which decreases with height, and background turbulence must be simulated.

The wind and turbulence profiles are crucial for dispersion modeling because they influence the size and location of flow characteristics around buildings. Also, the rate and direction of dispersion is highly dependent on the wind and turbulence profile. Early wind tunnel modeling demonstrated that plume spread and recirculation zones around buildings vary greatly depending on the characteristic profiles.

In non-steady state CFD modeling such as LES modeling, dynamic boundary conditions would need to be established for the modeling effort. The incoming wind would need to represent the actual atmosphere with incoming turbulent eddies appropriate to those generated by the general upstream land characteristics under the atmospheric conditions being simulated. Again, at scales approaching 10 km, the incoming turbulent eddies begin to be better defined as organized large eddies, which even LES cannot handle.

This chapter primarily deals with a steady-state solution used in RANS modeling. With a steady-state solution, the atmospheric wind profiles and turbulence profiles can be defined with no actual rolling vortices or other structures of turbulence. Turbulence is parameterized as TKE, and in a steady state solution, the wind profile can simply be represented by the mean wind profile of the atmosphere.

3.1 Steady-State Approach Flow

In the surface layer of the atmosphere, a number of characteristics of the atmosphere can be ignored and some assumptions can be made if we are going to be modeling airflow at a micrometeorological scale.

Pressure can be assumed to be constant. The top of the modeling domain will generally be lower than 200 meters (Richards and Hoxey, 1993), which is about a 25 mb pressure difference in a standard atmosphere from surface to top of the domain. The atmosphere can be assumed to be hydrostatic as the pressure force upward is balanced by the gravitational force downward, so that the vertical pressure field is irrelevant. In this respect, gravity can be ignored. Buoyancy forces can be simulated using a Bousinessq assumption that simulates buoyancy simply as a function of temperature difference. Also, the scale must be kept small enough that the Coriolis force can be ignored.

A commonly accepted set of boundary conditions for the K- ϵ model is described by Richards and Hoxey (1993). Assuming a steady state equilibrium boundary layer, the incoming atmosphere can be described by a profile of wind speed, TKE, and dissipation rate of TKE. The derivation of these is described in Easom (2000).

The Harris and Deaves (1981) model states that the wind profile of the atmospheric boundary layer, $U(z)$, can be described by a logarithmic equation dependent on friction velocity (u_*) and the depth of the surface layer (δ), where κ is the Von Karmon constant (~ 0.41), z height above the surface, and z_o the surface roughness length:

$$U(z) = \frac{u_*}{\kappa} \left[\ln \left(\frac{z + z_o}{z_o} \right) + 5.75 \frac{z}{\delta} \right] \quad (3.1)$$

The friction velocity, u_* , can be estimated from this equation if the surface roughness length, z_o , and the windspeed at a reference height are known:

$$u_* = \frac{\kappa U_{ref}}{\ln\left(\frac{z_{ref}}{z_o}\right)} \quad (3.2)$$

Assuming that in the equilibrium boundary layer shear stress decreases with height, an expression can be derived for TKE, where C_μ is the turbulence constant.

$$TKE = \frac{u_*^2 \left(1 - \frac{z}{\delta}\right)^2}{\sqrt{C_\mu}} \quad (3.3)$$

The dissipation rate can be assumed to equal the rate of generation of TKE, which is described by the equation:

$$\varepsilon(z) = \text{generation of TKE} = \frac{\tau_z}{\rho} \frac{\partial u}{\partial z} \quad (3.4)$$

Using the derivative of the wind profile equation, an expression for dissipation can be resolved from the TKE generation equation:

$$\varepsilon(z) = u_*^2 \left[1 - \frac{z}{\delta}\right]^2 \frac{u_*}{\kappa(z+z_o)} \left[1 + 5.75 \frac{(z+z_o)}{\delta}\right] \quad (3.5)$$

The depth of the boundary layer can be estimated using the equation (Huser, 1997):

$$\delta = 0.4 \sqrt{\frac{u_* L}{f}} \quad (3.6)$$

where L is the Monin-Obukov length and f is the Coriolis parameter (0.000125/second). A typical L is 10^4 for neutral atmospheric conditions, and a typical neutral boundary layer depth may be 500 - 1500 meters.

Richards and Hoxey (1993) assumed that when modeling very near to the surface, as would be the case in urban microenvironment studies, the height variation is much smaller than the depth of the boundary layer ($z \ll \delta$) so that shear stress is virtually the same at the top and bottom of the modeling domain. With this assumption, the term $z/\delta \approx 0$ and our 3 equations now become:

$$\text{Wind Profile: } U(z) = \frac{u_*}{\kappa} \left[\ln \left(\frac{z + z_o}{z_o} \right) \right] \quad (3.7)$$

$$\text{TKE Profile: } K = \frac{u_*^2}{\sqrt{C_\mu}} \quad (3.8)$$

$$\text{TKE Dissipation Profile: } \varepsilon(z) = \frac{u_*^3}{\kappa(z + z_o)} \quad (3.9)$$

These equations for the steady-state wind and turbulence profiles can be used for the air inlet and initial conditions in the CFD domain. This is an advantageous set to use because all equations are simply dependent on friction velocity, estimated easily from Equation 3.2 if the roughness length is known. However, this may only be applicable to small-scale studies with short buildings because TKE will decrease with height above the surface layer. In that case, Equation 3.3 should be used for the TKE profile and Equation 3.5 for the dissipation rate profile.

3.2 Surface Roughness Lengths

With the wind and turbulence profiles determined by friction velocity, z_o is the most important parameter in the neutral boundary layer since the u_* equation is a function of z_o and U at a reference height. Values for z_o have been well documented by studies of wind profiles and friction element distributions in various geography and land use situations. Typical values for z_o are provided in Figure 10.5 of Arya (1988). A few of the entries from that figure are given in Table 2.

If the typical friction element height can be easily estimated for a region in question, the ratio between roughness length and friction element height can be useful in determining the surface roughness length for the region. Arya states that the ratio of the roughness length and the average friction element height (z_o/h_o) varies from 0.03-0.25, increasing gradually with rougher surfaces. For grasslands a typical value of z_o/h_o is 0.15.

Table 2. Typical Surface Roughness Lengths.

Terrain	Surface roughness length, z_o
Level grass plains	0.01
Farmland	0.1
Rural, few buildings	0.2
Centers of small towns	0.5
Centers of large towns	1.0

Grimmon and Oke (1999) derive a set of surface roughness lengths for varying urban densities that is useful for determining which z_o to use in an urban micrometeorological study. It includes various measurements and estimates of z_o and other aerodynamic properties from a database of studies. That paper includes a typical set of aerodynamic properties for varying urban densities. They are given in Table 3.

In Table 3, the surface roughness lengths provided are a range of values dependent on the density of vegetation. A city such as Phoenix, Arizona, with sparse vegetation, will have z_o near the lower end of the range. A city such as Seattle, Washington, with dense vegetation in urban areas, will have z_o near the upper end of the range. Grimmond and Oke also point out that sites with deciduous tree cover will have 20% - 30% smaller z_o values during the time of year with no leaves on the trees.

Table 3. Typical Urban Surface Roughness Lengths.

Urban surface form	Surface roughness length, z_o
Low height and density: Residential one and two story houses, mixed houses and small shops, or light industrial and warehouses	0.3 - 0.8
Medium height and density: Residential two and three story apartment buildings, shops, schools, churches, and light industry	0.7 - 1.5
Tall height and high density: Closely spaced <six story apartment buildings, universities, heavy industry, town center.	0.8 - 1.5
High-rise Urban core and dense urban surroundings.	> 2.0

As a general rule of thumb, the estimate that $z_o \sim 0.1 \bar{z}_h$ is generally valid. Grimmond and Oke explored several different methods of calculating z_o from literature, and compared the results of these methods to databases of observations. The ratio, z_o/\bar{z}_h , generally ranged around 0.1 for surface element densities found in real cities.

3.3 Urban Wind Profile Displacement Height

In a micrometeorological study using CFD, the local wind climate must be analyzed and wind scenarios must be selected to represent various meteorological conditions that may occur. Wind data are collected at surface meteorological

towers at airports, universities, agricultural sites, air quality observation sites, elementary schools and a variety of other locations. A graph known as a “wind-rose” can be developed from the annual data set of wind speed and direction to display observation frequencies.

Most meteorological surface data are purposely collected at locations clear of obstacles, such as trees and buildings, to ensure that local winds are representative of the wider area. Because of this, the nearest meteorological data set to the site of your micrometeorological study often will have wind speed data that is higher on average than that of the study site. The higher density of obstacles will slow the average wind speed. Meteorological datasets nearest to the study site should be selected so that wind direction is approximately the same. If the density of friction elements near the study site warrants it, a “displacement height” for the approach wind profile should be used. The displacement height is a “lifting” of the wind profile to a height above the surface determined by the influence of the obstacles at the site. It is used for the approach flow in a CFD study to account for the differences in wind profiles from the data collection site and the CFD study site.

The displacement height, z_d , is a function of the surface friction element average height, \bar{z}_h . The simplest approximation of displacement height has been the assumption that it is a linear relation to surface friction element height (Grimmond, 1999).

$$z_d = C_d \bar{z}_h \quad (3.10)$$

Measurements of C_d range from 0.64 in field crops to 0.8 in forests. Hanna and Chang (1992) suggest $C_d \sim 0.5$ in their review of urban dispersion parameters. Grimmond and Oke (1999) argue that C_d varies depending on the density, arrangement, and shape of the surface roughness elements.

In terms of density, as friction elements become more compact, there is less room for momentum to penetrate into the canopy and the flow begins to “skip”. Thus, in the case of high density, z_d approaches \bar{z}_h . This can be observed walking through an urban center on windy days as the flags atop buildings are outstretched in the strong winds while the surface remains relatively windless.

In terms of shape, Grimmond and Oke note that trees and buildings will have profoundly different influences on the mean flow, even if they are the same average height. Buildings are solid objects with sharp edges that cause flow separation and vortex shedding, whereas trees are porous and pliable to the wind. Arrangement of the surface roughness elements can also influence z_d as buildings are arranged in grids that provide more or less open area for wind passage depending on the direction of wind flow.

Grimmond and Oke (1999) analyze several different equations from the literature developed to determine z_d and they compare the equations' performance to observations. They note that z_d/\bar{z}_h increases with increasing density of friction elements for each method analyzed, and that each method provides reasonable estimates.

A simplified technique can be used to estimate z_d using the results of Grimmond and Oke's sensitivity analysis (from Figure 3 of Grimmond and Oke). This can be done by fitting a mean line through results of z_d/\bar{z}_h based on plan areal fraction (λ_p), where A_p is the area covered by buildings, trees, and other surface friction elements and A_t is the total area.

$$\lambda_p = \frac{A_p}{A_t} \quad (3.11)$$

$$C_d = \frac{z_d}{\bar{z}_h} = 0.2 + \lambda_p \quad (3.12)$$

Estimate λ_p from at least a $\frac{1}{2}$ mile upstream 30° sector of urban landform. These equations can be assumed to fit closely to the average C_d from the various methods analyzed in Grimmond and Oke for $0.1 < \lambda_p < 0.7$, which covers the range of most real cities.

Grimmond and Oke also include a table of typical displacement heights as observed in varying urban landscapes. These values are given in Table 4.

Table 4. Typical displacement heights.

Urban surface form	Displacement height, z_d
Low height and density: Residential one and two story houses, mixed houses and small shops, or light industrial and warehouses	2 - 4 m
Medium height and density: Residential two and three story apartment buildings, shops, schools, churches, and light industry	7 - 14 m
Tall height and high density: Closely spaced < six story apartment buildings, universities, heavy industry, town center.	11 - 20 m
High-rise: Urban core and dense urban surroundings.	> 20 m

In Table 4, the displacement heights provided are a range of values dependent on the density of vegetation. A city such as Phoenix, Arizona with sparse vegetation will have z_d near the lower end of the spectrum compared to a city such as Seattle, Washington with dense vegetation in urban areas.

The displacement height can be applied to the incoming wind-flow equation so that the wind profile is raised. Equation 3.7 is altered to account for the newly calculated displacement height. This is expressed in Equation 3.13, where δ is the displacement height:

$$U(z) = \frac{u_*}{\kappa} \left[\ln \left(\frac{z + z_o - \delta}{z_o} \right) \right] \quad (3.13)$$

The wind speed reference height, z_o , that is commonly at 10 meters (the common wind measurement height), is now displaced 10 meters above the displacement height. According to this new wind profile, the wind-speed approaches zero at the displacement height and it is undefined below the displacement height. Therefore, below the new wind reference height, the wind profile is no longer valid. We must apply another wind profile equation to account for wind from the surface up to 10 meters above the displacement height (if 10 meters is the original height of the wind reference).

We can calculate this wind profile using the logarithmic Equation 3.7 and a new friction velocity. Using the same z_o as measured for the above-displacement wind profile, a new, lower zone friction velocity can be calculated using Equation 3.14. This equation solves for the friction velocity by using the reference wind speed at its new height:

$$u_{* \text{ canopy}} = \frac{\kappa U_{(ref+\delta)}}{\ln \left(\frac{z_{(ref+\delta)}}{z_o} \right)} \quad (3.14)$$

The final incoming wind profile will contain two parts, as illustrated in Figure 4:

1. A wind profile extending from the displaced wind-speed reference height (usually 10 meters above the displacement height) to the top of the domain, determined from Equation 3.13.
2. A wind profile extending from the surface to the displaced wind-reference height using Equation 3.7, but using the friction velocity calculated from Equation 3.14.

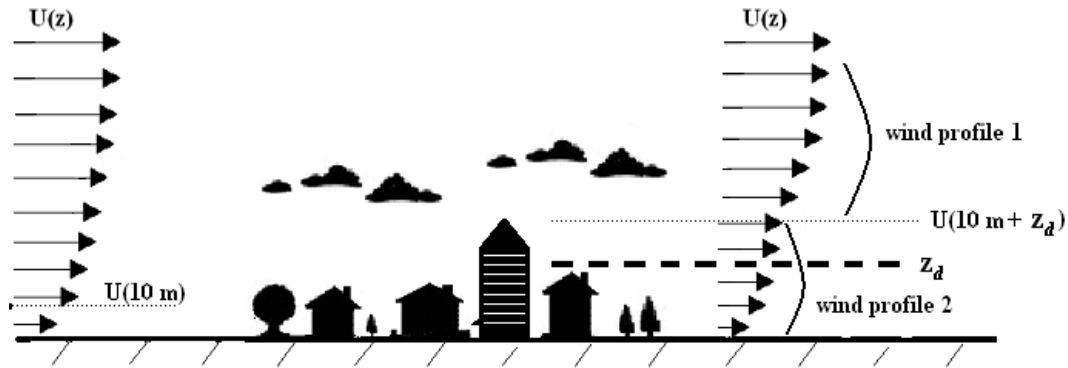


Figure 4. Illustration of the two wind profiles used if an urban displacement height of the main wind profile is necessary. Wind profile 1 uses the standard equation displaced upward by the displacement height. Wind profile 2 extends from the surface to the wind observation height: the displacement height + the wind observation height (usually 10m).

3.4 K- ϵ Constants

Richards and Hoxey (1993) argue that the standard K- ϵ modeling constants are not universally applicable and new constants must be determined to apply the model to the neutral atmospheric boundary layer. By analyzing the conservation equations of TKE and ϵ , they note that the boundary equations satisfy the conservation equation for ϵ only if:

$$\sigma_\epsilon = \frac{\kappa^2}{(C_2 - C_1)\sqrt{C_\mu}} \quad (3.15)$$

σ_ϵ , σ_K , C_2 , C_1 , and C_μ are the constants of the TKE and ϵ conservation equations that were originally estimated by Launder and Spalding (1974), and κ is the Von Karmon constant. Constant C_μ is the constant of proportionality that relates the turbulent viscosity to the length and time scales of TKE (from Equation 2.15). Constants σ_ϵ and σ_K are the turbulent Prandtl numbers for TKE dissipation and TKE, respectively. These constants relate the advection of TKE and ϵ through the atmosphere to the viscosity. Constants C_2 and C_1 are proportionalities that determine the production and loss of TKE dissipation rate.

The commonly used values for the constants are based on an evaluation of plane turbulent free jets and mixing layer simulations (Adaptive Research, 1997). They represent a “consensus” parameter set and can be assumed to represent a flow dependent model accuracy of 10-50%. The constants are:

$$\sigma_\epsilon = 1.3 \quad \sigma_K = 1.0 \quad C_1 = 1.44 \quad C_2 = 1.92 \quad C_\mu = 0.09$$

where κ is the Von Karmon constant estimated to be about 0.433 to satisfy the equation with the Launder and Spalding constants.

While these constants are commonly used in general engineering applications of the K- ϵ model, they are not necessarily applicable to the atmospheric boundary layer. The description of atmospheric turbulence is highly dependent on the value of C_μ since it is directly related to the equation for viscosity. Constant σ_ϵ is, in turn, dependent on the value of C_μ as can be seen in Equation 3.7, but it has been shown that modeling results are insensitive to σ_ϵ (Bottema, 1997). Chen and Kim (1987) suggest that σ_K should be less than 1, recommending a value for σ_K of 0.75 to satisfy observations of ϵ dissipating lower in the boundary layer than TKE. C_1 and C_2 are evaluated in Deterling and Etling (1984) for use in the boundary layer and are taken to be 1.13 for C_1 and 1.90 for C_2 . These values are similar to Chen-Kim values of $C_1=1.15$ and $C_2=1.9$. Huser et al. (2000) suggest the use of $C_2=1.83$ to limit the destruction of ϵ to conform to observed phenomena.

It is likely that C_μ is observed to be lower in the atmospheric boundary layer flows due to “inactive” turbulence (Bottema, 1997). Inactive turbulence can be defined as the large eddies in the flow that contain a significant amount of the turbulent kinetic energy but do not actively represent Reynold’s stresses at the grid scale that is being modeled. That is, they are considered turbulent but are not as fully active in local turbulent mixing as smaller eddies. These large eddies are produced by gravity waves, flow over objects, convective cells and other atmospheric phenomena. The representation of TKE as a scalar is the main culprit in this problem – an inability to account for the size spectra of eddies and directional qualities of TKE in eddies.

To account for the inactive turbulence, C_μ must be altered. Richards and Hoxey (1993) observed that with the commonly used C_μ of 0.09, Equation 3.8 gives K/u_*^2 as 3.3 in the surface layer of the neutral atmosphere. They further observed that the data from five different studies of the surface layer suggest a K/u_*^2 value greater than 3.3. Table 5 shows the values of K/u_*^2 from those studies and the calculated values of the constants C_μ (from equation 3.8) and σ_ϵ (from equation 3.15).

Table 5. K/u_*^2 Observed Values and Corresponding Calculated Constants.

Study	K/u_*^2	C_μ	σ_ϵ
Klebanoff (1955)	3.35	0.089	1.23
Panofsky & Dutton (1984)	5.48	0.033	2.02
Hagen et al. (1981)	6.2	0.026	2.28
ESDU (1985)	7.26	0.019	2.67
Silsoe (Richards and Hoxey, 1993)	8.75	0.013	3.22

Table 5 supports the value of 0.03 for C_μ estimated by Bottema (1997). However, such a low value for C_μ may only be appropriate in some portions of an urban

modeling domain. In a typical flow around a cubical building, several re-circulation zones will occur, as illustrated in Figure 3. The large re-circulation zone at the roof of the building and in the wake of the building will contain a large amount of turbulent kinetic energy, most of which is stored in larger eddies. In these regions, a lower value of C_μ may be justified. This suggests that different C_μ values may be needed within one domain, varied by the characteristics of a zone. Bottema (1997) recognized this by examining the roughness sublayer that is typically above the layer of buildings at the surface. Above the obstacle tops, inactive turbulence becomes significantly less, justifying a higher C_μ value. Varying the C_μ value is a feature of the Realizable K- ϵ variant model, with a resulting improved performance over the standard K- ϵ model.

Based on these papers, a set of constants for the K- ϵ model and its variants in the neutral boundary layer can be recommended:

$$\sigma_\epsilon = 2.12 \quad \sigma_K = 1.0 \quad C_1 = 1.15 \quad C_2 = 1.83 \quad C_\mu = 0.03$$

3.5 Domain Turbulence Distribution

One of the more important initial conditions that must be defined for a CFD model of the urban environment is an accurate wind and turbulence structure of the atmosphere. And this wind and turbulence structure must be maintained throughout the domain, except as it is modified by the structures and other blockages. However, it has been observed by many researchers (e.g., Hanna et al., 2004 and Riddle et al., 2004) that the TKE tends to dissipate too much in K- ϵ models, resulting in domain-exiting wind and TKE profiles that are not consistent with the incoming profiles, even in domains of consistent flat terrain.

It is a common recommendation, as described below, that CFD modelers conduct an initial model run in their domain with all internal obstacles temporarily removed. The results should confirm that the wind and turbulence profiles exit with almost the same profiles as the incoming air.

One approach to alleviate this problem has been suggested by Tang et al. (2005). A two-step approach involves initial modeling with a wind and turbulence profile estimate. The inlet and outlet of the model are coupled using “periodic” boundary conditions, which is part of most commercial CFD software packages. In this method, the outlet profile is used to iteratively modify the inlet profile until a stable boundary layer is obtained. Then, the user alters the mass flow into the domain until the desired friction velocity is achieved. From this process, profiles of velocity, TKE, and ϵ are calculated, which can be used as inlet conditions for the main modeling.

Another method to prevent TKE decay is to include a turbulence source term throughout the whole domain. From our observations with various projects, the TKE tends to dissipate fastest near the surface because of the higher initialized

dissipation rate of TKE at the surface. Our first attempt at a turbulence source term was to add a domain wide source term equal in rate to the dissipation term. However, this tended to overproduce TKE within the domain.

Through experimentation we have found that a turbulence source term of 60-80% of the TKE dissipation rate tends to help secure a constant wind profile and TKE profile in the domain. The coefficient will vary depending on the wind, turbulence magnitudes and choices for the K- ϵ model constants. This ad-hoc method is useful, but it should be noted that a domain wide source term will include production of TKE within areas of wind interaction with the structures and other boundary conditions within the domain. A possible alternative may be to contain the source region at the windward lead to the obstacles, ignoring the downwind region if dispersion of pollutants is unimportant there.

3.6 Pollutant Dispersion

Dispersion of pollutants in the atmosphere is due to advection, molecular diffusion, and turbulent diffusion. Molecular diffusion is irrelevant in the short time scales used in urban microenvironment studies. Advection of pollutants by wind will be fairly accurate if a proper wind profile has been prescribed and the flow patterns around the structures are improved by the use of a variant K- ϵ model or an advanced CFD model such as LES. Dispersion by advection can also be improved if modeling is conducted using an unsteady state model that allows for small time scale variances in wind speed and direction.

Turbulent diffusion is the primary process that determines pollutant dispersion in the atmospheric boundary layer. Therefore, when modeling dispersion, careful attention must be directed towards the parameterization of turbulence to obtain accuracy. Turbulent fluxes of momentum are not equal in all directions near the surface. In a stable and neutral atmosphere, turbulent flux in the vertical is less than that in the horizontal because the presence of the earth's surface and the wind velocity gradient tend to suppress vertical turbulence.

In a typical CFD study of the urban microenvironment, we are going to be interested in modeling the most common case, a neutrally stratified boundary layer. In this case, turbulence is entirely from mechanical forcing due to surface friction and vertical wind shear. Typical surface layer observations indicate that in neutral conditions, the three direction-dependent ratios are $\sigma_u/u_* \approx 2.5$, $\sigma_v/u_* \approx 1.9$, and $\sigma_w/u_* \approx 1.3$ (Arya, 1988). Considering these observations, it would be important to model dispersion based on independent, directionally-dependent turbulence parameters. Unfortunately, the standard K- ϵ model and most K- ϵ variants only consider turbulent kinetic energy as a directionally-independent scalar. A Reynold's Stress Model (RSM) would be a more appropriate model for dispersion modeling, since it is able to account for the individual, directionally-dependent Reynold's stresses (Riddle, 2004).

3.6.1 Diffusivity in the K- ϵ Model and Schmidt Numbers

When the K- ϵ model or K- ϵ variants are used, special approaches may be incorporated to account for the anisotropic turbulence of the actual environment. Tang et al. (2005) point out that the greater standard deviation of horizontal wind speed is due to turbulent dispersion and small changes in wind direction. To account for this, they modeled steady-state solutions and then smoothed the results over the expected range in wind direction.

Another option to simulate dispersion may be to modify the diffusivity of a pollutant in the vertical in order to restrict diffusion in the vertical. This can be done by assigning a higher Schmidt number to vertical diffusion than to horizontal diffusion. The Schmidt number is a coefficient that relates the turbulent viscosity to the diffusivity of a pollutant by the equation,

$$D = \frac{\nu_T}{Sc} \quad (3.16)$$

where D is the diffusivity of the pollutant, ν_T is the turbulent viscosity, and Sc is the Schmidt number. One would expect that in an atmosphere free of significant buoyancy forces, the diffusivity of a pollutant is entirely dependent on the diffusivity of momentum. With higher Schmidt numbers, the dispersion of the pollutant will be suppressed, or in other words, the pollutant will disperse slower than the diffusion of momentum. Typical dimensional Schmidt numbers may be $\sigma_y = 0.55$, $\sigma_x = 0.77$, and $\sigma_z = 0.77$, where z is vertical, x is with the flow, and y is perpendicular to the flow (Scanlon, 1997). Based on these values, a good base ratio of vertical dispersion to horizontal dispersion would be 5/7. These concepts are illustrated in Figure 5.

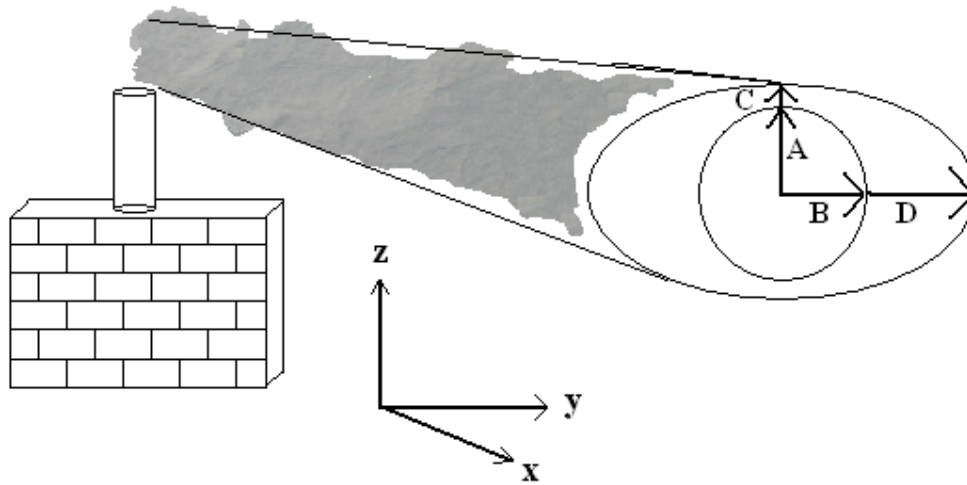


Figure 5. Illustration of the use of Schmidt numbers to parameterize dispersion. In this figure, a plume is dispersing downwind. The boundaries of the plume at a point downwind are illustrated in a vertical slice of the plume. Diffusivity of the plume is based on the turbulent diffusivity. Vertical spread A and horizontal spread B are equal in the case where no Schmidt number is used because turbulent diffusivity is not directionally dependent, being a non-dimensional scalar. Schmidt numbers can be applied (Equation 3.16) to enhance or limit dispersion in the x,y, or z direction to conform with realistic conditions. Spread C and D demonstrate the plume spread in the vertical and horizontal after different Schmidt numbers have been applied.

Some field studies and experiments have shown that the Schmidt number is fairly constant in the atmospheric boundary layer in the absence of significant buoyancy effects (Baik, 2003). So, the assumption of a constant Schmidt number may be valid for the general CFD case discussed in this chapter. Schmidt number values ranging from 0.18 to 1.34 have been measured in field observations under a variety of atmospheric conditions (Tang et al., 2006), but Schmidt numbers of 0.7 to 0.9 have traditionally been used in CFD models of the neutral atmosphere.

In a recent study, various Schmidt numbers were used in CFD simulations to compare with the Project Prairie Grass field dispersion study (Tang, 2006). CFD simulation results were compared to the plume centerline concentrations. In this study, the researchers found that a Schmidt number near 1.3 performed best for more near range dispersion (50 meters), and Schmidt number near 1.0 performed best for the longer range dispersion (100m – 800 m).

Based on the findings of the Tang et al. study, we recommend a higher Schmidt number than the typical range of 0.7 - 0.9 generally used in short range CFD studies. Values ranging from 1.0 - 1.3 would be more conservative numbers to use.

3.7 CFD Domain, Meshing, and Recommended Modeling Specifics

There is a consensus among urban wind engineering CFD researchers on certain aspects of the setup of the CFD domain and settings. The distance of the domain sides to the buildings, the resolution of cells within regions of interest, and the numerical settings of the model can all have significant influence on the quality of the modeling project. Recommendations for these settings are provided in this section.

3.7.1 Domain Size

It is important to ensure that the walls of the domain, which contain your inlet and outlet boundary conditions, are far from the subject buildings, sources, and significant topography. If they are too close, interactions between the boundaries can distort results.

In our earlier paper (McAlpine and Ruby, 2004) we provided a recommendation for domain size and the placement of buildings and obstructions in the domain that is based on air quality modeling rules. We have found that a rule based on the maximum modeled wind speed and building dimensions is effective in avoiding edge effects. Others have focused more specifically on the building height.

Hall (1997) recommends that the domain walls upwind of the building should be $5H$ in distance from the building with H being the height of the building. The top of the domain and sides of the domain should also be $5H$ in distance from the building faces or top. For multiple buildings, the height of each building needs to be taken into account to determine the distance as illustrated in Figure 6. Downwind, the outflow boundary should be at least $15H$ beyond from the buildings to allow the development of the flow behind the structures, which may extend some distance downwind (Franke et al., 2004).

If extensive topography is present in a model, it is advantageous to extend the domain boundary out to a region of relative flatness so that significant topographical features don't interact directly with the domain wall boundary conditions.

Buildings upwind of the site of interest need to be included in the modeling if they will have significant effects on the airflow at the site. This is especially true in high wind cases where significant "skipping flow" may occur. A general guideline is to include buildings upwind and downwind that are $6-10H_n$ in distance from the site of interest, where H_n is the height of the upwind/downwind buildings (Franke, 2004). For greater wind speeds, use the higher standard up to $10H_n$, and for lower windspeeds use $6H_n$.

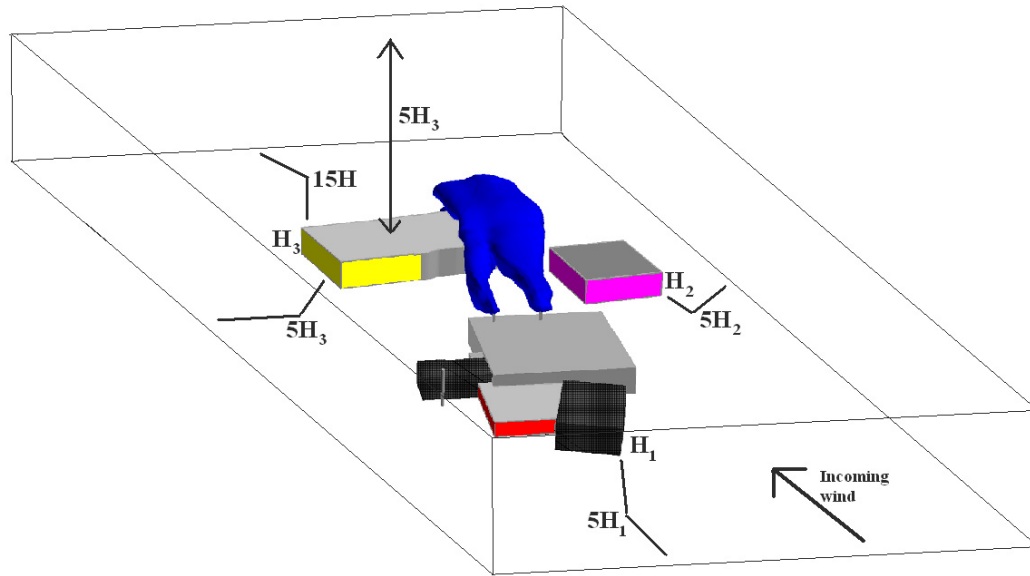


Figure 6. Illustration of domain wall distancing. The domain includes several buildings and one wind condition. Pollutants from two stacks are illustrated from the source building as blue plumes. H_1 , H_2 , and H_3 label the heights of the respective buildings.

3.7.2 Meshing and Cell Size

When building a model, careful attention needs to be directed towards determining the number of cells in the domain. With too few cells, the model may not be able to resolve the complex flow around objects or may result in excessive numerical diffusion. With too many cells, the computing resources may be limited, extending the time of model runs beyond the scope of your project.

A few sets of guidelines have been suggested for mesh sizing. Most of these are focused on structured hexagonal meshing of domains. Other types of meshing schemes may require other insight, but this does not mean they are not any better nor any worse than hexagonal meshing. Unstructured grids may be especially useful when grid refinement is needed near areas of concern or variability. However, the ERCOFTAC Best Practice Guidelines (ERCOFTAC, 2000) do recommend the use of hexagonal meshing over tetrahedral meshing when boundary layer modeling is critical.

The number of cells needed in the model can be estimated by the size of objects in the domain. One system of estimation is to include 10 cells per cube root of the building volume (Franke, 2004). For a cubical building of 10-meter sides, the building would have a volume of 1000 m^3 . The cube root of this is 10, so 100 cells per building side would be warranted. This is, of course, a vague guideline and would not be applicable to all scales.

Number of cells per unit length may be decreased further from the area of interest to limit the number of total cells in the domain. One recommendation is that the number of cells between buildings should be at least ten (Franke, 2004). Other minimum grid sizes suggested have been $0.025H$ (Cowen, 1997), $0.01H$ (Scaperdas, 2004), or $0.2H$ in the horizontal and $0.05H$ in the vertical (Bartizis, 2004).

There is relative flexibility in the number of cells chosen for a model. One must include enough cells to resolve the important flow features and site detail in the model. We have had some experience modeling large buildings with very small lab hood stacks. Our goal in these cases was to attempt to use 3 - 6 cells per smallest size of element so that the flow out of the stack would at least be partially resolved. If the element of importance, such as a small stack, is too small, then parameterization may be needed for pollutant release. One parameterization strategy may be using a "box model" that would define a zone around the stack outlet and modeling the flow and pollutant release from a specified distance from the stack. With a "box model", the correct volume and momentum of stack exhaust are modeled without the need of modeling the details of the stack itself.

Regardless of cell size, a mesh independence study must be conducted initially to get an idea of how the cell size influences the flow. Details such as TKE magnitude, recirculation zone location and size, or velocity magnitudes can be observed to judge mesh influence. The goal is to find the largest cell size that resolves the flow without significant changes from a slightly smaller cell size grid.

3.7.3 Modeling Time Steps

The length of time necessary for a steady-state solution in a micro-scale meteorological project will vary depending on the size of the domain and complexity of the model. A first-guess time estimate can be based on the 10-meter wind speed and the length of the model. For example, if your domain is 200 meters long and the wind speed is 4 m/s, then it would take 50 seconds for the incoming air to reach the other side of the domain in a flat, obstacle-free domain. This would be the first-guess minimum time and results every 5-10 seconds in a time series could be observed after 50 seconds until a steady state solution is qualitatively observed.

For most bluff body flows, a steady state solution may not be completely obtainable due to vortex shedding in the wakes of objects. For an air quality study, it is most desirable to try to use the set of results that most resembles the flow average. When observing an unsteady state solution, vortex shedding can be observed in the wake of the building. The solution can be frozen as a final result in the middle of a vortex shedding cycle so that the wake is near average size.

Overall, in our experience for typical flows of 2 m/s to 8 m/s in a domain size covering a city block or so, we tend to see a quasi-steady state solution around 100 - 200 seconds. We would recommend using at least a 90-second run for most typical modeling runs of this scale. After a steady state solution is obtained, it can be frozen and the model can be re-run with the species transport equation to model the dispersion of the pollutant throughout the domain.

3.7.4 Selection of Wind Scenarios for Modeling

When selecting the scenarios for modeling for a project, one needs to avoid redundancy and limit the number of runs. This is especially important for large complex domains where a single CFD run may take many days with desktop PC computing resources.

The most important wind directions are obviously those that blow directly from source to receptor. Receptors may include air intakes, operable windows, doorways, pedestrian walkways, and other sensitive locations where persons may be exposed to the contaminant. For each wind direction, a sensitivity analysis should be conducted by adjusting the wind direction by 3° - 7.5° clockwise and counterclockwise. The differences in concentrations at receptors should be noted for each alteration. A sensitivity analysis may also be needed even if your modeling approach includes an unsteady-state time averaged solution with incoming wind of varying wind directions.

For a pedestrian comfort or natural ventilation study, wind directions must be more uniformly distributed with perhaps a total of 16 wind directions analyzed to cover all the major wind directions (Ratcliff, 1990).

For wind speed, a good variety is needed to assess the distribution of mean wind speed and gusts. For pedestrian comfort studies, the higher wind speeds should be studied since high wind gusts will be the main cause of nuisance. For air pollution studies, lower magnitudes will need study since the most problematic situations occur when receptors are impacted for longer lengths of time.

Generally for air quality studies, the 99.5th percentile, 95th percentile, 75th percentile, and mean wind speeds for each wind direction are a good basis for wind speed selection. For example, for a meteorological data set in the Seattle area for a southwest wind, the 99.5th percentile is 9 m/s, 95th percentile is 6 m/s, 75th percentile is 3 m/s, and mean wind is 2 m/s. A good spread of wind speed is needed in a project to cover the variety of conditions that may occur. It is also advantageous to conduct a sensitivity analysis for a wind speed for each direction by varying the wind speed by 0.2 m/s or so.

4 Industry Opinion and Guidelines

Overall, the general opinion in the industry is that engineers and scientists should use caution in applying CFD to air quality questions. User skill continues to be an important element in model success. More validation work and continued improvement of turbulence models are needed. A number of guidelines and recommendations have been established to guide the practitioner, but they tend to differ from one another. This section reviews the current opinion of practitioners and outlines the various guidelines available at this time. The section concludes with a set of recommendations based on the available advice.

4.1 Industry Opinion

Much of the current opinion on the use of CFD is based on comparisons to physical modeling results, mainly wind-tunnel modeling. Reviewers admit that even though CFD has great promise in replacing the wind tunnel for micro-scale modeling, it is still in a learning stage. However, it is quickly maturing and its current use as an analysis tool is appropriate if used with caution and awareness of its weaknesses. Some of the complaints about CFD accuracy seem excessive and pedantic.

A review by Stathopoulos (1997) concluded that “practitioners should be warned about the uncertainties of the numerical wind tunnel results and urged to exercise caution in their utilization.” He is concerned that there is an “ever-increasing confidence in the results obtained by CFD codes and more and more papers propagate the idea that the numerical wind tunnel does exist today and produces results ready to be used by practitioners.” He reviews several of the more prominent current studies that compare CFD results to experimental data. He notes that while some results are quite good, others deviate greatly. Most of his criticism focuses on the poor pressure distribution on bluff bodies estimated by the standard $K-\epsilon$ model, which is widely acknowledged to be inadequate. For environmental flows and flow over complex terrain, the models perform better, but some problems are still evident. For air quality analysis projects, he again notes the poor performance of the standard $K-\epsilon$ model. An improved model better predicts the results in study he reviewed, with a tendency towards a conservative solution (over-prediction of pollutant concentration), which is beneficial for air quality planning.

In a review by Murakami (Murakami, 2002) of the CFD related research papers in the Computational Wind Engineering 2000 Symposium, he observes that, for his taste, the direction of research in the field is too focused on applications and not on improving the models themselves. He directs attention to the inadequacy of the log-law type wall boundary condition, the potential for high numerical error with the standard $K-\epsilon$ model, and the errors caused by poor modeler choice of gridding and boundary conditions.

While these authors note that “none of the existing models. . . [have] an overall high prediction accuracy”, “the prediction accuracy is sometimes insufficient” or the models “are not perfect”, they also observe “remarkable progress” in the development of CFD models. They note that “the predictions . . . are in good agreement with the experimental data.” They cite some papers with results in good agreement with the experimental data but also report a paper that “fails to predict” the experimental observations. Looking at each of the figures in the Stathopoulos paper, one can see close, but not precise, correspondence between the experimental data and the CFD results, with the range of CFD results similar to the spread in the experimental data.

Despite the acknowledged shortcomings of CFD modeling, there are some advantages to using it as an analysis tool. One benefit is that CFD can provide data at many more points than a wind tunnel and can work at full scale. This is a significant advantage over wind tunnels for urban dispersion (Wright, 2004), particularly when an area wide distribution of pollutant concentration is desired. The ability to model full scale allows for interactions between building interiors and exteriors, and in atmospheric boundary layers with various stability conditions, which is another advantage over a wind-tunnel.

Overall, the critics recommend that CFD be used as an analysis tool rather than a design tool in conjunction with another analysis method. Modeling might be conducted in conjunction with an alternative form of air quality analysis such as Gaussian modeling or theatrical fog release. In any case, careful scrutiny of the results is needed. Careful attention must be directed to the atmospheric boundary layer setup, preferably using a setup scheme and validation as suggested in this chapter. Any study should also include a grid independence run and sensitivity analysis of variations due to boundary conditions or wind speed and direction. Lastly, the shortcomings of the study should be communicated in the report.

4.2 Published Guidelines

There are several sets of CFD guidelines that can be applied to micro-scale urban air quality studies. In this section we will discuss the details of three distinct sets. It is recommended that any practitioner in the application of CFD for air quality analysis follow strictly the first of these sets (the ERCOFTAC set) of guidelines, and refer closely to the recommendations of the last two sets of guidelines (COST and QNET-CFD). An additional set of guidelines of best practice are presented in the Project EMU final report, which is based on the results of that study.

4.2.1 ERCOFTAC Guidelines

A set of best practice guidelines were published in 2000 for general use of CFD for industrial applications by the European Research Community on Flow, Turbulence and Combustion (ERCOFTAC, 2000). Practitioners frequently cite these guidelines as a foundation for industrial CFD practices. Though it is a

general set of guidelines, and does not contain any specific recommendations for computational wind engineering, it is a good basic protocol to follow for any CFD application.

The ERCOTAC guidelines were published by the Special Interest Group on “Quality and Trust in Industrial CFD.” They were commissioned following an “extensive consultation with European industry which revealed an urgent demand for such a document”. The guidelines claim that they offer about 20% of the most important general rules of advice and cover about 80% of applications. The content of the document is quite applicable to air quality studies considering the types of flows it focuses on. The majority of the document covers topics such as meshing, quality assurance, time-stepping, CFD settings, boundary conditions, and validation/verification.

Some of the more important guidelines from the document that can relate to most micro-scale air quality project are included here in an overview. Guidance for inlet/outlet and related boundary conditions for the atmosphere are not included, but the guidance recommends careful attention to the setup of these to correspond to the reality of the process being modeled. The setup procedures for the atmosphere discussed earlier in this paper generally comply with these guidelines.

One should obtain the document and follow its guidance if performing or reviewing a CFD project. Following is a discussion of a selection of the guideline’s topics that have not already been discussed in this paper:

- A. Validation - Guideline 11.5: “Validate it against test data for a similar application with similar flow structures and flow physics.”

Before beginning a CFD project, the user should conduct several sets of validation tests to establish the user’s ability and ability of the software to accurately model the type of problems being examined. This is important because it has been demonstrated that CFD project results can vary greatly from user to user simply due to personal choices for meshing and boundary condition setup, even using the same CFD code and prescribed conditions (Stathopoulos, 2002). Conducting the validation exercises is alone a valuable learning opportunity for the new CFD practitioner.

A good first validation exercise is to model the flow around a simple cube in an atmospheric boundary layer. A good set of data to use is that of velocity measurements from Minson (1995). Also, the lengths of re-circulation zones behind the block can be examined by comparing to those observed in wind tunnel tests conducted by Snyder (Snyder, 1994).

B. Model Choice - Guideline 11.6.1:

Be aware of the weaknesses of the standard K- ϵ model and use an alternative model if possible using the guidance this chapter has discussed. Conduct a sensitivity run by using a different model and comparing the results to your original model. For dispersion, a method must be used to account for the inability of the K- ϵ model to handle the anisotropy of turbulence in the surface layer of the atmosphere.

C. Guidelines on wall functions - Guideline 11.6.2:

Wall functions are used by CFD to parameterize the transition from laminar flow to turbulent flow at the wall boundary. The common log-law wall function calculates flow near a wall assuming that each cell is within the turbulent layer. Therefore, meshing must account for this, making sure that the center of the first cell is outside of the laminar layer. Not doing so can have an impact on the accuracy of the flow in terms of heat transfer and turbulence dissipation. The y^+ value is a measurement of distance from the wall with relation to the laminar layer calculated using the friction velocity of the layer. The guideline states that a y^+ value of 30 is a good goal. Considering the high Reynold's number of atmospheric flows, higher values of y^+ up to 50 or 100 are acceptable.

The y^+ value is calculated by:

$$y^+ = \frac{u_*^* y}{\nu} \quad (4.1)$$

where y is the distance to the center of the first cell from the surface, u_* is the friction velocity, and ν is the kinematic viscosity of air.

D. Guidelines on grid design - Guideline 11.8:

For hexahedral cells, gridlines should be optimized in an effort to achieve $\sim 90^\circ$ for all sides. Included angles of less than 40 or more than 140 degrees deteriorate the results. Avoid non-orthogonal cells near boundaries (surfaces and domain boundaries). Avoid aspect ratios that are too high (ratio of one edge of the cell to the perpendicular edge). The goal should be to maintain an aspect ratio of near 1:1 in areas of importance in the domain, but no greater than 5:1 (CFD2000, 2002). The ERCOFTAC guidelines state that ratios as high as 20 - 100 can be satisfactory, and we have found this acceptable for regions near the outer edge of the domain. Expansion ratios of cells (the increase in cell length from one layer of cells to the next) should also be kept at a minimum, following recommendations by the code creator (1.3 is the maximum expansion ratio recommended for CFD2000).

E. Guidelines on temporal discretization - Guideline 11.10.4:

Second order accuracy is recommended in both space and time. Also conduct sensitivity analyses by varying the time step, changing grid size, and by trying higher order schemes for convection.

4.2.2 Guidelines from the COST Action C14 Working Group 2

COST (European COoperation in the field of Scientific and Technical research) is a framework for the cooperation of research institutions in Europe on a matter of pressing subjects. Action C14 is the study of the “Impact of Wind and Storms on City Life and the Built Environment,” and is part of the Urban Civil Engineering group of COST. Working Group 2 of Action C14 is dedicated to CFD techniques involving the analysis of urban wind climate. The main focus of the group is pedestrian climate, but its efforts can be applied to other urban applications such as air quality modeling. Their set of guidelines is also based off of recommendations from the QNET-CFD and ERCOFTAC guidelines.

The following list includes some of the more important guidelines from their publications available at <http://www.costc14.bham.ac.uk>. (Franke, 2004):

- Use of the RNG model is suggested over K- ϵ or K- ϵ variants, in order to use an anisotropic turbulence model
- Area of radius for a project: ~ 300 m around a region of interest
- Buildings within 6-10 times their own height distance from a project should be included in the model
- Geometrical details with size > 1 m should be included in the model in the region of most interest
- Surrounding buildings should be simple blocks with less detail
- The domain sides should be $5H$ in distance upwind and laterally
- Domain top should be $6H$ above ground
- Domain outlet downwind should be $15H$ in distance from the last structure
- Blockage ratio of buildings for incoming wind should be $\leq 3\%$
- Lateral and top boundaries should include symmetry and no re-entry of the flow
- The domain outlet should have a zero gradient for all variables
- Use of the Richards and Hoxey (1993) equations for wind, TKE, and ϵ profiles
- Smooth walls for pedestrian comfort study with a higher density of cells nearer the surface
- For pedestrian comfort, the height region of interest for pedestrian wind speed should be at the 3rd or 4th cell from the surface
- Use second order methods for advection and diffusion for a final solution
- Demonstrate grid independent solutions: refine model by 50% more nodes in each direction.

4.2.3 QNET-CFD

QNET-CFD is the “Thematic Network on Quality and Trust for the industrial applications of Computational Fluid Dynamics.” It is a European program formed to provide industry with guidance on CFD techniques and quality control for industrial applications. QNET-CFD guidance is divided into 6 thematic areas. Two of these areas of focus, “Environmental Flows” and “Construction and HVAC”, involve micro-scale air quality evaluation problems. Because of this direct focus on selected applications, QNET-CFD is a good reference for guidelines on any CFD project (QNET, 2005).

The guidelines for each thematic area were developed by different teams performing baseline type projects and recommending engineering advice based on their research and experience with these baseline projects. Each baseline project involved a physical test where data was gathered on physical properties of the flow. The QNET project involved simulating each physical study using CFD and comparing the results.

There are some differences in the guidelines for each application. A user should be able to judge by reviewing the baseline project if the provided guidance is applicable to his/her study. The following sub-sections contain specific guidelines for both related Thematic Areas.

4.2.3.1 Thematic Area 4: Best Practice Advice for Civil Construction and HVAC

Although this section covers both hydraulics and transport infrastructure, the main portion of it focuses on the built environment for both external and internal flow. Five applications were demonstrated for this thematic area, each concluded with best practice advice. For micrometeorological air quality studies, only one of these projects was directly similar - “Wind Environment Around an Airport Terminal Building” (Scaperdas and Gilham, 2004).

The following best practice advice is recommended in the discussion of this project:

- A 3-D calculation should always be used.
- The computational domain should be no smaller than 5H upstream, 15H downstream, and 4H on either side.
- Simplification of building geometry is necessary and a refinement of all details down to 0.01H is recommended if the details may have influence on the region of interest.
- A gradual expansion ratio of 1.2 can be applied.
- The inlet boundary conditions should use the wind, TKE, and ϵ profiles recommended by Richards and Hoxey (1993), and Castro and Apsley (1997). Both sets of profile equations have logarithmic wind profiles. Castro and Apsley’s conditions contain a distinction for TKE based on a

surface layer (up to $0.9H$) and above the surface layer. The ϵ profiles are similar.

- The ground boundary should be applied with a rough wall with appropriate z_0 value.
- Unsteady RANS equations give better results. LES is the best option.

4.2.3.2 Thematic Area 5: Best Practice Advice for Environmental Flows

For this thematic area, five applications were demonstrated for practice advice, four of which directly relate to urban microenvironment applications. Each application and the best practice advice for each are discussed below:

1. Flow and Dispersion in the Presence of an L-shaped Building:

This application concerns the experience of a firm with the EMU project described earlier in this paper. This project concerned the dispersion of a non-buoyant tracer gas around an L-shaped building. The best practice advice for this type of application is:

- Computational domain with sides at: $8H$ upstream, $15H$ downstream, and $6H$ vertical
- $0.2H$ horizontal grid spacing in the region of the source and building.
- $0.05H$ vertical grid spacing in the region of the source and building
- Expansion ratio of no more than 1.2
- Maximum horizontal grid resolution of $2H$
- Maximum vertical grid resolution of $0.5H$
- 2nd order accurate numerical schemes, under-relaxation factors avoided
- Advanced RANS or LES

2. Dense Gas Release over flat terrain with and without obstructions:

This project involved the continuous jet release of a cold dense gas over flat ground. Dispersion over the flat surface and around an obstacle on the surface was simulated. The best practice advice for this project was as follows:

- Vertical velocity at the top of the domain should be kept at zero.
- Ground heat transfer should be limited to conduction.
- Size of the domain should be at least $8H$ upstream, $15H$ downstream, and $6H$ vertically.
- Expansion ratio of 1.2
- Underground domain should be a depth of $1H$ with 10 cells vertically.

3. Urban Scale Problems:

This effort involved modeling the dispersion of exhaust in a 2D array of buildings with emphasis on the concentrations in the canyons between the buildings.

- 2-D idealization is suitable for street canyon modeling when the wind is perpendicular to the street axis.

- An asymptotic roughness and displacement height is needed to reflect the urban nature of the domain.
 - Domain including 2 canyons upstream and two downstream is adequate.
 - A horizontal resolution $< H/10$ has little further effect on accuracy (i.e., $0.1H$ resolution is good enough to accurately model the flow).
 - A vertical resolution of $H/10$ is adequate.
4. Flow and Dispersion over isolated hills and valleys:
This project involved modeling the dispersion of pollutants from a stack located in the wake of a hill. The physical test was conducted in the EPA wind tunnel. The Best Practice Advice for this project is as follows:
- Upper boundary should be $10H$ above the hill.
 - Surface should be fully rough.
 - Downstream outlet should be at $20H$ behind hill (depends on area of interest for exposure to pollutant).
 - 2nd-order differencing for convective terms is crucial.
 - Horizontal mesh of $0.1H$ at hill summit is best.
 - Vertical mesh of $0.01H$ at hill summit is best.
 - Proper wind and turbulence profiles are necessary.
 - Avoid using the standard $K-\epsilon$ model - more advanced model needed.
 - Unsteady flow should be used.

The environmental flow thematic area discussion is wrapped up with a discussion on best practice advice that is common for all projects of this type. Some of these points are as follows:

- Coriolis force can be ignored for small-scale surface layer flow modeling.
- Modeling of buoyant forces is necessary for realism.
- Larger scale modeling will make the incompressible assumption invalid.
- 2nd-order accuracy is necessary.
- LES is recommended over RANS modeling.
- 3-D pollutant dispersion modeling requires non-isotropic turbulence parameters to account for the differences in directional dispersion.

4.2.4 Project EMU Conclusions - Best Practice Advice

Based on the results of Project EMU, which is described in more detail in section 5 of this chapter, the authors were able to provide a set of best practice advice. However, they are rather vague compared to the other guideline sets. They note that as the scenarios became larger and more complex, it was increasingly more difficult for the teams to satisfy common best practice advice. Due to this, problem size limits the applicability of best practices. The list of recommended guidelines is summarized as follows:

- Objectives: The user should have a clear pre-modeling plan with emphasis on how uncertainty is to be handled. The plan should include detail on

how the domain setup will fit to the test with more detail in regions of interest.

- Preliminary “scoping” calculations: Domain size and modeling time should be estimated to give a proper estimate of cost and time to the client.
- Domain size: Follow the common 5H rules for domain side distance from obstacles and be careful to have a long enough domain to account for pollutant transport.
- Mesh Architecture: Finer mesh is needed near sources and around buildings. The author points out that mesh independent solutions are “generally not achievable with this class of problem.”
- Boundary conditions: Realistic atmospheric boundary layer profiles of wind and turbulence are needed.
- Numerics: Use of higher-order differencing (2nd order or greater).
- Turbulence model: standard K-ε model is adequate near the building, but a model tuned for atmospheric flows would be better for far-field dispersion.
- Time accuracy: It is important to pay attention to the Courant number. This is a limit on the time step of the calculation and is defined by:

$$C = \frac{\Delta t}{\Delta x_{cell} / u_{fluid}} \quad (4.2)$$

- Quality assurance: QA plan should be prepared before the project and followed closely.
- Output: Careful planning before project to ensure that analysis methods are correct.
- Resources: CFD user experience with software, code, and dispersion science is crucial. They found 4 to 6 months of experience with the CFD code was necessary to achieve reasonable results.

5 Validation and Verification

Computational modeling of any type is absolutely worthless without a rigorous effort to validate the approach to the physical phenomena it is meant to simulate. This is a critical issue in CFD today when we consider that CFD itself is extremely complex and that the physical processes being modeled (turbulence, heat transfer, diffusion, etc.) are not entirely understood or resolved mathematically. Thus, an ongoing effort of model improvement through verification is necessary before any claim can be made about the predictability of a model.

CFD, under its various forms, has been validated for many different types of flow phenomena. For computational wind engineering and micro-scale urban dispersion, this has been somewhat of a challenge. Verification studies have

demonstrated a number of difficulties in micro-scale meteorological modeling using CFD in its various forms, but also significant and useful results.

The main difficulty has been in the complexity of bluff body flows. Flow around a fixed object is inherently transitory and characterized by vortex shedding. This fact considerably impairs the credibility of steady state modeling. It has been observed that “separation and re-circulation regions develop, wash away resulting in uniformly down-wind flows over the roof, and then the circulation zone redevelops” (Meroney, 1999). Also, bluff body flows can contain separation zones and re-circulation zones that can not be accounted for well in the standard log-law wall functions.

The isotropic turbulence assumption is problematic in the surface layer of the atmosphere. In the atmosphere, the size and scale of turbulent eddies is dictated by the presence of the ground and the static stability of the atmosphere. Thus, eddies have an easier time moving laterally than vertically. Pollutant dispersion is mainly determined through turbulent diffusion, so directional spread of the turbulent eddies is very important.

5.1 Flow Around a Block

Much of the validation work of CFD for wind engineering involves studying the simulated flow around a simple cube. This is a great validation exercise for buildings because most buildings consist of groups of cubes and rectangles. Even though the geometry is simple, the flow around a simple block is quite complex involving strong pressure gradients, streamline curvature, separation and reattachment, and re-circulation zones (Scanlon, 1997). Also, a great deal of wind-tunnel data is available to ensure that the details of the flow around a block are well described, such as that by Castro and Robins (1977), which is a common study referred to for CFD validation.

Murakami and Mochida (1989) were among the first to conduct validation studies of CFD modeled flow around a block. They carried out a series of CFD runs and compared them to wind-tunnel studies of flow around a 200 m cube. Their studies demonstrated that meshing of around $0.17H$ produced poor results in velocity direction and magnitude around all parts of the block. Best results were produced when mesh resolution was increased to about $0.04H$ around the entire block, including the lee of the block where re-circulation zones were sensitive to the mesh interval. They demonstrated that with sufficient mesh resolution the flow around the block and surface pressure distributions, including recirculation zone position and magnitude, was simulated rather well.

As previously described, Murakami and Mochida also found that the $K-\epsilon$ model had difficulties in accurately predicting TKE and ϵ . First, they found that the mesh in the lee of the block had to be fine enough to accurately promote the production of TKE and ϵ . Under-prediction of TKE tends to elongate the size of the re-circulation zone. They also noted the common over-production of TKE at

the windward sharp edge of the block, and attributed it to the inability of the wall function to handle separation at this point.

K- ϵ variant models such as the MMK model, discussed earlier, were found to improve model performance at the sharp edge, but it did not improve flow in the wake, as it tended to over-predict the lengths of the recirculation zones. The Chen-Kim and RNG models showed more success at improving the predictability of the flow around a building.

The findings of Murakami and Mochida suggest that the K- ϵ model is good at predicting flows around a block, but needs improvement if dispersion around the block is going to come into play, considering that accurate representation of TKE is needed to model the dispersion correctly. Many studies have been conducted that involve the dispersion of exhaust around a cube. Generally, they have found that in neutral flow conditions the K- ϵ model reasonably predicts ground concentrations of pollutants released at the roof level (Zhang, 1996 and Scanlon, 1997). Concentrations tend to be overestimated on average, which is good for a conservative air quality evaluation.

5.2 Dispersion in a Street Canyon

The case of dispersion of pollutants in a street canyon, both with the source inside and outside of the canyon, has been a significant focus of air quality study. It is important because of the high concentrations of carbon monoxide and diesel particulate matter in dense urban topography that consists primarily of street canyon grids. In these arrangements, “skipping flow” often occurs, trapping the pollutants in the canyon. Because of these concerns and the relatively simple geometry of the case, it is a useful baseline case for CFD validation studies.

Most validation studies involve analyzing the positioning of streamlines within the canyon and the magnitude of velocity at certain points within the canyon. Also, TKE within, above, and at the walls of the canyon can be compared to experiments. Since the dimensions of street canyons can vary in width and building wall heights, a lot of attention has been directed to the difference in flow and dispersion with varying dimensions. The common aspect ratio, which is the ratio of canyon width to building wall height (the baseline case always considers canyon wall buildings to be the same height), is often the focus of attention in studies.

Baik and Kim (1999) conducted a numerical study of flow and dispersion in street canyons with different aspect ratios using the “Realizable” K- ϵ variant model. The study focused more on the nature of the flows rather than comparison to experimental results. However, their results did indicate that the vertical velocities at the canyon walls in a canyon with aspect ratio Height/Width = 1.2 was close in magnitude to that of a wind-tunnel study. They also say the locations of TKE maxima and minima are the same as found in experimental studies.

Sagrdado et al. (2002) conducted a numerical study of pollutant dispersion in a street canyon as a validation, with their results directly compared to experiment. The numerical simulations were conducted using the “Realizable” K- ϵ variant model. This study was conducted using blocks separated by an aspect ratio of 1, with both canyon walls the same height for the first case and the lee canyon wall higher in the second case. The study also took into account a case where an upstream building influenced flow at the canyon. The results of the numerical simulation are qualitatively quite similar to that of the experiment; the streamlines, re-circulations, and separation points are almost identical in most cases. However, the velocity magnitudes and pollutant concentrations differ quantitatively. The authors indicate that the discrepancies may be due to the weaknesses of the 2-D steady state solution, suggesting it cannot account for the 3-D, unsteady characteristics of real flow.

5.3 Dispersion Over a Flat Field

Another baseline validation study is the dispersion of a tracer in the atmosphere over a flat field. This is an important validation effort because it tests the model’s scheme to disperse pollutants within the atmospheric boundary layer. As discussed earlier, models with isotropic turbulence assumptions cannot account for the directional differences in turbulent flux in the surface layer.

Most validation studies have involved comparing numerical CFD results to measurements from the famous “Project Prairie Grass,” consisting of 70 scenarios of neutrally buoyant gas releases over an open agricultural field. This and several other studies were combined to determine the standard Gaussian vertical and horizontal dispersion coefficients that are still used in many of today’s air quality models, such as EPA’s SCREEN and ISCST3.

Tang et al. (2005) have been active in validating RANS modeling for dispersion over a flat field by comparing their numerical results to the “Project Prairie Grass” results. Their work involves not only comparisons at plume centerline, which is common of many studies, but also of measurements away from the centerline, along an arc. Since they use the standard K- ϵ model in their study, they accounted for anisotropic turbulence in the atmosphere by modeling a spread of wind direction to include the variance in wind direction for a standard average wind. In the study, the centerline and arc concentrations compare very well to the experiment when Schmidt numbers of around 1.0 are used.

5.4 Project EMU

Project “Evaluation of Modelling Uncertainty” (EMU) (Hall, 1996) is likely the most well known “CFD as a micro-scale air quality model” validation exercise. The Project was conducted for the European Commission’s Science, Research, and Development section to explore the usefulness of CFD as a tool to model

atmospheric dispersion around buildings. The goal of the project was to investigate the variance in results from different modelers given the same CFD problem and the accuracy of those results when compared to experimental measurements. The same cases were modeled in a wind-tunnel and the results compared to each CFD run.

This project has been referred to as an indication of the significant variability that can occur due to user choices concerning gridding, boundary conditions, numerical scheme, and other variables. In this project, four separate teams were given the details of a project and were asked to conduct CFD modeling using the same commercial CFD code. The project involved three different stages, increasing in complexity:

- Stage A: Dispersion of a gas around an L-shaped building under a neutrally stable atmosphere at 5m/s wind speed. Gas was released in several different scenarios: a continuous release of neutrally buoyant gas, a semi-continuous buoyant jet, and an instantaneous release of dense gas.
- Stage B: A second building, a cliff, and a trench were added to the domain with a stably stratified atmosphere at 2 m/s. A denser gas was used in several different release scenarios.
- Stage C: Full industrial site with many buildings and complex terrain. Dense gas released under different scenarios in a neutral atmosphere.

The teams were only given the dimensions, gas release scenarios, and atmospheric conditions. The goal of the project was to examine how each team set up their domains, meshing, atmosphere, and boundary conditions, and to see how the results varied based on their decisions. Overall, there was substantial difference in all factors. Meshing, boundary condition setup, and numerical differencing were found to have a lot of influence on the accuracy of the solutions. In the literature, emphasis has been placed on reviewing the results of Stage A because if the simple case is problematic, then the results from a more complex case will be even more suspect.

In general, for Stage A, two of the teams conducted their modeling more in line with the common best practice advice discussed in the next section of this paper and had better results compared to the teams that deviated from it. Teams #1 and #2 used second-order differencing terms as well as a denser mesh nearer the buildings, with Team #2 using the densest mesh. Team #3 used a small domain, only extending 2H upwind, whereas the other teams have domains that extended to 5H or greater upwind, as indicated in common best practice advice. Teams #3 and #4 used a smooth ground, which leads to elongated plumes along the surface. Teams #1 and #2 used more realistic atmospheric boundary layer profiles of turbulence (#1 used a wind tunnel profile, #2 used the Richards and Hoxey [1993] equations).

For results for a neutrally buoyant plume, Team #2 performed very well with estimated concentrations at different points downwind of the building very near to

the wind tunnel measurements. Team #1 had poorer concentration results, but the plume dimensions (5% iso-concentration field) were close to experimental results. Teams #1, #3, and #4 deviated from the experimental results substantially.

For Stage A with a buoyant jet, Team #1 accidentally applied a neutrally-buoyant jet, so the results are not comparable. Teams #2 and #4 had fairly similar plumes and #3 had a shorter, less spread plume. Plume dimensions are fairly close to the experimental results for Teams #2, #3, and #4, with Team #3 predicting the downwind hazard length a bit better due to less plume spread.

For Stage A with a dense cloud release, Team #1 again specified a neutrally buoyant gas so that the plume blew over the building roof instead of sagging around the building as observed by the other teams. Team #3 deviated a bit with their cloud not sinking around the building as much as #2 and #4. Teams #2 and #4 have fairly similar results. This case was not modeled in the wind tunnel so a comparison could not be made.

Overall, Project EMU demonstrated the high potential for inaccuracy of CFD results due to the many degrees of freedom a user has in selecting parameters that affect the quality of the solution. Human error, such as in the selection of ground roughness, the selection of a neutrally buoyant gas instead of a buoyant gas, or the wrong direction of heat flux at the surface, proved to be the greatest cause of errors. In addition, a number of mistakes were made in concentration calculations in post-processing. Domain size and cell size variance had a large influence on the accuracy of the results, generally with higher resolution and following the 5H domain rule leading to more accurate results. Turbulence profiles in the atmospheric simulation had influence on the results, with some of the teams applying unrealistic conditions. The teams using realistic turbulence profiles tended to have more accurate results.

Some important overall conclusions were made based on the project results. An important detail discovered from this effort was that the CFD solution most free from numerical error was not necessarily the most accurate CFD solution. Hazard ranges were often over-predicted. The results of the stable atmospheric cases were quite poor with substantial spread in the teams' results.

The Project EMU conclusions illustrate the degree of caution that must be used when reviewing atmospheric urban environment CFD results. However, the degree of variability found in this study is not inevitable. When user error is limited by active quality control and the guidelines provided here are followed, then much of the variability found in the Project EMU study can be avoided. One could conclude from the study that gas dispersion in a neutral atmosphere can be done accurately with CFD if the proper approach is followed.

5.5 Validation Exercise Recommendations

Before conducting a CFD study, it is important to validate and verify the user/code combination. One should first conduct several validation studies using baseline scenarios. The document “How to verify, validate, and report indoor environment modeling CFD analyses” (Chen, 2001) is a good document for reference. It discusses the importance of validation before attempting to use CFD for a specific project, with an emphasis on indoor problems. The document also suggests several studies with adequate data that can be used for indoor validation work. Since no similar document exists for external flow at the scale we are concerned about in this chapter, we suggest that the four types of studies explored above be used as a first step verification/validation:

- Flow around a block: Possibly use data from Minson (1995), Snyder (1994), or Castro and Robbins (1977)
- Flow within a street canyon
- Flow over a flat field: Horizontal and Vertical dispersion coefficients are available in Turner (1970)
- Project EMU, Case A1 and A2: Good measurement details for flow and dispersion around a simple building (Hall, 1996)

5.6 Example Validation Exercise

This is an example of a quick qualitative validation exercise. Snyder and Lawson (1994) conducted a wind-tunnel study of the flow around a simple cube in the EPA wind tunnel. Wind vectors were measured at certain points along the center of the domain and streamlines were estimated by a plotting algorithm. The results of this study include generally good estimates of streamlines, separation points, and reattachment lengths. However, some of the length estimates of the block wakes are not especially accurate because of the sparse velocity measurements downwind of the block.

Our intention in this validation exercise is to simulate the wind tunnel experiment using the wind and turbulence equations, and setup procedures discussed in section 3 of this chapter. Boundary conditions and settings will be set up appropriately to follow the guidance and methods described in this paper, ensuring that the domain, wind and turbulence profiles, and other parameters match the experiment as closely as possible.

We begin our validation exercise by constructing the domain. The cube itself was the standard 200 mm surface mounted cube that is generally used in bluff body flow validation (Castro and Robbins, 1970). A description of the EPA wind tunnel is available in Snyder (1979). For a CFD domain we apply a space of 8H upstream, 15H downstream, and 6H laterally to the domain walls. This domain has larger dimensions than recommended to provide extra room to examine the boundary layer. The top of the domain was 9H above the top of the cube to provide a 2 meter high boundary layer to coincide with the wind tunnel

dimensions. The outlet boundary was a standard pressure outlet that has no effect on the upstream flow. The sides and top of the domain are frictionless walls. The inlet is set at the upstream boundary with incoming wind and turbulence profiles nearly identical to those of Snyder and Lawson (1994). The wind and turbulence profiles and domain setup are illustrated in Figure 7.

It is important to ensure that the wind profile and turbulence profiles match the experiment as closely as possible. It has been demonstrated that upstream turbulence has significant effect on the size and positions of flow characteristics around a building. Higher turbulent energy in the flow will result in a reduced building re-circulation cavity (Zhang, 1992).

Snyder and Lawson include in their paper a plot of wind velocity measured at four different points along the stream in the wind-tunnel before the block was placed in the stream (two upstream of the block position and two downstream of the block).

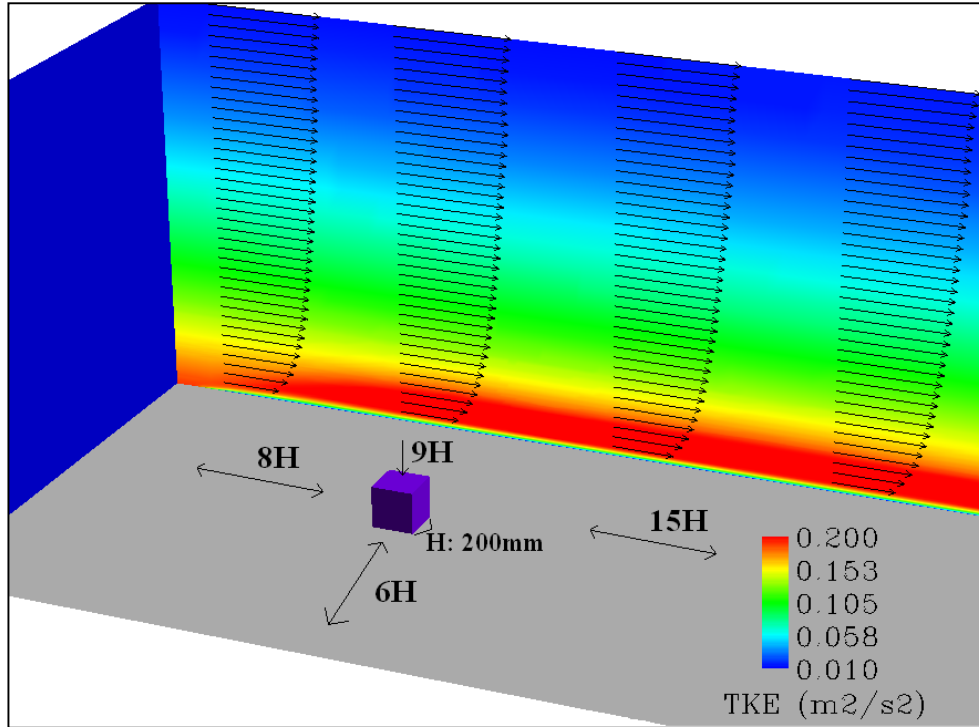


Figure 7. Illustration of the CFD domain setup for the sample qualitative validation study. Domain boundary distances from the 200 mm cube are indicated. Wind profiles at various points along the domain are illustrated. Turbulent Kinetic Energy values are illustrated in scalar coloring.

The plot demonstrates that the wind profile is quite continuous across the domain with very little deviation. They indicate that the profile is consistent with a 0.16 coefficient power law profile. However, by our examination of the data, a power law coefficient of 0.176 seems to fit with the data better. The power law equation is often used to describe a wind profile instead of the log law equation. The common power law equation is:

$$\frac{U(z)}{U_{z_0}} = \left(\frac{z}{z_0} \right)^n \quad (5.1)$$

where U_{z_0} is the windspeed at a reference height z_0 and n is the coefficient. Typical values of n for different types of terrain can be found on Figure 10.5 of Arya (1988).

Snyder and Lawson compare the turbulence intensity profile to the bounds suggested by the Engineering Sciences Data Unit (ESDU) for turbulence in a neutral atmosphere with full-scale roughness lengths between 5 and 50 cm. The wind-tunnel is set up to simulate a full scale friction element length of 20 cm (actual roughness length in the wind-tunnel was 1mm), so it is assumed that the turbulence profile will fit within this range.

Turbulence intensity is a bit more variable along the domain at the center of the domain, about H to 4H above the surface (0.2 to 0.8 m). Turbulence intensity diminishes in this region along the domain so that the incoming intensity is greater than the ESDU bounds and the outgoing intensity is less than the ESDU bounds. The average of the intensities fit well within the ESDU bounds, and the intensities nearer to the block position are near the average.

For the CFD domain profile equations we use the Richard and Hoxey equations (3.2, 3.7, 3.8, and 3.9 in this chapter). We begin by calculating the profiles using these equations and compare them to the Snyder and Lawson profiles to ensure that they are the same. The first step is to calculate friction velocity using Equation 3.2 in this chapter since the profile equations are based on it. The friction velocity should be constant throughout the layer for a neutral boundary layer. Twelve different elevations are selected for measurement and we calculate friction velocity at each level using the velocity and height at each level with the roughness element height of $z_o = 0.001$ m. The values are given in Table 6 using a von Karmon constant κ of 0.42. The experimental measurements used for our calculations may not be exact; they were picked off the graph in Figure 1 of Snyder and Lawson (1994).

Table 6. Wind Profile Setup Calculations.

Height (m)	Wind speed measured (m/s)	Friction Velocity (m/s) from Eq. 3.2	Calculated from Eq. 3.7 using 0.24m/s u_*	Wind speed: power law Eq. 5.1
0.05	2.3	0.246	2.25	2.30
0.1	2.7	0.246	2.64	2.60
0.2	3.1	0.246	3.03	2.94
0.4	3.4	0.238	3.43	3.32
0.6	3.7	0.243	3.66	3.56
0.8	3.8	0.239	3.82	3.75
1.0	3.9	0.237	3.95	3.90
1.2	4.0	0.237	4.05	4.02
1.4	4.1	0.238	4.14	4.13
1.6	4.2	0.239	4.22	4.23
1.8	4.3	0.241	4.28	4.32
2.0	4.4	0.243	4.34	4.40

The friction velocity for the layer averages about 0.24 m/s, which corresponds to u_*/U_R (U_R is the velocity at the top of the boundary layer) of about 0.05, which was the value calculated by Snyder and Lawson. Using this friction velocity, we can now calculate the wind profile and compare it to the experimental data. The calculated winds, included in Table 6, fit well to the experimental winds, justifying the use of the log-law wind Equation 3.7. The results are also compared to a power law wind equation using an exponent of 0.176 in Table 6.

Comparing turbulence intensities is a bit more difficult since turbulence intensity and turbulent kinetic energy are not exactly related. Turbulent kinetic energy can be estimated from turbulence intensity. Turbulent intensity is (u'/\bar{u}) , so mean turbulent kinetic energy can be estimated from the magnitude of u' . The kinetic energy equation can be used to estimate turbulent kinetic energy per unit mass:

$$TKE = \frac{3u'^2}{2} \quad (5.2)$$

The estimated TKE from this equation is included in Table 7. Observing the resultant TKE profile, we see that TKE decreases with height. This means we cannot use the Richards and Hoxey equation for TKE (Equation 3.8), which is based on the assumption of constant TKE in the surface layer. Their assumption is often only valid when the boundary layer is deep and the roughness elements are small. Therefore, the alternative TKE and ϵ equation (Equations 3.3 and 3.5) from Huser et al. (1997) are used. The TKE curve with a C_μ of 0.024 fits the TKE profile best using Equation 3.3. TKE calculated from the equation fits well to the ESDU bounds and wind-tunnel TKE profiles.

Table 7. TKE Profile Setup Calculations.

Height (m)	Turbulent Intensity (measured)	Wind Speed measured (m/s)	Estimated TKE (m^2/s^2) Eq. 5.2	TKE Eq. 3.3 (m^2/s^2) Using $\delta=3.4$ m and $C_\mu = 0.024$
0.05	0.22	2.3	0.384	0.361
0.1	0.18	2.7	0.354	0.350
0.2	0.15	3.1	0.324	0.329
0.4	0.13	3.4	0.293	0.289
0.6	0.11	3.7	0.248	0.252
0.8	0.10	3.8	0.217	0.217
1.0	0.09	3.9	0.185	0.185
1.2	0.08	4.0	0.154	0.156
1.4	0.07	4.1	0.124	0.129

The first test runs reveal that the TKE profile does not maintain itself throughout the domain, fading slightly from inlet to outlet. Therefore, a constant source boundary condition is applied to the domain to supply TKE at a specified rate to balance the excess dissipation. Tests demonstrated that a source equal to amount 70% of the dissipation rate in TKE production would maintain a constant profile throughout the domain. A source above 70% produced an exiting profile with higher TKE values than the entering profile, while a source below 70% of the dissipation rate did not compensate fully for the excess dissipation.

Simple mesh sensitivity runs were conducted beginning with a mesh of 0.0625H at the cube with expansion ratios of up to 1.4 near to the cube. This original mesh was used to account for the y^+ value near the ground. Expanding to a mesh of 0.125H dramatically reduced the predictive quality of the flow around the block and seemed to alter the nature of the turbulence profile. Concentrating the mesh down to 0.03H did not significantly improve the results; the flow around the block did contain more evident re-circulation on the roof, but other details such as the consistency of the TKE profile did not improve significantly.

All final runs were conducted using the Chen-Kim K- ϵ model with second-order terms, and the PISO differential equation solver in CFD2000 by Adaptive Research. Local time-stepping was used to accelerate convergence. Steady state was usually reached around 30 - 40 seconds for most cases, and all runs were run out to 60 seconds. The constants of the Chen-Kim K- ϵ model were set at $C_\mu = 0.024$ and $\sigma_\epsilon = 2.37$, with the others set to their defaults.

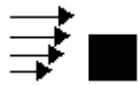
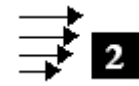
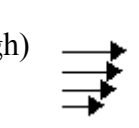
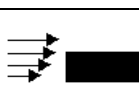
The results of the modeling runs were compared to the results of Snyder and Lawson (1994). Ten different runs were conducted with the incoming wind perpendicular to the windward face of the cube. Each run involved different block dimensions varying in three different orientations: varying in length parallel to the wind flow, varying in length normal to wind flow, and varying in height.

For each case, the separation point at the windward side of the block and the length of the re-circulation zone behind the block were estimated and compared to those of Snyder. The results are provided in Table 8. It compares the results of our CFD runs and the Snyder and Lawson wind-tunnel results to a commonly used set of empirical equations based on observations from Hosker (1984). Hosker developed the equations from earlier wind-tunnel studies of flow around different sized blocks. The equations are used to estimate the length of the wake behind the block.

The first equation is used for block buildings where $L/H \leq 2$:

$$\frac{X_r}{H} = \frac{L}{H} + \frac{A(W/H)}{1+B(W/H)} \quad (5.3)$$

Table 8. Results of the Sample CFD Validation Exercise.

Scenario	Snyder Wake length/ Height	Hosker Wake length/ Height	CFD validation example Wake length/Height
Cube 	1.4	1.5	1.7
2W 	2.1	2.6	2.5
4W 	3.5	4.2	3.5
10W 	5.6	6.7	5.5
Plate (1H high) 	2.3	not applicable	2.5
½ L 	1.5	2.2	1.5
2L 	1.2	1.4	1.5
4L 	1.4	1.4	1.5
2H 	0.75	1.2	1.4
3H 	0.5	1.0	0.8

where X_r is the wake length, L is the building along-wind length, W is the width, H is the height and A and B are scaling functions of L and H :

$$A = -2.0 + 3.7(L/H)^{-1/3} \quad (5.4)$$

$$B = -0.15 + 0.305(L/H)^{-1/3} \quad (5.5)$$

Hosker compared this curve to other studies and found that most data is within $\pm 15\%$ of the equation estimate.

For buildings where $L/H \geq 2$, the equation is:

$$\frac{X_r}{H} = \frac{1.75(W/H)}{1 + 0.25(W/H)} \quad (5.6)$$

All of the CFD results showed fair agreement with the wake lengths and very good agreement for separation points on the windward wall. Overproduction of TKE at the sharp windward edge was evident in every run, likely leading to error in flow magnitudes downwind. The recirculation zone on the top of the block is minimized in some of the cases. Qualitative comparison of the streamlines showed some deviation when compared to the Snyder and Lawson results, though the center of circulation was often in approximately the same location. A graphical comparison of the base case (the simple cube) is shown in Figure 8.

This example has been a demonstration of the simplest form of validation exercise. A more exhaustive set of validation exercises must be conducted to confirm the user-code combination before conducting an actual project. As well as qualitative comparison of streamlines, the validation exercise should involve comparison of separation and re-attachment lengths and centers of circulation. Quantitative comparisons of surface pressures, TKE, and velocity are also recommended. A good set of validation exercises are suggested in section 5.5.

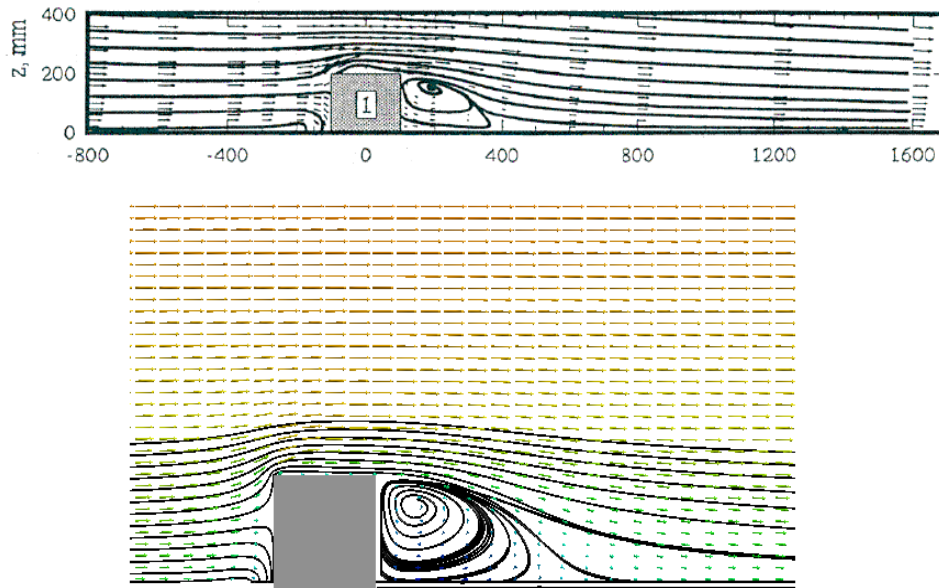


Figure 8. Graphical comparison of the streamlines around the simple cube. The top graphic is the results of Snyder and Lawson (1994). The bottom graphic is the illustration of the simple validation exercise results using CFD.

6 Conclusion

In this chapter we have discussed applying CFD to local-scale urban air quality dispersion studies. The purpose of this document is to supply the typical environmental scientist or engineer with an overview of the methods and details of CFD modeling for urban micro-environments.

The methods and guidelines that have been presented are best used for simpler small air quality studies around a single building or several buildings. We have reviewed the general methods of setting up and conducting a study using the $K-\epsilon$ model and its variants. This involves setting up proper boundary conditions to simulate the atmosphere, proper meshing and mesh sensitivity tests to ensure grid independent solutions, selection of wind scenarios, and visualization techniques.

The discussions presented in this chapter can be utilized as best practice guidance based on the most recent computational wind engineering studies using simpler $K-\epsilon$ methods.

References

Adaptive Research. 1997. *CFD2000 - Theoretical background*. Adaptive Research, Division of Simunet Corporation, Alhambra, CA.

- Adaptive Research. 2002. *STORM/CFD2000 User Guide*. Adaptive Research, Division of Simunet Corporation, Alhambra, CA.
- Apsley, D., 2003. Lecture notes for Introduction to CFD, Spring 2003. University of Manchester, School of Mechanical, Aerospace and Civil Engineering.
- Arya, P., 1988. *Introduction to Micrometeorology*, 1st edition. Vol. 42 of Int. Geophysics Series. Academic Press, New York.
- Baik, J. and J. Kim, 1999. A Numerical Study of Flow and Pollutant Dispersion Characteristics in Urban Street Canyons. *Journal of Applied Meteorology*, Vol. 38, pp. 1576-1589.
- Baik, J., J. Kim, and H. Fernando, 2003. A CFD Model for Simulating Urban Flow and Dispersion. *Journal of Applied Meteorology*, Vol. 42, pp. 1636-1648.
- Bartis, J., D. Vlachogiannis, and A. Sfetsos, 2004. Thematic Area 5: Best Practice Advice for Environmental Flows. *QNET-CFD Network Newsletter*, Vol. 2, No. 4, July 2004.
- Bottema, M., 1997. Turbulence closure model “constants” and the problems of “inactive” atmospheric turbulence. *Journal of Wind Eng. and Ind. Aerodynamics*, Vol. 67 & 68, pp. 897-908.
- Brown, R., 1991. *Fluid Mechanics of the Atmosphere*. Vol. 47 of Int. Geophysics Series, Academic Press, San Diego.
- Castro, I. and A. Robins, 1977. The flow around a surface-mounted cube in uniform and turbulent streams. *Journal of Fluid Mechanics*, vol. 79, part 2, pp. 307-335.
- Castro, I. and D. Apsley, 1997. Flow and dispersion over topography: a comparison between numerical and laboratory data for two dimensional flows. *Atmospheric Environment*, Vol. 31, No. 6, pp. 839-850.
- Castro, I., 2003. CFD for External Aerodynamics in the Built Environment. *QNET-CFD Network Newsletter*, Vol. 2, No. 2 – July 2003.
- Chen, Y. and S. Kim, 1987. Computation of Turbulent Flows Using an Extended K- ϵ Turbulence Closure Model. *NASA Contractor Report 179204*.
- Coirier, W., 2004. Validation of CFD-Urban using Accepted Open Field and Urban Area Transport and Dispersion Test Data. *8th Annual George Mason U. Conf. on Transport and Dispersion Modeling*. July 14, 2004, Fairfax, Virginia.
- Delaunay, D., 1996. Numerical simulation of atmospheric dispersion in an urban site: Comparison with field data. *Journal of Wind Eng. and Ind. Aerodynamics*, Vol. 64, pp. 221-231.
- Deterling, H. and D. Etling, 1984. Application of the E- ϵ Turbulence Model to the Atmospheric Boundary Layer. *Boundary Layer Meteorology*, Vol. 33, pp. 113-133.
- Duynkerke, P., 1987. Application of the E-, Turbulence Closure Model to the Neutral and Stable Atmospheric Boundary Layer. *Journal of the Atmospheric Sciences*, Vol. 45, no. 5, pp. 865-880.
- Easom, G., 2000. *Improved Turbulence Models for Computational Wind Engineering*. Doctoral Thesis: University of Nottingham, School of Engineering.

ERCOFTAC, 2000. *Best Practices Guidelines for Industrial Computational Fluid Dynamics*, Version 1.0. Ed. Casey, M. and Wintergerste, T.

Franke, J., C. Hirsch, A. Jensen, H. Krus, M. Schatzmann, P. Westbury, S. Miles, J. Wisse, and N. Wright, 2004a. Recommendations of the use of CFD in Predicting Pedestrian Wind Environment. *COST Action C14*, Working Group 2.

Franke, J., C. Hirsch, A. Jensen, H. Krus, M. Schatzmann, P. Westbury, S. Miles, J. Wisse, and N. Wright, 2004b. Recommendations of the use of CFD in Wind Engineering. *Proceedings of Urban Wind Engineering and Buildings Aerodynamics*, Brussels.

Garratt, J., 1992. *The Atmospheric Boundary Layer*. Cambridge University Press. New York.

Gao, Y. and W. Chow, 2005. Numerical Studies on Air Flow Around a Cube. *Journal of Wind Eng. and Ind. Aerodynamics*, vol. 93, pp. 115-135.

Grimmond, C. and T. Oke, 1999. Aerodynamic Properties of Urban Areas Derived from Analysis of Surface Form. *Journal of Applied Meteorology*, vol. 38, pp. 1262-1292.

Hall R., 1996. Evaluation of modelling uncertainty – CFD modelling of near-field atmospheric dispersion, *Project EMU final report*, WS Atkins Consultants Ltd, UK.

Hanna, R., O. Hansen, and S. Dharmavaram, 2004. FLACS CFD air quality model performance evaluation with Kit Fox, MUST, Prairie Grass, and EMU observations. *Atmospheric Environment*, vol. 38, pp. 4675-4687.

Hosker, R., Jr., 1984. Flow and diffusion near obstacles. *Atmospheric Science and Power Production*, Chapter 7. D. Randerson, ed. Department of Energy DOE/TIC-27601 (DE84005177), pp. 241-287.

Huber, A., W. Tang, A. Flowe, B. Bell, K. Kuehlert, and W. Schwarz, 2004: Development and Applications of CFD Simulations in Support of Air Quality Studies Involving Buildings. *Proceedings of 13th Conference on Applications of Air Pollution Meteorology*, AWMA/AMS.

Huser, A., P. Nilsen, and H. Skatun, 1997. Application of the K- ϵ Model to the Stable ABL: Pollution in Complex Terrain. *Journal of Wind Eng. and Ind. Aerodynamics*. vol. 67 & 68, pp. 425-436.

Kato, M. and B.E. Launder, 1993. The modeling of turbulent flow around stationary and vibrating square cylinders, *Proc. 9th Symposium on Turbulence and Shear Flows*, Kyoto.

Kantha, L. and C. Clayson, 2000. *Small Scale Processes in Geophysical Fluid Flows*. Academic Press, San Diego, CA.

Kim, S. and F. Boysan, 1999. Application of CFD to environmental flows. *Journal of Wind Eng. and Ind. Aerodynamics*, vol. 81, pp. 145-158.

Kim, H. and V. Patel, 2000. Test of Turbulence Models for Wind Flow over Terrain with Separation and Re-circulation. *Boundary-Layer Meteorology*, vol. 94, pp. 5-21.

Lakehal, D. and W. Rodi, 1997. Calculation of the flow past a surface-mounted cube with two-layer turbulence models. *Journal of Wind Eng. and Ind. Aerodynamics*. vol. 67-68, pp 65-78.

Launder, B. and D.B. Spalding, 1974. The numerical computation of turbulent flows, *Computational Methods of Applied Mechanical Engineering*, vol. 3, pp. 269-289.

McAlpine, J.D. and M. Ruby, 2004. Using CFD to Study Air Quality in Urban Microenvironments. Chapter 1 of *Environmental Science and Environmental Computing*, Vol. II (P. Zannetti, Ed.) The Envirocomp Inst.

Meroney, R., B. Leidl, S. Rafailidis, and M. Schatzmann, 1999. Wind-tunnel and numerical modeling of flow and dispersion about several building shapes. *Journal of Wind Engineering and Industrial Aerodynamics*, vol. 81, pp. 333-345.

Minson, A., C. Wood, and R. Belcher, 1995. Experimental Velocity Measurements for CFD Validation. *Journal of Wind Eng. and Ind. Aerodynamics*, vol. 58, pp. 205-215.

Murakami, S. and A. Mochida, 1989. Three-Dimensional Numerical Simulation of Turbulent Flow Around Buildings using the K- ϵ Turbulence Model. *Building and Environment*, Vol. 24, No.1, pp. 51-64.

Murakami, S., 1998. Overview of turbulence models applied in CWE-1997. *Journal of Wind Engineering and Industrial Aerodynamics*, vols. 74-76, pp. 1-24.

Murakami, S., 2002. Setting the scene: CFD and symposium overview. *Wind and Structures*, Vol 5, No. 2-4, pp. 83-88.

QNET-CFD website, 2005. <http://www.qnet-cfd.net/>. Accessed 12-10-2005.

Ratcliff, M. and J. Peterka, 1990. Comparison of Pedestrian Wind Acceptability Criteria. *Journal of Wind Eng. and Ind. Aerodynamics*, vol. 36, pp. 791-800.

Richards, P. and R Hoxey, 1993. Appropriate Boundary Conditions for Computational Wind Engineering Models Using the K- ϵ Turbulence Model. *Journal of Wind Eng. and Ind. Aerodynamics*, vol. 46 & 47, pp. 145-153.

Riddle, A., D. Carruthers, A. Sharpe, C. McHugh, and J. Stocker, 2004. Comparisons between FLUENT and ADMS for atmospheric dispersion modeling. *Atmospheric Environment*, vol. 38, 1029-1038.

Sagrado, A., J. van Beeck, P. Rambaud, and D. Olivari, 2002. Numerical and experimental modelling of pollutant dispersion in a street canyon. *Journal of Wind Eng. and Ind. Aerodynamics*, vol. 90, pp. 321-339.

Scanlon, Thomas J., 1997. A Numerical Analysis of Flow and Dispersion Around a Cube. *Proceedings of IBPSA Building Simulation '97 conference*, Prague, Sept. 8-10, 1997.

Scaperdas, A. and S. Gilham, 2004. Thematic Area 4: Best Practice Advice for Civil Construction and HVAC. *QNET-CFD Network Newsletter*, Vol. 2, No. 4, July 2004.

Shih, T., W. Liou, A. Shabbir, Z. Yang, J. and Zhu, 1994. A New K- ϵ Eddy Viscosity Model for High Reynolds Number Turbulent Flows. *Computers and Fluids*, Vol. 24, No. 3, pp. 227-238.

Snyder, W., 1979. *The EPA Meteorological Wind Tunnel: Its Design, Construction, and Operating Characteristics* (EPA-600/4-79).

Snyder, W., 1981. *Guideline for Fluid Modeling of Atmospheric Diffusion* (EPA-600/8-81-009).

Snyder, W. and R. Lawson, 1994. Wind-tunnel Measurements of Flow Fields in the Vicinity of Buildings. *Proceedings of the 8th AMS/AWMA Joint Conference on Applications of Air Pollution Meteorology*. Jan. 23-28, 1994. Nashville, Tennessee.

Stathopoulos, T., 2002. The numerical wind tunnel for industrial aerodynamics: Real or virtual in the new millennium? *Wind and Structures*, Vol. 5, No. 2-4, pp. 193-208.

Stull, R., 1988. *An Introduction to Boundary Layer Meteorology*. Kluwer Academic Publishers, Netherlands.

Tang, W., A. Huber, B. Bell, K. Kuehlert, and W. Schwarz, 2005. Example Application of CFD Simulations for Short-Range Atmospheric Dispersion over the Open Fields of Project Prairie Grass. *Proceedings of AWMA 98th Annual Conference*. Minneapolis, MN. June 21-25, 2005.

Tang, W., A. Huber, B. Bell, and W. Schwarz, 2006. Application of CFD Simulations for short-range atmospheric dispersion over open fields and within arrays of buildings. *Proceedings of AWMA/AMS 14th Joint Conference of the Applications of Air Pollution Meteorology*, Atlanta, GA, Jan. 30-Feb 2, 2006.

Tsuchiya, M., S. Murakami, A. Mochida, K. Kondo, and Y. Ishida, 1996. Development of New K-, Model for Flow and Pressure Fields Around Bluff Body. *2nd Int. Symposium on Computational Wind Engineering*, Col. State U. August 4-8, 1996.

Turner, D.B., 1970. *Workbook on Atmospheric Dispersion Estimates*. U.S. Environmental Protection Agency (AP-26).

Zhang, Y., S. Arya, A. Huber, and W. Snyder, 1992. *Simulating the Effects of Upstream Turbulence on Dispersion Around a Building* (EPA/600/A-92/228).

Zhang, Y., S. Arya, and W.H. Snyder, 1996. A Comparison of Numerical and Physical Modeling of Stable Atmospheric Flow and Dispersion Around a Cubical Building. *Atmospheric Environment*, Vol. 30, No. 8, pp. 1327-1345.

BRANK
P
e

Chapter 6

Plume Rise

A chapter dedicated to the topic “Plume Rise” was presented in Volume I of this book series.

For additional information, the reader can visit:

- http://www.cerc.co.uk/software/pubs/ADMS3-1TechSpec/P11_02.pdf
Comprehensive discussion on plume rise formulas.
- <http://www.epa.gov/scram001/7thconf/iscprime/tekpr1.pdf>
Interaction of plume rise and building downwash.
- <http://www.weblakes.com/aermodvol1/652.html>
Plume rise in the stable boundary layer.

BRANKLEY
PAPER

Chapter 7

Gaussian Plume Models

A chapter dedicated to the topic “7A - Introduction to Gaussian Plume Models” was presented in Volume I of this book series. In the following pages we include:

7B – Simulation Algorithms in Gaussian Plume Models

BRANKENBACH

Yamartino, R. 2008. *Simulation Algorithms in Gaussian Plume Modeling*. Chapter 7B of *AIR QUALITY MODELING - Theories, Methodologies, Computational Techniques, and Available Databases and Software. Vol. III – Special Issues* (P. Zannetti, Editor). Published by The EnviroComp Institute (www.envirocomp.org) and the Air & Waste Management Association (www.awma.org).

Chapter 7B

Simulation Algorithms in Gaussian Plume Modeling

Robert J. Yamartino

Integrals Unlimited, Portland, Maine (USA)
rjy@maine.rr.com

Abstract: This chapter focuses on the development of various Gaussian modeling techniques with an emphasis on the relevant mathematical and numerical details. Beginning with the diffusion equation in one-dimension, we show how one solution of this differential equation for pollutant mixing ratio involves the Gaussian function. The three-dimensional Gaussian plume solution is then constructed via consideration of the advection terms and the use of the separation of variables technique. Influences of the ground and other “reflecting” barriers is then added via the method of images and alternative mathematical formulations of this summation of images is considered, both from theoretical and numerical accuracy viewpoints. The issue of air density varying with height is then discussed as it complicates the solution expressed in terms of mass concentration (e.g., g/m^3) versus the more-fundamental mixing ratio (e.g., ppm) formulation. Having an impact on computed results in the 5-15% range, this density complication is presently nearly-universally overlooked. Focus then shifts to extending the point source formulation to various integrated forms that accommodate line and area sources, and including wind shear. Removal processes, particularly dry deposition, are then treated in some detail.

Key Words: Gaussian methods, atmospheric dispersion modeling.

1 Introduction

As introduced in Volume 1, Chapter 7A by Venkatram and Thé (2003), the Gaussian plume expression, given by their Eq.(1), serves as the starting point for much of the air pollution modeling that has taken place during the past half-century. First applied to the atmospheric diffusion problem for a steady-state source by Sutton (1932, 1953), this equation states that a time-independent, mass concentration distribution, $C(x,y,z)$, of:

$$C(x, y, z) = \frac{Q}{2\pi \cdot U \cdot \sigma_y(x) \cdot \sigma_z(x)} \cdot \exp\left[-\frac{(z - z_s)^2}{2\sigma_z(x)^2} - \frac{y^2}{2\sigma_y(x)^2}\right] \quad (1)$$

results when a steady source of strength Q (mass/time) positioned at coordinates $(0, 0, z_s)$ emits into a uniform flow U (m/s) moving in the $+x$ horizontal direction. This emitted material is free to spread out (or diffuse) in the two perpendicular directions y (horizontally transverse to the flow direction) and z (vertically), with the “dispersion coefficients”, σ_y and σ_z , representing the standard deviation widths (m) of the distribution in the y and z directions, respectively.

Given the dimensions of the above expressions, one thing to note is that a Q expressed in g/s will give rise to a mass per unit volume (mass/volume) concentration C having units of g/m^3 ; thus, clarifying use of the terminology mass concentration. This terminology is worth clarifying because the word “concentration” is alternatively employed to indicate a mass concentration C or a mixing ratio concentration ϕ , frequently quoted in non-dimensional units of parts per million (ppm) or parts per billion (ppb), with the further qualification that these fractional mixing ratio “concentrations” represent fractional compositions on a mass basis, rather than a volumetric basis. These two pollutant measures, mass concentration C and mass mixing ratio ϕ , are related by the simple expression $C = \phi \cdot \rho$, where $\rho(\text{g/m}^3)$ is the local density of air. However, this simple relation gives rise to one of the many problems that often lie hidden and unresolved within the framework of the Gaussian plume formulation, and even within other air pollution modeling frameworks, such as numerical Eulerian models.

This chapter will examine various issues and simplifications intrinsic to the derivation of the Gaussian plume formulation and will point out various measures that are, or have been, suggested to correct these simplifications. The chapter will then proceed to consider numerous mathematical extensions of the simple plume formalism to account for real-world complexities, such as barriers to plume mixing, pollutants emitted from area and line sources, deposition of plume material to surfaces, wind directional shear, and concentration fluctuations. Emphasis will be placed on mathematical and algorithmic details rather than on considering the features and merits of specific Gaussian models that currently continue to be applied.

2 Theoretical Background

2.1 Diffusion and Advection

2.1.1 Diffusion in One-Dimension

Sir Isaac Newton is often credited with introducing the notion of gradient transfer of heat by noting that heat will move from hotter to cooler environments. This notion of “down-gradient” transfer accounts for the minus sign one sees in the heat conduction proportionality relation $q \propto -dT/dx$. Apparently, clarification of the units of the needed proportionality constant k , to yield the modern flux relation, $q = -k \cdot dT/dx$, was introduced many decades later in 1822 by the French mathematician, Joseph Fourier. Nevertheless, this notion of down-gradient transport is intrinsic to the second law of thermodynamics (variously attributed to Carnot, Clausius, or Lord Kelvin), which states that: in any physical process the entropy (or disorder) of an isolated system never decreases. This second law really forces the time arrow to have a single (forward) direction and explains why pollutant concentrations, fortunately for all of us, always move in the direction of greater, rather than lesser, dilution. We now know that counter-gradient transport can occur and can be important in convective mixing, but that is beyond the focus of this chapter.

The flux-gradient relation for heat was extended to diffusive mass transfer flux, F_d , by Adolf Fick in 1855 and was originally expressed as:

$$F = -K \cdot (dC/dx) \quad (2a)$$

where the diffusivity K , having units of m^2/s , gives rise to the flux, F_d , having units of $g/m^2/s$. As Fick’s paper dealt with salt concentration diffusion in water, it was not concerned with density issues, but one would reformulate this to include density as:

$$F = -K \cdot \rho \cdot \frac{\partial \phi}{\partial x} \quad (2b)$$

This flux-gradient relation, known as Fick’s First Law, serves as the basis of the time-dependent diffusion equation, also known as Fick’s Second Law, which is expressed in flux-conservative form (and updated to include density) in one-dimension for the mixing ratio as:

$$\frac{d(\rho \cdot \phi)}{dt} = + \frac{\partial}{\partial x} \cdot K(x) \cdot \rho \cdot \frac{\partial \phi}{\partial x} \quad (3a)$$

where t is, of course, time. It is important to note that it is the mixing ratio which diffuses, and not the mass concentration per se. Thus, in an environment where the domain is bounded, maximum entropy or disorder is achieved when the mixing ratio is the same everywhere, such that any gradients in ϕ vanish. Also, the

ρ in Eq.(3a) may be a function of both x and t , though temporal changes in density usually occur on much longer time scales and do not involve diffusive processes. Equation (3a) may also be expressed as a diffusion equation for mass concentration as:

$$\frac{dC}{dt} = + \frac{\partial}{\partial x} \cdot K(x) \cdot \rho \cdot \frac{\partial(C/\rho)}{\partial x}. \quad (3b)$$

In the case of a space-time uniform density field, Eqs.(3a) and (3b) are identical; however, differences emerge when the air density, $\rho(x)$, becomes a function of x or more significantly, a function of z in the comparable 1D equation for vertical diffusion.

One of the simplest, non-trivial solutions of Eq.(3a) is given for the y direction and spatially uniform K as:

$$\phi(y, \sigma) = \frac{1}{\sqrt{2\pi\sigma}} \cdot \exp\left[-\frac{y^2}{2 \cdot \sigma^2}\right] \quad (4a)$$

$$\text{where } \sigma^2 \equiv \sigma_0^2 + 2 \cdot K_y \cdot (x/U) \quad (4b)$$

where σ_0 is an arbitrary constant, and the diffusivity has been given the subscript y to differentiate it from the appropriate diffusivities in other dimensions. It should be noted that Eq.(4a) satisfies the differential Eq.(3a) only if $\frac{d\sigma^2}{dx} = \frac{2 \cdot K}{U}$, which is realized for the constant K , appropriate for Brownian or molecular diffusion, by σ being constrained by Eq.(4b). However, the added unit normalization condition, expressed below through the constraint that the integral on y over all values from $-\infty$ to $+\infty$ yields one, or

$$\int_{-\infty}^{+\infty} dy \cdot \phi(y, \sigma) = 1. \quad (5)$$

This is valid for any definition of σ and is ensured by the factor $\sqrt{2\pi}$ in the denominator of Eq.(4a).

Assuming an Eq.(4a) solution to apply for both y and z dimensions, abandoning the constraint on σ provided by Eq.(4b), and blindly swaping C for ϕ enables one to come close to attaining the Gaussian plume of Eq.(1), except for the absence of the factor Q/U .

2.1.2 The Advection Term and Building the 3D Plume Solution

In order to understand the origin of the Q/U factor, one must expand Eqs.(3a) and (3b) to include the advective flux term, $F_a = U \cdot \rho \cdot \phi = U \cdot C$, and write:

$$\frac{\partial(\rho \cdot \phi)}{\partial t} = -\frac{\partial}{\partial x} \cdot (U \cdot \rho \cdot \phi) + \frac{\partial}{\partial x} \cdot K(x) \cdot \rho \cdot \frac{\partial \phi}{\partial x} + (S - D) \quad (6a)$$

or

$$\frac{\partial C}{\partial t} = \frac{\partial}{\partial x} \cdot [-U \cdot C + K(x) \cdot \rho \cdot \frac{\partial(C/\rho)}{\partial x}] + S - D \quad (6b)$$

where source, S , and depletion, D , terms have been added for completion and would have volumetric units of $\text{g}/\text{m}^3/\text{s}$.

Now in the steady-state limit, defined as existing when $dC/dt = 0$, and neglecting losses D and along-wind or x diffusion by setting K to zero, Eq.(6b) can be easily integrated in x to yield $C = C_0 + (\int dx \cdot S) / U$, where C_0 is an arbitrary integration constant or, more physically, a background concentration. Now just to minimize sleight of hand trickery, it must be pointed out that as the concentration C and source term S are both by definition volumetric, or 3D, entities, reconciling their 3D nature with the 1D nature of the equation demands that one integrate over y and z dimensions as well to encompass the entire source. Further postulating the source distribution S as the 3D delta function, $Q \cdot \delta^3(\underline{x}) = Q \cdot \delta(x) \cdot \delta(y) \cdot \delta(z-z_S)$, for a true point source located at $(0,0,z_S)$, and recalling that the normalization condition of Eq.(5) just yields unity for the y and z integrations over C , one obtains the result:

$$\overline{\overline{C}} = \frac{Q}{U} \quad \text{or} \quad \overline{\overline{\phi}} = \frac{(Q/\rho_0)}{U} \quad (7)$$

where ρ_0 is the presently-assumed-constant air density and the double overbar denotes integration over y and z dimensions. The fact that Eq.(7) becomes infinite as $U \rightarrow 0$ is simply a consequence of ignoring alongwind diffusion (i.e., setting $K(x)$ to zero in Eq.(6)) and should not be viewed as something that happens in nature. Nevertheless, the history of Gaussian plume modeling is so littered with concern over this infinity, that regulatory modelers are urged to use a minimal U of about 1 m/s to avoid serious overestimation. This subject of alongwind diffusion will be re-visited in detail in Chapter 8a.

Combining the result of Eq.(7) plus the Eq.(4) functional forms for the y and z dimensions, one “constructs” the 3D Gaussian plume solution for the mixing ratio, ϕ , due to a source located at $(0,0,z_S)$ as:

$$\phi(x, y, z) = \frac{(Q/\rho_0)}{U} \cdot P(y, \sigma_y) \cdot P(z - z_S, \sigma_z) \quad (8a)$$

where x distance and time are inextricably linked via the relation $x \equiv U \cdot t$,

$$P(y, \sigma_y) = \frac{1}{\sqrt{2\pi}\sigma_y} \cdot \exp\left[-\frac{y^2}{2 \cdot \sigma_y^2}\right], \quad P(z - z_s, \sigma_z) = \frac{1}{\sqrt{2\pi}\sigma_z} \cdot \exp\left[-\frac{(z - z_s)^2}{2 \cdot \sigma_z^2}\right] \quad (8b)$$

and where:

$$\sigma_y^2 \equiv \sigma_{y0}^2 + 2 \cdot K_y \cdot t \quad \text{and} \quad \sigma_z^2 \equiv \sigma_{z0}^2 + 2 \cdot K_z \cdot t \quad (8c)$$

are the appropriate dispersion coefficients for the constant diffusivities associated with molecular/Brownian diffusion.

As indicated in the discussion of Eq.(4), other expressions for σ_y and σ_z are possible, provided that they satisfy the relation:

$$\frac{d \sigma^2}{dx} = \frac{2 \cdot K(x)}{U} \quad \text{or} \quad \frac{d \sigma^2}{dt} = 2 \cdot K(t) . \quad (8d)$$

However, downwind-distance or transport-time dependent diffusivities have traditionally created discomfort among modelers, due to the questionable causal mechanism. Nevertheless, more modern understanding of turbulent spectra and the multiple turbulent length scales contributing to plume growth suggests that diffusivities proportional to the current plume size, that is, $K(x) = V_T \cdot \sigma$, where the proportionality constant, V_T , has the dimensions of a turbulence velocity, may not be unreasonable. In this case, appropriate solution dispersion coefficients would take the forms:

$$\sigma_y \equiv \sigma_{y0} + V_{Ty} \cdot t \quad \text{and} \quad \sigma_z \equiv \sigma_{z0} + V_{Tz} \cdot t \quad (8e)$$

or equivalently,

$$\sigma_y \equiv \sigma_{y0} + (V_{Ty}/U) \cdot x \quad \text{and} \quad \sigma_z \equiv \sigma_{z0} + (V_{Tz}/U) \cdot x. \quad (8f)$$

Note that here the terms add linearly, rather than in quadrature as in Eq.(8c). This is because the appropriate "addition rule", derived based on pseudo-transport times, can be shown to involve the reciprocal of the growth exponent, p , in x^p . Thus, sigmas that grow as $x^{1/2}$ or $t^{1/2}$ will have a $1/p = 2$, or quadrature addition rule, while those linear in x (i.e., $p=1$) will have a $1/p = 1$, or linear addition rule. A yet wider range of dispersion coefficient forms, such as those involving various powers of x or t , or even more complex algebraic forms, have been used over the decades of Gaussian modeling, with their prime justification being that they provide viable predictions relative to tracer experiments or other measurements. Though many of these empirical dispersion coefficient forms lack a clear link to the diffusivity formulation of the advection-diffusion equation, their utility and

retained characteristic of mass conservation (i.e., with respect to integrations over y and z) have been sufficient to justify their use in applied modeling.

It is important to note that Eq.(8a) is appropriate for the mixing ratio, ϕ ; however, it is more frequently applied in its concentration form:

$$C(x, y, z) = \frac{Q}{U} \cdot P(y, \sigma_y) \cdot P(z - z_s, \sigma_z) \quad (9)$$

even though this expression can lead to underestimation of ground level concentrations for air density falling off with height, as will be discussed in a following subsection.

It is also worth noting that Eqs.(8a) and (9) do not contain the added “reflection” terms associated with the presence of the ground or inversion lids. These factors will be discussed later.

The only other seeming mystery involved in this construction of the 3D solution arises if one questions why a product solution or dimensionally-factorized form was chosen. This product factorization arises from the full 3D form of the advection-diffusion equation and the multi-dimensional solution methodology known as “separation of variables”.

Finally, it should be noted that the form of Eq.(9) is also often simply conjectured or derived on intuitive grounds. That is, consider the mass of emissions, $Q \cdot \Delta t$, emitted during a time increment, Δt , and filling a box of along-wind length $U \cdot \Delta t$. Let this pollutant also uniformly fill-out the box’s transverse dimensions of L_y and L_z to yield a concentration, $C = (Q \cdot \Delta t) / [(U \cdot \Delta t) \cdot L_y \cdot L_z]$, where the expression in brackets is recognized as simply the volume of the box. Noting that the Δt terms cancel, the resulting “box-normalized” concentration, $C = Q / [U \cdot L_y \cdot L_z]$, can be converted to Eq.(8g), by replacing the box normalizations of $1/L_y$ and $1/L_z$ with the Gaussian normalization forms given by Eq.(8b). This simple approach recognizes the key elements of mass conservation and flow uniformity, as well as the neglect of any along-wind diffusion stretching of the box’s length. Furthermore, this box normalization highlights the fact that for 1D flow, that is the flow vector $(U, 0, 0)$, there is no distinction between the average wind speed and the vector mean wind speed, and this average wind speed is simply the arithmetic mean wind, $U = \langle u_i \rangle$, where $\langle \rangle$ denotes the averaging operation, and not some more exotic average, such as the “harmonic mean”, $U = \langle 1/u_i \rangle^{-1}$.

Box models and the box normalization principle continue to play a large role in pollutant dispersion modeling and will re-appear later in this chapter.

2.1.3 Advection-Diffusion in Three-Dimensions

For completeness, the 3D expressions of the advection-diffusion equation are:

$$\frac{\partial(\rho \cdot \phi)}{\partial t} = -\underline{\nabla} \cdot (\underline{V} \cdot \rho \cdot \phi) + \underline{\nabla} \cdot (\underline{K} \cdot \rho \cdot \underline{\nabla} \phi) + (S - D) \quad (10a)$$

and

$$\frac{\partial C}{\partial t} = \underline{\nabla} \cdot [-(\underline{V} \cdot C) + (\underline{K} \cdot \rho \cdot \underline{\nabla}(C/\rho))] + (S - D) \quad (10b)$$

where scalar variables, C , ϕ , ρ , S and D , vector wind field \underline{V} , and tensor (or 2D matrix) diffusivity \underline{K} may all be 3D functions of x , y , and z . In these 3D forms, the $\underline{\nabla}$ symbol represents the vector 3D gradient operation, whereas the \cdot symbol denotes the vector dot product operation. At various points in this chapter and in the subsequent chapter on puff modeling, it may be convenient to revisit these 3D equations.

Returning again to the solutions provided by Eq.(8), we note that these results only represent a solution of the 3D advection-diffusion equation in the simplified case of $\underline{V} = (U, 0, 0)$, with U uniform in space and time, and the sparse diffusivity

$$\text{matrix of } \underline{K} = \begin{bmatrix} 0 & 0 & 0 \\ 0 & K_{yy} & 0 \\ 0 & 0 & K_{zz} \end{bmatrix}, \text{ containing only the "diagonal" diffusivity elements,}$$

K_{yy} and K_{zz} (or in their compressed notation form, K_y and K_z).

2.2 Normalization, Reflections, and Their Summation

Equation (5) showed that the normalization of the Gaussian form, $\phi(y,t)$, given by Eq.(4a), or its Eq.(8) equivalent, $P(y,\sigma_y)$, when integrated over all y -space from $-\infty$ to $+\infty$ yields unity. This normalization is valid for any functional form of the σ , such as σ provided that σ is not itself a function of y . However, this normalization becomes problematic in the z -direction, where any $z < 0$ implies that one is considering material "below ground", where it cannot possibly be.

Again, considering the Eq.(8) Gaussian z distribution function as:

$$P(z - z_s, \sigma_z) = \frac{1}{\sqrt{2\pi} \cdot \sigma_z} \cdot \exp\left[-\frac{(z - z_s)^2}{2 \cdot \sigma_z^2}\right] \quad (11)$$

where $\sigma_z = \sigma_z(t)$, one notes that its integral from $z=z_1$ to $z=z_2$ is just:

$$N(z_s, z_1, z_2) \equiv \int_{z_1}^{z_2} dz \cdot P(z - z_s, \sigma_z) = \frac{1}{2} \cdot \left[\text{erf}\left(\frac{z_2 - z_s}{\sqrt{2}\sigma_z}\right) - \text{erf}\left(\frac{z_1 - z_s}{\sqrt{2}\sigma_z}\right) \right] \quad (12)$$

where erf is the symbolic notation for the “error function”, and it is defined by its integral expression. While the erf is often referred to as a “tabulated function”, it is no more so than the more familiar sine and cosine functions. Like the sine function, the erf is an odd function, such that $erf(-x) = -erf(x)$, so $erf(0) = 0$. For small x , $erf(x) \approx 2 \cdot x / (\pi)^{1/2}$, whereas for $x \rightarrow +\infty$, $erf(x) \rightarrow +1$. Also, there is a “complementary error function”, $erfc(x)$, defined such that $erfc(x) = 1 - erf(x)$.

One may evaluate the plume mass residing “above ground” by considering the integration limits of $z_1 = 0$ and $z_2 = \infty$. The result is just $N(z_S) \equiv N(z_S, 0, \infty)$ or

$$N(z_S) = \frac{1}{2} \left[1 - erf\left(\frac{-z_S}{\sqrt{2}\sigma_z}\right) \right] = \frac{1}{2} \left[1 + erf\left(\frac{z_S}{\sqrt{2}\sigma_z}\right) \right]. \quad (13a)$$

This result says that $N(z_S) < 1$ for all finite source heights z_S , which falls short of the goal of accounting for 100% of the emitted mass. Now, imagine a source of identical strength located “below ground” at a depth of $z = z_S$. Immediately, one notes that this “image source” will lead to an above ground mass, $N(-z_S)$ of

$$N(-z_S) = \frac{1}{2} \left[1 - erf\left(\frac{+z_S}{\sqrt{2}\sigma_z}\right) \right] \quad (13b)$$

and that the sum of Eqs.(13a) and (13b) yields the desired result of:

$$N(z_S) + N(-z_S) = \frac{1}{2} \cdot (1 + 1) = 1. \quad (13c)$$

That is, the erf terms cancel and 100% of the mass now resides above ground in the domain defined by the limits of $z_1 = 0$ and $z_2 = \infty$.

In addition to this desirable mass accounting property, the distribution function associated with this below-ground “image source” is such that its magnitude at $z = 0$ is just equal to the magnitude of the original above-ground source, and it tapers off above-ground in the same manner as the original above-ground source tapers off below-ground. That is, the below-ground “image source” gives rise to a mass distribution above ground of $P(z+z_S, \sigma_z)$ that appears to “reflect” material upwards that attempts to diffuse across the $z = 0$ boundary.

This “ground reflection” term is given as:

$$P(z + z_S, \sigma_z) = \frac{1}{\sqrt{2\pi} \cdot \sigma_z} \cdot \exp\left[-\frac{(z + z_S)^2}{2 \cdot \sigma_z^2}\right]. \quad (14)$$

This is the only other term that need be considered if the ground represents the only possibility for reflecting plume mass. In this case, the original Eq.(8a) solution for the mixing ratio, ϕ , due to a source located at $(0, 0, z_S)$ now becomes:

$$\phi(x, y, z) = \frac{(Q/\rho_0)}{U} \cdot P(y, \sigma_y) \cdot [P(z - z_S, \sigma_z) + P(z + z_S, \sigma_z)]. \quad (15)$$

This is consistent with the analogue to mirror images, in that if one stands in front of a single mirror, there will only be a single reflection that appears to be at a depth “behind” the mirror equal to our distance from the front of the mirror.

Just as with mirrors, the situation becomes more complicated, and infinitely so, if a second parallel mirror is placed behind us. One observes an infinite series of reflections (Pasquill, 1974; 1976) receding ever further into the distance.

An elevated thermal inversion at height $z = h$ positioned above the source at $z = z_S$ constitutes such an equivalent “second parallel mirror” impediment to vertical diffusion, and in this case, the single terms given by Eqs.(11) and (14) are replaced by two infinite series (i.e., one series for the direct term involving $z-z_S$, and one for the reflection term involving $z+z_S$) of distribution functions to yield:

$$\phi(x, y, z) = \frac{(Q/\rho_0)}{U} \cdot P(y, \sigma_y) \cdot [P(z - z_S, \sigma_z, h) + P(z + z_S, \sigma_z, h)] \quad (16)$$

where

$$P(z \pm z_S, \sigma_z, h) = \frac{1}{\sqrt{2\pi} \cdot \sigma_z} \cdot \sum_{j=-\infty}^{j=+\infty} \exp\left[-\frac{(z \pm z_S + 2jh)^2}{2 \cdot \sigma_z^2}\right]. \quad (17a)$$

It turns out that these series can be re-expressed in terms of the Jacobi theta function of the third kind as:

$$P(z \pm z_S, \sigma_z, h) = \frac{1}{\sqrt{2\pi} \cdot \sigma_z} \cdot \exp\left[-\frac{(z \pm z_S)^2}{2 \cdot \sigma_z^2}\right] \cdot \theta_3\left[\frac{i \cdot (z \pm z_S) \cdot h}{\sigma_z^2}, \alpha\right] \quad (17b)$$

where $i \equiv (-1)^{1/2}$ and $\alpha \equiv \exp(-2 \cdot h^2/\sigma_z^2)$. However, this re-expression of the infinite series might be of little more than academic interest except for another transformation, discovered in 1893 by Landsberg, which enables one to write:

$$P(z \pm z_S, \sigma_z, h) = \frac{1}{2 \cdot h} \cdot \theta_3\left[\frac{\pi \cdot (z \pm z_S)}{2 \cdot h}, \beta\right] \quad (17c)$$

where $\beta \equiv \exp[-(\pi \cdot \sigma_z)^2 / (2 \cdot h^2)]$. Expanding Eq.(17c) for small β , or large σ_z/h , then enables one to approximate the rightmost bracketed term in Eq.(16) to yield the final mixing ratio result:

$$\phi(x, y, z) \cong \frac{(Q/\rho_0)}{U \cdot h} \cdot P(y, \sigma_y) \cdot (1 - \beta^2) \cdot [1 + \beta^2 + 2\beta \cdot \cos(\frac{\pi \cdot z}{h}) \cdot \cos(\frac{\pi \cdot z_S}{h})] \quad (18a)$$

or to yet higher accuracy via the expression:

$$\phi(x, y, z) \cong \frac{(Q/\rho_0)}{U \cdot h} \cdot P(y, \sigma_y) \cdot (1 - \beta^2) \cdot (1 - \beta^4) \cdot \frac{1}{2} \cdot \left\{ \begin{aligned} & [1 + \beta^2 + 2\beta \cdot \gamma_-] \cdot [1 + \beta^6 + 2\beta^3 \cdot \gamma_-] + \\ & [1 + \beta^2 + 2\beta \cdot \gamma_+] \cdot [1 + \beta^6 + 2\beta^3 \cdot \gamma_+] \end{aligned} \right\} \quad (18b)$$

where $\gamma_{\pm} \equiv \cos[\pi \cdot (z \pm z_s) / h]$. It is clear from Eqs.(18a) and (18b) that the mixing ratio distribution becomes uniform in z as $\beta \rightarrow 0$.

Figure 1 shows the worst case percentage error experienced (i.e., generally achieved with receptor and source separated by the layer depth, h) using the various techniques considered, and one is struck by how rapidly this error varies with σ_z/h . The “Sum 6” and “Sum 10” curves refer to using Eq.(16), with the sums in Eq.(17a) ranging from $j = -1$ to $j = +1$ for 6 terms and from $j = -2$ to $j = +2$ for 10 terms; whereas the “Uniform Mix” assumption is just $\phi \propto 1/h$, or equivalently Eq.(17c) with $\beta = 0$ to yield $\theta_3 = 1$. The “Jacobi 1” and “Jacobi 2” term curves refer to refining the uniform mixing assumption via use of Eqs.(18a) and (18b), respectively.

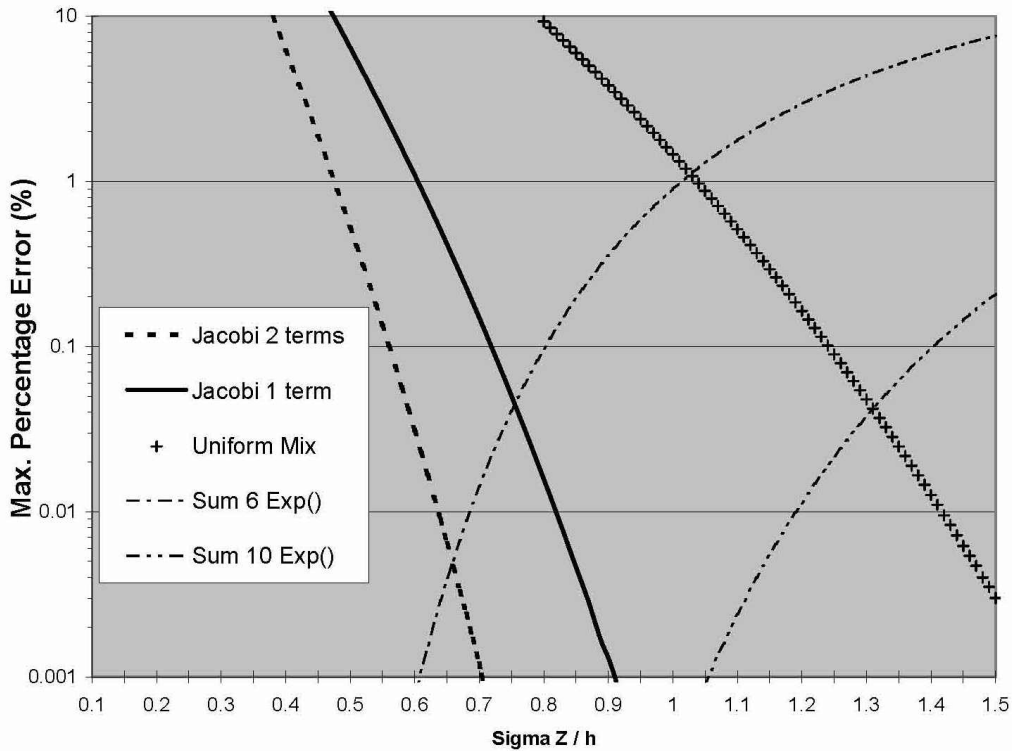


Figure 1. Maximum Computational Errors for Various Gaussian Plume Methods.

Various curve crossover points in Figure 1 provide strategies for building computational algorithms that guarantee a desired maximum error. For example,

if one could tolerate errors as large as 1.12%, one could choose the “Sum 6” method for $\sigma_z/h \leq 1.03$ and then switch over to the uniform mixing calculation for $\sigma_z/h > 1.03$. Alternatively, one could incur the higher computational cost of the “Sum 10” method, transition to the uniform mixing calculation for $\sigma_z/h > 1.31$, and never suffer errors exceeding 0.042%. Neither of these two strategies employ the Jacobi theta function expansions of Eq.(18). However, using the simpler, 1-term Jacobi expansion of Eq.(18a) for the limited interval of $0.76 \leq \sigma_z/h \leq 1.30$ in-between the “Sum 6” and uniform mixing calculations yields maximum computation errors below 0.05%. Similarly, using the 2-term Jacobi expansion of Eq.(18b) for the somewhat larger interval of $0.66 \leq \sigma_z/h \leq 1.47$ in-between the “Sum 6” and uniform mixing calculations yields maximum computation errors below 0.005%. These algorithmic crossover points and maximum errors differ somewhat from those originally recommended by Yamartino (1977), as those earlier calculations were found to contain a programming bug that discarded some of the contributing “Sum 6” terms.

2.3 Ground Level Concentrations and the Air Density Issue

Accepting the limitations that are already-stated, one can feel relatively comfortable about using Eq.(15) (i.e., for $h = \infty$) or Eqs.(16) through (18) (i.e., for vertical mixing limited by a lid at $z=h$) to compute mixing ratios aloft and at ground level. However, transitioning from these expressions for the mixing ratio field φ to the original and widely-used Gaussian plume formula [e.g., Eq.(1) or Eq.(9)] for mass-based concentrations means that one must accept that air density remains constant throughout space. Yet, we clearly know that air density varies considerably throughout the depth of a mixed layer – especially if that mixed layer is several kilometers deep. To grasp the problem at hand, imagine that the atmosphere is divided into two vertically stacked boxes of equal depth. Furthermore, suppose that the pollutant is completely diffused vertically, giving rise to a mixing ratio $\varphi = 1.0$ everywhere. Now suppose that the density in the upper box is 0.85, but the density in the lower box has a higher value of 1.15. This means that the vertically-averaged density throughout this two-box atmosphere is $\langle \rho \rangle_z = 1.0$, as is the vertically-averaged concentration, that is, $\langle C \rangle_z = 1.0$. However, as discussed previously, the actual concentration in the individual boxes is computed as $C = \rho \cdot \varphi$, so that the concentration in the upper box is $C_u = 0.85$ and in the lower box is $C_l = 1.15$. Nevertheless, the 2D version (i.e., well-mixed vertically) of the Eq.(1) Gaussian plume equation would yield $C_l = 1.0$. Is a 15% difference worth worrying about given the known uncertainties in the key mixing depth determination? Perhaps not, but it is surprising that this issue and its correction has been ignored for so long.

A more detailed look at this problem begins by invoking the hydrostatic assumption for an isothermal atmosphere, such that the density falloff with height is given as $\rho(z) = \rho_0 \cdot \exp(-z/L)$, where L is the “scale height” of the atmosphere, known to be about 8 km. The exact solution for mixing ratio from K -theory may then be written as:

$$\phi(x, y, z) = \frac{A \cdot Q}{[U \cdot \rho(z_S)]} \cdot P(y, \sigma_y) \cdot \left\{ \begin{array}{l} P[z - \delta - z_S, \sigma_z, h] + \\ P[z - \delta + z_S, \sigma_z, h] \end{array} \right\} \quad (19a)$$

where A is a normalization constant with $A \approx 1$ very near the source, and where the “receptor shift distance”, δ , is given as:

$$\delta \equiv \frac{K_{zz} \cdot x}{U \cdot L} = \frac{\sigma_z^2}{2 \cdot L} \quad (19b)$$

and with choice of the + sign in the vertical term corresponding to the mirror image density function, $\rho(z) = \rho_0 \cdot \exp(+z/L)$. This “receptor shift distance”, δ , accommodates the variable density with no other alteration to the “method of images” summation. The expression for concentration may then be written as:

$$C(x, y, z) = \frac{A \cdot Q \cdot \exp[-(z - z_S)/L]}{U} \cdot P(y, \sigma_y) \cdot \left\{ \begin{array}{l} P[z - \delta - z_S, \sigma_z, h] + \\ P[z - \delta + z_S, \sigma_z, h] \end{array} \right\} \quad (19c)$$

where the normalization “constant”, A , is obtained by integrating C over all y , the positive z domain of $(0, +h)$, and requiring a final integrated result of Q/U .

This normalization integration is best performed by completing the square in z , and this leads to the more convenient crosswind-integrated form:

$$\bar{C}(x, z) = \frac{A \cdot Q}{U} \cdot \sum_{j=-\infty}^{+\infty} \exp\left(\frac{2 \cdot j \cdot h}{L}\right) \cdot \left\{ \begin{array}{l} \exp\left[\frac{-1}{2} \cdot (z + \delta - z_S + 2 \cdot j \cdot h)^2 / \sigma_z^2\right] + \\ \exp\left(\frac{2 \cdot z_S}{L}\right) \cdot \exp\left[\frac{-1}{2} \cdot (z + \delta + z_S + 2 \cdot j \cdot h)^2 / \sigma_z^2\right] \end{array} \right\} \quad (19d)$$

While for arbitrary h , the resulting integration in z yields a not-so-convenient infinite series of error function differences, the case of the unbounded atmosphere (i.e., $h \rightarrow \infty$) involves only the $j = 0$ term, and performing this integration yields the exact result:

$$A^{-1} = \frac{1}{2} \cdot \left\{ \operatorname{erfc}\left(\frac{\delta - z_S}{\sqrt{2} \cdot \sigma_z}\right) + \exp\left(\frac{+2 \cdot z_S}{L}\right) \cdot \operatorname{erfc}\left(\frac{\delta + z_S}{\sqrt{2} \cdot \sigma_z}\right) \right\} \quad (20a)$$

which for small arguments for the $\operatorname{erfc}(\dots)$ expands to yield a form consistent to lowest order in σ_z/L with the approximation:

$$A^{-1} \approx \exp\left(\frac{+z_S}{L}\right) \cdot \left[1 - \frac{\sigma_z}{\sqrt{2 \cdot \pi \cdot L}} \right] \quad (20b)$$

In the far field where $\sigma_z \geq h$, we revert back to Eq.(19c) and use the series expansion of the Jacobi theta function¹. Integrating in z from 0 to h yields:

$$A^{-1} \approx \exp\left(\frac{+z_S}{L}\right) \cdot \left\{ \begin{array}{l} \frac{L}{h} \cdot \left[1 - \exp\left(\frac{-h}{L}\right) \right] + \frac{2}{\pi} \cdot \sum_{k=1}^{+\infty} \beta^{k^2} \cdot \cos\left(\frac{k \cdot \pi \cdot z_S}{h}\right) \cdot \\ \left[1 - (-1)^k \cdot \exp\left(\frac{-h}{L}\right) \right] \cdot \left[\frac{\sin(b_k) + a_k \cdot \cos(b_k)}{k \cdot (1 + a_k^2)} \right] \end{array} \right\} \quad (20c)$$

where, as before, $\beta \equiv \exp[-(\pi \cdot \sigma_z)^2 / (2 \cdot h^2)]$, $a_k \equiv h / (k \cdot \pi \cdot L)$, $b_k \equiv k \cdot \pi \cdot \delta / h$, and δ is given by Eq.(19b). Now Eq.(20c) hardly represents a convenient normalization “constant”, but noting that in the truly well-mixed regime, where $\beta \rightarrow 0$, one may expand the first term in Eq.(20c) to obtain:

$$A^{-1} \approx \exp\left(\frac{+z_S}{L}\right) \cdot \left[1 - \frac{h}{2 \cdot L} \right]. \quad (20d)$$

Thus, one may construct a continuous normalization “constant” by combining Eq.(20b) for small σ_z with Eq.(20d), or, better yet, the first term of Eq.(20c), for larger σ_z . This final, somewhat-optimized synthesis for A (i.e., not A^{-1}) is:

$$A \approx \exp\left(\frac{-z_S}{L}\right) / \left\{ W + (1-W) \cdot \frac{L}{h} \cdot \left[1 - \exp\left(\frac{-h}{L}\right) \right] \right\}$$

where (20e)

$$W \approx \left[1 - \frac{3.16 \cdot \sigma_z}{L} \right] \text{ for } \sigma_z / L \leq 1/3.16, \text{ and } W \equiv 0 \text{ for larger } \sigma_z.$$

¹ Justifying this conclusion requires using the series expansion for the Jacobi theta function of the third kind and summing the two θ_3 terms to yield:

$$P(z, \sigma_z) = \frac{\exp[-(z - z_S)/L]}{2 \cdot h} \cdot \left\{ 2 + 2 \sum_{k=1}^{\infty} \beta^{k^2} \cdot \left[\begin{array}{l} \cos\left(\frac{k \cdot \pi \cdot (z - \delta - z_S)}{h}\right) \\ \cos\left(\frac{k \cdot \pi \cdot (z - \delta + z_S)}{h}\right) \end{array} \right] + \right\}$$

In integrating over z from 0 to h , all terms in the k sum vanish for $L = \infty$ (and hence $\delta = 0$); however, for finite L , and trigonometric expansion to isolate the z term, the integral over $\sin(k \cdot \pi \cdot z/h)$ for odd k values survives, as seen in the resulting Eq.(20c).

Also, noting that the $\exp(z_S/L)$ terms cancel when A from Eq.(20e) is inserted into Eq.(19c), one finds that the far-field effect of a realistic density profile on concentrations is effectively to multiply them by an overall factor, F , of:

$$F \approx \exp\left(\frac{-z}{L}\right) \cdot \left[1 + \frac{h}{2 \cdot L}\right] \quad (20f)$$

which is exactly the magnitude of effect envisioned at the outset. That is, for well-mixed conditions, a convective mixing height of $h \approx 2.4$ km, and an atmospheric scale height, L , of 8 km, ground-level mass concentrations should be increased by 15%, with smaller effects seen for shallower mixing heights. As decades of regulatory modeling rests upon the presumed validity of the simpler Eq.(1) (i.e., with $F \equiv 1$ presumed), the sub-sections which follow will not further consider inclusion of this atmospheric density refinement.

3 Extending the Plume Formulation Beyond Point Sources

Returning to Eq.(1) as the basic Gaussian plume equation arising from a point source, one naturally is led to ask how this result can be extended to sources having various and more complex distributions in space, such as lines and areas (e.g., see Turner, 1970), or in space and time, such as moving point sources.

3.1 Line Source Models

The straight-line source is a natural choice if one wishes to estimate impacts from roadway segments. In Volume 1, Chapter 7A by Venkatram and Thé (2003), the equation for line source impacts under perpendicular wind flow conditions (i.e., where the wind direction defines the $+x$ direction and the straight roadway defines the y axis), is presented for the infinite length line. This is accomplished by summing the concentration increments, dC , arising from infinitesimal sources of length dy and source strength $q \cdot dy$, where q is the line's emission density having units of mass/length/time. The total line's direct impact is then computed as the integral over these infinitesimal point elements as:

$$C(x, y, z) = \int dC = \frac{q}{U} \cdot P(z - z_S, \sigma_z) \cdot \int_{y_1}^{y_2} dy \cdot P(y, \sigma_y) \quad (21a)$$

where the integration limits, y_1 and y_2 , represent the endpoints of the line, and $P(z - z_S, \sigma_z)$ and $P(y, \sigma_y)$ are as in Eqs.(8b), except that σ_y and σ_z are typically taken as functions of x rather than travel time t , and are written:

$$P(y, \sigma_y) = \frac{1}{\sqrt{2\pi}\sigma_y} \cdot \exp\left[-\frac{y^2}{2 \cdot \sigma_y^2}\right], \quad P(z - z_S, \sigma_z) = \frac{1}{\sqrt{2\pi}\sigma_z} \cdot \exp\left[-\frac{(z - z_S)^2}{2 \cdot \sigma_z^2}\right]. \quad (21b)$$

Just as with the normalization integral of Eq.(12), one is able to express the result of the integration in Eq.(21a) as:

$$N(y_1, y_2) \equiv \int_{y_1}^{y_2} dy \cdot P(y, \sigma_y) = \frac{1}{2} \left[\operatorname{erf}\left(\frac{y_2}{\sqrt{2}\sigma_y}\right) - \operatorname{erf}\left(\frac{y_1}{\sqrt{2}\sigma_y}\right) \right] \quad (21c)$$

where *erf* is again the symbolic notation for the “error function”, as previously discussed in Section 2.2. Note that for an infinite line, $y_1 \rightarrow -\infty$ and $y_2 \rightarrow +\infty$, so that $N(y_1, y_2) \rightarrow 1$.

Thus, for the typical line source at $z_s = 0$, where the effect of adding in the ground reflection term is simply a factor of 2, the final result for the concentration due to perpendicular flow across an infinite, ground-level line is:

$$C(x) = \frac{2 \cdot q}{\sqrt{2\pi} \cdot \sigma_z \cdot U} \cdot \exp\left[\frac{-z^2}{2 \cdot \sigma_z^2}\right] \quad (21d)$$

3.1.1 Arbitrary Wind Angle Solutions

The great simplicity associated with the perpendicular wind is that the downwind distance, x , does not vary as one integrates along the line. Hence, the values of the dispersion coefficients, σ_y and σ_z , remain constant along the line source and the integrations can be performed as shown in Eq.(21). If instead the wind crosses the roadway at an angle θ away from perpendicular, the problem becomes far more difficult, as the σ_y and σ_z values vary with y position along the line and the integrals cannot be performed analytically for arbitrarily varying functions, $\sigma_y(x')$ and $\sigma_z(x')$, where x' is now the downwind distance as depicted in Figure 2 below. For the receptor located a perpendicular distance $x = x_R$ from the roadway, this receptor is now located a distance x'_R , directly downwind of a point declared to be $l = \theta$ along the roadway. Thus, at other points l along the line, the downwind distance, x' , and crosswind distance, y' , will be given as:

$$\begin{aligned} x' &= x'_R + l \cdot \sin(\theta) = x_R / \cos(\theta) + l \cdot \sin(\theta) \\ y' &= l \cdot \cos(\theta) \end{aligned} \quad (22)$$

These definitions make the dependence of x' and y' explicit as l varies during the integration along the line. As the dispersion coefficients, $\sigma_y(x')$ and $\sigma_z(x')$, are often defined as piecewise, power-law functions, or some other awkward functional form, we know that general attempts to evaluate the concentration as:

$$C(x, y, z) = \int dC = \frac{q}{U} \cdot \int_{\ell_1}^{\ell_2} d\ell \cdot P(z - z_s, \sigma_z) \cdot P(y', \sigma_y) \quad (23a)$$

where l_1 and l_2 are the end points of the integration, are likely to require numerical evaluation. Note that as “downwind” portions of the line’s emissions cannot contribute, the lower (or leftmost) limit l_1 must be greater than (or equal to) the point seen shown in the drawing as l_0 , where

$$l_0 = -x'_R / \sin(\theta) = -x_R / [\cos(\theta) \cdot \sin(\theta)] \quad . \quad (23b)$$

As mentioned, solution of Eq.(23a) must generally be performed numerically; however, it can be evaluated analytically if one makes the reasonable assumption that the key contribution to the integral comes primarily from the portion of the line nearly directly upwind of the receptor. In this case, one may linearize the dispersion coefficient dependence on downwind distance and write:

$$\begin{aligned} \sigma_z(x') &= \sigma_z(x_R' + x_0) + i_z \cdot (x' - x_R') \\ \sigma_y(x') &= \sigma_y(x_R') + i_y \cdot (x' - x_R') \end{aligned} \quad (24a)$$

where the pseudo-distance, x_0 , has also been added to allow for initial mixing, $\sigma_{z0} \equiv \sigma_z(x_0)$, at the line source due to various effects (e.g., vehicle induced mixing of exhaust). As $\sigma_y(x')$ dependence generally plays a minor role in line source integrations, disappearing, in fact, for the long crosswind line, we make an additional assumption that:

$$\sigma_y(x') = (i_y / i_z) \cdot \sigma_z(x') \quad (24b)$$

for all x' . This has the relatively minor impact of forcing the equality condition,

$$\sigma_y(x_R') = (i_y / i_z) \cdot \sigma_z(x_R' + x_0) \quad (24c)$$

on the value of $\sigma_y(x_R')$ at the upwind point of maximum impact. This then allows the Eq.(24a) expressions for the dispersion coefficients to be rewritten simply as:

$$\begin{aligned} \sigma_z(x') &= i_z \cdot [a' + l \cdot \sin(\theta)] \\ \sigma_y(x') &= i_y \cdot [a' + l \cdot \sin(\theta)] \end{aligned} \quad (24d)$$

where $a' \equiv \sigma_z(x_R' + x_0) / i_z$.

This then permits the integral expression of Eq.(23a) to be expressed as:

$$C(x, y, z) = \frac{q}{2 \cdot \pi \cdot U \cdot i_y \cdot i_z} \cdot I_0 \quad (24e)$$

where

$$I_0 \equiv \int_{\ell_1}^{\ell_2} d\ell \cdot \exp \left\{ -\frac{1}{2} \cdot \frac{[(b^2 + (\ell \cdot \cos \theta)^2)]}{i_y^2 \cdot (a' + \ell \cdot \sin \theta)^2} \right\} / (a' + \ell \cdot \sin \theta)^2$$

has dimensions of (m^{-1}) and

$$b \equiv (i_y / i_z) \cdot (z - z_S) \quad (24f)$$

represents the appropriately scaled z -coordinate for the direct plume term. In most cases, the source and receptor will be located near enough to ground level that b can be set to zero and the overall expression for C in Eq.(24e) can be multiplied by two to account for the ground reflection, but for now we will carry the b term and consider only the direct plume impact.

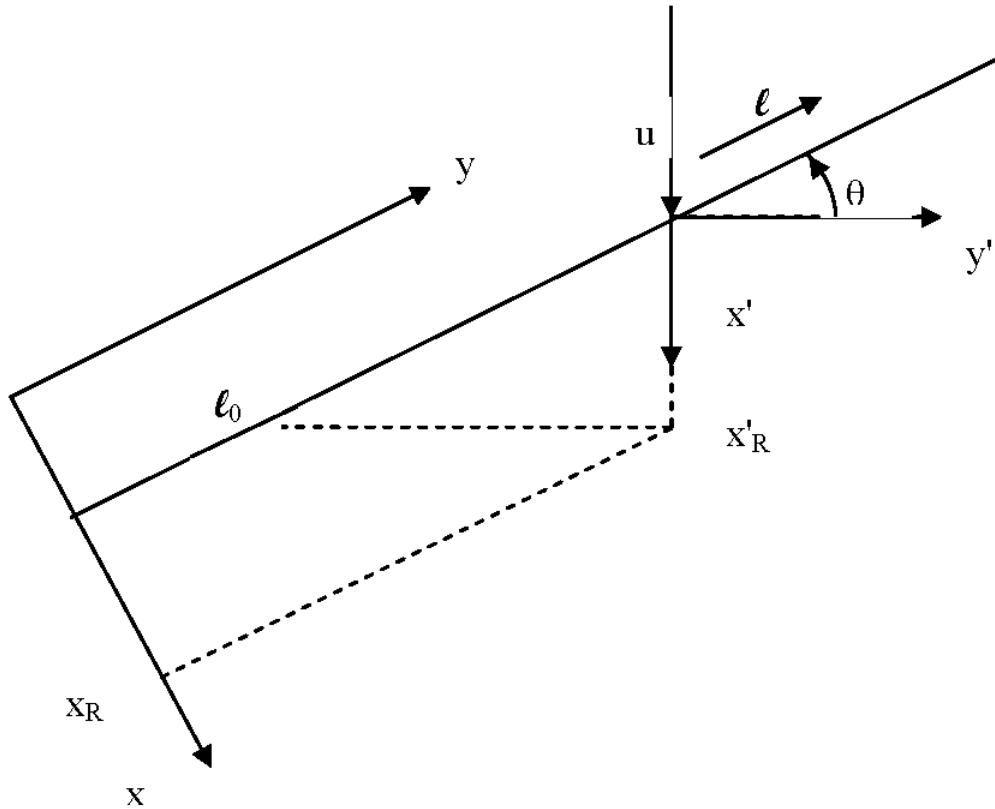


Figure 2. Roadway Coordinate System (x, y) rotated by the Angle θ relative to the Downwind-Crosswind System (x', y'). The receptor is located a perpendicular distance x_R from the roadway and a distance x'_R directly downwind of the line.

The variable substitution, $p \equiv [a' + l \cdot \sin(\theta)]^{-1}$, such that $l = (p^{-1} - a') / \sin(\theta)$, transforms I_0 in Eq.(24e) to:

$$I_0 \equiv \frac{-1}{\sin \theta} \cdot \int_{p_1}^{p_2} dp \cdot \exp \left\{ - \frac{[1 - 2 \cdot a' \cdot p + b'^2 \cdot p^2]}{2 \cdot i_y^2 \cdot \tan^2 \theta} \right\} \quad (24g)$$

with

$$b'^2 \equiv b^2 \cdot \tan^2(\theta) + a'^2 \quad (24h)$$

and integration limits, p_1 and p_2 , corresponding to limits l_1 and l_2 , respectively.

The subsequent change of variables from p to s via $s \equiv b' \cdot p - a' / b'$ transforms the numerator within the exponential from the expression within the brackets [...] to $[s^2 - (a' / b')^2 + 1]$; thus, “completing the square” and yielding the I_0 solution:

$$I_0 = \frac{i_y \cdot \exp \left\{ - \frac{b^2}{2 \cdot i_y^2 \cdot b'^2} \right\}}{b' \cdot \cos \theta} \cdot \frac{\sqrt{2 \cdot \pi}}{2} \cdot \left\{ \operatorname{erf} \left[\frac{s_1}{\sqrt{2} \cdot i_y \cdot \tan \theta} \right] - \operatorname{erf} \left[\frac{s_2}{\sqrt{2} \cdot i_y \cdot \tan \theta} \right] \right\} \quad (24i)$$

and hence, the solution for the time-averaged concentration at (x, y, z) is:

$$C(x, y, z) = \frac{q \cdot \exp \left\{ - \frac{b^2}{2 \cdot i_y^2 \cdot b'^2} \right\}}{\sqrt{2 \cdot \pi} \cdot U \cdot b' \cdot i_z \cdot \cos \theta} \cdot \frac{1}{2} \cdot \left\{ \operatorname{erf} \left[\frac{s_1}{\sqrt{2} \cdot i_y \cdot \tan \theta} \right] - \operatorname{erf} \left[\frac{s_2}{\sqrt{2} \cdot i_y \cdot \tan \theta} \right] \right\} \quad (25a)$$

where

$$s_1 = b' \cdot [a' + l_1 \cdot \sin(\theta)]^{-1} - a' / b' \quad \text{and} \quad s_2 = b' \cdot [a' + l_2 \cdot \sin(\theta)]^{-1} - a' / b' \quad (25b)$$

The final result given by Eq.(25) [i.e., with symbols a' , b , and b' defined in Eqs.(24d, f, and h)] is not very intuitively appealing, but it becomes more recognizable when one considers the limit of small θ . In this case, $b' \rightarrow a' = \sigma_z(x_R' + x_0) / i_z$, $s_1 / [i_y \cdot \tan(\theta)] \rightarrow -l_1 \cdot \cos(\theta) / \sigma_y(x_R')$, and $s_2 / [i_y \cdot \tan(\theta)] \rightarrow -l_2 \cdot \cos(\theta) / \sigma_y(x_R')$, yielding the more familiar solution:

$$C(x, y, z) = \frac{q \cdot \exp \left\{ - \frac{(z - z_s)^2}{2 \cdot \sigma_z^2(x_R' + x_0)} \right\}}{\sqrt{2 \cdot \pi} \cdot U \cdot \sigma_z(x_R' + x_0) \cdot \cos \theta} \cdot \frac{1}{2} \cdot \left\{ \operatorname{erf} \left[\frac{-l_1 \cdot \cos \theta}{\sqrt{2} \cdot \sigma_y(x_R')} \right] - \operatorname{erf} \left[\frac{-l_2 \cdot \cos \theta}{\sqrt{2} \cdot \sigma_y(x_R')} \right] \right\} \quad (26)$$

where $\sigma_y(x_R')$ is dictated by Eq.(24c). For a very long line, $l_1 \rightarrow -\infty$, $l_2 \rightarrow +\infty$, and the odd property of the *erf* yields the condition that the expression $\frac{1}{2} \cdot \{\dots\} \rightarrow +1$. Furthermore, recalling that Eq.(21d) is for a ground level line (i.e., $z_S = 0$) and includes the ground reflection term as a multiplicative factor of two, leads one to the conclusion that Eqs.(21d) and (26) are identical except for the fact that the line source strength, q , in Eq.(21d) is replaced with $q/\cos(\theta)$ in Eq.(26). This means that as the wind shifts from the perpendicular wind flow situation (i.e., $\theta = 0$), one dominant effect is that the foreshortened line is effectively “seen” by the receptor as being unrotated, but having an increased line-source emission density, $q/\cos(\theta)$. However, this effect is countered by the facts that: (i) the “error function” terms roll off at large angles, and (ii) the centerline, upwind distance, $x'_R = x_R/\cos(\theta)$, is also increasing. For typical, urban dispersion (i.e., neutral stability), the near-field vertical growth of a plume is quite linear with downwind distance, and for the case of no initial mixing (i.e., $x_0 = 0$) in the vertical, one has simply: $\sigma_z(x_R' + x_0) = i_z \cdot x'_R = i_z \cdot x_R/\cos(\theta)$. Thus, the two factors of $\cos(\theta)$ cancel exactly and one is left with little wind angle dependence in the concentrations estimated by Eq.(26). Of course, Eq.(26) was developed assuming small θ ; however, a numerical study of Eq.(25) under comparable conditions, shown in Figure 3 below, displays modest angular dependence in $C(\theta)/C(0)$ for angles less than about 40 to 50 degrees, with almost none of this arising from the *erf* terms. This rather weak angular dependence was first described by Calder (1973) as part of his numerical integration studies of line source impacts.

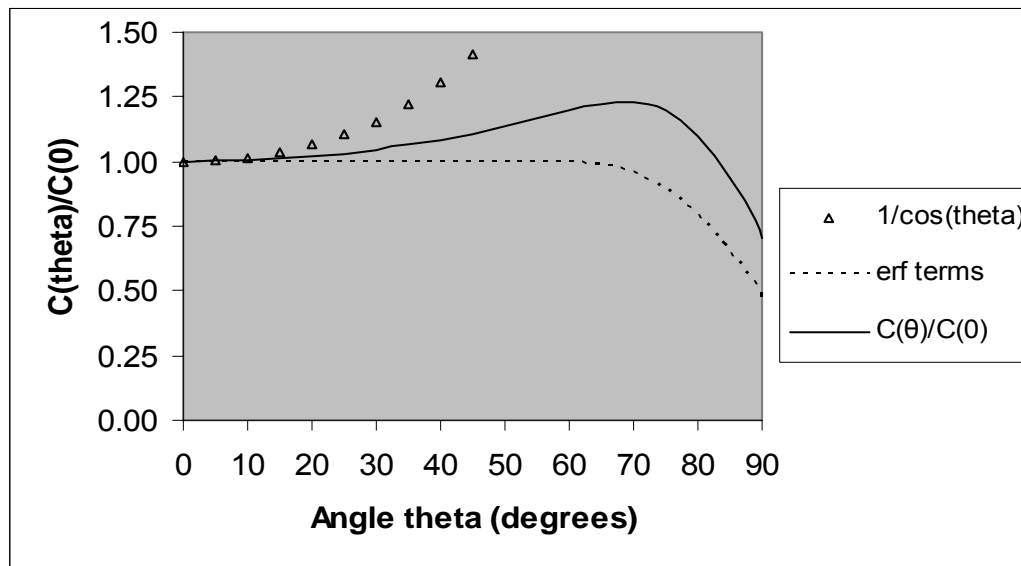


Figure 3. Angular dependence of Eq.(25). The dotted line shows only the sum of error function terms, whereas the solid line depicts the full ratio $C(\theta)/C(0)$. Parameter values assumed include: $\sigma_z(x_0) = 1m$; $x_R = 10m$; and $i_z = i_y = 0.2$.

Another way to view Figure 2 is to imagine that the x'_R is held fixed and the line source itself is rotated by θ . For line sources that are short relative to the value of

the appropriate Y-diffusion coefficient, that is, $L \equiv l_2 - l_1 \ll \sigma_y(x_R')$, the $erf()$ terms in Eq.(26) can be expanded using the small argument approximation, $erf(x) \approx 2 \cdot x / \pi^{1/2}$.

Inserting $l_2 = L/2 = -l_1$ into Eq.(26) and expanding yields the result:

$$\begin{aligned}
 C(x, y, z) &= \frac{q \cdot \exp \left\{ -\frac{(z - z_S)^2}{2 \cdot \sigma_z^2(x_R' + x_0)} \right\}}{\sqrt{2 \cdot \pi} \cdot U \cdot \sigma_z(x_R' + x_0) \cdot \cos \theta} \bullet \\
 &\quad \frac{1}{2} \cdot \frac{2}{\sqrt{\pi}} \left\{ \left[\frac{-(-L/2) \cdot \cos \theta}{\sqrt{2} \cdot \sigma_y(x_R')} \right] - \left[\frac{-(L/2) \cdot \cos \theta}{\sqrt{2} \cdot \sigma_y(x_R')} \right] \right\} \quad (27) \\
 &= \frac{q \cdot L \cdot \exp \left\{ -\frac{(z - z_S)^2}{2 \cdot \sigma_z^2(x_R' + x_0)} \right\}}{2 \cdot \pi \cdot U \cdot \sigma_z(x_R' + x_0) \cdot \sigma_y(x_R')}
 \end{aligned}$$

which is recognized as the Y-centerline value of a point source concentration (i.e., ignoring reflections). This is a reasonable result, because if a line source is small enough, it should be equivalent to a point source of strength $q \cdot L$ and the line's orientation angle, θ , should vanish from consideration.

3.1.2 Extension to Lines of Finite Width

Most line sources of interest, such as highways, have a finite width, W , that may be significant relative to the distance, x_R , of the receptor from the centerline of the roadway or lane. For the case of perpendicular wind flow, finite roadway width may be accommodated in Eq.(25) or Eq.(26) through the use of a multiplicative integral-averaging correction factor, F_W , defined such that:

$$F_W \equiv \frac{\sigma_z(x_R'')}{W} \cdot \int_{x_1}^{x_2} \frac{dx}{\sigma_z(x)} \quad (28)$$

where $x_1 = x_R'' - W/2$, $x_2 = x_R'' + W/2$, $x_2 - x_1 = W$, and the distance, x_R'' , includes all pseudo-distance effects as well (i.e., $x_R'' = x_R' + x_0$). Equation (28) has the simple solution:

$$F_W \equiv \frac{\sigma_z(x_R'')}{i_z \cdot W} \cdot \ln \left[\frac{\sigma_z(x_R'' + W/2)}{\sigma_z(x_R'' - W/2)} \right]. \quad (29a)$$

Now at first glance, Eq. (29a) seems to blow-up as $W \rightarrow 0$, but if one multiplies both numerator and denominator inside the log with $1/\sigma_z(x_R'')$ and linearizes the

expansion of $\sigma_z(x_R'' \pm W/2) / \sigma_z(x_R'') \approx 1 \pm \varepsilon$, where $\varepsilon \equiv \frac{1}{2} \cdot i_z \cdot W / \sigma_z(x_R'')$, then Eq.(29a) becomes:

$$F_W \approx \frac{1}{2 \cdot \varepsilon} \cdot \ln \left[\frac{1 + \varepsilon}{1 - \varepsilon} \right]. \quad (29b)$$

Equation (29b) only serves to bring the apparent problem into a clearer focus, which in turn demands expansion of the natural log as: $\ln(1 \pm \varepsilon) \approx 1 \pm \varepsilon - \varepsilon^2/2 \pm \varepsilon^3/3$. Provided all terms up to ε^3 are retained, one arrives at the final result of:

$$F_W \approx 1 + \frac{\varepsilon^2}{3} = 1 + \frac{1}{12} \cdot \left[\frac{i_z \cdot W}{\sigma_z(x_R'')} \right]^2 \quad (29c)$$

where this result is strictly valid only for $|\varepsilon| < 1$ or $|i_z \cdot W / \sigma_z(x_R'')| < 2$. Equation (29c) is primarily useful for showing that F_W does not have problems as the roadway width, W , shrinks to zero, but it should not be used for values of ε beyond about $\frac{1}{2}$. Instead, the more robust equation [i.e., Eq.(29a) or Eq.(29b)] should be used. Taking a rather wide roadway width of $W = 20$ m, and a vertical turbulent intensity of $i_z = 0.5$ over the turbulent roadway environment, a roadside receptor might experience a near-field plume as shallow as say $\sigma_z(x_R'' - W/2) \approx 1$ m, However, given the assumed level of turbulence suggests that $\sigma_z(x_R'' + W/2) \approx 11$ m and $\sigma_z(x_R'') \approx 6$ m, thus, yielding a value of $\varepsilon \equiv 0.833$. Using these values, both Eqs.(29a) and (29b) yield $F_W = 1.44$, whereas Eq.(29c) yields the smaller value of $F_W = 1.23$ as the expansion of $\ln(1 \pm \varepsilon)$ converges rather slowly for these larger values of ε .

Additionally, one notes that the Eq.(29a) [or Eq.(29b)] correction factor for Eq.(25) or Eq.(26) might also be approximately extended to arbitrary angles, by replacing W with $W/\cos(\theta)$.

Finally, one may think that, with the ever-increasing speed of computers, one might just leave all these line source issues to numerical integration. In fact, the AERMOD regulatory model does just this and does not presently include explicit formulae for line sources. One consequence of this is that individuals running long-term simulations (e.g., one-year) for airports and/or highway systems containing many line elements continue to complain of long run times.

3.1.3 The Moving Point Source Solution

The source strength, q , considered in the subsections above, including Eqs.(21) through (27), represented a steady-state source having a linear emission density of q (mass/length/time). Typically, q might be given in units of g/m/s. Suppose instead, that the source consists of small point sources traveling along the line, such as depicted in Figure 2, at speed V_0 . If there are N (#/s) sources passing a fixed point each second, then the separation between sources is just $\Delta l = V_0 / N$. In

addition, if each of these sources emits pollutant at a rate, E (g/s), then the emission density is just:

$$q = E / \Delta l = N \cdot E / V_0 \quad (30a)$$

and all the equations developed above [i.e., Eqs.(21) through (27)] are still valid.

Suppose instead that there is just one source traveling along this same line over the interval of the concentration averaging period, τ , with starting and ending times chosen such that the source's concentration impact at a given receptor is fully realized between these start/end times. In this case, one could compute an N of $N = 1 / \tau$, so that the emission density, q , to be used in the case of a single point source traverse, would be:

$$q = E / (V_0 \cdot \tau). \quad (30b)$$

While it seems odd to have the concentration averaging time appear in expressions for the average concentration, such will be the case when only a single source passes by during the duration of the concentration-averaging period.

The above discussion may appear obvious to many, but now consider the case where the single source of strength E moves along the line l as some function of time. For example, for a constant velocity source, $l(t)$ is given as:

$$l(t) = l_0 + V_0 \cdot t \quad (31a)$$

so that then
$$dl = V_0 \cdot dt. \quad (31b)$$

The integration yielding the average concentration, as given by Eq.(24e), could just as well have been written as:

$$C(x, y, z) = \frac{E}{2 \cdot \pi \cdot U \cdot i_y \cdot i_z} \cdot \frac{I_C}{\tau} \quad (32a)$$

where

$$I_C \equiv \int_{t_1}^{t_2} dt \cdot \exp \left\{ -\frac{1}{2} \cdot \frac{[(b^2 + (\ell(t) \cdot \cos \theta)^2]}{i_y^2 \cdot (a' + \ell(t) \cdot \sin \theta)^2} \right\} / (a' + \ell(t) \cdot \sin \theta)^2 \quad (32b)$$

has units of (s/m²), and the time-integration, end-point limits, t_1 and t_2 , are given simply as: $t_1 = [l_1 - l_0] / V_0$ and $t_2 = [l_2 - l_0] / V_0$.

Performing the integration in time t now requires replacing all the appearances of $l(t)$ in Eq.(32b) with the explicit function of t given in Eq.(31). By now everyone is demanding that this madness be stopped and the change be made back to the

more convenient integration variable dl . Substituting dt with dl / V_0 and resetting the integration limits to l_1 and l_2 , one notes that the integral, I_C , for a constant speed source returns to the solution form I_0 of Eq.(24e), except for the appearance of a factor of $(1/V_0)$ inside of I_C . Of course, this constant factor can be taken outside the integral, so $I_C = I_0 / V_0$, thus permitting the average concentration to again be expressed as:

$$C(x, y, z) = \frac{E / (\tau \cdot V_0)}{2 \cdot \pi \cdot U \cdot i_y \cdot i_z} \cdot I_0 \quad (33)$$

where a final form for I_0 is given by Eq.(24i). Again, this solution is identical to simply substituting the q in Eqs.(25) through (27) with $E/(V_0 \cdot \tau)$, as discussed previously. The motivation for these seemingly trivial changes of variables will become clear in the next subsection.

3.1.4 The Accelerating Point Source Solution

Let us now consider a source of strength E (g/s) that is accelerating at some constant acceleration rate, A (m²/s), along the line depicted in Figure 2, with $A > 0$ corresponding to positive acceleration toward the right of the figure.

Lest one thinks that this is merely a problem of academic interest, I note that a present-day automobile's emission rate is very high during "hard" accelerations (i.e., as the catalytic reactor is intentionally bypassed), and jet aircraft emit most of their ground-level NO_x during their high-thrust, rapid-acceleration takeoff mode.

For these accelerating source cases, we redefine the relationship between $l(t)$ and time to be:

$$l(t) = V_0 \cdot t + \frac{1}{2} \cdot A \cdot t^2 \quad (34a)$$

where V_0 , rather than uniform along the line as before, is now defined as the velocity at point $l = t = 0$ corresponding to the line element directly upwind. Now, when one changes from integration variable dt to dl , it must be noted that:

$$dl = (V_0 + A \cdot t) \cdot dt = (V_0^2 + 2 \cdot A \cdot l)^{1/2} \cdot dt \quad \text{or} \quad dt = (dl / V_0) \cdot (1 + 2 \cdot A \cdot l / V_0^2)^{-1/2} \quad (34b)$$

so the accelerating source integral, I_A , with units (s/m⁻²) becomes:

$$I_A \equiv \frac{1}{V_0} \cdot \int_{l_1}^{l_2} dl \cdot \exp \left\{ -\frac{1}{2} \cdot \frac{[(b^2 + (\ell \cdot \cos \theta)^2)]}{i_y^2 \cdot (a' + \ell \cdot \sin \theta)^2} \right\} \frac{(1 + 2 \cdot A \cdot \ell / V_0^2)^{-1/2}}{(a' + \ell \cdot \sin \theta)^2} \quad (35a)$$

where, as before, $a' \equiv \sigma_z(x_R' + x_0) / i_z$.

Following the same transformations from l to p to s that accompanied Eqs.(24) and (25), one finds that the relations between l and s are just:

$$\ell = \frac{b' - a' \cdot (s + a' / b')}{(s + a' / b') \cdot \sin \theta} \quad \text{and} \quad s = \frac{b'}{(a' + \ell \cdot \sin \theta)} - \frac{a'}{b'} \quad (35b)$$

where, as before, $b \equiv (i_y / i_z) \cdot (z - z_s)$ and $b'^2 \equiv b^2 \cdot \tan^2(\theta) + a'^2$, and this leads to the substitution:

$$(1 + 2 \cdot A \cdot \ell / V_0^2)^{-1/2} = \frac{1}{\gamma^{1/2}} \cdot \left[\frac{(s + a' / b')}{(s + \delta / \gamma)} \right]^{1/2} \quad (35c)$$

with

$$\gamma = 1 - \left[\frac{2 \cdot A \cdot a'}{V_0^2 \cdot \sin(\theta)} \right] \quad \text{and} \quad \delta = \frac{a'}{b'} + \left[\frac{2 \cdot A \cdot b'}{V_0^2 \cdot \sin(\theta)} \right] \cdot \left[1 - \left(\frac{a'}{b'} \right)^2 \right] \quad (35d)$$

Then, reversing the limits of integration, the final integral expression in s is:

$$I_A = \frac{\exp\left\{-\frac{b^2}{2 \cdot i_y^2 \cdot b'^2}\right\}}{V_0 \cdot b' \cdot \sin \theta} \cdot \int_{s_2}^{s_1} ds \cdot \exp\left[\frac{-s^2}{2 \cdot i_y^2 \cdot \tan^2 \theta}\right] \cdot \frac{1}{\gamma^{1/2}} \cdot \left[\frac{(s + a' / b')}{(s + \delta / \gamma)} \right]^{1/2} \quad (35e)$$

While it does not appear that this integral is solvable analytically, the fact that most of the contribution to the integral occurs near $l \approx 0$, or $s_p \approx b'/a' - a'/b'$, suggests detailed consideration of the factor, F , defined as:

$$F \equiv \frac{1}{\gamma^{1/2}} \cdot \left[\frac{(s + a' / b')}{(s + \delta / \gamma)} \right]^{1/2} = \left[\frac{1 + (a' / b') \cdot A' \cdot (s - s_p)}{1 + (a' / b') \cdot (1 - A') \cdot (s - s_p)} \right]^{1/2} \quad (36a)$$

where

$$A' \equiv \frac{2 \cdot A \cdot a'}{V_0^2 \cdot \sin(\theta)} \quad \text{is a dimensionless acceleration factor.} \quad (36b)$$

One may expand F around small values of $(s - s_p)$ to obtain:

$$F \approx 1 + \frac{1}{2} \cdot (a' / b') \cdot A' \cdot (s - s_p) \equiv F_C + F_S \cdot s \quad (36c)$$

where

$$\begin{aligned}
 F_C &= 1 - \frac{1}{2} \cdot (a'/b') \cdot A' \cdot s_p = 1 - \frac{A'}{2} \cdot \left(1 - \left(\frac{a'}{b'}\right)^2\right) \\
 &= 1 - \frac{A \cdot a'}{V_0^2 \cdot \cos^2(\theta)} \cdot \frac{b^2 \cdot \sin(\theta)}{b^2 \cdot \sin(\theta) + a'^2}
 \end{aligned} \tag{36d}$$

and

$$F_S \cdot s = + \frac{1}{2} \cdot (a'/b') \cdot A' \cdot s = \frac{A \cdot a'^2}{b' \cdot V_0^2 \cdot \sin(\theta)} \cdot s. \tag{36e}$$

Noting that F_C is independent of s and the linear s dependence in $F_S \cdot s$ leads to an integral that can be transformed to the integral of a simple exponential, one may write the solution as:

$$\begin{aligned}
 I_A &= F_C \cdot I_C + \\
 &F_S \cdot \frac{\exp\left\{-\frac{b^2}{2 \cdot i_y^2 \cdot b'^2}\right\}}{V_0 \cdot b' \cdot \sin\theta} \cdot i_y^2 \cdot \tan^2 \theta \cdot \left\{ \exp\left[\frac{-s_2^2}{2 \cdot i_y^2 \cdot \tan^2 \theta}\right] - \exp\left[\frac{-s_1^2}{2 \cdot i_y^2 \cdot \tan^2 \theta}\right] \right\}
 \end{aligned} \tag{36f}$$

with the concentration given as:

$$C(x, y, z) = \frac{E / \tau}{2 \cdot \pi \cdot U \cdot i_y \cdot i_z} \cdot I_A. \tag{37}$$

Referring back to the Eqs.(36d) and (36e) definitions of F_C and F_S , recalling that $I_C = I_0 / V_0$, and examining Eq.(36f), one notes that if $A = 0$, one immediately recovers the Eq.(33) solution for the constant velocity source. Also, one can see that if the wind flow is perpendicular to the line (i.e., $\theta = 0$), I_A reverts to I_C , which simply means that one is insensitive to acceleration or deceleration under such perpendicular flows, and only the velocity at the upwind point on the line is important. This implies that the lower speed, higher emission density, left-of-centerline (i.e., for $A > 0$) portion of the line's contribution is exactly offset by the higher speed, lower emission density, right-of-centerline contribution to the receptor concentration.

The Eq.(37) solution for the concentration due to an accelerating sources is appropriate for a wide variety of conditions. However, in some instances (e.g., when the upwind point does not lie on the physical line or when $V_0 = 0$), an alternative formulation of I_A must be considered, starting with a simple redefinition of the Eq.(34a) relationship between $l(t)$ and time t .

3.2 Area Source Models

Area sources are a natural extension of the line source problem. The direct concentration (i.e., not counting reflection terms) from a steady-state area source of emission strength, q_A (g/m²/s), can be written as:

$$C(x, y, z) = \frac{q_A}{U} \cdot \int_{x_1}^{x_2} dx \cdot P(z - z_S, \sigma_z) \cdot \int_{y_1}^{y_2} dy \cdot P(y, \sigma_y) \quad (38)$$

where x and y are the along-wind and cross-wind coordinates, respectively, and the integration may be performed over an arbitrarily shaped area for which one is able to define the cross-wind limits, y_1 and y_2 , as a function of increasing x .

Now as the y integration is purely a crosswind integration, σ_y remains constant, and Eq.(21c) may be invoked and Eq.(38) reduced to the single integration:

$$C(x, y, z) = \frac{q_A}{U} \cdot \int_{x_1}^{x_2} dx \cdot P(z - z_S, \sigma_z) \cdot \frac{1}{2} \cdot \left[\operatorname{erf} \left(\frac{y_2}{\sqrt{2}\sigma_y} \right) - \operatorname{erf} \left(\frac{y_1}{\sqrt{2}\sigma_y} \right) \right]. \quad (39)$$

However, as both $\sigma_y(x)$ and $\sigma_z(x)$ are functions of x , evaluation of the Eq.(39) integration in x is generally accomplished via an efficient numerical integration method (e.g., Romberg).

If one invokes the “narrow plume hypothesis” of Gifford (1959), or alternatively considers a very wide area source, such that the $\operatorname{erf}(\)$ terms saturate to 1 and -1, respectively, one is able to consider the simpler integral:

$$C(x, y, z) = \frac{q_A}{\sqrt{2\pi} \cdot U} \cdot \int_{x_1}^{x_2} \frac{dx}{\sigma_z(x)} \cdot \exp \left[-\frac{(z - z_S)^2}{2 \cdot \sigma_z^2(x)} \right]. \quad (40)$$

To solve this integral, one must choose an explicit form for $\sigma_z(x)$. Assuming the typical power-law form:

$$\sigma_z(x) = a \cdot (x + x_0)^b \quad (41a)$$

where x_0 is the pseudo-distance implicitly determined from the initial mixing, σ_{z0} , as $\sigma_z(x_0) = \sigma_{z0}$, one may transform to the variable s defined as:

$$s = \frac{(z - z_S)^2}{2 \cdot \sigma_z^2(x)}. \quad (41b)$$

After some algebra, one finds that:

$$\frac{dx}{\sigma_z(x)} = \frac{-ds}{2 \cdot s} \cdot \left[\frac{d\sigma_z(x)}{dx} \right]^{-1} = \frac{-ds}{2 \cdot s} \cdot \left(\frac{1}{b \cdot a^{1/b}} \right) \cdot \left[\frac{(z - z_S)^2}{2 \cdot s} \right]^{(1-b)/(2 \cdot b)}$$

or

$$\frac{dx}{\sigma_z(x)} = -\alpha \cdot ds \cdot s^{-1 + \frac{b-1}{2 \cdot b}} \quad (41c)$$

where

$$\alpha \equiv \left(\frac{1}{2 \cdot b \cdot a^{1/b}} \right) \cdot \left[\frac{(z - z_S)^2}{2} \right]^{(1-b)/(2 \cdot b)} \quad \text{is a dimensionless constant.} \quad (41d)$$

This change of variables permits Eq.(40) to be rewritten as:

$$C(x, y, z) = \frac{q_A \cdot \alpha}{\sqrt{2\pi} \cdot U} \cdot \int_{s_2}^{s_1} ds \cdot s^{-1 + \frac{b-1}{2 \cdot b}} \cdot \exp(-s) \quad (42a)$$

where $s_1 = \frac{(z - z_S)^2}{2 \cdot \sigma_z^2(x_1 + x_0)}$ and $s_2 = \frac{(z - z_S)^2}{2 \cdot \sigma_z^2(x_2 + x_0)}$, and the solution of Eq.(42a) can be written in terms of the incomplete Gamma function (Abramowitz and Stegun, 1972) as:

$$C(x, y, z) = \frac{q_A \cdot \alpha}{\sqrt{2\pi} \cdot U} \cdot \left[\Gamma\left(\frac{b-1}{2 \cdot b}, s_2\right) - \Gamma\left(\frac{b-1}{2 \cdot b}, s_1\right) \right]. \quad (42b)$$

While this solution may be useful, its form does not facilitate an easy grasp of the overall behavior of the solution. To achieve this understanding, it is preferable to consider the simplified case of a surface source and receptor (i.e., $z = z_S = 0$) and also add in the effect of the ground reflection. In this case, and assuming the same Eq.(41b) form for $\sigma_z(x)$, Eq.(40) reduces to the simpler expression:

$$C(x, y, z) = \frac{q_A}{\sqrt{2\pi} \cdot U \cdot a} \cdot \int_{x_1}^{x_2} dx \cdot (x + x_0)^{-b} = \frac{q_A \cdot [(x_2 + x_0)^{1-b} - (x_1 + x_0)^{1-b}]}{\sqrt{2\pi} \cdot U \cdot a \cdot (1-b)} \quad (43a)$$

for $b \neq 1$, and for $b = 1$ yields:

$$C(x, y, z) = \frac{q_A \cdot \log[(x_2 + x_0)/(x_1 + x_0)]}{\sqrt{2\pi} \cdot U \cdot a}. \quad (43b)$$

A disturbing aspect of Eq.(43) is that for $b \leq 1$, an infinite source (i.e., $x_2 \rightarrow \infty$) will cause infinite concentrations; however, infinite extent sources will also be a problem for $b > 1$, as the presence of the reflecting lid will eventually cancel out the seeming benefit of having $b > 1$. Studies performed for various real and idealized cities have shown (Hanna et al., 1982) that urban concentrations can range from about $50 \cdot q_A / U$ for unstable conditions to as much as $1000 \cdot q_A / U$ under stable atmospheric conditions.

3.3 Incorporation of Wind Shear

Of course there are many types of wind shears, $\partial u_i / \partial x_j$, where u_i might represent any of the three wind components and x_j any of the three spatial dimensions; however, in Gaussian plume modeling, the dominant shear that is generally ignored is due to the turning of the wind with height. To first order, one may represent such turning with height by injecting a plume transverse velocity, $v(z)$, of the form $v(z) = (\partial v / \partial z) \cdot (z - z_S)$, where $\partial v / \partial z$ is taken to be a constant in space. Walcek (2004, 2007) has recently obtained an analytic solution to the steady-state diffusion equation appropriate for this problem. The differential equation for the steady-state plume which Walcek solves is:

$$u \cdot \frac{\partial C}{\partial x} + v \cdot \frac{\partial C}{\partial y} = K_h \cdot \frac{\partial^2 C}{\partial y^2} + K_z \cdot \frac{\partial^2 C}{\partial z^2} \quad (44)$$

and the solution he obtains for a source at $x = y = 0$ can be written as:

$$C(x, y, z) = \frac{Q}{2\pi \cdot u \cdot \sigma_y \cdot \sigma_z \cdot f} \cdot \exp \left[-\frac{1}{2} \left\{ \frac{y^2}{f^2 \cdot \sigma_y^2} + \frac{(z - z_S)^2 \cdot (1 + s^2 / 3)}{f^2 \cdot \sigma_z^2} - \frac{(z - z_S) \cdot y \cdot s}{f^2 \cdot \sigma_y \cdot \sigma_z} \right\} \right] \quad (45a)$$

where

$$f^2 \equiv 1 + s^2 / 12 \quad \text{and} \quad s \equiv \frac{\partial v}{\partial z} \cdot \frac{x}{u} \cdot \frac{\sigma_z}{\sigma_y} = \frac{\partial v}{\partial z} \cdot \frac{x}{u} \cdot \sqrt{\frac{K_z}{K_h}} \quad \text{or} \quad s \equiv \frac{\partial \theta}{\partial z} \cdot x \cdot \frac{\sigma_z}{\sigma_y} \quad (45b)$$

The latter, alternative definition of s is expressed in terms of a constant rate of turning of the wind direction, $\partial \theta / \partial z$, with height, z .

This generalization to include plume transverse wind shear is a particularly important and timely development, especially as data on wind shears are now rather widely available.

4 Removal Processes in Gaussian Plume Modeling

Processes which can deplete the mass within a pollutant plume include: radioactive decay, chemical reactions, dry deposition and wet removal. The goal of this section will be to present adjustment factors and altered plume formulations to take these various depletion mechanisms into account.

Radioactive decay is accommodated quite simply by multiplying the source strength, Q , by the exponential factor $F = \exp(-t/\tau)$, where t , the travel time is given as, $t \equiv x/U$, and τ represents the relevant decay time scale. Such an approach is also appropriate for removal by first-order chemical reactions, such as irreversible destruction by sunlight or other transformation pathways not dependent on the concentration of another trace gas depleted by the reaction. Higher-order chemical reactions involving the reaction of two trace species with one another to produce one or more different species generally requires numerical grid approaches, which are beyond the scope of this section.

4.1 Wet Removal

The removal of tropospheric pollutants by cloud systems is accomplished primarily through rainout or washout. Rainout generally refers to in-cloud scavenging of gases or aerosols, whereas washout (or sweepout) generally refers to below cloud processes. Within-cloud processes can often involve vertical transport and mixing of the pollutant, especially in convective systems, making a detailed treatment difficult within the realm of Gaussian plume modeling; however, below cloud scavenging, and particularly irreversible scavenging, is a Poisson process that also leads to exponential depletion of the plume mass below the cloud. In this case, the factor k in the exponential factor, $F = \exp(-k \cdot t)$, is referred to as the scavenging coefficient. Computation of this scavenging coefficient is beyond the scope of this chapter, but it can entail detailed information on the spectrum of particle sizes and raindrop sizes for particulate plumes or, for gases, consideration of the Henry's law solubility constant and, of course, the rainfall rate. Some attempts are also made to deal with a fractional cloud/rain coverage fraction, f , by replacing the simple exponential, $\exp(-k \cdot t)$, with a factor $F = \{1 - f[1 - \exp(-k \cdot t)]\}$, which prevents the plume mass being depleted to zero by halting it at $F = 1 - f$.

4.2 Dry Deposition Removal

Removal of pollutants at the surface through dry deposition is generally modeled via the use of a deposition velocity, first formulated by more than fifty years ago by Chamberlain (1953). This approach states that the deposited pollutant flux, F_d , can be computed as:

$$F_d = v_d \cdot C_0 \quad (46)$$

where v_d is the deposition velocity and C_0 is the pollutant concentration at a reference height, typically not far above the surface. The actual value of the deposition velocity depends on the reference height used, as well as many surface-, species-, and meteorology-dependent variables that will not be discussed further here. However, once v_d is determined, the amount of plume mass, dM , removed per unit time in a distance interval dx is given as simply:

$$dM = dx \cdot v_d \cdot \bar{C}(x, z_{ref}) = dx \cdot v_d \cdot \int_{-\infty}^{+\infty} dy \cdot C(x, y, z_{ref}) \quad (47a)$$

where $\bar{C}(x, z_{ref})$ is the crosswind-integrated concentration at reference height z_{ref} . Substituting the Gaussian plume expression into Eq.(47a) then yields the following differential expression for dM :

$$dM = dx \cdot v_d \cdot \frac{Q}{U} \cdot D(z_{ref}, z_S, \sigma_z, h) \quad (47b)$$

where $D(z_{ref}, z_S, \sigma_z, h)$ signifies the desired vertical distribution function, such as:

$$D(z_{ref}, z_S, \sigma_z, h) = P(z_{ref} - z_S, \sigma_z, h) + P(z_{ref} + z_S, \sigma_z, h) \quad (47c)$$

where the couplings, such as $P(z_{ref} \pm z_S, \sigma_z, h)$, are the vertical couplings defined in Eq.(17) at height $z = z_{ref}$ for a plume at source height z_S , reflected by both the ground and inversion lid at height h .

The precise manner in which dM is removed from the pollutant plume gives rise to two, quite different plume depletion approaches.

4.2.1 Source Depletion

If one makes the simplifying assumption that information about the amount of pollutant mass, dM , removed at the surface is instantly communicated throughout the entire depth of the plume, then the removed amount might effectively be thought of as being removed from the source strength itself, that is, $dM = dQ$. This enables one to rewrite Eq.(47b) to yield the simple differential equation for $Q(x)$ as:

$$\frac{dQ}{Q(x)} = dx \cdot \frac{v_d}{U} \cdot D(z_{ref}, z_S, \sigma_z(x), h). \quad (48)$$

This has the simple formal solution:

$$\frac{Q(x)}{Q} = \exp \left[-\frac{v_d}{U} \cdot \int_{x_0}^{x+x_0} dx' \cdot D(z_{ref}, z_S, \sigma_z(x'), h) \right] \quad (49)$$

where x_0 is the pseudo-distance accounting for initial mixing, and Q is the initial or unmodified source strength $Q(0)$. The integral in Eq.(49) is often evaluated numerically and with the reference height, z_{ref} , set to zero; however, this choice of z_{ref} does not really simplify the problem, as the integral is over the x' dependence contained within the dispersion coefficient, $\sigma_z(x')$. A typical term in the D sum over couplings is expressed as:

$$P(Z, \sigma_z(x')) = \frac{1}{\sqrt{2\pi} \cdot \sigma_z(x')} \cdot \exp\left[-\frac{Z^2}{2 \cdot \sigma_z^2(x')}\right] \quad (50a)$$

where

$$\sigma_z(x') = a \cdot (x')^b \quad (50b)$$

and Z represents one of the infinity of terms, $Z_{\pm, j} = z_{ref} \pm z_S + 2 \cdot j \cdot h$, with j ranging from $-\infty$ to $+\infty$ [i.e., see Eq.(17a)]. Substituting Eq.(50a) into Eq.(49), and making use of the basic definition of the incomplete Gamma function, $\Gamma(a, x)$, yields:

$$\Gamma(a, x) \equiv \int_x^{\infty} dt \cdot \exp(-t) \cdot t^{a-1} \quad (50c)$$

which ultimately leads to the solution:

$$\frac{Q(x)}{Q} = F(Z_{\pm, j}) = \exp\{-\beta \cdot [\Gamma(p, t_2) - \Gamma(p, t_1)]\} \quad (51a)$$

where

$$\beta = \frac{v_d}{2 \cdot U \cdot \sqrt{\pi} \cdot b \cdot Z_{\pm, j}} \cdot \left(\frac{Z_{\pm, j}}{\sqrt{2 \cdot a}}\right)^{1/b}, \quad p = \frac{b-1}{2 \cdot b}, \quad (51b)$$

$$t_2 = \frac{Z_{\pm, j}^2}{2 \cdot \sigma_z^2(x + x_0)}, \quad \text{and} \quad t_1 = \frac{Z_{\pm, j}^2}{2 \cdot \sigma_z^2(x_0)}.$$

As a has units of $(m)^{1-b}$, one notes that β is dimensionless. Also, the computation of the sum over coupling coefficients becomes equivalent to a product over exponentials (i.e., given that the summation (\sum) and integration (\int) operators are interchangeable). Thus, a final form for the solution is:

$$\frac{Q(x)}{Q(0)} = \prod_{j=-\infty}^{j=+\infty} F(Z_{-, j}) \cdot F(Z_{+, j}) \approx F(Z_{-, 0}) \cdot F(Z_{+, 0}) \cdots \quad (51c)$$

where the product expansion generally converges quite rapidly; however, as with the sum over reflections (Section 2.2), nearly-well-mixed plumes require more terms. Actual computations of the $F(Z)$ terms in Eq.(51c) are aided by the series expansion,

$$\Gamma(p, t_2) - \Gamma(p, t_1) = \sum_{n=0}^{\infty} (-1)^n \cdot \left[\frac{t_1^{n+p} - t_2^{n+p}}{(p+n) \cdot n!} \right] \quad (51d)$$

and recursion relations, such as:

$$\Gamma(p, t) = \frac{1}{p} \left[\Gamma(1+p, t) - t^p \cdot e^{-t} \right]. \quad (51e)$$

Equation (51e) can be particularly useful, as the range $\frac{1}{3} < b < 1$ leads to $-1 < p < 0$. Note also that for the special case of $p = 0$, which arises for exponent $b = 1$, L'Hospital's rule gives the $n = 0$ term in Eq.(51d) as $\ln(t_1) - \ln(t_2)$.

For downwind distances beyond the point $x = x_m$, where the plume can be considered well-mixed, the x' integration in Eq.(49) can be broken up into two pieces. The first piece, from x_0 to $x_m + x_0$, would be computed as indicated in Eq.(51a), and the part beyond $x' = x_m$ would contribute the multiplicative factor:

$$F(x - x_m) = \exp \left[-\frac{v_d}{U} \cdot \frac{(x - x_m)}{h} \right] = \exp(-t_m / \tau) \quad (52)$$

where $t_m = (x - x_m)/U$ is the transport time while well-mixed, and $\tau = h/v_d$ is the depletion time scale for a pollutant, well-mixed within a layer of depth h and having a deposition velocity v_d . The Eq.(52) form of source depletion is widely used in simple models of long-range transport.

Equations (51) and (52) served as the primary approach for dealing with dry deposition removal for nearly two decades in some regulatory models, such as the German regulatory model, AUSTAL-86 (Fath and Luehring, 1986). However, a major problem with this source depletion methodology is that it assumes that the loss of material at the surface is instantly communicated throughout the entire plume, and this can create a significant problem, particularly under stable conditions where the material loss at the surface lowers the surface concentration substantially (and hence subsequent deposition), as the vertical mixing rate is not rapid enough to replenish depleted surface concentrations with plume material from aloft. Thus, surface depletion generally:

- depletes the plume mass too quickly;
- overpredicts the deposited mass flux, $F = v_d \cdot C$; and
- overpredicts near-surface concentrations.

A “poor-man’s way” of coping with this problem is to decrease the value of v_d by increasing the atmospheric resistance term (i.e., as deposition velocities are generally computed as the reciprocal of a sum of resistances, one of which is the atmospheric resistance term). This approach can eliminate the overdepletion of plume mass and lead to improved flux estimates; however, it cannot correct the profile of concentrations near the surface.

4.2.2 Surface Depletion

The surface depletion model was introduced by Horst (1977) to eliminate the problems associated with source depletion. In his approach, the concentration is defined as the concentration due to the unabsorbed plume minus the sum of concentration “deficits” due to all upwind surface depletions. These deficits, or “anti-matter” plumes, emitted from the surface are assumed to disperse the same as normal plume material; thus, yielding the integral equation:

$$\bar{C}(x, z) = \frac{Q}{U} \cdot D(z, z_s, \sigma_z(x), h) - \frac{v_d}{U} \cdot \int_{x_0}^{x+x_0} dx' \cdot \bar{C}(x', z_{ref}) \cdot D(z, 0, \sigma_z(x-x'), h) \quad (53)$$

where $\bar{C}(x, z_{ref})$ is the crosswind-integrated concentration at reference height z_{ref} , where deposition and “re-emission” as concentration deficits is assumed to occur.

As Eq.(53) involves the unknown, crosswind-integrated concentration inside an integral as well as on the left-hand side, it is referred to as a Volterra integral equation of the second kind. Additionally, the fact that the integral involves a convolution (i.e., containing both a function of x' and one of $x-x'$) that defies splitting into a product of x and x' terms complicates converting the problem to a simple differential equation. Equation (53) is generally solved using iterative numerical methods that can render the process excessively time-consuming for many dispersion modeling applications; however, Laplace transforms also provide a convenient way (Yamartino, 1981) to solve Eq.(53) because of several convenient properties. For example, with respect to convolution integrals, one finds that:

$$\mathcal{L} \cdot \int_0^x dx' \cdot f(x') \cdot g(x-x') = \mathcal{L} f(x) \cdot \mathcal{L} g(x) = F(s) \cdot G(s) \quad (54a)$$

and with respect to integrals:

$$\mathcal{L} \cdot \int_0^x dx' \cdot f(x') = F(s) / s. \quad (54b)$$

\mathcal{L} is the Laplace transform operator defined such that:

$$\mathcal{L} f(x) \equiv F(s) \equiv \mathcal{L} \cdot \int_0^{\infty} dx \cdot \exp(-s \cdot x) \cdot f(x) \quad (54c)$$

and \mathcal{L}^{-1} is the inverse Laplace transform operator defined as:

$$f(x) \equiv \mathcal{L}^{-1} F(s) \equiv \frac{1}{(2 \cdot \pi \cdot i)} \cdot \int_{a-i\infty}^{a+i\infty} ds \cdot \exp(s \cdot x) \cdot F(s) \quad (54d)$$

where “ a ” is chosen so the complex integration is performed to the right of all singularities. While evaluating inverse Laplace transforms can take one into the intricacies of contour integration, it is useful to know that Laplace transforms and their inverses exist for many common functions and are tabulated in various math reference works and can now be found on the Web as well.

Taking the Laplace transform of Eq.(53) at $z = z_{ref}$ yields:

$$\mathcal{L}\bar{C}(x, z_{ref}) = \frac{Q}{U} \cdot \mathcal{L}D(z_{ref}, z_S, \sigma_z, h) - r \cdot \mathcal{L}\bar{C}(x, z_{ref}) \cdot \mathcal{L}D(z_{ref}, 0, \sigma_z, h) \quad (55a)$$

where $r \equiv \frac{v_d}{U}$. Rearranging terms algebraically yields:

$$\mathcal{L}\bar{C}(x, z_{ref}) = \frac{Q}{U} \cdot \left\{ 1 - \frac{r \cdot \mathcal{L}D(z_{ref}, 0, \sigma_z, h)}{[1 + r \cdot \mathcal{L}D(z_{ref}, 0, \sigma_z, h)]} \right\} \cdot \mathcal{L}D(z_{ref}, z_S, \sigma_z, h) \quad (55b)$$

and taking the inverse transform yields the integral equation solution:

$$\bar{C}(x, z_{ref}) = \frac{Q}{U} \cdot \left\{ D(z, z_S, \sigma_z, h) - \int_{x_0}^{x+x_0} dx' \cdot D^*(z_{ref}, 0, \sigma_z(x), h) \cdot D(z, z_S, \sigma_z(x-x'), h) \right\} \quad (55c)$$

where D^* is now defined via the relation:

$$\mathcal{L}D^*(z_{ref}, 0, h, x) = \frac{r \cdot \mathcal{L}D(z_{ref}, 0, \sigma_z, h)}{\{1 + r \cdot \mathcal{L}D(z_{ref}, 0, \sigma_z, h)\}} \quad (55d)$$

or via the integral equation:

$$D^*(z_{ref}, 0, h, x) = r \cdot \left\{ D(z_{ref}, 0, \sigma_z(x), h) - \int_{x_0}^{x+x_0} dx' \cdot D^*(z_{ref}, 0, \sigma_z(x'), h) \cdot D(z, 0, \sigma_z(x-x'), h) \right\} \quad (55e)$$

One might question what has been accomplished in trading the integral equation, Eq.(53), evaluated at $z = z_{ref}$ to give the near-surface concentration, for the convolution solution of Eq.(55c) plus the subsidiary integral equation for D^* , Eq.(55e). The advantage is that convolution integrals may be evaluated quickly (i.e., without the iterative means needed for integral equations), and the one remaining integral equation, Eq.(55e), need only be evaluated once each modeling hour for the specific stability class and mixing height, h , as D^* is not a function of source height, z_s .

As another example of this approach, consider what happens when Eq.(53) is integrated over all appropriate z (i.e., from $z = 0$ to $z = h$). In this case, Eq.(53) becomes:

$$\frac{Q(x)}{U} \equiv \int_0^h dz \cdot \bar{C}(x, z) = \frac{Q}{U} - \frac{v_d}{U} \cdot \int_{x_0}^{x+x_0} dx' \cdot \bar{C}(x', z_{ref}) . \quad (56)$$

Invoking the Eq.(54b) property that $\int_0^x dx' \cdot \bar{C}(x', z_{ref}) = \frac{1}{s} \cdot \int \bar{C}(x, z_{ref})$, and utilizing Eq.(55b) for $\int \bar{C}(x, z_{ref})$, one obtains the solution:

$$\frac{Q(x)}{Q} = 1 - r \cdot \left\{ \int_{x_0}^{x+x_0} dx' \cdot D^{**}(z_{ref}, 0, \sigma_z(x), h) \cdot D(z_{ref}, z_s, \sigma_z(x-x'), h) \right\} \quad (57a)$$

where D^{**} is now defined via the relation:

$$\int D^{**}(z_{ref}, 0, \sigma_z, h) = \frac{(1/s)}{\{1 + r \cdot \int D(z_{ref}, 0, \sigma_z, h)\}} \quad (57b)$$

or via the integral equation:

$$D^{**}(z_{ref}, 0, h, x) = 1 - r \cdot \int_{x_0}^{x+x_0} dx' \cdot D^{**}(z_{ref}, 0, \sigma_z(x'), h) \cdot D(z_{ref}, 0, \sigma_z(x-x'), h) . \quad (57c)$$

What is again important here is that: (i) Eq.(57c) need only be solved once for each modeling hour involving a unique stability class and mixing height, and (ii) the convolution in Eq.(57a) for the remaining plume mass is as easy to solve as the source depletion equation, Eq.(49), and yet yields a result free of the objectionable assumption of instantaneous vertical re-mixing of the deposited mass deficit throughout the entire plume.

Despite the elegance of the surface depletion methodology and the extent to which its solution procedure can be simplified via the use of Laplace transforms, it is a methodology that has gone largely unused in regulatory dispersion models.

4.2.3 Surface-Corrected Source Depletion

Possibly recognizing the modeling community resistance to dealing with integral equations, Horst (1983) developed a modified methodology to incorporate a corrected plume profile into the source depletion methodology. This resulted in a hybrid approach which corrected for the major shortcoming of source depletion, but required invoking results from K-theory. This approach was incorporated into the ISC-2 and ISC-3 models, which served as the primary, U.S. EPA Guideline model for short-range applications for many years.

In this hybrid approach, Eq.(49) now becomes:

$$\frac{Q(x)}{Q} = \exp \left[-\frac{v_d}{U} \cdot \int_{x_0}^{x+x_0} dx' \cdot D(z_{ref}, z_S, \sigma_z(x'), h) \cdot P(x', z_{ref}) \right] \quad (58a)$$

where $D(\dots)$ is the dispersion function unmodified by deposition and $P(x, z_{ref})$ is the correction factor to the profile arising from the deposition. The crosswind-integrated concentration at downwind points becomes:

$$\bar{C}(x, z) = \frac{Q(x)}{U} \cdot D(z, z_S, \sigma_z(x), h) \cdot P(x, z) \quad (58b)$$

where mass conservation requires that the non-dimensional $P(x, z)$ be normalized such that:

$$\int_0^h dz \cdot D(z, z_S, \sigma_z(x), h) \cdot P(x, z) \equiv 1 \approx \int_0^h dz \cdot D(z, 0, \sigma_z(x), h) \cdot P(x, z). \quad (58c)$$

Horst argues that this approximation of a ground level source height is reasonable for downwind distances where dry deposition is significant as $\sigma_z > z_S$ at these distances, and thus, the actual source height assumed becomes unimportant. This normalization integral is important, as it is ultimately utilized to determine $P(x, z_{ref})$.

Further assuming that concentration variations close to the surface, in the constant flux layer, are due solely to this profile correction factor P , and not to variations in $D(\dots)$, 1D K-theory tells us that:

$$P(x, z) = P(x, z_{ref}) \cdot [1 + v_d \cdot R(z, z_{ref})] \quad (58d)$$

where the atmospheric resistance between z_{ref} and z are given from K-theory as:

$$R(z, z_{ref}) \equiv \int_{z_{ref}}^z \frac{dz'}{K(z')} = \frac{1}{U} \int_{z_{ref}}^z \frac{dz'}{\sigma_z(x) \cdot [d\sigma_z(x)/dx]} \quad (58e)$$

Note that the Eq.(58e) expression in terms of plume sigmas relies on the point-source, K-theory relation, $\sigma_z^2(x) = 2 \cdot K \cdot (x/U)$, for the second moment, and is attributable to Briggs' formulas for σ_z (Gifford, 1976). Nevertheless, this form for the resistance is peculiar in that $\sigma_z(x)$ is usually not an explicit function of z ; however, it can be seen to be an implicit function of z through the first moment relation, $z' = \bar{z} = \sqrt{2/\pi} \cdot \sigma_z$. Thus, before the integral on the right side of Eq.(58e) is evaluated, one must first replace all terms in x with its equivalent in terms of σ_z , and then replace σ_z with the first-moment relation in z' . As a check, one should note that the simple, stable dispersion expression, $\sigma_z = \sqrt{2K/U} \cdot \sqrt{x}$, results in the resistance, $R(z, z_{ref}) = (z - z_{ref}) / K$. The ISC3 User's Guide (EPA, 1995) presents results for these resistance integrals, $R(z, z_d)$, and the resulting profile functions, $P(x, z_{ref})$, for the unstable through stable dispersion functions used within ISC3. A typical result for the depletion factor, $P(x, z_{ref})$, and the profile correction factor, $[1 + v_d \cdot R(z, z_{ref})]$, is given in Figure 4.

It should also be noted that Eq.(58d) represents a simplification applicable to the case of negligible gravitational settling velocity, v_g . The more general expression is:

$$P(x, z) = P(x, z_{ref}) \cdot \left\{ 1 + \frac{v_d - v_g}{v_g} \cdot [1 - \exp[-v_g \cdot R(z, z_{ref})]] \right\} \quad (58f)$$

However, inserting this expression into the normalization integral [i.e., the right hand side of Eq.(58c)] essentially guarantees that a numerical integration must be performed, whereas the normalization integration associated with the simpler Eq.(58d) can often be performed analytically.

Horst has shown that use of the methodology prescribed by Eqs.(58a) through (58e) leads to suspended mass, $Q(x)/Q$, and surface concentration estimates that are generally within a few percent of the reference surface depletion values, and thus, far more accurate than source depletion approximated values, particularly for the stable dispersion cases.

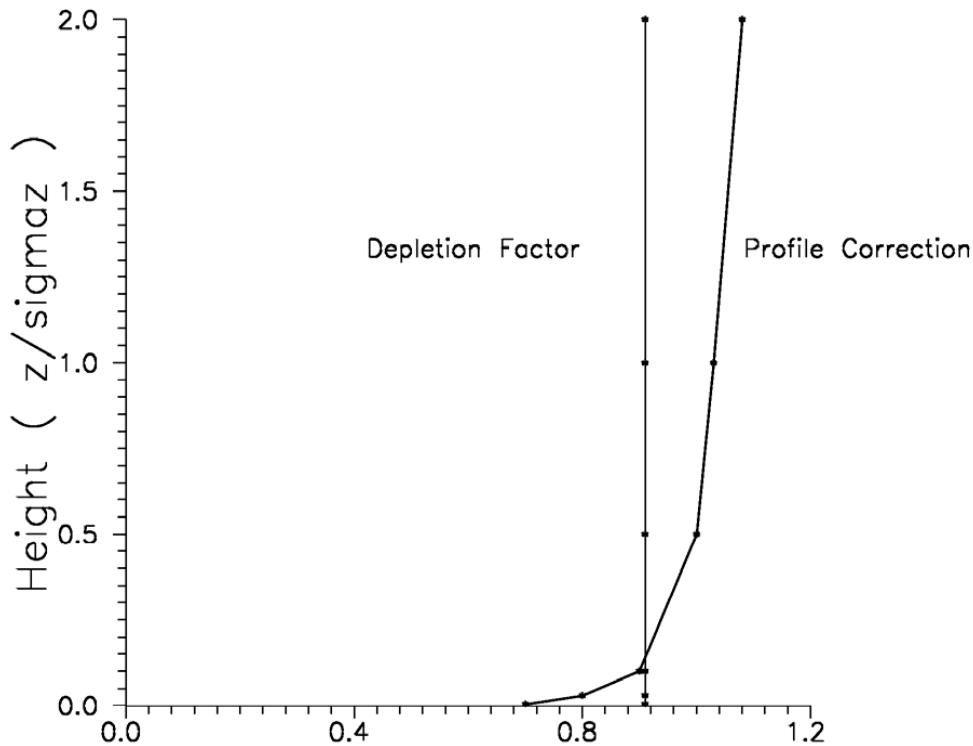


Figure 4. A typical for the Depletion factor, $P(x, z_{ref})$, and the associated Profile Correction factor, $[1 + v_d \cdot R(z, z_{ref})]$. Source: Fig. 1-7, U.S. EPA (1995).

4.2.4 Gravitational Settling and the Tilted Plume

Particles that are bigger than several microns are known to undergo dry deposition enhanced by their gravitational settling velocity, v_g . The terminal velocity of a particle of given physical (or Stokes) diameter, d_p , and density, ρ , is determined from the balance of gravitational and viscous drag forces to be:

$$v_g = \frac{g \cdot (\rho - \rho_A) \cdot d_p^2 \cdot C_S}{18 \cdot \mu} \quad (59)$$

where g is the gravitational acceleration, ρ_A is the ambient (air) density, C_S is the Cunningham slip factor (which is approximately 1.0 for particles larger than one micron), and μ is the viscosity of air. While this gravitational velocity is only about 0.03 cm/s for a unit density particle (i.e., $\rho = 1$ g/cc) of diameter 3μ , it increases with the square of particle diameter, such that a 10μ particle would settle at about 0.3 cm/s, and a more typical density 10μ particle might settle at about 1.0 cm/s. These velocities seem quite small relative to turbulent velocity scales, yet their persistent effect makes them hard to ignore when modeling the transport of particulate plumes over travel times of an hour or more.

Perhaps the simplest “fix” to plume modeling that one might imagine is correcting the effective source height z_S for such gravitational sinking via the “tilted” plume. That is, computing a corrected source height z_S' defined as:

$$z_S' = z_S - v_g \cdot t \quad (60)$$

where t is the downwind travel time, $t = x/U$. This simple idea works well until the effective source height reaches the ground and then effectively has the primary plume digging into the ground, and worse, has the ground reflection term simulating a plume climbing up from the ground at upward velocity, v_g . The simplest solution to this problem is to simply freeze the plume centerline at ground level once it reaches the ground, which is the solution that has been incorporated into many dispersion models. However, this approach erroneously suggests that gravity stops acting on these particles once the plume centerline reaches ground level. In the ISC-3 model, this subsequent settling has been incorporated as a correction to the plume’s vertical dispersion coefficient. For example, if the plume’s uncorrected plume spread is given as $\sigma_z(x)$ and $z_S' = 0$, then the mean plume centerline height $\langle z \rangle$ of this plume is just $(2/\pi)^{1/2} \cdot \sigma_z(x)$, so one can compute the gravitationally corrected dispersion rate as:

$$\sigma_z'(x) = \sigma_z(x) - (\pi/2)^{1/2} \cdot v_g \cdot (t - t_T) \quad (61)$$

subject to the additional constraint that $\sigma_z'(x)$ remains positive.

4.2.5 Deposition in K-Theory

K-theory continues to be used in numerical grid models. Exploiting the linkage between K-theory solutions and plume models dates back to the early days of modeling by Csanady (1955) and Smith (1962). While the substitution

$$\sigma_z^2(x) = 2 \cdot K \cdot (x/U) \quad (62a)$$

is strictly valid only for stable conditions, Rao (1981) has exploited the K-theory solution for depositing particles and developed a solution for the crosswind-integrated concentration as:

$$C(x,z) = \frac{Q}{\sqrt{2\pi} \cdot U \cdot \sigma_z} \cdot \exp \left[-\frac{v_g \cdot (z - z_S) \cdot x}{U \cdot \sigma_z^2} - \frac{v_g^2 \cdot x^2}{2 \cdot U^2 \cdot \sigma_z^2} \right] \cdot \left\{ \exp \left[-\frac{(z - z_S)^2}{2 \cdot \sigma_z^2} \right] + \exp \left[-\frac{(z + z_S)^2}{2 \cdot \sigma_z^2} \right] \cdot \left[1 - 2 \cdot \sqrt{2\pi} \cdot \frac{V \cdot x}{U \cdot \sigma_z} \cdot \exp(\xi^2) \cdot \text{erf}(\xi) \right] \right\} \quad (62b)$$

where

$$V = v_d - v_g/2 \quad (62c)$$

and

$$\xi = \frac{(z + z_s)}{\sqrt{2} \cdot \sigma_z} + \sqrt{2} \cdot \frac{V \cdot x}{U \cdot \sigma_z} \quad (62d)$$

For non-settling particles (i.e., $v_g = 0$ and $V = v_d$), Eq.(62) depletes only the image source, as one might intuitively expect from the notion that deposition is equivalent to imperfect reflection of matter from the surface, as was suggested quite early by Csanady (1955) and later by Overcamp (1976). While Eq.(62b) does not conserve mass for the general case where σ_z does not obey Eq.(62a), Rao forces the proper analytic normalization by integrating Eq.(62b) over z . Horst (1984) shows that Rao's solution is always intermediate in accuracy between the source depletion and surface depletion solutions. That is, it is superior to source depletion, but not as accurate as Horst's surface-corrected source depletion and the reference surface depletion solution.

Acknowledgments

I would like to thank Prof. Chris Walcek, Dr. Rainer Stern, and Mr. Gary Moore for their useful comments and careful readings of this manuscript.

References

- Abramowitz, M. and I. A. Stegun, 1972. Handbook of Mathematical Functions. NBS Applied Mathematics Series, Vol. 55, Tenth printing with corrections, Washington, D.C. Now available online at: <http://mintaka.sdsu.edu/faculty/wfw/ABRAMOWITZ-STEGUN/intro.htm> or at: <http://www.convertit.com/Go/ConvertIt/Reference/AMS55.ASP>.
- Calder, K.L., 1973. On estimating Air Pollution Concentrations from a Highway in an Oblique Wind. *Atmos. Environ.* **7**, 863-868.
- Chamberlain, A.C., 1953. Aspects of travel and deposition of aerosol and vapor clouds. Atomic Energy Research Establishment. AERE Report HP/1261.
- Csanady, G.Y., 1955. Dispersal of dust particles from elevated sources. *Aust. J. Phys.*, **10**, 558-564.
- Fath, J. and P.G. Luehring, 1986. Anwenderhandbuch zur Durchfuehrung von Ausbreitungsrechnungen nach TA Luft mit dem Programmsystem AUSTAL-86. UBA Forschungsbericht 10402575, Materialien 2/87, Erich Schmidt Verlag, Berlin.
- Fick, A., 1855. On liquid diffusion, *Phil. Mag. and Jour. Sci.*, **10**, 31-39.
- Gifford, F., 1959. Computation of pollution from several sources. *Int. J. Air Water Pollut.*, **2**, 109-110.
- Gifford, F., 1976. Turbulent diffusion typing schemes – a review. *Nuclear Safety*, **17**, 68-86.
- Hanna, S.R., G.A. Briggs, and R.P. Hosker, 1982. Handbook on Atmospheric Diffusion. U.S. Dept. of Energy Report DOE/TIC-11223.

Horst, T.W., 1977. A surface depletion model for deposition from a Gaussian plume. *Atmos. Environ.* **12**, 797-802.

Horst, T.W., 1983. A correction to the Gaussian source-depletion model. In *Precipitation Scavenging, Dry Deposition and Resuspension*, Vol. 2, H.R. Pruppacher, R.G. Semonin, and W.G.N. Slinn, Eds., Elsevier, 1205–1218.

Horst, T.W., 1984. The modification of plume models to account for dry deposition. *Boundary-Layer Meteor.* **30**, 413-430.

Overcamp, T.J., 1976. A general Gaussian diffusion-deposition model for elevated point sources. *J. Appl. Meteor.* **15**, 1167-1171.

Pasquill, F., 1974. *Atmospheric Diffusion*, 2nd Ed., John Wiley & Sons, New York.

Pasquill, F., 1976. The Gaussian Plume Model with Limited Vertical Mixing. U.S. EPA Report EPA-600/4-76-042.

Rao, K.S., 1981. Analytical Solutions of a Gradient-Transfer Model for Plume Deposition and Sedimentation. NOAA Technical Memorandum ERL ARL-109, Air Resources Laboratory, Silver Spring, MD.

Smith, F.B., 1962. The problem of deposition in atmospheric diffusion of particulate matter. *J. Atmos. Sci.* **19**, 429-434.

Sutton, O.G., 1932. A theory of eddy diffusion in the atmosphere. *Proc. Royal Soc. (London), Series A*, **135**: 143.

Sutton, O.G., 1953. *Micrometeorology*. McGraw-Hill Book Company, New York.

Turner, D.B., 1970. *Workbook of Atmospheric Dispersion Estimates*. U.S. EPA Publication AP-26, Research Triangle Park, NC, 84 pp.

U.S. EPA, 1992. User's guide for the Industrial Source Complex (ISC2) dispersion models. Vol. II, Description of model algorithms. EPA-450/4-92-008b, 82 pp. [NTIS PB-92-232446].

U.S. EPA, 1995. User's guide for the Industrial Source Complex (ISC3) dispersion models. Vol. II, Description of model algorithms. EPA-454/B-95-003b, 120 pp. [NTIS PB-95-222758].

Venkatram, A. and J. Thé, 2003. Introduction to Gaussian Plume Models. Chapter 7A in *Air Quality Modeling: Volume I – Fundamentals*. Paolo Zannetti, Ed., EnviroComp Institute and the Air and Waste Management Association.

Walcek, C.J., 2004. Accounting for wind shear in Gaussian dispersion models. American Meteorological Society 16th Symposium on Boundary Layers and Turbulence, Aug. 8-14. Portland, ME, Preprint 10.5.

Walcek, C.J., 2007. Accounting for wind shear in Gaussian dispersion models. *Atmos. Environ.*, In Press.

Yamartino, R., 1977. A new method for computing pollutant concentrations in the presence of limited vertical mixing. *J. Air Pollution Control Assoc.*, **27**, 467-468.

Yamartino, R.J., 1981. Solutions to the Equation for Surface Depletion of a Gaussian Plume. Proc. of the 12th NATO/CCMS International Technical Meeting on Air Pollution Modeling and Its Application, Menlo Park, CA.

Yamartino, R. 2008. *Gaussian Puff Modeling*. Chapter 8 of *AIR QUALITY MODELING - Theories, Methodologies, Computational Techniques, and Available Databases and Software. Vol. III – Special Issues* (P. Zannetti, Editor). Published by The EnviroComp Institute (www.envirocomp.org) and the Air & Waste Management Association (www.awma.org).

Chapter 8

Gaussian Puff Modeling

Robert J. Yamartino

Integrals Unlimited, Portland, Maine (USA)
rjy@maine.rr.com

Abstract: This chapter focuses on the development of various Gaussian puff modeling techniques, with an emphasis on the relevant mathematics. Beginning with the diffusion equation, we first discuss the linkage between the 3D puff and plume formulations and show how the puff approach overcomes many of the limitations associated with plume modeling, including the limit of calm winds. The focus then shifts to consideration of the integral over source emission time and the integral-average over receptor time, both of which must be accomplished in an applied puff model. Puff model enhancements, including consideration of incorporating true puff dispersion coefficients and a detailed evaluation of the effect of wind shears on puff dispersion, conclude the chapter. No attempt has been made to duplicate discussions from Chapter 7B (e.g., summation of images, dry deposition) that are also directly applicable to puffs.

Key Words: Gaussian puff methods, atmospheric dispersion modeling.

1 Introduction

In both the preceding Chapter 7B and Chapter 7A from a previous volume (Vol. 1), the great simplicity and versatility of Gaussian plume formulations is evident. Extensive use of the plume formulation preceded that of the 3D puff because most near-field, high-impact source-receptor situations are adequately modeled by the plume and because the plume calculation can often be as computationally-simple as a “back-of-the-envelope” calculation; however, from a mathematical point of view, it is the puff which is more fundamental, deserving to be described first.

To rationalize exploring the more computationally-intensive puff modeling approach, one must recall the significant simplifications and approximations that were invoked to reach the Gaussian plume, including:

- the steady-state assumption, implying time-independent flow and turbulence fields as well as source conditions;
- neglect of most spatial gradients in flow and turbulence, though some shears can be approximated and plumes can be treated in a spatially-segmented fashion; and
- neglect of along-wind diffusion, though this can be shown to be related to the steady-state assumption.

How can one avoid these approximations and simulate transport and diffusion as accurately as possible, especially in low-wind or meandering wind situations? As mentioned above, “segmented-plume” models provide some relief, in that they can accommodate changing wind speed (i.e., for speeds over 1-2 m/s), wind direction, and stability class. However, even segmented-plume models ignore along-wind diffusion, and are thus inappropriate for extended calm periods.

Before delving into the puff in detail, consider first the most-detailed, opposite extreme to plume modeling. Perhaps, the ultimate method is to characterize pollutant emissions as consisting of many mathematical point particles, with each particle carrying information about:

- its current coordinates (x,y,z);
- the pollutant species mass(es) it represents; and,
- other possible “markers”, such as its source name, emission time, and current density (i.e., for plume rise calculations).

Each particle can then be transported by the local flow (i.e., advective) and turbulent (diffusive) fields or conditions (e.g., statistical moments of turbulence) at each particle’s current location. Of course, this approach is very close to mimicking the real emission process and is exactly the approach taken in Lagrangian particle modeling: many of the advantages of which are described in detail by Anfossi and Physick in Chapter 11 (Vol. 2). Unfortunately, this approach also has an important limitation arising from the fact that in order to compute a concentration, one must essentially “count” the particles at or near a receptor, and this process implies a level of statistical uncertainty. The process of computing concentrations can either be done by: (i) adding up the point particle masses within some finite-volume box imagined surrounding a receptor, and then dividing by the volume of the box; or, (ii) assigning each particle a sphere-of-influence, considering only those particles whose sphere-of-influence includes the specific receptor point, and adding the “partial concentration contributions” from each particle to yield a total concentration at the receptor. These “partial concentration contributions” are explicitly computed using a kernel estimator function, and there are many types of such kernel functions. For example, imagine that the mass of a particle is smeared uniformly over some sphere of radius R . Given that the 3D integral over this volume of $V = 4\pi R^3/3$ must contain 100 % of the particle’s mass, m , one is led to assign a concentration contribution of $C = m/V = 3\cdot m/(4\pi R^3)$ to receptors falling inside this radius of R and $C = 0$ to receptors outside of this radius. This kernel, K , of $1/V$ is seen to be

little different from the coupling coefficient of box- or plume-modeling, except that its units of m^{-3} is appropriate for a particle of discrete mass rather than the usual coupling coefficient units of $\text{s}\cdot\text{m}^{-3}$ associated with a source having a continuous mass emission rate expressed in $\text{g}\cdot\text{s}^{-1}$. This uniform density distribution kernel is not ideal, as it creates an unacceptable level of statistical noise due to its sharp drop in density at radius, R . What is preferred instead is a kernel that peaks at the location of the particle and falls off rapidly with distance. De Haan (1997) describes a variety of such kernel estimators and relates their properties (e.g., second moments) to that of the Gaussian kernel in one, two and three dimensions. In three dimensions the spherical kernel is given as:

$$K(x, y, z) = \frac{1}{(2\pi)^{3/2} \cdot \sigma^3} \cdot \exp\left[-\frac{r^2}{2\sigma^2}\right] \quad (1)$$

where $r^2 = (x - x_0)^2 + (y - y_0)^2 + (z - z_0)^2$ and the particle's current center is located at coordinates (x_0, y_0, z_0) . Of course, this kernel is nothing more than a spherically symmetric Gaussian puff.

Thus, beginning with an emission of mathematical point particles, capable of precisely following the local flow and turbulence fields, coupled with the need to mitigate the statistical uncertainty noise associated with counting such particles, leads to a basic choice. One may either (1) increase the number of mathematical point particles emitted to a point where the statistical noise is acceptable, or (2) envision the particles as having their mass distributed over some volume in space. As the second choice is generally far less computationally intensive than the first, a rationale for puff modeling emerges. However, keep in mind that a weakness of this puff approach is that the larger the puff dimension, σ , the less the flow and turbulence sampling at the point (x_0, y_0, z_0) is representative of conditions over the entire puff. Thus, at the outset, one can realize the strength and weakness of the puff methodology in simulating air pollution problems.

In Chapter 7B, the 3D advection-diffusion equation (ADE) was given as:

$$\frac{\partial(\rho \cdot \phi)}{\partial t} = \underline{\nabla} \cdot [-(\underline{V} \cdot \rho \cdot \phi) + (\mathbf{K} \cdot \rho \cdot \underline{\nabla} \phi)] + (S - D) \quad (2a)$$

and

$$\frac{\partial C}{\partial t} = \underline{\nabla} \cdot [-(\underline{V} \cdot C) + (\mathbf{K} \cdot \rho \cdot \underline{\nabla}(C/\rho))] + (S - D) \quad (2b)$$

for the mixing ratio, ϕ , and mass concentration, C , respectively, and where scalar variables C , ϕ , ρ , S and D , vector wind field \underline{V} , and tensor (or 2D matrix) diffusivity \mathbf{K} may generally all be 3D functions of x , y , and z . However, for the

simplified case of $\underline{V} = (u, v, w)$, with components u , v , and w and density ρ_0 uniform in space and time, and the rather sparse, diffusivity matrix of

$$\mathbf{K} = \begin{bmatrix} K_{xx} & 0 & 0 \\ 0 & K_{yy} & 0 \\ 0 & 0 & K_{zz} \end{bmatrix}, \text{ containing only the diagonal and space-time uniform,}$$

diffusivity elements, K_{xx} , K_{yy} and K_{zz} (or in their compressed notation form, K_x , K_y and K_z), one may write the solution of Eq.(2) as:

$$C(x, y, z, t) = \rho_0 \cdot \varphi(x, y, z) = m \cdot P(X, t) \cdot P(Y, t) \cdot P(Z, t) \quad (3a)$$

where

$$X \equiv (x - x_0) - u \cdot (t - t_0), \quad P(X, t) = \frac{1}{\sqrt{2\pi\sigma_x}} \cdot \exp\left[-\frac{X^2}{2 \cdot \sigma_x^2}\right] \quad (3b)$$

and where, for example,

$$\sigma_x^2 \equiv \sigma_{x0}^2 + 2 \cdot K_x \cdot (t - t_0). \quad (3c)$$

Parallel expressions can be written for the corresponding Y and Z dependent variables, utilizing the velocity components v and w and the diffusivity components K_y and K_z , respectively. One also notes that the space-time zero point, (x_0, y_0, z_0, t_0) , and initial dimension, σ_{x0} , may correspond to either the conditions at the time of initial release of mass m from the source or some other intermediate point in time (e.g., the conditions existing at the end of the previous computational time step in a multi-step model).

The similarity between Eq.(1) and Eq.(3) is no accident. As both equations are simply expressions of mass conservation and basically show that, under the stated uniformity conditions leading up to Eq.(3), the 3D Gaussian kernel, sometimes employed rather *ad hoc* in Lagrangian particle modeling, is identical to the solution of the 3D ADE for constant isotropic diffusivities.

Equation (3) is the core equation for all puff models and it will be used as the starting point for many calculations in the sections that follow. Also, it should be noted that much of what follows evolved during the development of the MESOPUFF II and CALPUFF models. Much of the material for these sections has been drawn from the "Model Formulation and User's Guide for CALPUFF" prepared by Scire et al. (1990b) for the California Air Resources Board.

The CALPUFF model has continued to evolve for nearly two decades, though many of the basic puff and integrated-puff equations described herein remain unchanged since the Scire et al. (1990b) document. The current version of

CALPUFF serves as a U.S. EPA Guideline model and is primarily documented in Scire et al. (2000).

2 Theoretical Background

2.1 The Puff-Plume Relationship

While the ability of Eq.(3) to be a solution of the 3D ADE is important, the fact that the normalization of the distribution functions over all space yields unity (i.e., 1.0) turns out to be more important from most practical considerations. For example, the space integral of $P(Z,t)$ over z yields:

$$N(Z, z_1, z_2) \equiv \int_{z_1}^{z_2} dz \cdot P(Z, t) = \frac{1}{2} \left[\operatorname{erf} \left[\frac{(z_2 - z_0) - u \cdot (t - t_0)}{\sqrt{2}\sigma_z} \right] - \operatorname{erf} \left[\frac{(z_1 - z_0) - u \cdot (t - t_0)}{\sqrt{2}\sigma_z} \right] \right] \quad (4)$$

where

$$Z \equiv (z - z_0) - u \cdot (t - t_0).$$

In the limit of integrating over all space (i.e., $z_1 \rightarrow -\infty$, $z_2 \rightarrow +\infty$), $N(Z, -\infty, +\infty) \rightarrow 1$, independent of the dependence of σ_z on time, t .

This same sort of integration also helps to bridge the transition between the puff and plume formulations. Rather than considering a few discrete puffs of mass m , imagine now a continuum of infinitesimal releases of size $Q \cdot dt'$, where continuous emission time t' takes the place of the discrete t_0 . In order to achieve steady-state plume conditions, the source must have begun emitting long ago (e.g., at $t' = -\infty$) and still be emitting; whereas, the receptor might just have been turned on at time $t = 0$ and off at time $t = T$. Thus, to reach steady-state plume limit, one needs to consider Eq.(3) for the case where the vector wind aligns with the +x axis, so $\underline{V} = (u, 0, 0)$, and then compute the following double-time-integral of Eq.(3):

$$C(x, y, z) = \frac{Q}{T} \cdot \int_{-\infty}^{\infty} dt' \cdot \int_0^T dt \cdot P(X, t) \cdot P(Y, t) \cdot P(Z, t) \quad (5a)$$

where

$$X \equiv (x - x_0) - u \cdot (t - t') \quad (5b)$$

and the source is assumed to be located at $(x_0, y_0, z_0) = (0, 0, z_S)$.

While σ_y and σ_z may be some arbitrary function of puff age or transport time (i.e., $t-t'$), the plume material reaching the receptor will do so at a relatively constant transport time – an approximation that becomes more valid as the along-wind puff dimension, σ_x , is taken to be small relative to transport distance, $x = u \cdot (t - t')$, that is:

$$\sigma_x \ll u \cdot (t - t') = x. \quad (5c)$$

Thus, we may rewrite $P(Y,t)$ and $P(Z,t)$ as:

$$P(Y,t) = \frac{1}{\sqrt{2\pi}\sigma_y} \cdot \exp\left[-\frac{y^2}{2 \cdot \sigma_y^2}\right] \text{ and } P(Z,t) = \frac{1}{\sqrt{2\pi}\sigma_z} \cdot \exp\left[-\frac{(z - z_s)^2}{2 \cdot \sigma_z^2}\right] \quad (5d)$$

and consequently, take these two terms outside the integrations of Eq.(5a).

This just leaves the $P(X, t-t')$ term inside the integrals. Now Eq.(5a) shows the emission time integration running from $t' = -\infty$ to $t' = +\infty$, even though it is obvious that any emissions later than $t' = T$ cannot possibly (i.e., via causality) contribute to the receptor concentration, but we choose the $t' = +\infty$ limit for simplicity. Note that Eq.(5a) actually indicates that one is integrating over emission time but averaging over receptor time, t . This is done because the time integral over receptor time yields an integrated-dose, whereas in Eq.(5a), one desires the average concentration, C . Now there are two ways to perform the double-integration. The more formal way involves integrating over receptor time, t , and the rotated variable $t'' \equiv t - t'$; however, as the actual plume concentration reaches steady-state, we note that the result of the receptor time integration must be $T/T = 1$, which reduces Eq.(5a) to a 1D integration, the result of which we already know from Eq.(4) to be:

$$C(x, y, z) = \frac{Q}{u} \cdot P(Y, t) \cdot P(Z, t). \quad (6)$$

This is just the Gaussian plume equation of Eq.(1) in Chapter 7B, with the exception that the wind velocity is explicitly given as the vector mean wind speed, u , rather than the more commonly used scalar wind speed, U . This is somewhat of a moot point for wind speeds in excess of 1 m/s, where the difference between the vector and scalar magnitudes is only a few percent. For very low wind speeds, the condition expressed by Eq.(5c) is no longer met, so the derivation of Eq.(6) would no longer be valid. Note that for very low wind speeds, the time dependence of the growth of the three σ quantities becomes important, such that the σ size values cannot be taken as "frozen" during the time of significant contribution of a puff to receptor's concentrations, and thus, cannot be subsequently ignored in the evaluation of Eq.(5a).

One can actually obtain a clearer understanding of what happens as $u \rightarrow 0$ by considering the case of a receptor at $(0,0,0)$ and begin again with Eq.(5a). However, rather than assuming $\sigma_x \ll u \cdot (t - t')$, as in Eq.(5c), we will take the opposite limit of $\sigma_x \gg u \cdot (t - t')$, and further assume that early plume growth proceeds as $\sigma_x = \sigma_u \cdot (t - t')$, with σ_y and σ_z showing corresponding dependencies on turbulent velocities σ_v and σ_w , respectively. In this case, Eq.(5a) becomes:

$$C(x, y, z) = \frac{Q \cdot \exp[-\frac{1}{2} \cdot (\frac{u}{\sigma_u})^2]}{(2 \cdot \pi)^{3/2} \cdot \sigma_u \cdot \sigma_v \cdot \sigma_w \cdot T} \cdot \int_0^T dt \cdot \int_0^t dt'' \cdot \exp[-\frac{1}{2} (\frac{z_S}{\sigma_w \cdot t''})^2] / t''^3. \quad (7a)$$

The t'' integration yields $\Gamma(1)/t_0^2$ ¹, where Γ is the Gamma function, with $\Gamma(1) = 1$, and the time-scale, t_0 , is the diffusive transport time, $t_0 = z_S/\sigma_w$. Combining this result with the factor T coming from the receptor time integration, Eq.(7a) finally yields:

$$C(x, y, z) = \frac{Q \cdot \exp[-\frac{1}{2} \cdot (\frac{u}{\sigma_u})^2]}{[(2 \cdot \pi)^{1/2} \cdot \sigma_u] \cdot [(2 \cdot \pi)^{1/2} \cdot \sigma_v \cdot t_0] \cdot [(2 \cdot \pi)^{1/2} \cdot \sigma_w \cdot t_0]}. \quad (7b)$$

This result is very similar to the concentration estimated from Eq.(6), with the σ_y and σ_z values given as shown, except that the vector mean wind has been replaced by the quantity $(2 \cdot \pi)^{1/2} \cdot \sigma_u$. This factor of $(2 \cdot \pi)^{1/2}$ is somewhat unexpected, as the scalar wind speed, U , is generally given as $U = (u^2 + \sigma_u^2)^{1/2}$, but one must remember that as $u \rightarrow 0$, the diffusion occurs in both the "upwind" and "downwind" directions (i.e., if such directions can still be thought to exist at $u = 0$). In fact, this factor $(2 \cdot \pi)^{1/2}$ is exactly the conversion factor from Gaussian to the "box" normalization we have seen in Chapter 7B. That is, while advection will sweep out a dilutionary box of length $u \cdot \Delta t$ in a time Δt , the effect of a diffusive turbulent velocity will lead to a box length of $(2 \cdot \pi)^{1/2} \cdot \sigma_u \cdot \Delta t$. Hence, if one were to piece together an effective "dilutionary velocity" for the Gaussian plume model, it would not be U (i.e., what is commonly defined as the scalar wind speed), but rather the new velocity variable, $U' \equiv (u^2 + 2 \cdot \pi \cdot \sigma_u^2)^{1/2}$. Again, for moderate wind speeds, this second term is only a few percent of the contribution by u^2 . Equation (7b) was obtained without invoking the need for the "frozen σ " approximation; however, given the widespread applicability of this approximation for even low wind speeds, we will have occasion to revisit it often in this chapter.

2.2 Practicality Constraints for Puff Models

Now that we understand the theoretical linkage between the puff and plume model, the connection between puff and Lagrangian particle models, and some of

¹ $\int dt \cdot \exp(-a \cdot t^p) / t^q = a^{(1-q)/p} \cdot \Gamma((1-q)/p, a \cdot t^p) / p$ from <http://integrals.wolfram.com>, where $\Gamma(\alpha, x)$ is incomplete Gamma function. Definite integral from Prudnikov et al., Vol. 1, pg 345, #2.3.18.2.

the advantages and limitations of puff models relative to the modeling techniques at the simpler (i.e., the Gaussian plume) and more computationally intensive (i.e., particle modeling) ends of the modeling spectrum, we have to decide what we really expect a practical puff model to deliver. The feature wish list can indeed grow quite long, but to become a useful regulatory model, a viable puff model must:

- deliver predictions that closely match plume predictions when conditions appropriate to the plume formulation pertain (e.g., steady-state emissions and dispersion conditions);
- avoid pitfalls associated with requiring data that is rarely available (e.g., accurate fields of vertical velocities, w)
- allow at least as much flexibility as plume models to include a variety of source types (e.g., points, areas, lines, volumes), near-source dynamical effects (e.g., plume rise, building wake effects), and loss mechanisms (e.g., dry/wet deposition, exponential decay); and,
- permit realistic scenarios (e.g., involving hundreds of sources, thousands of receptors, on a domain as large as a few thousand kilometers) to be performed for time periods as long as five years using present-day and widely-available computers.

Though the latter of these constraints is clearly not static, as computers become faster and cheaper, other constraints, such as providing accurate 3D winds (including w), are also evolving over time. Thus, the design of a practical model must be flexible enough to facilitate evolution of the model's capabilities.

Much of the history of puff model development has been driven by the first of the above constraints, that is, to deliver predictions that closely match plume predictions when conditions appropriate to the plume formulation pertain. However, it is not immediately obvious that a finite series of discrete puffs will yield the continuous plume result. Early puff models (e.g., Ludwig et al., 1977; van Egmond and Kesseboom, 1983; Peterson, 1986) evaluated the contribution of a puff to the concentration at a receptor by a "snapshot" approach. Each puff was considered "frozen" at particular time intervals or sampling steps, and the concentration due to the "frozen" puff at that time was computed or sampled. The puff was then allowed to move and evolve in size and mass until the next sampling step. The total concentration at a receptor was then just the sum of the contributions of all nearby puffs averaged over all sampling steps within the basic time step. Depending on the model and the application, the sampling and averaging time steps could be one hour (or longer), indicating that only one "snapshot" of the puff is utilized each hour. In this case, a problem immediately arises because there will be holes (or gaps) in the plume concentration precisely where there are spaces between the discrete puffs.

Thus, a traditional drawback of the puff approach has been the need for the release of many puffs to adequately represent a continuous plume close to a source. Ludwig et al. (1977) have shown that if the distance between puffs

exceeds about $2 \cdot \Phi_y$, inaccurate results may be obtained. Figure 1 shows that reasonable results are obtained for puff separations of no more than Φ_y . If the puffs do not overlap sufficiently, the concentrations at receptors located in the gap between puffs at the time of the "snapshot" are underestimated. While the normalization used in Figure 1 fixes the concentration at unity at the puff center, an un-normalized plot would show that for puff separations exceeding Φ_y , concentrations near the puff centers are overestimated. Ludwig et al. (1977) recommended spacing puffs uniformly in space, rather than in time, with a puff merging/purging scheme to reduce the total number of puffs.

As visualized in Figure 2, Zannetti (1981) suggested tracking fewer puffs than necessary for adequate sampling, but then saturating the area near a receptor with synthesized, interpolative puffs, in order to provide the required puff overlap.

Although both schemes act to reduce the number of puffs carried by the model, considering puffs as "snapshots" in space and time still requires that an uneconomically large number of puffs be generated near the source. For example, at a receptor 100 meters from a source, and assuming Pasquill-Gifford-Turner (PGT) dispersion rates, puffs at a density corresponding to a release rate of over 1300 puffs/hour are required to meet the two- Φ_y criterion for F stability, 3 m/s wind conditions. During high wind speed, neutral conditions (10 m/s, D stability), nearly 2200 puffs/hour are needed. The more stringent, one Φ_y criterion, would double the number of puffs required.

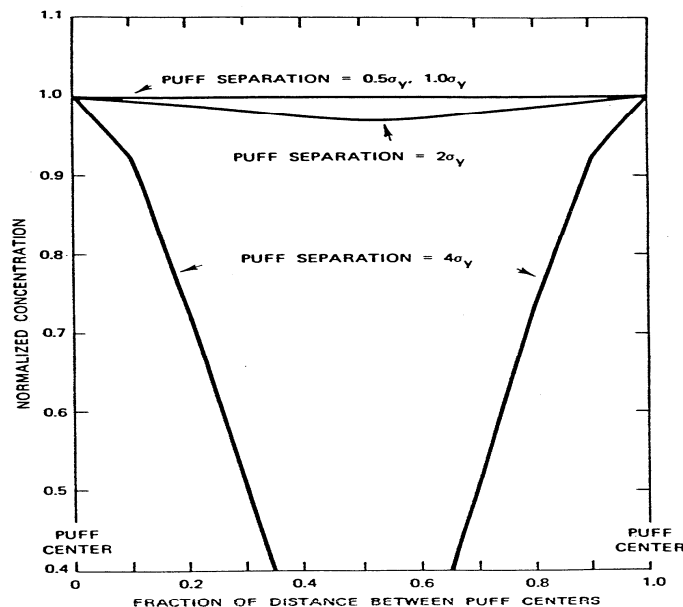


Figure 1. Normalized concentration between two puffs within a series of puffs having equal size and spacing. [From Ludwig et al., 1977.]

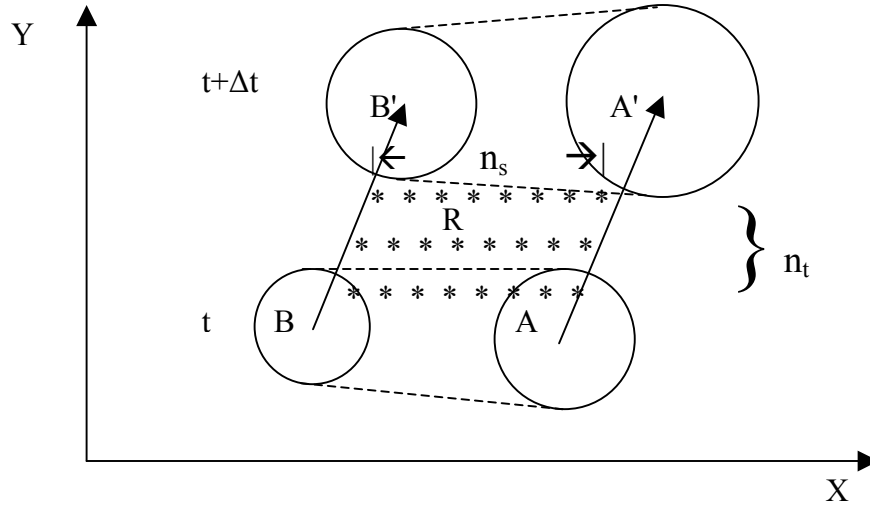


Figure 2. Illustration of the puff generation scheme of Zannetti (1981). A plume is represented by puffs A and B at time t . Subsequent transport moves these puff centers to locations A' and B' at time $t+\Delta t$. Concentrations at receptor R will not be well approximated by these four puffs, so they are subdivided into n_s puffs in space at n_t sub-time intervals. Such interpolative puffs are shown by the * symbol. [From Zannetti, 1981.]

2.3 Integral Approximations for Sampling and Continuous Emissions

Faced with the high computational cost of sampling so many puffs, something had to be done to simplify the problem for a majority of cases, including:

- the far field where many large size puffs contribute to each receptor; and,
- the near field of continuous point sources where many hundreds of puffs and sampling sub-time-steps might be needed to emulate a continuous point source to avoid incurring holes in the concentration field.

Where approximations must be made can be better seen by considering the snapshot concentration contribution from a puff to a receptor located at space-time coordinates, (x, y, z, t) . This instantaneous level can be simply written as:

$$C(x, y, z, t) = Q \cdot P(d_a, \sigma_a) \cdot P(d_c, \sigma_c) \cdot P_z \quad (8a)$$

where

$$P(d_\beta, \sigma_\beta) \equiv P(d_\beta, \sigma_\beta, t) \equiv \frac{1}{\sqrt{2\pi} \cdot \sigma_\beta} \cdot \exp\left[-\frac{d_\beta^2}{2 \cdot \sigma_\beta^2}\right] \quad (8b)$$

with subscript β denoting alongwind and crosswind axis subscripts a and c , respectively, such that d_a and d_c are the respective alongwind and crosswind distances from the puff center to the receptor, and where

$$P_z \equiv [P(z - z_S, h, \sigma_z, t) + P(z + z_S, h, \sigma_z, t)] \quad (8c)$$

with

$$P(z \pm z_S, h, \sigma_z, t) = \frac{1}{\sqrt{2\pi} \cdot \sigma_z} \cdot \sum_{j=-\infty}^{j=+\infty} \exp\left[-\frac{(z \pm z_S + 2jh)^2}{2 \cdot \sigma_z^2}\right]. \quad (8d)$$

Note that this is a slightly different use of the notation for the function P from previous use, in that the plume standard deviations are now explicitly referenced and explicit inclusion of the time variable has been suppressed. The time variable has been explicitly dropped as nearly every variable in Eq.(8), including Q , d_a , d_c , z_S , σ_a , σ_c , and σ_z , can be an explicit or implicit functions of time; thus, rendering explicit display of the time variable rather academic.

As in the case of Gaussian plume modeling (Chapter 7B), z_S is the effective source height of the puff above the ground and h is the mixed-layer depth. Similarly, the vertical term, P_z , includes the multiple reflections from the ground and inversion lid, and rapidly converges to the uniformly mixed limit of $P_z = h^{-1}$ for $\Phi_z > 1.6 h$. In general, puffs within the convective boundary layer meet this criterion within a few hours after release, permitting some level of simplification for models designed solely for mesoscale through long-range transport.

Nevertheless, having so many of the variables present in Eq.(8) being time-dependent suggests that performing integral summing over emission time and integral averaging over receptor time may be a formidable task. Two alternatives to the conventional snapshot sampling function are discussed below. Both utilize the previously-discussed "frozen Φ " approximation to avoid having time-dependence in the denominators of the exponential terms (i.e., due to time-dependent dispersion, Φ_s), though the rationales used for invoking this approximation differ.

2.3.1 The MESOPUFF Integrated Puff Sampling Formulation

The MESOPUFF II model (Scire et al., 1984a, b) introduced the notion of an integrated puff sampling function and also provided some simplifications for near-field applications. In the far-field, the developers assumed that over a given time step, puffs in the far-field grow fractionally by only a small amount such that frozen dispersion Φ_s might be presumed. They further assumed that these receptor-specific, frozen sigmas could be obtained by interpolating between the puff sigmas at the beginning and end of the time step to the downwind distance associated with the point of closest approach. In the cases where the downwind point of closest approach was beyond the beginning- or end-point of the puff trajectory segment, the nearest end-point sigma values were utilized. In addition, this integrated puff sampling scheme assumed radially-symmetric Gaussian puffs.

For a horizontally symmetric puff with $\Phi \equiv \Phi_a = \Phi_c$, Eq.(8a) reduces to:

$$C(x, y, z) = Q \cdot P(R, \sigma) \cdot P_z \quad (9a)$$

where

$$P(R, \sigma) \equiv P(d_a, \sigma_a) \cdot P(d_c, \sigma_c) = \frac{1}{2 \cdot \pi \cdot \sigma^2} \cdot \exp\left[-\frac{R^2}{2 \cdot \sigma^2}\right] \quad (9b)$$

where R is the receptor to puff center distance, such that, $R^2 = d_a^2 + d_c^2$. Now consider the parametric variable, p , conceived so that $p = 0$ at the beginning of the time step and $p = 1.0$ at the end of the time step. Consider a puff moving from initial coordinates (x_1, y_1) at $p = 0$ to final coordinates (x_2, y_2) for $p = 1$. Assuming the puff trajectory segment is a straight line, the radial distance to a receptor at (x, y) in terms of the parameter p is: $R^2 = (x_1 + p \cdot dx - x)^2 + (y_1 + p \cdot dy - y)^2$, where $dx \equiv x_2 - x_1$ and $dy \equiv y_2 - y_1$. Furthermore, one may assume that any changes in the puff's mass due to wet and dry removal processes can also be linearized such that, $Q(p) = Q(0) + p \cdot \Delta Q$, with $\Delta Q \equiv Q(1) - Q(0)$ typically being negative for loss mechanisms. Finally, freezing the value of the sigmas to their midpoint values at $p_m = 0.5$, such that $\Phi \equiv \Phi(p_m)$ and $\Phi_z \equiv \Phi_z(p_m)$, enables one to express the time-averaged receptor concentration over the time period T as:

$$\bar{C} \equiv \frac{1}{T} \int_t^{t+T} dt \cdot C(x, y, z, t) = \frac{P_z}{2 \cdot \pi \cdot \sigma^2} \cdot \int_0^1 dp \cdot Q(p) \cdot P[R(p), \sigma] \quad (10)$$

where P_z has been taken outside the integration for the most typical case, the puff centerline height does not change over the time averaging period, and the sole dependences on p remain in the puff mass Q and the radial distance function, R . Re-expressing R^2/σ^2 as $a \cdot p^2 + 2 \cdot b \cdot p + c$ within the exponential, with a , b and c given as:

$$a = (dx^2 + dy^2) / \sigma^2 ,$$

$$b = [dx \cdot (x_1 - x) + dy \cdot (y_1 - y)] / \sigma^2 , \text{ and}$$

$$c = [(x_1 - x)^2 + (y_1 - y)^2] / \sigma^2 .$$

“Completing the square” (see Chap 7B) within the integrand, one is left with integrands of the form $\exp(-x^2)$ and $x \cdot \exp(-x^2)$, that are known integrals, so the results may be expressed as:

$$\bar{C} = \frac{P_z}{2 \cdot \pi \cdot \sigma^2} \cdot [Q(0) \cdot I_1 + \Delta Q \cdot I_2] \quad (11a)$$

where

$$I_1 = \left[\frac{\pi}{2a} \right]^{1/2} \exp \left[\frac{b^2}{2a} - \frac{c}{2} \right] \left\{ \operatorname{erf} \left[\frac{a+b}{(2a)^{1/2}} \right] - \operatorname{erf} \left[\frac{b}{(2a)^{1/2}} \right] \right\}$$

and (11b)

$$I_2 = \frac{-bI_1}{a} + \frac{1}{a} \exp \left[\frac{b^2}{2a} - \frac{c}{2} \right] \left\{ \exp \left[\frac{-b^2}{2a} \right] - \exp \left[\frac{-1}{2} \left(a + 2b + \frac{b^2}{a} \right) \right] \right\}$$

As mentioned, both the horizontal dispersion coefficient, Φ , and the vertical term, P_z , are evaluated and held constant throughout the trajectory segment and are computed at the mid-point (i.e., $p = 0.5$) of the segment in MESOPUFF II.

Again, at mesoscale distances, the fractional change in the puff size during the sampling step is usually small, and the use of the mid-point values of Φ and P_z is adequate. This assumption also reduces the number of times that the dispersion coefficients and vertical reflection terms need to be computed to once per sampling step (independent of the number of receptors). However, this optimization for mesoscale distances may not be appropriate in the near-field where the fractional puff growth rate can be rapid and plume height may vary. For this reason, the integrated sampling function for the CALPUFF model (Scire et al., 1990b) was implemented with receptor-specific values of Φ and P_z , evaluated at the point of closest approach of the puff to each receptor. This point was initially limited to the $p = 0$ thru $p = 1.0$ physical segment of the puff's trajectory, although some extension beyond these end-points by a fractional amount of the end-point sigma values was implemented in the code to ensure self-consistent results.

2.3.2 The CALPUFF Slug Formulation and Sampling Functions

The integrated puff sampling function approach ensures that puffs are properly sampled by the receptor, but this does not ensure that the puffs are spaced closely enough to ensure proper representation of a continuously emitted plume. To accomplish this, one must either emit puffs at a rapid enough rate (i.e., the dilemma faced in earlier puff models) or develop a methodology to account for both continuous emission and integral-average receptor sampling. This latter methodology can be achieved only if one is able to perform the double-integral over both emission time, t' , and receptor time, t . This same double-integral was considered in Eq.(5) with the accompanying discussion showing the linkage between the puff and plume formulations; however, the same integrals are not considered using a finite emission duration beginning at time $t' = 0$ and ending at $t' = t_E$, with the understanding that the $t_E \leq t$, the current sampling time, and the latest time which causality tells us can contribute to any impact. For the case of a source located at (x_0, y_0, z_0) and wind aligned with the x-axis, the receptor concentration, $C(x,y,z,t)$, integrated over emission time, t' , is now:

$$C(x, y, z, t) = Q \cdot P(Y, \sigma_y) \cdot P(Z, \sigma_z) \cdot \int_0^{t_E} dt' \cdot P(X, \sigma_x, t - t') \quad (12)$$

where $X \equiv (x - x_0) - u \cdot (t - t')$, $Y = y - y_0$, and $Z = z - z_0$.

Note that the $P(Y, \sigma_y)$ and $P(Z, \sigma_z)$ functions have already been taken outside the integral. In the discussion accompanying Eq.(5), this was justified on the basis of assuming the condition of Eq.(5c), that is, that along-wind diffusion was much smaller than the relevant transport distance to the receptor, or $\sigma_x \ll x$. Shrinking σ_x has the effect of forcing all the impact of emissions at time t' to be experienced at the receptor at the fixed time difference, $t - t' = x/u$, which in turn forces the dispersion coefficients, $\sigma(t - t')$, to take on fixed (or “frozen”), receptor-specific values. In the more general case of larger σ_x , where a wider range of time differences (i.e., $t - t'$), and hence differing σ values, contribute to the concentration, we continue to apply the “frozen σ ” approximation, on the practical grounds that it links one back to the Gaussian plume formulation for which the empirical σ functions were determined from experiment in the first place. This insistence on a firm linkage to the Gaussian plume formulation is also a constraint imposed by regulatory agencies, which would be hard-pressed to explain why their puff model, run under conditions that emulate steady-state conditions, did not give the same answer as their plume model.

Performing the t' integration in Eq.(12) then yields the result:

$$C(x, y, z, t) = Q \cdot P(Y, \sigma_y) \cdot P(Z, \sigma_z) \cdot (F/u) \quad (13a)$$

where F is the causality factor given as:

$$F = \frac{1}{2} \cdot \left\{ \operatorname{erf} \left[\frac{x - u \cdot (t - t_E)}{\sqrt{2} \sigma_x(t - t_E)} \right] - \operatorname{erf} \left[\frac{x - u \cdot t}{\sqrt{2} \sigma_x(t)} \right] \right\}. \quad (13b)$$

Consistent with the discussion in Section 2.1, considering the limit of the vector mean wind, $u \rightarrow 0$, and to ensure a better match with the Gaussian plume, the factor $1/u$ is shifted to $1/U$ in terms of the scalar wind, and a factor, u/U is injected into the crosswind component to ensure that the sense of “crosswind” versus “downwind” vanish at $u = 0$.

The final expression for the snapshot concentration field due to such a pollutant “slug” then can be written as:

$$C(x, y, z, t) = Q \cdot P'(Y, \sigma_y) \cdot P(Z, \sigma_z) \cdot (F/U) \quad (14a)$$

where

$$P'(Y, \sigma_y) \equiv \frac{1}{\sqrt{2\pi}\sigma_y} \cdot \exp\left[-\frac{d_c^2}{2 \cdot \sigma_y^2} \cdot \frac{u^2}{U^2}\right] \quad (14b)$$

the causality factor F is re-expressed as:

$$F = \frac{1}{2} \cdot \left\{ \operatorname{erf}\left[\frac{d_{a2}}{\sqrt{2}\sigma_{y2}}\right] - \operatorname{erf}\left[\frac{-d_{a1}}{\sqrt{2}\sigma_{y1}}\right] \right\}. \quad (14c)$$

This form now matches the formulation used in the CALPUFF model (Scire et al., 1995). Note that to achieve this match, the additional assumption, $\sigma_x = \sigma_y$, was injected for simplicity, and the distances d_c and d_a introduced as the cross-slug (i.e., perpendicular to the slug axis) and along-slug distances, respectively, to the receptor. In particular, d_{a2} is the receptor distance from the “youngest” slug end 2 (with $d_{a2} > 0$ in the direction of end 1), that is $d_{a2} = x_R - x_2$, whereas the receptor distance from the “oldest” slug end 1 is defined as:

$$-d_{a1} = d_{a2} - \ell_{xy}, = x_R - x_2 - (x_1 - x_2) = x_R - x_1 \quad (14d)$$

where ℓ_{xy} is the length of the slug projection in the x - y plane, and where $\ell_{xy} = u \cdot t_E$ in this case. Again, the subscripts 1 and 2 on the dispersion coefficients refer to values at the “oldest” and “youngest” ends of the slug, respectively, while the absence of a numerical subscript indicates a value defined at the receptor.

This "slug" formulation retains many of the important properties of the circular puff model, while significantly reducing puff overlap problems associated with snapshot sampling of circular puffs. As it must, Eq.(14) explicitly conserves mass. As with circular puffs, each slug is free to evolve independently in response to the local effects of dispersion, chemical transformation, removal, etc. Also, the concentration distribution within the body of the slug, well away from the slug endpoints, approaches that of the Gaussian plume distribution. Finally, the concentrations near the endpoints of the slug (both inside and outside of the body of the slug) fall off in such a way that if adjacent slugs are present, the plume predictions will be reproduced when the contributions of those slugs are included (again, during steady-state conditions). This property can be proven by imagining that the previously emitted slug has ends labeled 0 and 1, with the #0 end being the oldest, and the newest end #1, coincident with the current #1 end representing the oldest part of the current release (i.e., the new end point of a previously released slug is co-located with the old end point of the slug subsequently released). This means that the summed concentration distribution from the two slugs will be:

$$C(x, y, z, t) = \frac{Q}{U} \cdot P'(Y, \sigma_y) \cdot P(Z, \sigma_z) \cdot \frac{1}{2} \cdot \left\{ \begin{array}{l} \text{erf} \left[\frac{x_R - x_2}{\sqrt{2}\sigma_{y2}} \right] - \text{erf} \left[\frac{x_R - x_1}{\sqrt{2}\sigma_{y1}} \right] + \\ \text{erf} \left[\frac{x_R - x_1}{\sqrt{2}\sigma_{y1}} \right] - \text{erf} \left[\frac{x_R - x_0}{\sqrt{2}\sigma_{y0}} \right] \end{array} \right\}$$

or, with cancellations, this becomes:

$$C(x, y, z, t) = \frac{Q}{U} \cdot P'(Y, \sigma_y) \cdot P(Z, \sigma_z) \cdot \frac{1}{2} \cdot \left\{ \text{erf} \left[\frac{x_R - x_2}{\sqrt{2}\sigma_{y2}} \right] - \text{erf} \left[\frac{x_R - x_0}{\sqrt{2}\sigma_{y0}} \right] \right\}. \quad (15)$$

Thus, assuming meteorology and emissions remain unchanged, consecutively released slugs combine to form a longer single slug, and ultimately, if the process is repeated, would form a complete Gaussian plume.

This fact illustrates the concept that the "causality" function, F , accounts for edge effects near the endpoints of the slug. For long emission times, such that $u \cdot t_E \gg \Phi_x$, and points well inside the body of the slug, evaluation of the error functions in Eq.(14c) produces: $F = 0.5 \cdot (1 - (-1)) = 1$ (i.e., no edge effects). For receptors well outside the slug, F becomes zero, indicating that the pollutant material has not yet reached the receptor or has already passed it. Near the endpoints, the causality factor produces a leading/trailing Gaussian-like tail on the distribution.

The factor (u/U) allows low wind speed and calm conditions to be properly treated. As u approaches zero, the exponential crosswind term becomes unity and $F \rightarrow -\text{erf}[d_a / (\sqrt{2}\sigma_y)]$. Under these conditions, the radial concentration dependence of the distribution is determined by the causality factor. For u greater than a few meters per second, (u/U) is very close to one, so that this ratio becomes unimportant. The factors (u/U) and F make the slug model more "puff-like" than segmented plume models (e.g., Hales et al., 1977; Benkley and Bass, 1979). Also, unlike the slug model, segmented plume models generally do not properly treat low wind speed conditions or segment edge effects.

Equation (14) represents a "snapshot" description of the elongated puff or slug at time t ; however, as with the "snapshot" puff equation, Eq.(14) must be integrally-averaged over the receptor's sampling time step to produce a time-averaged concentration, $\bar{C}(x, y, z)$. In the case where the emission rate and meteorological conditions do not vary during the sampling step, a generalized analytical solution to the integral can be obtained for "emitted" slugs (i.e., where the endpoint of the "youngest" end of the slug is at the source) as:

$$\bar{C}(x, y, z) = \frac{Q}{U} \cdot P'(Y, \sigma_y) \cdot P(Z, \sigma_z) \cdot \bar{F} \quad (16a)$$

where the time-averaged causality factor, \bar{F} , is given as:

$$\bar{F} = \frac{1}{2} \cdot \text{erf}(\phi_2) + \frac{1}{2} \cdot \frac{\sqrt{2} \cdot \sigma_y}{u \cdot \Delta t_S} \cdot \left\{ [\xi_e \cdot \text{erf}(\xi_e) - \xi_b \cdot \text{erf}(\xi_b)] + \frac{1}{2} \cdot [\exp(\xi_e^2) - \exp(\xi_b^2)] \right\} \quad (16b)$$

and where,

$\xi_b \equiv d_{a2} / (\sqrt{2} \sigma_y)$ accounts for the beginning of the sampling time step,
 $\xi_e \equiv (d_{a2} - u \cdot \Delta t_S) / (\sqrt{2} \sigma_y)$ represents the end of the sampling step, and
 $\phi_2 \equiv d_{a2} / (\sqrt{2} \sigma_{y2})$ represents the steady-state conditions at the source, with Φ_{y2} representing any initial lateral spread of the emissions at the source.

Note that Eq.(16) applies to the case where the sampling interval, $(0, \Delta t_S)$, is the same as the emission interval, $(0, t_E)$, as is normally the case for fresh, continuous emissions (i.e., since emissions for $t_E > \Delta t_S$ cannot causally contribute). However, as the indefinite integral, $\int dx \cdot \text{erf}(x) = x \cdot \text{erf}(x) + \exp(-x^2) / \sqrt{\pi}$ exists, the more general solution could have been written.

For older slugs, the endpoint of the slug is no longer fixed at the source and the long axis of the slug is not necessarily along the current advecting wind direction. Additionally, the two end points may experience different winds, causing rotation and stretching of the slug. In this general case, an analytical integration of Eq.(14) is not possible for such slugs unless restrictive conditions are imposed on the form of the puff growth equations. Because of the importance of generality in the puff growth equations, the time-averaged concentrations associated with older slugs are determined via numerical integration of Eq.(14) and such integration can generally be accomplished at reasonable computational cost. For example, Figure 3 displays the snapshot concentration isopleths of a slug at the beginning (left) and end (right) of a particular sampling time step, whereas Figure 4 shows the result of the numerical integral averaging over the same time interval.

The above development also ignores the effect of loss or production mechanisms; however, this can be handled in much the same "linearized" manner that MESOPUFF II invokes. This is accomplished by allowing the effective emission rate, Q , to vary linearly over time as:

$$Q(t) = Q_b + (Q_e - Q_b) \cdot (t / \Delta t_S) \quad (17)$$

where Q_b is the effective emission rate for the slug at the beginning of the time step (note that $Q_b = Q$ for fresh emissions), Q_e is the effective emission rate including loss or production which occurs during the time step, and Δt_S is the duration of the time step.

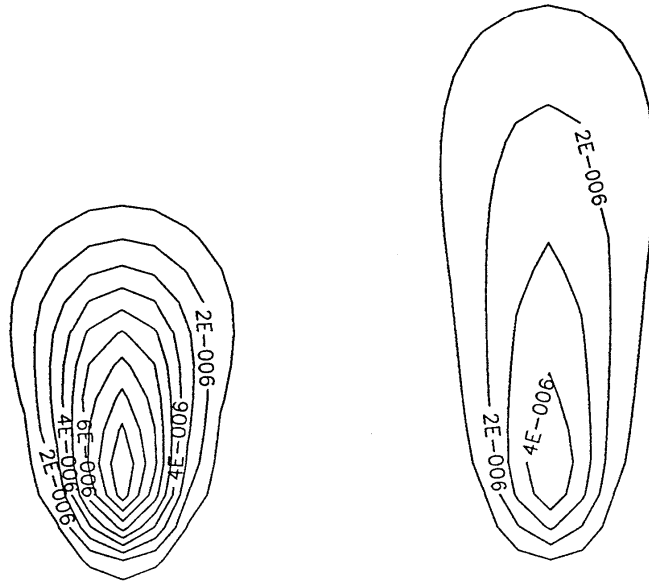


Figure 3. Isopleths of a slug "snapshot" at two points in time. The slug at left shows concentrations at some early time, whereas the snapshot at right shows the isopleths of the same slug at a later time. During the intervening time, the slug clearly experienced advection (to the right), diffusion, and some along-slug stretching due to wind shear. [From Scire et al., 1990b]

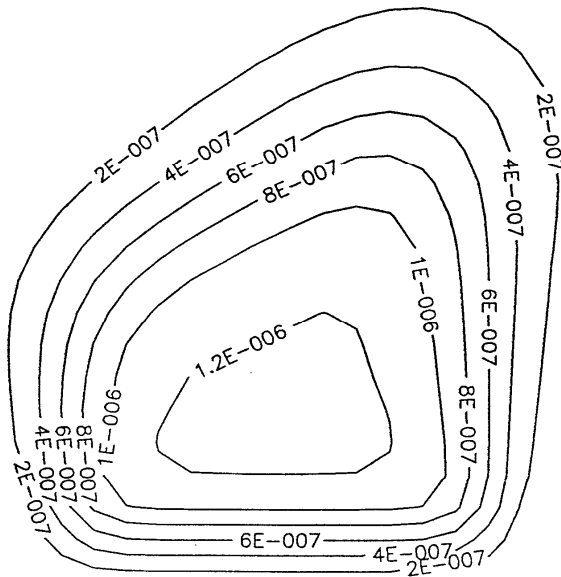


Figure 4. Receptor-time averaged concentrations resulting from numerical integration of the evolution of the slug depicted in Figure 3 from its initial (left) to its final (right) "snapshot" states. [From Scire et al., 1990b]

The variable ζ in Eq.(16) can also be written as the function:

$$\xi \equiv \frac{d_{a2} - u \cdot \Delta t_S \cdot (t / \Delta t_S)}{\sqrt{2}\sigma_y} \quad (18)$$

of the dimensionless time variable $(t/\Delta t_S)$, where $0 \leq t/\Delta t_S \leq 1$, such that $\zeta = \zeta_b + (\zeta_e - \zeta_b) \cdot (t/\Delta t_S)$, with $\xi_b \equiv \frac{d_{a2}}{\sqrt{2}\sigma_y}$ and $\xi_e \equiv \frac{d_{a2} - u \cdot \Delta t_S}{\sqrt{2}\sigma_y}$, as defined

following Eq.(16b), so that the causality function of Eq.(14c) can be written:

$$F = \frac{1}{2} \cdot \{erf(\phi_2) - erf(\xi)\} \quad (19)$$

Thus, the time averaging process yields:

$$\bar{C}(x, y, z) = \frac{1}{U} \cdot P'(Y, \sigma_y) \cdot P(Z, \sigma_z) \cdot \{Q_b \cdot \bar{F}_0 + (Q_e - Q_b) \cdot \bar{F}_1\} \quad (20)$$

where \bar{F}_0 is \bar{F} from Eq.(16b) and

$$\bar{F}_1 = \int_0^{\Delta t_S} \frac{dt}{\Delta t_S} \cdot \left(\frac{t}{\Delta t_S} \right) \cdot F(t) = \frac{1}{\Delta \xi} \int_{\xi_b}^{\xi_e} d\xi \cdot \left(\frac{\xi - \xi_b}{\Delta \xi} \right) \cdot F(\xi) \quad (21)$$

with $\Delta \xi \equiv \xi_e - \xi_b = \frac{-u \cdot \Delta t_S}{\sqrt{2}\sigma_y}$. Substituting in Eq.(19) into Eq.(21) then yields:

$$\bar{F}_1 = \frac{1}{4} \cdot erf(\phi_2) - \frac{1/2}{(\Delta \xi)^2} \left\{ \int_{\xi}^{d_{a2}} d\xi \cdot \xi \cdot erf(\xi) - \xi_b \cdot \int_{\xi}^{\xi_e} d\xi \cdot erf(\xi) \right\} \quad (22)$$

where the integral, $\int dx \cdot erf(x) = x \cdot erf(x) + \frac{1}{\sqrt{\pi}} \cdot \exp(-x^2)$, has already been used to obtain Eq.(16b) and where the integral, $\int dx \cdot x \cdot erf(x) = \frac{1}{2} \cdot x^2 \cdot erf(x) + \frac{1}{2} \cdot \frac{x}{\sqrt{\pi}} \cdot \exp(-x^2) - \frac{1}{4} \cdot erf(x)$, is a special case of the more general expression developed by Geller and Ng (1971) in terms of the generalized hypergeometric function ${}_2F_2$.

Generalizing the problem of dealing with older slugs is straightforward if one chooses a numerical integration (i.e., time-average) of Eq.(14). The time dependent expression $Q(t)$ given by Eq.(17) simply replaces Q and the numerical integration proceeds.

However, this numerical integration process has itself received special attention because it greatly influences the computing time needs of the slug model. First, all receptors lying outside of the slug's $\pm 3 \Phi_y$ envelope during the entire averaging time interval are eliminated from consideration. Second, for those receptors remaining, integration time limits are computed such that sampling is not performed when the receptor is outside of the $\pm 3 \Phi_y$ envelope.

Invocation of the "frozen Φ " methodology (i.e., Φ_y and Φ_z are fixed at receptor-specific values throughout the averaging time period) creates another class of situations which can be integrated analytically; however, the most general case involves indefinite integrals of the form:

$$\int dt \cdot \exp(-\beta^2 \cdot t^2) \cdot \text{erf}(a + b \cdot t) \quad (23)$$

which defy solution except in a few simple cases (e.g., $a = 0$ and $b = \exists$). In fact, integrability has proven not to be the sole criteria in these slug sampling problems. For example, the preceding work on linear time variation of loss (or production) mechanisms can also be evaluated for the more realistic exponential process; however, the analytic forms are found to be very volatile on a computer because subtraction of large numbers to obtain small numbers is required.

One tractable case involves the quite physical scenario of a slug passing rapidly over a receptor and with slug endpoints sufficiently far away that the along-slug causality factor, $F(t)$, is time independent. In this case, the causality factor also becomes fixed and can be taken outside the integral and approximated as:

$$\bar{F} = \frac{1}{2} \cdot (F_b + F_e) \quad (24)$$

which is just the average of values at the beginning and end of the time step. This approximation is, however, made only if F_b and F_e are within a specified small fractional tolerance of each other. A similar procedure enables one to move the vertical coupling factor, $P(Z, \sigma_z)$, outside the integral and replace it with the mean value, \bar{P} , provided that the initial and final values are within a small tolerance window (e.g., a few percent). Finally, the variability of the lateral coupling term of Eq.(14b) to temporal variation of the crosswind distance, $d_c(t)$, is checked and the integrals:

$$I_m = \int_0^{\Delta t_s} \frac{dt}{\Delta t_s} \cdot \left(\frac{t}{\Delta t_s} \right)^m \cdot P'[\eta(t), \sigma_y] \quad (25)$$

with $P'(\eta(t), \sigma_y) \equiv \frac{1}{\sqrt{2\pi}\sigma_y} \cdot \exp[-\eta^2(t)]$ and $\eta(t) \equiv \frac{1}{\sqrt{2}} \cdot \frac{d_c(t)}{\sigma_y} \cdot \frac{u}{U}$ evaluated for $m = 0$ and 1. These integrals can be solved to yield:

$$I_0 = \frac{\sqrt{\pi}}{2} \cdot \frac{[erf(\eta_e) - erf(\eta_b)]}{(\eta_e - \eta_b)} \quad \text{and} \quad I_1 = \frac{1}{2} \cdot \frac{[\exp(-\eta_e^2) - \exp(-\eta_b^2)]}{(\eta_e - \eta_b)^2} - \frac{\eta_b \cdot I_0}{(\eta_e - \eta_b)} \quad (26)$$

so that the final, time-averaged concentrations can be written as:

$$\bar{C}(x, y, z) = \frac{\bar{F} \cdot \bar{P}(Z, \sigma_z)}{\sqrt{2\pi} \cdot \sigma_y \cdot U} \cdot \{Q_b \cdot I_0 + (Q_e - Q_b) \cdot I_1\} \quad (27)$$

as an alternative to numerical integration for some older slugs.

Vertically integrated counterparts to Eq.(20) and Eq.(27) are also required in CALPUFF for evaluation of wet removal and wet fluxes at a ground level receptor; however, given the normalization properties of the Gaussian, these are obtained by replacing $P(Z, \sigma_z)$ with 1.0 in Eq.(20) or $\bar{P}(Z, \sigma_z)$ with 1.0 in Eq.(27).

It should also be noted that decision logic in CALPUFF allows slugs in the near-field to transition to puffs in the far-field. This decision process is based primarily on the eccentricity of the overall slug shape; that is, axial slug length relative to the size of the horizontal dispersion coefficients at the slug end points. It should be noted in such conversion that one must have retained both the slug's effective emission rate, Q , as well as the original emission duration, t_E , for that slug, so that the slug mass of $Q \cdot t_E$ is available for puff computation purposes.

Both the original California ARB documentation (Scire et al., 1990b) and the more recent report on CALPUFF Version 5 (Scire et al., 2000) contain extensive documentation on the absolute and comparative accuracy and computation times of the various slug and puff formulations discussed herein.

In addition, several model evaluations using hour-average tracer concentrations have been performed (e.g., IWAQM, 1998; Strimaitis et al., 1998; Chang et al., 2003) and CALPUFF was found to be more reliable predictor of ambient concentrations than ISC3.

3 Puff Model Enhancements

The integrals discussed in the previous section lie at the heart of the CALPUFF model, but this model is now a comprehensive code exceeding 50K lines and includes a full range of phenomena that must now be explicitly considered. For example, CALPUFF has modules for many, near-source effects (e.g., plume rise, stack and building downwash, partial lid penetration), complex-terrain plume dynamics, mass depletion (e.g., dry and wet deposition) and transformation mechanisms, and specialized meteorological conditions (e.g., fog). The CALPUFF modeling system also contains a graphical interface for setting up and managing runs; preprocessor programs for emissions, meteorology, land-use,

terrain and other input files; and postprocessor programs for various longer-term concentration averages and visibility. An exposition of most of these features is beyond the scope of this chapter; however, in the following subsections, we consider some phenomena that are fundamental to the puff model itself.

3.1 Dispersion Coefficients for Puff Modeling

Short duration pollutant releases and human exposures can have important consequences: toxic gas releases and odor impacts being among the clearer examples. Historically, puff models have been developed with an emphasis on predicting one-hour (and longer) average concentrations on meso- through regional-scale domains. Hence, the model's basic time step for taking in new meteorology (e.g., a specific wind speed and direction at each source) was one hour or longer, and the dispersion coefficients were tailored to reflect all dispersive mechanisms that contribute during a corresponding averaging time interval. That is, the dispersion rate of individual puffs is effectively convoluted with the lower frequency meandering of wind direction to yield overall dispersion coefficients that in-turn yield reasonable, hourly or multi-hour average concentrations. More specifically, in the case of CALPUFF, regulatory dispersion coefficient schemes were chosen so predicted concentrations would exactly match the results of the Gaussian plume ISC3 model (i.e., if CALPUFF is run using steady-state emissions and meteorology conditions for a sufficiently long time to avoid "transients" associated with initiation of emissions or the "causality" lag associated with source to receptor transport).

One way to account for shorter, time-average concentrations in CALPUFF is to allow input of peak-to-mean concentration ratio factors into CALPUFF's post-processor program (i.e., CALPOST). This feature improves the utility of CALPUFF in applications involving odor and short-term toxic exposure problems.

To more realistically simulate shorter averaging time periods when suitable meteorological data are available, the most recent version of CALPUFF (i.e., Version 6) permits updates of meteorological fields as often as once per minute. Optimal use of this rapid-update feature requires that the dispersion coefficients be appropriately matched to the meteorological field update interval.

Traditionally, such shorter averaging-time quantities have been estimated from longer-time-averaged measured data via the averaging-time power-law scaling:

$$\sigma(\tau_1) \approx (\tau_1/\tau_2)^p \cdot \sigma(\tau_2) \quad (28a)$$

where τ_1 and τ_2 are the two relevant averaging times, and p is the appropriate power-law exponent. For averaging times shorter than one hour, a value of $p = 0.2$ for τ in the range of 3 - 60 minutes has been suggested by Gifford (1975) for σ_y ; whereas, smaller exponents over a more limited range of averaging times

(e.g., 3 - 20 min.) are considered for σ_z (Pasquill, 1976). Discussion continues over the importance (Hanna et al., 2003) and appropriateness (Venkatram, 2002) of making such power-law corrections for averaging time. Currently, CALPUFF permits averaging time corrections, of the type expressed by Eq.(28a), to be made only for the Pasquill-Gifford σ_y dispersion curves. The other parameterized dispersion curves available for use in CALPUFF cannot be so scaled, as appropriate guidance does not appear in the literature.

Another dispersion coefficient alternative for short averaging times that is presently offered within CALPUFF is the ability to compute dispersion coefficients based on locally measured values of turbulence (i.e., σ_v and σ_w) and the formulae:

$$\sigma_y = \sigma_v \cdot t \cdot f_y(t/\tau_y) \quad \text{and} \quad \sigma_z = \sigma_w \cdot t \cdot f_z(t/\tau_z) \quad (28b)$$

where $f_y(t/\tau_y) = 1.0 / [1.0 + 0.9 \cdot (t/\tau_y)^{1/2}]$ and $f_z(t/\tau_z) = 1.0 / [1.0 + a \cdot (t/\tau_z)^p]$, with $(a, p) = (0.9, 0.5)$ for unstable conditions and $(0.945, 0.806)$ for stable conditions. This Eq.(28b) approach to dispersion uses Irwin's (1983) recommended implementation of Draxler's (1976) forms for the f_y and f_z functions, and currently incorporates a fixed value for τ_y of 1000s and fixed values for τ_z of 500s and 100s for unstable and stable conditions, respectively.

Unfortunately, the validity of Eq.(28b), including the appropriate forms for f_y and f_z and their accompanying coefficients and time scales, has not yet been extensively evaluated for short averaging times.

The most elegant approach to modeling short averaging times would be to build in a model option to choose true "puff sigmas"; however, appropriate formulations are not widely available over a significant range of transport times and dispersion conditions. A series of true puff tracer release experiments (e.g., BOREX89, BORRIS94, GUARDO, MADONA, FLADIS, COFIN) were recently performed, and an analysis by Mikkelsen et al. (2002) of several such experiments combined suggests a linear time-dependent puff growth law of:

$$\sigma_{puff}(t) \approx 0.73 \cdot U_* \cdot t \quad (29)$$

where U_* (m/s) is the surface friction velocity and t (s) is puff travel time. Equation (29) was found to be appropriate for near-surface releases and has been confirmed only for $\sigma_{puff}(t) \leq 25\text{m}$. Of course, such early-phase puff growth gives way to a period of accelerated $t^{3/2}$ growth (Richardson, 1926; Batchelor, 1950), which has been observed (Gifford, 1977), and concludes with Taylor's (1921) $t^{1/2}$ growth (i.e., which may or may not ever be observed due to the eventual dominance of wind shear induced growth).

It is interesting to note that the coefficient of 0.73 is about half of that used in typical, turbulence-based, dispersion coefficients [e.g., $\sigma_y = 1.6 \cdot U_* \cdot t \cdot f(t/\tau_y)$ and

$\sigma_z = 1.3 \cdot U_* \cdot t \cdot f(t/\tau_z)$] that may be computed within CALPUFF (i.e., when the turbulence-based dispersion option is chosen and the turbulence is computed from surface-layer formulae). These larger coefficients of $U_* \cdot t$ result from the fact that these larger dispersion coefficients include a significant wind-meander component along with the true puff dispersion.

Clearly, if puff sigmas are employed, then some explicit formulation of wind direction meander, such as that of Oetl et al. (2005), also ought to be available for the computation of the concentration cumulative frequency distribution and/or longer time averages.

3.2 Wind Shear Effects on Puffs

While puff models are often driven by a wind field model that allows for spatially and varying wind fields, the entire puff is usually just transported by the wind at the center of the puff, such that wind gradients or shears are ignored. In some cases, the accumulated wind shear is tracked and, when large enough, leads to a splitting of the puff into two or more puffs. However, the successful incorporation of shear into plume models [i.e., Walcek (2004) as discussed in Chap. 7B], leads one to ask if this could also be done for puff models.

The reason the puff model formulations generally ignore explicit shear is that they stem from the solution of the diffusion equation with an assumed diagonal diffusivity matrix. That is, they begin with the diagonal diffusivity matrix, \mathbf{K}_d , rather than the full diffusivity matrix, \mathbf{K} , where both are given as:

$$\mathbf{K}_d = \begin{bmatrix} K_{xx} & 0 & 0 \\ 0 & K_{yy} & 0 \\ 0 & 0 & K_{zz} \end{bmatrix} \quad \text{and} \quad \mathbf{K} = \begin{bmatrix} K_{xx} & K_{xy} & K_{xz} \\ K_{yx} & K_{yy} & K_{yz} \\ K_{zx} & K_{zy} & K_{zz} \end{bmatrix} \quad (30)$$

Now the \mathbf{K}_d form of the diffusivity matrix leads to the well-known puff solution:

$$C(x,y,z,t) = \frac{m}{(2\pi)^{3/2} \cdot \sqrt{8 \cdot K_{xx} \cdot K_{yy} \cdot K_{zz}} \cdot t^3} \cdot \exp \left[\frac{-1}{4 \cdot t} \left\{ \frac{(x-x_c)^2}{K_{xx}} + \frac{(y-y_c)^2}{K_{yy}} + \frac{(z-z_c)^2}{K_{zz}} \right\} \right] \quad (31)$$

where m is the mass within the puff. Replacing the terms $2 \cdot K \cdot t$ with their equivalent σ^2 then leads back to the Eq.(3) form introduced earlier.

Unfortunately, Eq.(31) does not allow for the introduction of puff-distorting wind shear terms; however, expansion of the basic advection-diffusion equation [i.e., Eq.(2)] in terms of Taylor series for the winds and concentrations shows (e.g., Yamartino, 2000) that one can include the effects of wind shears either through

purely advective terms or via diffusive terms involving the off-diagonal terms of the full \mathbf{K} matrix.

The less well-known solution to the full diffusivity matrix form (Anderson, 1984; Wegener and Schroeter, 1995) can be written for an arbitrary number of dimensions, n , as:

$$C(x, y, z, t) = \frac{m}{(2 \cdot \pi)^{n/2} \cdot |D|^{1/2} \cdot (2 \cdot t)^{n/2}} \cdot \exp\left[-\frac{1}{4 \cdot t} \mathbf{X}^T \mathbf{K}^{-1} \mathbf{X}\right] \quad (32a)$$

where for $n = 3$, $\mathbf{X} = \begin{bmatrix} x - x_c \\ y - y_c \\ z - z_c \end{bmatrix}$ is a column vector, $\mathbf{K}^{-1} = \begin{bmatrix} K_{xx} & K_{xy} & K_{xz} \\ K_{yx} & K_{yy} & K_{yz} \\ K_{zx} & K_{zy} & K_{zz} \end{bmatrix}^{-1}$ is the

inverse of the 3D diffusivity matrix \mathbf{K} , $\mathbf{X}^T = [x - x_c, y - y_c, z - z_c]$ is the transpose row vector, with (x_c, y_c, z_c) being the center coordinates of the puff, and $|D|$ is the determinant of matrix \mathbf{K} . It is also useful to know that Eq.(32a) can alternatively be written in terms of the dispersion sigmas as:

$$C(x, y, z, t) = \frac{q}{(2 \cdot \pi)^{n/2} \cdot |D|^{1/2}} \cdot \exp\left[-\frac{1}{2} \mathbf{X}^T (\boldsymbol{\sigma}^2)^{-1} \mathbf{X}\right] \quad (32b)$$

where $(\boldsymbol{\sigma}^2)^{-1} = \begin{bmatrix} \sigma_x^2 & \sigma_{xy}^2 & \sigma_{xz}^2 \\ \sigma_{yx}^2 & \sigma_y^2 & \sigma_{yz}^2 \\ \sigma_{zx}^2 & \sigma_{zy}^2 & \sigma_z^2 \end{bmatrix}^{-1}$ and $|D|$ is the determinant of matrix $\boldsymbol{\sigma}^2$.

Expanding the $n = 3$ solution for the inverse \mathbf{K}^{-1} yields the rather messy result:

$$\mathbf{K}^{-1} = \frac{1}{|D|} \begin{bmatrix} +(K_{yy} \cdot K_{zz} - K_{yz} \cdot K_{zy}) & -(K_{xy} \cdot K_{zz} - K_{xz} \cdot K_{zy}) & +(K_{xy} \cdot K_{yz} - K_{xz} \cdot K_{yy}) \\ -(K_{yx} \cdot K_{zz} - K_{yz} \cdot K_{zx}) & +(K_{xx} \cdot K_{zz} - K_{xz} \cdot K_{zx}) & -(K_{xx} \cdot K_{yz} - K_{xz} \cdot K_{yx}) \\ +(K_{yx} \cdot K_{zy} - K_{yy} \cdot K_{zx}) & -(K_{xx} \cdot K_{zy} - K_{xy} \cdot K_{zx}) & +(K_{xx} \cdot K_{yy} - K_{xy} \cdot K_{yx}) \end{bmatrix} \quad (33a)$$

where

$$|D| = [K_{xx} \cdot (K_{yy} \cdot K_{zz} - K_{yz} \cdot K_{zy}) - K_{yx} \cdot (K_{xy} \cdot K_{zz} - K_{xz} \cdot K_{zy}) + K_{zx} \cdot (K_{xy} \cdot K_{yz} - K_{xz} \cdot K_{yy})] \quad (33b)$$

One notes that the 2D, y - z plume solution appears much simpler as:

$$\mathbf{K} = \begin{bmatrix} K_{yy} & K_{yz} \\ K_{zy} & K_{zz} \end{bmatrix} \quad \text{and} \quad \mathbf{K}^{-1} = \frac{1}{|D|} \begin{bmatrix} +K_{zz} & -K_{yz} \\ -K_{zy} & +K_{yy} \end{bmatrix} \quad (34a)$$

with determinant,

$$|D| = (K_{yy} \cdot K_{zz} - K_{yz} \cdot K_{zy}) \quad (34b)$$

Comparison with the plume solution of Walcek [see Chapter 7B, Eq.(45)] suggests that:

$$\left(1 - \frac{K_{yz} \cdot K_{zy}}{K_{yy} \cdot K_{zz}}\right) = 1 + s^2 / 12 \quad \text{where} \quad s \equiv \frac{\partial v}{\partial z} \cdot \frac{x}{u} \cdot \sqrt{\frac{K_{zz}}{K_{yy}}} \quad (34c)$$

If one further assumes that $K_{zy} = -K_{yz}$, as is necessary to achieve the sign flip between the left and right sides of Eq.(34c), then one concludes that Walcek's plume solution requires²:

$$\frac{K_{yz}}{\sqrt{K_{yy} \cdot K_{zz}}} = \frac{1}{\sqrt{12}} \cdot \frac{\partial v}{\partial z} \cdot \sqrt{\frac{K_{zz}}{K_{yy}}} \cdot \frac{x}{u} = \frac{1}{\sqrt{12}} \cdot \frac{\partial v}{\partial z} \cdot \sqrt{\frac{K_{zz}}{K_{yy}}} \cdot t \quad (35)$$

This is fine, except that a K ratio proportional to travel time, t , shows that the needed solution for a constant crosswind velocity shear, $(\partial v / \partial z)$, does not simply involve the purely, space-time invariant K values usually assumed for the Eq.(32) solution of the time-dependent diffusion equation in n dimensions.

Nevertheless, for the puff, we consider the case of the two most important velocity shears: $u_z \equiv (\partial u / \partial z)$ and $v_z \equiv (\partial v / \partial z)$. This means that the determinant will now appear as:

$$|D| = [K_{xx} \cdot (K_{yy} \cdot K_{zz} - K_{zy} \cdot K_{yz}) - K_{xz} \cdot K_{zx} \cdot K_{yy}] = [K_{xx} \cdot K_{yy} \cdot K_{zz} \cdot \left(1 - \frac{K_{zy} \cdot K_{yz}}{K_{yy} \cdot K_{zz}} - \frac{K_{xz} \cdot K_{zx}}{K_{xx} \cdot K_{zz}}\right)] \quad (36a)$$

or

$$|D| = K_{xx} \cdot K_{yy} \cdot K_{zz} \cdot \left[1 + \frac{(s_u^2 + s_v^2)}{12}\right] \quad \text{and} \quad |D| = \sigma_x^2 \cdot \sigma_y^2 \cdot \sigma_z^2 \cdot \left[1 + \frac{(s_u^2 + s_v^2)}{12}\right]$$

for the \mathbf{K} and σ^2 representations, respectively,

² Symmetry suggests a full K_{yz} of: $K_{yz} = \frac{1}{\sqrt{12}} \cdot \frac{\partial v}{\partial z} \cdot \frac{x}{u} \cdot K_{zz} - \frac{1}{\sqrt{12}} \cdot \frac{\partial w}{\partial y} \cdot \frac{x}{u} \cdot K_{yy}$

where the added substitutions:

$$\frac{K_{xz}}{K_{zz}} = \frac{1}{\sqrt{12}} \cdot \frac{\partial u}{\partial z} \cdot \frac{x}{u} = \frac{1}{\sqrt{12}} \cdot \frac{\partial u}{\partial z} \cdot t, \quad (36b)$$

$$s_v \equiv \frac{\partial v}{\partial z} \cdot t \cdot \sqrt{\frac{K_{zz}}{K_{yy}}} = \frac{\partial v}{\partial z} \cdot t \cdot \frac{\sigma_z}{\sigma_y}, \text{ and } s_u \equiv \frac{\partial u}{\partial z} \cdot t \cdot \sqrt{\frac{K_{zz}}{K_{xx}}} = \frac{\partial u}{\partial z} \cdot t \cdot \frac{\sigma_z}{\sigma_x} \text{ are used.} \quad (36c)$$

Thus far, the 3D \mathbf{K} matrix approach is useful, as it has yielded the correct form of $|D|$; however, continuing further with the \mathbf{K} matrix strategy requires one to specify the K_{xy} term, and this is not obvious nor can it be neglected. Instead, we step back to the Walcek solution [Chapter 7B, Eq.(45)], add in the x -component ingredient of the puff formulation, and temporarily ignore uniform advection (i.e., as the principle of translational invariance will always permit us to re-inject uniform advection). Without uniform advection, there is no preferred orientation for the x - y axes, except for the directionality dictated by shear. Thus, imagine a coordinate system where the effective total shear is aligned along the y' axis. In this case, one might guess the equivalent puff solution to be:

$$C(x,y,z) = \frac{m}{(2\pi)^{3/2} \cdot \sigma_x \cdot \sigma_y \cdot \sigma_z \cdot f} \cdot \exp \left[-\frac{1}{2} \left\{ \frac{x'^2}{\sigma_h^2} + \frac{y'^2}{f^2 \cdot \sigma_h^2} + \frac{(z-z_S)^2 \cdot (1+s^2/3)}{f^2 \cdot \sigma_z^2} - \frac{(z-z_S) \cdot y' \cdot s}{f^2 \cdot \sigma_h \cdot \sigma_z} \right\} \right] \quad (37a)$$

where σ_h is the lateral dispersion coefficient,

and as before,

$$f^2 \equiv 1 + s^2 / 12 \quad \text{and} \quad s^2 \equiv s_u^2 + s_v^2. \quad (37b)$$

Given that Walcek's 2D solution conserves mass, one can be quite sure that Eq.(37a) will at least conserve mass in 3D. Now, one simply rotates back from the (x', y') axes to the usual (x, y) frame via substitutions:

$$y' = y \cdot \cos(\theta) + x \cdot \sin(\theta) \quad \text{and} \quad x' = x \cdot \cos(\theta) - y \cdot \sin(\theta) \quad (37c)$$

where

$$\sin(\theta) = s_u / s \quad \text{and} \quad \cos(\theta) = s_v / s \quad (37d)$$

After expanding the substitutions, collecting terms, and re-inserting uniform advection, one recovers the full puff solution of:

$$C(x,y,z,t) = \frac{m}{(2 \cdot \pi)^{3/2} \cdot \sigma_x \cdot \sigma_y \cdot \sigma_z \cdot f} \cdot \exp \left[\frac{-1}{2 \cdot f^2} \left\{ \begin{array}{l} \frac{f_v^2 \cdot x''^2}{\sigma_x^2} + \frac{f_u^2 \cdot y''^2}{\sigma_y^2} + \frac{z''^2 \cdot (1+s^2/3)}{\sigma_z^2} \\ - \frac{x'' \cdot y'' \cdot s_u \cdot s_v}{6 \cdot \sigma_x \cdot \sigma_y} - \frac{x'' \cdot z'' \cdot s_u}{\sigma_x \cdot \sigma_z} - \frac{y'' \cdot z'' \cdot s_v}{\sigma_y \cdot \sigma_z} \end{array} \right\} \right] \quad (38a)$$

where

$$f_u^2 \equiv 1 + s_u^2 / 12, \quad f_v^2 \equiv 1 + s_v^2 / 12, \quad (38b)$$

$$x'' \equiv x - \{x_0 + [u_0 + 1/2 \cdot (\partial u / \partial z) \cdot w_0 \cdot t] \cdot t\}, \quad y'' \equiv y - \{y_0 + [v_0 + 1/2 \cdot (\partial v / \partial z) \cdot w_0 \cdot t] \cdot t\},$$

and

$$z'' \equiv z - (z_0 + w_0 \cdot t) \quad (38c)$$

with (x_0, y_0, z_0) and (u_0, v_0, w_0) being the coordinates and winds at time $t = 0$. These initial values are typically the coordinates and winds at the source. Note also that any vertical velocity component, w_0 , is assumed to be constant over the time period t .

Verification that Eq.(38) is indeed a solution of the diffusion equation requires that one switch back to the K representation by substituting $\sigma^2 = 2 \cdot K \cdot t$ everywhere (and with appropriate subscripts). The number of terms involving time, t , is quite intimidating, such that evaluation of whether Eq.(38) is a solution of the diffusion equation,

$$\frac{\partial C}{\partial t} + u \cdot \frac{\partial C}{\partial x} + v \cdot \frac{\partial C}{\partial y} + w \cdot \frac{\partial C}{\partial z} - K_{xx} \cdot \frac{\partial^2 C}{\partial x^2} - K_{yy} \cdot \frac{\partial^2 C}{\partial y^2} - K_z \cdot \frac{\partial^2 C}{\partial z^2} = 0 \quad (39a)$$

is best accomplished using a computer algebra program, such as Maple (i.e., a software package sold commercially by Waterloo Maple, Inc.) or Mathematica (i.e., a software package sold commercially by Wolfram Research, Inc.). This has been done and Eq.(38a) is indeed an exact solution of Eq.(39a).

One might immediately question why the off-diagonal diffusivity terms don't appear in Eq.(39). The answer is that the off-diagonal terms, such as:

$$K_{xz} \cdot \frac{\partial^2 C}{\partial x \cdot \partial z} + K_{zx} \cdot \frac{\partial^2 C}{\partial z \cdot \partial x} = 0 \quad (39b)$$

all vanish for pure wind-shear related diffusivities, as $K_{xz} = -K_{zx}$ are antisymmetric in their subscript indices, and the equality of the partial second derivatives, such as:

$$\frac{\partial^2 C}{\partial x \cdot \partial z} = \frac{\partial^2 C}{\partial z \cdot \partial x} \quad (39c)$$

is almost always guaranteed for C given by analytic functions. Note that if the off-diagonal diffusivity terms contained true diffusion components, these portions of the off-diagonal K elements would be symmetric, and addition rather than cancellation would occur.

The solution provided by Eq.(38) is quite interesting and worthy of further analysis. First, one notes that the shear-altered, puff-center concentration, C_c' , (i.e., at $x'' = y'' = z'' = 0$) is reduced by the factor $1/f$ (i.e., $C_c' = C_c/f$). Thus, even though shearing per se is distortional and not diffusive, the combination of shear in concert with diffusion leads to the reduced puff-center concentration.

It is also interesting to note what has happened to the standard deviations of the sheared distribution (i.e., $\sigma'_x, \sigma'_y, \sigma'_z$) relative to the original, unsheared moments (i.e., $\sigma_x, \sigma_y, \sigma_z$). Actually, there can be several different interpretations of what is meant by the second moment. For example, if one were to evaluate the effective σ'_x in Eq.(38a) through the puff center, as defined by the line $y'' = z'' = 0$, simple inspection of Eq.(38a) would show an increased standard deviation of:

$$\sigma'_x = \sigma_x \cdot f / f_v \xrightarrow{s_v \rightarrow 0} \sigma_x \cdot (1 + s_u^2 / 12)^{1/2} \quad (40a)$$

in agreement with the result presented by F. B. Smith (1965), and in agreement with along-wind diffusion parameterizations employed by Wilson (1981) and Hanna and Franzese (2000). Similarly the effective σ'_y through the puff center, as defined by the line $x'' = z'' = 0$, would yield the increased value of:

$$\sigma'_y = \sigma_y \cdot f / f_u \xrightarrow{s_u \rightarrow 0} \sigma_y \cdot (1 + s_v^2 / 12)^{1/2}. \quad (40b)$$

However, the effective σ'_z through the puff center, defined by the line $x'' = y'' = 0$, would surprizingly yield the reduced value of:

$$\sigma'_z = \sigma_z \cdot \frac{(1 + s^2 / 12)^{1/2}}{(1 + s^2 / 3)^{1/2}} \quad (40c)$$

How could the plume shrink in this vertical dimension as there is no shear stretching or enhanced diffusivity in this dimension? The truth is that the plume has not physically shrunk in the z -dimension, but the fact that the diffused ellipsoid has been rotated away from its original principal axes means that the line specified by $x'' = y'' = 0$ is no longer along a major/minor axes, but rather cuts obliquely through the ellipsoid.

However, if one first integrates Eq.(38a) over the entire x'' - y'' plane and then re-evaluates the vertical second moment, one would find that this projection of the entire distribution onto the z'' -axis was indeed associated with an unchanged standard deviation of:

$$\sigma'_z = \sigma_z . \quad (41a)$$

Performing similar analyses on the integrated projections onto the x'' and y'' axes, respectively, yields standard deviations of :

$$\sigma'_x = \sigma_x \cdot (1 + s_u^2 / 3)^{1/2} \quad \text{and} \quad \sigma'_y = \sigma_y \cdot (1 + s_v^2 / 3)^{1/2} . \quad (41b)$$

As these standard deviations represent a full projection of the entire puff distribution rather than a slice through a single point (i.e., the puff center), it is not surprising that each of these three standard deviations are larger than the corresponding standard deviation presented in Eq.(40). Thus, the moments one obtains are sensitive to the constraints placed upon the computational procedure, and more specifically, sensitive to the specific projection that is being considered. As a final example of this, consider Eq.(38a) on the plane $z'' = 0$, then integrate over y'' , and finally evaluate the variance in x'' . This will lead to the exact results:

$$\sigma'_x = \sigma_x \cdot (1 + s_u^2 / 12)^{1/2} \quad \text{and} \quad \sigma'_y = \sigma_y \cdot (1 + s_v^2 / 12)^{1/2} \quad (42)$$

where the σ'_y result arises from the corresponding consideration of $z'' = 0$, integration over x'' , and finally evaluation of the variance in y'' .

The solution of the sheared puff problem may also be approached using Fourier Transforms (FT). Recently, R. B. Smith (2005) has done a thorough analysis of the sheared puff solution in FT space, and obtains a general solution of the FT of the concentration distribution in terms of the spatial FT of the source distribution. Inversion of this solution via rapid inverse transform algorithms (i.e., Fast Fourier Transform or FFT software) provides an efficient means for evaluating concentration distributions as well as obtaining interesting results on the distribution of tracer ages within a sheared puff. Smith also finds that the FT approach yields first and second concentration distribution moments in agreement with the earlier work of Saffman (1962). While there is agreement between their estimate of the vertical standard deviation σ'_z and the unchanged standard deviation of Eq.(41a), their estimates for the altered σ'_x and σ'_y are considerably smaller [i.e., $(7/30-\pi/16)/2 \approx 0.018491$ versus the $1/12 \approx 0.0833333$] than those presented in Eq.(40b). This factor of 4.5 difference in the σ^2 (i.e., a factor of 2.12 in the σ) was also derived by F. B. Smith(1965) (see also Pasquill and Smith, 1983) and can be understood by recognizing that Eq.(38a) is the solution for the unbounded puff, such that shear can be viewed as symmetric about the puff's center; however, Saffman (1962) and R. B. Smith (2005) treat the case of the semi-bounded puff (i.e., a ground level release described by the unbounded puff solution above ground plus its reflection term below ground). To compute the

reflection term equivalent to Eq.(38a), one must recognize that the shears, s_u and s_v of Eq.(36c), flip sign in the ground reflection terms. Thus, rather than a puff sheared symmetrically about its center, one has a half-puff shape sheared asymmetrically and subjected to net overall transport. Intuitively, one might imagine that the shear sign flip in the reflection term would yield a factor-of-two smaller, shear-induced sigma (rather than the factor of 2.12 mentioned above); however, the asymmetry of this sheared, “half-puff” shape accounts for the deviation from a strict factor-of-two. Note that when evaluating the standard deviation of this half-puff shape, one must account for the net advective displacement via the computational rule: variance equals mean-square minus the mean squared, or:

$$\sigma_x^2 = [\langle C \cdot x^2 \rangle - \langle C \cdot x \rangle^2] / \langle C \rangle \quad (43)$$

where $\langle \rangle$ denotes integration over the domain and variable (i.e., dx) of interest.

Finally, returning briefly to Eq.(38), one notes that the formulation includes mean velocity components, u_0 , v_0 , and w_0 , and that the coordinates x , y , z , represent an arbitrary orthogonal system and do not reflect a “preferred” frame, such as used in plume modeling, where x is meant to imply the along-wind direction. Thus, Eq.(38) can easily be adapted to a multi-time-step model where u_0 , v_0 , and w_0 can change with each new time step. This adaption is accomplished through the use of “initial sigmas” and various pseudo-times, t_0 , such that the $t = 0$ point at the beginning of the next time step is associated with the $t = \Delta t$ state of the Eq.(38a) distribution at the end of the previous time step. Thus, Eq.(38a) can be advanced over many time steps with varying meteorology without needing to consider computationally-expensive measures such as puff-splitting. Of course, at some point, the puff may become so sheared that its top and bottom are in different meteorological grid cells (i.e., possibly having totally different flow and turbulence characteristics), and, in such cases, it will be necessary to split the puff. In this case, it may be most appropriate to break the single ellipsoid, characterizing the distribution, into two (or more) ellipsoids.

3.3 Modeling of Higher Concentration Moments

As far back as the mid-1980s, Sykes and co-workers at Aeronautical Research Associates of Princeton (ARAP) were working on developing a series of higher-order closure based plume and puff models. One primary feature of this approach is that by expanding the concentration and velocity fields into mean and fluctuation components, Sykes *et al.* (1984) were able to develop a partial differential equation for the mean-square concentration, $\langle C^2 \rangle$. This implies that one is able to predict concentration variance, σ_c^2 (i.e., as $\sigma_c^2 = \langle C^2 \rangle - \langle C \rangle^2$), along with the traditional mean concentration, $\langle C \rangle$. The resulting puff model, SCIPUFF, employs second-order turbulence closure theory and solves the PDEs for mean and mean-squared concentration via numerical methods. The SCIPUFF model has undergone refinement and evaluation for more than a decade. Thus,

any attempt to fully and fairly describe SCIPUFF's equations and features and the technical aspects of yet other modeling approaches to predicting higher concentration moments and fluctuation measures would require an additional chapter and will not be attempted here. For those interested in SCIPUFF, the model and its extensive documentation are available online at:
http://www.titan.com/products-services/336/download_scipuff.html .

Acknowledgments

I would like to thank Prof. Ronald B. Smith and Mr. Gary Moore for their useful comments and careful readings of this manuscript.

References

- Abramowitz, M. and I.A. Stegun, 1972. Handbook of Mathematical Functions. NBS Applied Mathematics Series, Vol. 55, Tenth printing with corrections, Washington, D.C. Now available online at: <http://mintaka.sdsu.edu/faculty/wfw/ABRAMOWITZ-STEGUN/intro.htm> or at: <http://www.convertit.com/Go/ConvertIt/Reference/AMS55.ASP> .
- Anderson, T.W., 1984. An Introduction to Multivariate Statistical Analysis, 2nd Edition, John Wiley and Sons, New York, 675 pp.
- Batchelor, G.K., 1950. The application of the similarity theory of turbulence of atmospheric diffusion. *Quart. J. Roy. Meteorol. Soc.*, **76**, 133-146.
- Benkley, C.W. and A. Bass, 1979. Development of Mesoscale Air Quality Simulation Models. Volume 3. User's Guide to MESOPUFF (Mesoscale Puff) Model. EPA 600/7-79-XXX, Environmental Protection Agency, Research Triangle Park, NC, 124 pp.
- Chang, J.C., P. Franzese and S.R. Hanna, 2000. Evaluation of CALPUFF, HPAC, and VLSTRACK with the Dipole Pride 26 Field Data. Proceedings, 11th Joint Conference on the Applications of Air Pollution Meteorology with the AWMA. American Meteorological Society, 45 Beacon St., Boston, MA 02108, pp. 340-346.
- Chang, J.C., P. Franzese, K. Chayantrakom, and S.R. Hanna, 2003. Evaluations of CALPUFF, HPAC, and VLSTRACK with Two Mesoscale Field Datasets. *J. Appl. Meteor.*, **42**, 4, 453-466.
- EPA, 1993. Interagency Workgroup on Air Quality Modeling (IWAQM) Phase I report: Interim recommendations for modeling long range transport and impacts on regional visibility. U.S. EPA, Research Triangle Park, NC.
- Geller, M. and E. Ng, 1971. Tables of Integrals of the Error Functions - II: Additions and Corrections. *J. Res. National Bureau of Standards, Part B, Mathematical Sciences*, **75B**, 149-163.
- Gifford, F.A., Jr., 1975. Atmospheric Dispersion Models for Environmental Pollution Applications, in *Lectures on Air Pollution and Environmental Impact Analyses*, Boston, MA, Sept. 29-Oct. 3, pp. 35-38, American Meteorological Society, Boston, MA.
- Gifford, F.A., Jr., 1976. Turbulent Diffusion - Typing schemes: A Review. *Nucl. Saf.*, **17**, 68-86.
- Gifford, F.A., Jr., 1977. Tropospheric relative diffusion observations. *J. Appl. Meteorol.*, **16**, 311-313.

Hales, J.M., D.C. Powell and T.D. Fox, 1977: STRAM - An Air Pollution Model Incorporating Non-linear Chemistry, Variable Trajectories, and Plume Segment Diffusion. EPA 450/3-77-012. Environmental Protection Agency, Research Triangle Park, NC, 147 pp.

Hanna, S.R. and P. Franzese, 2000. Alongwind dispersion - A simple similarity formula compared with observations at 11 field sites and in one wind tunnel. *J. Appl. Met.*, **39**, 1700-1714.

Hanna, S.R., R. Britter, and P. Franzese, 2003. A baseline urban dispersion model evaluated with Salt Lake City and Los Angeles tracer data. *Atmos. Environ.*, **37**, 5069-5082.

Interagency Workgroup on Air Quality Modeling (IWAQM), 1998. Phase 2 Summary Report and Recommendations for Modeling Long Range Transport Impacts, EPA-454/R-98-019, U.S. Environmental Protection Agency.

Ludwig, F.L., L.S. Gasiorek and R.E. Ruff, 1977. Simplification of a Gaussian puff model for real-time minicomputer use. *Atmos. Environ.*, **11**, 431-436.

Mikkelsen, T., H. Jørgensen, M. Nielsen, and S. Ott, 2002. Similarity scaling of surface-released smoke plumes. *Boundary-Layer Meteorology*, **105**, 483-505.

Oettl, D., A. Goulart, G. Degrazia, and D. Anfossi, 2005. A new hypothesis on meandering atmospheric flows in low wind speed conditions, *Atmos. Environ.*, **39**, 1739-1748.

Pasquill, F., 1976. Atmospheric Dispersion Parameters in Gaussian Plume Modeling. Part II. Possible Requirements for Change in the Turner Workbook Values. EPA-600/4-76-030b, 44 pp.

Pasquill, F. and F.B. Smith, 1984. Atmospheric Diffusion, 3rd Edition, Halsted Press Division of John Wiley and Sons, New York, 437 pp.

Prudnikov, A.P., Yu. A. Brychkov, and O.I. Marichev, 1986. Integrals and Series, Volume 1, Elementary Functions. USSR Academy of Sciences, Moscow. Translated from the Russian by N.M. Queen, Gordon and Breach Science Publishers, New York.

Richardson, L.F., 1926. Atmospheric diffusion shown on a distance-neighbour graph. *Proc. Roy. Soc. London*, **A110**, 709-737.

Saffman, P.G., 1962. The Effect of Wind Shear on Horizontal Spread from an Instantaneous Ground Source, *Quart. J. Roy. Meteorol. Soc.*, **88**, 382-393.

Scire, J.S., E.M. Insley and R.J. Yamartino, 1990a. Model formulation and user's guide for the CALMET meteorological model. Prepared for the California Air Resources Board by Sigma Research Corporation, Concord, MA.

Scire, J.S., D.G. Strimaitis and R.J. Yamartino, 1990b. Model formulation and user's guide for the CALPUFF dispersion model. Prepared for the California Air Resources Board by Sigma Research Corporation, Concord, MA.

Scire, J.S., D.G. Strimaitis and R.J. Yamartino, 2000. User's guide for the CALPUFF dispersion model (Version 5). Earth Tech, Inc., Concord, MA.

Scire J.S., F.R. Robe, M.E. Fernau, and R.J. Yamartino, 1998. A User's Guide for the CALMET Meteorological Model (Version 5.0). Earth Tech, Inc., Concord, MA.

Scire, J.S., F.W. Lurmann, A. Bass and S.R. Hanna, 1984a. Development of the MESOPUFF II dispersion model. EPA-600/3-84-057, U.S. EPA, Research Triangle Park, NC.

- Scire, J.S., F.W. Lurmann, A. Bass and S.R. Hanna, 1984b. User's guide to the MESOPUFF II model and related processor programs. EPA-600/8-84-013, U.S. Environmental Protection Agency, Research Triangle Park, NC.
- Smith, F.B., 1965. The role of wind shear in horizontal diffusion of ambient particles. *Quart. J. Roy. Meteor. Soc.*, **91**, 318-329.
- Smith, R.B., 2005. An analytical approach to shear dispersion and tracer age. *Boundary-Layer Meteorology*, **117**, 383-415.
- Strimaitis, D.G., J.S. Scire and J.C. Chang, 1998. Evaluation of the CALPUFF Dispersion Model with two Power Plant Data Sets. Preprints 10th Joint Conference on the Applications of Air Pollution Meteorology, January 11-16, Phoenix, AZ.
- Sykes, R.I., S.F. Parker, D.S. Henn, C.P. Cerasoli and L.P. Santos, 1998. PC-SCIPUFF Version 1.1PD.1 Technical Documentation. ARAP Report No. 718. Titan Corporation, Titan Research & Technology Division, ARAP Group, P.O. Box 2229, Princeton, NJ, 08543-2229. Available at: http://www.titan.com/products-services/336/download_scipuff.html.
- Sykes, R.I. and D.S. Henn, 1995. Representation of velocity gradient effects in a Gaussian puff model. *J. Appl. Met.*, **34**, 2715-2723.
- Sykes, R.I., W.S. Lewellen and S.F. Parker, 1984. A turbulent-transport model for concentration fluctuations and fluxes. *J. Fluid Mech.*, **139**, 193-218.
- Taylor, G.I., 1921. Diffusion by continuous movements. *Proc. London Math. Soc.*, **20**, 196-211.
- van Egmond, N.D. and H. Kesseboom, 1983. Mesoscale air pollution dispersion models - II. Lagrangian Puff model and comparison with Eulerian grid model. *Atmos. Environ.*, **17**, 267-274.
- Venkatram, A., 2002. Accounting for averaging time in air pollution modeling. *Atmos. Environ.*, **36**, 2165-70.
- Walcek, C.J., 2004. Accounting for wind shear in Gaussian dispersion models. American Meteorological Society 16th Symposium on Boundary Layers and Turbulence, Aug. 8-14. Portland, ME, Preprint 10.5.
- Walcek, C.J., 2007. Accounting for wind shear in Gaussian dispersion models. *Atmos. Environ.*, In Press.
- Wegener, R. and J. Schroeter, 1995. Correlational Kinetics, Part I: General Theory. *Physika A*, **219**, 159-188.
- Wilson, D.J., 1981. Along-wind diffusion of source transients. *Atmos. Environ.*, **15**, 489-495.
- Yamartino, R.J., 2000. Refinement of Horizontal Diffusion in Photochemical Grid Models. *Proc. 11th Joint AMS/AWMA Conference on the Applications of Air Pollution Meteorology*, Long Beach, CA, January 9-14.
- Zannetti, P., 1981. An improved puff algorithm for plume dispersion simulation. *J. Appl. Meteor.*, **20**, 1203-1211.

Chapter 9

Special Applications of Gaussian Models

A brief introduction to the topic “Special Applications of Gaussian Models” was presented in Volume I of this book series. A full chapter on this topic is expected to be published in Volume IV.

For additional information, the reader can visit:

- http://www.epa.gov/scram001/dispersion_prefrec.htm#other
http://www.epa.gov/scram001/dispersion_alt.htm
US EPA site where models developed for special applications are listed.

BRANKLEY
PAPER

Chapter 10

Eulerian Dispersion Models

A chapter dedicated to the topic “Eulerian Dispersion Models” was presented in Volume I of this book series.

For additional information, the reader can visit:

- <http://www.epa.gov/asmdnerl/CMAQ/CMAQscienceDoc.html>
The US EPA site describing the Models-3 project. Models-3 and Community Multi-scale Air Quality (CMAQ) software in combination form a powerful third generation air quality modeling and assessment system that enables users to execute air quality simulation models for their specific problem domain and visualize the results.
<http://www.ntis.gov/products/bestsellers/cpn8867.asp?loc=4-2-0>
- <http://www.ce.gatech.edu/~todman/24itm.pdf#search='air%20pollution%20grid%20models>
A research paper on adaptive grids in air pollution modeling.
- <http://parallel.bas.bg/~ceco/ps/boro02pap.pdf#search='air%20pollution%20grid%20models>
A research paper on “Flexible Two-Level Parallel Implementations of a Large Air Pollution Model” that also describes The Danish Eulerian Model (DEM).
- <http://www.epa.gov/scram001/photochemicalindex.htm>
Grid models for photochemical simulations.

- <http://www.aironline.info/haifa/tekster.cfm?id=6892>
The Air Quality Information System (AirQUIS) is a professional management tool for Air Quality developed by Norwegian Institute for Air Research (NILU) together with GIS-experts.
- http://www.nilu.no/AQM/1m_episode.htm
The NILU-developed source oriented numerical dispersion model EPISODE calculates spatially distributed hourly concentrations from point, line and area sources.
- http://www.cmar.csiro.au/research/tapm/docs/tapm_v3infosheet_nov07.pdf
The Air Pollution Model (TAPM V3) is a PC-based 3-D prognostic model for air pollution studies.

Chapter 11

Lagrangian Particle Models

A comprehensive chapter on “Lagrangian Particle Models” was published in Volume II. For additional information, the reader can visit:

- http://users.frii.com/uliasz/modeling/ref/lpd_bib.htm
A list of useful references.
- <http://files.harc.edu/Projects/AirQuality/Projects/H044.T117.2004/H044.T117FinalReport123.pdf>
A Web-Based Lagrangian Particle Model.
- <http://biocycle.atmos.colostate.edu/~marek/archive/models/cloud98.pdf>
Large-Eddy Simulation of Air Pollution Dispersion in the Nocturnal Cloud-Topped Atmospheric Boundary Layer.

BRANK
P
e

Chapter 12

Atmospheric Transformations

A comprehensive chapter on “Atmospheric Chemistry and Chemical Transformations” was published in Volume II. For additional information, the reader can visit:

- http://en.wikipedia.org/wiki/Atmospheric_chemistry
From Wikipedia, the free encyclopedia.
- <http://physchem.ox.ac.uk/~wayne/atmos.html>
Lectures on atmospheric chemistry.
- <http://www.cac.yorku.ca/intro.html>
Introduction to atmospheric chemistry.
- <http://www.shsu.edu/~chemistry/Glossary/glos.html>
Atmospheric Chemistry Glossary.

BRANK
P
e

Chapter 13

Deposition Phenomena

A comprehensive chapter on “Atmospheric Deposition Phenomena” was published in Volume II. For additional information, the reader can visit:

- <http://nadp.sws.uiuc.edu/>
The National Atmospheric Deposition Program/National Trends Network (NADP/NTN) is a nationwide network of precipitation monitoring sites. The network is a cooperative effort between many different groups, including the State Agricultural Experiment Stations, U.S. Geological Survey, U.S. Department of Agriculture, and numerous other governmental and private entities.
- <http://www.maine.gov/dep/air/monitoring/Atmosdepos.htm>
Fundamentals of atmospheric deposition phenomena.
- <http://www.epa.gov/glnpo/glindicators/air/airb.html>
Atmospheric deposition in the Great Lakes.
- <http://www.epa.gov/oar/oaqps/gr8water/handbook/index.html>
Frequently asked questions about Atmospheric Deposition: A Handbook for Watershed Managers.

BRANK
P
e

Chapter 14

Indoor Air Pollution Modeling

A comprehensive chapter on “Indoor Air Pollution Modeling” was published in Volume II. For additional information, the reader can visit:

- <http://www.epa.gov/iaq/>
US EPA web site for indoor air pollution.
- <http://www.epa.gov/iaq/pubs/hpguide.html>
Indoor Air Pollution: An Introduction for Health Professionals.
- <http://www.who.int/indoorair/en/>
World Health Organization web site for indoor air pollution.
- <http://www.epa.gov/appcdwww/iemb/model.htm>
US EPA web site for indoor air pollution modeling.
- <http://exposurescience.org/research-topic/indoor-air-quality>
Mathematical models for indoor air quality.

BRANKLEY
PAPER

Chapter 15

Modeling of Adverse Effects

A brief introduction to the topic “Modeling of Adverse Effects” was presented in Volume I of this book series. A Chapter on this topic (“15A – Modeling of Health Risks Associated with Combustion Facility Emissions”) was included in Volume II. Two additional chapters are included in the following pages:

15B - Odor Modeling

15C - Climate Change - An Introduction to Atmosphere-Ocean General Circulation Modeling

BRANKLEY
PAPER

Diosey, P.G. and M. Buono. 2008. *Odor Modeling*. Chapter 15B of *AIR QUALITY MODELING - Theories, Methodologies, Computational Techniques, and Available Databases and Software. Vol. III – Special Issues* (P. Zannetti, Editor). Published by The EnviroComp Institute (<http://www.envirocomp.org/>) and the Air & Waste Management Association (<http://www.awma.org/>).

Chapter 15B

Odor Modeling

Phyllis G. Diosey⁽¹⁾ and Maureen E. Buono⁽²⁾

⁽¹⁾ *Malcolm Pirnie, Inc., White Plains, NY (USA)*

pdiosey@pirnie.com

⁽²⁾ *Malcolm Pirnie, Inc., White Plains, NY (USA)*

Abstract: Atmospheric dispersion modeling is an invaluable tool in the control and management of air pollution. It has been used for many years in the regulatory arena for the assessment of the air quality impacts from a wide variety of sources of air pollution, such as powerplant stacks, industrial chimneys, and mobile sources. Dispersion models apply mathematical equations, often modified with empirical factors, to convert a mass emission rate from a source of air pollution to an ambient air concentration at some distance downwind of the source. It has been found that atmospheric dispersion modeling can also be an extremely useful tool in the assessment of offsite impact to evaluate control and better manage odors. However, there can be significant differences between the traditional pollutant-specific modeling and modeling that is performed for odor assessment. Modeling used for air quality compliance purposes, for example, is usually concerned with fixed time-averaged concentrations for direct comparison to ambient air quality standards and criteria (generally 1 hour to 1 year). Odors, on the other hand, can be recognized on the order of seconds or minutes. In addition, unlike air quality standards which have been quantified based upon exposure and health related responses, the response to odors can be very subjective and are historically based on nuisance. This chapter discusses the techniques used to model odors, and details the differences that must be addressed from both theoretical and practical points of view when applying dispersion models to odor assessment.

Key Words: Odors, odor modeling, odor dispersion modeling, air quality modeling, odor impacts.

1 Modeling for Odors in the Atmosphere

The quality of the air we breathe has traditionally been based on levels of ambient air concentrations of pollutants known to have adverse health effects. However, as “quality of life” emerges as a strong public concern, odor is increasingly linked

to air quality. A difficult problem with that association is that unlike specific air pollutants like sulfur dioxide or carbon monoxide, which have quantifiable levels protective of public health (i.e., ambient air quality standards), the perception of odor is subjective and not easy to quantify. For example, in the late 1970s, the United States Environmental Protection Agency (USEPA), given the responsibility of developing regulations for hazardous air pollutants, initially proposed odor regulations. However, these odor standards were never promulgated because the link between odor and health was not established, and odor was considered to be a local issue better left to the states.

Atmospheric dispersion modeling has been an invaluable tool in the control and management of air pollution. It has been used for many years in the regulatory arena for the assessment of the air quality impacts from a wide variety of sources of air pollution, such as power plant stacks, industrial chimneys, and mobile sources. Atmospheric dispersion models apply mathematical equations, often modified with empirical factors, to convert a mass emission rate from a source of air pollution (mass per unit time) to a mass-based ambient air concentration (mass per unit volume) at some specified distance downwind of the source.

Over the years, atmospheric dispersion modeling has also been used for offsite impact assessment in the control and management of odors. This type of odor impact analysis is important for determining effective control strategies, identifying key odor sources, and demonstrating reduced odor impacts within the community. Much of the basic understanding of odor transport can come from an understanding of atmospheric dispersion processes. However, there can be significant differences between the traditional pollutant-specific modeling and modeling that is performed for odor impact analysis. For instance, modeling used for air permit purposes is concerned with time-averaged concentrations for direct comparison to ambient air quality standards (generally 1 hour to 1 year), whereas recognition of an odor can occur on the order of seconds. In addition, air quality standards, developed to protect the public, are based upon quantifiable health effects, whereas nuisance odor thresholds are highly dependent upon the receiving population, so that one person's nuisance odor can be another person's sweet perfume or fondest memory. These differences must be understood before selecting a dispersion model and modeling methodology for predicting odor impacts.

2 Odor Measurement

One distinction between standard dispersion modeling and odor modeling is in the characterization of the odors themselves. Modeling performed for air permits or environmental assessments generally evaluate the transport of known pollutants and use pollutant-specific mass emission rates. Emission rates or emission fluxes, in units of mass emitted per unit time and mass per unit time per unit area, are determined from source sampling, emission factors, or theoretical

emission formulas. Likewise, concentrations at the receptor are generally in terms of mass concentration in units of mass per unit volume. Odorous emissions, on the other hand, may often be complex combinations of compounds, where the components can sometimes be identified, but are not necessarily quantitative indicators of the odor itself. In addition, odor-emitting facilities, such as wastewater treatment plants or animal feedlots, may generate a number of different odors from a number of different processes, and the fate of these odors as they are transported with the wind is difficult to determine. In the face of such complex emissions, a single indicator compound with a low odor threshold and high emission rate has sometimes been used as representative of the sources under consideration; however, this approach can lead to significant underestimation of odor impacts offsite (Duffee and O'Brien, 1992).

Odor is currently evaluated by five parameters:

Character Odor *character* or odor quality is reported in terms of standard descriptors, such as "fruity," "earthy," "musty," etc. Odor observers are trained to use such standardized descriptive terminology in order to identify an odor.

Hedonic Tone *Hedonic tone* measures the pleasantness or unpleasantness of the odor, independent of the character. Different scales may be used. The most common is a 20-point scale, where 0 would be neutral, +1 to +10 would be pleasant, and -1 to -10 would be unpleasant. This is a subjective parameter since the pleasantness or unpleasantness of an odor is often based on the experience and memory of the person smelling the odor.

Intensity Odor *intensity* is the relative strength of the odor above the threshold. This is often referenced against a standard odorous gas, such as n-butanol. Using the standard n-butanol method, a device called a butanol wheel delivers varying concentrations of butanol in odor-free air to eight sniffing ports. The concentration of n-butanol in the mixture at the ports has an increasing concentration ratio of 2 on a binary scale. The odor *intensity* is then expressed in terms of parts per million of n-butanol by volume of air.

Concentration The *detection threshold* can be defined as the lowest concentration of a substance that can be detected above a blank (odor-free) sample by an odor panel. The *recognition threshold* (RT), on the other hand, is the lowest concentration of a substance that can be recognized based upon the character of the odor. Published *odor threshold* values for specific compounds have generally been derived in the laboratory, and represent the concentration at which the "average" person can detect a compound. These *odor threshold* values can vary widely for a given population and a given odor. Hydrogen sulfide (H₂S), for example, has reported *odor thresholds* that vary from 1 ppb to 130 ppb (IAH, 1989). Another method of presenting odor concentration is the concept of a dilution to threshold ratio. The *dilution ratio* (D/T, dilutions to threshold value) is the estimated number of dilutions with equal volumes of clean air needed to make

the odor non-detectable. When dealing with odors that are complex mixtures of compounds, concentration is denoted in terms of dilutions or odor units per unit volume.

The highly subjective nature of our response to odors makes odors very difficult to assess and quantify. Odors can trigger both physiological and psychological responses. While research continues in an effort to develop instrumentation that can objectively measure odors, the industry standard for measuring odors today is with the use of a trained *odor panel* using a *dynamic olfactometer*. The olfactometer has a sniffing port supplied alternately with three samples; one sample contains a diluted sample of the odorous gas, the remaining two are odor-free air. Trained individuals making up the odor panel are asked individually to select which of three samples presents an odor different from the other two (Figure 1). The concentration of odorous gas is then increased until the odor is detected or recognized.



Figure 1. Dynamic dilution olfactometer test (courtesy of St. Croix Sensory).

Another odor sampling device, called a field olfactometer (or *scantometer*), measures odors directly in the field by varying the proportions of ambient air and air filtered through activated carbon (to remove the odors) that is introduced to the individual using the instrument. The ratio of the ambient air to the carbon-filtered air at the point where the odor is detected is the *dilution to threshold* value of the odor. Figure 2 shows one of the newest versions of the field olfactometer.

Persistence The rate of change of intensity with odor concentration is called the *persistence*. While it seems logical to assume that the intensity of an odor is related to its concentration, the rate of change of intensity with odor concentration is not the same for all odors. Intensity and odor concentration (in D/T) are plotted on a log-log scale and the flatter the slope, the more persistent the odor.



Figure 2. Field olfactometer (courtesy of St. Croix Sensory).

Field olfactometers commonly have D/T ratios set at 2, 4, and 7, which are in the range of existing standard ambient odor guidelines. Additional D/Ts such as 15, 30, 60 and higher dilution ratios are also available.

3 Odor Modeling-Related Issues

Differences between traditional dispersion modeling and odor modeling appear in at least three areas: at the source of the odors (wastewater treatment plant, rendering plant, etc.), en route from the source of the odors to the receptor, and at the receptor (i.e., the human nose). Often, the methodology used for an odor assessment will be based upon consideration of only one of these factors (e.g., the short detection or recognition time characteristic of odors at the receptor) without regard for the effect of the other factors. This can lead to results that appear to overlook the physical phenomena associated with the project. Therefore, it is important to look at the “big picture” before deciding on the appropriate approach when planning an odor assessment.

3.1 Source Characteristics

In general, most sources can be categorized as a point, area, or volume source. Sources responsible for odor complaints are generally continuous sources (e.g., stacks, scrubbers, or basins); although routine but instantaneous or very short-term releases (e.g., from digester pressure release valves at wastewater treatment plants) can also pose problems at nearby receptors. Depending upon the rate of release relative to odor perception's short time frame, intermittent sources can be classified as either continuous sources (release rate on the order of minutes or longer), or instantaneous sources (release rate on the order of seconds).

If the odors can be characterized by distinct chemicals, or if different odorous sources at a facility can each be characterized by distinct chemicals, then the model emissions can be put in terms of the individual mass emission rates.

Assuming that there are no significant chemical reactions that occur during the transport process, the odor model is not much different from the traditional air quality model. When dealing with complex odorous emissions, the odor emission rates are generally modeled as D/T or odor units (ou) per unit time (for point or volume sources), or per unit time per unit area (for area sources). This “odor emission rate” is based upon determining a source concentration in D/T or odor units and multiplying this concentration by a volume flowrate or flux at the source. An important distinction between modeling a single odorous compound, such as H₂S, as opposed to a complex odor comprised of multiple compounds is the interactive nature of odors. Models can easily and appropriately assess single compound-specific odors in terms of mass concentrations. However, it may not be appropriate to use models to assess the cumulative offsite odor impacts from different sources or different processes at a single facility (e.g., odors from the headworks and odors from the digestion process at a wastewater treatment plant), in units of D/T, unless the odors from these sources and processes are similar.

Whatever the method used to determine the odor emission rate at the source, it is important that the emission rate is truly representative of that particular source, whether the emissions are stated in terms of mass per unit time, or as D/T or odor units per unit time. This generally will require that site-specific source sampling be conducted in order to determine the odor emission rate.

3.2 Effect of Averaging Time

There are a number of locations where time and time-averaging come into play in odor modeling and odor assessment.

At the source A source emits odors at some rate, duration, and frequency. The odors can be emitted on a continuous basis (for example, odors from an odor control stack), or on a sporadic basis (odors from a pressure relief valve). Continuous odors may be emitted at a single rate, or at a rate that varies over time. Sporadic odors may be emitted for a short or long duration, frequently or infrequently, and regularly or irregularly. Depending upon the rate of release relative to odor perception's short time frame, intermittent sources can be classified as either continuous sources (release rate on the order of minutes or longer), or instantaneous sources (release rate on the order of seconds).

At the receptor At the receptor (e.g., the nose of someone in the community), there is a time associated with detecting an odor, recognizing the odor, and ultimately, a time frame after which the odor is so annoying that the person feels that they must lodge a complaint. Parameters associated with an odor include the concentration, intensity, character, and degree of pleasantness or unpleasantness of the odor, but time-related issues such as frequency and the duration of the odor are also important considerations. A person may detect an odor in a matter of seconds, but the difficult question is what combination of parameters leads to an odor being annoying or offensive enough to complain?

During transport The time it takes for the odors to reach the receptor can play a major role in the perceived nature of that odor. Surface obstructions like buildings and trees, terrain effects like valleys or mountains, and meteorological conditions like wind speed and turbulence during the transport process can have significant influence on the odor levels at the receptor. The effects of travel path and time should be a consideration when designing a modeling analysis.

During sampling In addition to the time scales described above, there are time scales associated with the sampling of odor. The time that is used to fill Tedlar® sampling bags or Summa® canisters, for example, can be varied from minutes to hours depending upon the sampling flowrate. This controls the range of fluctuations that can be measured using such techniques since high fluctuations that occur at smaller time steps will be blended with lower concentrations as the sample is collected. Hence, the sampling time can influence the characterization of source emission rates along with interpretation of the community monitoring results, and should be another consideration in the design of an odor study.

The fact that odor can be perceived in a very short time is often noted; however, what that short time period is and what it represents in odor modeling analyses varies. Important, but not so easily answered questions include:

1. What constitutes an odor impact? Is it exceeding odor detection, exceeding odor recognition, or exceeding some enhanced factor based upon one of these that considers a complaint level?
2. What time frame is most representative of odor impact? While most researchers agree in principle that the perception of odor occurs in a short time, what constitutes “short” in an odor analysis varies significantly.

The question of the appropriate time considerations has been one of the primary distinctions cited for modifying standard dispersion modeling methods for use in odor assessment, or for applying specialized models with features that attempt to account for the concept of time. Since most of the currently used dispersion models incorporate empirical factors which are time-averaged values, such as the turbulent diffusion coefficients, the model output is also related to these averages. If we photograph a plume of smoke from a stack, an instantaneous snapshot of a smoke plume will primarily show the plume meandering around its centerline under the influence of larger scale atmospheric turbulence. As the exposure time increases, the photograph will capture both the meander and the internal spread of the plume; detail within the plume is smeared (from the small scale atmospheric turbulence), and the boundary of the plume will spread with increasing distance and time to account for the plume meander. Far downwind, even the boundary of the time-averaged plume can meander around the centerline under the influence of very large-scale atmospheric turbulence. Figure 3 is a schematic showing the meander and crosswind spread of a smoke plume visualized at increasing averaging times from an instantaneous view to a 2 hour time-averaged view.

Crosswind concentration profiles of the plume would show that the centerline concentration for the instantaneous plume is significantly higher than that for the time-averaged plume, that is, the shorter the sampling time (exposure time following the camera analogy), the larger the fluctuations from the longer (exposure) time mean concentration. In short, the use of a fixed averaging time filters out the very high (peak) and very low concentration fluctuations. Since odors can be perceived within seconds, the issue of averaging time can play a much greater role than in traditional dispersion modeling where longer term averaging is the objective.

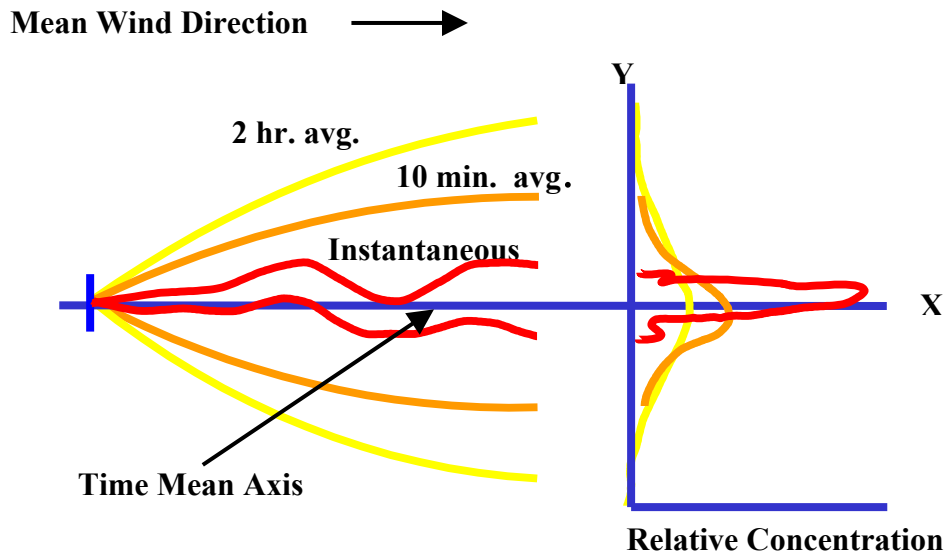


Figure 3. Plume vs. Averaging Time (adapted from Slade, 1968).

Traditional atmospheric dispersion modeling generally assumes that the emissions from a stack are continuous, and that the mass emission rate (mass per unit time) does not vary over the travel time from the source to the receptor. As Figure 3 indicates, measurements of time-averaged concentration profiles downwind of such sources have been shown to approach a bell-shaped, or Gaussian distribution. An instantaneous, or short-term release, such as a puff of gas from a pressure relief valve, however, may have a different release pattern, especially in the near-field region, where the puffs are transported bodily by large-scale turbulent eddies in the atmosphere. Measurement of concentration profiles downwind of these instantaneous or intermittent releases may produce periods of high concentration alternating with periods of zero or very low concentration. Alternative methods may need to be developed to determine these peak concentrations.

The literature presents an assortment of time scales used in odor modeling (Mahin, 1997). Frequent mention is made of the fact that odor can be perceived in a very short time; what that short time period is and what it represents in odor

modeling analyses varies. Table 1 presents a listing of some of the time periods that have been used in recently published odor analyses (Diosey, 2001).

Table 1. Examples of Time Scales Used in Odor Modeling.

Time Scale	Criterion	Source
2 second	Odor recognition	Compost facility
30 seconds	4 D/T	Compost facility
< 1 minute	Odor complaint	Compost facility
2 minutes	4 D/T	Wastewater treatment plant
3 minutes	“Nuisance-causing odor complaint”	Wastewater treatment plant
5 minutes	3 D/T	Portland cement plant
5 minutes	5 D/T	Wastewater treatment plant
10 minutes	Odor threshold	Hazardous waste landfill
1 hour	50 dilutions	Compost facility
1 hour	2 D/T	Composting facility
1 hour	1 ppb H ₂ S	Local environmental quality review odor threshold (NYCDEP, 2001)

Table 1 indicates there is currently a significant variation in both the “effective” time scale used to characterize an odor impact as well as variation in the odor criteria. It is clear that while most researchers agree in principle that the perception of odor occurs in a short time, what constitutes “short” in an odor analysis varies significantly.

Many of the empirical factors used in the dispersion equations are based upon field sampling data collected over finite sampling duration. Most of the models currently approved for regulatory purposes are the so-called Gaussian models. Gaussian models are empirically based and rely on sampling data that are time-averaged, such as the turbulent diffusion parameters, σ_y and σ_z . In addition, Gaussian models assume a steady-state condition. This makes Gaussian-based dispersion models, such as the Industrial Source Complex – Short Term (ISCST3) model and AERMOD model, appropriate for averaging times of 3 minutes to 1

hour. If the odor criterion for a particular odor assessment is on the order of seconds, then the time-averaged formulas could conceivably underestimate a shorter-term peak odor impact.

4 Odor Criteria

In the United States, there are currently no federal odor standards. A number of states and some localities have odor regulations; the majority of these are nuisance laws. However, growing concern over odors from sources such as concentrated animal feeding operations (CAFOs), composting facilities, rendering plants, landfills, wastewater treatment plants, and geothermal energy facilities, especially in an age of development where the traditional buffer zones between such facilities and the community are shrinking or non-existent, has led to surge of interest in measuring and managing odors. Recent surveys of odor standards and criteria used within the United States and in other countries around the world (Mahin and Pope, 1999; Mahin, 1997; and Malcolm Pirnie, 2002) indicate that there are a number of different odor levels currently being used to regulate odors, including the *detection threshold*, the *recognition threshold*, and *odor threshold* (See Table 2).

Table 2 - Odor Standards and Criteria.

Location	Compound	Standard/Criteria
California	Hydrogen sulfide	30 ppbv (1 hr average)
Connecticut	Hydrogen sulfide	6.3 $\mu\text{g}/\text{m}^3$
"	Methyl mercaptan	2.2 $\mu\text{g}/\text{m}^3$
"	N/A	7 D/T
Illinois	N/A	8 D/T (residential), 24 D/T (industrial), 16 D/T elsewhere
Kentucky	N/A	7 D/T (state standard)
Michigan	Hydrogen sulfide	1 $\mu\text{g}/\text{m}^3$ (24 hr average)
"	Methyl mercaptan	10 $\mu\text{g}/\text{m}^3$ (1 hr average)
Minnesota	Hydrogen sulfide	30 ppbv, 50 ppbv (30 min average)
Nebraska	Total reduced sulfur	100 ppbv (30 min average)
New Jersey	N/A	5 D/T (wastewater/solids handling)
New York	Hydrogen sulfide	14 $\mu\text{g}/\text{m}^3$ (1 hr average, state standard)

Location	Compound	Standard/Criteria
North Dakota	Hydrogen sulfide	# 50 ppb
"	N/A	7 D/T non-H ₂ S
Pennsylvania	Hydrogen sulfide	100 ppbv (1 hr average)
"	"	5 ppbv (24 hr average)
Texas	Hydrogen sulfide	80 ppbv (30 min average, residential/commercial area)
"	"	120 ppbv (industrial or vacant lands)
Quebec	Hydrogen sulfide	10 ppbv (1 hr average)
Alberta	Hydrogen sulfide	10 ppbv (1 hr average)
"	Ammonia	2,000 ppbv (1 hr average)
Ontario	N/A	1 ou/m ³ (10 min average)
WHO (Europe)	Hydrogen sulfide	1.3 ppbv (30 min average, guideline)
Denmark	N/A	0.6 - 1.2 ou/m ³ (1 min average)
Hong Kong	NA	5 ou (5 sec average)
Japan	Hydrogen sulfide	20-200 ppbv (depending on location)
"	Dimethyl disulfide	9-100 ppbv
"	Methyl mercaptan	2-10 ppbv
"	Butyric acid	1-6 ppbv
"	Ammonia	1,000-5,000 ppbv
Taiwan	N/A	50 ou/m ³ (petrochemical park)
Victoria, Australia	Hydrogen sulfide	0.1 ppbv
"	Methyl mercaptan	0.42 ppbv
"	Ammonia	830 ppbv
"	Chlorine	33 ppbv

Due to the subjective nature of odor perception, odor criteria are often site-specific, and developed from actual field sampling data and community-based odor panel assessment. Regulatory odor criteria are sometimes receptor-specific as well. Some criteria are to be met at the fence line, others at a residence, still others at sensitive receptor locations including homes, schools, nursing homes, churches, etc. Other odor criteria are activated only upon receipt of one or more

official complaints. Consideration of what the target level should be and where this target level needs to be met must be included in the odor modeling methodology, since the odor criterion will set the threshold and often the timescale of concern, while the receptor will determine the locations that must be modeled and range of the analysis.

Most odor assessments are performed to either prevent or mitigate odor complaints. Willhite and Dydek (1991) questioned whether the odor threshold is the same as the nuisance level, which is a level that would generate complaints. They noted that the nuisance level appears to be related to the "odor acceptability", which is based upon an individual's attitude and experience with the odor. The results of a field study (Ontario Ministry of Environment, 1988) that they reported implied that people will complain, in general, when the odor reaches approximately four times the odor threshold. They also noted that the levels at which people complain differ for unpleasant and pleasant odors. In this case, those chemicals with unpleasant odors have a complaint level approximately three times the odor threshold, while pleasant odors will not be recognized as a nuisance until the ambient odor levels exceed five times the odor threshold.

5 Odor Models and Modeling Techniques

As with other air pollutants, the dispersion of odors in the atmosphere is primarily a result of turbulence, or eddies in the atmosphere. Atmospheric eddies range from small-eddies on the order of a centimeter, to very large scale eddies, tens of meters across. When there is a continuous plume from a source of odors or pollutants, the smaller eddies in the atmosphere (i.e., smaller than the size of the plume) work to expand the plume around its center, diluting the plume internally as it travels downwind. Field observation of dispersion in the atmosphere also indicates the presence of large-scale, short-term fluctuations in concentration, which is a characteristic feature of atmospheric dispersion. Larger-scale atmospheric eddies work to transport the plume bodily, primarily in the crosswind and vertical directions (meander), while providing little in the way of dilution. In between the smaller and larger scale eddies, those equivalent to the size of the plume both dilute and transport the plume.

If the effects of plume spread and meandering are viewed at a fixed location, (e.g., sampling location along the X-axis in Figure 3), the monitor would "see" periods of turbulent concentration fluctuations as the plume travels past the monitor, and periods of zero concentration, or intermittency, when the plume meanders away from the monitor (see Figure 4). Based upon these observations, the dispersion of the plume can be viewed as the result of two distinct processes: the instantaneous spreading out of the plume in the vertical and crosswind directions (from the small-eddy turbulence), and the meandering, or fluctuation of the entire plume about its mean position as it travels downwind (from the large-scale eddy turbulence). A "true" model of atmospheric dispersion should be able

to correctly simulate both of these processes. The mean, or average concentration, can be significantly less than the peak concentrations measured by the monitor.

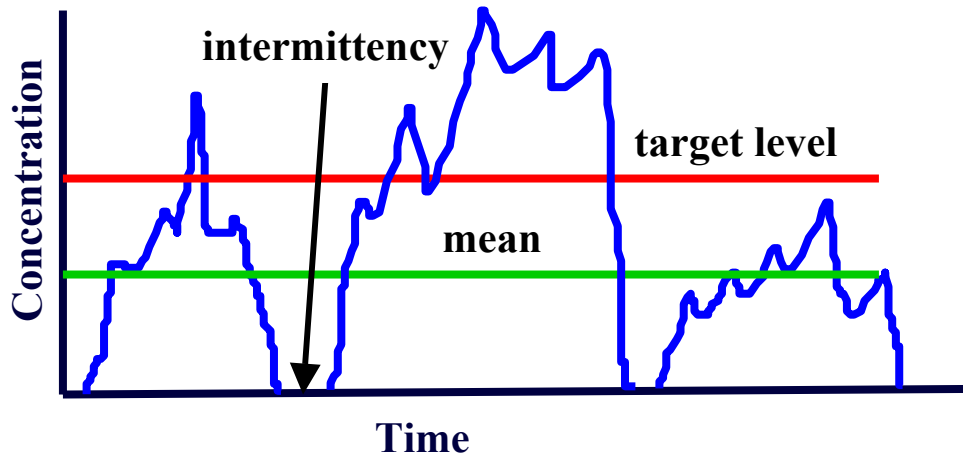


Figure 4. Concentration Timeline (at a fixed monitor).

The ultimate goal of a dispersion model is to accurately predict the odor or concentration of a contaminant as it travels downwind of a source (or sources) under any and all atmospheric conditions. While our understanding of atmospheric processes is increasing rapidly, the complexities are so great that all currently-used models have limitations on their applicability. Models have been developed to evaluate different source types (point, area, volume), different terrain (simple or complex), different locales (urban, rural, coastal), different release rates (plume, puff), different meteorological conditions (stable, convective), and different ranges (short-range and long-range transport). As with other forms of modeling, the model(s) that most closely approximates the parameters of the odor source and the characteristics of the dispersion process under analysis should be selected, and the limitations should clearly be recognized.

5.1 Odor Models

Similar to the decision process used to select the appropriate model for regulatory air quality modeling, the selection of the appropriate dispersion model for odor assessment starts with the source type and release scenario. In general, most sources can be categorized using the traditional designations of point, area, or volume sources. The sources responsible for most odor complaints tend to be from continuous sources (e.g., stacks, scrubbers, or basins); although routine but instantaneous or very short-term releases (e.g., from digester release valves) can also pose problems at nearby receptors. Depending upon the rate of release relative to odor perception's short time frame, intermittent sources can be classified as either continuous sources (release rate on the order of minutes or longer), or instantaneous sources (release rate on the order of seconds). Other

practical considerations may also come into play, such as matching the model to the objective of the analysis. The use of very conservative models and modeling techniques provide a level of safety for regulatory compliance analyses, but may result in costly over-design if the model is being used as part of the design process. Similarly, the model output must be able to match the criteria of concern.

5.1.1 Puff Models

Quasi-instantaneous and short-term releases are frequently viewed as "puff" releases. A puff release scenario assumes that the release time and sampling times are very short compared to the travel time from the source to the receptor. Högström (1972) considered the total spread (sigma, σ , to be a combination of the meandering of the puffs (σ_r) about a relative axis and the spread relative to the puff centroid (σ_c). He performed a series of field experiments and was able to give estimates of σ_r and σ_c in the downwind, crosswind and vertical dimensions for a sampling time of 30 seconds. In light of the limited data available to estimate the diffusion coefficients for puff diffusion, a number of models use the Pasquill-Gifford values. Since these coefficients were developed specifically for plumes, their use in puff models is questionable. In addition, most puff models assume a normal, or Gaussian concentration distribution within the plume. This assumption overlooks fluctuations within the puff. CALPUFF and AUSPUFF are examples of two currently used non-steady-state puff models.

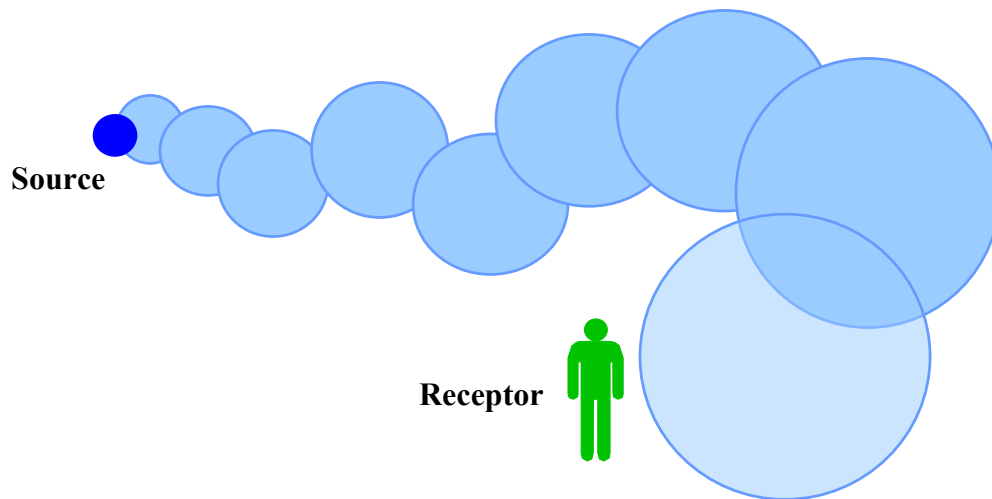


Figure 5. Schematic of Puff Dispersion.

5.1.2 Plume Models

Continuous releases are generally modeled as a plume. The assumption here is that the release time is much greater than the time of travel from the source to the

receptor. There are a number of approaches to modeling plumes, each with its own focus, assumptions, and limitations. These approaches can be categorized as (Hanna et al., 1982):

- Meandering (fluctuating) plume models
- Gaussian plume models
- Probability distribution function (pdf) models
- K models
- Statistical models
- Similarity models
- Second order closure and eddy simulation models

Within these categories are a number of different models. However, not all of the models using these approaches are at a developmental stage where they can be practically applied. Some, like the statistical and second-order closure approaches, are too computer-intensive for routine use. Many of the other model types have little in the way of the field validation needed in order to be confidently applied to real-world situations. The most frequently used types for dispersion model used for odor modeling among the list are the fluctuating plume-puff model and the Gaussian model.

5.1.2.1 Fluctuating Plume-Puff Model

The fluctuating plume-puff model, first developed by Gifford (1960), is a hybrid model that simulates the emissions from a source as a series of continuously emitting puffs. The model assumes that the dispersion is separated into two separate parts: one due to the instantaneous spreading out of the Gaussian plume in the crosswind and vertical directions, and another due to the meandering, or fluctuation of the entire plume around its mean position. Gifford visualized the fluctuating plume as an infinite series of overlapping disks. The model tries to follow the path of the puffs (or disks) of contaminant under the influence of varying wind fields and stability conditions, and attempts to predict the peak concentration as a discrete puff passes a given receptor.

One problem with this type of model is that limited data are available to help in determining the diffusion coefficients, σ_y and σ_z , needed to estimate the spread of the disks. Högström (1972) developed a form of the fluctuating plume-puff model from his field experiments (noted above) to determine the values of the diffusion coefficients. As with most of these types of models, it was assumed that the concentration distribution within the instantaneous plume relative to the centerline to be constant and Gaussian (i.e., fluctuations within the instantaneous plume are not considered).

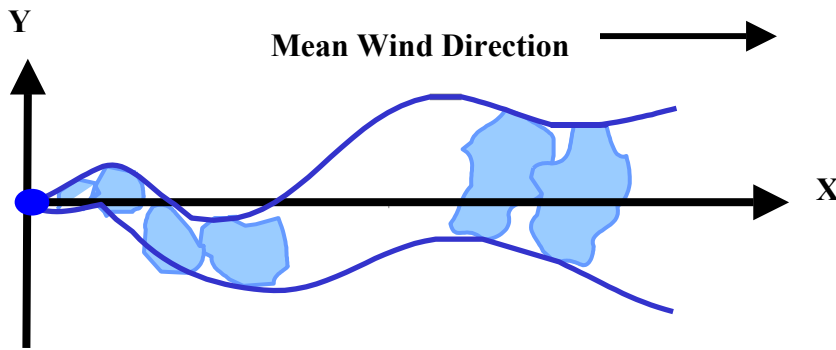


Figure 6. Fluctuating Plume-Puff Model.

5.1.2.2 Gaussian Plume Model

The Gaussian model of diffusion is the most widely used model for atmospheric dispersion modeling. Gaussian models currently used include the Industrial Source Complex - Short Term (ISCST3) model and AUSPLUME. Stable conditions in the AERMOD model are also described in Gaussian terms. One of the most attractive features of Gaussian models is that they were designed to fit what we see and experience in the real world for a range of conditions. In addition, the mathematics of the model is fairly straightforward. On the other hand, Gaussian models need significant empirical input in order to be used for practical dispersion estimates, making the model results highly dependent upon the conditions of the sampling used to derive the empirical values.

The basic assumptions of the Gaussian models are:

- conservation of mass
- continuous emissions
- steady-state conditions
- lateral and vertical concentration profiles follow normal distribution

A problem with the Gaussian model arises because the model assumes a time-averaged distribution in the plume and assumes that the meteorological conditions (including wind direction) are constant during the time required for the plume to travel from the source to the receptor. Under these conditions, results are applicable for time periods from approximately 3 minutes to 1 hour. This time averaging may not fully account for the turbulent concentration fluctuations within the plume, or the meander of the plume from the mean direction. Therefore, using this approach could lead to underprediction of the short-term concentration.

However, Gaussian models have significant advantages. They have been widely applied and modified to consider numerous source types with an assortment of site-specific characteristics, such as terrain and building wake. The ISCST3 model, for example, underwent extensive field-testing and validation so that it has

widespread regulatory approval. In addition, many of the Gaussian models are in the public domain, and the source codes can be obtained from regulatory agencies or through governmental electronic bulletin board systems. This significantly reduces the cost of an odor assessment, and allows the modeler the opportunity to match the model to the specific project.

5.2 Peak to Mean Ratio

In general, most of the concentration and turbulence field data used to determine empirical factors found in many dispersion models are collected over relatively long sampling times (on the order of minutes) because of the difficulty of measuring high-speed fluctuations in the atmosphere. For any fixed sampling time, the mean concentration (mean), which is assumed to remain nearly constant, can be determined. However, as Figure 4 shows, within that long-term sampling time, there may be significant short-term fluctuations. These short-term fluctuations may exceed the mean by as much as two orders of magnitude. If the averaging time of the modeled odor concentration (represented by the “mean” line in Figure 4), is greater than the averaging time of the odor criterion, then the odor level predicted by the model may be an underprediction.

Considerable effort has been spent trying to account for the difference between peak and mean concentration (Gifford, 1960; Singer et al., 1966; Hino, 1968; Islitzer and Slade, 1968; and Pasquill, 1975). Analysis of numerous field data have led to estimates of a “*peak to mean ratio*” for different source/receptor configurations. Once a *peak to mean ratio* appropriate for the project is determined, the averaged model output from the model can be used to estimate a peak concentration. One advantage of this approach is that the analysis retains the benefits of using the more standard dispersion models, which are commonly understood and have regulatory approval, while considering the short-term peak concentration that may be required by the odor assessment.

In those analyses where the model predictions are representative of averaging times greater than the selected odor criterion, many researchers have used a power law relationship to estimate a peak, short-term odor impact. The power law relationship is expressed as:

$$C_p = C_m * (t_p / t_m)^p \quad (1)$$

where,

- C_p = peak concentration
- C_m = mean concentration
- t_p = time period for C_p
- t_m = time period for C_m
- p = empirical constant

The values of p are generally determined empirically. Inoue (1950) postulated that the width of a smoke cloud increased in proportion to the $-1/2$ power of the sampling time, or $C \propto t^{1/2}$. Stewart et al. (1954) and Cramer (1957) reported a $-1/5$ -power law relationship between sampling time and concentration at heights near the height of release for short sampling times. Hino (1968) confirmed the $-1/2$ power law for sampling times between 10 minutes to 5 hours, but noted that the $-1/5$ power law reported by Nonhebel (1960) was valid for sampling times less than 10 minutes.

The concept of peak versus mean concentration has been studied in both the field and the laboratory, and it has been shown that there are a number of factors that must be considered in both (either determining or using such a factor in an odor modeling assessment). Factors such as distance, terrain, stack height, and turbulence-inducing obstructions have all been shown to affect *peak to mean* values.

5.2.1 Effect of Distance

Gifford (1960) studied a series of field studies for an elevated source (stack heights from 24 meters to 108 meters) and found that the ground level *peak to mean* ratio decreased with increasing distance downwind. Plots of the data indicated that the ratio reached its theoretical limit of 1 at some 20 to 50 stack heights downwind. Since distance is associated with increased travel time, it makes sense that atmospheric turbulence has more opportunity to disperse the plume with increasing distance, thus smoothing out the peak concentrations until ultimately, the peak concentration approximates the mean.

5.2.2 Effect of Stack Height

Peak to mean values were found to increase when the stack height increases (Gifford, 1960). Values of the *peak to mean* ratio from 50 to 100 were found to occur at the ground near a moderately tall (50 - 100 meter) stack. However, for sources and receptors at approximately the same height, the *peak to mean* ratio ranged from 1 to 5, at least one order of magnitude lower.

5.2.3 Effect of Elevated Terrain

In their review of field experiments performed at Brookhaven National Laboratory, and three other studies (Meade, 1960; Stewart et al., 1954; and Wipperman, 1961), Singer et al. (1963) concluded that the surface roughness, such as an urban geometry, “practically obliterates all short term fluctuations of concentration depending on the location of the receptor with respect to the source.” This is intuitively clear if we recall that concentration fluctuations are, for the most part, the result of turbulence in the atmosphere. Any physical obstruction that alters or modifies the structure of this turbulence, such as surface roughness, is likely to affect the structure of the concentration profiles.

5.2.4 Effect of Building-Induced Turbulence

Meroney (1982) considered the effects of building wakes on the *peak to mean* ratio. Flow around a simple structure can be divided into three zones: the free flow zone far upwind and downwind of the structure unaffected by the building; the wake zone where the flow recognizes the obstruction and bends around it; and the high turbulent and recirculating cavity wake region, attached to the top, back, and sides of the building. Because the flow must bend to flow around the building, the velocity along the streamlines changes, resulting in a corresponding change in pressure. In general, there is a positive pressure area upwind of the building, and a negative region along the top, sides, and leeward face of the building. This negative pressure entrains pollutants into these recirculation regions, leading to highly concentrated, highly fluctuating flow. It is clear that the location of the source and receptor with respect to these zones will affect the dispersion and resulting concentration.

If a stack emits odorous compounds high above the wake or cavity (i.e., within the free flow region), then there is little or no effect of the building on the dispersion (unless and until the plume intersects the building wake region farther downwind). A slightly lower stack may be affected by the contoured flow around the structure. In this case, the plume will be brought more quickly to the ground than if the structure were not there (i.e., the plume rise will be decreased due to the flow around the building), however, the plume keeps its distinct structure with the highest concentrations along the plume centerline. On the other hand, emissions from a very short stack, or vent, may be partially or entirely captured within the cavity. Due to the complicated flow within the cavity, even ground level sources within the cavity can cause high concentrations on the roof.

Meroney determined that the peak concentration in the wake of a building did not exceed the mean concentration by more than a factor of 2 more than 10% of the time at any reasonable distance downwind of a building. For highly noxious gases, a safety factor of 10 was recommended in order to prevent a specified concentration from occurring more than 1% of the time.

5.2.5 Peak to Mean Factors

If using this peak to mean approach, it is important to understand the timeframe that the mean impact represents. The 1-hour impact predicted by ISCST3 and other similar Gaussian models, for example, actually represented an averaging time of between 3 to 15 minutes (Pasquill, 1975). This is because the empirical data used in this model were based upon sampling times of 3 to 15 minutes (Pasquill, 1975). This added conservatism to the use of such models for regulatory purposes, since the 1-hour average is likely to be lower than the shorter time average, but it can cause confusion when used for odor modeling if the 1-hour impact is converted directly to shorter time averages with the use of a *peak to mean* factor.

Some odor analyses have made the conversion to shorter time averages by first setting the 1-hour output equal to a 15-minute average, and then converting from 15 minutes to a shorter averaging time (e.g., Engel et al., 1997). Others have taken the 1-hour model output as representative of a 1-hour average, and converted that impact directly to the shorter term impact. The Hong Kong Environmental Protection Department Guideline (Hong Kong Environmental Protection Department, 2000) recommends converting the 1-hour modeled concentration to a 3-minute concentration based upon a stability-dependent power-law relationship, then using a conversion factor to go from a 3-minute to 5-second averaging time. Other researchers have reported using a *peak to mean* conversion factor based upon other parameters, such as distance from the source and height of the source relative to the receptor. The CALPUFF model has incorporated the 1/5 power law for use in odor assessment (Scire et al., 2000). Table 3 lists *peak to mean* conversions from recently published odor modeling analyses (Diosey, 2001).

Table 3. Conversion Factors Used for Determining Short-term Impacts.

Time Scale	Conversion Factor	Conversion Method *
5 second	45 to 9	Power law (stability dependent) + conversion factor
30 second	1.97	Modified power law, $p = -0.2$
< 1 minute	6	Power law, $p = -0.30$
2 minutes	2	Power law
2 minutes	---	Power law, $p = -1/5$
3 minutes	4.47 to 1.65	Power law, p is stability dependent
5 minutes	1.7	Conversion factor
5 minutes	---	Power law, $p = 1/5$
5 minutes	2.29	Conversion factor
10 minutes	1.82	Conversion factor
10 minutes	1.35	Conversion factor
1 hour	1	None

6 Summary

Modeling the impact of odors downwind of a source can be performed using many of the same tools used for atmospheric dispersion analysis. However, there are some distinct differences that must be accounted for before proceeding with this approach. One difference is that odors are detected and recognized at timescales that are generally far shorter than the averaging times used in routine air quality analysis. Most standard dispersion models have not been validated for such short averaging times. However, a number of techniques developed to adapt the standard dispersion models for potentially shorter averaging times were discussed. Secondly, odors can be complex mixtures at a given source, can vary from source to source at a given facility, or can become more complex as they are transported downwind. Unlike the specific compounds that are studied in routine air quality analyses, such distinct odors are not necessarily additive at locations downwind of the source(s).

The key to selecting the appropriate odor modeling technique is to understand the objective of the odor analysis, and to understand the characteristics of the site itself. What are the criteria that must be met, what model and modeling techniques offer the best simulation of the odor transport process, and who will be reviewing the analysis. These are all questions that must be determined as part of a practical odor modeling analysis.

References

- AIHA, 1989. *Odor Thresholds for Chemicals with Established Occupational Health Standards*. American Industrial Hygiene Association.
- Cramer, H.E., 1957. A Practical Method for Estimating the Dispersal of Atmospheric Contaminants, in *Proceedings of the Conference on Applied Meteorology*, American Meteorological Society.
- Csanady, G., 1973. *Turbulent Diffusion in the Environment*, D. Reidel Publishing Co.
- Diosey, P.G., 2001. It's A Matter of Time: Odor Modeling and Averaging Time; Paper presented at the 94th Annual Air & Waste Management Association Meeting and Exhibition, Orlando, FL.
- Duffee, R.L. and M.A. O'Brien, 1992. Establishing Odor Control Requirements by Odor Dispersion Modeling; Paper presented at the 85th Annual Meeting of the Air and Waste Management Association, Kansas City, KS.
- Engel, P.L., T.O. Williams, and T. Muirhead, 1997. Utilizing ISCST to Model Composting Facility Odors. Paper presented at the 90th Annual Air & Waste Management Association Meeting and Exhibition, Toronto, Ontario, Canada.
- Gifford, F., 1960. Peak to Average Concentration Ratios According to a Fluctuating Plume Dispersion Model. *Int. J. Air Pollution*, 3, 253-260.

- Hanna, S.R., G.A. Briggs, and R.N. Hosker Jr., 1982. *Handbook on Atmospheric Diffusion*, DOE/TIC-11223; U. S. Department of Energy.
- Hino, M., 1968. Maximum Ground-Level Concentration and sampling Time. *Atmospheric Environment*, 2, 149-155.
- Högström, U., 1964. An Experimental Study on Atmospheric Diffusion. *Tellus*, 16, 205-251.
- Hong Kong Environmental Protection Department, 2000. *Guidelines for Local-Scale Air Quality Assessment Using Models*. <http://www.info.gov.hk/edp>.
- Inoue, E., 1950. On the Turbulent Diffusion in the Atmosphere. *J. Met. Soc. Japan*, 28.
- Islitzer, N.F. and D.H. Slade, 1968. *Meteorology and Atomic Energy*, D. H. Slade, Ed., U. S. Atomic Energy Commission, Office of Information Services.
- Mahin, T., 1997. Using Dispersion Modeling of Dilutions to Threshold (D/T) Odor Levels to Meet Regulatory Requirements for Composting Facilities. Paper presented at the 90th Annual Air & Waste Management Association Meeting and Exhibition, Toronto, Ontario, Canada.
- Mahin, T. and R.J. Pope, 1999. Overview of Different Approaches Used in Odor Regulations and Policies. Presented at the *Water Environment Federation 72nd Annual Conference & Exposition*, New Orleans, Louisiana.
- Malcolm Pirnie, Inc. (2002) Literature Search.
- Meade, P.J., 1960. The Effects of Meteorological Factors on the Dispersion of Airborne Material; *Elettronica e Nucleare*, Rome, July 1959.
- Meroney, R.N., 1982. *Engineering Meteorology*, E. Plate, Ed., Elsevier, Amsterdam, 481-526.
- Nonhebel, G., 1960. Recommendations on Heights for New Industrial Chimneys. *J. Inst. Fuel*, 33, 479-511.
- Ontario Ministry of Environment, 1988. *Procedure for the Determination of Odor Impact Models by the Binary Port Odour Panel Method*. Ontario Ministry of the Environment, Toronto.
- Pasquill, F., 1975. *Some Topics Related to Modeling of Dispersion In Boundary Layer*. Office of Research and Development, United States Environmental Protection Agency, Research Triangle Park, North Carolina. EPA-650/4-75-015.
- Ramsdell, J.V., and W.T. Hinds, 1970. *Atmospheric Environment* 5, 483-495.
- Scire, J.S., D.G. Strimaitis, and R.J. Yamartino, 2000. *A User's Guide for the CALPUFF Dispersion Model (Version 5)*. Earth Tech, Inc., Concord, Massachusetts.
- Singer, I.A., K. Imai, and R.J. Gonzalez del Campo, 1963. Peak to Mean Pollutant Concentration Ratios for Various Terrain and Vegetation Cover. *Air Pollution Control Association*, 13, 1, 40-42.
- Singer, I.A., J.A. Frizzola, and M.E. Smith, 1966. *Journal of the Air Pollution Control Association*, 16, 11, 594-596.
- Slade, D.H., 1968. *Meteorology and Atomic Energy*, D. H. Slade, Ed., U. S. Atomic Energy Commission, Office of Information Services.

Stewart, N.G., H.J. Gale, and R.N. Crooks, 1958. The Atmospheric Diffusion of Gases Discharged from a Chimney of the Harwell Pile (BEPO). *Int. J. Air Pollution*, 1, 87.

USEPA, 1995. *User's Guide for the Industrial Source Complex (ISC3) Dispersion Models. Volumes I and II*. USEPA Office of Air Quality Planning and Standards, Research Triangle Park, North Carolina. EPA-454/B-95-003.

USEPA (Draft), 2000. Guideline Document for Ambient Monitoring of 5-minute SO₂ Concentrations.

Willhite, M.T. and S.T. Dydek, 1991. Use of Odor Thresholds for Predicting Off-Property Odor Impacts, in *Recent Developments and Current Practices in Odor Regulations, Controls and Technology*. Transactions of the Air & Waste Management Association.

Wilson, D.J., 1976. *Contamination of Building Air Intakes from Nearby Vents*. Univ. Of Alberta, Dept. of Mech. Eng. Report No. 1, Edmonton, Canada.

BRANKLEY
PAPER

Freedman, F. 2008. Climate Change - *An Introduction to Atmosphere-Ocean General Circulation Modeling*. Chapter 15C of *AIR QUALITY MODELING - Theories, Methodologies, Computational Techniques, and Available Databases and Software. Vol. III – Special Issues* (P. Zannetti, Editor). Published by The EnviroComp Institute (<http://www.envirocomp.org/>) and the Air & Waste Management Association (<http://www.awma.org/>).

Chapter 15C

Climate Change - An Introduction to Atmosphere-Ocean General Circulation Modeling

Frank R. Freedman

The EnviroComp Institute, Fremont, CA (USA)
freedman@envirocomp.com

Abstract: This chapter provides an introduction to the formulation of Atmosphere-Ocean General Circulation Models (AOGCMs), the state-of-the-art tool for attributing and projecting of earth-atmosphere climate change. The formulation topics summarized in this review include gridding, numerical solution and the parameterizations of physical processes used for both atmospheric and oceanic components. A sampling of the results from attribution and projection studies using AOGCMs, presented in the IPCC Fourth Assessment Report (AR4), are then shown. Sources for further reading are listed at the end of the review.

Key Words: Atmosphere-Ocean General Circulation Models, Coupled General Circulation Models, Climate Change, Numerical Modeling.

1 Introduction

Atmosphere-Ocean General Circulation Models (AOGCMs) are the current state-of-the-art numerical tool for modeling the earth's climate system. They are most encompassing in representing the full suite of important processes affecting climate. By association, they are also the most computationally complex and expensive to run. It has been estimated that a full AOGCM would take between

25-30 person-years to code, and a multi-decadal simulation thousands of computer hours to run¹.

The main application of AOGCMs over recent years has been attribution and projection of climate change² due to the increased atmospheric concentrations of greenhouse gases (GHGs) that have built up over the last century and a half. This concentration increase is primarily made up of carbon dioxide (CO₂), which has built up in concentration primarily due to industrial emissions from fossil fuel combustion³. Attribution of climate change is addressed by running AOGCMs with and without anthropogenic radiative forcing⁴, and comparing the simulated climates resulting from the model runs for each case to the observed climate of the last century. Projection is addressed by investigating the future climates simulated by AOGCMs when run with user-specified levels of future anthropogenic radiative forcing.

AOGCM attribution and projection studies of climate change are published abundantly in peer-reviewed scientific literature, and the body of this work has been summarized in periodic reports by the UNEP International Panel of Climate Change (IPCC) for the purpose of communicating the findings of climate change research to global policymakers. The most recent IPCC report, Assessment Report 4 (AR4), was published in 2007⁵. Among the major findings in AR4 is that climate change since the beginning of the industrial era *is* due to increased anthropogenic GHG emissions and that future climate change *will amplify* assuming that current trends in these emissions persist. Also, it is found that climate change will most likely occur, albeit to a lesser degree, even without any additional future GHG emissions. This has prompted increasingly intense action on the part of policy makers to develop policies to limit future global GHG emissions and/or mitigate the effects of future climate change.

Given this importance, development and application of AOGCMs will grow in the future as the need for updated and more detailed understanding of climate change continues. This chapter is therefore aimed at providing an introduction to AOGCMs. First, the formulation of AOGCMs is summarized. Their evaluation and key results from the climate change attribution and projection studies

¹See Chapter 1 of McGuffie and Henderson-Sellers, *A Climate Modelling Primer*, 3rd Edition, 2005; and Appendix L of Washington and Parkinson, *An Introduction to Three-Dimensional Climate Modeling*, 2nd Edition, 2005.

²The most studied aspect of climate change is the gradual warming of global temperatures over the last century and a half. The term “global warming” has therefore been used synonymously with climate change.

³CO₂ emissions from land-use change and biomass burning are approximately 10% of the contribution from fossil fuel combustion; see Figure 2.3 of the IPCC “Assessment Report 4” (AR4).

⁴The primary components of anthropogenic radiative forcing are those due to increased atmospheric GHG concentrations and increased levels of aerosols, also due to anthropogenic emissions. The concept of radiative forcing is discussed further in Section 3 of this review.

⁵See <http://www.ipcc.ch/> for more details on the IPCC as well as links to AR4.

presented in AR4 are then briefly summarized. Areas where future development is needed as well as literature and weblinks for further reading are then listed.

2 AOGCM Formulation

Much of the material in this section is taken from Washington and Parkinson (2005), which we will hereafter refer to as WP05⁶.

2.1 Basic Equations

AOGCMs are based on the fundamental conservation equations for atmospheric and oceanic motion, mass and heat, along with equations of state for air and water. These equations comprise a coupled set of non-linear partial differential equations requiring numerical solution. This involves discretization of the equations over finite spatial grid volumes and solution of the equations over finite time steps. Finite-difference numerical methods are generally used for the atmospheric component, although some models apply spectral methods horizontally in space. Atmospheric components currently have horizontal spatial grids of approximately $3^\circ \times 3^\circ$, and oceanic components usually less than $1^\circ \times 1^\circ$.

These grid sizes are too large to explicitly resolve all atmospheric and oceanic motions. The effects of these “sub-grid scale” motions must therefore be parameterized in AOGCMs to approximate the effects of these motions on the resolved scale fields. In the atmospheric component, parameterized motions include turbulent and organized buoyant convection. The need for parameterization also extends to processes not involved directly with sub-grid motions, for example radiative transfer and hydrometeor (rain, snow, cloud drops, etc.) formation. The manner of parameterizing these and other processes in AOGCMs is summarized below.

Most AOGCMs now also include representations for the change in mass and aerial coverage of sea ice, as well as a hydrology sub-model to represent the change in the global water balance resulting from changes in the mass of land ice and snow. These are important processes for representing the effects of average earth surface albedo on the climate system as well as for examining the effects of/on climate change on/by the hydrologic cycle.

The formulation and numerical solution procedure for the resolved-scale (also referred to as “core”) equations common to most AOGCMs are presented in detail in Chapters 3 and 4, respectively, of WP05. Summarizing, most AOGCMs are hydrostatic, incompressible and Boussinesq in both atmospheric and oceanic

⁶Washington, W.M. and C.L. Parkinson, *An Introduction to Three Dimensional Climate Modeling*, 2nd Edition, University Science Books, 2005.

components. The equations are solved in the horizontal using spherical coordinates (special treatments are sometimes applied near the poles) and, in the atmospheric component, are solved in the vertical using various “sigma” type terrain-following coordinates. Ocean models employ various vertical coordinate systems, including depth, sigma and isopycnal. Numerical schemes are generally designed to globally conserve all or at least some of the following quantities: energy, mass, vorticity, heat, and moisture.

The atmosphere and ocean components are coupled through the vertical turbulent momentum, heat and moisture fluxes at the atmosphere-ocean interface. These comprise the lower boundary condition for ocean grid columns in the atmospheric component, as well as the upper boundary condition to the ocean component equations. These fluxes are computed by the turbulence parameterizations used in the atmosphere and ocean components.

For land grid columns, turbulent fluxes of momentum, heat and moisture at the land-air interface are computed through coupling the atmospheric turbulence parameterization within the lowest atmospheric grid layer to a land-surface parameterization scheme. The land-surface parameterization is based on the surface energy balance equation with coupling to parameterized equations to represent transfer of heat and moisture through the soil and vegetation canopy layer. Land-surface parameterizations are summarized in more depth below.

2.2 Parameterizations in the Atmospheric Component

2.2.1 Turbulence

Turbulent transport is a fundamental process in geophysical fluid flows. In the atmosphere, it is the primary process by which momentum, heat, moisture and other scalars are transported between the surface and atmosphere. Turbulence is a sub-grid scale motion, and therefore vertical turbulent fluxes must be parameterized. Most of the turbulence important for vertical transport is generated by wind shear and small scale thermal eddies in the lowest couple kilometers of the atmosphere, a layer called the “atmospheric boundary layer”. Turbulence schemes in atmospheric models are therefore also called “boundary-layer” schemes.

Vertical turbulent fluxes are parameterized in AOGCMs in a manner analogous to Fickian diffusion,

$$\text{Vertical turbulent flux of quantity “a”} = -K_a \partial A / \partial z \quad (1)$$

where z is used for the vertical coordinate and K_a is called the “eddy-diffusivity” for the arbitrary variable a . For momentum, the quantity is also called the “eddy-viscosity”. The rate of change of A due to turbulent transport is then the vertical flux-divergence of Equation 1.

Whereas molecular viscosity and diffusivities are essentially constant for typical atmospheric conditions, eddy-viscosity and diffusivities vary in time and space according to the local flow properties and density stratification of the background fluid. This leads to complex formulations for K_a , which, although having evolved over the years to a high degree of accuracy for common prototypical boundary-layer flow regimes, are still in an active state of research for more complex atmospheric situations. One important example is the strong interactions of flow and stratification with moisture and radiation fields involved in predicting stratocumulus cloud coverage over oceans. Marine stratocumulus prediction by AOGCMs is one of their biggest uncertainties^{7,8}.

2.2.2 Cumulus Convection

Whereas vertical turbulent fluxes in the atmosphere are due to relatively small or intermediate scale turbulent motions confined to the boundary layer, organized convective vertical motions due to strong buoyant instability can penetrate through the boundary layer and encompass the entire troposphere. Such motions are triggered by a combination of (a) surface forcing, for example surface heating or flow convergence near the surface, which initiates updrafts and (b) density instability, either absolute or conditional, which maintains vertical acceleration of updrafts once initiated. Such motions lead to cumulus cloud formation, and therefore organized convection is synonymously called “cumulus convection”. The main physical role of cumulus convection in the atmosphere is the vertical redistribution (“overturning”) of heat and moisture during times of density instability. The main mechanism for heat transfer is the latent heat release at higher levels in the troposphere by the cumulus cloud field. Important cumulus convection on the climatic scale occurs over the tropics due to trade-wind convergence. The persistent occurrence of this process over the tropics is one of the main drivers to the earth’s climate system.

Cumulus scale eddies are sub-grids in AOGCMs, and therefore the effects of cumulus convection on the resolved scale temperature and moisture fields must be parameterized. A variety of schemes exist, the basis of the main ones described in detail in Chapter 3 of WP05. The simplest scheme is the “convective adjustment” type, which simply resets the modeled vertical temperature and moisture profiles to theoretically or otherwise observationally constrained pre-set values during times when the resolved scale temperature profile is unstable. For temperature, for example, the pre-set value could be dry or moist adiabatic, or some other value determined from observations of cumulus cloud fields. More complex schemes are of the “mass flux” type, which attempt to parameterize cumulus convection according to the average vertical mass fluxes of individual updraft and downdraft

⁷Zhu et al., 2005, “Intercomparison and Interpretation of Single-Column Model Simulations of a Nocturnal Stratocumulus-Topped Marine Boundary Layer”, *J. Atmos. Sci.*, **133**, 2741-2758.

⁸Randall et al., 2003, “Confronting Models with Data: The GEWEX Cloud Systems Study”, *Bull. Am. Meteorol. Soc.*, **84**, 455-469.

cumulus cloud ensembles. The heat and moisture transport linked to each ensemble presents the main closure problem, and requires empiricism. Mass flux schemes are generally preferred due to their better appeal on physical grounds, as well as by the tendency of convective adjustment schemes to predict too much condensation in the upper troposphere.

2.2.3 Resolved-Scale Clouds

AOGCM results are very sensitive to their parameterization of cloud coverage, particularly stratocumulus. Clouds affect climate primarily through their feedbacks on the radiation balance. Clouds block sunlight as well as absorb and reemit longwave radiation back to the surface. Since these feedbacks are large and in opposite direction, the magnitude and sign of the cloud feedback computed by AOGCMs is still a matter of great uncertainty, with the different results produced by AOGCMs most likely due to differences in the details in the models' parameterizations of the process. The parameterization of clouds involves predicting their aerial coverage, hydrometeor type, height and optical thickness. All of these factors strongly affect the radiation field.

In modeling, “resolved-scale” clouds occur when the resolved-scale temperature and water vapor values in an AOGCM grid box are such to lead to saturated conditions. In theory, saturation occurs at 100% relative humidity, yet models tend to use a lower threshold value (~ 90%) based on observations that complete cloud coverage occurs at slightly sub-saturated conditions. Partial cloud coverage is assumed to occur starting at even lower relative humidity (~ 60%). Equations for fractional aerial coverage of clouds within a grid box are formulated in such a way as to monotonically increase cloud coverage as relative humidity increases between these two threshold values. Once the cloud coverage at each level in a given vertical model column is obtained, the total aerial cloud coverage can in turn be obtained. The possibility of overlapping clouds at different grid layers is accounted for in this step.

Resolved scale clouds tend to form in locally stably-stratified conditions, and are therefore also called “stratiform clouds”. Such clouds include tropospheric stratus and cirrus, as well as boundary-layer stratocumulus when mean conditions within the boundary layer are saturated at some vertical level within the boundary layer. “Resolved” stratocumulus is most common in primarily shear-driven marine boundary layer regimes.

More sophisticated schemes employ equations for aerial cloud coverage involving the grid-volume liquid water and ice content, rather than or in addition to relative humidity. Such schemes are used in conjunction with microphysical parameterizations, which are discussed below.

2.2.4 Sub-Grid Scale Clouds

Even though the resolved-scale moisture field may not be saturated, a portion of a model grid volume may still be cloudy due to sub-grid scale convection. This is the situation, for example, during unstable conditions when cumulus clouds form. Cumulus parameterizations, discussed above, must therefore output the amount of cloud coverage within and precipitation falling out of the vertical grid column due to cumulus processes. This is generally done through empirical equations relating cloud volume and precipitation to some property of cumulus convection involved in the closure. For example, for mass-flux schemes the cloud volume and precipitation could be related to the total upward mass-flux associated with the updraft, which, in turn, is parameterized empirically in this approach⁹.

In addition to cumulus, boundary-layer stratocumulus clouds also have an unresolved component since some of the turbulent updrafts in a given vertical column could reach saturation within the boundary-layer. Such conditions are common in primarily buoyantly-driven marine boundary layer regimes. Parameterization of cloud processes in this case is done through inclusion of additional empirically based equations in the turbulence parameterization¹⁰.

2.2.5 Radiation

The parameterization of radiation in AOGCMs is aimed at obtaining the total radiative flux (integrated over all wavelengths and incident directions) at each grid level in a vertical model column, including the surface. From this, the incident net radiative flux at the surface can be computed for use in the surface energy balance equation, employed in the land-surface parameterization, and to obtain the radiative heating rate at each vertical level of the atmosphere.

Schemes of various complexities have been developed to achieve this. In all schemes, solar (“shortwave”) and terrestrial (“longwave”) radiation are parameterized separately. This is because solar radiation is primarily in the ultraviolet and visible portions of the radiative spectrum and terrestrial radiation is primarily in the infrared part of the spectrum. Solar radiation is primarily affected by scattering of radiative energy by the surface, atmospheric gases and hydrometeors. Solar radiation is also affected by ozone absorption in the stratosphere and by water vapor absorption of near-infrared wavelengths within the troposphere. Terrestrial radiation is instead affected mainly by absorption by atmospheric gases and hydrometeors. Parameterizations of these scattering and absorption processes are the central part of radiation parameterizations. See

⁹ For further details, see Chapter 9 of Pielke, R. A., *Mesoscale Meteorological Modeling*, 2nd Edition, Academic Press, 2002.

¹⁰ See references in footnotes 6 and 7. In addition, see Lock, A., and J. Mailhot, 2006, “Combining non-local scalings with a TKE closure for mixing in boundary-layer clouds”, *Bound.-Layer Meteorol.*, **121**, 313-338, and references therein.

Appendix J of WP05 and Pielke (2002, see footnote 9) for a review of some of these parameterizations.

Another important aspect of radiation schemes is that the radiative calculations are not done at each individual wavelength (“line-by-line”), since this would involve overly burdensome computational expense. Instead, radiation schemes define radiative properties (absorptivity, reflectivity, emissivity) across discrete wavelength “bands” over which the variation of properties is small enough to achieve robust averages across the bands. This can require many bands, given the strong line-by-line variation of properties over many parts of the radiative spectrum.

Major absorbing gases in the atmosphere accounted for in AOGCMs radiation parameterizations are water vapor (near-infrared and infrared), carbon dioxide (infrared), methane (infrared), ozone (ultraviolet and small part of infrared), nitrous oxide and CFCs. Account is also taken for scattering and absorption by hydrometeors (cloud drops, snow, rain, and ice) as well as by natural and anthropogenic aerosols, the latter discussed in more depth below. Obtaining sufficiently detailed knowledge of the radiative properties of clouds and aerosols for use in radiation parameterizations is one of the major areas of future development need in AOGCMs.

2.2.6 Cloud Microphysics and Precipitation Processes

Cloud microphysics encompasses the processes involved in the formulation of hydrometeors (e.g., cloud and rain drops, snow and hail). Given the increasingly realized importance of hydrometeor type on the radiation field, as well as the desire to include more direct coupling of climate to the hydrologic cycle, most AOGCMs include parameterizations to calculate the amount of water mass contained in various hydrometeor types.

Most microphysics schemes are “bulk” schemes, that is, they do not attempt to calculate the size distribution of a given hydrometeor, but only its total mass integrated over all sizes. They also categorize the water mass across a limited set of hydrometeor types. Common bulk parameterizations calculate the total mass of four hydrometeor types: cloud liquid water, cloud ice, rain and snow. Resolved scale fields for each of these are calculated through prognostic equations. Sub-grid values are calculated diagnostically within the cumulus parameterization and turbulence parameterization, as discussed above.

The mass of water within these hydrometeor classes at each model grid volume is then passed to the radiation parameterization.

2.2.7 Land-Surface Processes

Differential surface heating from equator to pole is the primary driver of climate. Surface heating results in a partitioning of input radiative energy absorbed at the surface into upward directed sensible heat and latent heat fluxes. The sensible and latent heat fluxes provide the heat to the atmosphere responsible for driving climatic wind circulations. Associated with the latent heat flux is water vapor flux, which is the driver of the global atmospheric water vapor, cloud and precipitation fields. Proper representation land surface processes is therefore of utmost importance for accurate climate prediction.

The primary role of the land surface parameterization is, given an incident amount of net radiative flux absorbed at the surface, to properly partition this flux into the correct amount of sensible and latent heat flux. To do this accurately, land surface models must represent a number of processes associated with the transport of heat and moisture transport through soil and vegetation. The scheme must also be coupled to the atmospheric turbulence parameterization to provide proper coupling to atmospheric wind, temperature and humidity near the surface.

Land surface schemes are all based on the surface energy budget equation,

$$0 = R_n - H_s - H_l - G \quad (2)$$

where R_n is net radiation, H_s is the sensible heat flux, H_l is the latent heat flux, and G is the ground heat flux. R_n is computed by the radiation parameterization. The remaining fluxes - H_s , H_l and G - necessitate representations for soil, vegetation heat and moisture transport. Such representations are strongly dependent on soil heat and moisture transfer coefficients. These, in turn, depend strongly on soil moisture content, which is generally a prognostic variable computed over a finite-differenced soil layer incorporated into the model. The linkage between the land surface and precipitation parameterization, which determines the climatic soil moisture fields, is therefore an important coupling in AOGCMs. Further details of the sensitivity of climate projections to the soil moisture field can be found in Chapter 8 of the IPCC AR4 report¹¹.

Other important roles of the land surface parameterization include the calculation of the amount and fractional aerial coverage of snow cover in each surface grid box, which is important in calculating surface albedo, as well as the calculation of land surface carbon dioxide uptake. The latter will be an issue of increasing importance in the future as more AOGCMs employ representations of the carbon cycle in their future climate projections.

¹¹ <http://ipcc-wg1.ucar.edu/wg1/wg1-report.html>.

2.3 Ocean Component

2.3.1 Basic Formulation

The basic equations of the ocean component of an AOGCM are similar to the atmospheric component. The ocean model is formulated based on the standard conservation equations for momentum, heat and salinity, with the hydrostatic, incompressible and Boussinesq assumptions applied. An equation of state, analogous to the ideal gas law, is applied that relates density, pressure, temperature and salinity. The equations are solved numerically, usually using spherical coordinates in the horizontal, and height, sigma or isopycnal coordinates in the vertical. In some models, the computational pole is shifted to a location over land (usually in Northern Canada) to allow for better numerical treatment of the Arctic Ocean. Further discussion of these issues can be found in WP05.

2.3.2 Parameterizations

The number of parameterized processes involved in the ocean component is far less than in the atmospheric component, largely because radiation effects are much simpler and there is no need for cloud parameterization. The main parameterizations are turbulent transport and mesoscale motions. Turbulence parameterizations in the ocean component are generally first-order closures, similar to those discussed above in connection to the atmosphere component. Accuracy of the turbulence parameterization in ocean models has proved important, since one of its primary roles is to maintain proper vertical structure and depth of the ocean-mixed layer, which controls many important oceanic circulations.

Mesoscale circulations in the ocean are forced baroclinically (i.e., due to horizontal density gradients). The numerical grid in the ocean components of AOGCMs often does not resolve such circulations. A mesoscale contribution to the velocity components is therefore added to the resolved velocity to account for mesoscale transport. The mesoscale contribution is related to the resolved scale density gradients.

2.3.3 Linkage to Atmospheric Component

The ocean and atmospheric components are coupled through the vertical momentum, heat and water fluxes at the ocean-atmosphere interface. Ideally, the momentum and heat fluxes at the surface, produced as the lower boundary condition to the atmospheric model, would serve identically as the upper boundary conditions to the ocean model. Older versions of most AOGCMs (and current versions of some), however, have mitigated the effects of climate drift in their long-term climate simulations by applying artificial surface flux terms to the ocean model, a procedure called “flux-adjustment”. Certainly, this is not a desirable feature of these AOGCMs, and fortunately, most models have now

improved their formulations and initialization schemes to the point where flux adjustment is no longer needed.

2.4 Sea-Ice Component

Most AOGCMs have algorithms to predict the aerial coverage and depth of sea ice. The amount of sea-ice affects many important feedbacks on the climate system, most importantly the ice-albedo feedback, whereby reduced ice coverage caused by induced warming would allow an increased amount of solar radiation to be absorbed by the earth's surface, thereby leading to more warming.

The amount of sea ice within a given surface grid volume in the ocean is determined by parameterizing the energy balance across that volume, accounting for radiative inputs, turbulent heat transfer from the atmosphere to the surface, latent heating or cooling (due to evaporation, sublimation, freezing, melting, etc.), heat transfer across the lower and horizontally-adjacent ice-ocean interfaces, and heat transfer through the ice layer. These parameterizations account for cases where the ice is overlaid with snow.

Some models, furthermore, couple this thermodynamic treatment with a dynamic model in which the ice is allowed to move due to interactions with ocean currents as well as oceanic and atmospheric shear stresses. Some models furthermore incorporate parameterizations to allow for fractional aerial coverage of the ice over a grid surface (i.e., allowing for the existence of leads).

See Chapter 3.9 of WP05 for additional details on sea-ice modeling in AOGCMs.

2.5 River Hydrology Component

Some AOGCMs now include formulations to represent transport of fresh water into the oceans from continental river basins. This is important, for example, in determining ocean mixed layer salinity, which in turn impacts ocean circulations.

Continental regions are divided into distinct river basins. In each continental grid square, the inflow and outflow of river water as well as the amount of surface water runoff is computed. River inflow and outflow depend on the topography gradient across this and neighboring grid squares. Surface runoff is computed by coupling to the land surface parameterization as described above.

See Chapter 3.10 of WP05 for additional details on river hydrology modeling in AOGCMs.

2.6 Coupling to Carbon Cycle

To achieve more fundamentally based climate change projections, AOGCMs are beginning to implement models for land and ocean CO₂ exchange with the atmosphere. This allows for interactive coupling between climate change and the carbon cycle, since land and ocean carbon uptake is dependant on temperature as well as the amount of CO₂ accumulated in the land and oceans.

An example of a carbon cycle module is that of Doney et al. (2006)¹². Here, CO₂ concentration is a prognostic variable, transportable within the atmosphere by mean advection and turbulence. The lower boundary conditions are the fluxes into and out of the land and oceans (four terms), which must be parameterized. The land fluxes involve uptake by plants (net primary productivity) and release to the atmosphere by respiration and decay. These fluxes are the total of individual components for various carbon pool sources, corresponding to, among other things, leaves, roots, wood as well as various classes of “dead” plant matter that release CO₂ over time. The coefficients and time scales used in the parameterization of each of these processes are empirically based. The land-surface model, discussed above, provides land surface characteristics (plant and soil types), as well as the atmospheric turbulent transfer coefficients needed for surface-to-atmosphere CO₂ fluxes.

Fluxes into and out of the ocean involve parameterizations of biogeochemical processes of ocean CO₂ uptake (solubility and uptake by ocean biota). This module is coupled with the ocean component for transport of CO₂ into the deeper ocean layers. As with the land fluxes, empiricism is employed to obtain various transfer coefficients and time scales associated with biogeochemical CO₂ uptake in the ocean.

2.7 Interactive Aerosols

Naturally occurring aerosols in the atmosphere include sea salt, sand and mineral dust. Anthropogenic aerosols include sulfate and black carbon. The current understanding is that the presence of anthropogenic aerosols provides an important negative radiative forcing on the earth's climate relative to pre-industrial conditions through the direct and indirect (through their role as cloud condensation nuclei) effects of these aerosols on back-scattering solar radiation. This negative forcing partially offsets the positive forcing associated with GHG concentration increases. Up until recently, AOGCMs incorporated the effects of anthropogenic aerosol scattering simply by increasing the surface albedo of each surface grid square by an amount consistent with observed estimates of vertically integrated sulfate aerosol optical depth. However, AOGCMs are beginning to implement algorithms to interactively predict atmospheric aerosol concentrations

¹² Doney, S.C., K. Linsey, I. Fung and J. John, 2006: “Natural Variability in a Stable, 1000-year Global Coupled Climate-Carbon Cycle Simulation”, *J. Climate.*, **19**, 3033-3054.

across a range of important species. These concentrations are then passed to the radiation parameterization.

Aerosol modules can be classified according to the manner in which they represent various properties and processes associated with aerosols. Bulk schemes only predict the mass of a given aerosol species, whereas “modal” or “bin” schemes represent the size distribution of these species through either predicting parameters associated with prescribed algebraic distribution equations (“modal”) or by computing aerosol concentration in a finite number discrete size bins (“bin”). “External” schemes do not allow mixing of individual aerosol components, whereas “internal” schemes allow such mixing. Schemes also vary according to the degree and manner by which they represent removal processes (dry and wet deposition, sedimentation), interaction with the hydrometeor field (important in modeling the effects of aerosols on clouds), nucleation and coagulation. Advanced models also employ SO₂ rate equations to allow for a better fundamental treatment of sulfate formation.

Further details of several aerosol modules used in AOGCMs, along with an inter-comparison of several schemes, can be found in Textor et al. (2006)¹³. Also, the AERONET surface lidar observational network, which has been implemented at over 150 sites globally to monitor the concentration and optical properties of aerosols, is described in this paper and in Kinne et al. (2006)¹⁴.

3 Applications of AOGCMs

The primary application of AOGCMs in recent years has been the attribution and projection of climate change resulting from the increased concentrations of greenhouse gases (GHG) in the atmosphere over the last century and a half. These applications have been summarized since 1988 in a series of UNEP-IPCC “Assessment Reports”, the most current being Assessment Report 4 (AR4), which was published in 2007 (see footnote 5). Here, a small portion of the results of the AOGCM climate change attributions and projection studies of AR4 are presented. The complete presentation can be found in AR4¹⁵.

Before proceeding, it is helpful to review a few concepts involved in climate change research:

- **Climate Forcing** – The change in net equilibrium radiative energy (expressed in watts per meter-squared) input to the earth-atmosphere system (EAS) caused by some prescribed change in a chosen radiative

¹³ Textor, C. et al., 2006, “Analysis and Quantification of the Diversities of Aerosol Life Cycles within AeroCon”, *Atmos. Chem. Phys.*, **6**, 1777-1813.

¹⁴ Kinne, S. et al., 2006, “An AeroCon Initial Assessment – Optical Properties in Aerosol Component Modules in Global Models”, *Atmos. Chem. Phys.*, **6**, 1815-1834.

¹⁵ <http://ipcc-wg1.ucar.edu/wg1/wg1-report.html>.

forcing agent (e.g., GHGs, aerosols, solar energy, among others). Positive forcing occurs when the change in net radiation is positive (increased energy to the EAS), and negative forcing occurs when the change in net radiation is negative (decreased energy to the EAS). Climate forcing is generally computed at the tropopause.

- Climate Feedbacks – Physical processes that occur in the EAS as a result of climate forcing that either enhance or suppress the change in globally-averaged temperature caused by the climate forcing. Positive feedbacks are those processes that enhance the temperature change induced by the forcing (i.e., enhanced warming as a result of positive climate forcing, enhanced cooling as a result of negative forcing), while negative feedbacks are those processes that suppress the temperature change induced by the forcing (offsetting cooling as a result of positive forcing and offsetting warming as a result of negative forcing).
- Climate Sensitivity – The change of some EAS property per unit climate forcing after the EAS re-achieves equilibrium subsequent to the prescription of some climate forcing. The new state of equilibrium in the EOS subsequent to forcing is a result of both the forcing itself, and the feedbacks caused by the forcing. Most commonly, the chosen quantities to define climate sensitivity are the equilibrium globally-averaged surface temperature change due to a doubling of atmospheric CO₂ concentration relative to pre-industrial times. Most AOGCMs have climate sensitivities in the range of about 2 to 4.5 °C for a doubling of CO₂, a range that has stayed very consistent over the years of climate model development. This range is generally consistent with observationally-based estimates¹⁶.

The above definitions are conceptual. More formal definitions and other details related to climate forcing, feedbacks and sensitivity can be found in AR4 and references therein.

3.1 AOGCM Evaluation

AOGCM evaluation has traditionally focused on the ability of the models to simulate broad climate features, for example the latitudinal variation of surface temperature, pressure and precipitation patterns associated with the general circulation. AOGCMs are reasonably successful on this level. For example, the global distribution of the 1980-1999 average surface temperature as predicted by the contributing AOGCMs in AR4¹⁷ is shown in Figure 1. Figure 1a shows color contours of the difference between the model-mean (i.e., the average of all models) predictions versus observations, while Figure 1b shows color contours of the root-mean square of the difference between each model prediction individually versus observations. It is seen that in most parts of the globe, errors are within a couple degrees Celsius. Greater errors are seen in areas of high

¹⁶ See Chapters 8.6 and 9.6.2 of AR4 for further discussion.

¹⁷ There are 23 AOGCMs that contributed results to AR4, as listed in Table 8.1 of the report.

latitudes as well as on the eastern sides of the southern oceans, the latter probably due to problems in model representations of stratocumulus cloud. The fact that greater errors are exhibited in the root-mean square of the individual model error (Figure 1b) is an indication of a tendency that has been seen over the years in AOGCM analysis for the average of AOGCM predictions, as taken among models, to have better predictive skill than that of any individual model.

The successful prediction of the global surface temperature distribution is associated with successful prediction of zonally-averaged net (upward minus downward) shortwave and longwave radiation at the top of the atmosphere (Figure 8-4 in AR4), which have errors of 6% and 5% in multi-model mean, respectively. Correct zonal distribution of input radiation implies basically correct general circulation features, which largely control the zonally-averaged surface temperature distribution.

The global distribution of 1980-1999 average precipitation as predicted by the contributing AOGCMs in AR4 is shown in Figure 2. Figure 2a shows color contours of the observations, while Figure 2b shows color contours of the multi-model mean prediction. The broad expected features of the global precipitation pattern are reproduced by the models, with local maxima in the tropics and mid-latitudes, and local minima in the sub-tropics and poles. Again, this points to the model's ability to capture the overall general circulation. Deficiencies lie mostly in equatorial regions, where the models tend to underpredict precipitation, and in the southern-hemisphere oceans at mid-latitudes, where precipitation is overpredicted. The weaker skill in equatorial precipitation is probably related to problems in the ability of models to represent organized convective motions, which are parameterized in AOGCMs.

The model evaluation presented in AR4 goes much beyond evaluation of basic general circulation features. Additional focus is on inter-annual variability, frequency of El Nino events, spatial variability, the frequency of extreme weather events, the strength of semi-permanent regional scale climate features (e.g., the Indian Monsoon), among other aspects of the climate system. Less skill and greater differences from model to model are exhibited on this level, although there has been predictive improvement in several of these areas since TAR (Third Assessment Report, 2001). The observational database has a higher degree of uncertainty compared to that for basic general circulation features. Such a detailed evaluation is important because it more directly elucidates the skill of climate models to represent particular processes than would be the case if only broad features were focused on. This is particularly important in evaluating the skill of a model to represent important climate feedbacks, which are associated with individual processes. Also, the details of climate regarding temporal and regional variability are arguably more relevant for practical purposes, since people experience weather and climate at a local level.

3.2 AOGCM Attribution Studies

3.2.1 Climate Forcing

AOGCM attribution studies of climate change require specification of the temporally varying climate forcing for all important forcing agents since the beginning of the industrial era (circa 1750). The values of climate forcing for the main processes affecting global climate change are shown in Figure 3 for one of the AOGCMs used in the AR4, while Figure 4 shows a similar graph for the model used by Hansen et al. (2005)¹⁸. It is seen that the primary positive climate forcing is GHGs (labeled LLGHG in Figure 3), which results primarily from industrial emissions of CO₂. There is a high degree of confidence in the estimated GHG forcing values¹⁹.

The primary negative forcing is tropospheric aerosols, which is divided into “direct” (Aerosol Direct and Reflective Tropospheric Aerosols on figures) and “indirect” (Cloud Albedo and Aerosol Indirect Effect on figures) contributions. It is seen that there appears to be large differences in the values assigned to aerosol forcing (particularly the direct contribution) between the two shown models. The level of uncertainty of aerosol forcing is high, which is especially problematic considering the sensitivity of model results to the value of this forcing. The findings of Knutti et al. (2002)²⁰, in fact, suggest that AOGCMs with a variety of different climate sensitivities can produce surface temperature trends consistent with observations as long as aerosol forcing is allowed to vary within its range of uncertainty. Clearly, this prompts the need to better understand aerosol forcing.

3.2.2 Results of Attribution Studies

Surface temperature predictions of AOGCM simulations incorporating anthropogenic and natural forcing versus those incorporating only natural forcing are shown in Figure 5. The temperature warming experienced over the 20th century is predicted accurately when applying both anthropogenic and natural forcing, whereas the warming is not reproduced when only natural forcing is included. This is the most direct manner by which AOGCMs positively attribute the warming of the 20th century to increased GHG emissions.

Such attribution has also been shown through “fingerprint” analyses (see AR4, Section 9.4.1.4). Here, it is shown that the results of runs employing only GHG forcing explain the most variation in the 20th surface temperature trend compared

¹⁸ Hansen et al., 2005, “Earth’s Energy Imbalance: Confirmation and Implications”, *Science*, **308**, 1431-1435.

¹⁹ Figure 2-20 of AR4 shows the degree of scientific understanding assigned to various climate forcings.

²⁰ Knutti, R., T.F. Stocker, F. Joos, and G.-K. Plattner, 2002, “Constraints on radiative forcing and future climate change from observations and climate model ensembles”, *Nature*, **416**, 719–723.

to runs employing only natural or other forcing agents individually. By applying forcing individually, the result is free of the spurious correlation to observations that can occur in runs employing all forcings together, which can be subject to error cancellation. The use of fingerprint analysis is therefore an important exercise given the large uncertainties in aerosol forcing.

The predicted versus observed surface temperature trends over the individual continents, as well as over land versus ocean, are shown in Figure 6. It is seen that anthropogenic forcing is necessary for AOGCMs to reproduce global warming.

Other investigated topics in the AR4 AOGCM attribution study are contained in Chapter 9 of AR4. These topics include analyses of extreme events, tropical storm activity, ocean heat content and precipitation trends.

3.3 AOGCM Projection Studies

AOGCM projection studies of future climate change are commonly designed by specifying a prescribed change in atmospheric GHG concentration and evaluating model results over approximately 100 years of future projected time. The AR4 multi-model mean surface temperature projections from this exercise are shown in Figure 7. Projections are made for four cases: a constant future GHG concentration at the current-day level, and cases of “low” (B1), “medium” (A1B) and “high” (A2) future GHG emission increases²¹. As shown, the AOGCMs project further warming in all cases, even for the case of constant GHG concentrations. In the cases with future specified emissions, the amount of warming is projected to be greater than that already experienced during the 20th century.

The zonal distribution of future projected warming and precipitation change are shown in Figure 8. Results are shown for the “commitment” run (constant GHG concentration at current-day level) and “high” emission case, A2. The changes plotted are for the 2080-2099 projected means relative to the 1980-1999 simulated mean and scaled according to the globally-averaged change for each case. Model projections show that the abundance of future warming will be in high-latitudes in the Northern hemisphere. Increased precipitation is projected at these latitudes alongside this warming. Warming is spread more uniformly at other latitudes. Increased precipitation over the tropics and decreased precipitation over the sub-tropical latitudes is projected.

²¹ The design of these runs corresponds to estimated emissions resulting from purely economic considerations in determining future emissions (“low”, A2) to purely environmental considerations in determining emissions (“high”, B1). Case A1B is intermediate between these two. See <http://www.climate.unibe.ch/jcm/doc/emit/sres.html> for more details.

4 Future Development Needs and Further Readings

Areas of future development need in AOGCMs touched upon in this paper include the following:

- Better treatment of cloud processes, particularly relating to cumulus and stratocumulus cloud formation. This will potentially lead to better precipitation projections and more constrained evaluation of cloud feedback processes in AOGCMs.
- Better understanding of aerosol physics, including both their optical properties and processes determining their formation and size distribution. This will lead to more constrained evaluation of tropospheric aerosol forcing in AOGCM attribution and projection studies.

In addition to references already cited in this paper, the following websites provide other useful information on the topics of climate change and AOGCM modeling:

- The Intergovernmental Panel and Climate Change: <http://www.ipcc.ch/>
- Real Climate: <http://www.realclimate.org/>
- Website of Professor Steven Schneider: <http://stephenschneider.stanford.edu/>
- Website of Professor Roger Pielke: <http://climatesci.colorado.edu/>

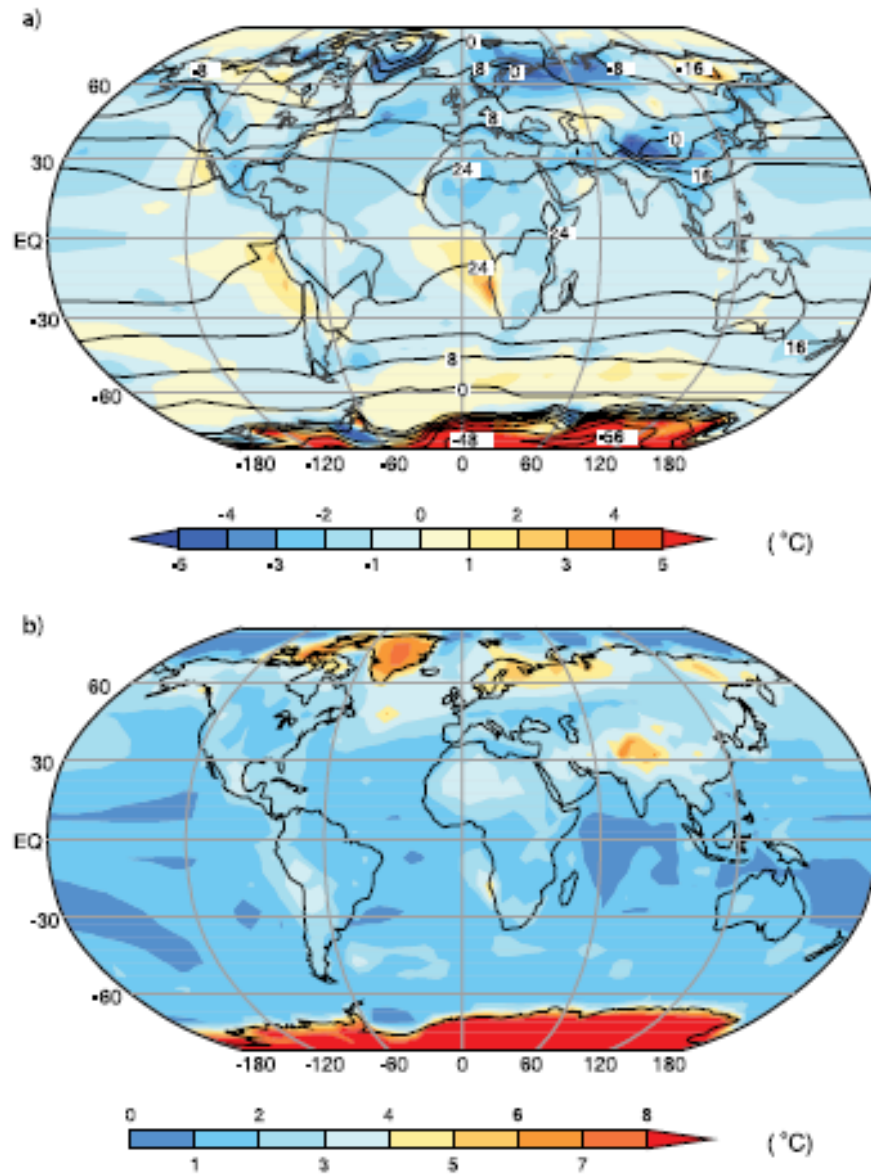


Figure 1. Figure 8.2 of AR4, showing predicted vs. observed surface temperature by the contributing AOGCMs in AR4. In (a), the solid-line contours are the observations, while the color contours are differences between the model-mean prediction vs. observations. In (b), the color contours are of the root-mean square of the difference between each model prediction vs. observations. See AR4 for more details.

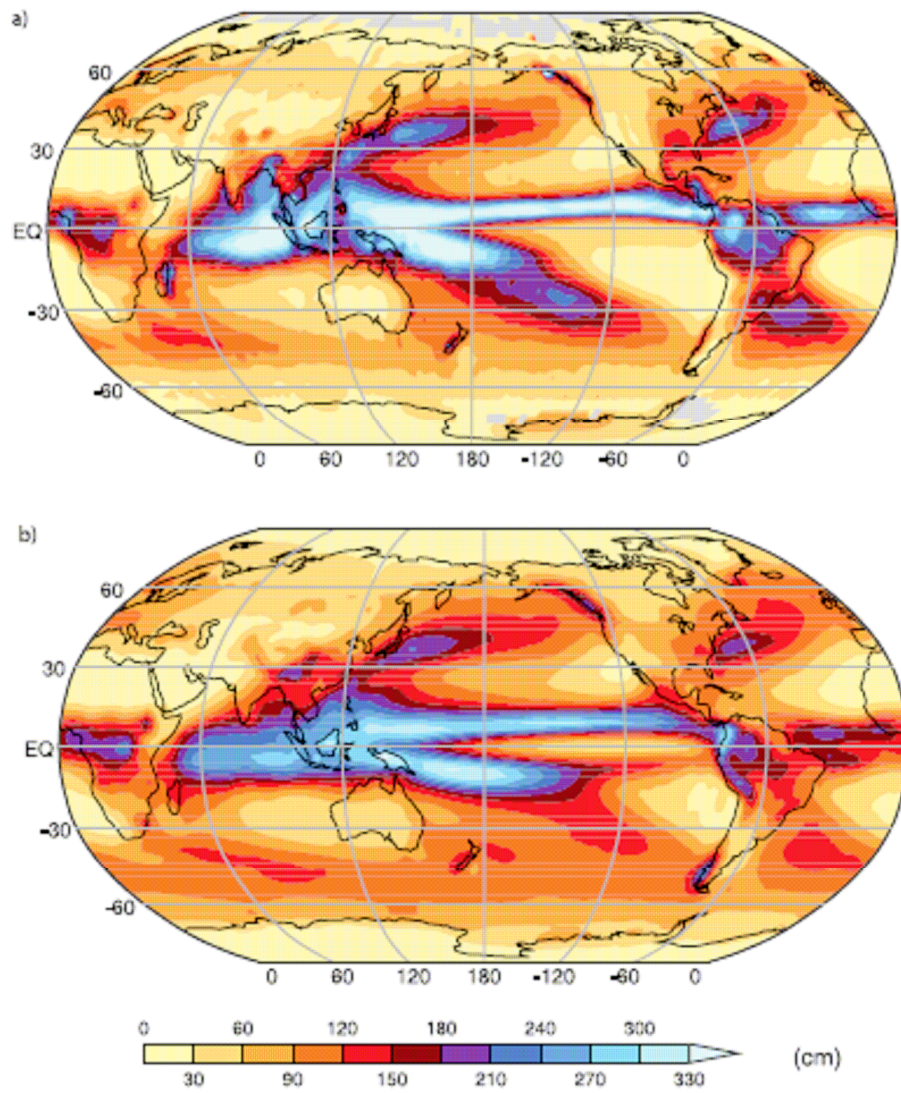


Figure 2. Figure 8.5 of AR4, showing (a) observed and (b) predicted precipitation by the contributing AOGCMs in AR4. See AR4 for more details.

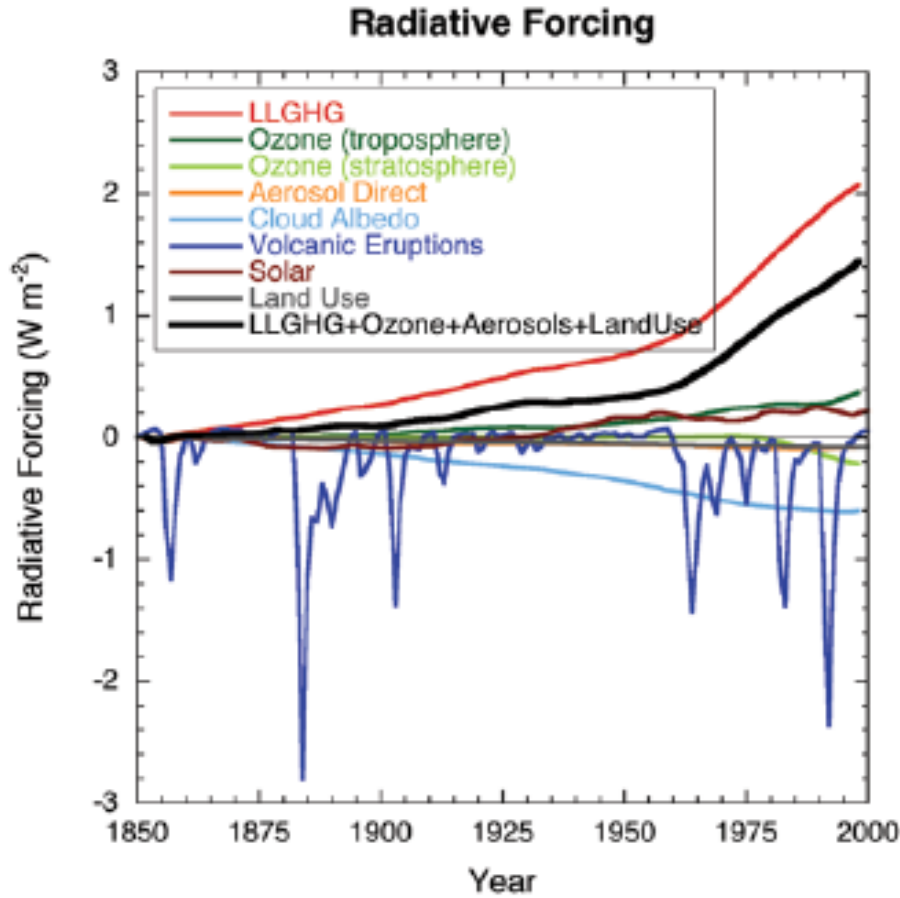


Figure 3. Figure 2.23 of AR4, showing the time-variation of radiative forcing used in one of the contributing models in AR4.

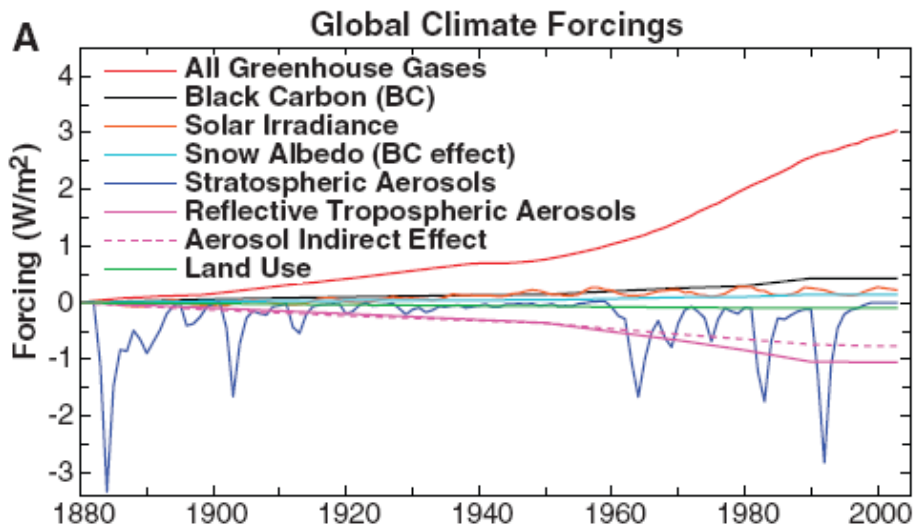


Figure 4. Figure 1 of Hansen et al. (2005, see footnote 18), showing the time-variation of climate forcing used in their AOGCM simulation.

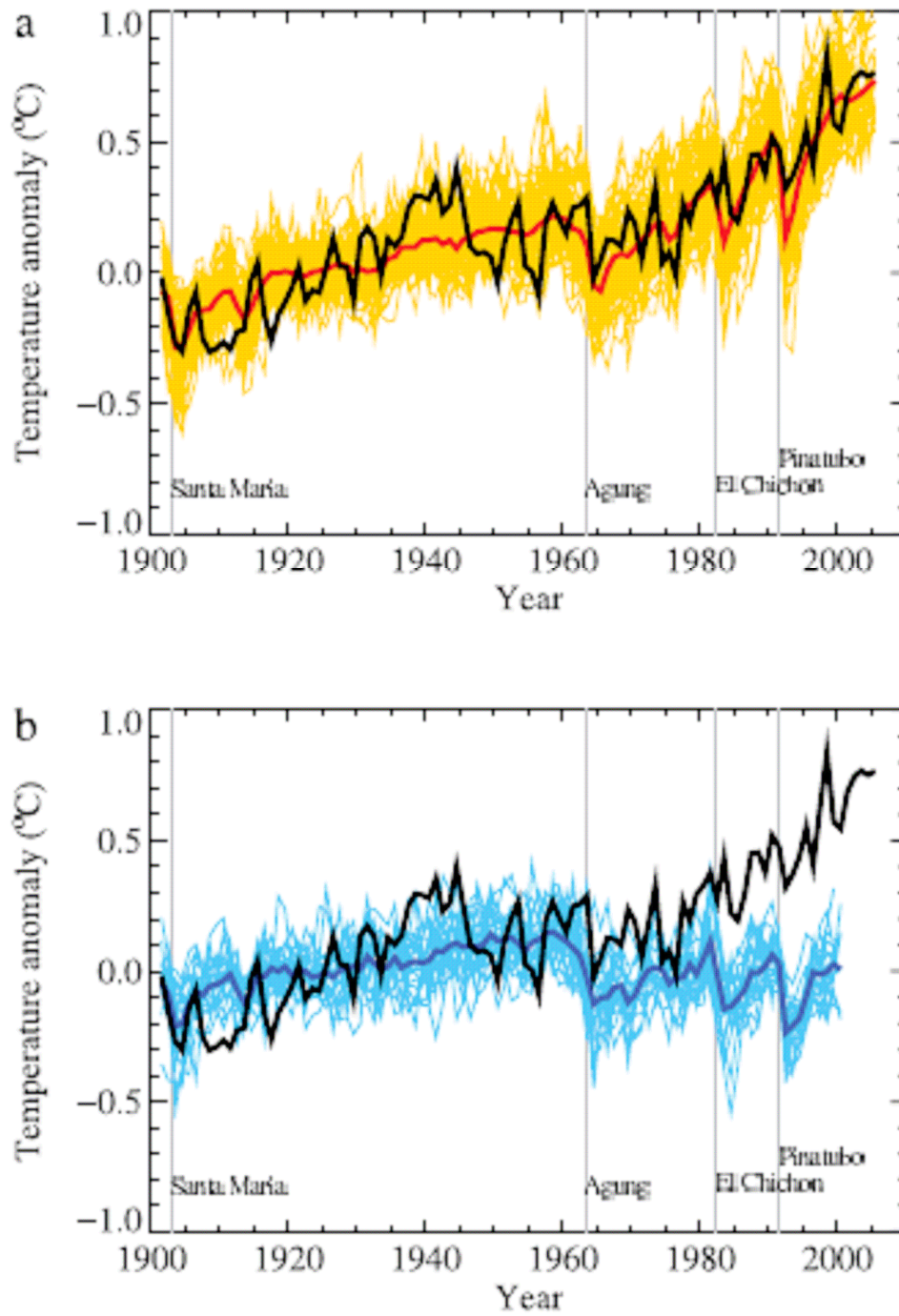


Figure 5. Figure 9-5 of AR4, showing the temperature anomaly relative to 1901-1950 mean versus year for runs of the contributing AOGCMs employing anthropogenic plus natural forcing (top) and natural forcing only (bottom). The black solid line is the observations. The thick red and blue lines are the multi-model mean, while the thin yellow and blue lines are the results of individual model runs (14 models and 58 runs). The vertical grey lines denote major volcanic eruptions. See AR4 for more details.

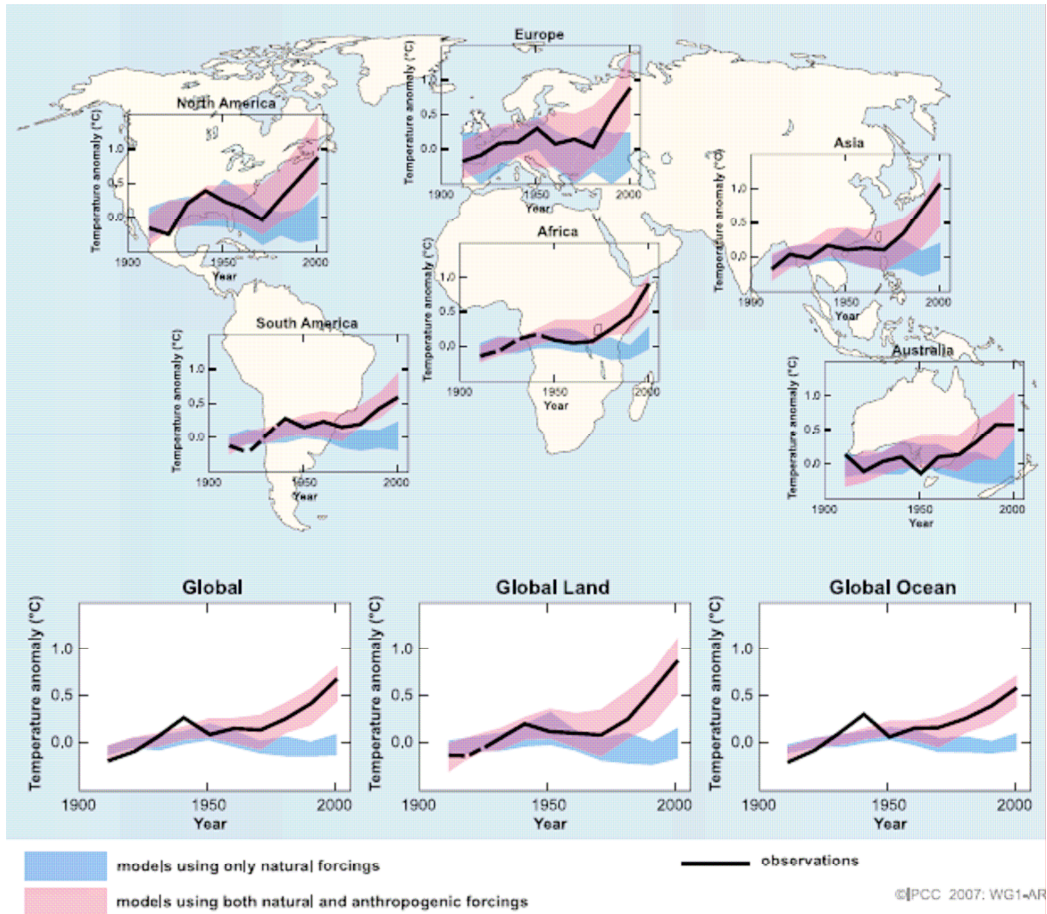


Figure 6. FAQ 9.2, Figure 1 of AR4, showing simulated vs. observed surface temperature trends over individual continents, land and ocean by the contributing AOGCMs in AR4. Blue, natural forcing only; red, anthropogenic and natural forcing. See AR4 for more details.

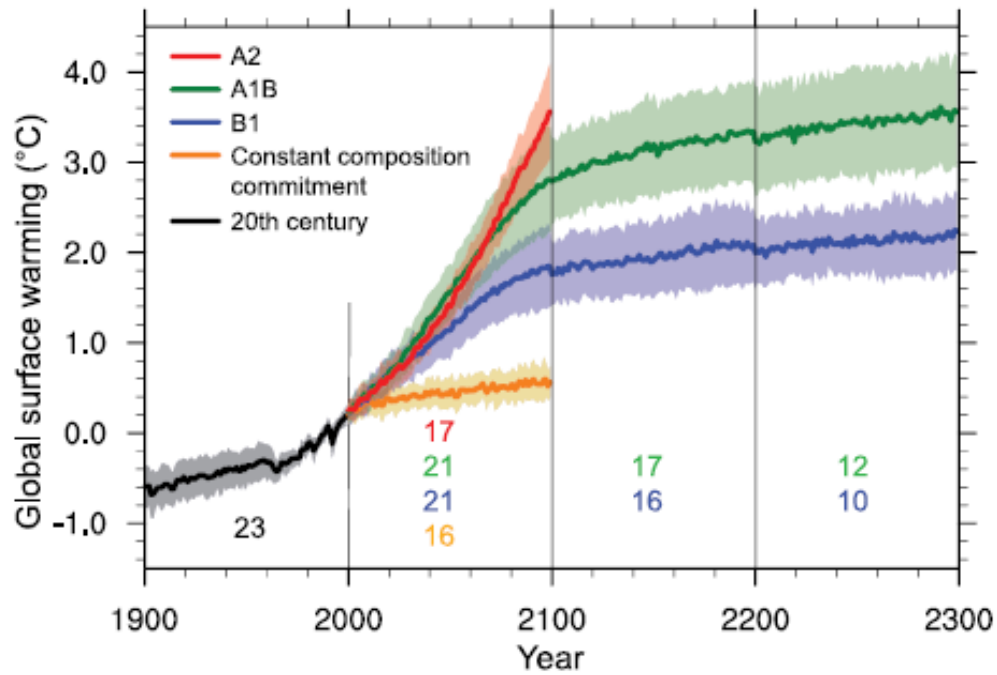


Figure 7. Figure 10-4 of AR4, showing projected surface temperature warming relative to the 1980-1999 mean value by the contributing AOGCMs to AR4. Trends for different future GHG concentration scenarios are shown. The yellow line is for CO₂ concentration held fixed at its current-day value, while the blue, green and red lines are for “low”, “medium” and “high” future GHG emission trends, respectively. The shading denotes plus and minus one standard deviation in the individual model runs, while the numbers denote the number of contributing AOGCMs to each scenario. See text and AR4 for more details.

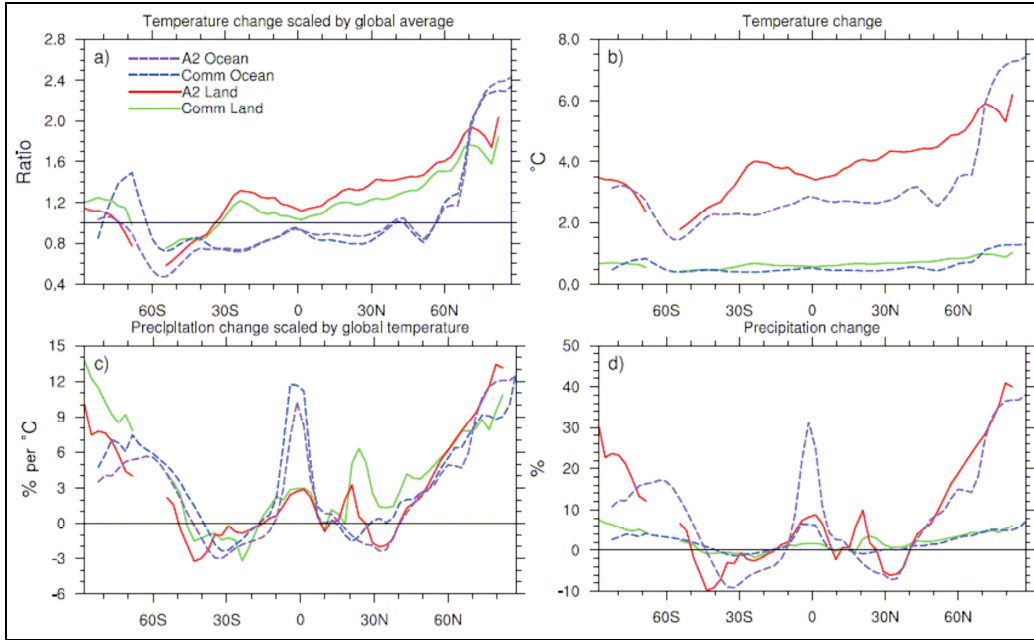


Figure 8. Figure 10-6 of AR4, showing the latitudinal variation of average surface temperature and precipitation change from 2080-2099 relative to 1980-1999 projected by the contributing AOGCMs to AR4. Results are shown for case of high future GHG emissions (A2) and constant concentrations at current-day levels (“Comm”). See AR4 for more details.

BRANK
P
e

Chapter 16

Statistical Modeling

A brief introduction to the topic “Statistical Modeling” was presented in Volume I of this book series. Two chapters on this topic (“16A – Air Quality Forecast and Alarm Systems” and “16B – Receptor Models”) were included in Volume II.

Additional information can be found at:

- <http://www.epa.gov/scram001/receptorindex.htm>
US EPA site on receptor modeling.
- http://www.ladco.org/tech/monitoring/presentations/Eberly_EPA_ORD.pdf
A PowerPoint presentation on Receptor and Hybrid Model Development and Applications.
- <http://airnow.gov/>
Air pollution forecasting in the US.
- <http://www.epa.gov/ttn/chief/conference/ei10/invval/vaughn.pdf>
AIRPACT: A Real-Time Air Quality Forecast System for the Pacific Northwest.
- <http://www.narsto.org/files/files/AQForecastingEPA.pdf>
A PowerPoint presentation on Air Quality Forecasting Activities in the United States.
- <http://www-stat.stanford.edu/~hastie/Papers/dominiciR2.pdf>
Improved Semi-Parametric Time Series Models of Air Pollution and Mortality.

- http://findarticles.com/p/articles/mi_m0CYP/is_5_113/ai_n13810603
A time-series analysis of air pollution and preterm birth in Pennsylvania, 1997-2001.
- <http://www.pubmedcentral.nih.gov/articlerender.fcgi?pubmedid=10656852>
A time-series analysis of acidic particulate matter and daily mortality and morbidity in the Buffalo, New York region.
- http://glwww.mst.dk/homepage/default.asp?Sub=http://glwww.mst.dk/udgiv/publications/2005/87-7614-617-0/html/default_eng.htm
Time Series Study of Air Pollution Health Effects in COPSAC Children.
- <http://citeseer.ist.psu.edu/637735.html>
Nonlinear Modelling of Air Pollution Time Series.

Chapter 17

Evaluation of Air Pollution Models

A comprehensive chapter on the “Evaluation of Air Pollution Models” was published in Volume II. For additional information:

- <http://www.epa.sa.gov.au/pdfs/modelling.pdf>
Evaluation of Air Pollution Model TAPM (version 2) for Adelaide, Australia.
- http://www.acd.ucar.edu/Events/Meetings/Air_Quality_Remote_Sensing/Presentations/Posters/krish.pdf
Evaluation of a Regional Air Pollution Model with Satellite Measurements.
- http://www.ofcm.gov/atd2/presentations/04-panel_evaluation/05-j_irwin2.ppt
A PowerPoint presentation “Evaluate Earth Science Models for What They are - Cartoons of Reality”.

BRANKLEY
PAPER

Chapter 18

Regulatory Modeling

A comprehensive chapter “18A – A Historical Look at the Development of Regulatory Air Quality Models for the United States Environmental Protection Agency” – was published in Volume II. For additional information:

- <http://epa.gov/ttn/scram/>
US EPA Support Center for Regulatory Atmospheric Modeling (SCRAM).
- <http://www.arb.ca.gov/html/soft.htm>
Air Quality Models and Documentation.
- <http://www.harmo.org/Conferences/Garmisch/ReportOn9Conf.pdf>
Report on the 9th conference on Harmonization within Atmospheric Dispersion Modelling for Regulatory Purposes.

BRANKLEY
PAPER

Chapter 19

Case Studies – Air Pollution Modeling at Local, Regional, Continental, and Global Scales

A chapter dedicated to the topic “Case Studies – Air Pollution Modeling at Local, Regional, Continental, and Global Scales” was presented in Volume I of this book series.

This topic will be further expanded in Volume IV.

BRANKLEY
PAPER

Chapter 20

The Future of Air Pollution Modeling

A chapter dedicated to the topic “The Future of Air Pollution Modeling” was presented in Volume I of this book series.

This topic will be further expanded in Volume IV.

BRANKLEY
PAPER

Chapter 21

Active Groups in Air Pollution Modeling

A chapter dedicated to the topic “Active Groups in Air Pollution Modeling” was presented in Volume I of this book series.

This topic will be further expanded in Volume IV.

BRANKLEY
P. 390

Chapter 22

Available Software

A chapter dedicated to the topic “Available Software” was presented in Volume I of this book series.

This topic will be further expanded in Volume IV.

BRANKLEY
PAPER

Chapter 23

Available Databases

A chapter dedicated to the topic “Available Databases” was presented in Volume I of this book series.

This topic will be further expanded in Volume IV.

BRANKLEY
PAPER

Chapter 24

Physical Modeling of Air Pollution

A chapter titled “Wind Tunnel Modeling of Pollutant Dispersion” is enclosed as Chapter 24A in the following pages. Other chapters on physical modeling of air pollution are expected in Volume IV.

BRANKLEY
P. 200

Petersen, R.L. and B. Cochran. 2008. *Wind Tunnel Modeling of Pollutant Dispersion*. Chapter 24A of *AIR QUALITY MODELING - Theories, Methodologies, Computational Techniques, and Available Databases and Software. Vol. III – Special Issues* (P. Zannetti, Editor). Published by The EnviroComp Institute (<http://www.envirocomp.org/>) and the Air & Waste Management Association (<http://www.awma.org/>).

Chapter 24A

Wind Tunnel Modeling of Pollutant Dispersion

Ronald L. Petersen ⁽¹⁾ and Brad Cochran ⁽²⁾

⁽¹⁾ *CPP, Inc., Fort Collins, Colorado (USA)*

rpetersen@cppwind.com

⁽²⁾ *CPP, Inc., Fort Collins, Colorado (USA)*

bcochran@cppwind.com

Abstract: This chapter provides a brief historical overview of wind tunnel modeling of pollutant dispersion. The theoretical basis behind wind tunnel modeling and why it can provide an accurate simulation of atmospheric flows and dispersion is discussed. In addition, typical methods used for setting up wind tunnel simulations are also discussed. Some example applications of wind tunnel modeling are discussed, such as, determining “Equivalent Building Dimensions” for input into EPA dispersion models; determining “Good Engineering Practice” stack height, numerical modeling testing and validation; and site specific concentration estimates.

Key Words: physical modeling, wind tunnel modeling, atmospheric dispersion, building and terrain wakes.

1 Introduction

For those who are unfamiliar with “wind tunnel” modeling of pollutant dispersion, a general description is first in order. The goal of wind tunnel modeling is to reproduce the important aspects of the atmospheric boundary layer and the resulting dispersion patterns of pollutants at a reduced scale. The theoretical basis for wind tunnel modeling can be derived from the basic equations of motion in dimensionless notation. If the important dimensionless parameters and dimensionless boundary conditions are identical at two different scales (i.e., full scale and model scale), the solution to the equations will be

identical. It should also be noted that these equations, if solved exactly, will yield a correct simulation. Unfortunately, an exact match of all of the dimensionless parameters is not physically possible. The challenge for the wind tunnel modeler is to find the appropriate dimensionless parameters and dimensionless boundary conditions such that a reasonably accurate simulation is conducted. This chapter will provide background information to help determine whether a simulation is reasonably valid and a brief historical summary of wind tunnel modeling. Also, it will discuss various applications related to modeling pollutant dispersion.

Wind tunnel modeling of pollutant dispersion has a long and varied history that is summarized by Cermak (1975), EPA (1981), and Meroney (2004). Cermak (1975) provides a good historical summary starting with the early 1900s going through 1974. Meroney's (2004) narrative complements the early history and extends it through 2002. The EPA (1981) historical summary is mainly focused on the effects of building and terrain wake effects. Some of the notable history is summarized below:

- Abe (1929) – studied air flow over small-scale model of Mt Fuji.
- Sherlock and Stalker (1940) – studied the effect of stack and building wakes on power plant exhaust dispersion. They found that stack tip downwash occurs when the exit velocity to wind speed ratio is less than 2.0.
- Golden (1961) – proposed a minimum acceptable building Reynolds number to obtain Reynolds number independence.
- Jensen and Frank (1963) – identified the importance of surface roughness and boundary layer turbulence when conducting wind tunnel simulations.
- Halitsky (1968) – conducted detailed wind tunnel tests around rectangular and rounded structures, and presented normalized concentrations on building surfaces for flush vent type releases.
- Snyder (1981) – wrote an EPA guideline for conducting wind tunnel modeling studies of atmospheric dispersion.
- Huber and Snyder (1982) – published the results of their research on stack dispersion downwind of rectangular buildings. Much of this research was used to develop the building downwash algorithms in the EPA ISC model.
- Hosker (1984) – published a detailed account of past wind tunnel and water flume modeling research on flow and dispersion near obstacles.
- Meroney (1986, 1988) – published a guideline for the simulation of liquefied natural gas cloud dispersion and dense cloud dispersion.
- Schulman et al. (2000) – developed an advanced building downwash model, PRIME, that made use of past extensive wind tunnel databases.

2 Theoretical Basis

2.1 Exact Similarity

An accurate simulation of the boundary-layer winds and stack gas flow is an essential prerequisite to any wind-tunnel study of diffusion. The similarity requirements can be obtained from dimensional arguments derived from the equations governing fluid motion. The basic equations governing atmospheric and plume motion (conservation of mass, momentum and energy) may be expressed using Einstein notation in the following dimensionless form (Cermak, 1975; Petersen, 1978):

$$\frac{\partial \rho^*}{\partial t^*} + \frac{\partial(\rho^* U_i^*)}{\partial x_i^*} = 0 \quad (1)$$

$$\begin{aligned} \frac{\partial U_i^*}{\partial t^*} + U_j^* \frac{\partial U_i^*}{\partial x_j^*} - \left[\frac{L_o \Omega_o}{U_o} \right] 2 \epsilon_{ijk} \Omega_j^* U_k^* = \\ - \frac{\partial p^*}{\partial x_i^*} + \left[\frac{\Delta T_o L_o g_o}{T_o U_o^2} \right] \Delta T^* g^* \delta_{i3} + \left[\frac{\nu_o}{U_o L_o} \right] \frac{\partial^2 U_i^*}{\partial x_k^* \partial x_k^*} + \frac{\partial}{\partial x_k^*} \overline{(U_i^* U_j^*)} \end{aligned} \quad (2)$$

$$\begin{aligned} \frac{\partial T^*}{\partial t^*} + \frac{U_i^* \partial T^*}{\partial x_i^*} = \\ \left[\frac{K_o}{\rho_o C_{p_o} \nu_o} \right] \left[\frac{\nu_o}{L_o U_o} \right] \frac{\partial^2 T^*}{\partial x_k^* \partial x_k^*} + \frac{\partial}{\partial x_i^*} \overline{(-T^* U_i^*)} + \left[\frac{\nu_o}{U_o L_o} \right] \left[\frac{U_o^2}{C_{p_o} (\Delta T)_o} \right] \phi \end{aligned} \quad (3)$$

where:

T	=	temperature
ρ	=	density
p	=	pressure
U	=	velocity
L	=	length scale
g	=	acceleration due to gravity
C_p	=	specific heat at constant pressure
x_i	=	Cartesian coordinates in tensor notation
ν	=	kinematic viscosity
K	=	thermal conductivity
Ω	=	angular velocity of earth
ϕ	=	dissipation

The dependent and independent variables have been made dimensionless (indicated by an “*”) by choosing the appropriate reference values. The prime (') refers to a fluctuating quantity, ϵ_{ijk} is the alternating unit tensor, and the subscript “o” denotes a reference quantity.

For exact similarity, the bracketed quantities and boundary conditions must be the same in the wind tunnel as they are in the corresponding full-scale case. The complete set of requirements for similarity is:

- undistorted geometry;
- equal Rossby number;

$$Ro = \frac{U_o}{L_o \Omega_o} \quad (4)$$

- equal gross Richardson number;

$$Ri = \frac{\Delta T_o g_o L_o}{T_o U_o^2} \quad (5)$$

- equal Reynolds number;

$$Re = \frac{U_o L_o}{\nu_o} \quad (6)$$

- equal Prandtl number;

$$Pr = \frac{\nu_o \rho_o C_{po}}{K_o} \quad (7)$$

- equal Eckert number;

$$Ec = \frac{U_o^2}{C_{po} (\Delta T)_o} \quad (8)$$

- similar surface-boundary conditions; and
- similar approach-flow characteristics.

For exact similarity, each of the above dimensionless parameters must be matched in the model and in full scale for the exhaust flow and ambient flow separately. To ensure that the exhaust plume dispersion is similar relative to the air motion, three additional similarity parameters are required (EPA, 1981) for modeling plume trajectories:

- velocity ratio;

$$R = \frac{U_s}{U_a} \quad (9)$$

- densimetric Froude number;

$$Fr = \frac{U_s}{\sqrt{(g\gamma L)}} \quad (10)$$

where

$$\gamma = \frac{\rho_s - \rho_a}{\rho_s} \quad (11)$$

and

- density ratio;

$$\lambda = \frac{\rho_s}{\rho_a} \quad (12)$$

where the subscripts “s” and “a” denote source and ambient quantity, respectively.

All of the above requirements cannot be simultaneously satisfied in the model and full scale. However, some of the quantities are not important for the simulation of many flow conditions. The parameters that can be neglected and those which are important will be discussed in the next section.

2.2 Scaling Parameters that Cannot be Matched

For most studies, simultaneously equating Reynolds number, Rossby number, Eckert Number and Richardson number for the model and the prototype is not possible. However, these inequalities are not serious limitations, as will be discussed below.

Reynolds number independence is an important feature of turbulent flows which allows wind-tunnel modeling to be used. The Reynolds number describes the relative importance of inertial forces to viscous forces in fluid flow. Atmospheric wind flows around buildings are characterized by high Reynolds numbers ($>10^6$) and turbulence. Matching high Reynolds numbers in the wind tunnel for the scale reduction of this type of study would require tunnel speeds 180 to 300 times typical outdoor wind speeds, which is impossible because of equipment limitations and since such speeds would introduce compressible flow (supersonic) effects. Beginning with Townsend (1956), researchers have found that in the absence of thermal and Coriolis (earth rotation) forces, the turbulent flow characteristics are independent of Reynolds number, provided that the Reynolds number is high enough. EPA (1981) specifies a Reynolds number criterion of about 11,000 for sharp-edged building complexes.

The Reynolds number related to the exhaust gas is defined by:

$$Re_s = \frac{V_e d}{\nu_s} \quad (13)$$

where d is the exhaust diameter. Plume rise becomes independent of the exhaust Reynolds number if the plume is fully turbulent at the stack exit (Hoult and Weil, 1972; EPA, 1981). Hoult and Weil (1972) reported that plumes appear to be fully turbulent for stack Reynolds numbers greater than 300. Their experimental data showed that the plume trajectories were similar for Reynolds numbers above this critical value. In fact, the trajectories appeared similar down to $Re_s = 28$ if only the buoyancy dominated portion of the plume trajectory was considered. Hoult and Weil's study was in a laminar cross flow (water tank) with low ambient turbulence levels and, hence, the rise and dispersion of the plume was primarily dominated by the plume's own self-generated turbulence. Arya and Lape (1990) showed similar plume trajectories for Reynolds numbers greater than 670 for buoyant plumes and greater than 2000 for neutrally buoyant plumes. Care should be taken to ensure Re_s exceeds the minimum values or trips should be installed in the stack to augment the turbulence.

The mean flow field will become Reynolds number independent and characteristic of the atmospheric boundary layer if the flow is fully turbulent (Schlichting, 1978). The critical Reynolds number for this criterion to be met is based on the work of Nikuradse, as summarized by Schlichting (1978), and is given by:

$$Re_{z_o} = \frac{z_o U_*}{\nu} > 2.5 \quad (14)$$

In this relation, z_o is the surface roughness factor and U_* is the friction velocity. If the scaled down roughness gives a Re_{z_o} less than 2.5, then exaggerated roughness would be required. The roughness elements should be larger than about $30z_o$. It should be noted that this guidance is based on a neutral atmosphere. For stable stratification, it has been often assumed that a similar limit applies, but no systematic studies have been conducted to confirm this assumption. In the event the Reynolds numbers are not sufficiently high, testing should be conducted to establish the expected errors.

Another scaling parameter that has been shown to be important is the Peclet-Richardson number ratio, Pe/Ri . The Peclet-Richardson number measures the relative rates of turbulent entrainment and molecular diffusion. If the wind-tunnel simulation is affected by molecular diffusion, the concentrations measured in the wind tunnel will be lower than those in the atmosphere for the same condition. Meroney (1987) reported that researchers at Shell concluded that molecular diffusion may play an important role in the laboratory when the scaled turbulent diffusivity is very small. They found that when the Pe/Ri number is less than a critical value, simulations were inaccurate. Their parameter was defined as follows:

$$\frac{Pe}{Ri} = \frac{U_r^3}{(g'\epsilon)} \quad (15)$$

where U_r is the reference wind speed, ϵ is a molecular diffusivity, and $g' = g(\rho_s - \rho_a)/\rho_a$. The criterion has a problem in that two flows with the same reference speed but different turbulence (i.e., neutral versus stable or grassland versus an urban area) will have the same criterion which does not seem appropriate. For this reason, Meroney (1987) suggests the following criterion:

$$\frac{Pe}{Ri} = \frac{U_*^3}{(g'\epsilon)} > 0.2 \quad (16)$$

Meroney (1987) found that errors in wind-tunnel simulations were noticed when Pe/Ri was less than 0.2; hence, all tests should be designed to meet or exceed this value. If tests are needed such that this restriction must be violated, additional tests should be conducted to assess the potential errors when using lower Pe/Ri values.

The Rossby number, Ro , is a quantity which indicates the effect of the earth's rotation on the flow field. In the wind tunnel, equal Rossby numbers between model and prototype cannot be achieved without a spinning wind tunnel. The effect of the earth's rotation becomes significant if the distance scale is large. EPA

(1981) set a conservative cutoff point at 5 km for diffusion studies. For most air quality studies, the maximum range over which the plume is transported is less than 5 km in the horizontal and 200 m in the vertical.

When equal Richardson numbers are achieved, equality of the Eckert number between model and prototype cannot be attained. This is not a serious compromise since the Eckert number is equivalent to a Mach number squared. Consequently, the Eckert number is small compared to unity for laboratory and atmospheric flows, and therefore can be neglected.

2.3 Typical Scaling Methods

This section discusses the methods commonly used to set up wind-tunnel model operating conditions. Based on the requirements in the EPA fluid modeling guidelines (EPA, 1981; 1985), the criteria that are frequently used for conducting wind-tunnel simulations of atmospheric dispersion are:

- match (equal in model and full scale) momentum ratio, M_o ;

$$M_o = \lambda \left(\frac{V_e}{U_H} \right)^2 \quad (17)$$

- match buoyancy ratio, B_o ;

$$B_o = \frac{gdV_e(\rho_a - \rho_s)}{\rho_a U_h^3} = \left(\frac{\rho_s}{\rho_a} \right) \left(\frac{(V_e/U_h)^3}{Fr_s^2} \right) \left(\frac{d}{z_r} \right) \quad (18)$$

where

$$Fr_s^2 = \frac{\rho_s V_e^2}{g(\rho_a - \rho_s)d} \quad (19)$$

- ensure a fully turbulent stack gas flow [stack Reynolds number ($Re_s = V_e d/\nu$) greater than 670 for buoyant plumes or 2000 for turbulent jets (Arya and Lape, 1990), or in-stack trip];
- ensure a fully turbulent wake flow [terrain or building Reynolds number ($Re_b = U_H H_b/\nu$) greater than 11,000 or conduct Reynolds number independence tests];
- identical geometric proportions;
- equivalent stability [Richardson number, $Ri = (g\Delta\theta H_b)/(T U_H^2)$, in model equal to that in full scale, equal to zero for neutral stratification]; and
- equality of dimensionless boundary and approach flow conditions

where:

V_e	=	stack gas exit velocity (m/s);
U_H	=	ambient velocity at building top (m/s);
d	=	stack diameter (m);
ρ_a	=	ambient air density (kg/m ³);
$\Delta\theta$	=	potential temperature difference between H_b and the ground (K);
T	=	mean temperature (K);
ρ_s	=	stack gas density (kg/m ³);
ν	=	viscosity (m ² /s);
H_b	=	typical building height (m); and
λ	=	density ratio, ρ_s/ρ_a (-).

For certain simulations, it is advantageous to conduct simulations at model scale Reynolds numbers less than 11,000. When this situation arises, Reynolds number independence tests can be conducted. The Reynolds number independence tests consist of setting up a simulation with a neutral density exhaust and an approach wind speed to exit velocity ratio of 1.5. Initial tests are conducted with a high model approach wind speed so that the building Reynolds number meets or exceeds 11,000. The simulation is subsequently repeated at incrementally lower approach wind speeds, thus, incrementally lower building Reynolds numbers. Concentrations during each of these simulations are measured at one or more receptor locations. The concentration distribution measured for the simulation with a building Reynolds number at or greater than 11,000 is used as the baseline. The concentration distribution from the subsequent, lower building Reynolds number simulations, are then compared to this baseline distribution. If the distributions are within $\pm 10\%$ of the baseline measured values, the two simulations are assumed to be equivalent. The building Reynolds number for the simulation with the lowest approach wind speed, which meets this criterion, is established as the site specific critical building Reynolds number. All subsequent simulations are conducted with building Reynolds numbers at least as great as this site specific building Reynolds number.

For buoyant sources, the ideal modeling situation is to simultaneously match the stack exit Froude number, momentum ratio and density ratio. Achieving such a match requires that the wind speed in the tunnel must be equal to the full scale wind speed divided by the square root of the length scale. For example, for a 1:180 length scale reduction, the wind speed ratio would be approximately 1:13, meaning the tunnel speeds would be 13 times lower than the full scale wind speeds. Such a low tunnel speed would produce low Reynolds numbers and is operationally difficult to achieve. Hence, Froude number scaling is typically not used. Instead, for buoyant sources, the buoyancy ratio defined above is matched between model and full scale. Using this criterion, the exhaust density of the source can be distorted, which allows higher wind-tunnel speeds.

Even with distorting the density, there may still be situations in which the buoyancy ratio can not be matched without lowering the wind-tunnel speed below

the value established for the critical building Reynolds number. When this conflict exists, the buoyancy ratio is distorted and the building Reynolds number criterion is not relaxed. The impact of distorting the buoyancy ratio will result in lower plume rise, which in turn will result in higher predicted ground-level concentrations. Hence, the results of the study will be conservative.

Testing in complex building environments is typically performed under neutral stability ($Ri = 0$). Meroney (1990) cites a Colorado State University report which determined that the effect of atmospheric stability on dispersion within five building heights of a building complex is relatively small due to the dominance of mechanical turbulence generated within the building complex.

Another factor to consider when setting up a wind-tunnel simulation is the blockage (model cross-sectional area perpendicular to the flow divided by wind tunnel cross-sectional area). EPA (1981) states that blockage should be limited to 5% unless the roof can be adjusted. If the roof can be adjusted, 10% blockage is acceptable.

3 Experimental Methods and Instrumentation

3.1 Wind Tunnel and Model Setup

3.1.1 Wind Tunnel Configuration

Wind tunnel modeling of pollutant dispersion should be conducted in a wind tunnel that is specifically configured to simulate the atmospheric boundary layer. Unlike an aerodynamic wind tunnel, which is designed to evaluate a moving body traveling through relatively non-turbulent air, an atmospheric boundary-layer wind tunnel is designed to evaluate the flow of air over a stationary body immersed in the earth's atmospheric boundary layer. In an aerodynamic wind tunnel, the desired air flow is homogenous in both the lateral and vertical directions and has very low turbulence. In an atmospheric boundary-layer wind tunnel, flow straighteners and screens at the tunnel inlet are used to create a homogenous, low turbulence entrance that is fairly similar to that of an aerodynamic wind tunnel. However, unlike an aerodynamic wind tunnel, the flow is then conditioned to simulate an atmospheric boundary layer. Spires and a trip downwind of the flow straighteners begin the development of the atmospheric boundary layer. A long boundary layer development region between the spires and the site model is filled with roughness elements placed in a repeating roughness pattern that is experimentally set to develop the appropriate approach boundary layer wind profile and approach surface roughness length.

When the approach conditions vary with wind direction (i.e., a site which is partially bounded by a large body of water or a site which is located on the outskirts of a large city), multiple roughness configurations may be necessary. Figure 1 shows a typical wind tunnel setup. Notice the roughness elements

upwind of the model turntable area and the spires and trip at the entrance to the wind tunnel.

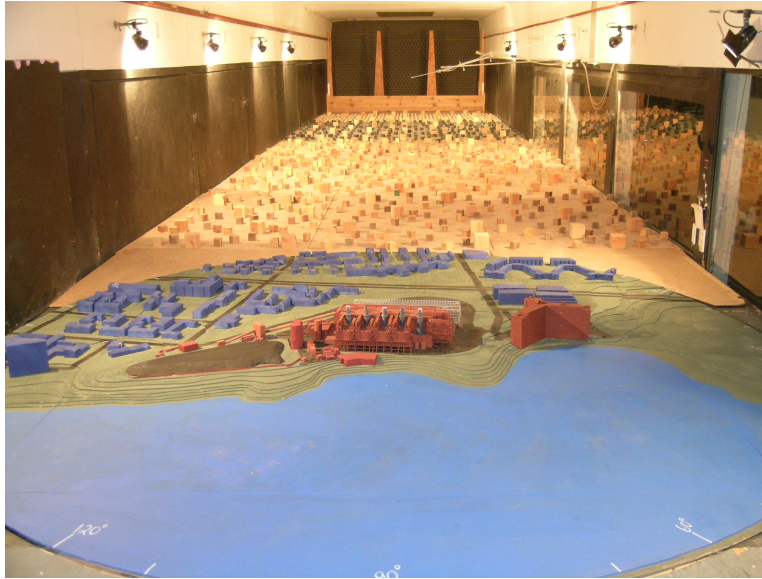


Figure 1. Typical wind tunnel setup for modeling power plant exhaust dispersion.

3.1.2 Scale Model

3.1.2.1 Scale Reduction Factor

Wind tunnel modeling of pollutant dispersion requires the construction of a reduced scale physical model. The scale at which the model is constructed can be of critical importance, and will depend upon the type of emission sources to be evaluated, the size of the wind tunnel, the area to be included in the model and the size of structures and/or terrain to be included in the model. Section 2 describes various similarity criteria that must be met to achieve an accurate simulation.

3.1.2.2 Test Model

Once the scale reduction factor has been defined, a physical model of the test building should be constructed by applying the scale reduction factor to the full scale dimensions in all three dimensions without distortion. The model should include all significant features that can impact the flow trajectories around and downwind of the test building. Corners of buildings directly adjacent to the emission source should be sharp to match the full-scale configuration. This can generally be achieved by constructing the test model out of wood, Plexiglas or other hard materials. For features near the stack location, special care should be taken to not only match the physical shape of the structure, but also its solidity. Examples of structures that might be found near exhaust stacks that are not necessarily solid include: screen walls, pipe racks, open-beam support structures tank farms, and electrical substations. When significant spherical or cylindrical

structures are nearby, the surface of these features should be roughened, or vertical trips should be placed along the structures to appropriately simulate the full-scale flow separation point.

3.1.2.3 Surrounding Model

The area surrounding the test model should be constructed to the extent that the air flow patterns approaching and downwind of the test model appropriately replicate the full-scale environment. This surrounding model may include man-made structures, terrain, and vegetation. The surrounding model should include all buildings whose height exceeds $1/20^{\text{th}}$ of its distance from the test building, or if its crosswind dimension is large compared to its height and the height is greater than $1/100^{\text{th}}$ of its distance from the test building (EPA, 1981). These structures can be modeled as massing models where the overall shape and size is of primary importance. Small building features such as parapet walls, sunshades, entryways, etc. do not need to be included. Similarly, terrain features should be included if the height of a ridge line is more than $1/100^{\text{th}}$ of the distance from the test building or if the height of a 3-dimensional hill is greater than $1/20^{\text{th}}$ of its distance from the test building (EPA, 1981). Vegetation should be included when it is the defining influence on the local surface roughness, that is, when no larger obstacles are present, and when they have the potential to influence the plume trajectory (e.g., tall trees near the emission source).

3.1.3 Emission Sources

Exhaust sources should be simulated by installing stacks constructed of tubes (typically brass) at appropriate locations. If the internal flow Reynolds number is insufficient (See Section 2.3), trips should be installed within the stacks to ensure that the stack flow is fully turbulent upon exit. The stack should include all architectural features or other impediments that might influence the flow of air out of the stack, such as rain caps or divergent or convergent cones. If the taper on the cones are such that fully-developed flow is maintained, the stacks can be modeled without the taper, using the exit diameter to define the tube diameter. The presence of stack shrouds or groupings of other stacks that might influence the local flow field should also be included in the model.

3.1.4 Receptors

Most receptor locations (concentration sampling points) positioned off of the test model can be evaluated by installing a point receptor at the specified location. One end of a sampling tube is installed at the receptor location. The other end of the tube is then connected to the inlet port of a concentration measuring device (discussed below) to determine the amount of tracer gas present at the receptor location. At point receptor locations, it is assumed that the plume is sufficiently large such that there is not a significant concentration gradient across the receptor

location. As such, the local concentration can be assessed by collecting a single point air sample at or near the receptor location of interest.

When a concentration gradient may exist across the receptor location, for example at a large nearby air handler unit, a single point air sample may not be sufficient to characterize the local concentrations. Also, the presence of air flow devices such as large air handler units or cooling tower intakes may influence the pressure distribution near the emission source, and thus, the trajectory of the emitted plumes. Therefore, to assure an accurate simulation of the plume trajectory and to obtain an area average concentration across an intake louver, the actual airflow into these units should be simulated using a vacuum source as part of the model.

3.2 Concentration Measurements

3.2.1 Data Collection Procedure

After the desired atmospheric condition has been established in the wind tunnel, a mixture of inert gas and a tracer of predetermined concentration is released from an emission source at the required rate to simulate the prototype plume rise. Typical tracer gases can include: ethane, methane, propane, carbon monoxide, and sulfur hexafluoride. The volume flow rate of the gas mixture should be controlled and monitored by a precision mass flow controller to ensure an accurate simulation.

An air sample is then collected to determine the percent of the released tracer gas that is present at each of the sampling points (receptors). In certain simulations, it is important to make sure that the presence of the sample tube does not influence the trajectory of the air flow. For these simulations, the velocity of the air sample into the receptor should not exceed the velocity of the air flow over the entrance of the receptor tube. An example of this situation is when one is interested in the time history of a finite duration release. Sampling at a higher volume flow rate will result in a slight decrease in pressure at the sample tube. This pressure gradient will distort the flow field, and thus the concentration distribution. For most simulations, however, the time averaged concentration is of greater importance than the time history. In this case, an intake velocity that exceeds the local lateral velocity will result in a time averaged concentration that corresponds to an area greater than the area of the receptor entrance, which may or may not be appropriate.

The collected air sample can be analyzed in one of two methods, either in real time or as a time averaged sample. In a real time application, the air sample is drawn directly into a concentration detector. The type of detector will depend upon the tracer gas used in the simulation. Either a flame ionization detector (FID) or photo ionization detector (PID) is commonly used for hydrocarbon (ethane, methane, propane, etc.) tracers. For a time averaged sample, the air sample is drawn into a collection chamber, such as a syringe or a Tedlar[®] bag.

After a complete sample has been collected, the air sample within the collection chamber is fed into a concentration detector.

The advantage of a real-time sampling system is that it allows the operator to collect time-dependent concentration measurements and/or get immediate feedback on the concentration levels at the receptor. The operator can use this direct feedback to search for the meteorological condition (wind speed and wind direction), which results in the highest concentration from a single source at a single receptor. The disadvantage of a real-time sample system is that most detectors can either only detect a single tracer gas, or cannot differentiate between a family of tracer gases. Therefore, it is not possible to distinguish concentration values from multiple emission sources. Also, if the experimental design requires multiple receptor locations to be evaluated simultaneously, a separate concentration detector is necessary for each sample location.

With a time averaged sampling system, there is a greater time delay between when the sample is collected and when the concentration results are available. Therefore, this system is less efficient when the objective is to evaluate a range of meteorological conditions from a single source at a single receptor location. However, when a time averaged sample is fed into a multi-gas concentration detector, such as gas chromatograph, a signal can be detected for a wide range of tracer gases. With this system, multiple emission sources can be evaluated concurrently. This can be particularly important when there is the potential for interaction between different plumes. Another advantage of the time averaged sampling system is that multiple samples can be collected simultaneously and then evaluated using a single concentration measuring device. For example, a time averaging sampling system with 50 collection ports can be used to simultaneously collect an array of data points that are sufficient to fully characterize an exhaust plume, without the need for 50 separate concentration measuring devices. This allows for a cost effective means of collecting large amounts of data where the interest is in evaluating the presence of the entire plume, rather than the plume concentration at a specific point in space.

3.2.2 Calculation of Full-Scale Concentrations

Measured model concentrations are converted to full-scale normalized concentrations by equating the non-dimensional concentration, $K = CUL^2/m$, in both model and full scale, as noted in the following equation presented in the Guideline for Use of Fluid Modeling of Atmospheric Diffusion (EPA, 1981):

$$\left(\frac{C}{m}\right)_f = \left(\frac{CU_r}{C_oV}\right)_m \left(\frac{1}{U_r}\right)_f \left(\frac{L_m}{L_f}\right)^2 \times 10^6 \quad (20)$$

$$C_m = \left[\left(\frac{E_{meas} - E_o}{E_{cal}} \right)_{rec} - \left(\frac{E_{meas} - E_o}{E_{cal}} \right)_{bg} \right] \times C_{cal} \quad (21)$$

where:

C_f	=	full scale concentration of pollutant ($\mu\text{g}/\text{m}^3$);
C_m	=	model scale concentration of tracer gas (ppm);
C_{cal}	=	calibration gas concentration (ppm);
C_o	=	tracer gas concentration at source (ppm);
E_{meas}	=	voltage reading from concentration detector (V);
E_o	=	concentration detector zero offset voltage (V);
E_{cal}	=	concentration detector calibration gas voltage reading (V);
L	=	length scale (m);
m	=	chemical mass emission rate (g/s);
U_r	=	reference wind speed (m/s);
V_m	=	model volume flow rate (m^3/s); and
10^6	=	conversion from g to μg .

The subscripts *rec* and *bg* denote measurements at the receptor and background, respectively.

Typically, concentrations measured in the wind tunnel are averaged over a period long enough to represent a steady-state average concentration. The required averaging time will vary with the speed set in the wind tunnel and typically ranges from 2 minutes for low wind speeds (i.e., 2 m/s) to 30 seconds for high wind speeds (> 8 m/s).

In the full scale, a steady-state average concentration is usually assumed to correspond to a 15 minute to 1 hour average concentration due to the natural fluctuations in both wind speed and wind direction present within the atmosphere. Full scale concentration estimates for averaging times less than 24 hours can be obtained using the following power law relationship defined by Turner (1994):

$$\left(\frac{C}{m} \right)_s = \left(\frac{C}{m} \right)_k \times \left(\frac{t_k}{t_s} \right)^p \quad (22)$$

where:

$(C/m)_s$	=	normalized concentration estimate for averaging time t_s ;
$(C/m)_k$	=	normalized concentration estimate for averaging time t_k ; and
p	=	power law exponent between 0.17 and 0.20.

Alternately, the wind tunnel average concentrations can be converted to 3-hr, 8-hr, 24-hr and annual average estimates using the scaling factors provided in EPA-

454/R-92-019 (1992). That reference states that “to obtain the estimated maximum concentrations for 3-, 8-, 24- or annual averaging times, multiply the 1-hour value by the indicated factor” shown below:

<u>Averaging time</u>	<u>Scaling or Multiplying Factors</u>
3 hours	0.9 (± 0.1)
8 hours	0.7 (± 0.2)
24 hours	0.4 (± 0.2)
Annual	0.08 (± 0.02)

Conservative 3-hr, 8-hr, 24-hr and annual average concentration estimates can be obtained using the above factors. More site specific annual average concentration can be obtained by correlating the actual wind frequency distribution at the site with the distribution of concentrations versus wind speed and wind direction obtained from the wind tunnel measurements.

For example, the annual average normalized concentration can be estimated by multiplying the hourly concentration values for each wind direction/wind speed category by the probability of the wind condition occurring using the following relationship:

$$\left[\frac{C}{m} \right]_{annual} = \sum_{i=1}^{15} \sum_{j=1}^{72} f(U_i, WD_j) \times \left[\frac{C}{m} \right]_{hourly U_i, WD_j} \quad (23)$$

where

$$\begin{aligned} f(U_i, WD_j) &= \text{frequency of wind speed } U_i \text{ and wind direction, } WD_j; \\ U_i &= \text{median anemometer wind speed in each of 15 wind speed} \\ &\quad \text{categories (m/s); and} \\ WD_j &= \text{median wind direction in each of 72 wind direction categories} \\ &\quad \text{(deg).} \end{aligned}$$

A similar method can be used to obtain 3-hr, 8-hr and 24-hour estimates. It should be noted that neutral stability is assumed for all hours for most wind tunnel modeling applications.

3.2.3 Error Analysis

The full-scale concentration results have certain experimental errors associated with them. To estimate the experimental error, referred to as uncertainty interval, the following equation is used:

$$\left(\frac{\Delta C}{C}\right)_f = \left[\left(\frac{\Delta C}{C}\right)_m^2 + \left(\frac{\Delta C_{cal}}{C_{cal}}\right)_m^2 + \left(\frac{\Delta C_o}{C_o}\right)_m^2 + \left(\frac{\Delta L}{L}\right)_m^2 + \left(\frac{\Delta U_r}{U_r}\right)_m^2 + \left(\frac{\Delta V}{V}\right)_m^2 \right]^{1/2} \quad (24)$$

where

$$\begin{aligned} (\Delta C/C)_m &= \text{uncertainty in measured concentration,} \\ &\quad \pm 0.15 \text{ for low concentrations, and} \\ &\quad \pm 0.05 \text{ for high concentrations;} \\ (\Delta C_{cal}/C_{cal})_m &= \text{uncertainty in calibration gas concentration, } \pm 0.02; \\ (\Delta C_o/C_o)_m &= \text{uncertainty in initial tracer gas concentration, } \pm 0.02; \\ (\Delta L/L)_m &= \text{uncertainty in length scale reduction, } \pm 0.01; \\ (\Delta U_r/U_r)_m &= \text{uncertainty in reference wind speed, } \pm 0.05; \text{ and} \\ (\Delta V/V)_m &= \text{uncertainty in volume flow setting, } \pm 0.02. \end{aligned}$$

Substituting the above uncertainty estimates into Equation 24 gives the following uncertainty for the full-scale concentrations:

$$\begin{aligned} (\Delta C/C)_f &= \pm 0.16 \text{ for low concentrations } (C_f < 100 \mu\text{g}/\text{m}^3) \\ &= \pm 0.08 \text{ for high concentrations } (C_f > 100 \mu\text{g}/\text{m}^3) \end{aligned}$$

3.3 Velocity Measurements

For most applications, split-film (dual hot-film sensor) and hot-film or hot-wire (single sensor) probes are used to measure velocity profiles. The dual sensor probe is used to measure mean velocity (U), longitudinal turbulence intensity (U'), vertical turbulence intensity (W') and surface friction velocity (U_*), while the single sensor probe is used to measure U and U' . The theory of operation for split-film and hot-film sensors is based on the physical principle that heat transferred from a sensor equals heat supplied to that sensor by an anemometer. This physical principle can be represented by the following equations.

For the hot-film sensor:

$$\frac{E_1^2}{K_1} = A + BU^c \quad (25)$$

and for the split-film sensor:

$$\left(\frac{E_1^2}{K_1}\right) + \left(\frac{E_2^2}{K_2}\right) = [A + B(U_n)^c] \quad (26)$$

and

$$\left(\frac{E_1^2}{K_1}\right) - \left(\frac{E_2^2}{K_1}\right) = (a + bU_n)(\theta_o - \theta) + c \quad (27)$$

where

E_i	=	output voltage from a sensor;
K_i	=	$R_{Hot, i} (R_{Hot, i} - R_{Cold, i})$;
U, U_n	=	the velocity sensed;
A, B, C, a, b, c	=	constants determined by calibration;
R_{Cold}	=	resistance across hot film with baseline voltage applied;
θ	=	angle formed by plane of sensor splits and the velocity vector;
θ_o	=	change in θ ; and
R_{Hot}	=	resistance across hot film with overheat ratio applied $\left(\frac{R_{Hot}}{R_{Cold}} = 1.5\right)$.

Sensor calibrations are accomplished immediately prior to each velocity measurement activity. For low flow calibrations (<1.5 m/s), the sensor can be placed inside a flow calibration nozzle that is connected to a mass flow meter that provides a metered air flow through the nozzle. High flow calibrations (> 1.5 m/s) can be accomplished by placing the sensor adjacent to a pitot-static tube mounted in the wind tunnel. The constants A and C (or A, B, C, a, b, c and θ_o) are obtained by calibrating the sensors over a range of known velocities (or velocities and angles), and determined by least squares analysis utilizing the appropriate previously referenced equations.

Lateral and vertical profiles of mean velocity and turbulence are obtained by affixing the probe to a traversing carriage that relates height (z) or lateral position (y) to voltage output. All data are obtained by sampling the probe output at sample rates ranging from 30 Hz to 400 Hz depending upon the approach wind speed.

Alternative methods exist to measure these quantities, such as cross wire or cross film sensors, multi-hole pressure probes or laser-Doppler equipment. The user must become thoroughly proficient with any of these systems to assure accurate measurements. All methods must be able to reproduce the characteristics of known boundary layer flows as presented in Section 3.5.

3.4 Volume Flow

The volume flow rate of tracer gas from the model stack is an important variable in any wind-tunnel study of atmospheric dispersion. Various volume flow rates are calculated prior to testing to simulate multiple wind speeds or source flow

rates. Mass flow controllers can then be used to supply the appropriate tracer gas mixture to obtain the desired volume flow rates at the stack exit.

3.5 Boundary Layer Verification

An important similarity criterion discussed in Section 2.4 is the similarity of the approaching wind and thermal conditions, particularly the variation of mean wind speed, temperature and turbulence intensity with height. Most atmospheric boundary-layer wind tunnels are specifically designed to simulate the mean wind speed and turbulence intensity profiles that occur in the atmosphere. Some wind tunnels are capable of heating and cooling the floor, and temperature profiles can also be simulated. The following discussion will mainly focus on simulating the neutral atmospheric boundary layer. EPA (1981) discusses methods for simulating the stratified boundary layer.

In order to document the appropriateness of the boundary layer, vertical profiles of mean velocity and longitudinal turbulence intensity are usually obtained upwind of the model test area. The profiles are normally collected using a hot-film anemometer mounted on a vertical traverse device. The procedures for measuring the velocity profiles are discussed in Section 3.3.

Figure 2 shows a typical mean velocity and longitudinal turbulence intensity profiles that have been collected within the test section of an atmospheric boundary layer wind tunnel, such as that shown in Figure 1. Each of the plots includes the measured data along with curves of the predicted profiles developed from the analysis described below.

An analysis of the mean velocity profile is conducted to determine whether the shape is characteristic of that expected in the atmosphere. The starting point in any analysis of the mean velocity profile characteristics is to consider the equations which are commonly used to predict the distribution of wind and turbulence in the atmosphere. The most common equation, which has a theoretical basis, is referred to as the “log-law” and is given by:

$$\frac{U}{U_*} = \frac{1}{k} \ln \left(\frac{z}{z_o} \right) \quad (28)$$

where:

- U = the velocity at height z ;
- z = elevation above ground-level;
- z_o = the surface roughness length;
- U_* = the friction velocity; and
- k = the von Kàrmàn’s constant
(which is generally taken to be 0.4).

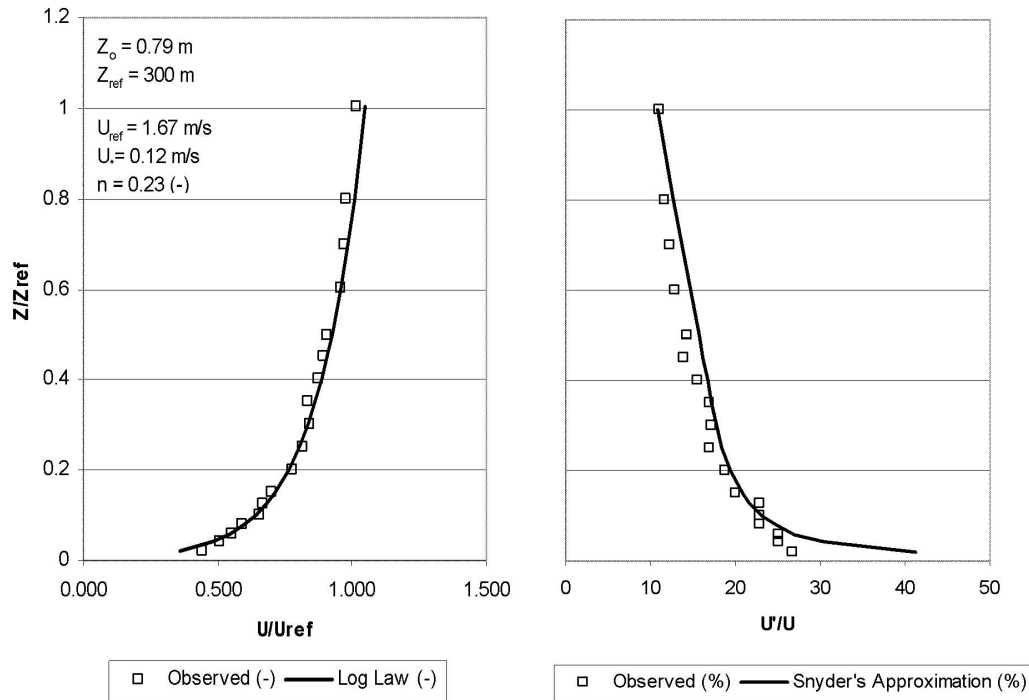


Figure 2. Mean and turbulent velocity profiles measured within the test section of an atmospheric boundary layer wind tunnel.

Another equation that is commonly used to characterize the mean wind profile is referred to as the “power-law” and is given by:

$$\frac{U}{U_r} = \left(\frac{z}{z_r} \right)^n \quad (29)$$

where:

- z_r = is some reference height;
- U_r = is the wind speed at the reference height; and
- n = is the “power-law” exponent.

Figure 2 shows the computed U_* and z_0 values obtained from the analysis of the mean velocity profiles. The analysis is undertaken using a least-squares technique to find the n , U_* and z_0 values, which give the least error to the above equations. The measured “power-law” exponent and the surface roughness length values are shown within the figure.

Another consistency check is to relate the power-law exponent, n , to the surface roughness length, z_0 . Counihan (1975) presents a method for computing the “power-law” from the surface roughness length, z_0 , using the following equation:

$$n = 0.24 + 0.096 \log_{10} z_o + 0.016 (\log_{10} z_o)^2 \quad (30)$$

When the value for z_o shown in Figure 2 is substituted into the above equation, a “power-law” exponent, n , is obtained. The power law wind profile was computed using this exponent and the result is shown in Figure 2.

The variation of longitudinal turbulence intensity with height has been quantified by the EPA (1981). The EPA gives the following equation for predicting the variation of longitudinal turbulence intensity in the surface layer:

$$\frac{U'}{U} = n \frac{\ln\left(\frac{30}{z_o}\right)}{\ln\left(\frac{z}{z_o}\right)} \quad (31)$$

where all heights are in full-scale meters. This equation is only applicable between 5 and 100 m (16 and 330 ft). Above 100 m, the turbulence intensity is assumed to decrease linearly to a value of 0.01 at a height of roughly 600 m (2000 ft) above ground level.

The goal of this analysis is to show that the mean velocity and turbulence intensity profiles established in the wind tunnel are representative of those expected for the site being evaluated.

3.6 Dispersion Verification

When the boundary layer has been adequately reproduced in an atmospheric boundary layer wind tunnel, the dispersion of pollutants should also be in good agreement between the field and the laboratory. This can be verified through a series of lateral and vertical concentration measurements that are designed to characterize the plume downwind of an isolated exhaust stack.

The concentration tests are typically conducted using a neutral density gas with an exit velocity ratio (V_e/U_h) of 1.5 to minimize plume rise and the potential for stack tip downwash (which occurs when a portion of the plume is caught in the downwind wake cavity created by the physical presence of the exhaust stack). Samples are collected along a horizontal and vertical grid placed at multiple locations downwind of the exhaust stack using the time averaging sampling system described above in Section 3.2, so that time averaged plume characteristics can be evaluated. The characteristic variables that are used to define the plume at each downwind location consist of the plume centerline, \bar{z} , the plume lateral offset, \bar{y} , and the lateral and vertical dispersion parameters σ_y and σ_z .

If the plume is behaving appropriately, the plume centerline should remain relatively constant and be consistent with the top of the exhaust stack, and the lateral offset in the plume should be minimal with little or no bias towards one side of the tunnel or the other. The dispersion parameters, σ_y and σ_z , can be compared against atmospheric values for either C or D stability developed by Pasquill/Gifford for a rural environment and McElroy/Pooler for an urban environment, as presented in Turner (1970).

As a final verification check on the dispersion comparability of the wind tunnel to the atmosphere, the ground-level concentrations observed in the wind tunnel can be compared with those generated using the Gaussian dispersion equation in the form:

$$\frac{CU_h}{m} = \left(\frac{1}{\pi\sigma_y\sigma_z} \right) \exp \left[-0.5 \left(\frac{z}{\sigma_z} \right)^2 \right] \quad (32)$$

The values for the normalized concentration CU_h/m are computed using a plume height corresponding to the height of the stack and the horizontal and vertical dispersion coefficients for either a C or D stability from either Pasquill/Gifford and/or McElroy/Pooler, depending upon the classification of the surrounding environment for the wind tunnel simulation.

4 Typical Applications

4.1 Numerical Model Testing and Development

Wind tunnel modeling is a very useful tool for use in testing and developing numerical models. As Snyder (EPA, 1981) so aptly put it,

“if a mathematical model is to be applied to the atmosphere, it should also be applicable to a fluid model, e.g., by eliminating or adjusting that portion of the model dealing with rotational effects, by reducing the Reynolds number, etc. If a mathematical model cannot simulate the results of an idealized laboratory experiment, how can it possibly be applicable to the atmosphere?”

Many examples can be cited where wind tunnel modeling has been used to help develop and test numerical models. A few examples will be mentioned here. Huber and Snyder (1976, 1982) conducted a series of wind tunnel tests to evaluate the effect of building wakes on plume downwash. They used the results to develop and test analytical equations that were subsequently used in the EPA Industrial Source Complex model (EPA, 1995).

Petersen (1978, 1987) used wind tunnel modeling to help develop and test an integral plume rise algorithm. This plume rise algorithm was then installed in the ISC model, and tested against field and wind tunnel databases (Petersen and Ratcliff, 1986; 1987).

Snyder et al. (1992, 1993) conducted wind tunnel testing to define the nature of the building wake and cavity. Schulman used these results to help develop an advanced plume downwash model referred to as PRIME. This model also includes an integral plume rise algorithm that had been tested by others (Petersen, 1987; Ohms, 1972) against wind tunnel and field databases. The PRIME algorithm was subsequently installed in the EPA approved model, AERMOD (Cimorelli et al., 2005).

Currently, the use of Computational Fluid Dynamic models for modeling the dispersion of pollutants in complex environments is being promoted (Huber et al., 2005; Tang et al., 2006; Hanna et al., 2006). Before these models can be used in a credible manner, extensive wind tunnel and field testing will be needed for validation purposes.

4.2 Equivalent Building Dimensions (EBD)

When the effects of building or terrain wakes on dispersion need to be accurately assessed using an appropriate dispersion model such as ISC or AERMOD, wind tunnel modeling can be used to determine the appropriate inputs. Typically, the building dimension inputs are obtained using an EPA program referred to as BPIP (Building Profile Input Program). BPIP uses various logic algorithms and the dimensions of structures at a site to specify a building height, width, length and position relative to the stack for each of 36 wind directions. The EBD approach uses wind tunnel testing of all the site structures and/or terrain to specify a single building for each of the 36 wind directions that produces the same dispersion. In other words, the EBD approach can make the model nearly “site specific”.

At present, the only method the Environmental Protection Agency (EPA) has concurred with for determining EBD is through the use of wind-tunnel modeling. Petersen et al., (1995, 2000, 2001, 2006) provides background on this approach, which has been reviewed and accepted by the EPA (Tikvart, 1994).

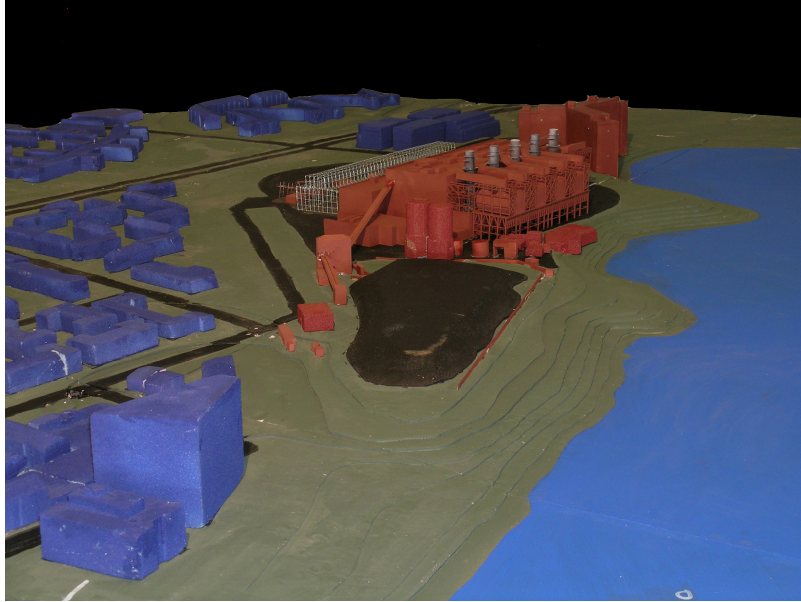


Figure 3. Photographs of wind tunnel setup with site structures in place for EBD testing.

The basic modeling approach for determining equivalent building dimensions is to first document, in the wind tunnel, the dispersion characteristics as a function of wind direction at the site with all significant nearby structure wake effects included (i.e., the setup shown in Figure 3). Next, the dispersion is characterized in the wind tunnel with an equivalent building positioned directly upwind of the stack in place of all nearby structures (i.e., the setup as shown in Figure 4). This testing is conducted for various equivalent buildings until an equivalent building is found that provides a profile of maximum ground-level concentration versus downwind distance that is similar (within the constraints defined below) to that with all site structures in place.

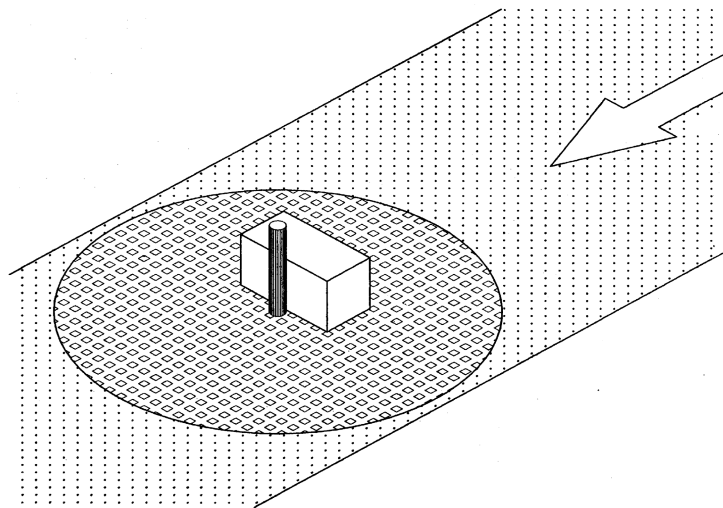


Figure 4. Drawing showing wind tunnel setup for EBD testing.

The criteria for defining whether or not two concentration profiles are similar is to determine the smallest building which: 1) produces an overall maximum concentration exceeding 90 percent of the overall maximum concentration observed with all site structures in place and 2) at all other longitudinal distances, produces ground-level concentrations which exceed the ground-level concentration observed with all site structures in place less 20 percent of the overall maximum ground-level concentration with all site structures in place. This criteria has been accepted in the past EPA approved EBD studies and is a suggested approach in Tikvart (1994).

To demonstrate the method for specifying the equivalent building, consider Figure 5 which shows a typical result from a past study. The figure shows the maximum ground-level concentration versus downwind distance for five different equivalent buildings and the maximum concentration measured with site structures in place. Within this figure, the concentration profile for EB2 meets the first criterion in that the maximum measured concentration is at least 90 percent of the maximum concentration measured with the site structures in place. However, the EB2 profile fails the second criterion at the third actual site data point (at approximately 200 m downwind) where the lower bound of the error bar exceeds the interpolated concentration value for EB2. Therefore, the equivalent building for the test case shown in Figure 3 is EB3, since EB3 is the smallest equivalent building which meets both criteria.

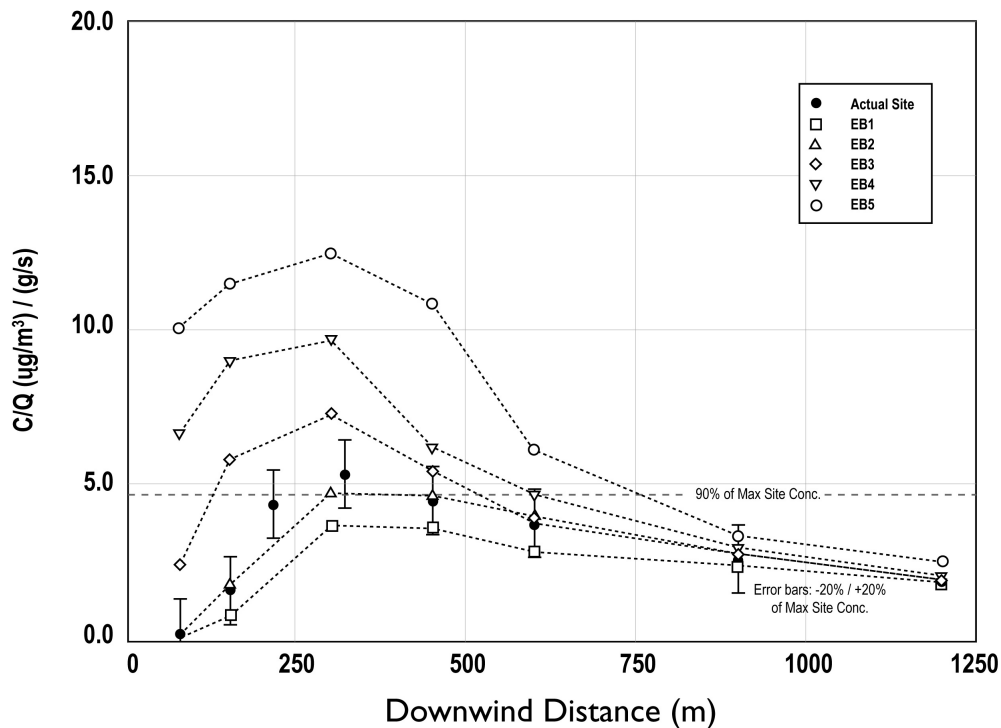


Figure 5. Typical results from EBD testing for one wind direction with actual site structures present and with equivalent buildings (EB1 to EB5) present.

4.3 Good Engineering Practice Stack Height Determinations

In the stack height regulation (40 CFR 51.100 (ii)), GEP stack height is defined to be the *greater* of:

- (1) 65 meters, measured from the ground level elevation at the base of the stack;
- (2) for stacks in existence on January 12, 1979, and for which the owner or operator had obtained all applicable permits or approvals required under 40 CFR Parts 51 and 52, $H_g = 2.5H$ provided that the owner or operator produces evidence that this equation was actually relied on in establishing an emission limitation;
- (3) for all other stacks, $H_g = H + 1.5L$ where:
 - H_g = good engineering practice stack height, measured from the ground-level elevation at the base of the stack
 - H = height of nearby structure(s) measured from the ground-level elevation at the base of the stack
 - L = lesser dimension, height or projected width, of nearby structure(s), provided that the EPA, State, or local control agency may require the use of a field study or fluid model to verify GEP stack height for the source or,
- (4) The height demonstrated by a fluid model or a field study approved by the EPA, State, or local control agency, which ensures that the emissions from a stack do not result in excessive concentrations of any air pollutant as a result of atmospheric downwash, wakes, or eddy effects created by the source itself, nearby structures or nearby terrain features.

For some situations, the EPA requires the use of wind tunnel modeling to determine the GEP stack height. These situations are typically for hyperbolic cooling towers, other unusual structures not covered by the formula, and nearby terrain features. To quantitatively determine the GEP height through physical modeling, the stack height regulation goes on to define an excessive concentration as:

“a maximum ground-level concentration due to emissions from a stack due in part or whole to downwash, wakes, or eddy effects produced by nearby structures or terrain features which individually is at least 40 percent in excess of the maximum concentration experienced in the absence of such downwash, wakes, or eddy effects and which contributes to a total concentration due to emissions from all sources that is greater than an ambient air quality standard.”

The above definition applies for complex terrain situations and standard building shape configurations. For structures not covered by the formula (i.e., cylindrical, spherical, lattice, etc.), the comparison with the National Ambient Air Quality Standards (NAAQS) required in the above definition is omitted.

To determine the GEP stack height using wind tunnel modeling, the maximum ground-level concentration from wind-tunnel testing with the site model configuration is first compared to the ambient standards. For this comparison, the background concentration due to other sources is added to the impact due to the unit being tested. If the total concentration is below NAAQS, a shorter stack must be considered. Once a stack height is found such that a lower stack would result in an exceedance of ambient standards, it is considered GEP if the concentration without nearby or buildings terrain present is at least 40 percent less than that with the terrain present (referred to as the 40 percent test). Figure 6 shows a wind tunnel setup for determining the GEP stack height due to upwind terrain affects.



Figure 6. Wind tunnel setup to evaluate GEP stack height based on upwind terrain effects.

4.4 Excessive Concentration Determinations

The EPA stack height regulation (40 CFR 51.100) allows facilities to seek credit for increases in stack height up to the “Good Engineering Practice” (GEP) stack height when it can be demonstrated by fluid modeling that emissions from the existing stacks result in “excessive” concentrations in the immediate vicinity of the source as a result of downwash created by nearby structures. For this situation, the stack height regulation gives the regulatory agency discretion to require that an excessive ground-level concentration be demonstrated for the existing stack. The two-part definition of excessive concentration requires that the downwash, wakes or eddies induced by nearby structures result in increases in ground-level pollutants that:

- 1) are at least 40 percent in excess of concentrations projected to occur in the absence of nearby structures; and
- 2) cause or contribute to an exceedance of the NAAQS.

To show whether excessive concentrations exist, tests must first be conducted for the existing stacks with all structures present and then with all nearby structures removed. If the ratio of the maximum concentration for each of the stacks under evaluation is at least 40 percent greater with the nearby structures present than without the structures present, the first criterion will have been satisfied.

Next, the maximum concentration due to the combined impact of all stacks is compared with the NAAQS. If this concentration is greater than the NAAQS, the second criterion for demonstrating an excessive concentration will have been satisfied. The EPA regulations then permit credit in regulatory modeling for stack height increases up to the GEP stack height. If a stack height taller than the formula is sought, a wind tunnel demonstration of the GEP height is required.

4.5 Laboratory and Hospital Exhaust and Intake Design

The design of exhaust stacks and air intakes for laboratories and hospitals needs careful consideration due to increasing public concern over air pollution in general, and because adverse exposure to air pollutants in the work place can affect employee health and productivity. In some cases, releases of toxic pollutants may lead to litigation. Some of these issues are illustrated by the following excerpts from newspaper articles:

Business Weekly (May 2, 1988) - "Local residents were frightened. New pharmacology laboratories at the University of California at San Francisco were investigating everything from AIDS to parasitic diseases. Could disease organisms or toxic chemicals from those labs escape and harm citizens?"

San Francisco Chronicle (September 5, 1996) - "A barrage of letters and concerns about toxic chemicals have forced a circuit board manufacturer to drop, at least temporarily, plans to move next door to a peninsula high school."

San Francisco Chronicle (May 20, 1997) - "An outpatient clinic was closed and six of its employees were treated for nausea after they were exposed to fumes from a 16 ounce spill of liquid phenol about noon yesterday."

Chicago Daily Herald (April 17, 1998) - "Suspicious confirmed. Public health officials say brain tumors at Amoco center more than coincidence. A study of Building 503 at the Amoco Research Center in Naperville indicates a rash of malignant brain cancers. Eighteen Amoco Research Center employees have developed brain tumors in the last 28 years."

Some challenges to specifying a good stack design include the existing building environment, aesthetics, building design issues, chemical utilization, source types, local meteorology and topography.

Figure 7 shows a depiction of the air flow around a simple rectangular building. The figure shows the highly turbulent recirculating region on the building roof, upwind of the building and in the building wake. It has been generally thought that stacks are poorly designed if the exhaust is caught in these highly turbulent regions because the pollutant is not able to escape the building cavity, and is thus re-entrained back into the building through air intakes, operable windows, and building entrances. However, stack designs may be acceptable even under this situation if the chemicals being emitted from the exhaust are not toxic or odorous, and/or if sufficient dilution occurs.

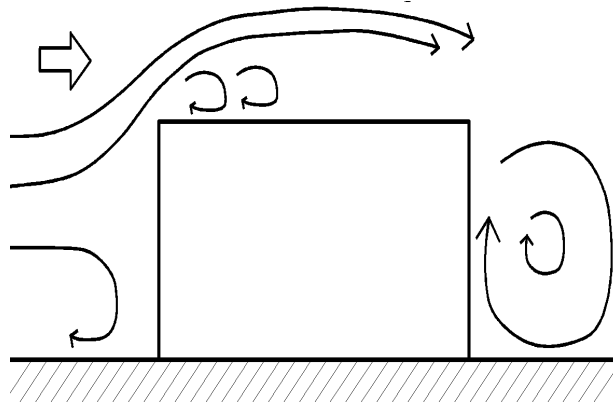


Figure 7. Schematic showing airflow around building.

The existing building environment presents a challenge when building heights vary significantly. If a new laboratory building is being designed that is shorter than surrounding buildings, it will be difficult to design a stack such that the exhaust will not impact neighboring buildings. The effect of a taller downwind building is illustrated in Figure 8. The figure shows how the plume hits the face of the downwind building. In addition, when the taller building is upwind, as shown in Figure 9, the wake cavity region of the taller building may trap the exhaust from the shorter building. In this case the plume once again impacts the face of the taller upwind building. Hence, the frequency of adverse concentrations on the face of the taller building face is augmented.

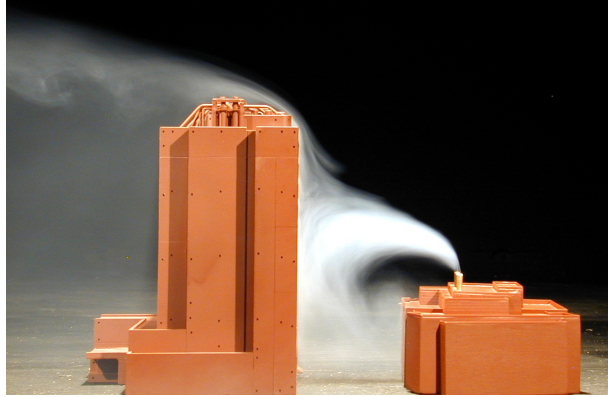


Figure 8. Plume impacting taller downwind building.



Figure 9. Plume caught in taller upwind building cavity.

Constraints are typically placed on laboratory stack design. The lowest possible stack height is desired for aesthetics and economy. The exit momentum (exit velocity and volume flow rate) is limited by capital and energy costs, noise, and vibration. The laboratory stack design then becomes a balance between these constraints and obtaining adequate air quality at surrounding receptors (air intakes, plazas, operable windows, etc.). If an exhaust stack is not properly designed, fumes from the exhaust may reenter the building, or adjacent buildings, or impact pedestrians at unacceptable concentration levels. To avoid reentry, taller stacks, higher volume flows and/or optimum locations on the roof may be necessary.

To determine the optimal exhaust design, predictions of the expected concentrations of pollutants in the exhaust stream at air intakes and other sensitive locations are needed to compare with health limits and odor thresholds. This near-field dispersion problem is ideally suited to wind tunnel modeling. More detailed information on this topic can be found in Petersen et al., (2002, 1991, 1987).

4.6 Other Applications

There are many applications of wind tunnel modeling that go beyond the scope of this chapter. These include:

- *Pedestrian wind evaluations* – In urban areas, the wind environment created by high rises can often lead to uncomfortable and even dangerous wind conditions. Wind tunnel modeling is frequently used by architects early in the design process to help ensure the intended usage of outdoor areas. These evaluations are even required by some cities such as Boston and San Francisco.
- *Hybrid modeling for accidental spills* – A combined wind tunnel and numerical modeling study can be carried out to provide more accurate information for complicated sites. The wind tunnel can be used to define the plume width and height at a facility property line, and then input into an appropriate dispersion model to estimate impacts farther downwind.
- *Water spray mitigation* – Wind tunnel modeling has been used to help assess the effectiveness of water spray systems at mitigating accidental spills of toxic chemicals. Figure 10 shows a wind tunnel simulation of a water spray mitigation system for accidental spills at a refinery.



Figure 10. Water spray mitigation system simulation for an accidental chemical spill at a refinery.

- *Dispersion of heavier than air gas clouds* – Often, accidental chemical or gas spills become super-cooled and heavier than air. This work is discussed in detail by Meroney (1986).
- *Wind loading on structures* – High rises are normally tested in the wind tunnel prior to construction to determine the design wind loads (usually a 50 or 100 year occurrence interval). These tests can also assess building dynamic response.
- *Snow loading assessment* – For unusually shaped buildings, snow accumulations on and around the building can be difficult to predict. Wind tunnel modeling can be used to provide qualitative information on drift

depths on the roof and near entrances. Figure 11 shows the results of a wind tunnel simulation of snow fall on a stadium roof.

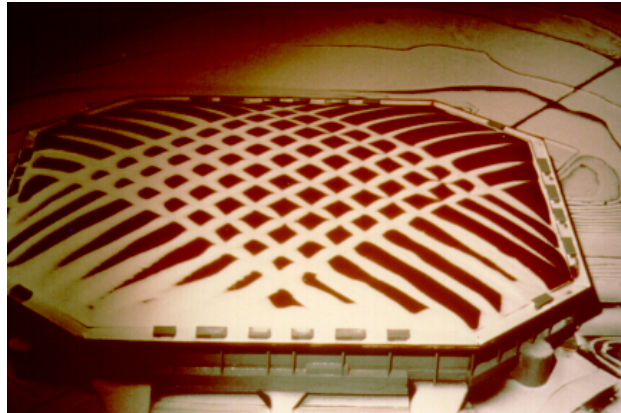


Figure 11. Roof snow deposition simulated in wind tunnel.

References

- Abe, M., "Mountain Clouds, Their Forms and Connected Air Currents," Bull. Cent. Meteor. Obs., Vol. 7, No. 3, Tokyo, 1929.
- Arya, S.P.S. and J.F. Lape, Jr., "A Comparative Study of the Different Criteria for the Physical Modeling of Buoyant Plume Rise in a Neutral Atmosphere," *Atmospheric Environment*, Vol. 24A, No. 2, pp. 289-295, 1990.
- Barbosa, P.H.A., M. Cataldi, and A. Freire, "Wind tunnel Simulation of Atmospheric Boundary Layer Flows," *J. Braz. Soc. Mech. Sci.*, July 2002, vol.24, no.3, p.177-185. ISSN 0100-7386.
- Cermak, J.E., "Applications of Fluid Mechanics to Wind Engineering," A Freeman Scholar Lecture, *Journal of Fluids Engineering*, Vol. 97, p. 9, 1975.
- Cimorelli, A.J., S.G. Perry, A. Venkatram, J.C. Weil, R.J. Paine, R.B. Wilson, R.F. Lee, W.D. Peters, and R.W. Brode. "AERMOD: A Dispersion Model for Industrial Source Applications. Part I: General Model Formulation and Boundary Layer Characterization," *JAM*, 44, 682-693. American Meteorological Society, Boston, MA. (2005).
- Counihan, J., "Adiabatic Atmospheric Boundary Layers. A Review and Analysis of Data from the Period 1880–1972," *Atmospheric Environment*, September 1975.
- EPA. Final Rulemaking on AERMOD. 70 *Federal Register* 68218. See http://www.epa.gov/scram001/guidance/guide/appw_05.pdf. (2005).
- EPA. "User's Guide for the Industrial Source Complex (ISC3) Dispersion Models, Volume I, Users Instructions," EPA-454/B-95-003A, EPA Office of Air Quality Planning and Standards, Research Triangle Park, 1995.
- EPA. "User's Guide for the Industrial Source Complex (ISC3) Dispersion Models. Volume II: Description of Model Algorithms," EPA-454/B-95-003b, 120 pp. [NTIS PB95-222758.] (1995).

EPA. "Screening Procedures for Estimating the Air Quality Impact of Stationary Sources, Revised," EPA-454/R-92-109, 1992.

EPA, "Guideline for Determination of Good Engineering Practice Stack Height (Technical Support Document for the Stack Height Regulation)," US EPA Office of Air Quality, Planning and Standards, Research Triangle Park, North Carolina, EPA-45014-80-023R, 1985.

EPA. *Guideline for Use of Fluid Modeling of Atmospheric Diffusion*. U.S. Environmental Protection Agency, Office of Air Quality, Planning and Standards, Research Triangle Park, North Carolina, EPA-600/8-81-009, April 1981a.

EPA. "Guideline for Determination of Good Engineering Practice Stack Height (Technical Support Document for the Stack Height Regulation)," US EPA Office of Air Quality, Planning and Standards, Research Triangle Park, North Carolina, EPA-450/4-80-023, 1981b.

Field, J.H. and R. Warden, "A Survey of the Air Currents in the Bay of Gibraltar in 1929-1930," Air Ministry Meteor. Office Geophys. Mem., No. 59.

Golden, J., "Scale Model Techniques," M.S. Thesis, College of Engineering, New York University, NY, 1961.

Halitsky, J., "Gas Diffusion Near Buildings," in *Meteorology and Atomic Energy*, D.H. Slade (Ed.), Chapter 5-5, 1968.

Hanna, S.R., M.J. Brown, F.E. Camelli, S.T. Chan, W.J. Coirier, O.R. Hansen, A.H. Huber, S. Kim, and R.M. Reynolds, "Detailed Simulations of Atmospheric Flow and Dispersion in Downtown Manhattan," BMAS, December 2006.

Hoult, D.P. and J.C. Weil, "Turbulent Plume in a Laminar Cross Flow," *Atmospheric Environment*, v. 6, pp. 513-531, 1972.

Hosker, R.P., "Flow and Diffusion Near Obstacles," Chapter 7 in *Atmospheric Science and Power Production*, Ed. Darryl Randerson, Technical Information Center, Office of Scientific and Technical Information, United State Department of Energy, DOE/TIC - 17601, 1984.

Huber, A., M. Freeman, R. Spencer, B. Bell, K. Kuehlert and W. Schwarz, "Applications of CFD simulations of pollutant transport and dispersion within ambient urban building environments: Including homeland security," AMWA 98th Annual Conference, Minneapolis, MN, Paper Number 1241, 2005.

Huber, A.H. and W.H. Snyder, "Wind Tunnel Investigation of the Effects of a Rectangular-Shaped Building on Dispersion of Effluents from Short Adjacent Stacks," *Atmospheric Environment*, Vol. 16, No. 12, pp. 2837-2848, 1982.

Huber, A.H. and W.H. Snyder, "Building Wake Effects on Short Stack Effluents," Preprint Volume for the Third Symposium on Atmospheric Diffusion and Air Quality, American Meteorological Society, Boston, Massachusetts, 1976.

Jensen, M. and N. Franck, "Model-Scale Tests in Turbulent Wind, Part I: Phenomena Dependent on the Wind Speed,": Danish Technical Press, Copenhagen, 1963.

Meroney, R.N., "Wind Tunnel and Numerical Simulation of Pollution Dispersion, A Hybrid Approach," Invited Lecture, Croucher Advanced Study Institute, Hong Kong University of Science and Technology, 6-10 December, 2004.

Meroney, R.N., "Bluff body Aerodynamics Influence on Transport and Diffusion," *Journal of Wind Engineering and Industrial Aerodynamics*, Vol. 33, p. 21, 1990.

Meroney, R.N., "Guidelines for Fluid Modeling of Dense Gas Cloud Dispersion," *Journal of Hazardous Materials*, Vol. 17, pp. 23-46, 1987.

Meroney, R.N., "Guidelines for Fluid Modeling of Liquefied Natural Gas Cloud Dispersion," Gas Research Institute Report No. GRI-86-0102.2, Chicago, IL, 1986.

Ooms, G., "A New Method for the Calculation of the Plume Path of Gases Emitted by a Stack," *Atmospheric Environment*, Vol. 6, 1972.

Paine, R.J. and R. Lew, "Project PRIME: Evaluation of Building Downwash Models Using Field and Wind Tunnel Data", Preprint Volume for the Tenth Joint Conference on Applications of Air Pollution Meteorology with A&WMA, American Meteorological Society, Phoenix, Arizona, 1998.

Petersen R.L. and J. Carter, "Evaluation of AERMOD/PRIME for Two Sites with Unusual Structures," 99th Annual AWMA Conference, New Orleans, Louisiana, June 20-23, 2006.

Petersen, R.L., B.C. Cochran, and J.J. Carter, "Specifying Exhaust and Intake Systems," *ASHRAE Journal*, August 2002.

Petersen, R.L., "Evaluation of ISC-PRIME for Stacks at Various Distances From Buildings," Paper 387 presented at the Air and Waste Management Associations 94th Annual Conference and Exhibition, Orlando, Florida, June 25-27, 2001.

Petersen, R.L., B.C. Cochran, and J.J. Carter, "Comparison of ISC and PRIME Model Predictions Versus Wind-tunnel Observations," Paper 1113 presented at the Air and Waste Management Associations 93rd Annual Conference and Exhibition, Salt Lake City, Utah, June 18-22, 2000.

Petersen, R.L., B.C. Cochran, D.E. Keen, and R.N. Walton, "Equivalent Building Dimensions for ISC2 Modeling Applications," presented at the 88th Annual Meeting and Exhibition of the Air and Waste Management Association, San Antonio, Texas, June 18-23, 1995.

Petersen, R.L. and M.A. Ratcliff, "An Objective Approach To Laboratory Stack Design," *ASHRAE Transactions*, Vol. 97, Pt. 2, 1991.

Petersen, R.L., "Performance Evaluation of Integral and Analytical Plume Rise Algorithms," *JAPCA*, Vol. 37, No.11, 1987.

Petersen, R.L. and M.A. Ratcliff, "Evaluation of Improvements to the Plume Rise Algorithms in the ISC Model," 80th Annual APCA Meeting, New York, NY, June 21-26, 1987.

Petersen, R.L., "Designing Building Exhausts to Achieve Acceptable Concentrations of Toxic Effluent," *ASHRAE Transactions*, Vol. 93, Pt. 2, 1987.

Petersen, R.L. and M.A. Ratcliff, "Evaluation of Modifications to the Plume Rise Algorithms in the Industrial Source Complex Mode," prepared for American Petroleum Institute, Washington, D.C., API Publication No. 4444, October 1986.

Petersen, R.L., "Plume Rise and Dispersion for Varying Ambient Turbulence, Thermal Stratification and Stack Exit Conditions," dissertation, CED77-78RLP25, Colorado State University, Fort Collins, CO, 1978.

Schlichting, H., "Boundary-Layer Theory," McGraw-Hill, NY, NY, 1978.

Sherlock, R.H. and E.A. Stalker, "The Control of Gases in the Wake of Smokestacks," ASME Journal, 62, 455-468, 1940

Schulman, L.L., D.G. Strimaitis, and J.S. Scire, "Development and Evaluation of the PRIME Plume Rise and Building Downwash Model," JAWMA, Vol. 50, pp. 378-390, March 2000.

Snyder, W.H. and R.E. Lawson, "Wind-tunnel Measurements of Flow Fields in the Vicinity of Buildings," Eighth Joint Conference on Applications of Air Pollution Meteorology with A&WMA. January 23-29, 1994.

Snyder, W.H., "Wind-Tunnel Simulation of Building Downwash from Electric-Power Generating Stations. Part II: Pulsed-Wire Measurements in Vicinity of Steam-Boiler Building." U.S. EPA, Research Triangle Park, NC, 1993.

Snyder, W.H., "Wind-Tunnel Simulation of Building Downwash from Electric-Power Generating Stations. Part I: Boundary Layer and Concentration Measurements." U.S. EPA, Research Triangle Park, NC, 1992.

Townsend, A.A., "The Structure of Turbulent Shear Flow," Cambridge University Press, Cambridge, England, 1956.

Tikvart, J., "United States Environmental Protection Agency, NC, letter to Brenda Johnson, Regional Modeling Contact, Region IV and Douglas Neeley, Chief Air Programs Branch, Region IV, July 25, 1994.

Turner, D.B., "Workbook of Atmospheric Dispersion Estimates," Lewis Publishers, Boca Raton, Florida, 1994.

BRANKLEY
PAPER

Chapter 25

Tracer Studies

A chapter on tracer studies (e.g., the use of tracer experiments to measure atmospheric dispersion parameters) is expected in Volume IV.

BRAND
PAPER

Daly, A. 2008. *Air Quality Modeling: Pre-Processing and Post-Processing*. Chapter 26 of *AIR QUALITY MODELING - Theories, Methodologies, Computational Techniques, and Available Databases and Software. Vol. III – Special Issues* (P. Zannetti, Editor). Published by The EnviroComp Institute (<http://www.envirocomp.org/>) and the Air & Waste Management Association (<http://www.awma.org/>).

Chapter 26

Air Quality Modeling: Pre-Processing and Post-Processing

Aaron Daly

EnviroComp Consulting, Inc., Fremont, CA (USA)
daly@envirocomp.com

Abstract: Environmental scientists now have an abundance of tools and data readily available to conduct and visualize air quality modeling simulations. Examples of using current tools for pre-processing and post-processing in air quality modeling are discussed, along with sources of data and the increasingly important role of Geographic Information Systems (GIS) in post-processing and visualization of modeling results.

Key Words: 2D visualization, 3D visualization, emission data, meteorological data, terrain data, land use/land cover data, aerial photography, satellite imagery, remote sensing, pollution roses, GIS, GUI, ESRI, ArcGIS, ArcExplorer, Global Mapper, Google Earth, SketchUp, georeferencing, geocoding.

1 Introduction

Since air quality models have been programmed in specialized computer languages such as FORTRAN, these programs require the input data to be in specific formats and contain certain meteorological parameters in order to run properly. After a user has collected the input data, or “raw data” that is required for running a model, the user needs to organize this data and also add additional inferred values so that the modeling program can read it and operate. The process of preparing raw data and inferring additional meteorological parameters to use in an air quality program is called the “Pre-processing of data”¹.

¹ <http://www2.dmu.dk/AtmosphericEnvironment/cost/fisher.htm>

After the data has been pre-processed and successfully read into the model, the output data from the modeling simulation needs to be evaluated for correctness, organized for clarity, and presented in a way so that the modeler and his/her colleagues and clients can understand the results. Sometimes, additional parameters and statistics need to be derived from the model output (e.g., averages or percentiles). This process of evaluating, organizing, presenting, and deriving additional values from the model output is called the “post-processing of data”². Post-processing is also used as a diagnostic examination of the modeling simulation to determine whether the results are plausible and the model is working properly.

The air quality models that are available from the United States Environmental Protection Agency (US EPA)³ and other regulatory agencies are usually composed of several modules. Besides the main module that performs the actual air dispersion simulation calculations, there are modules that perform pre-processing and post-processing tasks. These modules interact and share data with the main module.

Several private companies^{4,5,6} have developed program suites that serve as “front-ends” to modules of several widely-used air dispersion models such as AERMOD⁷ and CALPUFF⁸. These front-ends are usually graphical user interfaces (GUIs) that simplify the stages of pre-processing and post-processing and many other tasks such as setting up the modeling domain and assigning receptors.

2 Pre-Processing

The availability of front-ends for air dispersion models has reduced the amount of manual pre-processing work that is typically required for performing air dispersion simulations. However, users will usually still need to pre-process some data to enter into the front-ends. The following sections are examples and recommendations on how to handle data that may need pre-processing before it can be used in an air quality model.

2.1 Emission Data

Regulatory air dispersion models require the emission rate to be defined over regular time intervals that are typically one hour in length. If one is modeling a

² http://www.flame.org/~cdoswell/forecasting/human_role/future_forecasters.html

³ <http://www.epa.gov/scram001/>

⁴ <http://www.weblakes.com/>

⁵ <http://www.beeline-software.com/>

⁶ <http://www.breeze-software.com/>

⁷ http://www.epa.gov/scram001/dispersion_prefrec.htm#aermod

⁸ http://www.epa.gov/scram001/dispersion_prefrec.htm#calpuff

release scenario with emissions that vary in time or last for a short time, they should be averaged appropriately to fit the requirements of the model. For example, in simulating hourly averages, a release scenario that involves 2000 grams of pollutant released over a period of 6 minutes is averaged in the following way to produce an equivalent emission rate for the entire first hour of the release:

$$\text{Hourly Emission Rate} = \frac{2000 \text{ grams}}{3600 \text{ seconds}} = 0.5556 \text{ g/s} \quad (1)$$

Using an air dispersion model for accident reconstructions (e.g., fires or explosions) may require emission modeling as a separate step to characterize the substances that are being emitted and to develop a timeline of their emissions. The emission data used in air quality modeling are generally computed by an engineering evaluation of the release. Methodologies and guidelines are also provided by the US EPA^{9,10,11}.

2.2 Meteorological Data

Most regulatory air dispersion models require meteorological data from surface stations and upper-air stations. The front-ends to meteorological pre-processing modules, such as AERMET¹² and CALMET¹³, are able to read meteorological data in many formats, but it is likely that data from representative surface stations may be in an unreadable format. For example, currently, the National Climatic Data Center¹⁴ (NCDC) provides archived surface station data in different formats than SAMSON¹⁵ and SCRAM/MET144¹⁶, which are two conventional formats read by front-ends to meteorological pre-processors. If modelers require surface station data in formats such as SAMSON or SCRAM/MET144, they can try sources such as WebMET¹⁷ and WorldGeoData¹⁸. Also, the Weather Underground¹⁹ website has historical METAR records for weather stations worldwide. The advantage of purchasing data from a service like WorldGeoData is that the data has been quality-checked and missing data has been corrected in accordance with US EPA guidelines²⁰.

⁹ <http://www.epa.gov/otaq/ap42.htm>

¹⁰ <http://www.epa.gov/ttn/chief/efpac/index.html>

¹¹ <http://www.epa.gov/OMSWWW/models.htm>

¹² http://www.epa.gov/scram001/metobsdata_procaccprogs.htm#aermet

¹³ http://www.src.com/calpuff/download/CALMET_UsersGuide.pdf

¹⁴ <http://www.ncdc.noaa.gov/>

¹⁵ <http://www.webmet.com/MetGuide/Samson.html>

¹⁶ <http://www.webmet.com/MetGuide/SCRAMSurface.html>

¹⁷ <http://www.webmet.com>

¹⁸ <http://www.worldgeodata.com/home.aspx>

¹⁹ <http://www.wunderground.com/>

²⁰ <http://www.epa.gov/scram001/guidance/met/mmgrma.pdf>

The most commonly used weather stations for regulatory air quality modeling in the US have been nearby National Weather Service (NWS) stations, which are usually located at major airports. These airport observations may not be the most suitable data for an air quality modeling application, because even though the data is reported every hour, the wind observations are not hourly averages. Instead, the airport winds are only 2-minute averages²¹, and therefore may not properly characterize the winds over the entire hour.

Alternate sources of meteorological data that may have hourly-averaged winds or wind data collected over shorter intervals include monitoring stations maintained by environmental regulatory agencies (e.g., CARB²² and LDEQ²³); agricultural networks (e.g., CIMIS²⁴ and LSU AgCenter²⁵); academic institutions; and private industry²⁶. Data retrieved from these stations will usually have to be reformatted to a style compatible with the pre-processor. The front-end may have the ability to import data from a spreadsheet format (e.g., Microsoft Excel) and convert it to a common format like SAMSON²⁷. If one needs to compute hourly averages or standard deviations from wind data reported in smaller time intervals, the US EPA guidelines should be consulted.

One should also make an effort to understand several characteristics about a weather station, including its geographic coordinates, terrain height of its location, height of its sensors, the type of land use in the surrounding area (e.g., rural, urban, residential, industrial, wetlands, grasslands, forests, etc.). It is also useful to know how the instrument is sited. For example, a wind sensor located in an open area with no buildings nearby may give more suitable wind data than one located close to or on top of a building.

Upper-air radiosonde data is commonly reported in an FSL format²⁸, as well as different NCDC formats. Manual pre-processing is usually not needed for radiosonde data since these formats are understood by front-end programs. Historical worldwide radiosonde data is available at the FSL website²⁹ or NCDC.

If mixing height data is needed, it can be calculated from radiosonde data by using a program³⁰ from the US EPA. The version of this program that is available currently (98340) is an older utility (December 1998), which is not Y2K compliant, and may have to be recompiled for computers that were built after the

²¹ <http://www.ofcm.gov/fmh-1/pdf/E-CH5.pdf>

²² <http://www.arb.ca.gov/homepage.htm>

²³ <http://www.deq.louisiana.gov/portal/>

²⁴ <http://www.cimis.water.ca.gov/cimis/welcome.jsp>

²⁵ <http://www.lsuagcenter.com/weather/>

²⁶ Other U.S. states have similar websites for meteorological and air quality measurements. Here we cited California and Louisiana sites only.

²⁷ <http://www.webmet.com/MetGuide/Samson.html>

²⁸ http://raob.fsl.noaa.gov/intl/fsl_format-new.cgi

²⁹ <http://raob.fsl.noaa.gov/>

³⁰ http://www.epa.gov/scram001/metobsdata_procaccprogs.htm#mixing

year 2000. The source code and documentation are available with the program, so the mixing heights algorithm can be duplicated if the program does not work.

Mixing height data can also be purchased from NCDC and WorldGeoData³¹, and some historical data is available from the US EPA SCRAM website³².

2.3 Maps/Aerial Photography/Satellite Imagery

Front-end programs often allow the user to insert a basemap image into the modeling domain. The modeler can scan a paper document that contains a street map or industrial site map, and import the image into the program. In order to properly align the image in the domain, the modeler needs to have geographic coordinates of at least two points on the image. More details about this procedure (called georeferencing) are given in section 4.

Using a procedure similar to maps, aerial photography and satellite imagery can be scanned and imported into the modeling domain, provided that the modeler has accurate geographic information about them. It is preferred that imagery be “orthorectified”, which means that any distortion due to terrain or camera angle is removed. This results in an image with a uniform scale that can be used as a map in a modeling domain. Sources of orthophoto imagery are numerous, and include the United States Geological Survey (USGS)³³, DigitalGlobe³⁴, Terraserver³⁵, GeoEye³⁶, and MapMart³⁷.

The most common type of imagery has the camera aimed directly down at the ground, but imagery where the camera is at an angle (“oblique imagery”) is becoming more popular. Oblique imagery, also called “Bird’s Eye View” imagery, can be used for a three-dimensional perspective. Pictometry³⁸ specializes in oblique imagery, and they sell imagery along with specialized tools that can give geographic coordinates of ground locations and measure horizontal and vertical distances in the images.

2.4 Terrain and Land Use/Land Cover

Terrain data is freely available on the internet in several formats. The common format for U.S. terrain data is Digital Elevation Model (DEM), which has a resolution up to 1 arc-second, which is about 30 meters for the contiguous U.S.

³¹ <http://www.worldgeodata.com/home.aspx>

³² <http://www.epa.gov/scram001/mixingheightdata.htm>

³³ <http://www.usgs.gov/>

³⁴ <http://www.digitalglobe.com/>

³⁵ <http://www.terraserver.com/>

³⁶ <http://www.geoeye.com/>

³⁷ <http://www.mapmart.com/>

³⁸ <http://www.pictometry.com/>

One source of DEM is WebGIS³⁹. A source of highly accurate terrain data is the Shuttle Radar Topography Mission⁴⁰, which is available for the entire world. Depending on the location, this terrain data is in 90 meter or 30 meter resolution. Land use or land cover data is often used in conjunction with terrain data, and both are available from WebGIS, TRC⁴¹, the National Geophysical Data Center⁴², and the Global Land Cover Facility⁴³.

It can be challenging to convert terrain and land use data into the correct format required for a pre-processor. The program Global Mapper⁴⁴ is a useful tool for this task. It can retrieve, read, display, and convert many types of imagery and geophysical data into different formats, and it is relatively inexpensive and easy to use.

When a modeler imports any extra layers of data (i.e., imagery, terrain, land use/land cover) into pre-processors, he/she needs to be aware of the coordinate system and datum associated with the modeling domain and the data layers so that the data layers are placed properly in the domain. A common mistake is to confuse the two datums NAD27 and NAD83. NAD83 is a modern datum that was developed in 1983, but geographic data may still be archived in the older NAD27 datum developed in 1927. Not accounting for the correct datum could result in errors up to 100 meters. A program like Global Mapper or other Geographic Information Systems (GIS) programs are very useful in identifying the coordinate systems and datums of imported data and aligning them correctly. More information about GIS programs is given in section 4.

3 Post-Processing

After an air quality simulation has successfully run, it is often desirable to have a graphical representation of air pollutant concentrations. This visualization can be useful in determining the impact of a plume of pollutants on a nearby community and in determining if the simulation was a reasonable representation of the real world.

Many front-ends to air quality models have their own post-processing modules that display contours of concentrations in the modeling domain. If one has used an aerial photograph or streetmap as a basemap, one can then evaluate the impact and correctness of a plume.

Post-processing modules can be useful diagnostic and visual tools, but if a simulation project involves producing very accurately contoured data or high-

³⁹ <http://www.webgis.com>

⁴⁰ <http://srtm.usgs.gov/>

⁴¹ http://www.src.com/datasets/datasets_main.html

⁴² <http://www.ngdc.noaa.gov/>

⁴³ <http://glcf.umiacs.umd.edu/index.shtml>

⁴⁴ <http://www.globalmapper.com/>

quality graphical output, or knowing the relationships between the simulated plume and several other types of data, it is very useful to import the modeling results into a GIS workspace. This is a straightforward process if the modeling output is given as a text file with the coordinates and concentrations at each receptor used in the simulation. This is the case for models like AERMOD and CALPUFF. Other US EPA models, like ALOHA and SLAB, may give output in the form of the coordinates of each concentration contour curve, and extra steps are needed to import these contour levels into a GIS workspace.

Figure 1 below shows an example of a plume overlaid on an aerial picture in a GIS workspace.

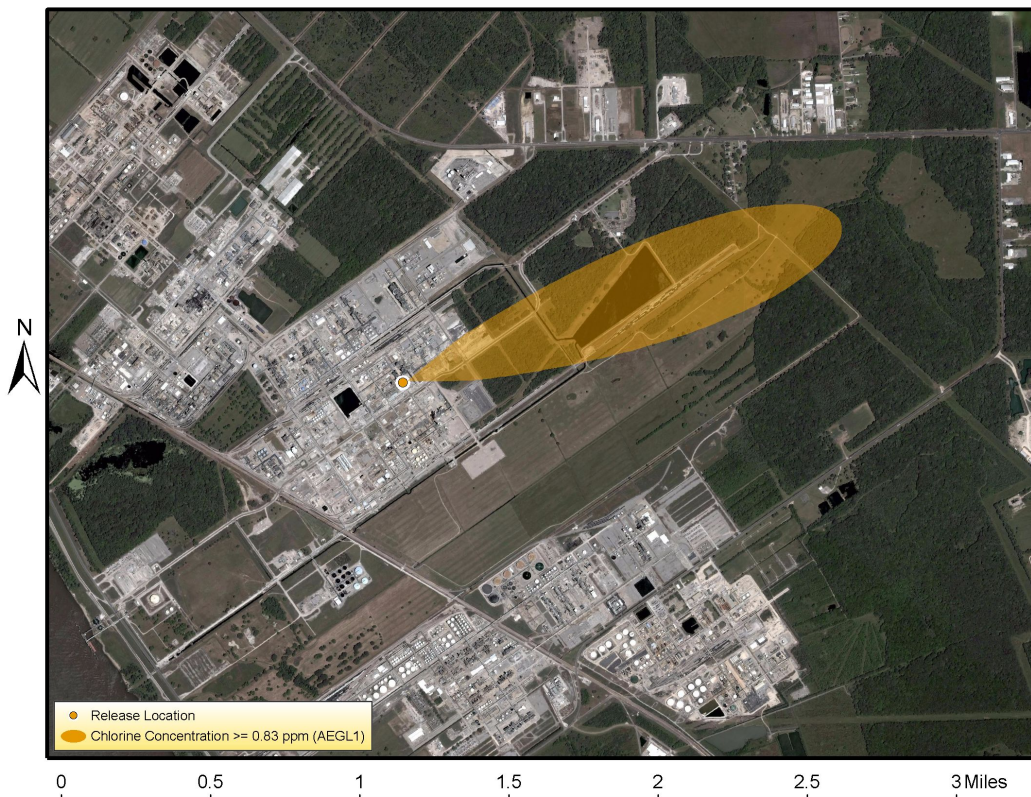


Figure 1. Post-processed plume in a GIS workspace.

The GIS environment allows the user to have significantly more control over how the plume is contoured and displayed than in typical post-processing modules, and the user can also overlay many other types of data along with the plume. Figure 2 below shows the same plume along with extra annotation that shows the time of the simulation and the wind direction.

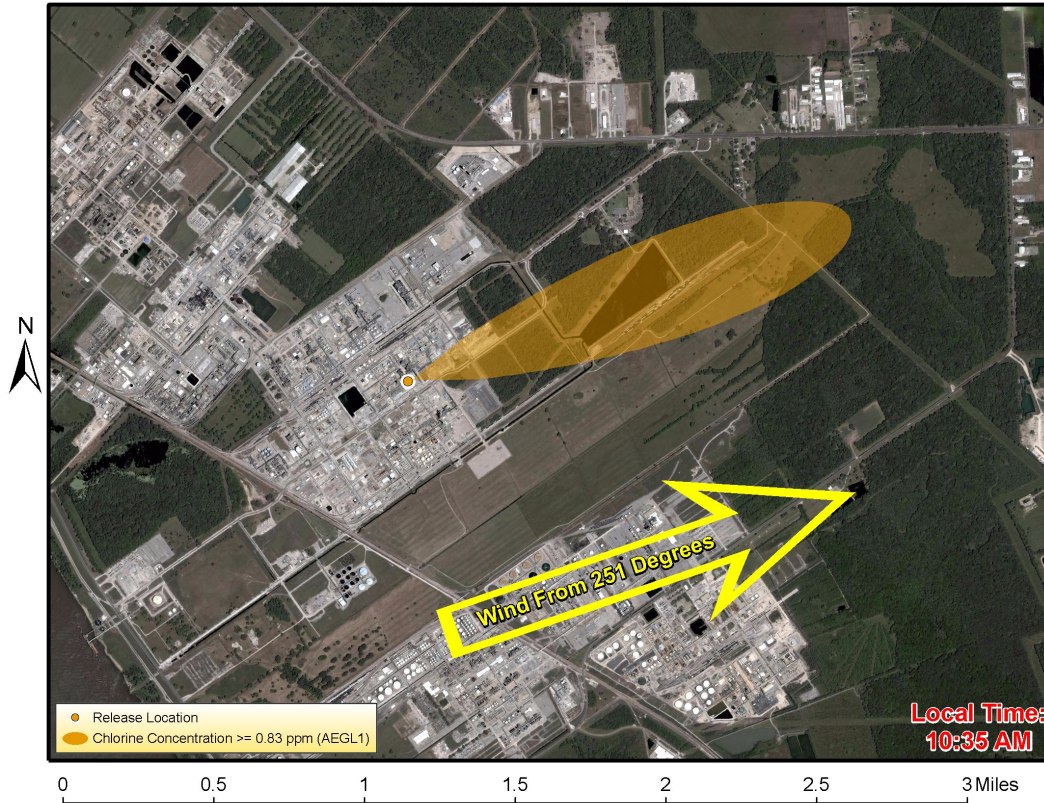


Figure 2. Post-processed plume in a GIS workspace with additional annotation.

Figure 3 shows the same plume with an overlay of the locations of several air quality measurements as a diagnostic exercise. Importing air quality measurements that have Global Positioning System (GPS) coordinates assigned to them is a straightforward task in the GIS environment.

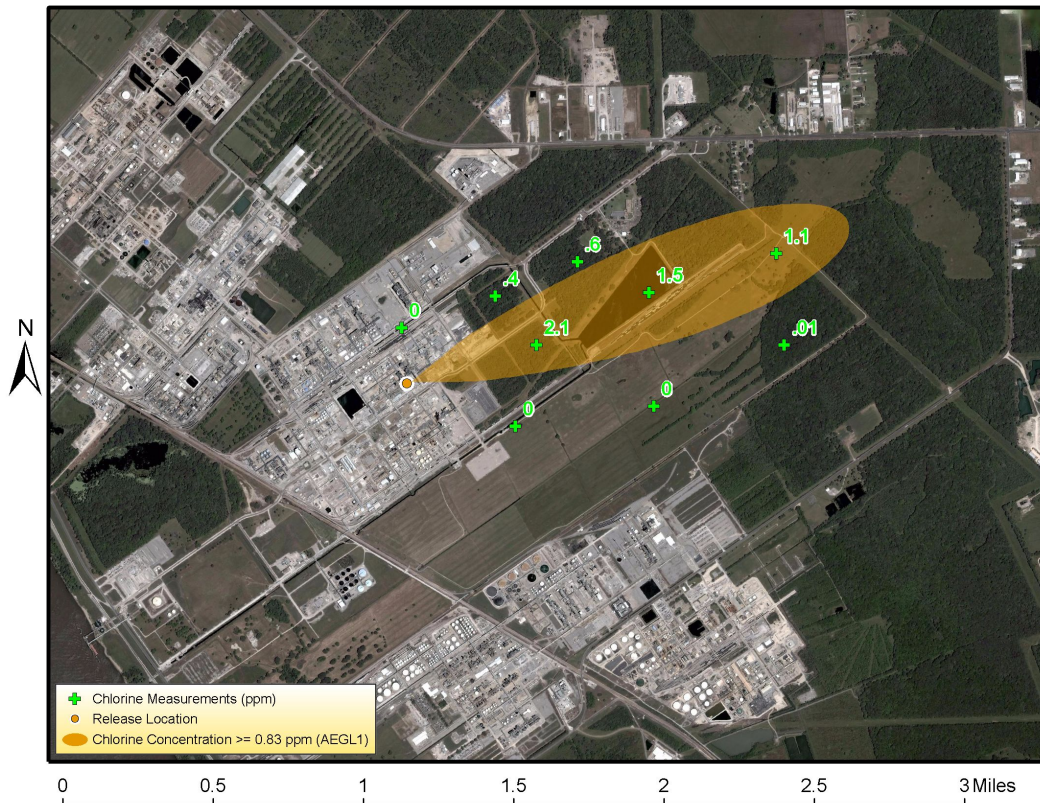


Figure 3. Post-processed plume in a GIS workspace displayed with locations of air quality measurements.

One may be interested in the subset of a data layer contained inside the plume. Figure 4 shows the same plume along with a layer that represents locations of claimants in a litigation case.

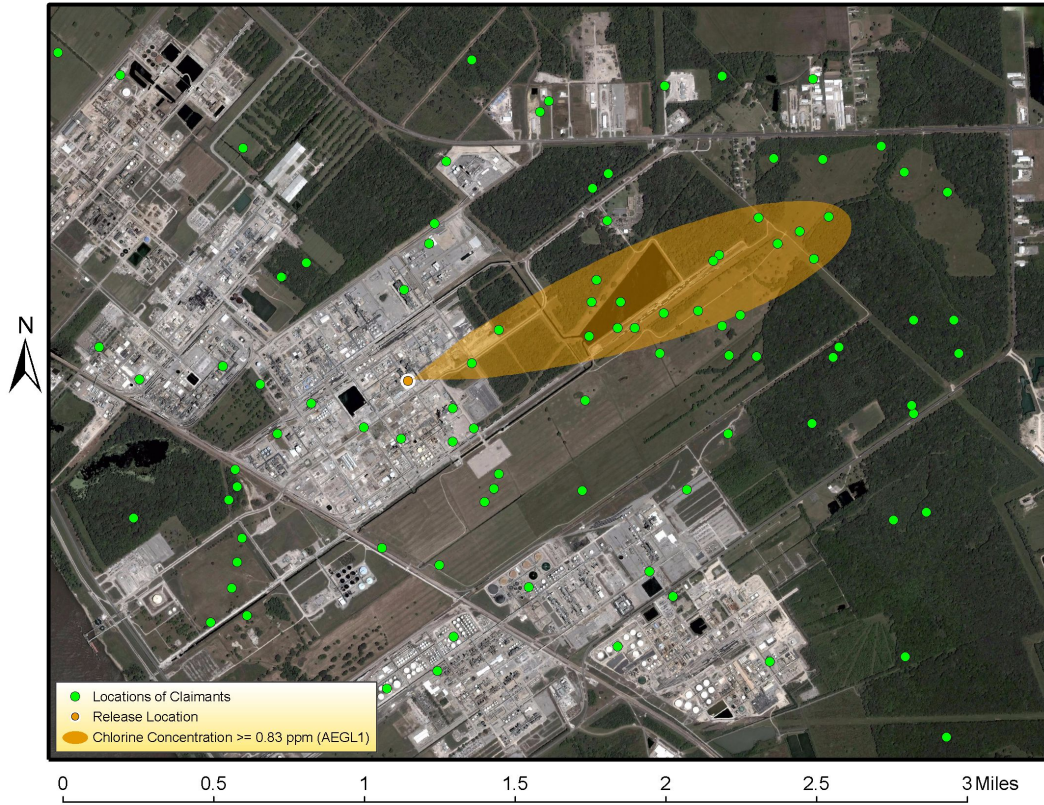


Figure 4. Post-processed plume in a GIS workspace displayed with claimant locations.

The GIS program can automatically extract the points inside the plume, which results in Figure 5. In this figure, the blue dots are the claimants inside the plume.

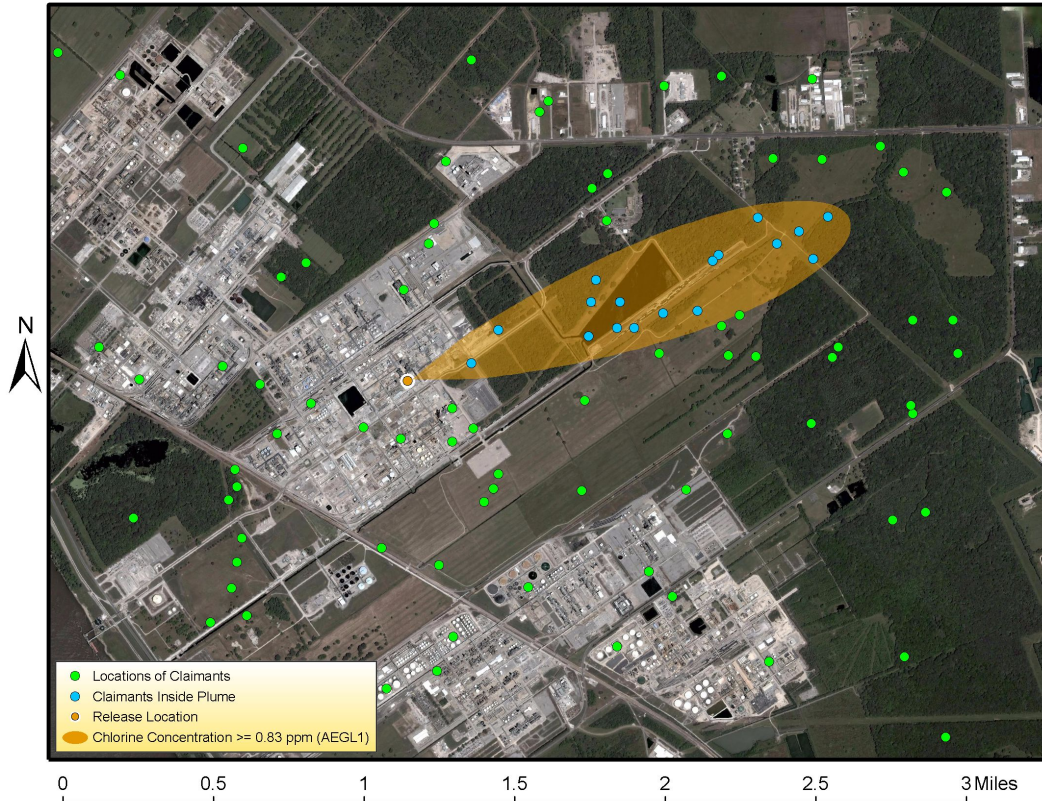


Figure 5. Post-processed plume in a GIS workspace displayed with locations of claimants in the area and also claimants inside the plume.

Since air quality models are often used to predict the impact of pollutants on people at ground level, two-dimensional (2D) representations like the preceding figures are often sufficient to tell the story. However, it may be useful to have a three-dimensional (3D) visualization of a plume if the simulation is over a very large area. Figure 6 is an image from a Google Earth⁴⁵ time animation of a 3D volcanic plume simulation of the Mount Etna eruption⁴⁶ on July 24, 2001. (Click on [Etna Animation](#) in the CD version of the book to view the full animation).

⁴⁵ <http://earth.google.com/>

⁴⁶ http://puff.images.alaska.edu/Google_Earth2/Etna_24_July_2001.gif



Figure 6. Post-processed plume of volcanic ash from the Mt. Etna eruption of July 24, 2001, in the Google Earth workspace.

Figure 7 is an image from a Google Earth time animation of a 3D volcanic plume simulation of the Mount St. Helens eruption⁴⁷ in May 1980. (Click on [St. Helens Animation](#) in the CD version of the book to view the full animation).

⁴⁷ http://puff.images.alaska.edu/Google_Earth2/StHelens_May_1980_side.gif

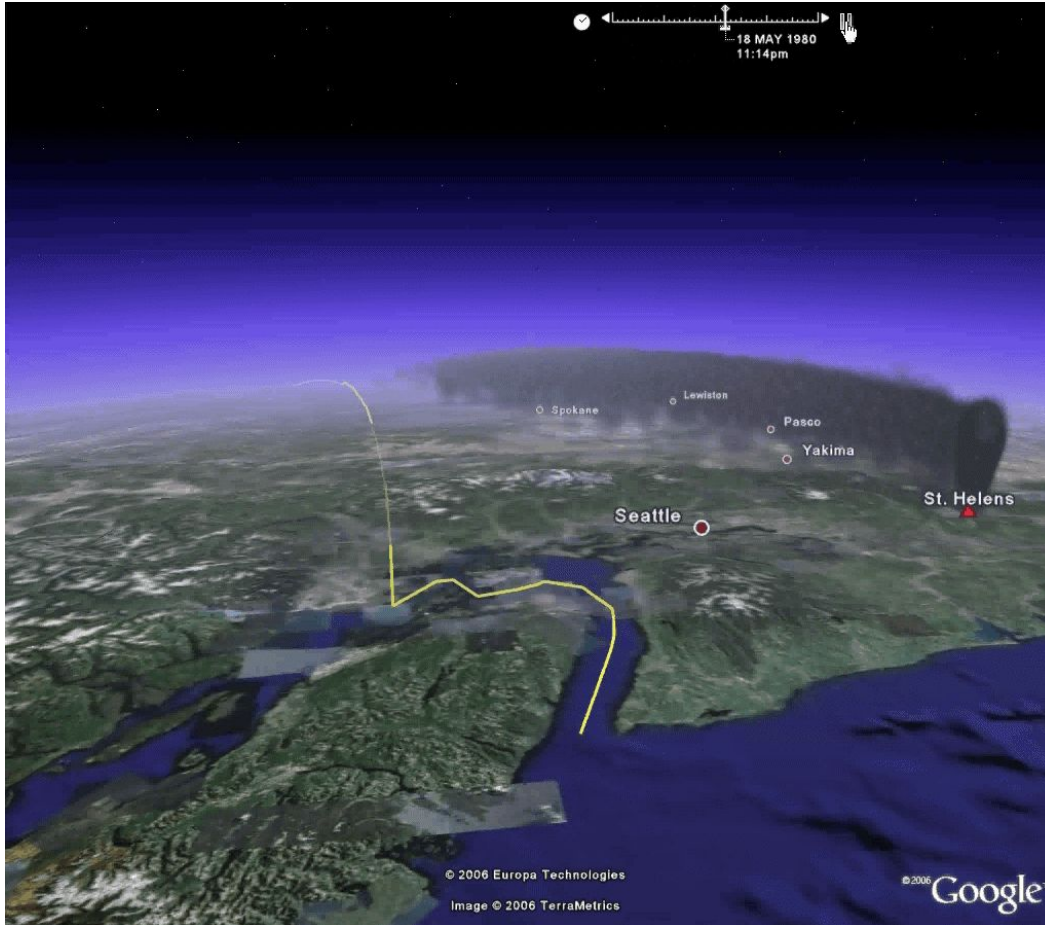


Figure 7. Post-processed plume of volcanic ash from the Mt. St. Helens eruption in May, 1980, in the Google Earth workspace.

Statistical analysis can be an important part of post-processing. For example, the output of air quality simulations are typically a sequence of air concentrations of a certain substance averaged over a period of time at each receptor. The average concentration values are used to create visualizations of plumes, but it can also be useful to look at concentrations over shorter intervals to see the range of concentration values. Figure 8 shows a timeline of concentrations at a single receptor in an air quality simulation. In this case, the peak 24-hour concentrations can be 25-30 times higher than the 5-year average concentrations. Also plotted is a Level of Concern (LOC) for this particular chemical. One can focus on days when the modeled concentrations exceeded this LOC as the next part of the modeling analysis.

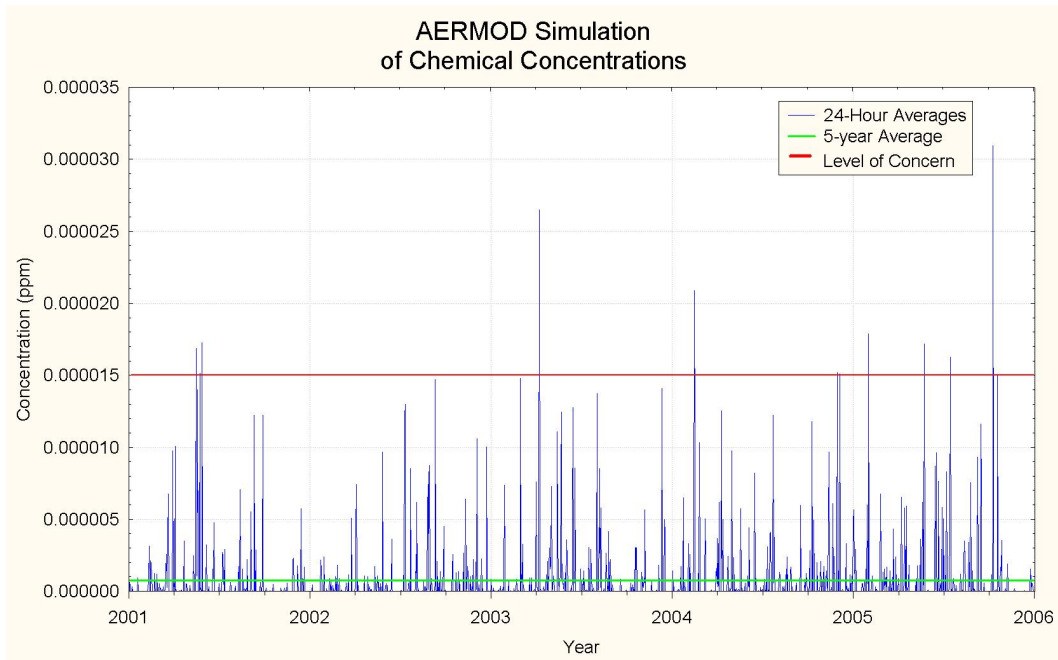


Figure 8. Timeline of simulated average concentrations from AERMOD.

Another useful statistical tool is a pollution rose. This tool combines wind direction data and air quality measurements to determine what directions the pollution is coming from. Figure 9 is a pollution rose for the tracer gas PTCH⁴⁸. The petals of the rose point to the directions the tracer is coming from, and a larger petal means that more tracer gas is coming from that direction. In the figure, the major source of PTCH is from the south.

⁴⁸ perfluoro-trimethylcyclohexane.

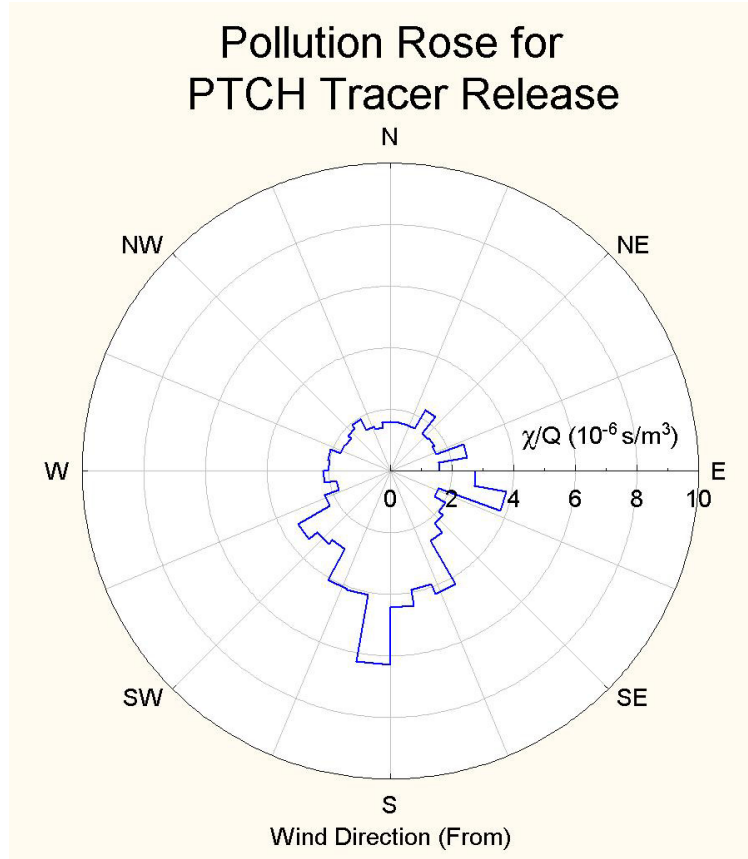


Figure 9. Pollution Rose for a Tracer Gas.

4 GIS in Air Quality Modeling

The field of GIS is constantly evolving and is gradually becoming more commonplace. The availability of free utilities like Google Earth and ArcExplorer⁴⁹ make GIS data and tools accessible to anyone with newer computers and fast internet access.

GIS can be used in an air quality modeling simulation from start to finish. For example, one may need to create an area source polygon for running AERMOD. A GIS user can view an aerial orthophoto, identify the source boundaries, and use tools to digitize the source polygon. The coordinates of the polygon source can then be entered into a front-end of an air quality model.

One can also use GIS to assign a scale and a coordinate system to an image. This process is called “georeferencing”. All that is needed are the coordinates of several locations in the image, and the GIS program georeferences the image so that it can be used as a basemap layer. Google Earth is useful for obtaining

⁴⁹ <http://www.esri.com/software/arcgis/explorer/index.html>

coordinates since it displays layers of georeferenced orthophotography for the entire Earth.

Some GIS programs can assign coordinates to street addresses. This process is called “geocoding”. Geocoding is useful when one has a large list of locations that need to be displayed on a map. Both Google Maps⁵⁰ and Google Earth can geocode addresses. The program ArcGIS⁵¹ developed by ESRI⁵² also geocodes addresses, and one example of an online geocoding service is EZ-Locate⁵³.

GIS programs are also useful for “geoprocessing” tasks. These tasks include extracting data that lie inside of another layer (e.g., the claimants inside the plume in Figure 5), extracting data that are a certain distance from another layer, converting discrete point data into continuous data surfaces and vice versa, and interpolating and contouring data.

One very powerful aspect of a high-end GIS program like ESRI’s ArcGIS is that it organizes many data layers such as discrete points, polygons, images, data surfaces, tables, and contours into a “geodatabase”. This geodatabase is in Microsoft Access format, which means that it is accessible to non-GIS users who can interact with the database and update its information. Previously-created Access databases can also be imported into ArcGIS and integrated with spatial data to create geodatabases.

High-end GIS programs like ArcGIS can also be programmed with customized tasks. It is feasible to create tasks for air quality modeling directly in the GIS environment so that with a click of a button, an air quality simulation runs and plumes of pollutants are displayed over imagery and terrain.

Another advanced use of GIS is remote sensing where multi-spectral imagery can be classified into different types of land use/land cover, which may play an important role in air quality simulations. An example is shown in Figure 10 below. The top picture is a USGS Landsat Thematic Mapper (TM)⁵⁴ image of Tippecanoe County, Indiana from July 17, 1986. The bottom picture is the same image classified into different types of crops⁵⁵. The program used for the classification is a freeware program called MultiSpec⁵⁶ that is developed by Purdue University.

⁵⁰ <http://maps.google.com/>

⁵¹ <http://www.esri.com/products.html>

⁵² <http://www.esri.com/>

⁵³ <http://www.geocode.com/>

⁵⁴ http://edc.usgs.gov/guides/landsat_tm.html

⁵⁵ Images are taken from http://cobweb.ecn.purdue.edu/~biehl/MultiSpec/Intro5_01.pdf

⁵⁶ <http://cobweb.ecn.purdue.edu/~biehl/MultiSpec/>

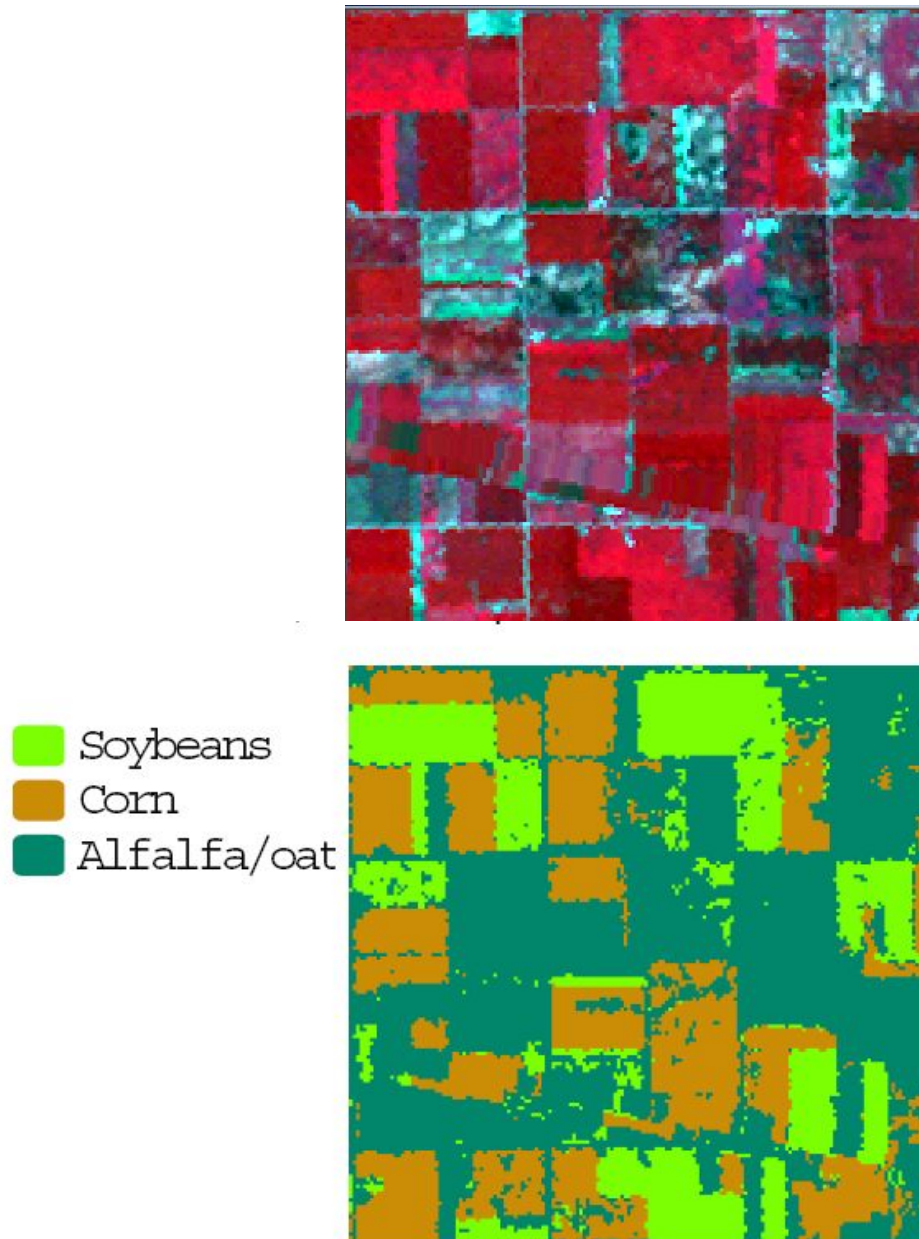


Figure 10. USGS Landsat TM image of fields in Tippecanoe County, Indiana (top), and the same image classified into different types of crop cover (bottom).

Computational Fluid Dynamics (CFD) models can also benefit from the use of GIS. The drafting tool SketchUp⁵⁷ can be used to create 3D buildings that can be georeferenced and exported to several formats, as well as visualized in Google Earth. Figure 11 shows an example of some buildings that were created in SketchUp, and later were georeferenced in Google Earth and used in FLUENT⁵⁸.

⁵⁷ <http://www.sketchup.com/>

⁵⁸ <http://www.fluent.com/>

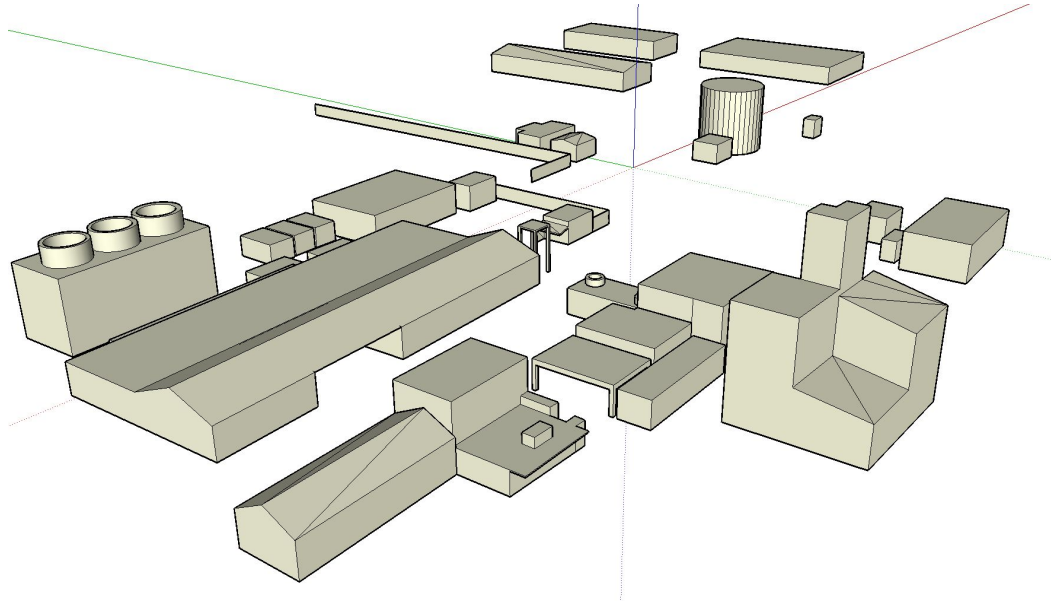


Figure 11. 3D buildings created with SketchUp.

5 Summary

Many tools and sources of data are available to an air quality modeler for pre-processing and post-processing. GIS is becoming indispensable as a tool, and with free programs like Google Earth and ArcExplorer, an air modeler can “visit” a site and look at the local terrain and land cover as a first step in their modeling project. The modeler can also “visit” the sites of nearby meteorological stations and determine which stations are most suitable for air quality modeling. GIS tools can also be used to create sources for air quality models and display the results of the simulations. If advanced spatial analysis like georeferencing, geocoding, creating geodatabases, or analyzing remotely-sensed imagery is needed, high-end programs like ArcGIS are available. Less expensive, “lightweight” GIS programs like Global Mapper are also available and can be very useful for visualization and small geoprocessing tasks.

Zannetti, P. 2008. *Air Quality Modeling Resources on the Web*. Chapter 27 of *AIR QUALITY MODELING - Theories, Methodologies, Computational Techniques, and Available Databases and Software. Vol. III – Special Issues* (P. Zannetti, Editor). Published by The EnviroComp Institute (<http://www.envirocomp.org/>) and the Air & Waste Management Association (<http://www.awma.org/>).

Chapter 27

Air Quality Modeling Resources on the Web

Paolo Zannetti ⁽¹⁾

⁽¹⁾ *The EnviroComp Institute, Fremont, CA (USA)*
zannetti@envirocomp.org

Abstract: This chapter presents a list of web addresses of useful sites for scientists, engineers, and managers using or developing air quality models.

Key Words: Air quality modeling, Internet sites, regulatory models, available software, courses online.

1 Introduction

The Internet revolution during the last 15 years has caused enormous progress in sharing data and information worldwide. The resources available on the Web today are enormous, and it is practically unthinkable, for a scientist, to work without this tool. However, some problems still remain. For example, 1) it is not always easy to identify the best and most reliable sources of information; 2) important sites often change address; and 3) the enormous amount of information on the web often provides a distraction more than a solid scientific support.

Nevertheless, the Internet revolution has changed scientists' lives - ways of operating, performing research and development studies. This has been particularly true for environmental sciences, in general, and air quality modeling, in particular.

This chapter presents a semi-organized list of topics and internet addresses that may be particularly useful to scientists, engineers, and managers using or

developing air quality models. The list is certainly incomplete and should be regarded like a collection of examples, more than a comprehensive catalog ; but in spite of its limitation, it represents a good starting point, especially for a researcher at the beginning or intermediate stage of his exploration of the world of air quality modeling.

Readers are encouraged to provide new Hyperlinks by contacting the author via email. All valuable suggestions will be included in possible future volumes.

2 Regulatory Issues

Title: Support Center for Regulatory Atmospheric Modeling (SCRAM)

Owner: US Environmental Protection Agency

Summary: This website is maintained by EPA's Air Quality Modeling Group (AQMG). The AQMG conducts modeling analyses to support policy and regulatory decisions in the Office of Air and Radiation (OAR) and provides leadership and direction on the full range of air quality models and other mathematical simulation techniques used in assessing control strategies and source impacts. Documentation and guidance for these air quality models can be found on this website, including downloadable computer code, input data, and model processors.

Hyperlink: <http://www.epa.gov/scram001/> and
<http://www.epa.gov/ttn/scram/guidanceindex.htm>

Title: Atmospheric Sciences Modeling Division (ASMD)

Owner: NOAA's Air Resources Laboratory (ARL) and US Environmental Protection Agency

Summary: ASMD implements the [Memorandum of Understanding](#) (MOU) and [Memorandum of Agreement](#) (MOA) between the Department of Commerce (DOC) and EPA, develops and evaluates predictive atmospheric models on all spatial and temporal scales for forecasting the Nation's air quality, and for assessing changes in air quality and air pollutant exposures, as affected by changes in ecosystem management and regulatory decisions. ASMD is responsible for providing a sound scientific and technical basis for regulatory policies to improve ambient air quality. The models developed by ASMD are being used by EPA, NOAA, and the air pollution community in understanding and forecasting not only the magnitude of the air pollution problem, but also in developing emission control policies and regulations.

Hyperlink: <http://www.epa.gov/asmdnerl/>

Title: Models Knowledge Base (KBase)

Owner: EPA's Council for Regulatory Environmental Modeling (CREM)

Summary: The CREM's Draft Guidance for Environmental Models provides recommendations for model development, evaluation, and application. The Models Knowledge Base is intended to be a living demonstration of the

recommendations from the Guidance for Environmental Models. In this way, these two products work in tandem to describe and document good modeling practices.

Hyperlink: http://cfpub.epa.gov/crem/knowledge_base/knowbase.cfm#overview

Title: National Exposure Research Laboratory (NERL)

Owner: US Environmental Protection Agency

Summary: **National Exposure Research Laboratory (NERL)** is comprised of several divisions with diversified research specialties. NERL conducts research and development that leads to improved methods, measurements and models to assess and predict exposures of humans and ecosystems to harmful pollutants and other conditions in air, water, soil, and food.

Hyperlink: <http://www.epa.gov/nerl/>

Title: Air Quality Modelling

Owner: Alberta Environment

Summary: Air dispersion modelling is a method of predicting the ground level concentration and deposition of air pollutants from one or more sources. The method may include relationships between emissions and air quality that incorporates the transport, dispersion and transformation of compounds emitted into the air.

Hyperlink: <http://www3.gov.ab.ca/env/air/AQModelling/index.html>

Title: California Air Resources Board

Owner: State of California

Summary: Collection of modeling software and some associated documentation

Hyperlink: <http://www.arb.ca.gov/html/soft.htm#modeling>

Title: Air Quality Assessment Division – Department of Environmental Quality (DEQ) Louisiana

Owner: State of Louisiana

Summary: The Air Quality Assessment Division manages a number of activities in support of the overall air program for the state.

Hyperlink: <http://www.deq.louisiana.gov/portal/tabid/2457/Default.aspx>

Title: UK Dispersion Modelling Bureau

Owner: UK Met Office

Summary: **The UK Dispersion Modelling Bureau** is part of the [Met Office](#) (originally an abbreviation for Meteorological Office, but now the official name in itself) which is the [UK's](#) national weather and meteorological service. The meteorologists in the bureau are among the UK's leading experts in areas such as:

- [meteorology](#)
- [air quality](#) studies and forecasting
- [air pollution dispersion modelling](#)
- [industrial emissions](#)

Hyperlink: <http://www.metoffice.gov.uk/>

3 Books

Title: Fundamentals of Stack Gas Dispersion

Author(s) : Milton R. Beychok

Summary: This is the new, fourth edition of the book on dispersion modeling of continuous, buoyant air pollution plumes which takes nothing for granted. Every equation is completely derived step-by-step without any complicated or advanced mathematics. Every constraint and assumption is fully explained. A set of self-study exercises is also included with the book.

Hyperlink: <http://www.air-dispersion.com/>

Title: Air Quality Modeling – Book Series

Author(s): Paolo Zannetti et al.

Summary: The EnviroComp Institute and the Air & Waste Management Association have joined forces to publish a new book series on air quality modeling, both traditional print and electronic formats. The first volume was published in December 2003. The second volume has been published in August 2005. And the third volume is expected to be published in late 2007.

Hyperlink: <http://www.envirocomp.org/aqm/>

Title: Air pollution dispersion modeling books

Author(s): Wikipedia

Summary: The information listed below for each of the [air pollution dispersion modeling books](#) includes the author(s), the publication date, the title, the edition, by whom published, and the [ISBN](#) or [ISSN](#) where available. The list is organized into two categories. One category is entitled "Books" and defined as books written by no more than three authors. The other category is entitled "Proceedings" and defined as books or other publications which are the proceedings of technical conferences or workshops.

Hyperlink:

http://en.wikipedia.org/wiki/Air_pollution_dispersion_modeling_books

4 Available Software

Title: Support Center for Regulatory Atmospheric Modeling (SCRAM)

Owner: US Environmental Protection Agency

Summary: This website is maintained by EPA's Air Quality Modeling Group (AQMGM). The AQMG conducts modeling analyses to support policy and regulatory decisions in the Office of Air and Radiation (OAR) and provides leadership and direction on the full range of air quality models and other mathematical simulation techniques used in assessing control strategies and source impacts. Documentation and guidance for these air quality models can be found on this website, including downloadable computer code, input data, and model processors.

Hyperlink: <http://www.epa.gov/scram001/>

Title: Software - Utilities and Modeling

Owner: California Air Resources Board

Summary: This page presents software and documentation available via the California Air Resources Board Information System (CARBIS).

Hyperlink: <http://www.arb.ca.gov/html/soft.htm>

Title: U.S. EPA Models

Owner: Lakes Environmental

Summary: U.S. EPA Models - Download EPA's Most Used Air Quality Models - MODELS, DOCUMENTATION, AND GUIDELINES

Hyperlink: <http://www.weblakes.com/lakeepa1.html>

Title: The GAIA Model Base

Owner: GAIA: A Multi-Media Tool for Natural Resources Management and Environmental Education.

Summary: Air quality simulation models

Hyperlink: <http://www.ess.co.at/GAIA/models/aria.htm>

Title: Air Pollution Software

Owner: Scientific Software Group

Summary: Air Pollution Software

Hyperlink: http://www.scisoftware.com/environmental_software/index.php?cPath=25

Title: CALPUFF Modeling System

Owner: Atmospheric Studies Group

Summary: CALPUFF is an advanced non-steady-state meteorological and air quality modeling system developed by ASG scientists. It is maintained by the model developers and distributed by TRC. The model has been adopted by the U.S. Environmental Protection Agency (U.S. EPA) in its *Guideline on Air Quality Models* as the preferred model for assessing long range transport of pollutants and their impacts on Federal Class I areas and on a case-by-case basis for certain near-field applications involving complex meteorological conditions. The modeling system consists of three main components and a set of preprocessing and postprocessing programs. The main components of the modeling system are CALMET (a diagnostic 3-dimensional meteorological model), CALPUFF (an air quality dispersion model), and CALPOST (a postprocessing package). Each of

these programs has a graphical user interface (GUI). In addition to these components, there are numerous other processors that may be used to prepare geophysical (land use and terrain) data in many standard formats, meteorological data (surface, upper air, precipitation, and buoy data), and interfaces to other models such as the Penn State/NCAR Mesoscale Model (MM5), the National Centers for Environmental Prediction (NCEP) Eta model and the RAMS meteorological model.

Hyperlink: <http://www.src.com/calpuff/calpuff1.htm>

Title: Air Quality Modeling

Owner: South Coast Air Quality Management District

Summary: The following models are available to assist the CEQA practitioner in calculating impact to air quality. The following links will take you directly to these models located on other websites.

Hyperlink: <http://www.aqmd.gov/CEQA/models.html>

Title: MM5

Owner: Penn State University and National Center for Atmospheric Research

Summary: The PSU/NCAR mesoscale model (known as MM5) is a limited-area, nonhydrostatic, terrain-following sigma-coordinate model designed to simulate or predict mesoscale atmospheric circulation. The model is supported by several pre- and post-processing programs, which are referred to collectively as the MM5 modeling system. The MM5 modeling system software is mostly written in Fortran, and has been developed at Penn State and NCAR as a community mesoscale model with contributions from users worldwide.

Hyperlink: <http://www.mmm.ucar.edu/mm5/mm5-home.html>

Title: Compilation of atmospheric dispersion models

Hyperlink:

http://en.wikipedia.org/wiki/Compilation_of_atmospheric_dispersion_models

Title: Selected Environmental and Biological Models

Hyperlink: <http://erda.rutgers.edu/resources/resources1.php>

Title: Polyphemus

Owner: Multiple Groups

Summary: Polyphemus is a Cyclops in Odyssey <http://en.wikipedia.org/wiki/Polyphemus> whose name roughly means "multiple speeches". It is consistent with the goals of the system, that is, gathering on the same platform:

- several models: with Gaussian, Eulerian, ... formulations;
- several scales: from small/local scale to continental scale; multiple pollutants: passive, radionuclides, photochemistry, aerosols, POP, ...
- processing from many inputs (meteorological models, ground data);
- many advanced methods: data assimilation, ensemble forecasting, models coupling, ...

It is written as much as possible with modern computer languages (mainly C++), and only perennial and scalable developments are included. Polyphemus is open. It is open source, distributed under GNU GPL, well documented (for users and developers), and released on a regular basis. Open also means that contributions from other teams are welcome.

Hyperlink: <http://cerea.enpc.fr/polyphemus/introduction.html> and <http://www.atmos-chem-phys-discuss.net/7/6459/2007/acpd-7-6459-2007.html>

Title: MERLIN (Multi-Pollutant Multi-Effect Modeling of European Air Pollution Control Strategies - an INtegrated Approach).

Owner: Cluster of European Air Quality Research ([CLEAR](#))

Summary: The aim of this proposed project is the development of a computer-based model system to determine the bundle of air pollution control measures, that is capable of achieving compliance with air quality limit and target values (for emission, concentrations and deposition) for specific pollutants at least-costs. Furthermore, the model will be used to calculate benefits, i.e. avoided damage costs by implementing air pollution control measures, first in a physical way, and in a second step - as far as possible - in monetary terms. Thus, costs and benefits of different bundles of measures can be estimated and cost-benefit analysis can be applied. In addition, macroeconomic effects and distributional impacts of pollution control strategies are determined.

Hyperlink: <http://www.merlin-project.de/>

5 Dispersion Models

Title: Dispersion Modeling

Owner: US Environmental Protection Agency

Summary: Dispersion modeling uses mathematical formulations to characterize the atmospheric processes that disperse a pollutant emitted by a source. Based on emissions and meteorological inputs, a dispersion model can be used to predict concentrations at selected downwind receptor locations.

Hyperlink: <http://www.epa.gov/scram001/dispersionindex.htm>

Title: The Air Pollution Model (TAPM) Technical descriptions and pricelist

Owner: CSIRO

Summary: The Air Pollution Model (TAPM) is a software package developed by CSIRO to estimate the spread and impact of air pollution. TAPM is a meteorological, prognostic air pollution model.

Hyperlink: <http://www.cmar.csiro.au/research/tapm/>

6 Photochemical Models

Title: Photochemical Modeling

Owner: US Environmental Protection Agency

Summary: Photochemical air quality models have become widely recognized and routinely utilized tools for regulatory analysis and attainment demonstrations by assessing the effectiveness of control strategies. These photochemical models are large-scale air quality models that simulate the changes of pollutant concentrations in the atmosphere using a set of mathematical equations characterizing the chemical and physical processes in the atmosphere. These models are applied at multiple spatial scales from local, regional, national, and global.

Hyperlink: <http://www.epa.gov/scram001/photochemicalindex.htm>

Title: CAMx

Owner: Environ

Summary: The Comprehensive Air quality Model with extensions is a publicly available open-source computer modeling system for the integrated assessment of gaseous and particulate air pollution. Built on today's understanding that air quality issues are complex, interrelated, and reach beyond the urban scale, CAMx is designed to:

- * Simulate air quality over many geographic scales
- * Treat a wide variety of inert and chemically active pollutants:
 - Ozone
 - Inorganic and organic PM_{2.5}/PM₁₀
 - Mercury and toxics
- * Provide source-receptor, sensitivity, and process analyses
- * Be computationally efficient and easy to use

Hyperlink: <http://www.camx.com/>

Title: EKMA/OZIP

Owner: The Shodor Education Foundation, Inc.

Summary: This exercise was designed for environmental professionals and educators by scientists and instructional design educators at the Shodor Education Foundation, Inc., in cooperation with the North Carolina Supercomputing Center and the North Carolina Industrial Extension Service (North Carolina State University). This project is being conducted under EPA Cooperative Agreement CR 822080 awarded to the Industrial Extension Service, North Carolina State University, with the North Carolina Supercomputing Center as the main technical partner. It represents the first step in a process of determining and recommending a comprehensive modeling curriculum which could be implemented by EPA through the Air Pollution Training Institute, by state and local agencies, and by universities.

Hyperlink: <http://www.shodor.org/ekma/>

Title: Air quality modeling in PREV'AIR

Owner: The Pierre-Simon Laplace Institute of the Centre National de Recherche Scientifique (IPSL/CNRS) and the INERIS for the CHIMERE Model, and Centre National de Recherches Météorologiques de Météo France (CNRM/Météo France) for the MOCAGE model

Summary: The three-day forecasts and air quality maps published on a daily basis on the PREV'AIR server are the result of numerical simulations carried out with the help of so-called 3D eulerian deterministic models ("chemistry-transport" models). For periods of time ranging from several days to several months, these tools allow to calculate changes in photochemical and specific pollution in the lower layer of the atmosphere, on different spatial scales.

Hyperlink: <http://prevair.ineris.fr/en/modele.php>

Title: Models-3/Community Multiscale Air Quality (CMAQ)

Owner: Community Modeling & Analysis System

Summary: The latest version of the Community Multi-scale Air Quality (CMAQ) model has capabilities for conducting urban to regional scale simulations of multiple air quality issues, including tropospheric ozone, fine particles, toxics, acid deposition, and visibility degradation. The primary goals for the Models-3/Community Multiscale Air Quality (CMAQ) modeling system are to improve:

1. the environmental management community's ability to evaluate the impact of air quality management practices for multiple pollutants at multiple scales
2. the scientist's ability to better probe, understand, and simulate chemical and physical interactions in the atmosphere

Hyperlink: <http://www.cmascenter.org/>

Title: Regional Modeling System for Aerosols and Deposition (REMSAD)

Owner: ICF International/Systems Applications International

Summary: Developed by ICF International/Systems Applications International to support a better understanding of the distributions, sources, and removal processes relevant to regional haze, particulate matter and other airborne pollutants, including soluble acidic components and toxics. REMSAD includes the streamlined micro-CB gas-phase chemical mechanism and an efficient transport algorithm that allow continental scale simulations of full calendar years. REMSAD provides spatially and temporally resolved air concentrations and (wet and dry) deposition values. Recent improvements to the modeling system include expanded treatment of mercury chemistry, the addition of a detailed secondary organic aerosol (SOA) treatment and improved performance under stagnant meteorological conditions. REMSAD calculates the concentrations of both inert and chemically reactive pollutants by simulating the atmospheric processes that affect pollutant concentrations over regional scales. It includes processes relevant to regional haze, particulate matter and other airborne pollutants, including soluble acidic components and mercury.

Hyperlink: <http://remsad.saintl.com/>

Title: Urban Airshed Model (UAM)

Owner: Sonoma Technology Inc.

Summary: The UAM is a 3-D grid model designed to calculate the concentrations of both inert and chemically reactive pollutants by simulating physical and chemical processes that take place in the atmosphere.

- The UAM uses a mass balance in which relevant emissions, transport, chemical reaction, and removal processes are expressed in mathematical terms.
- Simulations are usually 24- to 72-hour periods during which episodic meteorological conditions persist.
- Typical UAM application:
 - Select episode (usually widespread exceedance of ozone NAAQS, typical meteorological conditions).
 - Select modeling domain to encompass ozone monitors that reported exceedances and all major source regions.
 - Prepare model inputs using observed meteorological, emission, and air quality data for an episode.
 - Evaluate model performance.
- The UAM is used for analysis of spatially and/or temporally differentiated future emission control strategies and their effect on air quality in various parts of the modeling region.

Hyperlink: <http://epa.gov/oar/oaqps/pams/analysis/uam/uam.html>

7 Receptor Models

Title: Receptor Modeling

Owner: US Environmental Protection Agency

Summary: Receptor models are mathematical or statistical procedures for identifying and quantifying the sources of air pollutants at a receptor location. Unlike photochemical and dispersion air quality models, receptor models do not use pollutant emissions, meteorological data and chemical transformation mechanisms to estimate the contribution of sources to receptor concentrations. Instead, receptor models use the chemical and physical characteristics of gases and particles measured at source and receptor to both identify the presence of and to quantify source contributions to receptor concentrations.

Hyperlink: <http://www.epa.gov/scram001/receptorindex.htm>

Title: EPA Unmix receptor model

Owner: US Environmental Protection Agency

Summary: The EPA Unmix receptor model was developed under this project. Unmix is named for its function, which is to "unmix" the concentrations of chemical species measured in the ambient air to identify the contributing sources. The particular mathematical approach used by Unmix is based on a form of Factor Analysis, but its novelty is that physically-meaningful constraints are

imposed which are intended to remove the undesirable ambiguity of the multiple solutions that are characteristic of ordinary Factor Analysis. For a given selection of species, Unmix estimates the number of sources, the source compositions, and source contributions to each sample. Chemical profiles of the sources are not required, but instead are generated from the ambient data.

Hyperlink: <http://www.epa.gov/nerl/research/2004/g1-6.html>

8 Air Quality Forecast and Resources

Title: Regional Air Quality Modeling Systems

Owner: NASA Langley Research Center

Summary: Scientists use the Regional Air Quality Modeling System (RAQMS) computer model to predict air quality around the globe. RAQMS has been designed to address the atmospheric chemistry modeling needs for NASA's Earth Science Enterprise science missions and to prototype future NASA, National Oceanic and Atmospheric Administration (NOAA), and Environmental Protection Agency (EPA) operational air quality prediction systems. It is a portable, global to regional scale meteorological and chemical computer modeling system. RAQMS assimilates remote and in-situ observations of atmospheric chemical composition to predict the distribution of atmospheric trace gases (air quality) within any region of the Earth. The Global Climate and Environmental Quality area of Langley's Creativity and Innovation initiative supports RAQMS.

Hyperlink: http://asd-www.larc.nasa.gov/new_AtSC/raqms.html

Title: FLEXTRA and FLEXPART

Owner: Andreas Stohl

Summary: FLEXTRA and FLEXPART are an atmospheric trajectory and a particle dispersion model, respectively, that are used by a growing user community. A recent user survey resulted in [34 groups from 17 countries who have confirmed to actively use one of the models](#) for a variety of research purposes. There are also a few operational installations for emergency preparedness and similar objectives.

Hyperlink: <http://zardozi.nilu.no/~andreas/flextra+flexpart.html>

Title: AIRNow

Owner: U.S. EPA, NOAA, NPS, tribal, state, and local agencies

Summary: The U.S. EPA, NOAA, NPS, tribal, state, and local agencies developed the AIRNow Web site to provide the public with easy access to national air quality information. The Web site offers daily AQI forecasts as well as real-time AQI conditions for over 300 cities across the US, and provides links to more detailed State and local air quality Web sites.

Hyperlink: <http://airnow.gov/>

Title: International Air Quality

Owner: AIRNow

Summary: Air Quality information for various countries

Hyperlink: <http://cfpub.epa.gov/airnow/index.cfm?action=where.world>

Title: Atmospheric Pollution and Economic Development (APD)

Owner: IIASA

Summary: IIASA's work brings together geo-physical and economic aspects of pollution control into one assessment framework and implement it – together with a network of collaborators - for practical policy analyses in different regions of the world.

Hyperlink: <http://www.iiasa.ac.at/rains/>

Title: Experimental Chemical Weather Forecast over Italy

Owner: University of L'Aquila, Italy - [CETEMPS](#)

Summary: The system for the forecast of regional air quality relies on two main elements: a meteorological mesoscale model (the PennState/NCAR [MM5 model](#)) and a regional chemistry-transport model ([CHIMERE model](#)).

MM5 model is developed at the Pennsylvania State University and at the National Center for Atmospheric Research and is available for free. The meteorological model provides input data such as winds, temperature and humidity necessary to run the model of transport and chemistry. The meteo model is forced by daily [ECMWF](#) forecast and run on a grid with a horizontal resolution of 30 km.

The forecast of the evolution and transformation of chemical species is provided by the CHIMERE model. CHIMERE is developed in Paris (France) by a number of French institutions: Institut Pierre-Simon Laplace, C.N.R.S., INERIS, LISA (C.N.R.S.). It is a free software available under the [GNU General Public License](#).

Everyday a 72h run is performed starting at h 12:00 of the previous day. The MM5 meteo model is run first and then its output is used by the chemical model CHIMERE to predict pollutant levels over Italy and surroundings. At the end of the simulation process another automatic procedure updates the figures visible on this web site.

Hyperlink: <http://pumpkin.aquila.infn.it/forechem/>

9 Visibility Modeling

Title: VISTAS Phase I Regional Haze Modeling

Owner: University of California, Riverside

Summary: The Clean Air Act establishes special goals for protection of visibility in many national parks and wilderness areas. Through the 1977 amendments to the Clean Air Act (CAA), Congress set a national goal for visibility as "the prevention of any future, and the remedying of any existing, impairment of visibility in mandatory Class I Federal areas which impairment results from

manmade air pollution". The Clean Air Act defines mandatory Class I Federal areas as national parks (over 6000 acres), wilderness areas (over 5000 acres), national memorial parks (over 5000 acres), and international parks that were in existence as of August 1977. The CAA requires that natural visibility conditions be attained in Class I areas by 2064, and also establishes certain requirements for making progress toward attainment at that date. States and tribes have authority under the CAA to develop State and Tribal Implementation Plans (SIPs and TIPs) to attain the CAA visibility standards for these Class I Areas.

Hyperlink: <http://pah.cert.ucr.edu/vistas/>

Title: Plume Visibility Model (PLUVUE II)

Owner: National Technical Information Service

Summary: PLUVUE is a visibility model designed to predict transport, atmospheric diffusion, chemical conversion, optical effects, and surface deposition of point-source emissions. PLUVUE performs plume optics calculations in two modes. In the Plume-based mode, the visual effects are calculated for a variety of lines of sight and observer locations relative to the plume parcel; in the observer-based mode, the observer position is fixed and visual effects are calculated for the specific geometry defined by the positions of the observer, plume, and sun.

Hyperlink: <http://www.ntis.gov/products/bestsellers/cpn0041.asp?loc=4-2-0> or http://iaspub.epa.gov/edr/edr_proc_qry.navigate?P_LIST_OPTION_CD=CSDIS&P_REG_AUTH_IDENTIFIER=1&P_DATA_IDENTIFIER=90366&P_VERSION=1

10 Publications and Information Online

Title: Finding Air Quality Information on the Internet

Author(s): Envirometrics

Summary: This article is intended to provide a summary of the more useful air quality directory sites (i.e., sites with links to other sites) and sites with air quality information.

Hyperlink: <http://www.envirometrics.com/news/main.html#search>

Title: Uncertainty Analysis of Transport - Transformation Models (PhD dissertation)

Author(s): Sastry S. Isukapalli

Summary: Characterization of uncertainty associated with transport-transformation models is often of critical importance, as for example in cases where environmental and biological models are employed in risk assessment. However, uncertainty analysis using conventional methods such as standard Monte Carlo or Latin Hypercube Sampling may not be efficient, or even feasible, for complex, computationally demanding models.

This work introduces a computationally efficient alternative method for uncertainty propagation, the Stochastic Response Surface Method (SRSM). The SRSM approximates uncertainties in model outputs through a series expansion in normal random variables (polynomial chaos expansion). The unknown coefficients in series expansions are calculated using a limited number of model simulations. This method is analogous to approximation of a deterministic system by an algebraic response surface.

Further improvements in the computational efficiency of the SRSM are accomplished by coupling the SRSM with ADIFOR, which facilitates automatic calculation of partial derivatives in numerical models coded in Fortran. The coupled method, SRSM-ADIFOR, uses the model outputs and their derivatives to calculate the unknown coefficients.

The SRSM and the SRSM-ADIFOR are general methods, and are applicable to any model with random inputs. The SRSM has also been implemented as a black-box, web-based tool for facilitating its easy use.

The SRSM and the SRSM-ADIFOR have been applied to a set of environmental and biological models. In all the case studies, the SRSM required an order of magnitude fewer simulations compared to conventional methods, and the SRSM-ADIFOR required even fewer simulations. In addition to their computational efficiency, these methods directly provide sensitivity information and individual contributions of input uncertainties to output uncertainties; conventional methods require substantially larger numbers of simulations to provide such information. Thus, the SRSM and the SRSM-ADIFOR provide computationally efficient means for uncertainty and sensitivity analysis.

Finally, this research addresses uncertainties associated with model structure and resolution with application to photochemical air quality modeling. A three dimensional version of the regulatory Reactive Plume Model (RPM), RPM-3D, has been developed and applied to understand model uncertainty.

Hyperlink: <http://www.ccl.rutgers.edu/~ssi/thesis/thesis.html>

Title: GIS applications in air pollution modeling

Author(s): Niraj Sharma et al.

Summary: Motor vehicles have been closely identified with increasing air pollution levels in urban centers of the world (Mage et al, 1996; Mayer 1999). Besides substantial CO₂ emissions, significant quantities of CO, HC, NO_x, SPM and other air toxins are emitted from these motor vehicles in the atmosphere, causing serious environmental and health impacts. Like many other parts of the world, air pollution from motor vehicles is one of the most serious and rapidly growing problem in urban centers of India (UNEP/WHO, 1992; CSE, 1996; CRRI, 1998). The problem of air pollution has assumed serious proportions in some of the major metropolitan cities of India and vehicular emissions have been identified as one of the major contributors in the deteriorating air quality in these

urban centers (CPCB, 1999). Although, recently, improvement in air quality with reference to the criteria pollutants (viz. NO_x, SO₂, CO and HC) have been reported for some of the cities, the air pollution situation in most of the cities is still far from satisfactory (CPCB, 2000). The problem has further been compounded by the concentration of large number of vehicles and comparatively high motor vehicles to population ratios in these cities (CRRRI, 1998).

Hyperlink:

<http://www.gisdevelopment.net/application/environment/air/mi03220.htm>

Title: Air Quality Modeling Appendix - Final Statewide Oil and Gas Environmental Impact Statement and Proposed Amendment of the Powder River and Billings Resource Management Plans

Author(s): U.S. Department of the Interior - Bureau of Land Management

Summary: Environmental Impact Statement

Hyperlink: <http://www.mt.blm.gov/mcfo/cbm/eis/volume2/AirQualityApp.pdf>

Title: Using a “Wiki” to pool experiences on atmospheric dispersion

Author(s): Helge Rørdam Olesen, National Environmental Research Institute, University of Aarhus, Denmark

Summary: A “Wiki” is a certain type of Web site that is especially suited for collaboration. It allows users to easily create and edit Web pages. A “Wiki” has a very open structure where anyone can contribute. Recently, a “Wiki” has been established on the subject of Atmospheric Dispersion Modelling. A “Wiki” is potentially a very powerful tool for the community of atmospheric dispersion professionals. A “Wiki” provides something that we normally miss in the community of atmospheric dispersion professionals: An easy possibility to provide feedback and pool our experiences with procedures, data sets and models related to our work.

Hyperlink: <http://atmosphericdispersion.wikia.com>

11 Courses Online

Title: Air Quality Modeling – AOSS 563

Author(s): Prof. Perry Samson

Summary: Design of effective strategies for managing atmospheric resources requires the use of computer models to simulate the transport, dispersion, chemistry and deposition of airborne pollutants on scales from a few meters to thousands of kilometers. This course introduces fundamentals of air pollution modeling with an emphasis on hands-on application to real-world situations.

Hyperlink: <http://www.engin.umich.edu/class/aoss563/lectures/index.html>

Title: Air Quality Meteorology

Author(s): A Developmental Course of the US Environmental Protection Agency in conjunction with the US National Oceanic and Atmospheric Administration - Developed by The Shodor Education Foundation, Inc.

Summary: This course is designed for environmental decision-makers, scientists, technical advisors, and educators by scientists and instructional design educators at the Shodor Education Foundation, Inc., North Carolina Supercomputing Center, and the North Carolina Industrial Extension Service (North Carolina State University). It represents the first step in a process of determining and recommending a comprehensive modeling curriculum which could be implemented by EPA through the Air Pollution Training Institute, by state and local agencies, and by universities.

Hyperlink: <http://www.shodor.org/metweb/>

Title: Basic Concepts in Environmental Sciences – (Module 6: Air Pollutants and Control Techniques)

Author(s): US EPA

Hyperlink: http://www.epa.gov/eogapti1/toc/full_toc.htm

12 Case Studies

Title: OMNI - Air Pollution Modelling in Practice

Author(s): The South East Institute of Public Health (SEIPH)

Summary: This 'Virtual Assessment Tool' is here to help those people who work in the field of air pollution. The site is specific to the area bounded by the M25 motorway, and provides assessment tools and information required by the National Air Quality Strategy (NAQS).

Hyperlink: <http://www.seiph.umds.ac.uk/omni/frames/omniframe.htm>

Title: Air quality in South East Queensland

Author(s): The Environmental Protection Agency (EPA), which includes the Queensland Parks and Wildlife Service (QPWS), is a department of the Queensland Government.

Summary: The South East Queensland Regional Air Quality Strategy notes that in addition to changing vehicle design, emissions can be greatly reduced by reformulating fuel types or substituting other types. On hot days, the pollutants created by petrol vapour evaporating into the atmosphere contribute significantly to smog development.

Hyperlink:

http://www.epa.qld.gov.au/environmental_management/air/air_quality_monitoring/air_quality_modelling/

Title: Fall line Air Quality Study (FAQS) Meteorology, Emissions, and & Air Quality Models

Author(s): Yongtao Hu and Ted Russell

Summary: The FAQS research team is using a system of meteorological, emissions, and air quality computer models (note 1) to characterize the major and minor factors that affect air quality in Augusta, Macon, and Columbus, Georgia. The models are used to study past episodes of poor air quality and to evaluate potential future actions that, if implemented, may reduce the incidence of air pollution and its associated impacts.

Hyperlink: <http://cure.eas.gatech.edu/faqs/models/index.html>

Title: Air Quality Modeling Report Snowmobile and Snowcoach Emissions

Author(s): Air Resource Specialists, Inc.

Summary: In support of the Winter Use Plan Preliminary Draft Environmental Impact Statement (PDEIS) for Yellowstone National Park (Yellowstone), Grand Teton National Park (Grand Teton), and the John D. Rockefeller, Jr. Memorial Parkway (Parkway), Air Resource Specialists, Inc. (ARS) completed an analysis of potential air quality impacts from snowmobile and snowcoach operations. This report analyzes potential air quality impacts for several preliminary alternatives utilizing air dispersion modeling and other accepted methods and models.

Hyperlink:

http://www.nps.gov/yell/parkmgmt/upload/final_air_quality_report_11_06.pdf

Title: Florida Department of Transportation (FDOT) Air Quality Modeling Plan

Author(s): A Florida Department of Transportation (FDOT)

Summary: The Florida Department of Transportation (FDOT) is truly a concerned partner in Florida's air quality. On-road highway emissions from motorized vehicles ranging from a one-hundred pound motor scooter to an eighty-thousand pound double-trailer truck produce substantial quantities of volatile organic compounds (VOCs) and nitrogen oxides (NO_x). VOCs and NO_x combine in the presence of sunlight to produce ozone.

Hyperlink: <http://www.dot.state.fl.us/planning/systems/stm/aq.htm>

Title: AIR POLLUTION MODELING AND APPLICATIONS IN ESTONIA

Author(s): Marko Kaasik and Veljo Kimmel

Summary: The modeling of air pollution in Estonia during Soviet Union period was complicated both due to ignorance of decision-makers and deficiency of good tools affecting also current situation.

Current practice is divided roughly into two parts: 1) official side relying on obsolete and not validated Russian models from the eighties not enabling to model most important polluter in cities - the traffic and 2) researcher side-dealing with development and use of advanced computers and new modeling tools.

Hyperlink: <http://www.meteo.bg/EURASAP/39/marko.html>

Title: Institute for Multi-dimensional Air Quality Studies.

Author(s): University of Houston

Summary: We are a diverse group of researchers from fields of geosciences, math, computer science and chemistry committed to using premier scientific tools

to model the complex issues of air quality and climate change. Our modeling efforts address many critical components simultaneously including emissions inventories, meteorology, and atmospheric chemistry. We are currently developing atmospheric boundary layer measurement techniques. We work closely with national, state and local leaders to identify key scenarios to run on our modeling systems so that public policy is guided with the best science.

Hyperlink: <http://www.imaqs.uh.edu/>

13 Resources and lists of References

Title: Air pollution

Author(s): Wikipedia

Summary: Air pollution is a chemical, physical (e.g. particulate matter), or biological agent that modifies the natural characteristics of the atmosphere. The atmosphere is a complex, dynamic natural gaseous system that is essential to support life on planet Earth. Stratospheric ozone depletion due to air pollution has long been recognized as a threat to human health as well as to the Earth's ecosystems.

Worldwide air pollution is responsible for large numbers of deaths and cases of respiratory disease. Enforced air quality standards, like the Clean Air Act in the United States, have reduced the presence of some pollutants. While major stationary sources are often identified with air pollution, the greatest source of emissions is actually mobile sources, principally the automobile. Gases such as carbon dioxide, which contribute to global warming, have recently gained recognition as pollutants by some scientists. Others recognize the gas as being essential to life, and therefore incapable of being classed as a pollutant.

Hyperlink: http://en.wikipedia.org/wiki/Air_pollution

Title: Information about Air Quality Modeling

Author(s): Clean Air World - by The National Association of Clean Air Agencies (formerly STAPPA and ALAPCO)

Summary: Air Pollutants; Mercury and Other Toxic Air Pollutants; Ozone; Particle Pollution; Control Strategies; Mercury and Other Toxic Air Pollutants; Global Warming; Indoor Air Pollution; Measuring Air Pollution; Air Quality Modeling; Monitoring; Vehicles and Fuels; Cars, Trucks and Buses; Other Engines and Equipment

Hyperlink: <http://www.cleanairworld.org/TopicLinks.asp#23>

Title: Air Dispersion Modeling

Author(s): Open Directory Project

Summary: In the context of this "Air Dispersion Modeling" category, air dispersion models may be defined as computerized mathematical calculations for predicting the dispersion behavior of air pollutants emitted into the atmosphere.

Hyperlink:

http://dmoz.org/Science/Environment/Air_Quality/Air_Dispersion_Modeling/

Title: [Convention on Long-range Transboundary Air Pollution](#)

Author(s): UN Economic Commission for Europe

Summary: Since 1979 the [Convention on Long-range Transboundary Air Pollution](#) has addressed some of the major environmental problems of the UNECE region through scientific collaboration and policy negotiation. The Convention has been extended by [eight protocols](#) that identify specific measures to be taken by Parties to cut their emissions of air pollutants.

Hyperlink: <http://www.unece.org/env/lrtap/welcome.html>

14 Calculation Sites

Title: Air pollution model

Author(s): SouthWest Organizing Project

Summary: The air pollution model on this page is most popular for calculating the direction and rates that pollution will travel given weather, distance, and emission rates. The model is based on theories of statistical probability. The locations of particular chemical molecules are determined following a set of assumptions regarding weather, topographic features, characteristics of the various chemicals. This model works best for short term modeling. When looking at the long term, the model's results must be averaged to account for time.

Hyperlink: http://www.swop.net/intel/air_model.html

Title: [Combustion Calculations Spreadsheets](#)

Author(s): Envirometrics

Summary: These spreadsheets calculate sulfur dioxide, particulate matter, and chloride emissions by mass balance and nitrogen oxides from emission factors.

Hyperlink: <http://www.envirometrics.com/news/main.html#calcs>

Title: [Odor Sampling Dilution Spreadsheets](#)

Author(s): Envirometrics

Summary: If a sampled source has water content much higher than normal ambient humidity it may be necessary to dilute the sample with dry air to reduce the humidity and comply with the sampling protocols. This reduces condensation in the bag during shipment, which might adversely affect the measurement of the odor. A spreadsheet recently developed to compute the amount of pre-dilution dry nitrogen is available for [downloading](#) (about 20k).

Hyperlink: <http://www.envirometrics.com/news/main.html#odorcalcs>

Acknowledgements

I would like to thank the several colleagues from different countries who provided inputs and valuable suggestions. I look forward to expand this chapter in the future and encourage the readers to email me comments, corrections, and new material.

Table of Contents – Volume I¹

Preface	xi
About the Editor	xiii
About the Publishers	xv
About the Chapter Authors	xvii
1 The Problem – Air Pollution	1
1 Our Natural Environment	1
2 Air Pollution, Some Definitions	3
3 Primary and Secondary Pollutants	4
4 A Short History of Air Pollution Modeling	5
5 Air Pollution Regulations	8
2 The Tool – Mathematical Modeling	13
1 Why Air Quality Modeling	13
2 Modeling Categorized	14
3 Modeling the Atmosphere	19
4 Modeling Alternatives	20
5 Spatial and Temporal Scales	22
6 Spatial and Temporal Resolution	23
7 Uncertainty: Bias, Imprecision, and Variability	24
8 Evaluation of Model Performance	25
9 Data Needs	27
10 Uses of Models	29
3 <i>Emission Modeling</i>	33
4 Air Pollution Meteorology	37
1 Synoptic Meteorology	38
2 Boundary-Layer Meteorology	61
5 <i>Meteorological Modeling</i>	101
6 Plume Rise	103
1 Introduction	108
2 Semi-Empirical Formulations	112
3 Advanced Plume Rise Models	131
4 Particle Models for Plume Rise	137
5 Special Cases	157
7 <i>Gaussian Plume Models</i>	183

¹ Chapters in italics will be provided in subsequent volumes.

7A	Introduction to Gaussian Plume Models	185
1	Introduction	186
2	The Point Source in the Atmospheric Boundary Layer	186
3	The Atmospheric Boundary Layer	190
4	Dispersion in the Atmospheric Boundary Layer	193
5	Building Downwash	197
6	Terrain Treatment	199
7	Modifications to the Gaussian Framework	202
8	Concluding Remarks	206
8	<i>Gaussian Puff Models</i>	209
9	<i>Special Applications of Gaussian Models</i>	211
10	Eulerian Dispersion Models	213
1	Air Quality Modeling Methods	214
2	Eulerian Formulations	218
3	Analytical Solutions for Ideal Atmospheric Conditions	232
4	Numerical Solution Methods	237
5	Numerical Algorithms for Advection	244
6	Horizontal Diffusion Algorithm	251
7	Vertical Diffusion Algorithm	258
8	Simplified Eulerian Models	268
	Appendix A	272
	Appendix B	276
	Appendix C	279
11	<i>Lagrangian Particle Models</i>	293
12	<i>Atmospheric Transformations</i>	297
13	<i>Deposition Phenomena</i>	301
14	<i>Indoor Air Pollution Modeling</i>	303
15	<i>Modeling of Adverse Effects</i>	305
16	<i>Statistical Modeling</i>	307
17	<i>Evaluation of Air Pollution Models</i>	309
18	<i>Regulatory Air Quality Models</i>	311
19	Case Studies – Air Pollution Modeling at Local, Regional, Continental, and Global Scales	313
1	List of Case Studies	314
2	Additional Information on Case Studies Relevant to Air Pollution Modeling/Simulation	323

20	The Future of Air Pollution Modeling	325
1	Processor Technology and Air Pollution Modeling	325
2	Comprehensive Modeling Systems (CMS)	330
21	Active Groups in Air Pollution Modeling	355
1	List of Active Groups	356
2	Additional Information on Groups Working on Air Pollution Modeling Issues	360
22	Available Software	363
1	Short-Range Models	366
2	Urban and Regional Photochemical Models	380
3	Long-Range Transport Models for Acid Deposition, Visibility Impairment and Complex Terrain	387
4	Emergency Release and Dense Gas Models	394
5	Meteorological Models	406
23	Available Databases	409
1	Overview	409
2	The Challenges	411
3	Characteristics of Weather Data Sets	413
4	NCEP Gridded Data Products	414
5	Data Archival	416
6	Reanalysis Techniques	418
7	Mesoscale Prognostic Models	421
8	Future Developments	423
	Authors' Index	427
	Subject Index	429

Blank Page

Table of Contents – Volume II^{1, 2}

	Preface	xi
	About the Editor	xiii
	About the Publishers	xv
	About the Chapter Authors/Contributors for Volumes I and II	xvii
1	The Problem – Air Pollution	1
2	The Tool – Mathematical Modeling	3
3	<i>Emission Modeling</i>	5
4	Air Pollution Meteorology	7
5	Meteorological Modeling	9
	 <i>5A Mesoscale Meteorological Modeling</i>	
	 5B Large-Eddy Simulations of the Atmospheric Boundary Layer	11
	1 Introduction	11
	2 Theoretical Background	14
	3 The ABL Simulations	35
	4 Final Remarks	74
	 <i>5C Computational Fluid Dynamics of Microscale Meteorological Flows</i>	
6	Plume Rise	83
7	Gaussian Plume Models	85
	 7A Introduction to Gaussian Plume Models	
	 <i>7B Simulation Algorithms in Gaussian Plume Models</i>	
8	<i>Gaussian Puff Models</i>	87
9	<i>Special Applications of Gaussian Models</i>	89

¹ Chapters in italics will be provided in subsequent volumes.

² The table of contents of Volume I can be found on page 635 of this book.

10	Eulerian Dispersion Models	91
11	Lagrangian Particle Models	93
1	The Lagrangian Approach	94
2	Lagrangian Stochastic Models (LSM)	95
3	LSM Applications	128
12	Atmospheric Transformations	163
1	Introduction	164
2	Gas-Phase Transformations	165
3	Heterogeneous and Aqueous Processes	172
4	Chemical Transformations Involved in the Formation of Air Toxics	179
5	Chemistry of the Upper Atmosphere: Stratospheric Ozone	183
6	Modeling of Gas-Phase Chemistry	193
7	Modeling of Heterogeneous and Aqueous Processes	199
8	Modeling of Reactive Plumes	207
9	Eulerian Models	212
13	Deposition Phenomena	233
1	Introduction	234
2	Different Deposition Parameterizations	240
3	Examples of Deposition Monitoring Programs	248
4	Examples of Air Quality Models	251
5	Sensitivity Analysis by Using the OPANA Model	257
14	Indoor Air Pollution Modeling	267
1	Introduction	270
2	Fluid Flow Fundamentals	274
3	Contaminant Sources	284
4	Design Criteria	293
5	Simple Modeling Techniques	297
6	Dynamics of Particles and Gases/Vapors	310
7	Numerical Modeling – CFD	322
15	Modeling of Adverse Effects	349
15A	Modeling of Health Risks Associated with Combustion Facility Emissions	351
1	Introduction	351
2	Case Study	354
	15B Odor Modeling	
	15C Visibility Modeling	
	15D Ecological Adverse Effects	
	15E Global Issues	

16	Statistical Modeling	395
16A	Air Quality Forecast and Alarm Systems	397
1	Introduction	398
2	Some Literature Results	401
3	Time Series Modelling	405
4	Building a Model for Air Quality Forecast	419
5	Identification of Statistical Air Quality Models	426
6	An Operational Decision Support System	437
7	Conclusions	445
	Appendix	453
16B	Receptor Models	455
1	Introduction	455
2	Receptor Model Types	457
3	Multivariate Receptor Model Mathematics	465
4	Model Input Measurements	469
5	Receptor Model Assumptions, Performance Measures, and Validation Procedures	482
6	Summary and Conclusions	491
17	Evaluation of Air Pollution Models	503
1	Introduction	503
2	Terminology	504
3	Background	507
4	Framework	510
5	Performance Measures	516
6	Model Evaluation	526
7	Statistical Model Evaluation	528
8	Model Quality Assurance	543
9	Guidelines for Model Evaluation: Towards Harmonization in Model Evaluation Methodology	547
18	A Historical Look at the Development of Regulatory Air Quality Models for the United States Environmental Protection Agency	557
1	Introduction	557
2	Legislative History of Air Pollution Modeling	561
3	Air Quality Models for Individual Industrial Facilities	566
4	The Development of Urban-Scale Long-Term Air Quality Models	575
5	Development of Tropospheric Chemistry Models	579
6	Current Issues and Trends in Model Development	598
19	Case Studies – Air Pollution Modeling at Local, Regional, Continental, and Global Scales	623
20	The Future of Air Pollution Modeling	625
21	Active Groups in Air Pollution Modeling	627
22	Available Software	629

23	Available Databases	631
24	<i>Physical Modeling of Air Pollution</i>	633
	Table of Contents – Volume I	635
	In Memoriam – Philip M. Roth	639
	Authors’/Contributors’ Index for Volumes I and II	641
	Subject Index for Volumes I and II	643

Authors'/Contributors' Index¹ for Volumes I, II and III

Anfossi, Domenico.....	I – p 103 II – p 93
Builtjes, Peter J.H.....	I – p 1
Buono, Maureen E.	III – p 329
Byun, Daewon W.....	I – p 213
Canepa, Elisa.....	I – p 103 II – p 503
Carrington, David B.....	II – p 267
Chow, Judith C.....	II – p 455
Cochran, Brad.....	III – p 397
Daly, Aaron.....	III – p 435
Degrazia, Gervásio.....	II – p 93
Diosey, Phyllis G.....	III – p 329
Eastman, Joseph L.....	I – p 409
Ferrero, Enrico.....	II – p 93
Finzi, Giovanna.....	II – p 397
Freedman, Frank R.....	III – p 353
González Barras, Rosa M.....	II – p 233
Hibberd, Mark.....	II – p 93
Hurley, Peter.....	II – p 93
Irwin, John S.....	II – p 503, 557
Keen, Cecil S.....	I – p 409
Lacser, Avraham.....	I – p 213
Lee, Russell.....	I – p 363
Luhar, Ashok.....	II – p 93
Lyons, Walter A.....	I – p 409

¹ Readers are encouraged to use the CD-ROM version of the book for text searching.

McAlpine, J.D.	III – p 169
Michelsen, Hope	II – p 163
Moon, Dennis A.	I – p 409
Moussiopoulos, Nicolas	I – p 313, 355
Nelson, Thomas E.	I – p 409
Nunnari, Giuseppe.....	II – p 397
Oettl, Dietmar.....	I – p 325
Pepper, Darrell W.....	II – p 267
Pérez, Juan L.	II – p 233
Petersen, Ronald L.	III – p 397
Physick, William	II – p 93
Pun, Betty K.	II – p 163
Reynolds, Steven D.....	I – p 13
Richter, Richard O.	II – p 351
Roth, Philip M.....	I – p 13
Ruby, Michael	III – p 169
San José, Roberto	I – p 325 II – p 233
Sarma, Ananthakrishna	III – p 131
Seigneur, Christian.....	II – p 163
Sheehan, Patrick J.	II – p 351
Solomon, Douglas	III – p 5
Sorbjan, Zbigniew	I – p 37 II – p 11
Thé, Jesse	I – p 185, 363 III – p 5
Tourlou, Paraskevi-Maria.....	I – p 313, 355
Trini Castelli, Silvia	II – p 93
van Dop, Han	I – p 103 II – p 93

Venkatram, Akula	I – p 185
Watson, John G.	II – p 455
Yamartino, Robert J.	I– p 213 III – p 239 , 281
Zannetti, Paolo	I – p 213 II – p. 93 III – p 453

Blank Page

Subject Index¹ for Volumes I, II and III

2D visualization	III – p 435
3D visualization	III – p 435
Abatement	I – p 313, 355
Acid deposition	I – p 363
Advection	I – p 213
Aerial photography.....	III – p 435
AERMOD	I – p 185, 409
Aerodynamic resistance	II – p 233
Air dispersion models.....	I – p 363
Air pollution episode.....	I – p 313, 355
Air pollution model(s).....	I – p 185, 409
Air pollution modeling.....	I – p 1, 325
Air pollution regulations	I – p 1
Air pollution	I – p 1, 185, 313, 355
Air quality forecasting.....	I – p 313, 355
	II – p 397
Air quality modeling	I – p 13, 213
	II – p 233
	III – p 329 , 453
Air quality models.....	I – p 363
Air quality	I – p 185
	II – p 55
	III – p 169
Air-conditioning.....	II – p 267
Airflow	III – p 169
Algorithms.....	III – p 131
Ambient measurement.....	II – p 455
Ambient turbulence	I – p 103
Aqueous reactions	II – p 164
ArcExplorer.....	III – p 435
ArcGIS	III – p 435
Atmosphere	III – p 169
Atmosphere-Ocean General Circulation Models	III – p 353
Atmospheric boundary layer	I – p 37, 185
	II – p 11
Atmospheric chemistry.....	II – p 164
Atmospheric dispersion modeling.....	III – p 239 , 281
Atmospheric dispersion.....	III – p 397
Atmospheric motions	I – p 37
Available software	III – p 453
Building and terrain wakes.....	III – p 397
Building contamination	II – p 267
Building effects	I – p 185
Building safety	II – p 267
Buildings	III – p 169
Bulk resistance	II – p 233
Buoyant plumes.....	I – p 103
CALMET	I – p 409
CALPUFF	I – p 409
Canopy resistance.....	II – p 233

¹ Readers are encouraged to use the CD-ROM version of the book for text searching.

CFD	III – p 169
Chemical mass balance (CMB)	II – p 455
Chemical mechanisms	II – p 164
Chemical transformation	I – p 13
Chemical transport models	II – p 164
Chen-Kim	III – p 169
Clean Air Act Amendments	II – p 557
Clean Air Act	II – p 557
Climate change	III – p 353
Cloud-free boundary layer	II – p 11
Cloud-topped boundary layer	II – p 11
Combustion facilities	II – p 351
Compensation point	II – p 233
Complex terrain dispersion	I – p 185
Complex terrain	I – p 363
Computational fluid dynamics	III – p 169
Computational wind engineering	III – p 169
Constant flux layer	II – p 233
Convection	I – p 37
	II – p 11
Convective boundary layer	I – p 185
Coupled general circulation models	III – p 353
Courses online	III – p 453
Data needs	I – p 13
Decision support system	II – p 397
Dense gas models	I – p 363
Deposition of air pollutants	I – p 313, 355
Deposition	II – p 233
Diagnostic models	I – p 363
Diffusion	I – p 37, 213
Direct chemical exposures	II – p 351
Dispersion modeling	I – p 13, 103
Dispersion	I – p 185, 313, 355
	III – p 169
Eddy diffusivity	I – p 213
Effective plume heights	I – p 103
Emergency releases	I – p 363
Emission data	III – p 435
Emissions inventory	III – p 5
Emissions modeling	I – p 13
	III – p. 5
Emissions tools	III – p 5
ERCOFTAC	III – p 169
ESRI	III – p 435
Eulerian modeling	I – p 213
Fate modeling	II – p 351
Fluid dynamics	II – p 267
Footprint analysis	II – p 94
Four-dimensional data assimilation	I – p 363
Future modeling	I – p 325
Gaussian dispersion model	I – p 185
Gaussian methods	III – p 239
Gaussian model(s)	I – p 13, 363
Gaussian puff methods	III – p 281
Geocoding	III – p 435
Georeferencing	III – p 435

GIS	III – p 435
Global Mapper	III – p 435
Google Earth	III – p 435
Grid-based models	I – p 13
GUI	III – p 435
Guidelines	III – p 169
Hazardous air pollutants	II – p 164
Hazardous waste incinerators	II – p 351
Heterogeneous reactions	II – p 164
Human health	II – p 351
Indirect chemical exposures	II – p 351
Indoor air quality	II – p 267
Internet sites	III – p 453
Internet	I – p 325
Inventory preparation plan	III – p 5
ISC	I – p 185
Jet plumes	I – p 103
K-epsilon	III – p 169
Kinetics	II – p 164
Lab hood	III – p 169
Lagrangian air pollution modeling	II – p 94
Lagrangian models	I – p 363
Land use/land cover data	III – p 435
Langevin equation	II – p 94
Large-eddy simulations	II – p 11
Local and non-local closure	I – p 213
Long-range transport	I – p 363
	II – p 94
Mesoscale dispersion	II – p 94
Meteorological data	I – p 363, 409
Meteorological data	III – p 435
Micrometeorology	III – p 169
Mixed layers	I – p 37
	II – p 11
Mixing	I – p 37
	II – p 11
Model development	II – p 557
Model evaluation	II – p 503
Model performance evaluation	I – p 13
Model quality assurance	II – p 503
Modeling	I – p 313, 355
	III – p 169
Monin-Obukhov theory	II – p 233
Numerical algorithms	I – p 213
Numerical modeling	II – p 267
	III – p 131 , 353
Odor dispersion modeling	III – p 329
Odor impacts	III – p 329
Odor modeling	III – p 329
Odors	III – p 329
Ozone formation	I – p 313, 355
Parameterizations	III – p 131
Particle models	I – p 363
Particulate matter (PM)	II – p 164, 455
Particulate transport	II – p 267
Performance measures	II – p 503

Photochemical models.....	I – p 13, 363
Physical modeling.....	III – p 397
Plume models.....	I – p 363
Plume.....	III – p 169
Plume-in-grid.....	II – p 164
Pollution control.....	I – p 313, 355
Pollution roses.....	III – p 435
Pollution.....	III – p 169
Prognostic models.....	I – p 363
Project EMU.....	III – p 169
Puff models.....	I – p 363
QNET-CFD.....	III – p 169
Radicals.....	II – p 164
Receptor model.....	II – p 455
Regional models.....	I – p 363
Regulatory application.....	I – p 13
Regulatory model.....	I – p 185
Regulatory models.....	III – p 453
Remote sensing.....	III – p 435
Resolution.....	I – p 13
Resuspension.....	II – p 267
Risk assessment.....	II – p 351
RNG.....	III – p 169
RUC2.....	I – p 409
Satellite imagery.....	III – p 435
Secondary air pollutants.....	II – p 164
Second-hand smoke.....	II – p 267
Self-induced turbulence.....	I – p 103
Short-range models.....	I – p 363
Similarity theories.....	I – p 37
Simulation models.....	I – p 13
Simulation.....	I – p 313, 355
SketchUp.....	III – p 435
Source apportionment.....	II – p 455
Source profile.....	II – p 455
Stability conditions.....	I – p 103
Stable boundary layer.....	I – p 185
Stacks.....	III – p 169
Statistical indices.....	II – p 503
Statistical model evaluation.....	II – p 503
Steady state flow.....	III – p 169
Stochastic models.....	II – p 94, 397
Stratospheric ozone.....	II – p 164
Street canyon.....	I – p 313, 355
Surface fluxes.....	II – p 233
Surface layer.....	III – p 169
Terrain data.....	I – p 363
	III – p 435
Thermodynamics.....	II – p 164
Transport modeling.....	II – p 351
Transport.....	I – p 313, 355
Tropospheric ozone.....	II – p 397
Turbulence modeling.....	II – p 267
Turbulence.....	I – p 37
	II – p 11
	III – p 169

Uncertainty analysis	II – p 503
Uncertainty	I – p 13
Urban models	I – p 363
Urban ozone	II – p 164
Urban plume	I – p 313, 355
Urban	III – p 169
Validation	III – p 169
Ventilation	II – p 267
Visibility	I – p 363
Volatile organic compound (VOC)	II – p 455
Weather systems	I – p 37
Wind tunnel modeling	III – p 397

Blank Page

Additional Information About the Chapter Authors/ Contributors for Volumes I, II and III

Anfossi, Domenico

-  [CV](#)
-  [Picture](#)

Buono, Maureen E.

Builtjes, Peter J.H.

-  [Picture](#)

Byun, Daewon W.

-  [Bio](#)
-  [Picture](#)

Canepa, Elisa

-  [CV](#)
-  [CV-short](#)
-  [Picture](#)

Carrington, David B.

-  [CV](#)
-  [Picture](#)

Chow, Judith C.

-  [CV](#)
-  [Picture](#)

Cochran, Brad

-  [Bio](#)
-  [Picture](#)

Daly, Aaron

-  [CV](#)
-  [Picture](#)

Degrazia, Gervásio

-  [CV](#)
-  [Picture](#)

Diosey, Phyllis G.

-  [Resume](#)
-  [Picture](#)

Ferrero, Enrico

-  [Bio](#)
-  [Picture](#)

Finzi, Giovanna

-  [CV](#)
-  [Picture](#)

Freedman, Frank R.

-  [Resume](#)
-  [Picture](#)

González Barras, Rosa M.

-  [CV](#)

Hibberd, Mark

-  [Bio](#)
-  [Picture](#)

Hurley, Peter

-  [Bio](#)
-  [Picture](#)

Irwin, John S.

-  [CV](#)

Lacser, Avraham

-  [CV](#)

Lee, Russell

-  [CV](#)

Luhar, Ashok

-  [Bio](#)
-  [Picture](#)

Lyons, Walter A.

-  [CV](#)
-  [Bio](#)
-  [Picture](#)

McAlpine, J.D.

-  [Resume](#)
-  [Picture](#)

Michelsen, Hope

- [!\[\]\(95ab54620a11c027cf4c88809d671c27_img.jpg\) CV](#)
- [!\[\]\(429ccc6d924bc1a621a757712378f00f_img.jpg\) Picture](#)

Moussiopoulos, Nicolas

- [!\[\]\(8563419afdf108cfa131608a1cdd96e5_img.jpg\) Picture](#)

Nunnari, Giuseppe

- [!\[\]\(d82cf55f143759907302d315f7500cd9_img.jpg\) CV](#)
- [!\[\]\(36d817b4972a2b7700ebb469a71c65a6_img.jpg\) Picture](#)

Öetl, Dietmar

- [!\[\]\(bb4895c062450f5be2968f3d2315c288_img.jpg\) CV](#)
- [!\[\]\(2b396c3df7ae576573fa926d367a6d07_img.jpg\) Picture](#)

Pepper, Darrell W.

- [!\[\]\(ed9335bfc55e541c06c67e9dc3cb4b4a_img.jpg\) CV](#)
- [!\[\]\(28ecd8175bb5dfe455d3a87deb70671a_img.jpg\) Picture](#)

Pérez, Juan L.

- [!\[\]\(24cdc404b1fbd0e02d463bf9ae32b25d_img.jpg\) CV](#)
- [!\[\]\(f9e9797a5e681a1ba4b6f83e6e394495_img.jpg\) Picture](#)

Petersen, Ronald L.

- [!\[\]\(a41866822eaa6f07d8ded7419cb18b69_img.jpg\) Bio](#)
- [!\[\]\(10097573a7731a6abca8c2c69e3cfae8_img.jpg\) Picture](#)

Physick, William

- [!\[\]\(4a91a9d20a52ed2adf89642f82e53e7f_img.jpg\) Bio](#)
- [!\[\]\(ef671769684a36c0b96df0376590e466_img.jpg\) Picture](#)

Pun, Betty K.

- [!\[\]\(58f01cd2884f3548a9e936929177463f_img.jpg\) CV](#)
- [!\[\]\(9f80b85d066e3840bff0230c3d52e190_img.jpg\) Picture](#)

Richter, Richard O.

- [!\[\]\(8e4c81fc48a2655bb3c792a3279d115f_img.jpg\) CV](#)
- [!\[\]\(5ddfd9a694938f23d6f2c543eef32b85_img.jpg\) Picture](#)

Roth, Philip M.

- [!\[\]\(8aaebeff40947cda5f1c3eef0836ac38_img.jpg\) In Memoriam](#)

Ruby, Michael

- [!\[\]\(448286b5af6606ddbbc7ea48cff7260c_img.jpg\) Resume](#)
- [!\[\]\(730610ac282e4e36af0459d765457b2b_img.jpg\) Picture](#)

San José, Roberto

 [CV](#)
 [Picture](#)

Sarma, Ananthakrishna

 [CV](#)
 [Picture](#)

Seigneur, Christian

 [CV](#)
 [Picture](#)

Sheehan, Patrick J.

 [CV](#)
 [Picture](#)

Solomon, Douglas

 [Email](#)

Sorbjan, Zbigniew

 [CV](#)
 [Picture](#)

Thé, Jesse

 [CV](#)

Trini Castelli, Silvia

 [CV](#)
 [Picture](#)

van Dop, Han

 [CV](#)
 [Picture](#)

Venkatram, Akula

 [Picture](#)

Watson, John G.

 [CV](#)
 [Picture](#)

Yamartino, Robert J.

 [CV](#)
 [Picture](#)

Zannetti, Paolo



[CV](#)



[Picture](#)